Roman mining and metal production near the antique city of ULPIANA (Kosovo)

Dissertation

zur Erlangung des Doktorgrades

der Naturwissenschaften

vorgelegt beim Fachbereich 11

der Johann Wolfgang Goethe-Universität

in Frankfurt am Main

von

Katrin Julia Westner

aus Ingolstadt

Frankfurt 2016

vom Fachbereich 11 der

Johann Wolfgang Goethe-Universität als Dissertation angenommen.

Dekan: Prof. Dr. Ulrich Achatz

Erstgutachter: Prof. Dr. Gerhard Brey, Universität Frankfurt

Zweitgutachter: apl. Prof. Dr. Sabine Klein, Universität Frankfurt

Datum der Disputation: 25. Januar 2017

Zusammenfassung

Das *Metalla Dardanica* Projekt

Diese Dissertation wurde im Rahmen eines interdisziplinären Kooperationsprojektes (*Metalla Dardanica*) zwischen dem Deutschen Bergbau-Museum Bochum und der Goethe-Universität Frankfurt durchgeführt, welches sich mit römischen Bergbau auf Blei und Silber und der damit im Zusammenhang stehenden Metallproduktion im Hinterland des *municipiums* Ulpiana im Zentralkosovo beschäftigt. Ulpiana, etwa 8 km südöstlich von Prishtina / Priština gelegen, wird als Verwaltungszentrum oder sogar als eine Art Hauptstadt der Region Dardania (i.e. der südliche Teil der Provinz Moesia Superior) angesehen (Dušanić, 2004; Petrović, 2006; und Literaturangaben dort). Die herausragende Position der Stadt wird zum einen mit ihrer günstigen Lage nahe der Kreuzung zweier Hauptstraßen, der Nord-Süd-Verbindung von Scupi (Skopje) Richtung Naissus (Niš) mit dem an der Mittelmeerküste gelegenen Lissus (Lheza) erklärt, zum anderen aber auch mit den reichen Erzvorkommen des Zhegovc- / Žegovac-Gebirges im Hinterland Ulpianas begründet. Tatsächlich wird angenommen, dass Ulpiana der Zentralort eines Bergbaudistriktes (Janjevo) war und möglicherweise sogar seine Existenz der hiesigen Erzgewinnung verdankte (Dušanić, 2004; Petrović, 2006). Die seit 2009 von dem Deutschen Bergbau-Museum in Zusammenarbeit mit dem Archäologischen Institut des Kosovo (Instituti Arkeologjik i Kosovës) durchgeführten Surveys in der Umgebung des *municipiums* führten zur Lokalisierung eines zwischen den Weilern Shashkoc / Šaškovac und Janjevo gelegenen Bergbaurevieres mit zahlreichen Spuren vormoderner Erzgewinnung und -aufbereitung (Stollen, Pingen, Schächte, Abraumhalden, Aufbereitungseinrichtungen) sowie mehrerer Schmelzplätze, welche eine vorläufig römisch / spätantike bis mittelalterlich / frühmoderne Zeitstellung besitzen. Die reichhaltigen montanarchäologischen und archäometallurgischen Befunde im Untersuchungsgebiet eröffnen die Möglichkeit die gesamte lokale *chaîne opératoire* - i.e. von den abgebauten Erzrohstoffen und metallurgischen (Bei-) Produkten zu Metallartefakten als Endprodukten - zu untersuchen und mögliche chronologische Variationen über eine Zeitdauer mehrerer Jahrhunderte nachzuvollziehen. Ein zentraler Punkt des Projektes ist die enge Verzahnung montanarchäologischer Methoden (GPS-basierte Surveys, geophysikalische und geoelektrische Messungen, Ausgrabungen an ausgewählten Abbau- und Verhüttungsplätzen) und geochemischer Analytik (OM, XRD, EMP, MC-ICP-MS).

Das Revier von Shashkoc-Janjevo und die Erzrohstoffe

Die beprobten Erze stammen vor allem aus der sulphidischen Primärmineralisation, repräsentieren teilweise aber auch lokal gebildete sekundäre Kupfersulphide und oxidierte Phasen. Die sulphidische Vererzung ist hydrothermalen Ursprungs und typischerweise in Form von Gängen, als Imprägnationen und Stockwerk ausgeprägt (Monthel et al., 2002). Analog zu anderen Lager-

stätten des serbomazedonischen Rhodopengürtels, welcher sich durch Serbien, Kosovo, Mazedonien, Nordgriechenland und Südbulgarien erstreckt (Heinrich & Neubauer, 2002), steht auch das Erzvorkommen von Shashkoc-Janjevo im Zusammenhang mit tertiärer magmatischer Aktivität, welche durch post-kollisionale Dehnungstektonik nach Schließung des Vardar-Ozeans (ein Bereich der Tethys) und Konvergenz von Afrika und Eurasia ausgelöst wurde (bspw. Borojević Šoštarić et al., 2012; Kalogeropoulos et al., 1989; Marchev et al., 2005).
Die sulphidische Vererzung wurde in drei Phasen (mittels Pb-Isotopie nicht unterscheidbar; s. unten) mit folgenden Hauptmineralen ausgefällt: I) Pyrit, Arsenopyrit, Quarz, II) Galenit, Sphalerit, Pyrit, Arsenopyrit, Chalcopyrit, Fahlerz, Carbonat / Quarz und III) Galenit, Sphalerit, Pyrit / Markasit, Carbonat. Erz aus den beiden frühesten Phasen ist durch erhöhte Kupfer-, Arsen- und Antimon-Gehalte gekennzeichnet, während es sich bei der später gebildeten, weniger variablen Mineralisation im wesentlichen um ein Blei-Zink-Silber-Erz handelt. Der Quarzgang der Haupterzfällungsphase (II) ist laut Hyseni & Alliu (1999) goldführend. Erz der beiden ersten Bildungsphasen ist nahe magmatischer Gesteine tertiären Alters, deren Bildung im Zusammenhang mit der des Erzes steht (s. oben) und welche somit den zentralen und heißesten Teil des Mineralisationssystemes darstellen, relativ angereichert. Dadurch lässt sich eine leichte Zonierung innerhalb des Revieres feststellen. Während von alten Abbauen im nahe Shashkoc aufgeschlossenen Serpentinit oftmals ausgeprägt galenitreiches Erz der späten Bildungsphase (III) beprobt wurde, konnten unmittelbar oberhalb von Janjevo in andesitisch / dacitischem Wirtsgestein ausschließlich Erze der zuvorigen Fällungsphasen gesammelt werden. Sekundäre Kupfersulphide, v.a. Chalkosin[1], Digenit[2] und Covellin[3], haben sich lokal aufgrund supergener Prozesse gebildet und sind oftmals wiederum bereits vor allem zu Malachit und Azurit verwittert.
Silber ist ein wichtiges Nebenelement des Erzes. Es ist im allgegenwärtigen Galenit vorhanden (median 895 ppm), der einer der wichtigsten Silberträger ist. Höhere Gehalte des Edelmetalles konnten zumeist in Mineralen der mittleren Fällungsphase bzw. deren Umwandlungsprodukten nachgewiesen werden und somit zu einem bevorzugten Abbau dieses Erztypes geführt haben. Die mittleren Gehalte in Fahlerz, sekundären Kupfersulphiden und oxidierten kupferhaltigen Phasen (v.a. Malachit) betragen 2,96 Gew-%, 4040 ppm und 590 ppm.
Das geförderte Erz wurde offensichtlich in unmittelbarer Nähe der Abbaugruben zerkleinert und sortiert. Anhand von Ausgrabungen ließ sich belegen, dass das Rohmaterial für die Verhüttung zumindest an einem der untersuchten Schlackenplätze (Mramor Samakove) in Form von etwa erbsengroßen Stücken angeliefert wurde. Ob eine weitere Zerkleinerung (etwa durch Aufmahlen) und Aufbereitung, ggf. auch mit nassmechanischen Methoden, erfolgte, lässt sich bislang weder aufgrund des Probenmaterials noch der archäologischen Befunde klären. Ebenso erlauben die bisherigen Erkenntnisse keine genaue Aussage ob bzw. in welchem Umfang die Erze vor dem Schmelzverfahren geröstet wurden. Es kann allerdings ausgeschlossen werden dass Schwefel vollständig ausgetrieben wurde, da in allen Schlackenproben eine beträchtliche Menge an neugebildeten Sulphidverbindungen beobachtet werden konnte. Dadurch lässt sich auch eindeutig erkennen, dass sämtliche untersuchten Schlacken die Überreste primärer Verhüttungsprozesse (mehrheitlich) sulphidischer bleireicher Ofenchargen darstellen.

[1] Cu_2S
[2] $Cu_{1,8}S$
[3] CuS

Die Rohstoffversorgung der Schmelzplätze

Insgesamt zehn Verhüttungsplätze - davon drei mit vorläufig römisch / spätantiker (Voguçincë / Vogačića, Mirash / Miraš, Mirash Novo / Miraš Novo), sechs mit vermutlich mittelalterlich / frühmoderner Datierung (Mramor Samakove, Marec / Marevce, Hajkobile / Ajkobilia, Hanroc / Androvac, Akllap / Oklap, Ostri Vrh) sowie ein bislang nicht datierbarer Platz (Mramor Proni Butoçit / Mramor Proni Butočit) - welche sich in einem Radius von etwa 20 km um Ulpiana befinden wurden genauer untersucht. Basierend auf Bleiisotopenanalytik konnten metallurgische (Bei-) Produkte der vorläufig römisch / spätantik datierten Verhüttungsplätze von Voguçincë und Mirash Novo sowie der mutmaßlich mittelalterlich / frühmodernen Fundplätze Mramor Samakove, Akllap und Ostri Vrh und des bislang undatierten Mramor Proni Butoçit ganz oder teilweise Erzen aus dem Revier von Shashkoc-Janjevo ($^{206}Pb/^{204}Pb$ = 18,781 - 18,793; $^{207}Pb/^{204}Pb$ = 15,665 - 15,675; $^{208}Pb/^{204}Pb$ = 38,950 - 39,004; $^{207}Pb/^{206}Pb$ = 0,83382 - 0,83433; $^{208}Pb/^{206}Pb$ = 2,07268 - 2,07595; n = 10) zugeordnet werden. Daneben zeichnen sich Verhüttunsgrelikte, die an den genannten Plätzen beprobt wurden durch überdurchschnittliche Gehalte an Nickel, Chrom und Magnesium aus, die höchstwahrscheinlich von dem im Distrikt von Shashkoc-Janjevo teilweise als Wirtsgestein der Vererzungen vorhandenen Serpentinit eingetragen wurden. Schlacken aus Marec stimmen teilweise mit Erzen aus der mindestens seit dem Mittelalter abgebauten Vererzung von Novobërdë / Novo Brdo überein ($^{206}Pb/^{204}Pb$ = 18,617 - 18,625; $^{207}Pb/^{204}Pb$ = 15,656 - 15,659; $^{208}Pb/^{204}Pb$ = 38,788 - 38,789; $^{207}Pb/^{206}Pb$ = 0,84076 - 0,84096; $^{208}Pb/^{206}Pb$ = 2,08308 - 2,08350; n = 3). Die restlichen Verhüttungsprodukte besitzen Bleiisotopensignaturen zwischen denen der beiden genannten Lagerstätten und können somit durch eine Mischung von Erzen mit leicht unterschiedlicher Signatur, durch die Verhüttung eines bislang nicht charakterisierten Rohstoffvorkommens oder durch ein Zusammenspiel beider Effekte erklärt werden (ausgeschlossen werden können analytische Artefakte durch Isotopenfraktionierung sowie zu geringe Bleigehalte). Insgesamt vier Proben von den südlich des Distriktes von Shashkoc-Janjevo gelegenen Plätzen Voguçincë, Mirash und Akllap weisen eine in allen Isotopenverhältnissen überlappende Signatur auf. Diese Tatsache spricht für die Hypothese, dass diese metallurgischen Überreste tatsächlich durch Verhüttung von Erzen aus einem einzelnen, bislang nicht charakterisierten Vorkommen erzeugt wurden.

Rekonstruktion archäometallurgischer Prozesse anhand von metallurgischen (Bei-) Produkten

Während aus Mramor Samakove bislang nur Ofenschlacken bearbeitet werden konnten, handelt es sich bei den übrigen Proben um Basinschlacken. Die beiden Schlackentypen unterscheiden sich in ihrer Bildungsgeschichte. Während Ofenschlacken im oberen Teil des Ofens gebildet wurden, sind Basinschlacken in einem speziell angelegten Reservoir, welches sich entweder innerhalb oder außerhalb des Ofens befand, abgekühlt. Die Morphologie von Basinschlacken welche außerhalb des Ofens erstarrt sind, weist eindeutig darauf hin, dass die silikatische Schmelze abgestochen wurde. Wie ihr in der Regel mehrlagiger Aufbau belegt, wurde die Abstichöffnung periodisch geöffnet um die Schlacke abzulassen. Basinschlacken, welche sich in einem Reservoir innerhalb des Ofens gesammelt haben, bestehen dagegen stets aus nur einer Schicht und weisen aufgrund ihrer Bildungsbedingungen wenig oder keine Anzeichen von Fließbewegungen auf. Dieser

Schlackentyp konnte bislang lediglich an den vermutlich mittelalterlich / frühmodernen Schmelzplätzen von Akllap und Ostri Vrh gefunden werden; an den drei potentiell römisch / spätantiken Verhüttungsplätzen wurden dagegen nur Abstichschlacken aufgefunden. Die bei allen Basinschlacken stets überlappenden Paragenesen und Phasenzusammensetzungen implizieren, dass jeder Schlackenblock im Verlauf einer Schmelzoperation entstanden ist und dadurch einer Ofencharge entspricht. Im Allgemeinen scheint die Schweretrennung der verschiedenen Schmelzen ausreichend gewesen zu sein, da die Schlacken offensichtlich nicht zerschlagen wurden um manuell Metalleinschlüsse abzutrennen.

In den meisten Basin- und allen Ofenschlacken ist Olivin die Hauptphase. Daneben fanden sich aber auch Olivin + Klinopyroxen-, Klinopyroxen- und Melilith-dominante Typen sowie glasige Schlacken. Letztere scheinen teilweise Blei-Silikate zu enthalten, deren Zusammensetzung aufgrund ihrer geringen Korngröße allerdings nicht bestimmt werden konnte. Subtypen der Basinschlacken wurden auf Basis des Vorkommens von Eisenoxidphasen (i.e. Spinell *ss* und Wüstit) und spät gebildetem Klinopyroxen (nur in Olivin-dominanten Typen) sowie der Kristallisationsreihenfolge definiert. Die meisten Analysen von Olivinen zeigen eine sehr eisenreiche Zusammensetzung und können in Übereinstimmung mit den Ergebnissen der Diffraktometeraufnahmen als Fayalit klassifiziert werden. Daneben wurden zum Teil beachtliche Gehalte von Magnesium und Zink bestimmt. Spätkristallisierte Olivine aus einer zweiten Generation, aber auch Analysen aus Klinopyroxen-haltigen Basinschlacken sowie Ofenschlacken sind in der Regel stark an Calcium angereichert (bis hin zu Kirschsteinit[4]). Klinopyroxene treten entweder als Spätkristallisat in Olivin-dominanten Schlacken auf oder bilden sich nach Eisenoxiden in Klinopyroxen- und Olivin + Klinopyroxen-Schlacken. Die Klinopyroxene sind calcium- und eisenreich und konnten als Hedenbergite bzw. Augite identifiziert werden. Der Chemismus der Melilithe bewegt sich zwischen Hardystonit, Gehlenit und (Fe-)Åkermanit[5]. Spinell *ss* tritt teilweise in Olivin- und allen Olivin + Klinopyroxen-, Klinopyroxen-, Melilithschlacken und glasigen Typen als Erstkristallisat auf und bildet sich ansonsten nach Olivin. Die Zusammensetzung ist generell nahe der von Magnetit, wobei ein Teil des dreiwertigen und zweiwertigen Eisens von vor allem Aluminium bzw. Zink ersetzt ist. Während Wüstit in Ofenschlacken häufig auftritt, ist er in Basinschlacken aufgrund der oxidierenderen Bildungsbedingungen nur noch restitisch vorhanden und in der Regel bereits zu Magnetit umgewandelt. Iscorit[6] bildet sich in Schlacken durch Reaktion von Wüstit und Fayalit mit atmosphärischem Sauerstoff (Smuts, 1992; Van Aken et al., 2005) und kann daher in oberflächennahen Bereichen und in der Nähe von Poren beobachtet werden. Leucit ist die häufigste Kalium- und Aluminium-Trägerphase in den Schlacken und scheint häufig aus einer entmischten kaliumreichen Schmelze kristallisiert zu sein. Feldspatverbindungen oder Kalsilit können in Schlackenzonen mit (lokal) erhöhten Silizium- und / oder Aluminiumgehalten vorhanden sein. Glas wurde in allen untersuchten Schlacken beobachtet.

Die geringen Anteile von restitischen Galenitkörnern (der in der Regel sicherlich die Hauptkomponente der verhütteten Erzchargen darstellte) in den Schlacken weisen darauf hin, dass die Verhüttungsöfen bei Temperaturen deutlich über 1115 °C, dem Schmelzpunkt von Bleiglanz (bspw. Craig & Kullerud, 1968), betrieben wurden. Die Maximaltemperaturen in der alten Metallurgie

[4] $CaFeSiO_4$
[5] $Ca_2(Zn,Fe,Mg,Al)(Si,Al)_2O_7$
[6] $Fe^{2+}{}_5Fe^{3+}{}_2SiO_{10}$

hingegen dürften 1400 °C kaum überschritten haben (bspw. Hauptmann, 2014). Klinopyroxen-, Melilith- und glasige Schlacken wurden bei oxidierenden Bedingungen gebildet (-log pO_2 zwischen ca. 10 und 5; im Gegensatz dazu zwischen ca. 12 und 7 für Olivinschlacken), unter denen Fayalit zu Magnetit und SiO_2 zerfällt (FMQ-Puffergleichgewicht; cf. Lindsley, 1976). Generell ist von einer Zugabe silikatischen Materials zu den Ofenchargen auszugehen, um eine ausreichende Schlackenbildung und somit Bindung von Verunreinigungen aus der Ofencharge zu gewährleisten. Dieses fiel bei der Aufbereitung in Form von restitischem Gangmaterial bzw. Wirtsgestein an, war aber auch als Sand, der bspw. von Bachläufen gewonnen werden konnte, verfügbar. Während der Eisengehalt der Schlacken durch die Mineralogie des Erzes erklärt werden kann, ist für die Bildung von Klinopyroxen- und Melilith-Schlacken (Proben aus Akllap, Mramor Proni Butoçit und Ostri Vrh) die Zugabe eines calciumhaltigen Flussmittels erforderlich. Glasige Schlacken (Proben aus Mirash Novo und Voguçincë) werden als Produkte eines Schmelzverfahrens unter relativ hohen fO_2, aber ohne Calciumzuschlag interpretiert. Für Olivinschlacken mit einem überdurchschnittlich hohen Calciumanteil in der Hauptphase (Proben aus Hajkobile, Hanroc und Mramor Proni Butoçit) könnte neben ausgeprägter Wechselwirkung mit calciumhaltiger Ofenwandung und Holzkohlenasche auch ein gezielter Zuschlag verantwortlich sein. Im Vergleich mit den anderen untersuchten Proben stimmen die Schlacken aus Mramor Proni Butoçit demnach mineralogisch, chemisch und auch typologisch mit dem Fundmaterial mutmaßlich mittelalterlich / frühmoderner Schmelzplätze überein. Die Bildung von Schlacken der vorläufig römisch / spätantik datierten Plätze Voguçincë, Mirash und Mirash Novo, sowie teilweise der vermutlich mittelalterlich / frühmodernen Fundplätze Marec und Hanroc kann hingegen durch die Zugabe silikatischen Materials und Wechselwirkung der Schmelze mit Ofenwandung und Holzkohlenasche erklärt werden; im Gegensatz zu späterer Prozessführung wurde eindeutig kein Calcium zugesetzt. Die Vorteile eines Calciumzuschlages liegen in der geringeren Viskosität sowie niedrigerer spezifischen Dichte der Schlacken, wodurch eine bessere Segregation der verschiedenen Schmelzen erreicht wird. Zudem treibt Calcium Blei aus seinen Silikatverbindungen aus, wodurch die Metallausbeute gesteigert werden kann (bspw. Bachmann, 1980; Gowland, 1914). Für fO_2-Bedingungen außerhalb des Fayalitstabilitätsfeldes ist ein Calciumzuschlag unerläßlich um nicht ausgesprochen zähe glasige Schlacken, sondern Klinopyroxen- und Melilith-dominante Paragenesen zu erhalten.

Ein weiterer Unterschied zwischen dem Fundmaterial mutmaßlich römisch / spätantiker und Plätzen mit einer potentiell späteren Datierung besteht in der Anwesenheit der Beiprodukte Matte und Speise, welche in nennenswerten Mengen beinahe ausschließlich an den drei vermutlich römisch / spätantiken Plätzen (Matte: Voguçincë, Mirash, Mirash Novo, Mramor Proni Butoçit, Hajkobile; Speise: Mirash Novo) gefunden wurden. Als Sammelbegriff umfasst Matte generell alle Basismetallsulphide, welche bei metallurgischen Prozessen gebildet werden. Matte tritt allgegenwärtig als tröpfchenförmige Einschlüsse, als interstitielle sulphidische Cluster (Galenit und (Zn,Fe)S, tlw. Pyrrhotin[7]), Pb-Cu-Matte (Galenit und Chalkosin *solid solution (ss)*) und Matte sensu stricto (s.s.; Galenit und Bornit *ss*, tlw. Pyrrhotin und (Zn,Fe)S), der einzige Typ, der aus einer von den Schlacken- und Metallschmelzen segregierten sulphidischen Schmelze kristallisiert ist, auf. Die Kupfer-(Eisen)-Sulphide beinhalten bemerkenswerte Silbergehalte (median 1530

[7] $Fe_{1-x}S$

ppm und 2730 ppm in Bornit *ss* bzw. sekundärem Covellin; Chalkosin *ss* konnte nicht analysiert werden). Möglicherweise wurde Matte bei relativ kupferreichen Ofenchargen bewusst erzeugt indem die Erze nicht totgeröstet wurden, um zu verhindern dass Kupfer in das Rohblei eingeht. Dadurch würde der Schmelzpunkt des Metalles stark erhöht werden, wodurch die Kupellation und andere Raffinationsprozesse erheblich erschwert werden würden. Fraglich ist ob die Silberverluste in der Matte den Metallurgen bewusst waren und ob diese durch weitere Behandlung dieses Materials minimiert wurden. Bachmann (1993) schlug für besonders silberreiche Erze vor, dass diese in der Antike geröstet und unter Zugabe von Blei als Edelmetallsammler verhüttet wurden. Im Mittelalter ist die Extraktion des Edelmetalles aus Matte der Blei-Silber-Metallurgie bekannt (bspw. Goldenberg, 1996).
Speise tritt als eisenreiche Variante und als Basismetallspeise auf. Erstere besteht zumeist aus Fe_9As und Fe_2As, FeAs tritt untergeordnet auf. Es konnten nur selten geringe Gehalte von Silber nachgewiesen werden. Auch die Fundsituation spricht für eine Entsorgung dieses Materials. Basismetallspeise ist gekennzeichnet von ausgeprägter Substitution und kann chemisch annähernd als $(Cu, Ni, Fe, Ag)_x(Sb, Sn, As)_y$ beschrieben werden. Aufgrund der ähnlichen Dichte ist Basismetallspeise oft eng mit Rohblei assoziiert und konnte dadurch nur selten untersucht werden. Die Silbergehalte der Phasen sind teilweise beachtlich. In $(Cu,Ni)_2Sb$ wurden im Mittel 2450 ppm des Edelmetalles nachgewiesen, in Proben aus Mirash Novo konnte Dyscrasit[8] beobachtet werden. Wie von Keesmann (1993) postuliert, wurde Basismetallspeise aufgrund der engen Verwachsung wahrscheinlich zumeist automatisch zusammen mit dem Rohblei kupelliert. Obwohl Kupellationsüberreste bislang nur in Marec gefunden wurden, kann aufgrund des durchweg hohen Silbergehaltes der Erze von einer Raffination des Rohbleis ausgegangen werden; dabei würden auch potentielle Goldgehalte abgetrennt werden. Die Tatsache, dass bislang kaum Kupellationsüberreste gefunden werden konnten lässt sich dadurch erklären, dass die bei diesem Raffinationsprozess erzeugte Bleiglätte anschließend wieder zu elementarem Blei zurückreduziert wurde.
Die Häufung von v.a. Matte an mutmaßlich römisch / spätantiken datierten Verhüttungsplätzen weist auf einen ausgeprägt polymetallischen Charakter des in dieser Periode verhütteten Erzes hin. Im Bergbaudistrikt von Shashkoc-Janjevo besitzt Erz der beiden frühesten Bildungsphasen einen ausgeprägt Kupfer-Arsen-Antimon-reichen Charakter und konnte zumeist an Gruben oberhalb von Janjevo beprobt werden. Die höheren Silber- sowie potentiell vorhandene Goldgehalte (s. oben) lassen einen bevorzugten Abbau dieser Mineralisationen im früheren Stadium des lokalen Bergbaus wahrscheinlich erscheinen. In der Nähe von Shashkoc wurde dagegen typischerweise beinahe monomineralischer Bleiglanz, der in der Spätphase der Erzfällung gebildet wurde, beobachtet. Dieser Zusammenhang entspräche den Beobachtungen Davies' (1935), der von römischen Bergbau nahe Janjevo und mittelalterlicher Erzgewinnung bei Shashkoc ausging.

Metallartefakte und die (über-) regionale Bedeutung der örtlichen Metallproduktion

Insgesamt vier in Ulpiana geborgene Bleiartefakte - zwei Sarkophage für Kleinkinder, ein rechteckiger Block mit der Inschrift 'III' (möglicherweise ein Gewicht) und ein mit Ornamenten dekoriertes feines Blech - konnten beprobt werden. Das Metall weist nur geringe Verunreinigungen von

[8] Ag_3Sb

vor allem Schwefel und Antimon auf. Die in der Regel nicht nachweisbaren Silbergehalte deuten darauf hin, dass das Rohmetall vor seiner Weiterverarbeitung kupelliert wurde. Die beiden Sarkophage konnten isotopisch Erzen aus Rudnik (Šumadija-Distrikt, Serbien; Pernicka et al., 1993) bzw. dem Kopaonik-Gebirge (Serbien / Kosovo; Gale, 1990, pers. comm.; Pernicka et al., 1993; Veselinović-Williams, 2011) zugeordnet werden. Die beiden anderen Bleiartefakte können generell mit Rohstoffen aus der Region in Verbindung gebracht werden, zeigen aber keine direkte Überlappung. Daneben können die vier Objekte aufgrund der ähnlichen Bildungsgeschichte der Mineralisationen auch mit tertiären Erzen des serbomazedonischen Rhodopengürtels und südostspanischer Vorkommen in Verbindung gebracht werden (Amov (1974; 1979; 1983; 1993) zitiert in Gale et al., 2000; Arribas & Tosdal, 1994; Chalkias et al., 1988; Graeser & Friedrich, 1970; Kalogeropoulos et al., 1989; Marcoux et al., 2002; Oen et al., 1975; Stos-Gale et al., 1995; Stos-Gale et al., 1996; Stos-Gale et al., 1998). Aufgrund der reichen Erzvorkommen in der Region ist aber eine lokale Provenanz der Rohstoffe sicherlich am wahrscheinlichsten. Teilweise beobachtete intermediäre Bleiisotopensignaturen können bei Bleiobjekten generell zum einen bereits bei der primären Erzverhüttung, aber auch nachfolgend bei Raffinationsprozessen, bspw. der Kupellation, zustande kommen. Dazu passt die Hypothese von Merkel (2007), der annahm, dass das gesamte Rohblei welches an römischen Schmelzplätzen gewonnen wurde, gesammelt wurde und an zentraler Stelle unter staatlicher Aufsicht kupelliert wurde. Funde von Gussformen für Silberbarren und metallischem Blei nahe von Öfen in Ulpiana's Werkstattkomplex (Parović-Pešikan & Stojković, 1995) legen die Vermutung nahe, dass zumindest zeitweise Rohblei innerhalb des *municipiums* raffiniert wurde.

Neben den Bleiartefakten wurden zwei Münzfunde aus Voguçincë und Ulpiana untersucht. Dabei handelt es sich um eine Bronzemünze (5,36 - 6,67 Gew-% Sn[9]) aus der Zeit von Probus (276 - 282) und eine Kupfermünze (0,22 - 0,83 Gew-% Sn), welche unter Aurelian geprägt wurde (270 - 275; M. Berisha & E. Shala, pers. comm.). In der Bronzelegierung konnten geringe Anteile von Schwefel bestimmt werden (0,01 - 0,04 Gew-% S). Aufgrund der bestimmten Bleigehalte (median 0,06 und 0,07 Gew-%) können durch Isotopenanalytik nur Rückschlüsse auf potentielle Blei (-Silber)-Quellen gezogen werden. Beim Abgleich mit der Datenbank stellte sich aber heraus, dass die Isotopensignatur der Münzen nicht eindeutig bestimmten Lagerstättenregionen zugewiesen werden konnte. Da die Münzen aus offiziellen Prägeanstalten stammen, ist zu erwarten dass Rohmaterial verschiedener Herkunft gemischt und zudem Altmetall recycelt wurde.

Kupferisotopenverhältnisse wurden an Erzen und Metallartefakten bestimmt. Die Signaturen der Erze (zwischen -4,29 und 11,90 ‰) und daraus abgeleitete Fraktionierungsprozesse stimmen zumeist mit der Petrographie und den Mineralparagenesen überein. Abweichungen können durch eine teils komplexe Entstehungsgeschichte der Erze und daraus resultierenden An- und Abreicherungseffekten, welche durch die relativ große Oberfläche der aufbereiteten Erzstücke verstärkt wurden, erklärt werden. Die analysierten Metallartefakte besitzen δ^{65}Cu-Werte zwischen +0,44 und -0,77 ‰. Dieser Datenbereich entspricht den Werten, die für primäre Erze postuliert wurden (-1 bis +1 ‰; bspw. Markl et al., 2006). Somit kann angenommen werden, dass die Objekte aus sulphidischen Erzchargen erschmolzen wurden. Diese Schlussfolgerung stimmt mit den zumeist detektierbaren Schwefelgehalten (s. oben) und der Tatsache, dass sowohl Blei als

[9] Vgl. Stech (1999) zur Klassifikation von Kupfer- und Bronzeartefakten.

auch Kupfer in der Zeit des römischen Reiches überwiegend aus sulphidischen Erzen gewonnen wurden, überein.
Um die Bedeutung der lokalen Metallproduktion abschätzen zu können, wurde die mögliche Provenanz von Bleiartefakten bzw. bleihaltigen Objekten, welche aufgrund ihrer Inschriften bzw. Fundsituation aus örtlichen Vererzungen produziert worden sein könnten, mit der durch diese Studie erheblich vergrößerten Datenbank verglichen. Dazu wurden zwei Datensets ausgewählt: 1) Ein Schiffswrackfund aus Augusta Caesarea (Israel; Raban, 1999), welcher unter anderem Bleibarren mit der Inschrift '*MET DARD*' beinhaltet und 2) Bleiglasuren von spätantiker Keramik aus Serbien und Rumänien (Walton & Tite, 2010). Für beide Fundgruppen konnte eine mögliche Produktion aus lokalen Rohstoffen postuliert werden. Anhand der Provenanzstudien an diesen Datensets und den in Ulpiana gefundenen Bleiobjekten kann geschlussfolgert werden, dass a) ein als *Metalla Dardanica* bezeichneter Bergbaudistrikt existierte, b) die Römer, wie auch in anderen Regionen des Reiches, nach Möglichkeit auf örtliche Ressourcen für die Metallproduktion zurückgriffen und c) offenbar schwunghafter Handel mit Metallen aus lokaler Produktion getrieben wurde und der Erzreichtum der Balkanregion somit von hoher Relevanz für die Rohstoffversorgung des (späten) römischen Reiches gewesen sein muss.

Summary

This PhD thesis has been carried out within an interdisciplinary cooperational project between the Deutsches Bergbau-Museum Bochum and the Goethe-Universität Frankfurt, which is dedicated to ancient Pb-Ag mining and metal production in the hinterland of the *municipium* Ulpiana in central Kosovo. Geochemical analysis (OM, XRD, EMP, MC-ICP-MS) of ores, metallurgical (by-) products and metal artefacts allowed to reconstruct the local *chaîne opératoire* and to decipher significant chronological differences between presumably Roman / late antique and medieval / early modern metallurgical processing. Pb isotope provenance studies documented the relevance of local metal production within the Roman Empire and confirmed the actual existence of a *Metalla Dardanica* district, which until now solely has been suspected on basis of epigraphy. The predominant abundance of the by-products matte (consisting of base metal sulphides) and speiss (ferrous speiss: Fe-As compounds; base metal speiss: $\sim (Cu, Ni, Fe, Ag)_x(Sb, Sn, As)_y$) at smelting sites with a preliminary Roman / late antique dating points to treatment of complex polymetallic ore. Pb isotope analysis demonstrated that the mining district of Shashkoc-Janjevo (partially) supplied six of the ten investigated metallurgical sites. In this mineralisation, parageneses with elevated Cu, As and Sb abundances comprise significant proportions of particularly tennantite-tetrahedrite minerals, chalcopyrite, arsenopyrite and were generated during the early and main stages of ore formation. Later precipitated ore in contrast is marked by a significantly less versatile mineralogy and consists almost exclusively of galena, sphalerite and pyrite / marcasite. Early- and main-stage ore parageneses are due to their precipitation at higher temperatures comparably enriched in the vicinity of genetically related Tertiary igneous rocks (e.g. Janković, 1997) as the hottest central part of the mineralising system. Besides increased Cu, As and Sb contents, ore from the main formation stage also exhibits generally higher Ag abundances, which are mainly hosted by fahlore and locally abundant secondary Cu sulphides (chalcocite, digenite and covellite) and oxidised phases (e.g. malachite, azurite). The higher precious metal grades of this ore type, whose geochemical signature (i.e. higher proportions of Cu, As and Sb) is mirrored by the abundance of the metallurgical by-products matte and speiss (almost exclusively found at potentially Roman / late antique smelting sites; see above), presumably were a pivotal factor leading to its preferential exploitation in earlier times. Matte and base metal-rich speiss contain notable amounts of Ag, which are mainly present in Cu-(Fe) sulphides and particularly antimonides ($(Cu,Ni)_2Sb$, Ag_3Sb), respectively. While the speiss compounds due to their close association with Pb bullion presumably were cupelled automatically (cf. Keesmann, 1993), the metallurgical treatment of matte could not have been unambiguously proven, but overall certainly is highly likely.
The beneficiated ore (i.e. crushed and sorted, potentially also treated by more lavish techniques such as grinding, sieving or wet-mechanical methods) possibly was partially roasted and subsequently together with fluxes and charcoal submitted to the furnaces. The working temperatures

approximately ranged between 1100 and 1400 °C. Slags from all presumably Roman / late antique dated and few of their potentially medieval / early modern analogues were produced from smelting of (partially roasted) ore with charcoal and added siliceous material, thus resulting in fayalite-dominant phase assemblages or rarely observed glassy parageneses. Even though several subtypes of fayalite slags have been established on basis of the abundance of Fe-rich oxide phases (i.e. spinel *ss* and wüstite), late clinopyroxene and the general solidification sequence of the slags, the process conditions (i.e. temperature, fO_2, added fluxing agents) must have been widely similar; chemical variations could be explained by varying degress of interaction of the slag melt with charcoal ash and furnace material. The other investigated metallurgical remains indicate employment of a calcareous flux, which led to formation of Ca-rich olivine-, olivine + clinopyroxene-, clinopyroxene- or melilite-type slags. Slag compositions with a higher bulk Ca content are advantageously characterised by a lower viscosity and specific gravity (e.g. Bachmann, 1980; Gowland, 1914). These types as well as glassy slags were generated at more oxidising conditions outside the fayalite stability field (FMQ buffer equilibrium, cf. Lindsley, 1976; –log pO_2 between 10 and 5) than their olivine-dominant analogues (–log pO_2 between 12 and 7). Conclusions on the furnace construction could be drawn on basis of the typology of the slags, which mostly were tapped into a basin located outside the furnace, but partially (at two presumably medieval / early modern sites) also accumulated in a reservoir within the smelter.
Lead artefacts excavated in Ulpiana could be isotopically related to ores from mineralisations in its vicinity and demonstrate that the resources were at least utilised for local metal production. However, also ship wreck cargo from Israel - including several lead ingots with the inscription *'MET DARD'* (Raban, 1999) - and late antique lead-glazed pottery from Serbia and Romania (Walton & Tite, 2010) could be related to a possible Kosovarian / Serbian provenance of the raw material and thus indicate flourishing trade of metal from the *Metalla Dardanica* district within the Roman Empire.

Contents

Zusammenfassung I

Summary IX

I. Introduction 1

1. The *Metalla Dardanica* project 2

2. Ancient mining and metallurgy of lead and silver 4
2.1. Lead and silver ores . . . 4
2.2. Ore beneficiation . . . 5
2.3. Extraction of lead . . . 6
2.3.1. The roast-reduction process . . . 6
2.3.2. The roast-reaction process . . . 7
2.4. Extraction of silver . . . 7
2.5. The chemistry of smelting and metallurgical (by-) products . . . 8
2.5.1. Slag . . . 9
2.5.2. Matte . . . 14
2.5.3. Speiss . . . 15
2.5.4. Pig iron . . . 15
2.5.5. Native lead . . . 15

3. Regional metallogeny and ore deposits 17
3.1. Spatial categorisation and relationship with geodynamic processes . . . 17
3.2. Pb-Zn-Ag-(Cu-Au) deposits of the Kopaonik district . . . 18
3.2.1. Pb-Zn-Ag deposits of the Zhegovc Mountains . . . 18
3.2.2. Occurrences of other base and precious metals in central / southern Kosovo 20
3.2.3. Pb-Zn-Ag deposits of the Kopaonik Mountains . . . 21
3.3. Characterisation of ore resources with isotope analysis . . . 22
3.3.1. Lead isotopes . . . 22
3.3.2. Copper isotopes . . . 24

4. *Res metalla*: Imperial mining and metal production in Kosovo and Serbia 26
4.1. The Zhegovc Mountains . . . 26
4.1.1. Historical timeline of mining and metal production . . . 26
4.1.2. Archaeological evidence for local mining and metal working and its possible connection to Ulpiana . . . 28

4.2. The Kopaonik Mountains . . . 30
4.3. The Šumadija district . . . 30

5. Other lead and silver mining districts of the Roman Empire 32
5.1. Southeastern Europe . . . 32
5.1.1. Greece . . . 32
5.1.2. Romania . . . 33
5.1.3. Bulgaria . . . 34
5.1.4. Macedonia . . . 34
5.2. Southwestern Europe . . . 34
5.2.1. The Iberian Peninsula . . . 34
5.2.2. Italy . . . 36
5.3. Central Europe . . . 37
5.3.1. Britain . . . 37
5.3.2. France . . . 38
5.3.3. Germany . . . 38
5.4. Résumé: Chronology of relevant mining districts . . . 39

6. Results of mining archaeological and archaeometallurgical investigations 40
6.1. The mining district of Shashkoc-Janjevo . . . 40
6.2. Metallurgical sites in the vicinity of Ulpiana . . . 42

II. The *chaîne opératoire*: Typology, petrography and geochemistry of ores, metallurgical (by-) products and metal artefacts 46

7. Analytical techniques 47
7.1. Sampling strategy and sample preparation . . . 47
7.2. Optical microscopy . . . 48
7.3. X-ray diffraction . . . 48
7.4. Electron microprobe analysis . . . 48
7.5. Isotope analysis . . . 48

8. Ore resources 53
8.1. Petrography and paragenesis of ore mineralisation . . . 53
8.1.1. Primary sulphide mineralisation . . . 55
8.1.2. Supergene Cu ore . . . 59
8.2. Geochemistry of ore minerals . . . 59
8.2.1. Primary sulphide ore . . . 59
8.2.2. Secondary Cu ore . . . 63
8.3. Ore deposition and formation processes . . . 63
8.4. Résumé and implications for archaeometallurgical processes . . . 64

9. Slag **65**
9.1. Typology of slag samples . . . 65
9.1.1. Basin slags . . . 66
9.1.2. Furnace slags . . . 67
9.1.3. Smithing slags . . . 70
9.2. Petrography and geochemistry of phases in metallurgical slags . . . 70
9.2.1. Olivine [$(Fe,Zn,Mg,Mn,Ca)_2SiO_4$] . . . 71
9.2.2. Clinopyroxene [$(Ca,Fe^{2+},Mg,Mn,Zn,Al,Fe^{3+})_2(Si,Al,Fe^{3+})_2O_6$] . . . 75
9.2.3. Melilite [$(Ca,Na,K,Pb)_2(Al,Fe^{3+},Fe^{2+},Mg,Mn,Zn)(Si,Al)_2O_7$] . . . 78
9.2.4. Feldspar [$NaAlSi_3O_8$ - $CaAl_2Si_2O_8$ - $KAlSi_3O_8$] . . . 78
9.2.5. Leucite [$KAlSi_2O_6$] . . . 80
9.2.6. Kalsilite [$KAlSiO_4$] . . . 80
9.2.7. Spinel *ss* [$(Fe^{2+},Mg,Mn,Ni,Zn)(Al,Fe^{3+},Cr,Ti)_2O_4$] . . . 80
9.2.8. Wüstite [$Fe^{2+}{}_{1-x}O$] . . . 83
9.2.9. Iscorite [$Fe^{2+}{}_5Fe^{3+}{}_2SiO_{10}$] . . . 84
9.2.10. Glass . . . 84
9.3. Textures and phase assemblages of smithing slags . . . 87

10. Matte **90**
10.1. Petrography of matte types . . . 90
10.1.1. Smelting residues . . . 90
10.1.2. Spherical inclusions in slag . . . 90
10.1.3. Interstitial cluster . . . 94
10.1.4. Pb-Cu matte . . . 94
10.1.5. Matte sensu stricto (s.s.) . . . 94
10.2. Geochemistry of matte phases . . . 95
10.2.1. Pyrrhotite . . . 95
10.2.2. (Zn,Fe)S . . . 97
10.2.3. Galena . . . 98
10.2.4. Bornite *ss* . . . 99
10.2.5. Intermediate solid solution (iss) . . . 101
10.2.6. Covellite . . . 101
10.2.7. Base metal sulphide melt . . . 101
10.2.8. Fe-rich oxide . . . 102
10.3. Solidification sequences of matte . . . 102
10.3.1. Interstitial sulphide clusters . . . 102
10.3.2. Pb-Cu matte . . . 103
10.3.3. Matte s.s. . . . 103

11. Speiss and pig iron **105**
11.1. Ferrous speiss . . . 105
11.1.1. Fe_9As . . . 105
11.1.2. Fe_2As . . . 105

11.1.3. FeAs . . . 107
11.2. Pig iron . . . 107
11.3. Base metal speiss . . . 108
11.3.1. (Ni,Cu)(Sb,As) . . . 108
11.3.2. $(Cu,Fe)_3(Sn,Sb)$ . . . 109
11.3.3. $(Cu,Ni)_2Sb$ . . . 109
11.4. Temperature estimates . . . 109
11.4.1. Ferrous speiss and pig iron . . . 109
11.4.2. Base metal speiss . . . 110

12. Crude lead **111**

13. Cupellation remains **113**

14. Metal artefacts **114**
14.1. Lead objects . . . 114
14.2. Copper-rich objects . . . 114

15. Isotope analyses **118**
15.1. Lead isotopes . . . 118
15.1.1. Ore . . . 118
15.1.2. Metallurgical by-products . . . 119
15.1.3. Lead metal artefacts . . . 124
15.1.4. Copper-rich artefacts . . . 129
15.2. Copper isotopes . . . 129
15.2.1. Ore . . . 130
15.2.2. Metal artefacts . . . 130

III. Discussion and interpretation **133**

16. Reconstruction of archaeometallurgical processes: I. The ore basis **134**
16.1. The local ore mineralisation and extracted metal(s) . . . 134
16.2. The geochemical signature of the Shashkoc-Janjevo district . . . 134
16.3. Ore supply of the smelting sites . . . 137
16.4. Preparation of the ore charges . . . 139
16.4.1. Beneficiation . . . 139
16.4.2. Roasting . . . 140
16.4.3. Dressing . . . 141

17. Reconstruction of archaeometallurgical processes: II. Smelting of ores **142**
17.1. Deciphering of the process type indicated by the investigated slags . . . 142
17.2. Classification of slags . . . 143
17.2.1. Olivine-type . . . 143
17.2.2. Olivine + clinopyroxene-type . . . 146

17.2.3. Clinopyroxene-type . . . 146
17.2.4. Melilite-type . . . 147
17.2.5. Glassy type . . . 147
17.3. Relation of slag types to process parameters . . . 148
17.3.1. Temperature . . . 148
17.3.2. Furnace atmosphere . . . 149
17.3.3. Correlation of furnace atmosphere and bulk chemistry of the slag melt . . . 151
17.3.4. The smelting sites and the chemistry of the slags . . . 156
17.4. Type and construction of the smelting furnaces . . . 158
17.4.1. Slags with flow structures . . . 159
17.4.2. Slags without flow structures . . . 160

18. Technological changes and developments in relation to chronology 161
18.1. The choice of the slag system: Addition of calcareous material as fluxing agent . 161
18.2. Variations of the raw material: Evidence from the metallurgical by-products matte and speiss . . . 162
18.3. Reconstruction of metallurgical process schemes . . . 165
18.3.1. Potential re-use and treatment of metallurgical (by-) products . . . 165
18.3.2. Metallurgical process schemes in relation to the ore type smelted . . . 168

19. Economic relevance of the local metal production in Roman times 172
19.1. Processing of the raw metal and trade in relation to Ulpiana . . . 172
19.2. Case study on the provenance of Roman imperial lead-based objects . . . 173
19.2.1. The *MET DARD* shipwreck cargo . . . 174
19.2.2. Lead-glazed pottery . . . 175

20. Further implications for research 178

Conclusions 180

References 183

Danksagung 205

IV. Appendix 206

i. Abbreviations 207

ii. Samples and sampling locations 210

iii. X-ray diffractograms 217

iv. Electron microprobe analyses 246

v. Isotope analyses 425

Part I.

Introduction

1. The *Metalla Dardanica* project

This PhD thesis has been carried out in the framework of the interdisciplinary cooperational *Metalla Dardanica* project between the Deutsches Bergbau-Museum Bochum and the Goethe-Universität Frankfurt, which is dedicated to Roman Pb-Ag mining and metal production in the hinterland of the *municipium* Ulpiana in central Kosovo. The mineral wealth of the region ever since put it in the focus of geopolitical considerations of the dominating powers and closely intertwined its changeful past with the history of Roman, Serbian and Ottoman Empires. Indeed, Rome's conquest of the region - which was considered by contemporaries as the mining province par excellence (*in Mysia...ubi metalla sunt*; *Dig.* 48.19.16.9 - 10) - in the 1st century CE generally is attributed to the Empire's virtually insatiable hunger for metals. In the mountains rising within eyeshot to the east of Ulpiana, a mining district with numerous old workings (galleries, (collapsed) shafts, beneficiation installations) as well as several metallurgical sites dating from Roman imperial to early modern times is preserved. This offers the possibility to comprehensively study the local *chaîne opératoire* - i.e. from the mined ores to metallurgical (by-) products and metal artefacts as final goods - and to retrace its potential chronological variations over a timespan of several centuries. A central point of the project is the close interlocking of mining archaeological techniques (GPS-based surveys, geophysical and geoelectrical measurements, excavations at selected mining and smelting sites) and geochemical analysis (OM, XRD, EMP, MC-ICP-MS). With this approach, all material groups representing an individual element of the production sequence each could be investigated in an ensured mining archaeological and archaeometallurgical context (Fig. 1.1). Based on the elements of the *chaîne opératoire* the following aims have been defined:

- Characterise the ore resources of the ancient mining district in the hinterland of Ulpiana with specific regard to potentially present precious metal contents
- Investigate the complete array of metallurgical remains recovered from smelting sites located in the environs of the *municipium* to reconstruct the process schemes in relation to chronological differences, i.e. from Roman / late antique to medieval / early medieval times
- Verify a potential connection of metal artefacts excavated in Ulpiana with the resources in its hinterland by Pb isotope provenance analysis, assess the importance of mining and metal production for the city's economic foundation, its relevance within the region Dardania and retrace the spatial distribution and potential trade routes of locally produced metal within the Roman Empire

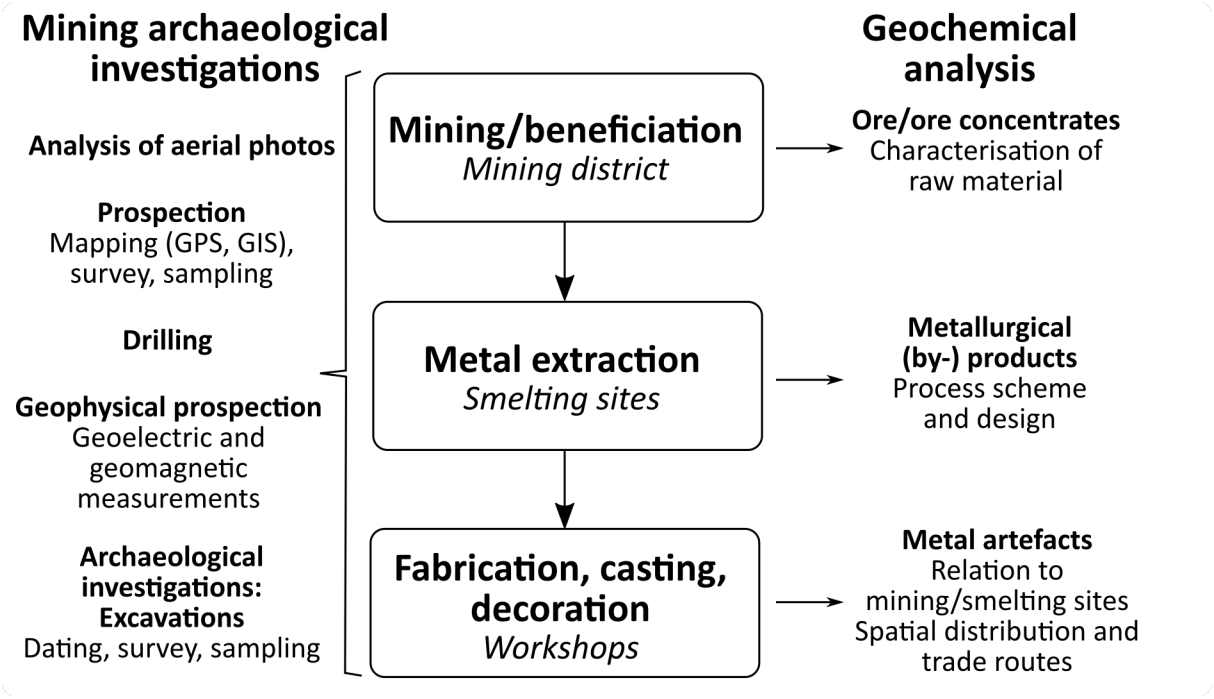

Figure 1.1.: Scheme depicting the in the Metalla Dardanica project applied mining archaeological and geochemical methods in relation to the individual elements of the *chaîne opératoire* investigated.

2. Ancient mining and metallurgy of lead and silver

The following chapter recapitulates the current state of research on the ancient metallurgy of lead and silver, including the occurrences of the elements as well as dressing and smelting of the ores and refining of produced metals. A chemical perspective on the complete array of metallurgical (by-) products, which potentially are generated by processing of a polymetallic ore comparable to the resources in the hinterland of Ulpiana (chapters 3 and 8), is given.
The mining and metallurgy of lead and silver are inseparable from each other - not only do the two elements mostly occur in the same mineralisation types, but also the extraction of silver was not possible without lead. Its low melting point (327 °C; Kullerud, 1969) and rather straightforward extraction - Tylecote (1964) after conducting smelting experiments pointed out that a campfire is virtually sufficient for this purpose - render lead the earliest metal smelted from its sulphide ores. Evidence is derived from findings from the neolithic settlements at Çatal Hüyük in Anatolia and Yarim-Tepe I in northern Mesopotamia, which have been assigned to the 6^{th} millenium BCE (Mellart, 1967; Muhly, 1989).
While prehistoric mining particularly focused on the silver contents of the ore and gathered lead as a by-product, the metal gained importance especially in the age of the Roman Empire (Gowland, 1901). Lead was used for a wide range of different applications such as water storage and transportation, coinage, kitchen ware, coffins and weights (Boulakia, 1972; Healy, 1978). Indeed, the metal was a bulk commodity and produced in industrially scaled operations with an estimated maximum output of 80,000 tons per year. The immense dimensions of the increased demand for the metal are recorded as the first hemispheric-scale pollution of the atmosphere in arctic ice cores (Hong et al., 1994).

2.1. Lead and silver ores

Although a wide variety of Pb-bearing phases exist, only galena occurs in large-scaled deposits (commonly associated with Zn sulphides) and hence is the principal source of the metal. Cerussite and anglesite as secondary minerals can be enriched in the uppermost weathered parts of the ore bodies. Galena also is the most important Ag ore, which either is hosted in solid solution or occurs as micro-scale inclusions of discrete minerals such as pyrargyrite [Ag_3SbS_3], proustite [Ag_3AsS_3] and stephanite [Ag_5SbS_4]. While the solubility of Ag_2S in galena is insignificantly low (0.6 mol. % at 600 °C; Van Hook, 1960), notable amounts of Ag can be incorporated by coupled substitution with Bi and / or Sb due to abundant solid solution in the Pb_2S_2 - $AgSbS_2$ - $AgBiS_2$ ternary system (Chutas et al., 2008). Other locally relevant carriers of the precious metal are fahlore minerals, particularly of the argentotennantite - freibergite series

$[(Ag, Cu)_{10}(Fe, Zn)_2(As, Sb)_4S_{13} - (Ag, Cu, Fe, Zn)_{12}(Sb, As)_4S_{13}]$ as well as Ag-bearing jarosites $[AgFe_3^{3+}(SO_4)_2(OH)$; argentojarosite], which are known to have been mined on a large scale in the Rio Tinto region in southwest Spain (e.g. Anguilano et al., 2010; Jones, 1980).
Besides these typically rather rare minerals, base metal sulphides common in Pb-Ag deposits minorly contribute to the Ag grade of the ore. Sphalerite, a main phase in most Pb deposits, was shown to contain notable Ag contents (up to several thousand ppm), the highest of which certainly are caused by discrete inclusions (Cook et al., 2009). Spectral analyses of sphalerite from deposits in the vicinity of Ulpiana reported by Grafenauer et al. (1969) yield up to 190 ppm of Ag. Bornite was shown to contain hundreds or thousands of ppm Ag in solid solution and thus might be a major carrier of the precious metal in certain occurrences. Chalcopyrite, however, comparatively is a rather poor host with clearly lower contents (Cook et al., 2011).
The descent of solutions carrying metal ions produced by sulphide dissolution to a zone with reducing conditions (i.e. near the groundwater table) leads to precipitation of Cu sulphides such as covellite [CuS], digenite $[Cu_{1.8}S]$, djurleite $[Cu_{1.97}S]$ and chalcocite $[Cu_2S]$, a process whose reaction rate supposedly is severely increased by bacterial activity (Sillitoe et al., 1996). These phases may contain several thousand ppm of Ag (up to around 1.1 wt % in digenite) present in solid solution as well as in the form of nanoparticles. A strong correlation of Ag and As contents suggests that As enhances the solubility of the precious metal (Cook et al., 2011; Reich et al., 2010). Interaction of oxidising fluids generated during gossan-forming processes with primary sulphides also may cause the precipitation of native Ag.

2.2. Ore beneficiation

Before the metal could be extracted by smelting, the ore was mechanically concentrated in a multi-stage process, which was described by Pliny (*Natural History* 33.69) and could be supported by mining archaeological research. Particularly the extensively studied mining district of Laurion with its well-preserved installations greatly contributed to the knowledge of ancient ore processing and metal extraction (cf. Healy, 1978 and references therein; Rehren et al., 2002).
The roughly sorted ore thus was crushed with stone mortars or anvil stones until the pieces had the size of peas (Wahl, 1993). Anguilano et al. (2010) state that a grain size between 10 to 20 mm is ideal for the extraction of Pb from galena ore since finer ground furnace feed has not proven to be more efficient for the smelting process. At least argentiferous and auriferous ore though was finely ground with stone mills to facilitate the liberation of the precious metals as archaeological investigations of Roman as well as medieval sites have proven (Hruby et al., 2007; Klemm & Klemm, 1989; Kudrnáč & Michálek, 1993; Wahl, 1993). Roman ore mills typically were of round shape with a diameter of 60 cm and a decentral handle. Hard and durable volcanic rocks such as granite, trachyte or andesite were used for the manufacturing of these stone tools. The grain size was controlled by sieving and, if necessary, the material was repeatedly milled until it was as fine as flour. The powder was subsequently washed to separate remaining amounts of barren host rock from the ore concentrate. According to Strabo (*Geography* 3.2.10), the sediment of Pb-Ag ore which was gained after five runs was eventually smelted.

2.3. Extraction of lead

Pb was extracted from its sulphide ores in ancient times either by the roast-reduction or roast-reaction process. The iron-reduction process, i.e. reduction of Pb sulphide ores with native Fe, was most widely used in 18th and 19th century Germany (particularly in the Upper Harz, Upper Silesia and Příbram). Earlier evidence for the application of this technique dating from the 7th to the 13th and to the 14th century CE, respectively, has been reported from China (Liu et al., 2015) and India (Dube, 2006). The following sections have been compiled on basis of the works of Gowland (1914), Hofman (1899), Iles (1904) and Tafel (1929).

2.3.1. The roast-reduction process

The roast-reduction process includes a prior roasting step to drive off sulphur from the ore (eq. 2.1). The generated PbO will partially react with the released SO_2 to form $PbSO_4$ (eq. 2.2); the rate for this reaction generally is higher at lower temperatures and is further increased by the presence of pyrite (Gowland, 1914). The formation of $PbSO_4$ is unwanted due to possible re-reaction to PbS during the smelting step (eq. 2.8; see below) but may be minimised by the presence of both $CaCO_3$ and CaO (eq. 2.3 and 2.4) as well as process temperatures exceeding 950 °C, i.e. the decomposition point of $PbSO_4$.

$$PbS + 3\,O_2 = 2\,PbO + 2\,SO_2 \tag{2.1}$$

$$2\,PbO + 2\,SO_2 + O_2 \rightleftharpoons 2\,PbSO_4 \tag{2.2}$$

$$PbSO_4 + CaCO_3 = PbO + CaSO_4 + CO_2 \tag{2.3}$$

$$PbSO_4 + CaO \rightleftharpoons CaSO_4 + PbO \tag{2.4}$$

The beneficiated ore pieces should be sufficiently small to accelerate the roast reaction but also large enough to avoid losses due to scattering. Maximum grain sizes of 4 mm and a process temperature of 800 °C are reported as ideal in modern metallurgy (Tafel, 1929).
The preliminary roasting step provides several advantageous side effects. The furnace charge is more homogeneous due to the oxidised nature of the roasted ore, which also can be, if necessary, crushed easier. Agricola (*De Re Metallica* 8, pp. 273 ff.) mentions an equivalent procedure involving fine grinding of the crushed ore after roasting it. Furthermore, the partial volatilisation of As and, to a lesser extent, Sb during the roasting step suppresses the formation of speiss, a generally unwanted by-product (cf. section 2.5.3). However, roasting also significantly reduces the Pb content of the ore (Tylecote et al., 1977). Roasting of polymetallic ore charges should not be carried out completely ('dead roasting') since potentially present Cu contents then are not diverted as a separate sulphide melt (matte; cf. section 2.5.2). In contrast, Cu then preferentially partitions into crude Pb, drastically increasing its melting point (e.g. 5 % Cu rises the liquidus temperature to approximately 700 °C; Hansen & Anderko, 1958) and hence impeding its further treatment, i.e. particularly cupellation. The presence of ZnS, a common component in Pb

ores, is unwanted due to its high thermal stability (it sublimates at normal pressure at 1185 °C; Kullerud, 1953) and consequently should be minimised. Complex Cu- and Zn-bearing Pb-Ag ores thus require a carefully balanced roasting step.
Smelting of the roasted ore under reducing conditions by usage of charcoal as fuel transforms PbO to native Pb (eq. 2.5 and 2.6). The reaction of PbO with CO already starts at temperatures between 160 and 185 °C. Possibly abundant $PbSO_4$ decreases the metal yield since it deprives the system of Pb (eq. 2.7 and 2.8).

$$PbO + CO \rightarrow Pb + CO_2 \tag{2.5}$$

$$PbO + C \rightarrow Pb + CO \tag{2.6}$$

$$PbSO_4 + Pb \rightarrow 2\,PbO + SO_2 \tag{2.7}$$

$$PbSO_4 + 4\,CO \rightarrow PbS + 4\,CO_2 \tag{2.8}$$

2.3.2. The roast-reaction process

The roast-reaction process is a single-stage operation in which the ore is oxidised by air supply within the uppermost furnace parts. The thus generated $PbSO_4$ and PbO (cf. eq. 2.1 and 2.2) react with primary galena from the smelter feed to SO_2 and native Pb, which accumulates at the bottom of the furnace. The reaction of PbS with PbO (eq. 2.9) starts at temperatures between 650 and 660 °C and reaches a considerable rate from 700 °C on. The minimum temperature for the reaction with $PbSO_4$ (eq. 2.10) is 550 °C; its rate drastically increases with higher temperatures, but is influenced by the SO_2 pressure.

$$PbS + 2\,PbO \rightleftharpoons 3\,Pb + SO_2 \tag{2.9}$$

$$PbS + PbSO_4 \rightleftharpoons 2\,Pb + 2\,SO_2 \tag{2.10}$$

The roast-reaction process is only suitable for relatively pure galena concentrates with a Pb content exceeding 58 % (Gowland, 1914) and no or only minor proportions of pyrite, chalcopyrite, sphalerite and As- and Sb-bearing phases as well as silica, calcite and baryte. The advantages of this process scheme are that volatilisation losses, especially of Ag, are small and that the gained Pb is particularly pure. According to Agricola (*De Re Metallica* 8, p. 275 ff.), Pb ores were not always roasted before the actual smelting step.

2.4. Extraction of silver

Ag as well as the other precious metals are effectively collected by native Pb, which either already is provided in sufficient amount by the smelted ore or has to be added to the furnace charge ('leaded smelting'), e.g. if jarosite minerals are treated. Pb metal also was used as an

additive in Au-Ag metallurgy to extract the precious metals from the ore (Baron et al., 2011). The precious metal-bearing crude Pb is subjected to cupellation, a process taking advantage of the less noble character of Pb, which hence is more readily oxidated. The liquid Pb metal is transformed by a constant airflow to PbO (melting point around 880 °C; Hansen & Anderko, 1958). Particularly Sn, but also Sb are oxidised as well; Bi, Te and Cu in contrast become enriched in the restitic native Pb during cupellation (Pernicka & Bachmann, 1983; cf. chapter 2.5.5). While Ag is to a certain extent readily dissolvable in native Pb, it is completely insoluble in PbO and hence remains in its native state segregated from the layer of oxidised Pb. The PbO floats on the surface of the liquid and thus can be easily skimmed off, but partially also is absorbed by the cupellation hearth until only pure native Ag is left over (German 'Silberblick'; Rehren & Klappauf, 1995).

The extraction of Ag from argentiferous Pb by cupellation is a long-known process, whose practice has been proven already for the 4$^{\text{th}}$ millennium BCE (Pernicka et al., 1998) and which was regularly used on a large scale in classical Laurion. Trace element analysis of Roman lead objects indicates that the cupellation process apparently was highly developed with residual Ag contents in the artefacts mostly scattering around 100 ppm (Bode, 2008; Merkel, 2007; Rehren & Prange, 1998; Wyttenbach & Schubiger, 1973). The limit of economically viable desilveration is due to its dependence on external factors (e.g. availability of skilled metalworkers, cost and abundance of fuel) rather difficult to estimate but is generally assessed to be in the range between 400 and 600 ppm (cf. Rehren & Prange, 1998). In the 16$^{\text{th}}$ century, a residual Ag content of 80 ppm in crude Pb is reported as minimum value (Nriagu, 1985).

2.5. The chemistry of smelting and metallurgical (by-) products

The nature of the smelting process is reflected by the abundance, composition and phase assemblage of the metallurgical (by-) products, i.e. slag and crude Pb as well as potentially matte, speiss and pig iron. Their properties and hence chemistry are characterised by the smelted ore and its gangue material, possibly added fluxes, charcoal ash and furnace lining:

Ore + gangue + charcoal ash + furnace lining (+ fluxes) → Slag + metallurgical (by-) products

The type of ore smelted is the most crucial factor since it dictates the type and abundance of metallurgical by-products and thus the design of the process scheme. A complex Pb-rich polymetallic ore similar to the resources in the Zhegovc / Žegovac mountains in the hinterland of Ulpiana (cf. chapter 8) may generate up to four different liquid fractions, which should gravitationally separate (Fig. 2.1): 1) slag, a siliceous melt which takes up unwanted impurities (e.g. from ore and restitic gangue material); 2) matte, a mixture of base metal sulphides; 3) speiss, consisting of arsenides, antimonides and stannides of base metals and Ag and 4) precious metal-bearing crude Pb.

The gangue material generally was largely removed during the beneficiation of the ores. However, some deposit types may be associated with host rocks of an advantageous composition and act as a fluxing agent itself ('self-fluxing ores'). Fluxes (see below) may be added to the furnace charge to increase the metal yield and generally optimise the process design. Furthermore, charcoal ash derived from the process fuel and the probably deliberately selected material of the furnace lining, which liquefies and interacts with the charge, as well influence the chemistry of the

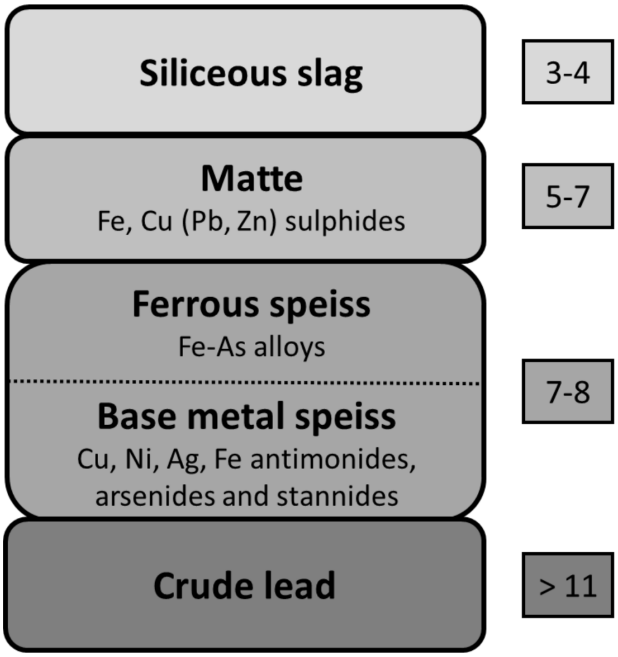

Figure 2.1.: Schematic overview of the different melts (and their typical specific gravities in g/cm³; Keesmann, 1993) potentially generated during smelting of a polymetallic Pb-rich sulphide ore similar to the resources of the Zhegovc Mountains.

smelting process. The following sections have been compiled on basis of the works of Gowland (1914), Hofman (1899), Iles (1904) and Tafel (1929).

2.5.1. Slag

The main purpose of a metallurgical slag is to collect unwanted impurities from the furnace feed in order to produce a crude metal as pure as possible. In addition, the overlying slag layer isolates the metal melt and thus prevents oxidation and quenching by storage of process heat. An ideal slag should be characterised by the following qualities:

- Its viscosity and specific gravity should be sufficiently low to ensure separation from the metal-rich liquids and to facilitate its tapping
- Its formation should require as few flux and fuel as possible
- Its liquidus temperature should be as low as possible, but high enough that the necessary reactions can take place in sufficient time

Whether a slag possesses these properties or not depends on its chemical composition which is defined by the furnace charge, influenced by technical necessities and which may be modified by the employment of suitable fluxing agents. The most common additives in ancient time were silica as well as iron and calcium oxide.

Chemical compounds of slags

Silica An appropiate amount of SiO_2 in the furnace charge is crucial for the success of smelting since it assures the formation of a sufficient amout of slag to take up impurities in the first place.

High SiO_2 contents, however, lead to a viscid slag and consequently poor liquid separation. Sandstones, quarzites and quartz are widely abundant as gangue material of mineralisations and as common country rocks.

Iron oxide The gossan zones of ore deposits readily provide FeO-bearing material, which often is marked by elevated base and precious metal contents due to abundant (restitic) ore minerals and potentially present newly-formed native Au and Ag. The presence of FeO generally decreases the viscosity; slags containing fayalite as the main silicate phase are highly fluid. However, the larger the amount of FeO is, the higher is the specific gravity of the slag thus impeding the gravitational separation of the different liquids. Exceptionally FeO-rich slags furthermore react highly corrosive towards the furnace lining. In Pb metallurgy, FeO prevents metal losses to the slag by driving it out from its silicate phases under release of PbO, which then can be reduced to native Pb. However, the ability of slags to retain metal sulphides increases with the amount of FeO present. Due to the similarity of their ionic radii, Mn^{2+} can directly substitute for Fe^{2+} and thus in Fe metallurgy enhances the amount of metal gained. Elevated contents of MnO give rise to particularly lowly viscid slags, but generally increase the liquidus temperature.

Calcium oxide CaO decreases the specific gravity and viscosity (Bachmann, 1980) of the typically rather Fe-rich slags and lowers their ability to dissolve base metal sulphides, particularly Cu_2S. CaO is able to drive off other basic oxides such as PbO, ZnO and FeO. Limestone as source for CaO is widely available as country rock and may be also present as host material of the mined ores. Dolomitic limestone leads to introduction of MgO in the furnace charge, which at elevated contents gives rise to highly viscous slags and also increases the liquidus temperature. Considerable proportions of CaO (i.e. several ten wt %) also are contained in charcoal ash (Angermann, 1989, cited by Heimbruch, 1990; Tylecote et al., 1977). Fluorspar is rendered by its low specific gravity (3.18 g/cm^3) and perfect cleavage a particularly well manageable fluxing agent, which drastically lowers the viscosity (as reflected by the German denomination 'Flussspat') and liquidus temperature of slags.

Barium oxide BaO may be introduced into the slag system by the mineral baryte, which often is abundant as gangue material of ore mineralisations. Due to its high specific gravity (4.5 g/cm^3) it is difficult to remove by wet-mechanical beneficiation techniques. BaO significantly lowers the melting point of slags but enhances their density, thus hampering gravitational segregation of the differing liquids in the furnace. Even more than CaO and FeO, BaO is able to drive off PbO from silicate phases.

Lead oxide PbO drastically lowers the melting point of slags. However, besides the Pb losses, the increased viscosity and specific weight have a negative impact on the metal extraction rate by impeding gravitational segregation.

Zinc oxide Zn easily substitutes other divalent cations (e.g. Fe^{2+}, Mn^{2+}, Mg^{2+}) due to similar ionic radii and thus is a typical constituent of silicate and oxide phases in slags generated by processing of Pb-Zn ores. The proportion of ZnO in slag positively correlates with the amount

of FeO present and further increases its specific gravity as well as its melting point. High losses of ZnO in the smelting process, however, are caused by the fact that native Zn is volatilised at 907 °C.

Aluminium oxide Elevated contents of Al_2O_3 (i.e. exceeding 8 - 10 %; Gowland, 1914), introduced by e.g. interaction of slag with the clayey furnace lining generally enhance the viscosity of slags.

Potassium oxide K_2O contents in slag derive from charcoal ash and to a lesser extent, furnace lining and lead to the formation of K-bearing foides (particularly leucite[1]) and feldspars. The amount of K in the smelting system varies with the type of wood used for charcoal production, but also depends on external factors such as the furnace temperature (e.g. Misra et al., 1993).

Phase assemblages of slags Olivine, whose composition typically is close to the Fe endmember fayalite [Fe_2SiO_4], commonly is the main phase in ancient slags regardless of the type of metal(s) extracted from the ore (Hauptmann, 2014). This predominance is based on the advantageously rather low viscosity and melting point of olivine slags, which facilitate tapping as well as segregation of the melts and ensure complete liquefaction of the furnace charge. Since Fe- and SiO_2-bearing material often is supplied by the exploited mineralisations themselves or can be easily accessed due to their wide occurrence (see above), the appropriate composition can be rather simply adjusted. The stability field of fayalite is delimited by the quartz-fayalite-magnetite (FMQ; eq. 2.11) and iron-quartz-fayalite (IQF; eq. 2.12) buffer equilibria (Fig. 2.2; cf. Lindsley, 1976):

$$3\,Fe_2^{2+}SiO_4 + O_2 = 2\,Fe^{2+}Fe_2^{3+}O_3 + 3\,SiO_2 \tag{2.11}$$

$$Fe_2^{2+}SiO_4 = 2\,Fe^0 + SiO_2 + O_2 \tag{2.12}$$

The transformation of fayalite with increasing fO_2 to generate magnetite and SiO_2 is an important mechanism observed in metallurgical slags. The freed silica mostly is bound by clinopyroxene-group phases (typically abundant as hedenbergite [$CaFeSi_2O_6$]) and, more rarely, by melilite-group phases, whose composition usually ranges between gehlenite [$Ca_2Al_2SiO_7$] and Fe-åkermanite [$Ca_2Fe^{2+}Si_2O_7$]. Consequently, clinopyroxene- and melilite-rich slags not only testify to generally elevated bulk Ca contents of the melt, but also to more oxidising conditions. The generation of native Fe by reduction of fayalite is unwanted in non-ferrous metallurgy and leads to the formation of so-called pig iron (cf. section 2.5.4). Magnetite also is formed by oxidation of wüstite (WM buffer; eq. 2.13) and with increasing fO_2 itself is oxidised to hematite (MH buffer; eq. 2.14).

$$3\,Fe_{1-x}^{2+}O + O_2 \sim Fe^{2+}Fe_2^{3+}O_4 \tag{2.13}$$

[1] Anthropogenic phases are not regarded as minerals (Nickel, 1995), but for the sake of better readability and comprehensibility are in the following labelled according to their natural occurring equivalents.

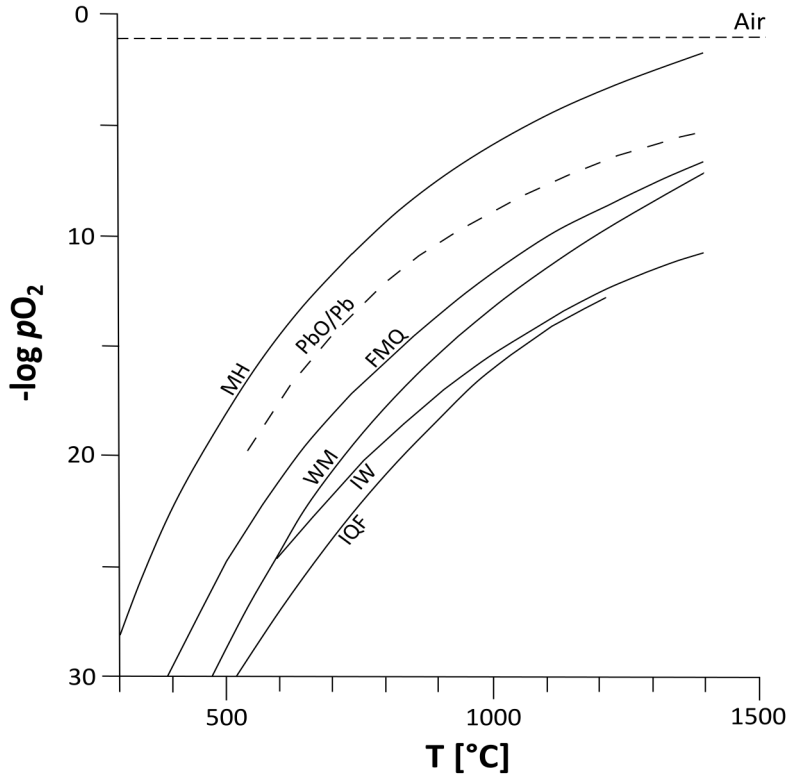

Figure 2.2.: Oxygen fugacities as a function of temperature for solid-solid buffer reactions relevant for Fe-rich slags (cf. Lindsley, 1976; redrawn from Bode, 2008). Abbreviations for the buffers are: MH – magnetite - hematite; FMQ – fayalite - magnetite - quartz; WM – wüstite - magnetite; IW – iron - wüstite; IQF – iron - quartz - fayalite.

$$4\,Fe^{2+}Fe_2^{3+}O_4 + O_2 = 6\,Fe_2^{3+}O_3 \tag{2.14}$$

The stability field of wüstite is delimited to lowered fO_2 by the reduction reaction to native Fe (IW buffer; eq. 2.15):

$$2\,(1-x)\,Fe^0 + O_2 = 2\,Fe_{1-x}^{2+}O \tag{2.15}$$

Iscorite [$Fe_5^{2+}Fe_2^{3+}SiO_{10}$], an Fe silicate phase containing both Fe^{2+} and Fe^{3+}, is generated by reaction of fayalite and wüstite with O_2 (eq. 2.16) under the stability conditions of magnetite and thus testifies to oxidation processes (Smuts et al., 1969; Smuts, 1992; Van Aken et al., 2005).

$$5\,Fe_{1-x}^{2+}O + Fe_2^{2+}SiO_4 + 0.5\,O_2 \rightarrow Fe_5^{2+}Fe_2^{3+}SiO_{10} \tag{2.16}$$

Consequently, the silicate and oxide phases abundant in Fe-rich metallurgical slags, which are precipitated in response to the composition of the smelter charge and the fO_2 conditions (i.e. the furnace atmosphere, but also oxidational processes), efficiently serve as indicators for the process scheme. Keesmann et al. (1984) developed a classification scheme for metallurgical slags, which is based on their phase assemblage in the system CaO - FeO - Al_2O_3 - SiO_2 (Fig. 2.3):

I Fayalite slags

II Fayalite-pyroxene slags

III Pyroxene slags

IV SiO_2-saturated slags contaminated by Al_2O_3 from furnace lining

V SiO_2-depleted, CaO-rich slags (with kalsilite instead of leucite)

The phase assemblages of slags related to Pb-Ag metallurgy are stunningly consistent from antique to modern times and typically comprise fayalitic olivine besides magnetite-rich spinel *ss* and partially wüstite as dominant phases. However, a trend to generally Ca-richer phase compositions is established from the medieval period on. Roman republican and imperial slags from Rio Tinto in southwest Spain (Anguilano, 2012) and Lüderich in Germany (Bode, 2008) related to smelting of oxidised and sulphide ores, respectively (cf. chapter 5), essentially consist of fayalite accompanied by varying proportions of magnetite-rich spinel *ss* and subordinate, lately precipitated clinopyroxene compositionally close to hedenbergite. Olivine-dominated slags as well have been reported from significantly earlier activities at e.g. the Agios Sostis site of Siphnos Island (Bronze Age, Archaic period; Pernicka et al., 1985) but also from medieval (Příbram / Czech Republic: Ettler et al., 2009c; Siegerland / Germany: Gassmann & Rehren, 1998; St. Marie-aux-Mines - Pfaffenloch / France: Goldenberg, 1996; Wiesloch / Germany: Ströbele et al., 2010) and modern (i.e. from the 18th to the 20th century) Pb-Ag production (Clayton smelter / USA: Piatak et al., 2004; Příbram / Czech Republic: Ettler et al., 2001; Santo Amaro / Brazil: De Andrade Lima & Bernardez, 2011; Sierra Almagrera / Spain: Navarro et al., 2008). Ca-richer bulk compositions leading to the formation of clinopyroxene- and melilite-dominated phase assemblages have been subordinately observed in pre-modern slags, e.g. at the Ari site of Laurion

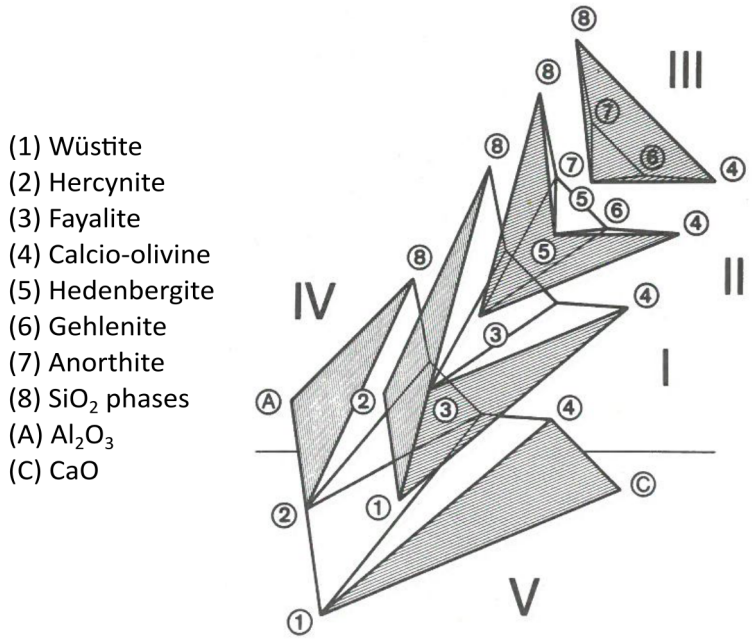

Figure 2.3.: Classification of Fe-rich slags in the system CaO - FeO - Al_2O_3 - SiO_2 (Keesmann et al., 1984).

(Tsaimou et al., 2015), Arialla and Rocchette Pannocchieschi (13^{th} / 14^{th} century, Colline Metallifere / Italy; Manasse & Mellini, 2002a) and Kutná Hora (14^{th} / 15^{th} century, Czech Republic; Manasse & Mellini, 2002b). Potentially deliberate addition of baryte and fluorspar as fluxing agents with consequently low to absent fayalite has been reported from metallurgical operations of the 12^{th} / 13^{th} century on in the German Erzgebirge and Schwarzwald districts (Eckstein et al., 1994; Goldenberg, 1996).

2.5.2. Matte

Matte as a sulphide melt is a common by-product in base metal smelting. In Pb metallurgy, the formation of a small amount of matte is highly desirable since it effectively binds the Cu contents of the smelter charge which otherwise would partition into the crude Pb and drastically rise its melting point (cf. chapter 2.3). Loss of a certain amount of Pb - Tafel (1929) mentions typical contents of 10 to 25 % in matte of modern metallurgy - is inevitable. The solubility of galena increases with higher FeS and decreases with rising Cu_2S contents. Ag also partially segregates into matte where it is almost exclusively hosted by Cu-bearing sulphides hence slightly diminishing its primary recovery. However, the major share of the precious metal though is collected by the accumulating native Pb (Tafel, 1929). Typical Ag contents in Cu-(Fe) sulphides of matte from medieval as well as modern Pb-Ag metallurgy scatter around 1000 ppm (Ettler et al., 2009b; c). According to Bachmann (1993), particularly Ag-rich matte was treated in antiquity by repeated roasting and smelting with added native Pb, which due to its greater affinity collected the freed Ag. The possible treatment technique for Ag-rich matte suggested by Bachmann (1993) is comparable to the medieval liquation process (*De Re Metallica* 9, pp. 400 ff.), in which argentiferous crude Cu was smelted with native Pb. Historical records prove the addition of matte from Pb metallurgy to furnace charges as well as its further treatment to

extract Cu in southern Germany in the 16th century (Goldenberg, 1996; and references therein).

2.5.3. Speiss

Speiss either occurs as ferrous or base metal variety, the latter due to its slightly higher specific density accumulates between matte or ferrous speiss, respectively, and crude Pb (Keesmann, 1993). Ferrous speiss is defined by Thornton et al. (2009) as a material with a base metal content below 2 to 3 % and may contain native Fe or As and the binary compounds Fe_2As, FeAs and $FeAs_2$. In situ analyses of these phases if any, did not determine notable amounts of Ag and Au (Keesmann, 1993; Photos et al., 1989). Precious metal contents generally described for speiss from Pb metallurgy (Gowland, 1914; Tafel, 1929) more likely originate from the contribution of base metal speiss and Pb bullion. Base metal speiss consists of arsenides, antimonides and stannides of mainly Cu, Fe, Ni and Ag. Typical phases include Cu_2Sb, $Cu_3(Sn,Sb)$, dyscrasite [Ag_3Sb] and koutekite [Cu_5As_2], which are marked by a wide range of possible substitutions.
Abundant Ag contents of base metal speiss - Kassianidou (2003) describes Phoenician-period speiss with a bulk content of 5000 ppm Ag - apparently mainly are hosted by dyscrasite as well as Cu antimonide, in which between 0.35 and 0.8 wt % Ag have been determined in medieval samples by Ettler et al. (2009b; c) and Rehren et al. (1999). The possible treatment of speiss to extract Ag and Au contents has been discussed controversially in the scientific community. Unusual bulk compositions of slags and crucibles led Craddock et al. (1987) to propose that ferrous speiss was desilverated at Rio Tinto under Roman rule. A later re-examination of these samples though caused Kassianidou (1998) to reject this hypothesis. Keesmann (1993) suggested repeated treatment of ferrous speiss in Roman period Spain to extract Ag hosted by trapped inclusions of crude Pb and, due to the close association of Pb bullion and base metal speiss, automatic desilveration of this speiss variety together with crude Pb. Apart from precious metal extraction, there is growing evidence for the usage of the As content of speiss throughout history, either by the intentional production of ferrous speiss or its use in metallurgy to generate arsenical Cu (Rehren et al., 2012; Thornton et al., 2009; and references therein).

2.5.4. Pig iron

Pig iron is generated during the smelting process if the SiO_2 content of the furnace charge is too low and the process conditions are due to high temperatures and excess charcoal extremely reducing. Its formation is further promoted by a rather high abundance of CaO which drives FeO out of its silicate slag phases. If the amount of speiss and matte is not sufficient to take up the Fe, a layer of impure pig iron is formed which according to its rather high specific gravity accumulates above the crude Pb. Pig iron is due to its high melting point and its ability to collect Au (as well as platinum-group elements) an unwanted by-product (Tafel, 1929).

2.5.5. Native lead

The ability of native Pb to act as a collector for precious metals is utilised in the cupellation process (see chapter 2.4). Chief impurities in Pb produced by modern metallurgy are S, Mn, Fe,

Co, Ni, Cu, Zn, As, Cd, Sn, Sb and Bi (Gowland, 1914; Tafel, 1929). Elevated contents of Fe, Cu, Zn and S and Cu, Sb, As, Cu, As, Ni, Co and Sn in crude Pb can be derived from trapped inclusions of matte and speiss, respectively. Sn, As, Sb, Fe and Zn are relatively easy oxidised and partially also form mixed compounds with PbO, which float on the liquid lead and thus can be easily removed during refining treatment.

3. Regional metallogeny and ore deposits

3.1. Spatial categorisation and relationship with geodynamic processes

The southeast European ore deposits belong to the Tethyan Eurasian metallogenic belt (TEMB), which stretches from southwestern Europe and the Alps throughout the Balkan region to Eurasia until ultimately joining the West Pacific metallogenic belt (Janković, 1997). The Alpine-Balkan-Carpathian-Dinaride sector (ABCD; Heinrich & Neubauer, 2002) of this transcontinental belt is Europe's premier ore province, whose rich metal resources not only substantiated ancient Greek and Roman Empires, but which indeed are linked to the beginnings of metallurgy itself (e.g. Jovanović, 2009; Pernicka et al., 1993; Radivojević et al., 2010; Ryndina et al., 1999; Schmitt-Strecker & Begemann, 2005). Notable occurrences include the Romanian Ag-Au deposits of the Baia Mare and Roşia Montană districts (Marcoux et al., 2002; Neubauer et al., 2005) and the As-Au-Ag bearing mineralisations of the Eastern Alps' Tauern window (Horner et al., 1997) as well as the Cu-(Au) deposits of the east Serbian Timok Massif (e.g. Bor, Majdanpek; Clark & Ullrich, 2004; Janković, 1990) and Cyprus (Stos-Gale et al., 1997). However, one of the most significant commodities are Ag-bearing Pb-Zn ores, which were or are, respectively, particularly mined in the Serbomacedonian-Rhodope belt (Heinrich & Neubauer, 2002). It stretches across Serbia, Kosovo, Macedonia, northern Greece and southern Bulgaria and includes among other mining regions the Šumadija-Kopaonik district (Janković, 1997). The Šumadija unit is located in central Serbia and comprises the mines of e.g. Rudnik, Avala and Kosmaj while Kopaonik refers to the ore deposits of the Trepça / Trepča Mining and Metallurgical Complex (Monthel et al., 2002), which occur in the eponymous Kopaonik Mountains in the northern and the Zhegovc Mountains (i.e. including the study area) in the southern part of the district.
The mines of the Kopaonik district are situated in the Vardar Zone - a Mesozoic suture bound by the Dinarides / Hellenides to the west and the Serbian-Macedonian Massif to the east (Dimitrijević, 2001) - which comprises various units of both continental and oceanic origin (Karamata et al., 1994) and is marked by extensive magmatic activity. The classification of the regional geological units and reconstruction of their formation history is the subject of intense scientific debate (e.g. Pamić et al., 1998; Robertson et al., 2013; Robertson & Karamata, 1994; Schmid et al., 2008; and references therein). Since a detailed approach of this topic is beyond the scope of this thesis, in the following a generalised scheme of the geodynamic processes related to ore deposit generation is summarised.

Intracontinental rifting: Late Permian to Middle / Early Triassic intracontinental rifting occurred in Gondwanaland or one of its fragments. Associated magmatic complexes and hydrothermal activity lead to formation of e.g. the Triassic Pb-Zn-(Ba) carbonate-hosted

deposits of the Alps.

Ocean-floor spreading: Rifting lead to development of an ocean basin (i.e. the Vardar Ocean, a branch of Tethys) in Late to Early Jurassic / Late Triassic times. The most significant related mineralisations are chromite occurrences in the Albanides / Dinarides and sea-floor sulphide deposits of the Cyprus type.

Subduction: Subduction of the Vardar Ocean basin towards the Serbo-Macedonian continent occurred during Late Jurassic / early Triassic times, resulting in pronounced magmatic activity and formation of hydrothermal base and precious metal deposits, particularly in the Carpatho-Balkanides.

Collision and post-collisional stage: Closure of the Vardar Ocean and suturing began in Late Jurassic times and finally terminated in the Palaeogene with the convergence of stable Africa and Eurasia. Extensional tectonics and widespread Oligocene / Early Miocene calc-alkaline post-collisional magmatic activity in the Vardar Zone is generally thought to have been caused by slab detachment (de Boorder et al., 1998; Wortel & Spakman, 2000) or lithosphere delamination (Cvetković et al., 2004; Schefer et al., 2011) and has been demonstrated to be related to the formation of base and precious metal deposits within the Serbomacedonian-Rhodope belt (Borojević Šoštarić et al., 2012; Borojević Šoštarić et al., 2013; Kalogeropoulos et al., 1989; Mankov, 2006; Marchev et al., 2005; Nesbitt et al., 1988; Palinkaš et al., 2013; Veselinović-Williams, 2011). Pb-Zn-(Ag-Au) deposits of the Carpathian Mountains in Romania are attributed to the Inner Carpathian-Alpine metallogenic belt and as well were formed as a result of hydrothermal activity initiated by mainly Miocene post-collisional magmatism (Marcoux et al., 2002; Neubauer et al., 2005). Detailed overviews of the metallogeny of the whole Balkan region are provided by e.g. Heinrich & Neubauer (2002), Neubauer (2002) and Palinkaš et al. (2008).

3.2. Pb-Zn-Ag-(Cu-Au) deposits of the Kopaonik district

The Kopaonik district comprises several Pb-Zn-Ag mines, occurrences and prospects in southern Serbia and Kosovo, whose most significant are briefly characterised in the following section.

3.2.1. Pb-Zn-Ag deposits of the Zhegovc Mountains

Kishnica / Kižnica

Kishnica, located in the heart of the investigated ancient mining district, is described as a low-sulphidation epi- to mesothermal polymetallic vein deposit occurring at the contact of serpentinite and Cretaceous flysh and hosted by serpentinite, andesite and schist or shale (Monthel et al., 2002). Stockwork and porphyry ore bodies are subordinate and of minor economic importance (Féraud & Deschamps, 2009). Kishnica has been exploited by surface and underground mining. The ore mineralogy is reported to be rather complex and particularly Cu-As-Sb-rich comprising besides ubiquitous galena, sphalerite, pyrite and pyrrhotite various sulphosalts and Cu-bearing sulphides. The main gangue phases are siderite, quartz, rhodochrosite, baryte and

chalcedony. The Pb, Zn and Ag reserves of the mine are stated as 126,000 t, 32,000 t and 142 t at average grades of 4.9 %, 1.2 % and 55 g/t, respectively (Monthel et al., 2002). Au, present in the ore in native form and as telluride compounds, is won as a by-product at Kishnica (Féraud & Deschamps, 2009). Test pittings, conducted by Hießleitner (1927) before the actual mine opened yielded Au contents of up to 3 g/t - the mining company then even reported maximum abundances of 19 ppm - which would render Kishnica the (formerly) most Au-rich Pb-Zn-Ag deposit of the Kopaonik district.

Badovc / Badovac

Badovc immediately adjoins Kishnica and also is classified as a low-sulphidation epithermal vein deposit, but possesses a slightly different host rock mineralogy with the ore being present at the contact serpentinite / schist and / or andesite and hosted by serpentinite, schist, phyllite, dacite, andesite and listwaenite. The deposit has been worked underground. Monthel et al. (2002) state the resources of the mine as 143,000 t Pb, 96,000 t Zn and 197 t Ag at average grades of 5.4 %, 3.6 % and 75 g/t, respectively.

Novobërdë / Novo Brdo

Novobërdë is one of the most renowned deposits of the Balkan Peninsula, which was exploited particularly for its auriferous Ag since the early 14th century and thus significantly contributed to the economic basis of the Serbian kingdom (e.g. Ćirković 1981; Gordus & Metcalf, 1969; cf. section 4.1.1). Mining currently is based on the Farbani Potok deposit, which is classified as replacement type with skarn and manto ore bodies. The main minerals are galena, sphalerite and pyrite besides accessorily present chalcopyrite and sulphosalts. The ore is hosted by Paleozoic metamorphites, Tertiary andesites and recrystallised limestone (Monthel et al., 2002). Resources are estimated as 118,000 t Pb, 131,000 t Zn and 366 t Ag at grades of 4.4 %, 4.9 % and 137 g/t, respectively. Furthermore, Novobërdë is a particularly Au-rich deposit with average contents of 1.1 g/t (mainly present in invisible form hosted by pyrite and arsenopyrite) amounting to a resource of 2.9 t (Monthel et al., 2002). Kaltrina and Kiseli Potok are unexploited Pb-Zn-Ag occurrences in the immediate vicinity, i.e. within a distance of 1 to 2 km of the current workings. Both are regarded as skarn and manto type mineralisations with a similar paragenesis as Farbani Potok. Average Pb, Zn and Ag grades are estimated as 4.4 % / 3 %, 4.5 % / 2.5 % and 129 ppm / 80 ppm, respectively (Monthel et al., 2002).

Hajvali / Ajvalija

Hajvali is the only major deposit of the Kopaonik district which has not yet been mined in antique or medieval times and was only discovered in 1929 (Trepca Kosovo under UNMIK administration, 2005). The mineralisation occurs as mantos and subordinate skarn hosted by marble layers of Palaeozoic schist. The main ore phases are galena, sphalerite and pyrrhotite with minor chalcopyrite and sulphosalts. The deposit is marked by an unusually high Zn : Pb ratio with reserves of Pb, Zn and Ag of 85,000 t, 167,000 t and 71 t and average grades of 8.4 %, 16.4 % and 70 g/t, respectively. For the past production average Au contents of 0.8 g/t have been reported (Monthel et al., 2002).

3.2.2. Occurrences of other base and precious metals in central / southern Kosovo

Zhegovcë / Žegovac

The occurrence Zhegovcë, situated few kilometres southeast of the ancient mining district, comprises four vein or veinlet ore bodies, respectively, which are associated with Cretaceous carbonates, Jurassic ultramafic rocks and Cenozoic magmatites. The Pb-Zn ore is described as polymetallic and in contrast to other occurrences in the Kopaonik district particularly Cu-Sb-rich, thus indicating elevated abundances of sulphosalts, e.g. fahlore minerals. Old workings as well as findings of slag in nearby valleys indicate former mining and metal production in the area (ICMM, 2011).

Slivovë / Slivovo

Slivovë is a Au-Ag occurrence within an outcropping gossan zone nearby the village Peshter / Pešter (Avrupa Minerals, 2016) and located few kilometres northeast the ancient mining district. The precious metal mineralisation is hosted by severely altered calcareous sandstone and presumably structurally controlled. The formation of the orebodies is assumed to be related to abundant intrusive rocks in the target area. Au mostly is present in its native state as free gold. Its emplacement is thought to postdate the formation of quartz-hosted epithermal Pb-Zn-rich sulphide veins. At a Au cut-off grade of 1 g/t, the indicated reserves amount to 640,000 t at Au and Ag grades of 4.80 g/t and 14.68 g/t (Avrupa Minerals, 2016) and estimate to 98,700 ozs Au (2.80 t) and 302,000 ozs Ag (8.56 t).

Gllama / Glama

Gllama, located immediately northwest of Gjilan / Gnjilane is a Ag-Au occurrence hosted within a gossan zone affiliated with Jurassic serpentinites, basalts and granitoids and metacarbonates (Dvorani et al., 2012; Féraud & Deschamps, 2009; Monthel et al., 2002). Reportedly mined since medieval times (Féraud & Deschamps, 2009), the name Gllama apparently is related to 'argentum de glama' (i.e. Au-bearing crude Ag won at medieval times from the local occurrences; cf. section 4.1.1) and thus memorises the particularly Au-rich character of the ore. The mineralogy of the deposit mainly comprises Cu-bearing sulphides (chalcopyrite, pyrite, chalcocite, covellite, bornite, galena and sphalerite) of both primary and secondary origin which are associated with oxidised phases (e.g. malachite, Fe oxides and hydroxides). Drill sampling yielded Ag and Au contents of up to 77 and 24 ppm, respectively (Dvorani et al., 2012), as well as maximum Sn abundances of 1200 g/t (Féraud & Deschamps, 2009).

Prekovc / Prekovce

In the Prekovc area, around 6 km southwest of the deposit of Novobërdë, small amounts of placer Au are reported in alluvial sediments of the rivulets Kriva Reka, Ciganski Potok, Kiseli Potok and Bostanska Reka (Barth et al., 2005).

3.2.3. Pb-Zn-Ag deposits of the Kopaonik Mountains

Stan Tërg / Stari Trg

The Stan Tërg mine, located approximately 7 km northeast of Mitrovica / Kosovska Mitrovica, was exploited since at least medieval times (1303; Ćirković 1981; Gordus & Metcalf, 1969). Ancient workings surrounding the modern mine primarily to the north and east in a radius of 1 to 2 km (Schumacher, 1950) testify to these earlier activities. Stan Tërg is considered a classical example of a structurally controlled distal Pb-Zn-Ag skarn deposit (Guilbert & Park, 1986; Palinkaš et al., 2012; Schumacher, 1950; Schumacher, 1954) with its mineralisation - primarily consisting of galena, sphalerite, pyrite, pyrrhotite and subordinate chalcopyrite - being hosted by recrystallised Upper Triassic limestone. The reserves of Pb, Zn and Ag are estimated as 215,000 t, 112,000 t and 495 t at average grades of 3.9 %, 2 % and 90 g/t. Past production of Cd and Bi amounted to 1,655 t and 4,115 t, respectively. Au has been recovered as a by-product with an average yearly production of 250 kg between 1950 and 1985 (Monthel et al., 2002), consistent with reportedly low grades of less than 0.2 g/t in the mined ore (Schumacher, 1950).
Melenica / Meljenica is a Pb-Zn-Ag occurrence c. 2 km to the northeast of the Stan Tërg deposit and is interpreted as a lateral mineralisation of the giant main complex. The ore is present at joints within limestone and forms lenses and chimneys while the contact limestone-schist and limestone-quarzite is not mineralised. Melenica was intensively exploited during earlier times and has been considered as exhausted by Schumacher (1950).

Bellobërdë / Belo Brdo

The beginnings of mining in Bellobërdë date back to at least medieval times (opened 1438; Ćirković, 1981). The economically most important mineralisation type is of hydrothermal replacement style and occurs at or close to the contact of Cretaceous carbonates and Tertiary volcanic rocks and / or Jurassic serpentinites. Quartz-carbonate-sulphide veins are hosted by Tertiary andesites. Skarn mineralisation was present in Cretaceous carbonates distant to the manto and vein occurrences, but now is completely exhausted. The sulphide ore assemblage predominantly consists of pyrite, galena and sphalerite and is complemented by minor chalcopyrite and arsenopyrite. The vein ore additionally contains subordinate baryte and stibnite (Sb_2S_3; Veselinović-Williams, 2011). Bellobërdë contains reserves of Pb, Zn and Ag of 51,000 t, 56,000 t and 95 t at average grades of 4 %, 4.4 % and 75 g/t, respectively. The deposit is considered to be one of the most Au-rich mineralisations of the Kopaonik district with high-grade Pb-Zn ore containing 1 g/t on average, while for the mined out skarn 2.7 g/t Au are reported (Monthel et al., 2002).

Crnac

The ore is present as epithermal veins (and economically insignificant porphyry mineralisation) hosted in Jurassic amphibolite and within mineralised listwaenites occurring at the contact between serpentinite and amphibolite. The sulphide mineralogy is rather versatile in comparison to the skarn and replacement type deposits of the Kopaonik district and mainly comprises galena, sphalerite, pyrite, arsenopyrite, pyrrhotite, tetrahedrite [$(Cu,Fe,Ag,Zn)_{12}Sb_4S_{13}$] and stephanite

(Borojević Šoštarić et al., 2011). The Pb, Zn and Ag reserves are stated as 115,000 t, 45,000 t and 170 t at average grades of 8.1 %, 3.2 % and 120 g/t (Monthel et al., 2002). Crnac allegedly was already exploited in medieval times (Trepca Kosovo under UNMIK administration, 2005).

3.3. Characterisation of ore resources with isotope analysis

Pb isotope ratios initially have been exclusively applied for geological questions, particularly to track down melt sources by deciphering isotopic reservoirs, but also to reconstruct the formation history of sulphide ore deposits. Soon the potential of Pb isotope analysis for the provenance of metal objects has been recognised and now is an essential tool of archaeometallurgical research with a huge collection of ore deposit reference data being available to the scientific community. Non-traditional stable isotope systems since several years increasingly attract the attention of archaeometric researchers and have been scrutinised for their possible application. Cu isotopes ratios as a reflection of the oxidation state of ore minerals this far appear to bear the greatest potential to become established as a beneficial supplement to Pb isotope provenance studies.

3.3.1. Lead isotopes

Pb possesses four naturally occurring isotopes of which ^{208}Pb, ^{207}Pb and ^{206}Pb are formed by radioactive decay of ^{232}Th, ^{235}U and ^{238}U while the abundance of ^{204}Pb remains constant. The amount of the daughter isotopes ^{208}Pb, ^{207}Pb and ^{206}Pb (approximately 52.3 %, 22.1 % and 24.1 %, respectively) therefore steadily increases with time in comparison to the proportion of ^{204}Pb (c. 1.4 %; De Bièvre & Taylor, 1993). Since sulphide minerals only take up Pb but neither Th nor U, their isotope composition always reflects the one present when they were formed; it hence generally records the formation age since younger phases are marked by higher proportions of ^{208}Pb, ^{207}Pb and ^{206}Pb compared to ^{204}Pb. Mining districts with a similar geological history thus possess comparable Pb isotope ratios clustering around major ore-forming events. However, the signature may be significantly influenced by tectonic and geological factors, e.g. due to remobilisation of earlier formed mineralisations. In archaeometry, the potential of applying Pb isotope signatures for the provenance analysis of metal artefacts has been discovered in the 1960's and has since been widely utilised.

The attention of the scientific community has been directed towards the ore source region of metal objects since the 19$^{\text{th}}$ century, which in the beginnings has been tried to retrace by chemical methods and later by Pb isotope analysis (see Pernicka, 2014; for a historical and methodological overview). The pioneering studies of Brill & Wampler (1967) and Grögler et al. (1966) first compared ore Pb isotope ratios with those of metal artefacts. The application of Pb isotope analysis since then has been expanded for a broad array of ores and metals as well as alloys relevant for ancient metallurgy (Cu, Sn, Ag, Au and even Fe; see e.g. Cattin et al., 2009; for an extensive compilation of published data) and by now is a routinely applied standard technique. In the beginnings, Pb isotope ratios have been determined by TIMS (thermal ionisation mass spectrometry), which required a few micrograms of sample material and had an accuracy of ± 1 % (Stos-Gale & Gale, 2009). Due to adjustment of measurement protocols and technological advancement, the analytical error could be improved to ± 0.1 % (Baker et al., 2006). The

application of MC-ICP-MS (multi-collector inductively coupled plasma mass spectrometry) further decreased uncertainties to ± 0.01 % and the amount of sample material necessary to a few nanograms (Hirata, 1996). The accuracy and precision of MC-ICP-MS measurements thus are comparable to TIMS double- / triple-spike procedures (Baron et al., 2014).
Besides the availability of fast and reliable instrumentation, the stability of Pb isotope ratios concerning subsequent processes such as weathering (Gulson & Mizon, 1979) and corrosion (Snoek et al., 1999), but also towards the amount of Pb present in the smelting system (Pernicka, 2014) and the deposit mineralogy (Gulson & Mizon, 1979) has significantly contributed to its success story. The effect of heat treatment on the elements' ratios, however, has been, provoked by calculations of Budd et al. (1995), who proclaimed notable isotope fractionation due to non-equilibrium Pb losses exceeding 40 %, controversially discussed in the past. Indeed, high removal rates of Pb (e.g. by volatilisation) might theoretically influence the ratios. Stos-Gale & Gale (2009) report Pb isotope data of argentiferous galena, metal smelted from this ore and litharge from cupelled metal which are within analytical errors. Similarly, Baron et al. (2009) in their experiments on Pb smelting from sulphide ores could not detect measurable isotope fractionation between ore, slag and smoke from the metallurgical operations, but named fluxes and heterogeneous furnace charges as significant influences on the signature. Cui & Wu (2011) could confirm the results of former experiments since even at non-equilibrium Pb losses of 99 %, fractionation does not exceed 0.1 % and thus also is well within the range of isotopic variation within ore bodies (Gulson, 1986; Stos-Gale, 1993).
Archaeometrical studies often relied on the ratios $^{207}Pb/^{206}Pb$ and $^{208}Pb/^{206}Pb$ due to the former rather high analytical uncertainty of the rarer ^{204}Pb, which though leads to a loss of information and hence renders provenancing more difficult. However, high-precision analysis technically made the abdication of this isotope obsolete (Baron et al., 2014; Villa, 2009). Generally, Pb isotope ratios should not be treated as abstract numbers alone but the geological background of the mining districts has to be kept in mind, i.e. to consider them as representatives of typically supraregional metallogenetic events, to know the associated deposit type (including its mineralogy, which is a crucial factor controlling the trace element signature commonly applied as an additional tool for provenancing; see below) and its host rocks as well as the regional geology of the area studied to gather as much information as possible from the very beginning of the metal smelting operations, i.e. from the raw material source on.
The application of Pb isotope provenance analysis is impeded if the investigated samples are Pb- and sulphide-poor or even non-sulphidic, respectively, since the isotope ratios then are easily influenced by e.g. later addition of Th and U as described by Pernicka et al. (1993) for the Eneolithic Cu mine site Rudna Glava, which under modern criteria is de facto classified as an Fe skarn deposit (Monthel et al., 2002). Generally, if Pb-poor mineralisations are investigated, it always has to be questioned where the analysed Pb content is derived from since the bulk isotope signature of Pb-poor material might be significantly altered by foreign Pb (derived e.g. from the gangue material of ore bodies or fluxes added during metallurgical processing). Mixing of primary metal from several sources, but also recycling of scrap metal (e.g. Boni et al., 2000; Klein et al., 2004) for the production of artefacts are other factors potentially blurring the Pb isotope ratio and may render successful provenancing a virtually impossible task. Considering

the massive benefits of Pb isotope analysis for provenance studies, it has to be kept in mind that it only can be used as an exclusion method, but not to positively assign a metal artefact to a distinct district. Trace element analysis may provide additional information on the source region (cf. Hauptmann et al., 1992; for a combined Pb isotope and trace element provenance study). Their theoretical behaviour during metallurgical processing has been tried to grasp by means of thermodynamic calculations (e.g. Pelton et al., 2015; Yazawa, 1980) and experimental studies (e.g. Pernicka & Bachmann, 1983; Merkel, 1990; Tylecote et al., 1977). Overall, the archaeological and historical context of the investigated objects should be considered as crucial when finally interpretating the gathered data.

3.3.2. Copper isotopes

Cu possesses two stable isotopes, ^{63}Cu and ^{65}Cu, which make up 69.17 % and 30.83 % of the element's population, respectively (Shields et al., 1964). Isotope fractionation is based on slightly different chemical and physical properties which are caused by mass differences. It generally tends to zero at very high temperatures and is much greater at lower temperatures (Allègre, 2008). Cu isotope data traditionally is noted as δ^{65}Cu calculated as

$$\delta^{65}\mathrm{Cu} = \left(\frac{\left(\frac{^{65}\mathrm{Cu}}{^{63}\mathrm{Cu}}\right)_{\mathrm{sample}}}{\left(\frac{^{65}\mathrm{Cu}}{^{63}\mathrm{Cu}}\right)_{\mathrm{standard}}} - 1 \right) \times 1000 \tag{3.1}$$

NIST SRM 976 (Shields et al., 1964) conventionally is used as a standard. Consequently, if δ^{65}Cu is positive, the sample is enriched in ^{65}Cu; if δ^{65}Cu is negative, it is enriched in ^{63}Cu.
The beginnings of Cu isotope geochemistry date back to Walker et al. (1958), who first reported ratio variations in minerals and plants. However, only the advent of plasma-coupled mass spectrometry instruments established the possibility to precisely determine the isotope ratios (Maréchal et al., 1999). Among the transitional metals, Cu isotopes are regarded as the most promising tool for geochemical process reconstruction since they are comparatively easily analysed and display distinct fractionation in varying environments.
While primary sulphides formed by high-temperature magmatic or hydrothermal processes generally appear to possess homogeneous Cu isotope ratios (i.e. δ^{65}Cu close to zero; see above), phases precipitated during redox processes at comparably low temperatures from aqueous solutions are marked by highly variable δ^{65}Cu values, which have been attributed to mass fractionation processes rather than a heterogeneous metal source (Larson et al., 2003; Markl et al., 2006; Zhu et al., 2000). High variation on meter- to partially sample-scale exclude the possibility to use Cu isotopes as a fingerprint since the significant heterogeneity of δ^{65}Cu values within single deposits exceeds possible differences between occurrences. Generally, Cu isotope ratios probably are influenced by several parameters, including temperature, ph, fO_2, salinity and Eh conditions (Asael et al., 2012; Larson et al., 2003).
Dissolution experiments demonstrated that supergene phases and the leachate of primary sulphides from which they originated are isotopically heavy in comparison to primary phases. ^{65}Cu thus gets preferentially oxidised and hence is enriched in supergene phases ($\delta^{65}\mathrm{Cu} > 0$) precipitated at the groundwater table while phases in the leached cap consequently exhibit higher

abundances of ^{63}Cu (δ^{65}Cu < 0). Primary sulphides are marked by a narrow δ^{65}Cu range between -1 and +1 ‰ (see Braxton & Mathur, 2011; Klein et al., 2010; Markl et al., 2006; Mathur et al., 2009; Wall et al., 2011; for an overview of data). However, bacterial activity may either suppress or even reverse the fractionation signature observed in abiotic experiments (Fernandez & Borrok, 2009; Kimball et al., 2009; Mathur et al., 2005). Due to their dependance on redox-controlled enrichment and leaching processes, Cu isotope ratios possess considerable exploration potential to indicate underlying enriched mineralisation and their primary source region (Braxton & Mathur, 2011; Mathur et al., 2009).

The relation of Cu isotope signatures to ore types (primary sulphides, phases related to secondary enrichment and oxidation) also has been applied to further delineate the possible provenance of archaeological metal artefacts (e.g. Artioli et al., 2008; Desaulty et al., 2011; Klein et al., 2004; Klein et al., 2010). However, besides the highly intricate task to correctly interpretate Cu isotope ratios due to a potentially complicated geological history of the raw material, it has also not yet been fully deciphered whether the isotope signature is sensitive to metallurgical processing. Only a small pilot study of Gale et al. (1999) has been published so far, but a thorough experimental investigation of the potential fractionation behaviour of Cu isotopes during smelting and refining treatment is in preparation (Th. Rose, Goethe-Universität Frankfurt). Surficial weathering of the artefacts, but also alteration during soil deposition in contrast certainly influences the isotope signature and might eliminate the pristine information related to the ore type the object has been manufactured from. The significance of Cu isotope data for the provenance analysis of archaeological metal artefacts to date thus is marginal but, however, may be increased by further research.

4. *Res metalla*: Imperial mining and metal production in Kosovo and Serbia

Ancient Pb-Ag mining activities in Kosovo and Serbia are known from the Zhegovc (Kosovo, comprising the study area) and Kopaonik Mountains (southern Serbia and Kosovo; both constitute the Kopaonik district in local economic geology) and Šumadija district (central Serbia). All of these mining regions are located within the Serbomacedonian-Rhodope belt (cf. section 3.1) extending across northern Greece, southern Bulgaria, Macedonia, Serbia and Kosovo. They hence share an identical formation history - the deposits are genetically related to Miocene calc-alkaline volcanism - resulting in overlapping Pb isotope signatures and similar mineralisation styles, i.e. carbonate-hosted skarns and mantos or hydrothermal veins (also see chapter 3).

4.1. The Zhegovc Mountains

4.1.1. Historical timeline of mining and metal production

Rome's expansional politics greatly shifted the borders of the Empire particularly in the 1st century CE and gradually put the Balkan Peninsula under Roman rule. The Kosovo region was conquered by Licinius Crassus in 29 / 28 CE and in the beginning presumably constituted an administrative unit together with Makedonia. Moesia was installed as a separate province probably in 45 / 46 CE and subdivided into Moesia Inferior and Superior. The latter part comprised what today is southern Serbia, Kosovo and northern Macedonia. Moesia Superior had four administrative units, namely Tricornenses, Pincenses and Moesi in the northern part and Dardania covering the entire south of the province (Ptolemy, *Geography* 3.9.2).
Ulpiana is assumed to have been an administrative centre or even some sort of capital of Dardania (Dušanić, 2004; Petrović, 2007; and references therein). The settlement was founded in the 1st century CE and gained the status of a *municipium* in the 2nd century CE, either during the reign of Trajan (98 - 117 CE; Mirdita, 1978) or Hadrian (117 - 138 CE; Mócsy, 1970). Due to the similarity of names it has long been thought that Ulpiana is identical to the modern settlements Lipjan / Lipljan or Llappllasallë / Laplje Selo (Mócsy, 1970). However, systematic excavations led to the discovery of the remains of the ancient city in 1954 (Popović & Čerškov, 1956), which in fact have been found close to the town of Graçanica / Gračanica and c. 8 km southeast of Prishtina / Priština, in the fertile land of the Kosovo basin (Fig. 4.1). Ulpiana's outstanding position in Dardania commonly is explained by its advantageous location nearby the junction of the road from Scupi (Skopje) with the road Naissus (Niš) - Lissus (Lheza), but also is related to the mineral wealth of the Zhegovc Mountains, which rise within eyeshot to the east of the *municipium* (e.g. Hirt, 2010; Mócsy, 1970). Indeed, the whole region seems to have been well-known for its rich ore abundances in antiquity and particularly Moesia obviously was considered

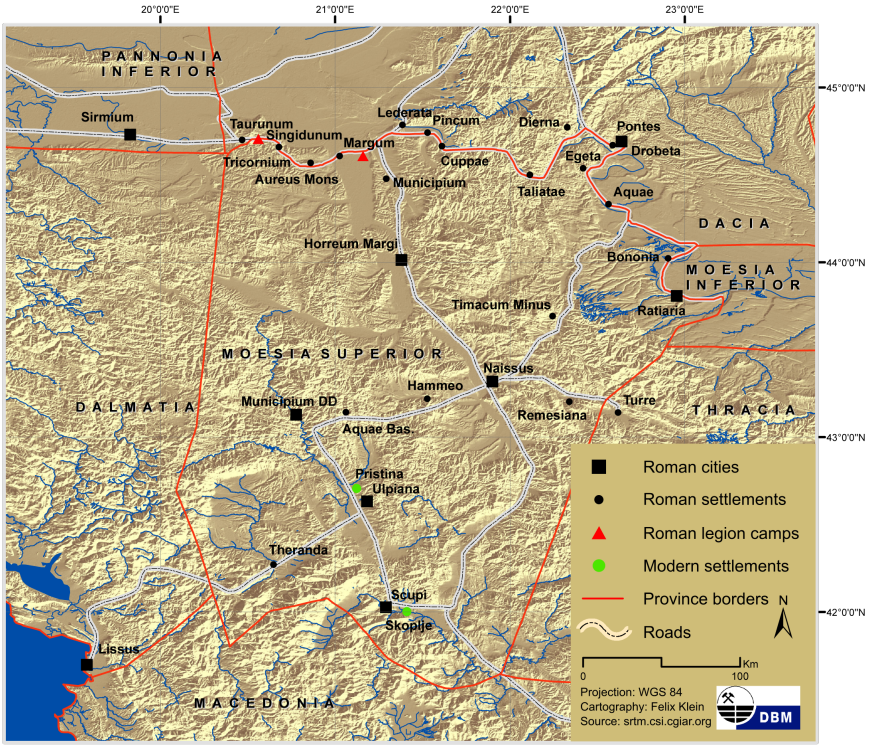

Figure 4.1.: Map of Moesia Superior and surrounding provinces displaying the location of Roman cities, settlements, legion camps and roads. Map: Deutsches Bergbau-Museum; cartography: Felix Klein.

as the mining province par excellence (*in Mysia...ubi metalla sunt*; *Dig.* 48.19.16.9 - 10). Rome's urge for expansion often is attributed to the mineral wealth of the Balkan region and to generally declining yields of the Ag mining districts of the Iberian Peninsula (cf. section 5.2.1). In fact, epigraphic and archaeological evidence (see chapter 4.1.2) strongly suggest that Ulpiana was – as well as supposedly Municipium DD, Lopate, Remesiana and Timacum Minus (cf. Fig. 4.1) - the administrative centre of a prosperous mining district (Janjevo; Dušanić, 2004; Petrović, 2007). The mentioning of Dardanian procuratores metallorum in the *Codex Theodosianus* (1.32.5; 386 CE) proves that local mining and metal production continued to at least the late 4th century CE. After struck by an earthquake in 518 CE, Iustinian I (527 - 565 CE) restored Ulpiana from its ruins as Iustiniana Secunda and the city experienced a last flourishing period (Procopius, *De Aedificiis* 4, 1, 29) during which precious metal mining in the region is thought to have persisted (Evans, 1996). The finding of a solidus attributed to the Byzantine Emperor Leo I (457 - 474 CE) in a gallery nearby Janjevo (Ivanišević & Špehar, 2005) testifies to mining activities in the region after division of the Roman Empire.

The advent of skilled 'Saxon' miners in 13th century Serbia marked the beginning of a new era of intense mining and metallurgical activities in the region. Several mines were opened during that time, e.g. Stan Tërg 1303 and the district of Novobërdë between 1304 and 1319 (Mrkobrad, 1994; and references therein). The latter included the workings around Janjevo and Graçanica, where mining activities started in 1346 and 1303, respectively (Ćirković, 1981). Silver won from the ores of Novobërdë and Janjevo contained a certain percentage of gold and was traded

as 'argentum de glama' (Ćirković, 1981) throughout Europe and the Near East - a fact which is memorised by medieval mine names such as Gllama (cf. section 3.2.2). The Ag and Au deposits of the Serbian Empire, praised by contemporaries for their fabulous wealth (Jireček, 1879), constituted its economical backbone with the most important district of Novobërdë alone reportedly yielding revenues of 200,000 ducats per year (Vryonis, 1962). When Ottoman Turks began conquering the region at the end of the 14^{th} century, they gradually also gained control of the mining centres in Serbia, Macedonia and Bosnia. Some ten years later they owned the most important deposits of the Balkan Peninsula, including Novobërdë and Janjevo besides e.g. Stan Tërg and Rudnik (Stoianovich, 1994). The new rulers quickly took advantage of the region's mineral wealth and continued exploiting the resources and minted their own coinage, e.g. at Novobërdë (Pamuk, 2000). During the second half of the 15^{th} and early 16^{th} century, the yields of the mining operations already decreased steadily and when the New World's cheap silver began to flood the market in the mid-16^{th} century, the European mines were largely rendered unprofitable (Stoianovich, 1994). The region experienced an anew revival of mining activities in the early 20^{th} century, when exploration campaigns and re-evaluation of older workings lead to the opening of numerous mines and establishment of the Trepça mining complex in 1926. With its rich history dating back to at least Roman times, the Kosovarian and Serbian Pb-Zn-Ag mining districts of the Kopaonik and Zhegovc Mountains are among the most productive and long-living in Europe.

4.1.2. Archaeological evidence for local mining and metal working and its possible connection to Ulpiana

Ancient mining remains around Janjevo have been first mentioned by Hießleitner (1927) who examined the profitability of the local mineralisation and came across numerous old workings tracing the partially Au-bearing Pb-Ag veins in an area exceeding 12 km^2. Inspecting a gallery, he discovered a variety of mining tools (hammer and pick), a wooden trough with handles on each end, a pan perhaps used for gold washing as well as fascines and torches used for illumination underground. Hießleitner (1927) describes several smelting sites with though rather small-scaled slag heaps - which he attributed to re-smelting in newer times - in the vicinity of Janjevo. However, he only mentions the site in the valley of the Kishnica stream by name, which now would be situated at the facility premises of the homonymous modern mine. The finding of litharge near Janjevo indicates Ag extraction via cupellation from the local ore. Besides Hießleitners detailed description, Davies (1935) briefly refers to the mining district and mentions ancient workings for Au and Ag at Janjevo - which he identified as 'the Roman mines of Dardania' - and medieval mining nearby the settlement Shashkoc / Šaškovac. He does not exclude that the rich deposit of Novobërdë could have been discovered by the Romans. In a later article, Davies (1938) expressed a rather cautious view and stated that there is no evidence for Roman activities at Janjevo but rather at Graçanica, where he though could not discover any kind of smelting remains. However, traces of Archaic settlements (e.g. at the mountain Veletin overlooking the village Shashkoc; Jovanović, 2003) and a hoard or grave assemblage of Iron Age bronze bracelets (9^{th} - 8^{th} century BCE) discovered nearby Janjevo (Vasić, 1990) date the beginnings of possibly related local mining activity to already prehistoric times. Damastian silver coins from the second half of the

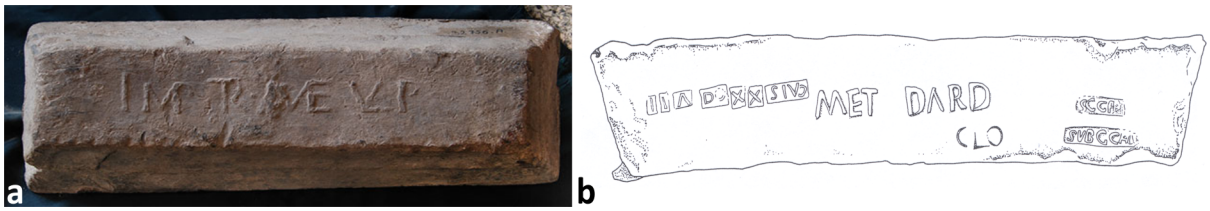

Figure 4.2.: a) Lead ingot from the 2nd century CE (106 - 117 CE) with stamp '*IMP (eratoris) TR (aiani) ME (talla) ULP (iana)*' discovered at the *forum vetus* of Sarmizegetusa / Ulpia Traiana (central city of the province Dacia, modern Romania; lupa 10895). b) Lead ingot, dated to the 1st century CE (83 - 96 CE), with stamp *MET (alla) DARD (anica)* retrieved from the harbour of Augusta Caesarea (Israel; Raban, 1999).

4th century BCE found at the mountain Veletin and at Janjevo in conjunction with the nearby ore district lead Ujes (2002) to include the area around Kishnica, Janjevo and Prishtina among possible locations for the Hellenistic settlement.
Similarly to Municipium DD, evidence for the relationship of Ulpiana itself to mineral exploitation has been assumed by Mócsy (1970) and Dušanić (2004) on basis of the caption '*METALLUM ULPIANUM*' on Traianic *nummi metallorum* (i.e. mining coinage) and lead ingots and caused them to suggest that Ulpiana was the central city of a mining district (*metalla*) or that the city even owed its existence to it (cf. section 4.1.1). The stamp '*IMP (eratoris) TR (aiani) ME (talla) ULP (iana)*' on a lead ingot (Fig. 4.2a) indicates that the local mines were property of the Empire and hence precious metals, in particular Ag, were won from the local ore (cf. chapter 4.2). The fact that lead ingots with a presumably Dardanian origin dated to the 2nd to 4th centuries CE were found in Romania (lupa 10895), Israeli territorium (Raban, 1999), Rome and Novae (Moesia Inferior; Dušanić, 2004) documents intense and flourishing trade and indicates the high importance of the region for the (late) Empire's metal supply. The collection of a tax or toll linked to mining activities is strongly suggested by toll stations which are mostly situated on the main road connecting Naissus, Ulpiana and Scupi in the vicinity of mining areas; the inscription *vilicus stat (ionis) Ulp (ianensis)* has been discovered in Llapplasallë 3 km to the west of Ulpiana. Whether these stations were positioned on the borders of a mining district or inside it, e.g. at strategic points such as bridges or passes, has yet to be clarified (Hirt, 2010).

Within the city limits of Ulpiana[1], a metallurgical workshop with four furnaces as well as tuyeres, appropriate tools, ores, slags and a stone mill have been excavated (Parović-Pešikan & Stojković, 1995). A lead lump adhering to one of the furnaces and the discovery of a mould probably designed for the manufacturing of standardised silver bars indicates that mainly argentiferous Pb was treated in the workshop. A casting mould for imitation of the Empire's official currency under Constantine (318 - 322 CE) has been retrieved from the ground of the Graçanica monastery. Indeed, various coins dating from the 1st to the second half of the 5th century CE have been discovered in the vicinity of the metallurgical workshop (Parović-Pešikan & Stojković, 1995). Similarly to other Roman settlements in Moesia Superior (e.g. Viminacium, Naissus; Golubović, 2002), lead sarcophagi have also been found in Ulpiana. The two sarcophagi are

[1]Detailed descriptions of the settlement archaeology of Ulpiana are provided by Berisha et al. (2012) and Teichner (2015).

undecorated and were obviously used for the burial of children. Further lead objects for everyday use from Ulpiana include a lead block (potentially a weight) and an ornamentally decorated part of a platelet (cf. section 14.1). Besides the lead objects, various silver artefacts such as cosmetic boxes, spindles and fibulae, mostly dating to the 2nd or 3rd , but also to the 4th or 5th century CE, have been found in the remains of Ulpiana itself or at the nearby settlement Graçanica (Petković, 2003; Popović, 1994). The presence of the metallurgical installations and tools documents a direct association of the city with metal working and implies that the lead and silver objects excavated on site might have been produced from local ore resources.

4.2. The Kopaonik Mountains

Evidence for Roman mining in the Kopaonik district this far mainly is based on epigraphic sources. Municipium DD (Dardanicum or Dardanorum; Dušanić, 1977), located in the Ibar valley close to the modern settlement of Soqanica / Sočanica (c. 20 km northwest of Mitrovica), was the central settlement of the region and promoted to its title during the reign of the Severan dynasty (193 - 235 CE; Mócsy, 1970). A close association of the city with mining activities is generally accepted. The captions '*(METALLUM) DARDANICUM*', '*DARDANICI*' and '*MET DARD*' found on *nummi metallorum* (one coin has been discovered in the immediate vicinity of the modern Stan Tërg mine) and lead ingots (Fig. 4.2b) from the late 1st and early 2nd century CE, respectively, have been related by Mócsy (1970) and Dušanić (1977; 2004) to a homonymous mining district nearby Municipium DD or interpreted as a labeling for the Dardanian mines in their entity. Three inscriptions found in the city dating from the 2nd to the 3rd century CE (Hirt, 2010; Dušanić, 1977), including *proc(urator) mm(etallorum) D(ar)d(anicorum)*, indicate imperial control of the mining district (see above). Similarly, stations of *beneficiarii consulares* found in the Sitnica valley at Vushtrri / Vučitrn, Novopazarska Banja, Slatina and Mitrovica might have been used for administrational control of the precious metal mines in the vicinity (Hirt, 2010).

Mining archaeological evidence to date has been scarcely reported from the region. Davies (1935; 1938) does not exclude the possibility of Roman workings in the Kopaonik district, particularly in the vicinity of the famous deposit of Stan Tërg. Slag heaps have been reported in the vicinity of Soqanica (Davis, 1938). Golubović (2002) mentions the presence of installations related to the metallurgical treatment of ores and the discovery of metal artefacts in the vicinity of Municipium DD. Further north the Ibar Valley, a Roman period metallurgical site with roasting installations, smelting furnaces and a workshop dated to the 4th century CE has been discovered near Zajačak. Evidence for another smelting complex has been found at Trsove Bare (Bogosavljević-Petrović, 2006).

4.3. The Šumadija district

Roman mining remains in Šumadija (probably *metalla Tricorn(i)ensia*; Dušanić, 2000; Dušanić, 2004) have been reported from Rudnik, Mt. Kosmaj and Avala and dated from the 2nd - the district has been opened during the reign of Marcus Aurelius (161 - 180 CE; Mócsy, 1970) - to the 4th century CE (Merkel, 2007). Rudnik is the only mine still in operation today. However,

an exploration campaign has led to the discovery of significant Pb-Zn-Ag-(Au) ore bodies in the vicinity of Mt. Kosmaj (Parlozi property; Tunningley, 2011). Traces of ancient activity - according to Tomović (1994), 5000 old workings have been mentioned in the literature of the early 20^{th} century - there cover an area of 5 km^2 and mainly include rows of collapsed mining shafts besides galleries and shafts. Drilling showed that ancient mining was limited by the water table, but reached a maximum depth of c. 150 m below the surface (Tunningley, 2011). An inscription found at Rudnik documents the presence of a *procurator* (*metallorum*; Hirt, 2010) and thus state-controlled extraction of precious metals. Smelting was carried out in the immediate vicinity of the mines, as indicated by the waste heaps, which range over an area of several km^2. 6000 g Ag are reported to have been won by the Romans from each ton of exceptionally rich ore smelted (Tomović, 1994). The amount of slags at the smelting sites has been diminished due to modern re-working for their Pb and Zn content by the Trepça company (Tunningley, 2011), but nevertheless is stated as 1,000,000 tons, thus putting the output of the ancient Šumadija district in a similar range than Laurion and second only after the giant complex of Rio Tinto in Roman times (Merkel, 2007). 14 lead ingots attributed to the district so far further emphasize the important role of the mines regarding the Empire's mineral supply (Tomović, 1994).

5. Other lead and silver mining districts of the Roman Empire

When the Roman Empire reached its biggest extension during the reign of Trajan, it possessed access to all major Pb and Ag mineralisations known at that time in the western world. Several examples demonstrated that the Romans after gaining control of the deposits began exploiting the ores shortly afterwards, often benefitting from earlier workings established by the native population (see below). However, since local mining generally could not fully meet the demand, metal produced from deposits located throughout Europe, including the previously detailed described supraregionally important mining districts of Kosovo and Serbia, was widely traded throughout the Empire. The following chapter lists the Pb-Ag districts most relevant for the metal supply of the Roman Empire and discusses their importance in relation to chronology, thus serving as a supplement to the compilation of Pb isotope reference data utilised for isotope provenance studies.

5.1. Southeastern Europe

5.1.1. Greece

Pb-Ag-(Au) ores are plentiful in Greece with Laurion and northern Greece (i.e. the regions Macedonia and Thrace) as the most relevant ancient districts (Healy, 1978). This far, however, no Roman lead objects could be clearly assigned to a Greek ore source so far thus suggesting that the mines must have been of only local relevance in later times (Bode, 2008).

Attica (Laurion)

Laurion is a Pb-Zn-Ag-(Au) carbonate replacement deposit, which is genetically related to Miocene andesite volcanism with mantos, chimneys and veins as the main mineralisation types (Skarpelis, 2007; Voudouris et al., 2008a; b). It is famous for its rich mining archaeological and archaeometallurgical remains, such as old workings as well as ore beneficiation and smelting sites (Healy, 1978; Rehren et al., 2002). Mining already began in the Neolithic period (late 4^{th} millenium BCE; Nriagu, 1983), but the most intensive exploitation phase is assigned to the Classical era during the 5^{th} and 4^{th} centuries BCE (Rehren et al., 2002). Strabo (*Geography*, 9.1.23) and Pausanias (*Description of Greece*, 1.1) report the district as abandoned in the 1^{st} and 2^{nd} century CE, respectively. However, while mining in Laurion apparently ceased, smelting activities, i.e. re-working of ancient slags, are mentioned by Shepherd (1993) for the time of the Roman Empire. Archaeological findings document a later anew period of mining activities in the 4^{th} to 6^{th} centuries CE (Rehren et al., 2002; and references therein). However, throughout the era of

both the Roman Republic and Empire, the dimension of the operations at Laurion must have been of no comparison to its earlier heydays and of only local relevance.

Northern Greece: Makedonia and Thrace

Makedonia is a region in northeast Greece, which includes the Chalkidiki Peninsula, the island Thasos and the Palaia Kavala area on the opposite mainland (Thasian Peraia). Thrace is the easternmost part of the country, which is bordered by Turkey to the east and Bulgaria to the north. Thasos, the Thasian Peraia and Thrace are attributed to the Rhodope Mountain chain, whose largest part belongs to Bulgaria (Nesbitt et al., 1988; chapter 5.1.3). Ore deposit formation apparently is related to Tertiary magmatism linked to extensional tectonics. Major mineralisation types include polymetallic veins, carbonate-hosted skarn and manto ore bodies and Cu-enriched base metal sulphides associated with serpentinite and amphibolite rocks (Nesbitt et al., 1988).

Polymetallic Tertiary skarns, mantos and veins are abundant in the area of the modern Kassandra mines in northeast Chalkidiki (Kalogeropoulos et al., 1989). Ancient mining in the region dates back to at least the 4th century BCE, but is suspected to have begun in the Bronze Age (Meier, 1995; and references therein). Thasos was widely renowned in ancient times for its Au occurrences in the northern and eastern part (Wagner et al., 1981). Furthermore, rich stratabound and stratiform carbonate-hosted Pb-Zn ores with Ag contents of up to 1500 g/t (Pernicka et al., 1981) are reported to occur in the western part (Nesbitt et al., 1988; Wagner & Pernicka, 1982). Roman mining and smelting is proven by radiocarbon dating of charcoal from old workings and by thermoluminescence analysis of ceramic found at a smelting site, which yielded ages grouping around 300 CE $\pm$ 120 and the 1st millenium BCE (Pernicka et al., 1981). Skapte Hyle, a famous ancient Au-Ag mine, is suspected to have been situated in the Pangeon Mountains in the Palaia Kavala region, which is located on the mainland opposite to Thasos (Photos et al., 1989). The deposit seems to have been largely exhausted in times of the early Roman Empire (Nriagu, 1983). However, smaller-scaled mining activities according to Domergue (2008) were consistent until the 2nd century CE. Geological proof for the location of Skapte Hyle is reported by Eliopoulos & Kilias (2011), who describe a Au-bearing mineralisation (carbonate-hosted vein and supergene gossan ore) in the Asimotrypes area at Mt. Pangeon to be situated among extensive ancient workings. Nesbitt et al. (1988) further mention abundant skarn-type base metal occurrences in the region.

Thrace's base metal mineralisations often are hosted by mafic rocks, i.e. serpentinites, amphibolites and greenschists and hence are marked by a predominantly Cu-enriched mineralogy. The ore mainly is present as polymetallic veins, stratiform lenses or porphyry bodies. Carbonate-hosted Pb-Zn replacement deposits (see above) are known from the region as well (Nesbitt et al., 1988).

5.1.2. Romania

Romania is particularly famous for its Au-Ag-(Cu) deposits in the Carpathian Mountains with the main mining areas being in the Maramureş region (Baia Mare and Baia Borşa) and the Apuseni Mountains, e.g. Roşia Montană (the Roman Alburnus Maior), whose ore bodies have been intensively mined for Au by the Romans (Baron et al., 2011; Hauptmann et al., 1995). The

formation of the ore bodies is linked to igneous activity caused by collisional and extensional processes in the Miocene. Pb-dominant ores generally are of subordinate character and present as polymetallic veins or, in the Apuseni Mountains, also as skarn, porphyry and VMS deposits (Marcoux et al., 2002). The geological conditions as well as the documented import of metal (see chapter 4.1.2) suggest that the local Pb production only must have been of regional relevance.

5.1.3. Bulgaria

Bulgaria is dappled by several mountain ranges, including the Stara Planina, Sredna Gora, Sakhar, Osogovo (see below) and Rhodope Mountains (section 5.1.1; see Gale et al., 2000; for an overview of Bulgarian deposits). Nriagu (1983) refers to the Ustrem district of the Sakar Mountains, Eastern Rhodope Mountains and Stara Planina in particular as the most important ancient mining districts. Indeed, a number of studies (e.g. Guénette-Beck & Furger, 2004; Kuleff et al., 2006; Walton & Tite, 2010) testify a Bulgarian provenance for (pre-) Roman lead-based artefacts.
The mining districts located in the Rhodope Mountains are the most intensively studied so far and mainly comprise hydrothermal vein and replacement deposits of Oligocene to Miocene age. Marchev et al. (2005) state the typical Ag contents of Central Rhodopian ore fields (Davidkovo, Laki, Madan, Eniovche, Ardino) between 12 and 53 g/t. Mineralisations located in the eastern part of the mountain range are characterised by elevated Cu and Au contents.

5.1.4. Macedonia

The Osogovo Mountains are situated in the border triangle Bulgaria-Serbia-Macedonia and possess characteristics comparable to those of the Rhodope deposits (Mankov, 2006). In one of its main ancient mining districts, the Macedonian Zlatovo-Kretovo region, hydrothermal Pb-Zn veins, which partially possess significant Ag and Au contents were worked. The town of Kratovo also had a mint where a coin from the 1st century CE has been discovered (Meier, 1995; and references therein).

5.2. Southwestern Europe

5.2.1. The Iberian Peninsula

For centuries – mainly from the 2nd century BCE to the 1st century CE – the Iberian Peninsula was the most important source region for metals for the Roman civilisation (Meier 1995; Nriagu, 1983) with the huge dimension of the operations according to Rosman et al. (1997) even recorded within Greenland ice. The decline of mining in imperial times is commonly thought to be related to exhaustion of technologically viable resources and the opening of other districts, e.g. Britain with its easily accessible ore bodies (see below).
The most important districts were located in the southern part of the peninsula in the Sierra Morena in southwest Spain and Portugal (Los Linares - La Carolina, Azuaga - Fuente Obejuna, Valle Alcudia, Los Pedroches) and in the Betic Cordillera in southeast Spain (Sierra Cartagena, Sierra de Gádor, Sierra Almagrera, Sierra del Cabo de Gata, Sierra Alhamilla; Bode, 2008; Meier,

1995; Nriagu, 1983). The mineralisations in the Cantabrian Mountains of northern Spain were of subordinate relevance for ancient Pb-Ag production, the area rather is known for Au and Sn exploitation (e.g. Lewis & Jones, 1970; Pérez-García et al., 2000).

Sierra Morena

Ancient mining in the Sierra Morena mostly is dated from the 2nd to the 1st century BCE, but locally is thought to have been continuous until the 4th century CE (Meier, 1995). The geological history of the mountain chain is complex with ore formation related to several geodynamic regimes (Tornos & Chiaradia, 2004). Besides Pb-Zn occurrences of various mineralisation styles, the district also hosts abundant Sn, W, Hg, Ni, Bi and particularly Cu-bearing ore types (cf. Klein et al., 2009).
The mineralisations range from late Neoproterozoic to Permian age resulting in a complex Pb isotope signature and include several deposit types such as Pb-Zn-(Cu-Ag-Ba-F) veins, stratabound Pb-Zn-(Ba) ore bodies, massive Zn-Cu-(Pb) sulphides and Zn-(Pb-Sn) skarns (Tornos & Chiaradia, 2004). Late- to post-Variscan Pb-Zn-(Cu-Ag) veins are particularly abundant at Azuaga-Fuente Obejuna, but also occur at Linares-La Carolina, where late Hercynian stratabound mineralisation types are present as well (Lillo, 1992).

Betic Cordillera

Carthago Nova, whose location is identical to the modern city of Cartagena in Spain's Murcia province, was the central harbour for the export of metals gained from local resources in southeast Spain. Based on findings of lead ingots, its heydays must have been at the end of the 2nd and particularly in the 1st century BCE (Trincherini et al., 2009).
Pb mineralisations of the Sierra Alhamilla and Sierra de Gádor occur as Triassic carbonate-hosted strata-bound F-Pb-Zn-(Ba) ore bodies, which are widely similar to alpine-type and MVT deposits (Arribas & Tosdal, 1994). The generally Ag-poor galena ore presumably was only smelted for its Pb content. Mining activities locally could be proven until the 6th century CE (Meier, 1995).
The ancient mining districts of the Sierra de Cartagena, Sierra del Cabo de Gata and Sierra de Almagrera exploited ore bodies formed by hydrothermal processes related to Tertiary volcanism. Mineralisation in the Sierra de Cartagena and Sierra de Almagrera is hosted by polymetallic Pb-Zn-Fe-Ag-(Ba-Cu-Sn-Sb) veins and mantos (Arribas & Tosdal, 1994; Graeser & Friedrich, 1970; Oen et al., 1975). Galena as well as sulphosalt minerals of the Sierra de Cartagena ore bodies contain significant amounts of Ag. Both the Sierra de Cartagena and Sierra de Almagrera districts were particularly long-lived and were mined until the 2nd and early 4th century CE, respectively (Meier, 1995). In the Sierra del Cabo de Gata district, two different vein types have been described, low-sulphidation Pb-Zn-(Ag-Cu-Au) and high-sulphidation Au-(Cu-Te-Sn) epithermal veins (Arribas & Tosdal, 1994).

Silver and copper mining in the Iberian Pyrite Belt

Although having been mined already since primeval times, the Iberian Pyrite Belt (IPB) still hosts ore reserves exceeding 1,500 Mt abundant in eight supergiant and numerous smaller deposits

including the largest individual massive sulphide ore bodies to be known. Currently, exploitation is based on base metal sulphides (i.e. Pb-Zn-Cu), Ag-Au in gossan zones, pyrite and locally on Cu and Sn (Sáez et al., 1999). The IPB is part of the Hercynian belt and was formed due to Late Devonian to Early Carboniferous extensional tectonics, which caused crustal thinning and rise of isotherms. These processes resulted in the ascent and emplacement of basic magmas, which activated and substantiated a hydrothermal system responsible for the precipitation of massive sulphide bodies between the Late Famennian and Early Visean (Sáez et al., 1999; Tornos, 2006; Yesares et al., 2015; and references therein).
The primary sulphide ore of the IPB deposits mostly consists of massive pyrite with polymetallic sulphides (mainly chalcopyrite, sphalerite and galena; Marcoux, 1998). Ancient mining focused on the weathered part of the ore bodies where Ag, Au and Cu are enriched (Leistel et al., 1998), but which also was technologically accessible to the old workers. Important phases for the ancient metallurgists formed by weathering processes are supergene Cu phases, Ag-bearing jarosite minerals (cf. chapter 2.1) as well as native Ag and Au. Precious metals often were the focus of the old workings. According to Rothenberg & Blanco-Freijeiro (1981), the Romans in Rio Tinto exploited secondary chalcocite from the supergene level of the sulphide orebody to extract both Ag and Cu. The ore often had to be smelted with externally added Pb to collect the precious metals ('leaded smelting'). Roman activities in the Rio Tinto region of the IPB have been dated from the 1^{st} century BCE to the 5^{th} century CE (Salkield, 1987). However, similarly to other mining districts of the Iberian Peninsula, revenues are expected to have been declining from the 1^{st} / 2^{nd} century CE on.

5.2.2. Italy

The Pb-Ag deposits of Italy are concentrated in Tuscany and Sardinia, no occurrences are known from the central and southern parts of the country.

Tuscany

Numerous Pb-Ag mineralisations are abundant in the districts of Massa Marittima, Campiglia Marittima and Bocchegiano in the Colline Metallifere, a portion of the Apennine Mountains formed during the Alpine orogeny. Tuscany was the centre of Etruscan metallurgy with the beginnings of local metal production dating back until the Bronze Age (Chiarantini et al., 2009; and references therein). In Roman republican and imperial times mining is generally thought to have been ceased (Nriagu, 1983). While Pliny (*Natural History*, 33.21) states that a senate's edict prohibited mining activities in the Italian mainland, according to Strabo (*Geography*, 5.1.12) the deposits simply were not as profitable as the districts of the Iberian Peninsula and of the Transalpine Celti. However, local Cu and Pb-Ag mining and production resigned in the 10^{th} and 11^{th} century CE (e.g. Manasse & Mellini, 2002a).

Sardinia

Sardinia possesses exceptionally rich ore resources with numerous Pb and Ag deposits spread throughout the eastern, northwestern and, most importantly, southwestern part (Iglesiente-Sulcis

district) of the island. The Cambrian mineralisations in the southwest are stratiform and / or stratabound, carbonate-hosted and are either classified as SEDEX type or MVT (De Vivo et al., 1998; and references therein). The occurrence of Hercynian veins in contrast is not restricted to a certain part of the island. They generally are marked by elevated Ba and F contents and are genetically associated with the emplacement of the calc-alkaline Corsican-Sardinian Batholith. Stratabound polymetallic sulphide lenses of the Correboi type possess a complex mineralogy with pronounced Cu and Ag as well as local Au contents and highly varying Pb isotope systematics (Boni & Koeppel, 1985; Valera & Valera, 2005; Valera et al., 2005). While galena of Cambrian deposits generally is rather Ag-poor (approximately 300 ppm), in polymetallic deposits it may contain up to 8000 ppm of the precious metal due to sulphosalt inclusions (Boni & Koeppel, 1985).
Exploitation of the local ore resources could be traced back until the Bronze Age (Valera et al., 2005) with the oldest lead ingots dating from the 12^{th} to the 8^{th} century BCE (Rothenhoefer & Hanel, 2013). While the Sardinian ore deposits are not mentioned by Greek and early Roman writings, the mines seem to have experienced a renaissance particularly in the beginning of the 2^{nd} century CE and were an important lead producer in the 4^{th} century CE (Boulakia, 1972) - a fact which certainly also is caused by the vicinity of Sardinia to the mainland in the troubled times of the late Empire. Traces of Roman mining can be found throughout the island and are reported from the east at Monte Narba and Baccu Arrodas and, further north, at Lula and Orosei (Davies, 1935). However, the deposits in the southwest clearly must have been most relevant for Roman mining and metal production. Hirt (2010) refers to the Iglesiente-Sulcis district as 'the heartland of Roman mining on Sardinia'.

5.3. Central Europe

5.3.1. Britain

Shortly after the first parts of Britain were conquered by the Romans under Claudius in 43 CE, Pb production from ores of the Mendips, a range of hills located in the southwest is proven by ingots dated to 49 CE (Tylecote, 1964). Other important mining districts were Flintshire and Shropshire in northern Wales and the western part of the British Isle, respectively, as well as Yorkshire and Derbyshire in the Pennines (Gardiner, 2001; Tylecote, 1964). The deposits mostly are classified as MVT and vein-style mineralisations, which were mainly formed during Late Carboniferous to Triassic times (Bau et al., 2003; Bouch et al., 2006; Ixer & Vaughan, 1982; Moorbath, 1962; Stanton, 1991).
The Pb ores must have been so plentiful and easily accessible due to the shallow position of the mineralisations that mining temporarily was restricted by law, as Pliny reports (*Natural History* 34, 49). The Ag content of the ores, however, is notoriously low and in several districts (Derbyshire, Yorkshire and Shropshire) might not have been worth desilveration (Tylecote, 1964). Findings of lead artefacts imply a production hiatus between 170 and 280 CE, which may indicate exhaustion of the advantageously located ore bodies. However, coins and inscriptions document continuity of mining activities until the end of the 3^{rd} century CE (Nriagu, 1983).

5.3.2. France

Pb-Ag mineralisations are widespread throughout France and mainly occur in the Massif Central, Pyrenees, Alps and Vosges. Most deposits (e.g. Mont Lozère, Mont Faulat) are located in the Massif Central and the Cévennes (i.e. the southeastern part of the Massif Central), and were intensively mined in medieval time (Baron et al., 2006). Traces of former antique activities thus often are extinguished or difficult to prove. However, Trincherini et al. (2001) identify the deposits of Le Bleymard, Vialas, La Rabasse and Mont Faulat – some of its workings have been dated to the 1st centuries BCE and CE, respectively - in the Cévennes as Roman districts with supraregional importance. The deposits of the Massif Central can be assigned to two different metallogenetic epochs (Brevart et al., 1982): Contemporaneous formation with Cambrian carbonate host rocks or relation to circulating hydrothermal fluids linked to often granitoid magmatic activity during the Hercynian orogeny, respectively. The remobilisation of earlier formed mineralisations in some cases may have also influenced the Pb isotope signature of the ore bodies. Common mineralisation styles of the Massif Central include MVT deposits and hydrothermal veins (e.g. Baron et al., 2006; Charef & Sheppard, 1988; Le Guen et al., 1992).

5.3.3. Germany

The most important Pb deposits in Germany are situated in the Rheinisches Schiefergebirge, i.e. in the northwestern Eifel, Sauerland, Bergisches Land and the Lahn area. Smaller occurrences are present in the Kraichgau and Schwarzwald. Roman mining activities in Germany mostly have been assigned to the 1st to 3rd century CE (Meier, 1995).

Rheinisches Schiefergebirge

Traces of Roman mining in the Eifel have been found in the Mechernich Trias depression (most distinctively at the Mechernicher Bleiberg and Kommerner Tanzberg) and in the Stolberg-Aachen district (Bode, 2008; Nriagu, 1983). The Eifel Pb ore district generally is of post-Variscan formation age. At Maubach-Mechernich, the mineralisation is present in the form of Triassic sandstone hosted Ag-poor galena impregnations (2 - 3 ppm on average; Gottschalk & Baumann, 2001; Krahn & Baumann, 1996; Large et al., 1983) while at Aachen-Stolberg the ore occurs as epigenetic carbonate-hosted Pb-Zn veins and stockwork (Krahn & Baumann, 1996; Large et al., 1983). Medieval mining of oxidised Ag-poor Pb-Zn ore (i.e. particularly cerussite and smithsonite) at the Briloner Hochfläche (Sauerland) is proven, Roman activities assigned to the 1st century CE are suspected (Bode, 2008; and references therein). In the district of Bensberg-Engelskirchen (Bergisches Land), archaeological investigations revealed pronounced traces of Roman mining dated from the 1st to 2nd century CE at the Lüderich hill near Rösrath. The vein ore is particularly Zn-rich and is marked by elevated Ag contents (350 g/t on average, up to 700 g/t; Körlin & Gechter, 2003; and references therein). Particularly traces of Roman smelting and less evidence for mining are reported from the Lahn area near Bad Ems. High average Pb contents of 35 wt % in the smelting slags according to Bode (2008; and references therein) indicate that the local metal extraction focused on Ag.

Southern Germany

Roman mining of the Wiesloch-Nußloch (Kraichgau) Miocene MVT Pb-Zn deposit has been dated by coins from the 1st to the mid-2nd century CE (Ströbele et al., 2010; Ströbele et al., 2014). Provenance analysis of Roman lead objects found in the vicinity suggests that they were exclusively produced from local resources (Ströbele et al., 2014). In the Schwarzwald, Permian Pb-Zn-Ag veins supposedly already were exploited by the Romans (Goldenberg, 1996 and references therein; Ströbele et al., 2012).
Bode et al. (2009) argue that due to the declining yields of the Spanish mines and the fact that Britain, one of the most relevant imperial Pb sources, has not yet been conquered the German mining districts at least in the early 1st century CE were of supraregional importance. Indeed, ingots recovered from the Rena Maiore shipwreck nearby Sardinia with a 'Germanic' stamp can be related to Eifel and Sauerland ores based on their Pb isotope signature (Bode, 2008; Bode et al., 2009). The local relevance of the German ores has been confirmed by several Pb isotope provenance studies (Bode, 2008; Bode et al., 2009; Durali-Müller, 2005; Durali-Mueller et al., 2007; Gottschalk & Baumann, 2001; Ströbele et al., 2014).

5.4. Résumé: Chronology of relevant mining districts

The relevance of the individual mining regions primarily due to exhaustion of easily accessible ore bodies and territorial changes naturally varied during the centuries. While the Iberian Peninsula surely was the main source of Pb and Ag in the early Empire, it was gradually replaced by particularly Britain with its easily reachable ore bodies in the 1st century CE due to declining metal yields. The districts of France and Germany, at least until Britain was conquered, presumably also contributed to the Empire's metal supply on a supraregional scale. The Greek ore mines in contrast assumably only produced metals on a regional scale, while the occurrences of the Italian mainland in Tuscany have not been exploited in imperial, but only in pre-Roman and medieval times.
However, when the Balkan Peninsula was conquered in the 1st century CE, its extensive Pb-Zn-Ag mineralisations (particularly in modern-day Bulgaria, Kosovo, Macedonia and Serbia) became increasingly important for the Empire's metal supply from the 2nd century CE on. The growing relevance of these resources certainly also is based on the notoriously low Ag contents of the British deposits. The remarkable dimensions of the Roman mining and smelting remains in the region (see above) are consistent with the contemporary appraisal of Moesia as the mining province of the Empire. In the early 2nd century, also the mineral wealth of the Sardinian mines experienced a renaissance, for which the small distance to the Roman mainland surely also was an important factor in the increasingly troubled times. For the era of the later Empire, the Balkan Peninsula and Sardinia hence are assumed to have been (among) the most important Pb and Ag suppliers. While Sardinia's mining archaeological and archaeometallurgical past has been thoroughly investigated, this project aims to contribute to the rather scarce previous research of the Kosovo region.

6. Results of mining archaeological and archaeometallurgical investigations

The results of the mining archaeological and archaeometallurgical surveys and excavations are shortly summarised in the following chapter. Detailed information on this part of the project can be found in Gassmann et al. (2011), Gassmann et al. (2015) and Körlin & Gassmann (2016).

6.1. The mining district of Shashkoc-Janjevo

The mining district of Shashkoc-Janjevo is located approximately 5 to 7 km east of Ulpiana and covers an area of circa 12 km². Remains of ancient workings are, despite the extent of modern mining, still clearly visible and omnipresent. Most common are mining depressions generated by the collapse of shafts besides still preserved shafts and galleries. Several hundred collapsed shafts have been exactly located by a GPS handheld device during the systematic surveys of the last years. They either occur in rows and thus suggest targeted exploitation of mineralised veins or are, more rarely, inordinately distributed in mining fields, then probably aiming for ore impregnations in the country rock. Ceramic sherds allow to date the workings in the mining district from Roman / late antique to medieval / early modern. Stone hammers discovered at the 'Mondlandschaft' (one of the mining centres in the district) opposite to Veletin, however, indicate beginning of local mining already since at least the late Bronze Age. The workings initially presumably tracked down outcropping typically brightly-coloured secondary oxidised minerals in the gossan zone at the uppermost weathered parts of the ore bodies until later reaching the primary sulphide mineralisation.
Mining tools have been rarely found suggesting that the workers used ironclad instruments which they brought along to the sites. Small lumps of gangue material (mostly less than the size of a fist) on the waste heaps indicate that the ore was roughly crushed and sorted in the immediate vicinity of the mines, as proven by frequently found anvil stones which were manufactured from locally present igneous rocks (i.e. andesite and dacite). Large-scaled terraces in the vicinity of the old workings presumably served as central beneficiation places (i.e particularly to crush the raw material), at which the ore of several nearby workings was processed. Slightly to the west of Veletin and nearby a small creek, several troughs with and without inlets are directly carved into the outcropping andesite. They can be interpreted to have been used for wet-mechanical beneficiation. Andesite also was utilised for the manufacturing of mill stones, as hundreds of negatives impressively document. The diameters of the mill stones apparently ranged between 45 and 60 cm and hence agree with the typical proportions of Roman ore mills (cf. section 2.2). A mill stone fragment discovered nearby the metallurgical workshop of Ulpiana (cf. section 4.1.2) possesses a similar size and hence suggests an association with metal production.

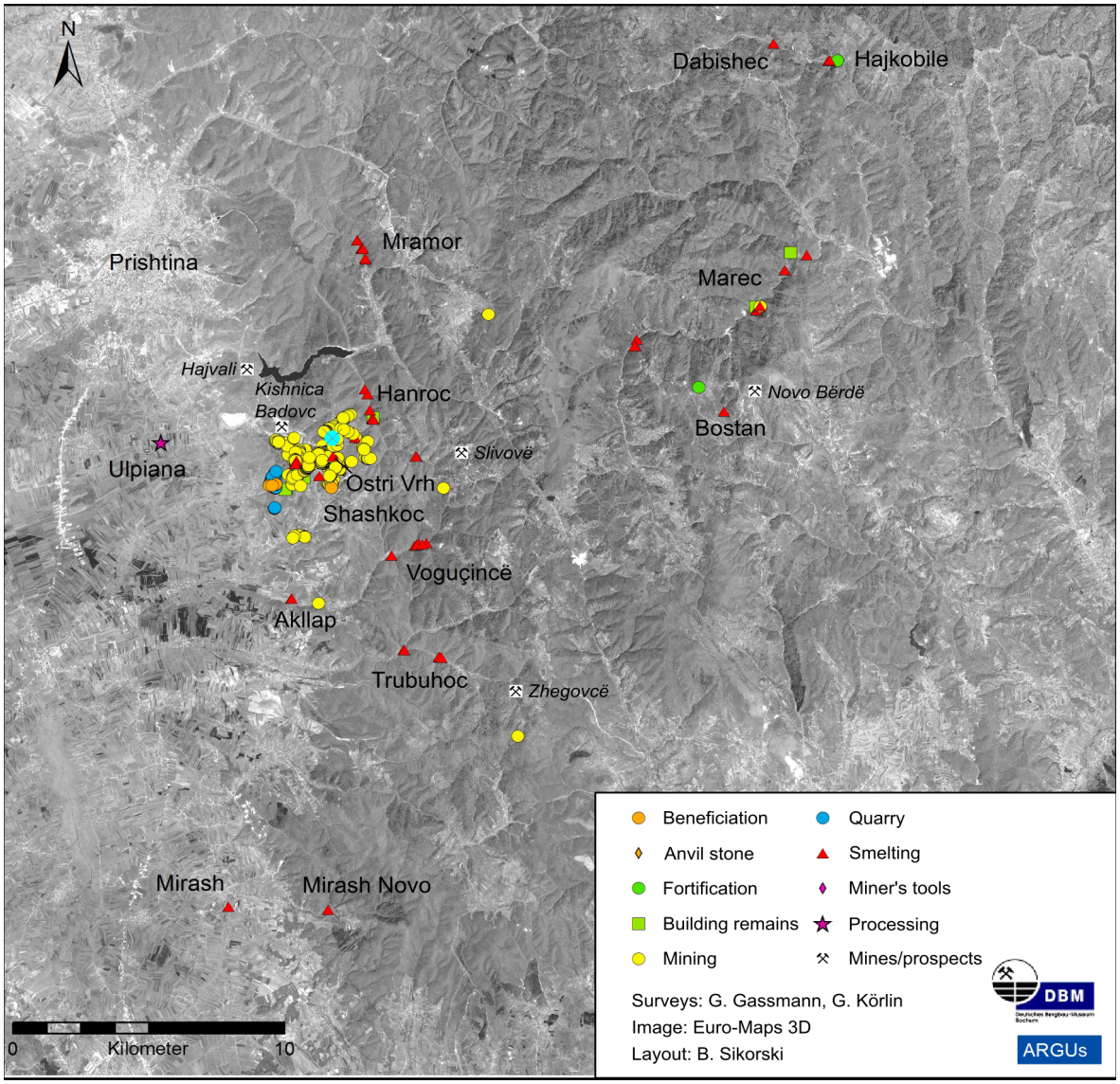

Figure 6.1.: Map of the study area showing the mining district of Shashkoc-Janjevo, the investigated smelting sites as well as modern mines and prospects. Map: Deutsches Bergbau-Museum; surveys: G. Gassmann, G. Körlin; layout: B. Sikorski.

6.2. Metallurgical sites in the vicinity of Ulpiana

Ten metallurgical sites (Fig. 6.1) situated within a radius of approximately 20 km from Ulpiana have been sampled and investigated in detail. Workshops with a preliminary Roman / late antique as well as medieval / early modern dating have been selected for analytical examination to retrace organisational and technological changes and developments. The sites often have been affected by modern activities, which led to general disturbance as well as the removal of significant quantities of the originally present waste heaps for re-smelting. Notable organisational differences characterise the presumably Roman / late antique and medieval / early modern sites investigated so far. While supposedly earlier workshops are large-scaled and remotely located, i.e. in wide stream valleys distant to mining sites and settlements, their later analogues commonly possess significantly smaller dimensions and often were discovered nearby building remains, partially even in the midst of villages. Another possible chronological difference concerns the array of metallurgical material, which generally appears to be more versatile, but nevertheless consistent at all examined presumably Roman / late antique sites (cf. sections 9, 10 & 11). The appearance of smelting wastes from supposedly medieval / early modern complexes in contrast seems rather monotonous. In contrast to presumably Roman/late antique sites, the metallurgical by-products matte and speiss have been rarely found. However, the location nearby rivulets, which presumably provided clayey sediments for furnace construction as well as sand acting as a silica source for the smelting operations, but possibly also water power to be utilised by the old metallurgists, is a commonality shared by all investigated workshops.

Voguçincë / Vogačića

The site nearby the hamlet of Voguçincë, where several slag heaps stretch throughout a valley along a small rivulet is one of the most large-scaled discovered so far. The amount of waste material generated by the metallurgical operations though is virtually impossible to estimate since the heaps have been partially overbuilt by modern houses and removed for re-smelting. Besides these large quantities of slag, a small piece of matte and several pieces of slagged furnace lining have been found. The furnace debris partially is covered by bright green and blue encrustations which are interpreted as precipitates from Cu-rich smoke released during the metallurgical operations. A coin with the portrait of Emperor Probus (reigning from 276 to 282 CE) discovered at the eastern end of the site allows a precise preliminary dating. Further investigations, i.e. excavations, sondages and geophysical measurements are envisaged for the future.

Mirash / Miraš

Notable quantities of slag and slagged furnace debris found in a crop field indicate the presence of a smelting site nearby the settlement Mirash. Ceramic sherds yield a preliminary antique dating of the site.

Mirash Novo / Miraš Novo

Mirash Novo is a large-scaled production site with its smelting remains (slag, matte, speiss) extending several hundred meters along the banks of a small creek. Archaeological findings from

the site include slagged furnace lining and sherds of late antique ceramic.

Mramor Proni Butoçit / Mramor Proni Butočit

The extensive smelting complex at the banks of a small rivulet comprises several waste heaps with varying dimensions and types of material. However, the severe disturbance of the locality due to partial removal of the waste heaps for re-smelting largely impedes an exact discrimination. The southern end of the site (Mramor Samakove) is located at a knoll and around 20 m higher than the northern end (Mramor Proni Butoçit), from which it is only c. 400 m away. Findings at Mramor Proni Butoçit include basin slags, a fragment of a tuyere and pieces of furnace lining with adhering slag. The operations at Mramor Proni Butoçit could not have been dated yet. However, envisaged excavations in the next project phase are expected to yield appropriate material.

Mramor Samakove

The smelting wastes sampled at Mramor Samakove so far comprise furnace slags and pig iron and thus already are macroscopically highly different from those collected at Mramor Proni Butoçit. The presence of a furnace complex has been already assumed during the surveys due to the unusual high quantities of slagged furnace material and has been further strengthened by an excavation. It revealed the presence of a channel running several meters downhill, which is filled with predominantly basin slags besides restitic galena ore and a small piece of crude lead. The channel is interpreted to have been used to dispose discharged slag liquid and consequently should be directly connected with a furnace complex located somewhat higher. The discovery of Ottoman ceramic indicates a rather young dating of this site.

Marec / Marevce

Several slag heaps are piled up nearby the Novobërdë Pb-Zn-Ag ore deposit along the rivulet Kriva, whose despite modern re-smelting for Zn recovery (according to an employee of the mine) large volumes testify to extensive metal production. Abundant galleries and shafts in the immediate vicinity may have provided the furnace feed for these operations. Remains of a cupel (cf. chapter 13) document extraction of precious metal. A variety of archaeological findings - including several fragments of slagged furnace lining - has been discovered at or nearby the smelting sites. Ceramic discovered so far points to a medieval / early modern dating of the operations. However, during the last survey (March 2016) a further smelting site situated between the already known workshops has been discovered and preliminary assigned to a late antique dating. Due to its late finding, samples from this locality could not have been examined yet, but are planned to be investigated in the next project phase.

Hajkobile / Ajkobilia

The site near the settlement of Hajkobile is situated in the very east of Kosovo, only about 2 km south of the Serbian border and thus is rather unlikely to have obtained its smelter feed from the mining district of Shashkoc-Janjevo. Widespread occurrence of greenish patinas on the slag

surfaces and the finding of a small lump of matte indicate treatment of a comparably Cu-rich ore. The waste heaps also comprised several sherds of furnace lining and coarse pieces of quartz, which might have been used as furnace construction material or as a fluxing agent for metallurgical processing. A supposedly medieval / early modern ceramic sherd allows a preliminary estimation of the site's production period.

Hanroc / Androvac

The valley of the rivulet Androvacka includes several small-scaled smelting sites (situated around 4 km northeast of Shashkoc), which appear to have been preserved in their original state. Indeed, at one of the sites the remains of a complete village with several houses, a sacral building and the smelting site with metallurgical installations (indicated by a notable quantity of furnace debris) in the immediate vicinity have been verified. The operations are documented by the findings of slag, a lump of native Pb and negative crop marks at an adjacent field. Several ceramic sherds clearly argue for a preliminary medieval / early modern dating.

Akllap / Oklap

Amid the hamlet of Akllap smelting slags have been found along a small rivulet. A slight unevenness of the terrain possibly marks the position of the main waste heap, whose volume renders it a rather small-scaled site. The fact that no archaeological findings have been discovered so far is coherent with the profound disturbance of the site due to modern building activities.

Ostri Vrh

The smelting site is situated about halfway between Shashkoc and Janjevo in the heart of the ancient mining district at a plateau of the mountain Ostri Vrh close to the Kishnica mine and overlooks an only seasonally water-bearing rivulet. Two small-scaled accumulations of smelting slag document the metallurgical operations, whose ore feed might have been won from collapsed shafts in the immediate vicinity. The good accessibility of the site via a nearby dirt road along with its central position offer an explanation for the small quantities of slag, which likely have been diminished by re-smelting in modern time. Archaeological findings are scarce and solely comprise furnace lining debris and several sherds of medieval / early modern ceramic, which allow a preliminary dating of the operations.

Ancient smelting at Janjevo?

Amid the modern settlement of Janjevo, several pieces of basin as well as furnace slags have been located in e.g. building pits or in the vicinity of old workings at the border of the village. Since the lack of assured archaeological context renders these findings difficult to interpretate, they have not been further investigated. Prospection of slags and metallurgical by-products in the small rivulet traversing the village has been abandoned due to the severe water pollution. However, the hand samples retrieved so far optically generally are similar to specimens from Voguçincë, Mirash and Mirash Novo (presumably Roman / late antique dating). The proximity to the mining district certainly renders Janjevo – similarly to Ostri Vrh and Hanroc – a particularly on a logistic

perspective advantageously located site for smelting activities, whose dimensions and working periods are due to the finding situation virtually impossible to estimate.

Part II.

The *chaîne opératoire*: Typology, petrography and geochemistry of ores, metallurgical (by-) products and metal artefacts

7. Analytical techniques

7.1. Sampling strategy and sample preparation

Samples of ore and smelting remains have been taken during the surveys of the last years. In order to gain material comparable to that extracted by the ancient miners, restitic ores displaying a strong archaeometallurgical context have been sampled, i.e. taken in the immediate vicinity of (collapsed) shafts, galleries and beneficiation as well as smelting sites. The samples also have been selected with regard to geographic considerations to adequately cover the whole extent of the investigated ancient mining district (cf. appendix, chapter ii). The complete inventory of metallurgical workshops (remains of ores, furnace / basin slags, matte, speiss, crude metal, cupels, technical ceramic and furnace lining) has been tried to fully cover. The exact location of all samples taken during the field campaigns has been recorded with a handheld GPS device. A potential disadvantage of the ore sampling strategy is that the collected specimens might not necessarily correspond to the ore eventually smelted, but rather represent waste material, which has been discarded due to its poor grade of the desired metal(s). However, the nature of the ore treated is mirrored by the chemistry of the (by-) products (i.e. matte, speiss, cupellation remains, crude metal) of the metallurgical operations. Unlike ores from modern mines and prospects or specimens from museum's collections, the material sampled on-site is more likely to match the original smelter feed processed by the ancient metallurgists. Due to the systematic prospection of the mining district, mineralogical variations of the exploited ore bodies and consequently the metallurgically treated raw material could be satisfyingly comprehended.
Ore and smelting product samples were cut in two halves - a slice was taken from the middle of larger ones, respectively - to select appropriate material for further analysis. One part of it has been utilised for the manufacture of polished thick sections or, if the samples were very small, polished mounted sections. The sections have been used for electron microprobe analysis. The second part of the samples has been used for X-ray diffraction and isotope analysis. For these measurements, the samples have been further crushed and subsequently ground in a vibratory disc mill equipped with a tungsten carbide container. Some ores also have been sampled for isotope analysis with a customary power drill. Drilling chips of lead (children's sarcophagi, a 'weight', ornamentally decorated platelet) and copper-rich artefacts (coins) discovered on-site in Ulpiana and Voguçincë, respectively (cf. chapter 14), have been taken with a customary power drill. Due to their comparatively large size and to check whether the side and bottom parts have been produced from metal from different sources, the lead sarcophagi have been sampled threefold. A polished mounted section has been prepared from each sampled metal artefact and analysed by electron microprobe. Material from the drilling chips taken from the metal objects has been prepared for isotope analysis.

7.2. Optical microscopy

In order to decipher the phase assemblages, textures and crystallisation sequences of ores and metallurgical (by-) products, the sections have been examined under transmitted and reflected light using a Zeiss Axiophot microscope equipped with an AxioCam MRc camera. Photographs have been taken and edited with the AxioVision software supplied by Zeiss.

7.3. X-ray diffraction

X-ray powder diffraction (XRD) has been employed to identify the major phases of selected samples of smelting products. The sample holders were filled using the back-loading technique. The analyses have been carried out at the Institut für Geowissenschaften of the Goethe-Universität Frankfurt using a PANALYTICAL X'Pert Pro diffractometer equipped with a Cu anode and automatic divergence slit. The samples have been analysed at a measurement range from 3 to 70° 2ϑ at a step width of 1.2 ° 2ϑ/min. The diffractograms have been processed with the software X'Pert Pro and the PDF-2 database. The XRD data can be found in the appendix.

7.4. Electron microprobe analysis

The major and minor element chemistry of the phases has been determined in situ by electron microprobe (EMP) analysis using a JEOL Superprobe JXA 8900-RL at the Institut für Geowissenschaften of the Goethe-Universität Frankfurt. Two different measurement setups have been designed for silicates, oxides and glass as well as sulphides, alloys and metals, respectively (cf. Tab. 7.1 and 7.2). The abundances of Na_2O, MgO, Al_2O_3, SiO_2, P_2O_5, K_2O, CaO, TiO_2, Cr_2O_3, MnO, FeO, NiO, CuO, ZnO and PbO have been determined in silicates, oxides and glass by applying an acceleration voltage of 15 kV, beam current of 20 nA and focused beam (Tab. 7.1). Foides (i.e. leucite and kalsilite) and feldspar-group phases have been measured with a beam diameter of 5 µm and a beam current of 12 nA to avoid evaporation of alkali metals (cf. Siivola, 1969). Sulphides, alloys and metals have been analysed for their contents of Mn, Fe, Co, Ni, Cu, Zn, As, Ag, Cd, Sn, Sb, Pb and S with an acceleration voltage of 20 kV, beam current of 30 nA and focused beam (Tab. 7.2). The electron microprobe analyses are given in the appendix. A mapping of the relative Cu, Fe and S abundances of a bornite *ss* grain (80×80 px; sample 11027(1)) has been carried out at X and Y pixel sizes of 0.2. The dwell time was 50 msec.

7.5. Isotope analysis

Pb isotope ratios of ores from the mineralisations of Shashkoc-Janjevo, Novobërdë and Melenica and metallurgical (by-) products from smelting sites in the vicinity of Ulpiana have been analysed to substantiate potential connections and to estimate the sources of the processed furnace feed. The established isotope signature subsequently has been compared to that of sampled lead artefacts retrieved from the *municipium* to fully cover the local *chaîne opératoire* and to assess the importance of local mining and metal production for Ulpiana's economic foundation. Additionally, the provenance of two copper-rich imperial coins collected at Ulpiana and

Element	Line	Standard	Spectrometer	Crystal	Mode	Measurement position [mm]			Measurement time [sec]		
						Peak position	Background +	Background -	Peak	Background +	Background -
Si	Kα	$CaSiO_3$	1	TAP	DIFF	77.895	4	0	40	40	0
Al	Kα	Al_2O_3	1	TAP	DIFF	90.669	2	0	40	40	0
K	Kα	$KTiOPO_4$	2	PETJ	INT	119.872	1.7	1.7	30	15	15
Ca	Kα	$CaSiO_3$	2	PETJ	INT	107.586	2	2	30	15	15
P	Kα	$KTiOPO_4$	2	PETJ	INT	197.238	1.5	1.8	30	15	15
Na	Kα	$NaAlSi_3O_8$	3	TAP	DIFF	129.805	3	0	20	20	0
Mg	Kα	Mg_2SiO_4	3	TAP	DIFF	107.517	3	0	40	40	0
Cr	Kα	Cr_2O_3	4	PETJ	INT	73.068	2	2	40	20	20
Ti	Kα	$MnTiO_3$	4	PETJ	INT	87.906	2	2	40	20	20
Pb	Mα	PbS_PH	4	PETJ	DIFF	169.2	0	2.5	60	0	60
Mn	Kα	MnO	5	LIFH	DIFF	146.325	1.5	0	30	30	0
Fe	Kα	Fe_2SiO_4	5	LIFH	INT	134.837	3	3.8	30	15	15
Ni	Kα	NiO	5	LIFH	INT	115.683	1.5	1.5	30	15	15
Cu	Kα	S4_Cu	5	LIFH	INT	107.547	2	1.5	30	15	15
Zn	Kα	0_ZnO	5	LIFH	INT	100.244	3	1.5	30	15	15

Table 7.1.: EMP measurement setup SlAP for analysis of silicates, oxides and glass in metallurgical slags.

Element	Line	Standard	Spectrometer	Crystal	Mode	Measurement position [mm]			Measurement time [sec]		
						Peak position	Background +	Background -	Peak position	Background +	Background -
Sb	Lα	S4_Sb	2	PETJ	INT	110.1	3.6	0	60	60	0
Zn	Kα	0-ZnO	2	LIF	INT	99.873	1.5	1.5	40	20	20
Ag	Lα	S4_Ag_bgu	2	PETJ	INT	133	2.3	0	60	60	0
Fe	Kα	S4_FeS	2	LIF	INT	135	1.4	0	40	40	0
Cu	Kα	S4_Cu	2	LIF	INT	107.2	2	1.5	40	20	20
As	Lα	S4_As	3	TAP	DIFF	105.5	4	0	60	60	0
Sn	Lα	S4_Sn	4	PETJ	INT	115.2	1.52	1.5	30	15	15
Pb	Mα	PbS_PH	4	PETJ	DIFF	169.2	0	2.5	90	0	90
S	Kα	PbS_PH	4	PETJ	DIFF	172.1	1.7	0	60	60	0
Ni	Kα	S4_Ni	5	LIFH	INT	115.7	1.5	1.5	40	20	20
Co	Kα	S4_Co	5	LIFH	INT	124.8	3	4.5	40	20	20
Mn	Kα	S4_Mn	5	LIFH	DIFF	146.479	1.5	0	40	40	0

Table 7.2.: EMP measurement setup Cuprico 2 for analysis of sulphides, alloys and metals.

Voguçincë, respectively, has been tried to reconstruct. The ore Pb isotope data furthermore has been utilised to test a potential connection with Roman imperial lead (-bearing) objects, which are due to their inscriptions or finding locations suspected to might have been produced from local resources. Two datasets have been selected for this case study: a) shipwreck cargo from Israel, including a lead ingot stamped *MET DARD* (Raban, 1999), and b) Pb-glazed ceramic from modern-day Serbia and Romania (Walton & Tite, 2010). Cu isotope data of the sampled ores and metal artefacts has been utilised to delineate the formation history of the ore specimens and to tentatively retrace potential raw material types the objects have been manufactured from. Sample preparation for isotope analysis has been carried out at the clean laboratory of the Universität Frankfurt using ultrapure chemicals only. The samples (powdered or as drilling chips; see above) have been dissolved in 1 ml 6 M HCl and HNO_3, respectively, under heat for several hours and subsequently evaporated. No HF to break down the silicate phases in slag has been applied since the bulk Pb content of the material is expected to be mainly hosted within sulphides and native Pb. Therefore, the amount of Pb dissolved by HNO_3 and HCl certainly is sufficient for analysis. Furthermore, the isotope signature determined in the silicate matrix of slags is prone to alteration by 'foreign' Pb, whereas the metal prills should reflect the ratios of the ore charge (Baron et al., 2014).

The residue has been taken up with 0.6 M HBr and centrifugalised to remove insoluble phases. Cu and Pb have been separated in ion-exchange columns (using Dowex 1*8, 100-200 mesh as resin) by 0.6 M HBr and 6 M HCl, respectively. Both Cu and Pb solutions have been evaporated, taken up by 2 % HNO_3 and diluted to a concentration of around 500 ppb of the respective metal. The Cu and Pb isotope sample solutions have been spiked with 1 ppm Ni (NIST SRM 986) and 100 ppb Tl (NIST SRM 997) standards, respectively, to correct for mass fractionation. Measurements have been carried out with a MC-ICP-MS (Neptune^{TM}, Finnigan MAT; Goethe-Universität Frankfurt) at low resolution ($\Delta m/m = 400$). Pb and Cu have been analysed using 9 blocks of 9 integrations and 5 blocks of 9 integrations, respectively, of c. 8.4 sec each followed by 40 sec baseline measurement. Interferences of Hg (^{202}Hg) and Ni (^{60}Ni) on Pb and Cu isotopes, respectively, have been constantly checked during the measurements. Precision and accuracy of the measurements have been continuously monitored by repeatedly analysing the NIST SRM 976 and 981 standards (standard bracketing method). If necessary, the elemental ratios have been corrected for instrumental drift by comparing them to the standard ratios. Average analytical uncertainties (two times standard deviation; 2σ) of the performed Pb isotope analyses are 0.015 for $^{206}Pb/^{204}Pb$, 0.014 for $^{207}Pb/^{204}Pb$, 0.039 for $^{208}Pb/^{204}Pb$, 0.00022 for $^{207}Pb/^{206}Pb$ and 0.00078 for $^{208}Pb/^{206}Pb$ (corresponding to 0.08 RSD %, 0.09 RSD %, 0.10 RSD %, 0.03 RSD % and 0.04 RSD %, respectively), which are in good agreement with generally accepted values (cf. chapters 3.3.1 and 15.1). 2σ values for $\delta^{65}Cu$ data ranges between 0.121 and 0.536 with the exception of a Cu-poor ore sample (11043(3)) consisting almost exclusively of arsenopyrite and quartz, which exhibits a 2σ value of 2.850 (cf. chapter 15.2). The Cu isotope composition of the ore sample 14018 could not be determined due to its elevated bulk Ni content. Pb and Cu isotope data are given in the appendix. Further information on the analytical setup and in-house precision of Pb and Cu isotope measurements can be found in Durali-Müller (2005), Durali-Mueller et al. (2007), Klein et al. (2004), Klein et al. (2009), Klein et al. (2010) and

Müller et al. (2015).

8. Ore resources

The mineralisation in the study area is mostly present as veins hosted by serpentinite as well as Tertiary andesite and dacite, whose occurrence analogous to the other deposits of the Vardar Zone apparently is genetically related to the formation of hydrothermal ore bodies (cf. chapters 3 and 5.1; Fig. 8.1). Particularly within serpentinite rocks outcropping nearby Shashkoc, a pronounced gossan zone with typical reddish colour must have clearly indicated the underlying mineral wealth to the early miners. To the east and south of Shashkoc (i.e. towards Janjevo), igneous rocks predominate as hosts of the mineralisation and the waste heaps thus mostly are of lighter and greyish colour. Yellow encrustations of secondary jarosite group minerals (presumably beaverite [$Pb(Fe^{3+}Cu^{2+}Al)_3(SO_4)_2(OH)_6$]) are common.

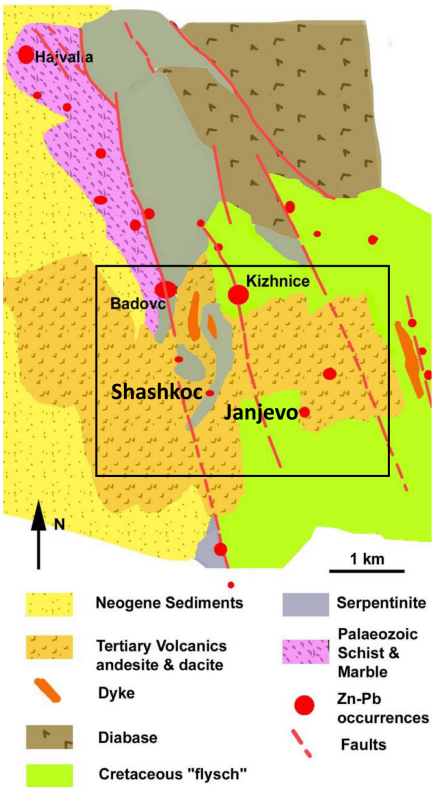

Figure 8.1.: Geological sketch map of the ore field Hajvali-Badovc-Kishnica (modified from Trepca Kosovo under UNMIK administration, 2005). The approximate location of the investigated ancient mining district of Shashkoc-Janjevo and the two settlements is indicated.

8.1. Petrography and paragenesis of ore mineralisation

Since the sampling strategy focused on gathering ore specimens displaying a context with historical mining, a thorough geoscientific characterisation of the local mineralisation is somewhat impaired. However, due to an observed potentially chronologically dependant correlation between ore geochemistry and the overall design of the metallurgical process scheme (see chapter 18.2), discrimination between varying ore types proved to be an important factor when interpreting smelting remains. Hence, a rough paragenetic overview of the ore mineralisation based on petrography and mineral chemistry is tentatively outlined. Generally, the sampled material mainly can be classified as primary

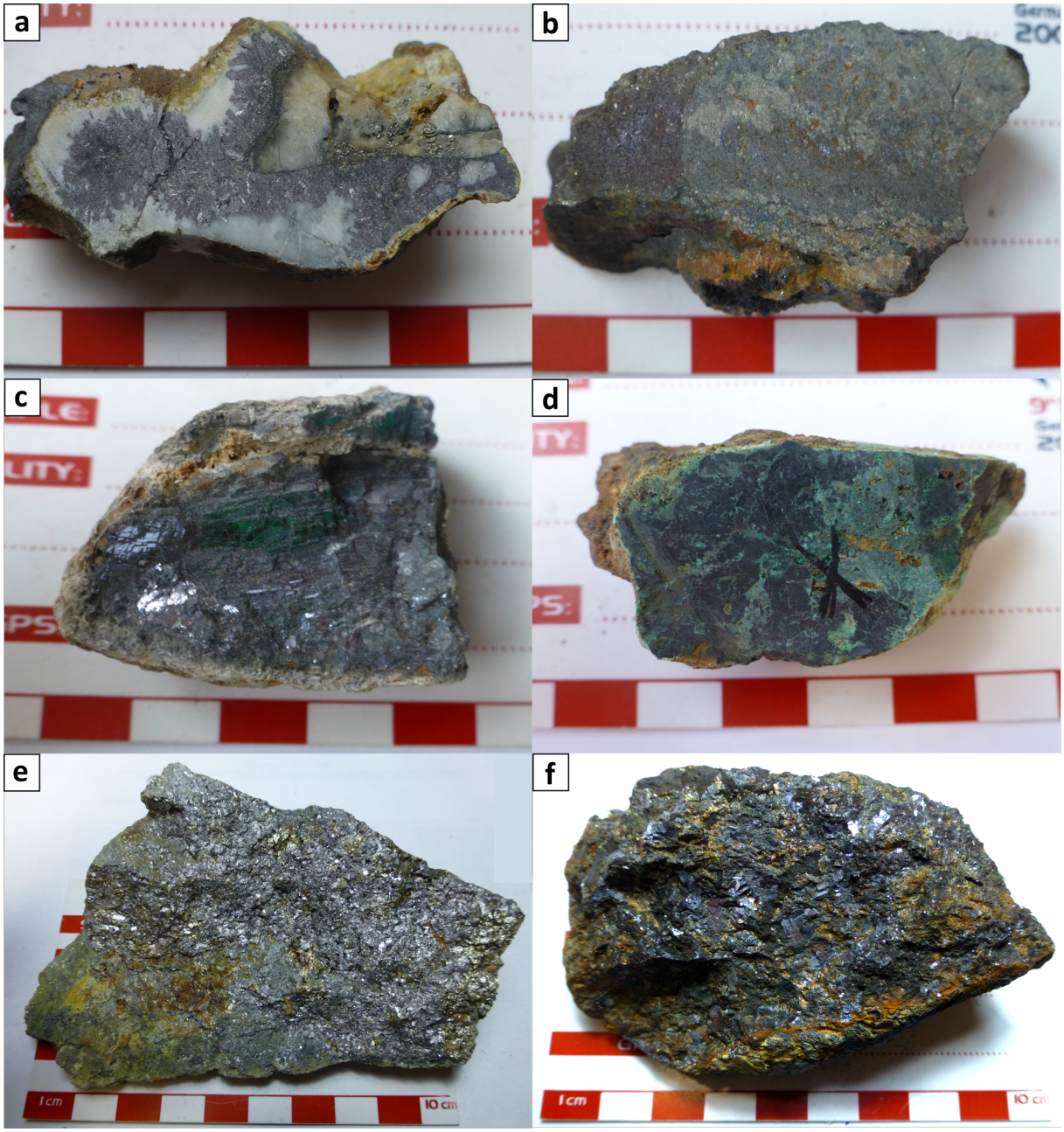

Figure 8.2.: Handsamples of ores. a) Early- to main-stage ore: A veinlet of arsenopyrite with minor pyrite and chalcopyrite is hosted by quartz [sample 11043(4), Shashkoc-Janjevo district]. b) Early- to main-stage ore: The rhythmically banded sulphide ore sample mainly consists of pyrite, sulphosalts and galena [sample 11015, Shashkoc-Janjevo district]. c) Main- to late-stage ore: The virtually monomineralic galena ore is covered by a thick whitish patina of oxidised Pb-bearing phases [sample 11090(4), Shashkoc-Janjevo district, 'Mondlandschaft']. d) Secondary Cu ore: Secondary supergene Cu sulphides (dark blue) partially are altered to oxidised Cu phases, particularly malachite. e) Massive sulphide ore [sample 13130(1), Novobërdë, modern mine]. f) Sulphide ore with a high proportion of galena, partially exhibiting typical cubic cleavage [sample 13105(1), Melenica].

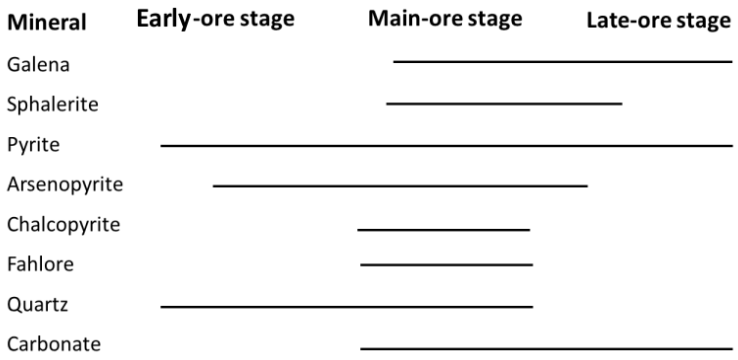

Figure 8.3.: Parageneses of main minerals associated with the early-, main- and late-ore stages of the primary sulphide mineralisation.

sulphide ore, which may be extensively weathered to oxidised Fe-, Pb- and Cu-bearing phases. Supergene enrichment processes locally led to the formation of secondary Cu sulphide ore.

8.1.1. Primary sulphide mineralisation

Optical (reflected light microscopy) and chemical (electron microprobe) analysis revealed a differentiation of the mineralisation (see appendix, chapter ii for further information on the respective ore samples). Roughly in the north and west of the study area (i.e. including the workings near Shashkoc), the samples mainly consist of galena, sphalerite and pyrite / marcasite and thus render it a rather 'pure' Pb-Zn-(Ag) ore. In the southern part (i.e. towards Janjevo) in contrast, the phase assemblage exhibits a more versatile, polymetallic character with an increased abundance of chalcopyrite and complex sulphosalts, e.g. tennantite-tetrahedrite minerals (i.e. fahlore) and boulangerite [$Pb_5Sb_4S_{11}$]. The in comparison to other deposits of the region elevated proportion of Cu-bearing phases potentially is related to interaction of hydrothermal ore-forming fluids with abundant serpentinite (cf. Nesbitt et al., 1988). Indeed, samples of distinctly Cu-rich (secondary) ore (i.e. 11043(3) and 13020(1)) have been collected from old workings near the contact zone between andesite / dacite – which analogous to other base metal occurrences of the Serbomacedonian-Rhodope belt is thought to be related to the development of the ore-forming hydrothermal system - and serpentinite. The observed zonation of the mineralisation apparently is caused by a temperature-dependance of the phase assemblages with three main ore precipitation stages (Fig. 8.2 and 8.3):

- Early-ore stage: pyrite and arsenopyrite with quartz gangue
- Main-ore stage: arsenopyrite, pyrite, galena, chalcopyrite, sphalerite and tennantite-tetrahedrite minerals with mixed quartz-carbonate gangue
- Late-ore stage: sphalerite, galena, pyrite / marcasite with carbonate gangue

The mineralogy of the precipitation stages generally is in agreement with the study of Hyseni & Alliu (1999), who reported pyrrhotite, chalcopyrite and arsenopyrite hosted by quartz to make up the early precipitated ore assemblage. The polymetallic second and third stages

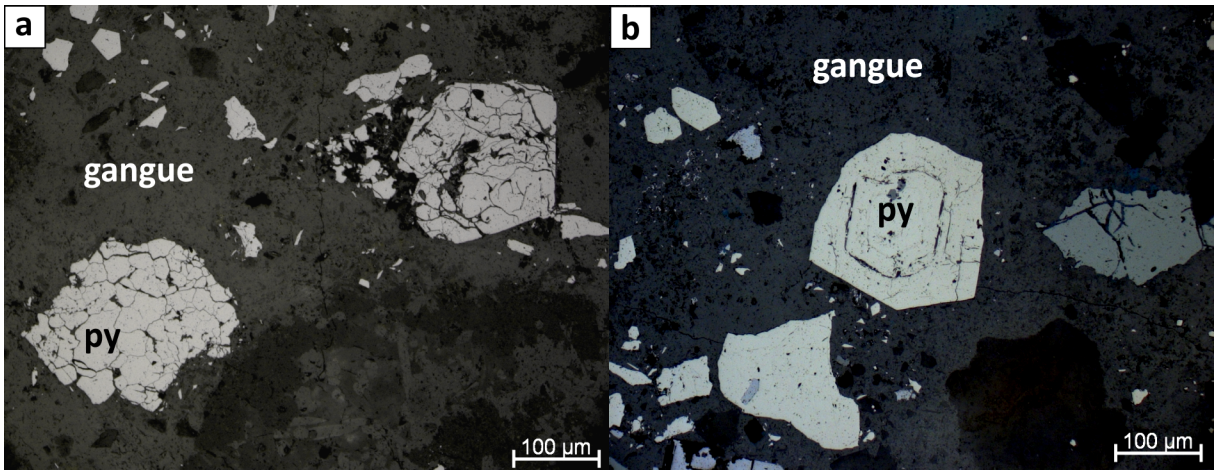

Figure 8.4.: a) Pseudomorphous late-stage pyrite grains replace an earlier phase [sample 12055(1), RL, PPL]. b) A pyrite grain shows multiple growth zoning [sample 12055(1), RL, PPL].

comprise sphalerite, galena, chalcopyrite, tetrahedrite and pyrite with quartz gangue and sphalerite, chalcopyrite, arsenopyrite, galenite, pyrite / marcasite, bornite, tetraedrite, boulangerite and rhodochrosite, respectively. The quartz gangue of the second ore stage reportedly is auriferous. The differences between the parageneses delineated in this study and the scheme depicted by Hyseni & Alliu (1999) can be explained by the comparably low number of ore specimens investigated, which furthermore have not been sampled in a geological, but mining archaeological context (chapter 7.1). The sampled ores rarely record only one deposition sequence. Indeed, overlapping with a dominant paragenesis[1] is far more common. The transition from one stage to another occurs gradually with formation of typical replacement textures such as growth zoning reflecting differing ore formation conditions, pseudomorphs and corroded boundaries of earlier formed minerals (Fig. 8.4[2]). Samples dominated by an early- or main-ore phase assemblage this far have been exclusively retrieved from areas with andesitic / dacitic host rock while specimens dominated by a later precipitated paragenesis have been predominantly collected from serpentinite zones within the district. This general temperature-dependant trend potentially is related to the proximal / distal location of the sampled ores to the andesite / dacite body, whose generation is thought to have established and sustained the hydrothermal ore-forming system. The igneous host rock as the hottest central part of the mineralised area thus likewise should contain ore parageneses indicative of formation at comparably higher temperatures. Generally, vein mineralisations related to igneous centres often are zoned with enrichment of Cu and Au proximal to igneous bodies and laterally or vertically increasing Pb-Zn-Ag grades (Plumlee et al., 1995).

Early-ore stage

The early-ore stage mainly comprises eu- to subhedral micro- to millimetre-sized pyrite and arsenopyrite associated with quartz gangue. Pyrite typically is of cubic cross-section while ar-

[1] The samples always could be attributed to a dominant ore precipitation stage.
[2] Abbreviations of minerals and phases, if possible, have been taken from Whitney & Evans (2010) and are given in the appendix, section i

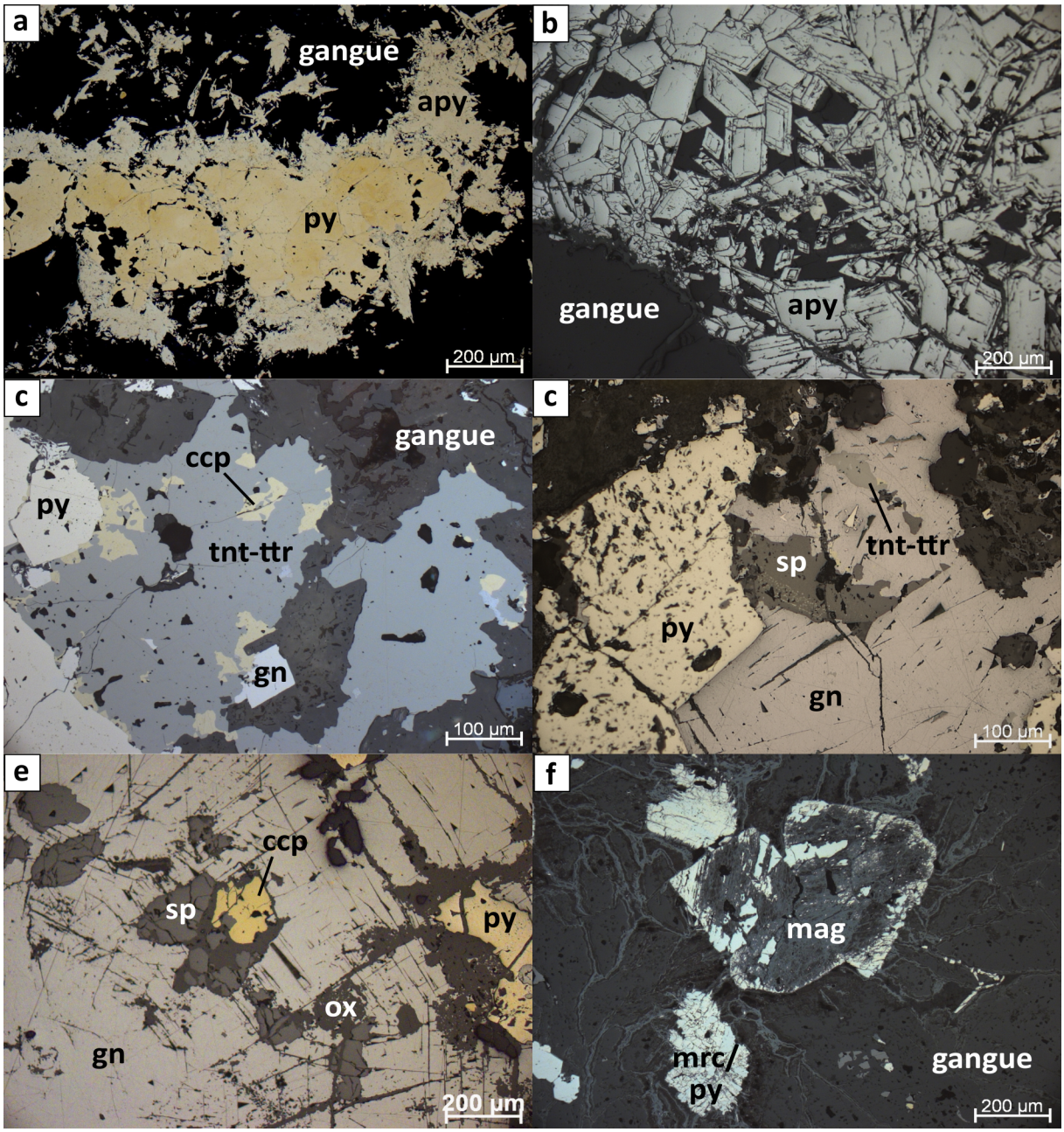

Figure 8.5.: Primary sulphide ore. a) Early-ore stage: Small-scaled arsenopyrite grains (often euhedrally lozenge-shaped) surround pyrite aggregates. The gangue consists of carbonate and quartz [sample 13099(4), RL, PPL]. b) Early-ore stage: Euhedral lozenge- and columnar-shaped arsenopyrite grains are embedded in quartz gangue [sample 11043(3), RL, PPL]. c) Main-ore stage: Grains of fahlore host chalcopyrite and pyrite, euhedral galena precipitated somewhat later. The gangue is dominated by quartz accompanied by minor carbonate [sample 13098(1), RL, PPL]. d) Main-ore stage: Anhedral sphalerite contains crystallographically orientated blebs of chalcopyrite (chalcopyrite disease) and is enclosed in galena, which also hosts fahlore and is intergrown with pyrite [sample 11015, RL, PPL]. e) Late-ore stage: The sample almost exclusively consists of galena, which contains inclusions of sphalerite, chalcopyrite and pyrite [sample 11090(6), RL, PPL]. f) Late-ore stage: Marcasite (cream with rose tint) replaces earlier pyrite (cream) whose former euhedral grain shape partially still is preserved. Magnetite is present as network within the sulphide phases. The siderite-rich carbonate gangue is slightly darker grey than magnetite [sample 14018, RL, PPL].

senopyrite occurs as two different forms, which were regularly observed within single samples (Fig. 8.5a, b): It either is present as discrete rhombs often exhibiting skeletal growth or forms typically radial, large-sized aggregates (diameters approaching several hundred micrometres) consisting of countless, mostly lozenge-shaped rather small grains (several ten micrometres long). While the individual arsenopyrite grains apparently were deposited somewhat later than pyrite, the close association of pyrite and arsenopyrite aggregates suggests contemporaneous crystallisation. Quartz grains often contain fluid inclusions or comprise early pyrite and arsenopyrite and typically possess an eu- to subhedral prismatic or columnar shape recording - as well as pyrite and arsenopyrite - open-space growth. Samples dominated by an early-ore paragenesis (i.e. 11015, 11043(3), 11043(4) and 13099(4)) mainly have been found within igneous host rocks in the southern part of the district (cf. appendix, chapter ii).

Main-ore stage

The phase assemblage of the main-ore stage is more versatile (i.e. galena, sphalerite, chalcopyrite, pyrite, arsenopyrite and sulphosalts) compared to the earlier precipitated mineralisation and is embedded in gangue dominated by quartz or carbonate (Fig. 8.3). The gradually more anhedral grain shapes reflect the decreasing amount of space. The first phase to crystallise in the main-ore stage typically is chalcopyrite,which partially replaces earlier arsenopyrite. The Fe-As sulphide also in the main-ore stage often is present as euhedral lozenge-shaped grains, which sometimes reach diameters of several hundred micrometres. Fahlore (Fig. 8.5c, d) as well precipitates in the beginning of the main-ore phase and may be intimately intergrown with other sulphosalts (e.g. bournonite, boulangerite). Sphalerite typically is closely associated with chalcopyrite and may also be affected by chalcopyrite disease, which manifests as inclusions of (crystallographically orientated) blebs of the Cu-Fe sulphide (Fig. 8.5d). Pyrite often forms coarse, large-scaled aggregates (with a diameter of some hundred micrometres to a few millimetres) consisting of several sub- to anhedral grains, but is also present as individual, often particularly large-sized grains, which typically contain several inclusions. Galena usually appears somewhat later in the main-ore stage after the early phases crystallised. Large grains or aggregates similar to these formed by pyrite may contain several inclusions of previously precipitated arsenopyrite, chalcopyrite, sphalerite and sulphosalts (Fig. 8.5d). Ore samples in which the paragenesis of the main-ore stage is dominant (i.e. 13098(1), 13099(2), 13099(5); secondary ores 11043(2) and 13020(1) contain restitic main-stage sulphides) have been, analogous to the early-ore stage phase assemblage (see above), particularly retrieved from ancient workings within igneous rocks in the southern part of the mining district (cf. appendix, chapter ii).

Late-ore stage

The late-ore stage comprises galena, sphalerite and pyrite or its low-temperature equivalent marcasite. The gangue is made up of carbonate, whose dark colour points to an Fe- and Mn-rich composition (i.e. siderite and rhodochrosite, respectively; Fig. 8.3). Galena often is particularly coarse-grained and partially reaches millimetre- to centimetre-sized diameters. Large grains typically contain several inclusions (Fig. 8.5e). Late-formed sphalerite may be rather coarse-grained (partially possessing diameters of several millimetres) and is characterised by a dull

dark grey colour. Pyrite is present as aggregates and individual, often comparatively large grains. It is partially replaced by its low-temperature analogue marcasite (samples 11090(6) and 14018), which often exhibits typical lamellar twinning and forms coarse aggregates. In one sample (14018), magnetite is exsolved as networks within intergrowths of pyrite and marcasite (Fig. 8.5f). Pyrrhotite has only been observed as few anhedral, possibly restitic grains occurring in the same specimen (14018). Ore samples in which the late-stage phase assemblage is the dominant paragenesis (11079, 11090(6), 12025, 12055(1) and 14018) have been mostly found in the northern and western part of the mining district, particularly within serpentinite outcropping nearby Shashkoc (cf. appendix, chapter ii).

8.1.2. Supergene Cu ore

Partially massive pieces of secondary supergene Cu ore have been sampled from old workings at outcrops of particularly Cu-rich ore bodies (samples 11043(2), 13020(1); see appendix, chapter ii). Their phase assemblage fully reflects the formation process from the protore to enriched sulphides and eventually oxidised minerals (e.g. carbonates, oxides, silicates). Secondary Cu sulphides were formed by precipitation of previously leached Cu in a reducing environment, i.e. below the groundwater table. Relictic primary ore present comprises mainly chalcopyrite, pyrite and tennantite-tetrahedrite minerals accompanied by minor sphalerite and galena. Secondary Cu sulphides are present either as a fine-grained intergrowth of chalcocite and digenite (the characteristic cleavage points to a higher proportion of the first-mentioned phase) - or covellite (Fig. 8.6a), which often surrounds a core of relictic chalcopyrite or fahlore. The formation of covellite also is promoted by the presence of galena due to precipitation by cation exchange between Cu-rich fluids and the Pb sulphide (Dill, 2015). Exposure of these sulphide ores to atmospheric (i.e. oxidising) conditions led to transformation to predominantly malachite and minor azurite (Fig. 8.6b).

8.2. Geochemistry of ore minerals

The most relevant Ag carriers in the analysed samples are galena and tennantite-tetrahedrite minerals in primary ore and secondary Cu phases (sulphides, oxidised species) in weathered mineralisations. The other phases only contain low to typically not detectable amounts of Ag.

8.2.1. Primary sulphide ore

Galena

Galena is ubiquitous and in varying quantities present in each of the sampled ores. Ag is a highly common minor element with roughly only 15 % of the analyses being below the detection limit (i.e. < 250 ppm). While the precious metal is somewhat depleted in early-stage dominated samples (0.02 to 0.10 wt %, median 0.04 wt %), notable contents have been determined in galena from both main- (0.02 to 2.23 wt %, median 0.12 wt %) and late-stage dominated ore (0.03 to 0.56 wt %, median 0.09 wt %). Sb as well could be mostly detected and is notably enriched in galena from late-stage ore (early-ore stage: 0.04 to 0.18 wt %, median 0.08 wt %;

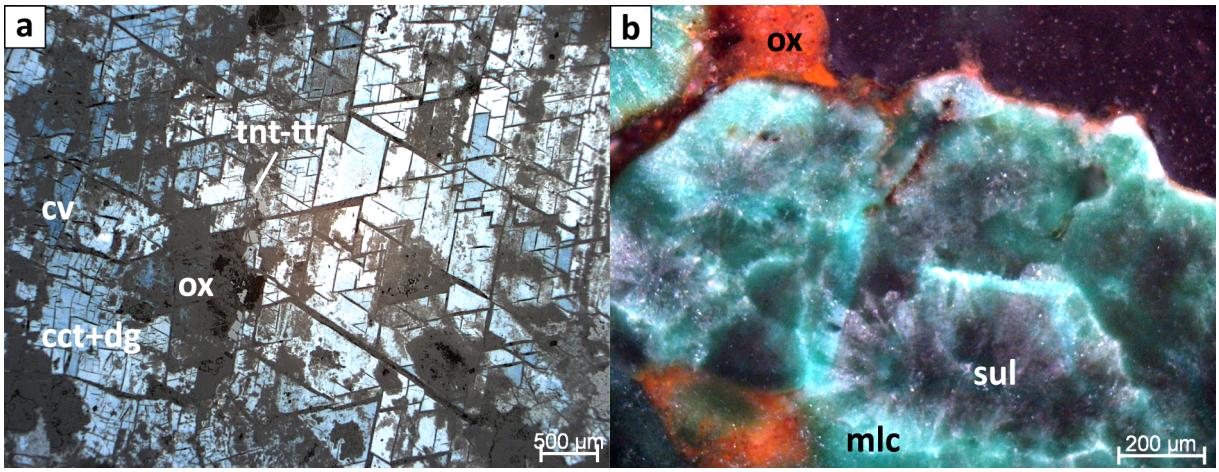

Figure 8.6.: Supergene Cu ore. a) Intimately intergrown digenite (light blue) and chalcocite (white with bluish tint) is accompanied by minor covellite (indigo blue). The sulphides partially are weathered to dull grey oxidised phases. Relictic primary fahlore acted as one of the protore minerals [sample 11043(2), RL, PPL]. b) Fibrous malachite forms botryoidal aggregates around cores of secondary Cu sulphide phases. Fe oxide and hydroxide phases also are of secondary origin [sample 13020(1), TL, XPL].

main-ore stage: 0.04 to 0.92 wt %, median 0.08 wt %; late-ore stage: 0.08 to 0.74 wt %, median 0.15 wt %). While Sb and Ag are strongly positively correlated in galena from late-stage ore ($R^2 = 0.96$) only a slightly positive or no relationship at all are discernible in early- and main-stage samples ($R^2 = 0.40$ and 0.10, respectively; Fig. 8.7b). However, a positive correlation with S ($R^2 = 0.57$; Fig. 8.7a) in galena from main-stage samples suggests that the determined precious metal abundances rather derive from analysis of micro-inclusions of Ag-bearing sulphosalts and sulphides than being hosted in solid solution due to coupled substitution with Sb (cf. chapter 2.1), as proposed for Pb sulphide in late-stage ore. Incorporation of Ag in sulphide form within galena from main-stage samples can be widely excluded since several analyses significantly exceed the solubility limit of Ag_2S at typical formation temperatures of hydrothermal ore (e.g. 0.6 mol % at 600 °C; cf. section 2.1). Further typically present elements are Mn (median contents of 0.03 wt %, 0.02 wt % and 0.02 wt % in early-, main- and late-stage ores, respectively) and Cd (median abundances of 0.06 wt % in main- and late-stage, typically not detectable in early-stage samples), whose distribution appears to be unrelated to the paragenetic classification of this mineral.

Sphalerite

Sphalerite is rather Fe-poor with higher contents of the element typically determined in late- (1.95 to 11.11 wt %, corresponding FeS from 3.5 to 19.5 mol %) than main-stage samples (0.27 to 0.62 wt %, FeS between 0.5 and 1.1 mol %). Cu, whose abundances range between 0.15 and 0.48 wt % in main- and, if detected, between 0.03 and 0.52 wt % in late-stage ore, generally is an important minor element. Other commonly present impurities are Mn (main-stage ore: typically not detected; late-stage ore: median 0.14 wt %) and Cd (median abundances in grains of main- and late-stage samples: 0.06 wt % and 0.20 wt %, respectively), which both are notably enriched

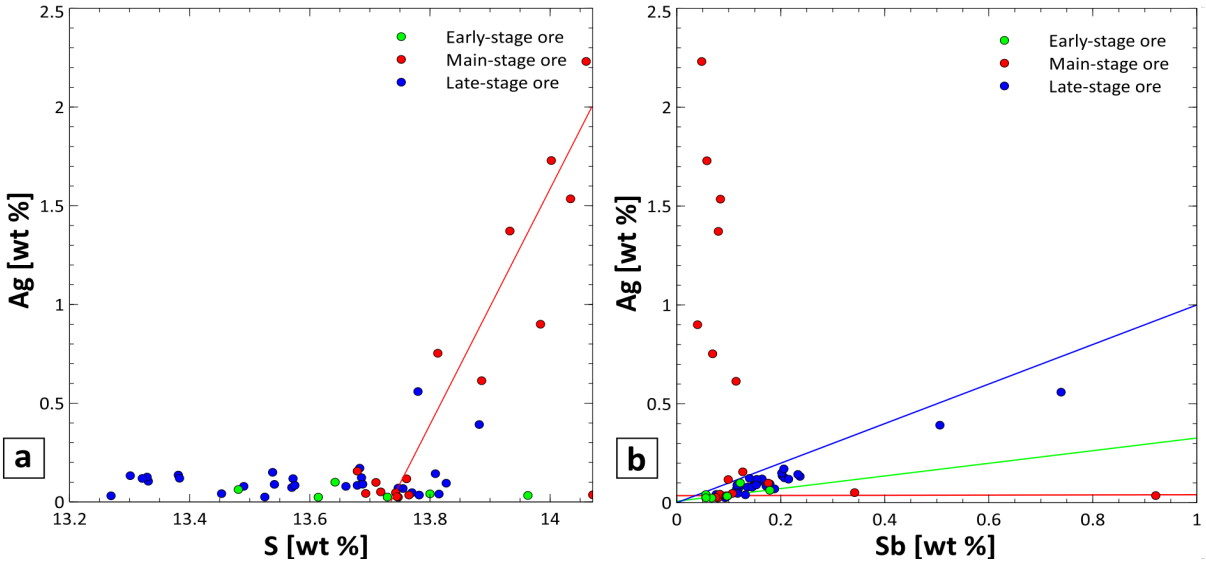

Figure 8.7.: Correlation plots of Ag contents in galena from early, main and late stage-dominated ore samples. a) Ag [wt %] versus S [wt %] abundances. Correlation coefficients of early, main and late stage-dominated ore samples are -0.15, 0.57 and 0.06. b) Ag [wt %] versus Sb [wt %] abundances. Correlation coefficients of early, main and late stage-dominated ore samples are 0.40, 0.10 and 0.96. b)

in samples dominated by a late-stage phase assemblage.

Pyrite

The most common minor element in pyrites of early-, main- and late-stage ore samples is As (0.02 to 0.96 wt %, 0.04 to 1.62 wt % and 0.02 to 1.61 wt %, median 0.45 wt %, 0.93 wt % and 0.72 wt %, respectively). Variations of the As content might have caused growth bands (see chapter 8.1.1). Particularly Co - whose median contents irrespective of the paragenetic classification of the samples consistently amount to 0.08 wt % - Mn and Cd are typically abundant minor elements.

Marcasite

The refractory elements Co and in particular Ni are more common in marcasite than pyrite and their contents typically are higher (median abundances of 0.09 wt % and 0.16 wt %, respectively). The median content of As (0.50 wt %; 0.35 to 1.90 wt %) in contrast is somewhat lower than in pyrite.

Pyrrhotite

Since pyrrhotite is very scarce in the investigated ores, only one analysis in sample 14018 has been possible. The obtained composition is Fe-rich (59.60 wt %) with a corresponding formula of $Fe_{0.86}S$. The only minor elements detected are Mn, Co and Sb (0.29 wt %, 0.10 wt % and 0.03 wt %, respectively).

Arsenopyrite

Only arsenopyrite analyses which yielded compositions between $FeAs_{0.9}S_{1.1}$ and $FeAs_{1.1}S_{0.9}$ (cf. Morimoto & Clark, 1961) have been accepted for examination. Arsenopyrite from samples predominated by an early-stage phase assemblage generally is Fe-poorer and As-richer (35.04 to 35.99 wt % and 41.10 to 44.19 wt %, respectively) than grains analysed in main-phase ore (34.06 to 35.54 wt % and 41.45 to 43.90 wt %, respectively). This finding matches the fact that the As contents of arsenopyrite synthesised from constant bulk compositions increase relative to its formation temperature (Kretschmar & Scott, 1976). Data from main-stage samples furthermore is enriched in Sb and Mn (median 0.05 wt % and 0.04 wt %, respectively) when compared to earlier formed specimens (median 0.22 wt % and 0.03 wt %, respectively). Analysis of arsenopyrite from the late stage-dominated sample 12055(1) yielded the lowest As content (40.90 wt %; Fe: 35.30 wt %) determined in the investigated ores and thus points to comparably low formation temperatures, which are in accordance with the assumed deposition stage of the specimen.

Chalcopyrite

The composition of chalcopyrite is relatively pure with generally low to not detectable minor element contents. No correlation between the mineral chemistry and the overall paragenetic classification of the samples is evident. Mn is a ubiquitous minor element with a median abundance of 0.02 wt %. It is highly enriched in sample 14018 (median 0.88 wt %), where however no significant correlation with any other element has been observed. Co is a common minor element in the analysed chalcopyrite (median content 0.05 wt %) while Sn has only been detected in some of the sampled ores (particularly in samples 11043(2), 11079 and 14018) with an overall maximum abundance of 0.32 wt %.

Tennantite-tetrahedrite minerals

The analysed fahlore generally is rather enriched in the Sb-bearing tetrahedrite component (0.20 to 28.51 wt % Sb), while As scatters between 0.14 and 18.80 wt %. The Cu content ranges between 32.50 and 41.87 wt % and correlates positively with As ($R^2 = 0.48$) but negatively with Sb and Ag (R^2 = -0.49 and -0.88, respectively). Both Fe (0.91 to 6.36 wt %) and Zn (0.54 to 7.57 wt %) have been continuously detected. Ag is an important constituent of the fahlore chemistry with abundances ranging between 0.20 and 7.94 wt % and a median content of 2.96 wt %. Tennantite-tetrahedrite analyses from late stage-dominated ore samples clearly exhibit the lowest Ag abundances ($<$ 0.02 to 0.62 wt %). Typical impurities are Mn, Cd and Sn with median contents of 0.02 wt %, 0.06 wt % and 0.10 wt %.

Bournonite

Bournonite has been only observed in sample 11015 and is compositionally pure with low As contents (median 0.57 wt %) and minor Mn, Fe and Sn abundances (median 0.03 wt %, 0.07 wt % and 0.10 wt %).

8.2.2. Secondary Cu ore

Supergene Cu sulphides

Due to the fine intergrowth no exact analyses have been possible. The obtained impure composition ($Cu_{1.82}S$ to $Cu_{2.03}S$) ranges between digenite, djurleite and chalcocite. The Ag contents (0.08 to 1.16 wt %, median 0.40 wt %) are particularly noteworthy and agree very well with those of secondary supergene Cu minerals described by Cook et al. (2011) and Reich et al. (2010). However, the relationship of solid-solution contained Ag and As contents in digenite (Reich et al., 2010) could not have been applied to the analysed sulphides since As always is below the detection limit of the electron microprobe (i.e. < 250 ppm). This observation in conjunction with the enriched Ag abundances strongly points to the presence of Ag-rich nano- or micro-inclusions, e.g. native Ag generated during supergene processes. Besides Ag, Fe, Cd and Sb are the only other minor elements regularly detected in the secondary sulphides with median contents of 0.03 wt %, 0.04 wt % and 0.10 wt %.

Oxidised Cu minerals

Oxidised Cu minerals possess Cu abundances between 52.17 and 58.74 wt % (median 55.48 wt %), which thus are somewhat similar to the composition of stoichiometric malachite (56.20 wt % Cu). The Ag contents are depleted (0.02 to 0.86 wt %, median 0.06 wt %) when compared to those determined in supergene sulphides, but still are among the highest analysed in ore samples from the district. Elevated S abundances (0.01 to 1.54 wt %) potentially derive from micro-inclusions of restitic sulphides. Fe is the only other relevant impurity routinely detected in the oxidised minerals (median 0.04 wt %).

8.3. Ore deposition and formation processes

The As content in arsenopyrite (29.61 to 32.54 at %) associated with pyrite and precipitated during the early and main stages of ore formation yields temperatures between circa 330 and 475° C (Kretschmar & Scott, 1976). It thus records high crystallisation temperatures in early samples and formation of late-stage ore at temperatures below 330 °C. This generally is in accordance with the results of Dangić (1985), who calculated temperatures between 438 and 486 °C using Cd-Mn thermometry on galena-sphalerite pairs of high-temperature ore samples from Kishnica. In general, the mineralogy of main stage-dominated samples is more versatile and also comprises uncommon ore assemblages, e.g. arsenopyrite, pyrite, chalcopyrite and wolframite [$(Fe^{2+},Mn)WO_4$] with quartz gangue (sample 13099(5), not chemically analysed). The typical main-stage phase assemblage (chalcopyrite + pyrite + tennantite-tetrahedrite) and the FeS content of associated sphalerite (median 0.8 mol %) proves an intermediate sulphidation state of the mineralising fluids. In the late-ore assemblage in contrast, the FeS abundance determined in sphalerite (median 15.4 mol %) and the partially present pyrrhotite indicate a low sulphidation state (cf. Einaudi et al., 2003). Partial replacement of pyrite by marcasite (Fig. 8.5f) in this stage documents in addition to the general petrography and phase assemblage of the samples decreasing temperatures. The sample with the highest FeS content in sphalerite also contains

pyrite-marcasite intergrowths in which the sulphides partially are replaced by magnetite, whose presence points to increasing fO_2 and consequently testifies to a decaying hydrothermal ore-forming system (Fig. 8.5f).

8.4. Résumé and implications for archaeometallurgical processes

The mining district of Shashkoc-Janjevo generally is classified as Pb-Zn-Ag mineralisation. However, a certain variation related to temperature-dependant ore forming processes is evident. Early-stage ore mainly consists of arsenopyrite and pyrite hosted by quartz. The main-stage mineralisation is embedded in quartz-carbonate gangue and exhibits a rather polymetallic character with elevated contents of Cu, Ag, As and Sb caused by the increased presence of arsenopyrite, fahlore and chalcopyrite. Later precipitated ore in contrast possesses a phase assemblage mainly made up of galena, sphalerite and pyrite / marcasite hosted by carbonate gangue. The different mineralisation types are slightly unevenly distributed. Main- and early-stage predominated ore has been rather retrieved from the southern part of the district while late-stage samples typically have been collected in the northern and western part of the study area. Similar distribution patterns have been described from other occurrences (e.g. Plumlee et al., 1995) and presumably are linked to the relative distance of the ore bodies from the igneous host rock as the hottest central part of the mineralised area.

The Ag content of the primary sulphide ore mainly is hosted by galena and tennantite-tetrahedrite minerals. Particularly fahlore phases, similarly to other districts (e.g. in the Mosel region: Kronz, 2005; in general for the medieval and early modern period: Bartels, 2014) significantly contributed to the precious metal grade of the mined ore. Weathering of Cu-enriched main-stage ore lead to generation of secondary Cu sulphides (particularly chalcocite, digenite and covellite), which in turn have been altered to oxidised phases (i.e. predominantly malachite besides minor azurite). In situ analysis detected notable Ag abundances, which are somewhat depleted in oxidised phases compared to their sulphidic predecessors.

Ore from the Shashkoc-Janjevo district hence generally supplies suitable raw material for Pb-Ag metallurgy. Abundant galena mainly provided the Pb content to be extracted, which in its reduced form acted as a collector for Ag mainly originating from galena, fahlore and secondary Cu phases. The higher Ag and reportedly abundant Au contents (Hyseni & Alliu, 1999) in main-phase mineralisation (and its weathering products) predominantly sampled in the southern area of the district could have been pivotal factors for preferential exploitation of this mineralisation in the earlier stages of local mining. However, the pronounced As, Sb and Cu contents of this ore type, if present in sufficient amounts, bear the potential to generate the by-products matte (a mixture of base metal sulphides) and speiss (arsenides, antimonides and stannides of mainly Cu, Fe, Ni and Ag; cf. sections 2.5.2 and 2.5.3) and consequently may necessitate modification of the metallurgical process scheme.

9. Slag

Slags are the most relevant material for the reconstruction of metallurgical processes. As discarded waste material, they are widely abundant and serve as primary indicators for e.g. smelting, refining and smithing activities. Their importance for archaeometric research is based on the multitude of parameters and general conditions they record by both their outer shape and at micro-scale. For slags related to non-ferrous metallurgy, the following aspects are relevant:

- Associated metallurgical operation, i.e. primary smelting, refining etc.
- Nature of the ore, e.g. oxidised or sulphide species, chemistry of the ore
- Extracted metal(s)
- General process design, i.e. single- or multi-stage operations
- Viscosity of the slag melt
- Process temperature
- Furnace atmosphere (i.e. fO_2) and potential subsequent oxidation
- Addition of fluxes or self-fluxing charges
- Interaction with furnace material and charcoal
- Furnace construction
- Efficiency of the process

9.1. Typology of slag samples

Three different types of slags have been sampled: a) basin, b) furnace and c) smithing slags. While basin and furnace slags have been collected at the investigated smelting sites and thus represent metallurgical waste material, smithing slags have been retrieved from blacksmiths' workshops at the 'Mondlandschaft' in the Shashkoc-Janjevo district and from excavations in Ulpiana. Basin and furnace slags are distinguished by their formation history. Furnace slags have been solidified within the furnace while the former have accumulated in a specifically designed basin, which could be located either within or outside the furnace.

9.1.1. Basin slags

The sampled basin slags can be roughly subdivided on the basis of differing morphology, i.e. particularly the presence or absence of flow structures. Slags with flow structures have been collected at all smelting sites except Akllap and Ostri Vrh and thus represent the vast majority of the investigated samples.

Slags with flow structures

Slags of this type either exhibit a blocky or platy shape and are covered by several distinct, finger-like flow structures (Fig. 9.1a-c) or consist of only one, thin finger-shaped structure (Fig. 9.1d).

Blocky / platy type Slags of the blocky / platy type possess a mid to dark grey colour, partially with a greenish or brownish tint, and an often pronounced metallic lustre. Their shape and size is rather variable and includes thin platy types as well as larger, relatively thick slag cakes. Particularly large-scaled samples may reach diameters of several ten centimetres and heights of up to c. 10 cm (Fig. 9.1c). Most slags, however, are up to 5 cm thick and possess diameters of maximum 10 cm. The slags do not show any evidence for crushing, i.e. particularly to manually remove trapped metal prills. Top and bottom sides can be clearly distinguished due to the flow structures. The bottom side of all handsamples is coarse and sandy, partially with a knotty structure, which resulted from reaction of the slag melt with the substrate. The flow structures are present at the upper side of the specimens and possess a finger-like shape (Fig. 9.1a, c). They often exhibit a glassy surface due to comparatively rapid cooling. Single finger-shaped flow structures typically are between 1 and 3 cm wide, but may reach extents of up to 5 cm. The flow structures observed at specimens from Mramor Proni Butoçit often exhibit pronounced parallel wrinkles (Fig. 9.1c). Several slags show marks of the cooling basin or related installations, i.e. potentially present channels connected with these reservoirs. In cross-section, commonly several layers can be distinguished (Fig. 9.1b). With the exception of a partially abundant black to dark grey glassy layer at their uppermost region, they appear to be crystalline. The porosity of the slags is varying from very dense with small pore diameters in the range of a few millimetres to rather porous with pores possessing centimetre-scaled diameters. Inclusions of charcoal in the slag matrix have been commonly found. Several slags comprise veinlets or layers of matte (Fig. 9.1b) and, more rarely, ferrous speiss. They are present at the bottom of the layers and hence indicate gravitational separation of the different melts. Matte has been observed within samples 12015(5) and 14032 from Voguçincë, 11027(1) and 11027(2) from Mirash, 11029(5) from Mirash Novo and 10024(4) from Mramor Proni Butoçit. Ferrous speiss is abundant within specimen 11029(4) from Mirash Novo. With the exception of the not yet dated site of Mramor Proni Butoçit, slags with segregated matte and ferrous speiss thus solely have been retrieved from metallurgical complexes with a preliminary Roman / late antique dating. Droplets of exsolved native Pb partially are visible to the naked eye (e.g. in sample 10024(5) from Mramor Proni Butoçit). Similarly to matte and ferrous speiss, inclusions of native Pb as well accumulate in the lower zones of the slag layers. Weathering generated partially pronounced reddish, yellowish and whitish patinas (Fig. 9.1a, c), which are attributed to the formation of secondary Fe- and

Pb-bearing phases. The presence of matte layers or veinlets is indicated by greenish and bluish oxidised Cu phases.

Finger-shaped type Finger-shaped slags have been collected at the sites of Voguçincë (no samples analysed) and Mirash Novo (11029(2) and 11029(3)). Slags of this type are characterised by a black colour with a strong glassy lustre and thus are optically similar to obsidian (Fig. 9.1d). They possess a finger-like shape and are comparably flat (< 3 cm high). Their width scatters around 1 or 2 cm and their length may be up to c. 10 cm. Analogous to blocky / platy slag types, their bottom side is coarse and partially knotty due to interaction of the slag liquid with the substrate. Top and bottom of the specimens hence can be unambiguously distinguished. The slags apparently do not have been crushed after their solidification. They always consist of only layer and appear glassy in cross-section. The specimens are very dense with only a few, small pores with diameters of a few millimetres. Sample 11029(3) possesses a matte layer, which has accumulated below the slag zone due to the differing specific gravities. This slag type seems to be comparably resistant to atmospheric weathering and rarely exhibits a slight whitish patina, which indicates the presence of oxidised Pb-bearing phases (Fig. 9.1d). Matte, if present, in contrast is strongly altered to greenish and bluish secondary phases.

Slags without flow structures

The specimens typically exhibit a mid to dark grey colour and partially possess a metallic lustre. Some of the samples are optically similar to obsidian and show a black colour with glassy lustre and conchoidal fracture (Fig. 9.1f). The shape and size of the specimens is comparably uniform. All samples are rather flat - their height does not exceed c. 3.5 cm – and typically exhibit a platy shape. With the exception of sample 12016(1) from Akllap, which is approximately 10 cm long (Fig. 9.1e), the slags possess a length of only a few centimetres. Analogous to slags with flow structures, they show no evidence for crushing. Slags without distinct, i.e. finger-like flow structures, exhibit either only few wrinkles on their upper surface (Akllap: 12016(1), 12016(2)) or do not show any such textures at all (Ostri Vrh: 13030(1), 13031(1)). The bottom sides of the slags, if discernible, are coarse and sandy, but in contrast to some samples with flow structures show no evidence for liquid reaction with the substrate (see above). The top and bottom sides of this slag type consequently often are difficult or virtually impossible to distinguish unambiguously. All investigated samples possess only one tap layer (Fig. 9.1e). The slag matrix is rather dense with small, typically millimetre-sized pore diameters. The samples appear to be fine-grained or even glassy in cross-section. Neither matte nor speiss have been observed within these slags. Samples of this type, analogous to finger-shaped specimens, seem to be comparably resistive towards weathering and appear relatively fresh (Fig. 9.1f).

9.1.2. Furnace slags

Furnace slags commonly are scarce and have been mostly found at large-scaled smelting sites (Voguçincë) or supposedly in the immediate vicinity of furnace complexes (Marmor Samakove). Thus only two samples (10021(2) and 10021(21)) from the latter site have been investigated. Sample 10021(21) conforms to the typical properties of furnace slags (see below; Fig. 9.2a).

Figure 9.1.: *Basin slags: Handsamples of slags with flow structures.* a) Blocky / platy type: Large slag with distinct finger-like flow structures, partially covered by a whitish patina [sample 12015(12), Voguçincë]. b) Blocky / platy type: Cross-section of a roughly rectangular multi-layered specimen with segregated matte [sample 11027(1), Mirash]. c) Blocky / platy type: The large platy slag with flow structures, which possess pronounced parallel wrinkles, is partially covered by whitish oxidised phases generated by atmospheric weathering [sample 10024(5), Mramor Proni Butoçit]. d) Finger-shaped type: Thin, blackish finger-shaped slag with isolated spots of whitish, presumably Pb-bearing secondary phases [sample 12015(10), Voguçincë]. *Handsamples of slags without flow structures.* e) Cross-section of a dense, single-layered specimen [sample 12016(1), Akllap]. f) Particularly glass-rich slag, due to its black colour and conchoidal fracture optically similar to obsidian [sample 13030(1), Ostri Vrh].

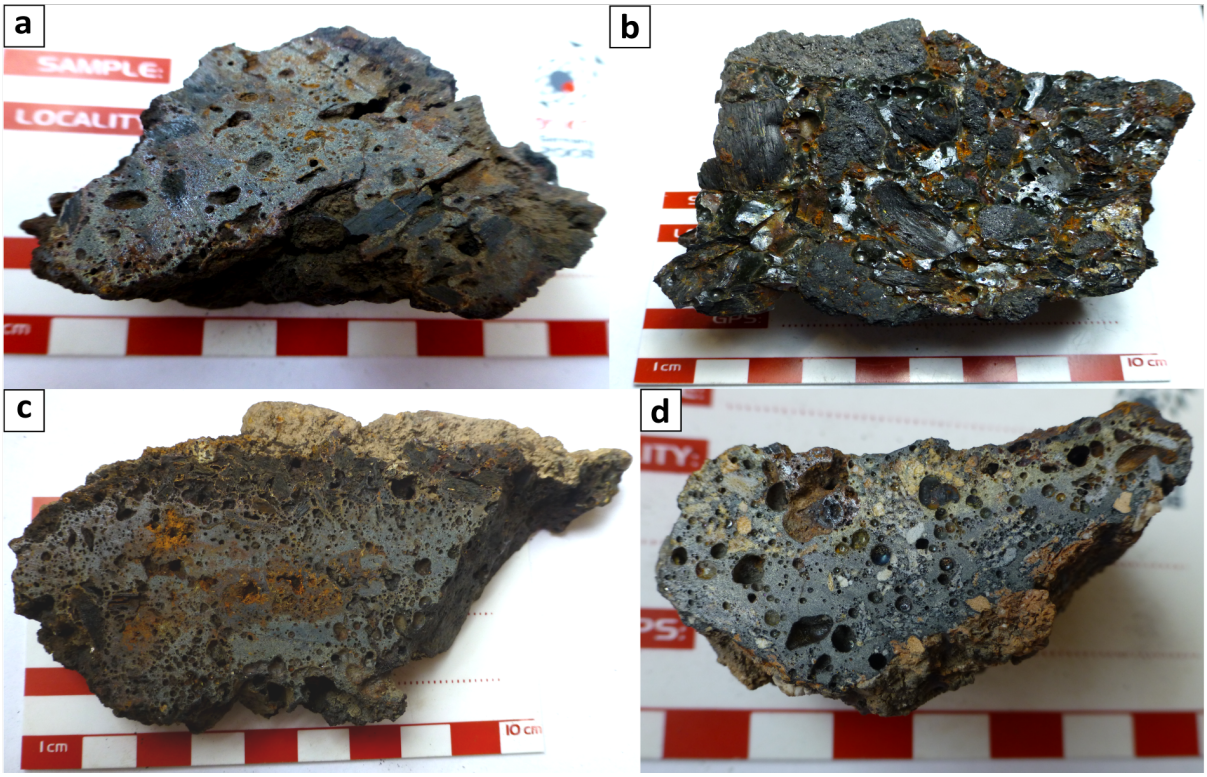

Figure 9.2.: *Furnace slags.* a) Furnace slag with steel-grey colour and rather high amount of pores containing several charcoal inclusions [sample 10021(21), Mramor Samakove]. b) Furnace slag with glassy surface and abundant charcoal pieces [sample 13361(1), chance find from a building pit in Janjevo]. *Smithing slags.* c) Highly porous plano-convex smithing slag exhibiting a pronounced metallic lustre. Reddish and whitish parts of the specimen are of secondary origin [sample 10041, 'Mondlandschaft' close to Shashkoc]. d) Specimen of an impure smithing slag comprising several grains of SiO_2-bearing phases, e.g. feldspar and silica [sample 12059(4), Ulpiana].

Specimen 10021(2), however, possesses characteristics - a platy, flat shape with subtle flow structures and an overall low porosity - which are typically rather assigned to basin slags. Since the phase assemblages and geochemistry though are highly similar to sample 10021(21), which has been unambiguously identified as furnace slag, 10021(2) is interpreted as being intermediate between basin and furnace slag types and due to its paragenesis and chemistry is treated as a furnace slag.

Furnace slags typically roughly possess the size of a fist, are of steel-grey colour and thus typically are lighter coloured than basin slags of any type. The furnace slags possess an irregular, rough surface and are relatively porous, partially with a sponge-like appearance and hence are prone to weathering, which particularly generates Fe oxides and hydroxides (Fig. 9.2a, b). Scraps of whitish to brick-red furnace debris are a typical constituent of their matrix. Another characteristic is the widespread occurrence of charcoal, nearby which Fe phases may have been reduced to droplets of native Fe. Generally, while basin slags often are optically similar to pahoehoe, furnace slags strongly resemble aa lava.

9.1.3. Smithing slags

Smithing slags have been found at the 'Mondlandschaft', a particularly intensively mined area of the ancient mining district nearby the settlement Shashkoc, and within the city limits of Ulpiana, supposedly within the *municipium's* workshop complex. While the blacksmith amid the old workings presumably mainly served to sharpen and repair the miner's ironclad tools[1], its tasks in Ulpiana certainly were more diverse. One specimen from Shashkoc (10041) and two samples from Ulpiana (12059(4) and 12059(8)) have been investigated by OM and XRD to substantiate the suspected presence of a blacksmith at the 'Mondlandschaft' and to umabiguously clarify the nature of the slags found in Ulpiana. The smithing slags have not further analysed (e.g. in situ measurements of phases by EMP) since the focus of this work explicitly lies on non-ferrous metal mining and production.
In general, the investigated smithing slags possess a similar morphology than the examined furnace slags. Freshly cutted surfaces typically show a strong metallic lustre and charcoal inclusions have been often observed. Samples 10041 and 12059(8) both are characterised by a high porosity and dark grey colour with metallic lustre. Specimen 10041 (Fig. 9.2c) possesses a plano-convex shape and a porous, spongy appearance. It partially is severely altered to reddish Fe oxide and hydroxide phases. The slag sample 12059(8) from Ulpiana optically generally is highly similar to the one from Shashkoc, but is significantly smaller and exhibits an irregular shape. Specimen 12059(4) from Ulpiana in contrast is heterogeneous in cross-section. It consists of a dark grey slag matrix, which merges into a zone containing a high proportion of milky white and brownish-yellow grains of SiO_2-bearing phases (e.g. feldspar and silica; Fig. 9.2d) hence indicating compositional differences presumably related to contamination by siliceous material, e.g. furnace lining.

9.2. Petrography and geochemistry of phases in metallurgical slags

A general petrographic classification of the sampled metallurgical slags can be, analogous to the approach of Keesmann et al. (1984) described in section 2.5.1, made on basis of the predominant silicate phase(s): a) olivine-type, b) olivine + clinopyroxene-type, c) clinopyroxene-type, d) melilite-type and e) glassy type (Tab. 9.1). In olivine + clinopyroxene-type slags, both silicate phases are present in approximately equal proportions. In specimens classified as glassy type, the phase assemblage mainly consists of glass besides spinel *ss* as well as potentially present Pb silicate phases.
Furnace slags always contain olivine as the predominant silicate phase. Blocky / platy basin slags with flow structures occur as olivine-, olivine + clinopyroxene- and clinopyroxene-type. Finger-shaped basin slags with flow structures always can be assigned to the glassy type. Basin slags without flow structures are classified as olivine + clinopyroxene-, clinopyroxene- and melilite-type, respectively. Slags with olivine as the main phase clearly are the most common type investigated and have been collected at the presumably Roman / late antique sites of Voguçincë

[1] An overview of medieval mining tools discovered in the Kopaonik-Šumadija district is presented by Bogosavljević (1994).

(samples 12015(5), 12015(7), 12015(12) and 14032), Mirash (11027(1), 11027(2)) and Mirash Novo (11029(4), 11029(5)), the potentially medieval / early modern workshops of Marec (10-6, 10032(1), 10032(4)), Hajkobile (10-1A) and Hanroc (3(1), 3(2)) and the not yet dated site of Mramor Proni Butoçit (10024(4)). Furnace slags retrived from Mramor Samakove (10021(2), 10021(21)) also are classified as olivine-type. The occurrence of samples containing predominantly clinopyroxene apparently is restricted to distinct smelting sites, i.e. Mramor Proni Butoçit (samples 10024(4) and 10024(5)), Akllap (12016(2)) and Ostri Vrh (13030(1)). Olivine + clinopyroxene- and melilite-types each have been solely retrived from Akllap (sample 12016(1)) and Ostri Vrh (13031(1)), respectively. The only specimen classified as glassy type which has been chemically analysed, has been collected at Mirash Novo (sample 11029(3)), where also more glassy slags have been observed. However, similar slags as well have been found at Voguçincë (cf. Fig. 9.1d).

While in olivine-dominant slags, either olivine or Fe-rich oxides (i.e. wüstite and spinel *ss*) precipitate first, in clinopyroxene- and melilite-type slags spinel *ss* always crystallises as first phase (Tab. 9.1). Late-crystallised clinopyroxene (i.e. after olivine and / or Fe-bearing oxide phases) has been observed in slags from the southernmost smelting sites Mirash and Mirash Novo and from Mramor Proni Butoçit. Further subdivision of the four main slag types can be done on the basis of the presence of Fe oxide phases and clinopyroxene as well as the general crystallisation sequence and is discussed in detail in chapter 17.2.

9.2.1. Olivine [$(Fe,Zn,Mg,Mn,Ca)_2SiO_4$]

Olivine is the dominant silicate compound in the homonymous slag type and often the first phase to crystallise. Some specimens (e.g. 10032(4)) even may exclusively consist of intimately intergrown olivine and glass. In olivine + clinopyroxene-type slags, olivine precipitates after spinel *ss* and together with clinopyroxene, is the main phase in these specimens. In slags predominated by clinopyroxene, olivine, if present at all, typically occurs subordinate as accessory, lately precipitated phase. Olivine has not been observed in melilite-dominated and glassy slag types. The morphology of the crystals records the cooling rate of the melt and the degree of supercooling. A typical sequence, ordered according to decreasing cooling rate is (Fig. 9.3 a-d; Donaldson, 1976): Feathery, snowflake shapes - H chains - skeletal laths - polyhedral grains with different degrees of skeletal growth - sub- to euhedral grains. Grains associated with rapid cooling often are elongated and may reach extents of several millimetres or even centimetres, but are extremely narrow and only a few micrometres wide. Polyhedral grains typically possess diameters ranging from several ten to hundreds of micrometres. In transmitted light, olivines possess a brownish or greenish colour and are slightly anisotropic (Fig. 9.6c). Zoning typically is manifested by greenish cores and whitish rims in cross-polarised reflected light (Fig. 9.3e) and has been commonly observed regardless of the crystal morphology. If leucite is present, olivine typically forms cotectoid intergrowths with this phase (Fig. 9.3f). A second generation of lately crystallised small micrometre-sized olivine dendrites within restitic glass has been often found (Fig. 9.3b, d, f).

The composition of olivines within one slag specimen generally is rather homogeneous and overlaps within the separate layers. Grains with a pronounced zonation or from differing gener-

Slag type	Smelting site	Preliminary dating	Sample	ol	ol II	cpx	mll	fsp	lct	kls	spl *ss*	wus	isc	Symplectite
ol	Voguçincë	R/la	12015(5)	xxx	x				x		xx		acc	[ol lct]
ol	Voguçincë	R/la	12015(7)	xxx	x			acc	xx		x			[ol lct]
ol	Voguçincë	R/la	12015(12)	xxx	x				x		xx		acc	[ol lct]
ol	Voguçincë	R/la	14032	xxx	x				xx		acc			[ol lct]
ol	Mirash	R/la	11027(1)	xxx	x	x			acc		acc			
ol	Mirash	R/la	11027(2)	xxx	x	x					acc			
gl	Mirash Novo	R/la	11029(3)								xx			
ol	Mirash Novo	R/la	11029(4)	xxx	x	acc			acc		x		acc	
ol	Mirash Novo	R/la	11029(5)	xxx	x	x		acc	acc		acc			
cpx	Mramor Proni Butoçit	-	10024(2)	x		xxx		acc	x		xx	x	acc	[ol lct], [lc wus]
ol	Mramor Proni Butoçit	-	10024(4)	xxx	x	acc			x		xx			[ol lct]
cpx	Mramor Proni Butoçit	-	10024(5)	acc		xxx			xx		xx	x		[lc wus]
ol	Mramor Samakove	M/em	10021(2)	xxx	xx				xx		x	xx		[lc wus]
ol	Mramor Samakove	M/em	10021(21)	xxx	xx			xx	xx					
ol	Marec	M/em	10-6	xxx							acc			
ol	Marec	M/em	10032(1)	xxx	x						acc			
ol	Marec	M/em	10032(4)	xxx										
ol	Hajkobile	M/em	10-1A	xxx					xx		xx	xx	x	[ol lct], [lc wus]
ol	Hanroc	M/em	3(1)	xxx	x							acc		
ol	Hanroc	M/em	3(2)	xxx					xx		x	xx	xx	[lc wus]
ol+cpx	Akllap	M/em	12016(1)	xx		xx		acc	x		xx			[ol lct]
cpx	Akllap	M/em	12016(2)	acc		xxx					xx			
cpx	Ostri Vrh	M/em	13030(1)			xxx		acc	x		xx		acc	
mll	Ostri Vrh	M/em	13031(1)				xx			x	xxx			

Table 9.1.: Classification and phase assemblages of the investigated basin and furnace (i.e. samples 10021(2) and 10021(21)) slags. The following abbreviations have been used: xxx = main phase, xx = common phase, x = abundant phase, acc = accessory phase; R/la = Roman/late antique, M/em = medieval/early modern. Analogous to Kronz (1997), symplectitic intergrowths are denoted as [phase A phase B]. See chapter i of the appendix for abbreviations of the phases.

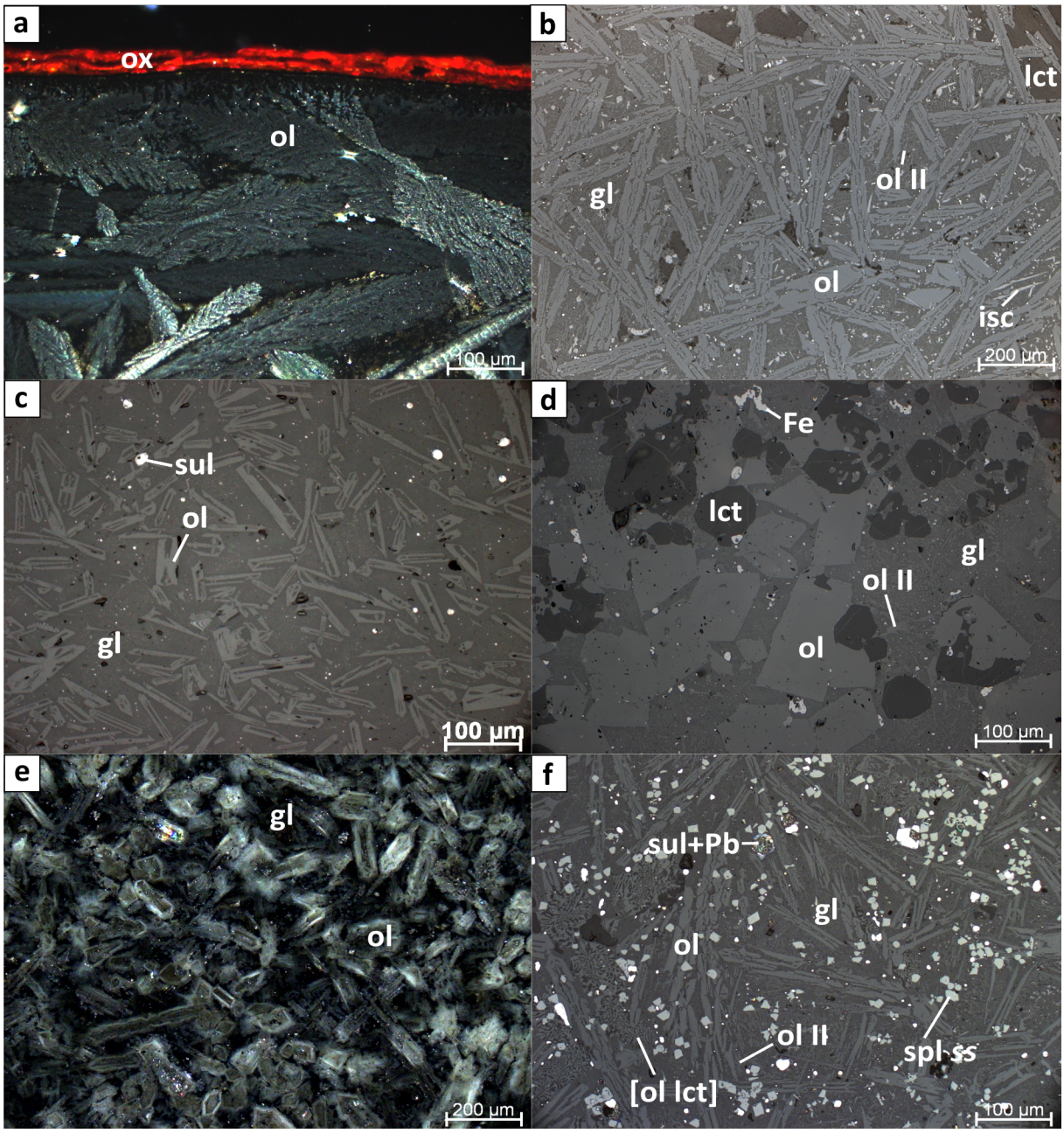

Figure 9.3.: a) Feathery, snowflake olivine is the only crystalline phase present at the surficial rim of a basin slag, which shows incipicient weathering to oxidised Fe-bearing phases [sample 10-6, Marec, RL, XPL]. b) Olivine, present as skeletal H-chain laths, is the main phase in a basin slag sample, which furthermore comprises thin iscorite rods, minute skeletal spinel *ss* rhombs, a second generation of late dendritical olivine II and an unidentified silicate phase, probably leucite (dark grey), all surrounded by glass [sample 11029(5), Mirash Novo, RL, PPL]. c) Skeletal olivine grains are embedded in glass, which contains several sulphide inclusions [sample 3(1), Hanroc, RL, PPL]. d) A slowly cooled furnace slag consists of a first generation of prismatic euhedral olivine grains, late dendritic olivine II, granular leucite and droplets of native Fe (i.e. pig iron) surrounded by silicate glass [sample 10021(21), Mramor Samakove, RL, PPL]. e) Eu- to subhedral olivine grains show compositional zoning with typically greenish cores and whitish rims [sample 10032(1), Marec, TL, XPL]. f) Olivine is present as skeletal laths, as late dendritical olivine II within glass and in symplectites with leucite. Spinel *ss* typically occurs as euhedral lozenge-shaped grains which partially exhibit skeletal growth. The glass contains several droplets of base metal sulphides with or without crude Pb [sample 12015(5), Voguçincë, RL, PPL].

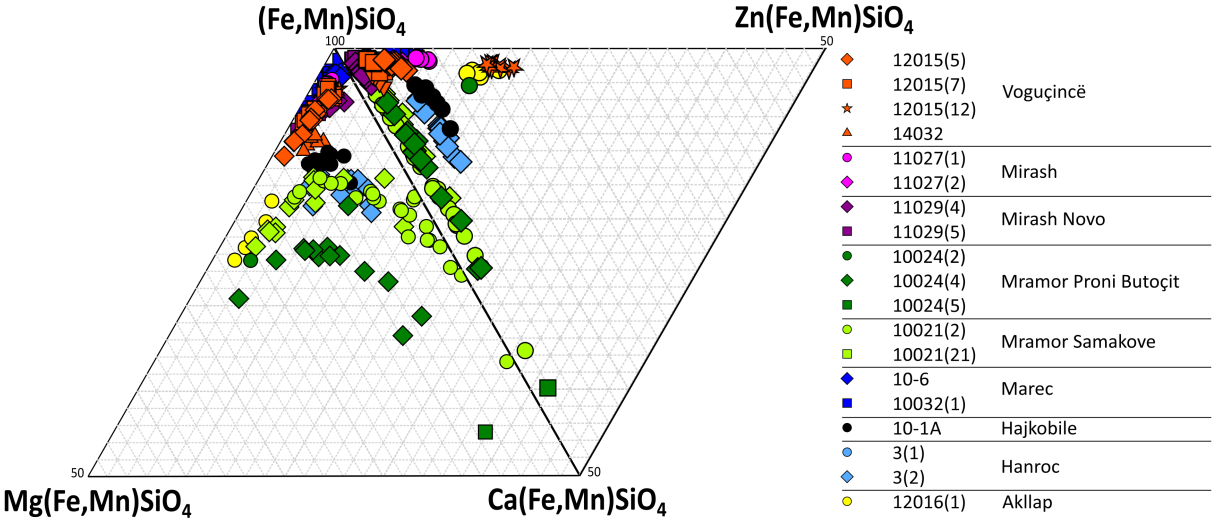

Figure 9.4.: Plot of olivine analyses in the double ternary systems $Mg(Fe,Mn)SiO_4$ - $Ca(Fe,Mn)SiO_4$ - $(Fe,Mn)SiO_4$ and $Zn(Fe,Mn)SiO_4$ - $(Fe,Mn)SiO_4$ - $Ca(Fe,Mn)SiO_4$.

ations (i.e. early and late olivine) naturally show a greater compositional variability. In the majority of slags, the analyses clearly are predominated by the Fe_2SiO_4 component containing minor amounts of Mn. In accordance with experimentally determined olivine crystal chemistry (Bowen et al., 1933; Bowen & Schairer, 1935; Brown, 1982; Ericsson & Filippidis, 1986; Glasser, 1961; Glasser & Osborn, 1960; Jak et al., 2001; Sarver & Hummel, 1962; Warner & Luth, 1973), miscibility is exhibited towards Mg_2SiO_4, Ca_2SiO_4 and Zn_2SiO_4 compositions (Fig. 9.4). Olivines from slags of Mramor Proni Butoçit (10024(2), 10024(4), 10024(5)), Mramor Samakove (10021(2), 10021(21)), Hajkobile (10-1A), and Hanroc (3(2)) are comparably enriched in the Ca_2SiO_4 component, while single samples from Voguçincë (12015(12)), Mramor Proni Butoçit (10024(2)) and Akllap (12016(1)) are marked by elevated Zn_2SiO_4 contents. Particularly in the clinopyroxene-type samples from Mramor Proni Butoçit (10024(2) and 10024(5)), the olivine geochemistry apparently reflects a Ca-richer bulk composition. In the furnace slag samples from Mramor Samakove, significant amounts of Ca certainly have been introduced by interaction of the siliceous slag melt with the furnace lining. Increased Zn contents determined in olivine are mirrored by the spinel *ss* compositions in the respective samples (section 9.2.7). Firstly crystallised olivine generally is Fe-richer and possesses a more homogeneous composition (Fe_2SiO_4 component ranging from 84.6 to 94.1 mol %, median 89.3 mol %) than grains from samples in which Fe-rich oxides (i.e. spinel *ss* and wüstite) precipitated first (Fe_2SiO_4 component ranging from 51.4 to 85.7 mol %, median 78.0 mol %), hence reflecting the differing bulk major element chemistry of the slag melts. MgO, MnO, CaO and ZnO have been always detected and often are important constituents of the phase's chemistry with contents ranging from 0.04 to 10.56 wt %, 0.12 to 7.46 wt %, 0.35 to 22.07 wt % and 0.85 to 13.16 wt %, respectively. The commonly observed zonation is caused by differing chemistry of the grains with relative enrichment of Mg in the core and of Fe and particularly Ca and Zn in the rim, thus resulting in minor variation of the main element chemistry (Fig. 9.4). The composition of lately precipitated olivine typically is enriched in Ca and extends towards the $Ca(Fe,Mn)SiO_4$ compound in the respec-

tive ternary. Analyses from samples with a large population of earlier Fe- and late Ca-enriched olivines (i.e. 10021(2), 10021(21) and 10024(4)) plot as distinct arc-shaped distribution patterns in the $Mg(Fe,Mn)SiO_4$ - $Ca(Fe,Mn)SiO_4$ - $(Fe,Mn)SiO_4$ diagram (Fig. 9.4).
Between the smelting sites, partially significant chemical differences exist. Olivine compositions from the presumably Roman / late antique sites of Voguçincë, Mirash and Mirash Novo largely overlap with those from Marec (with the exception of sample 10032(4), where the extremely small grain size prohibited in situ analysis), particularly in the $Mg(Fe,Mn)SiO_4$ - $Ca(Fe,Mn)SiO_4$ - $(Fe,Mn)SiO_4$ range. Sample 12015(12) from Voguçincë, however, is - comparable to 12016(1) from Akllap - significantly enriched in Zn and (Fig. 9.4). The highest proportion of the Zn_2SiO_4 component determined in olivine grains (sample 12015(12); 17.2 mol % in the ternary plot of Fig. 9.4, equivalent to 18.2 mol % in the Fe_2SiO_4 - Zn_2SiO_4 binary) approaches the solubility limits reported by Ericsson & Filippidis (1986) and Jak et al. (2001). The analyses from Marec are rather Fe-rich with Zn being the most notable impurity. Olivine grains from Akllap, Mramor Proni Butoçit and Mramor Samakove are comparably enriched in Mg. The elevated abundances of the element in sample 12016(1) from Akllap coincide with significant Ni contents (median 0.09 wt %) and thus point to simultaneous introduction, potentially by serpentinite rocks partially hosting ore bodies in the study area (more detailed in sections 9.2.7and 16.2). Olivine analyses from Mramor Proni Butoçit and Mramor Samakove due to their bulk composition and the presence of two grain populations (see above) generally are Ca-richer and show a comparable chemical trend (Fig. 9.4). Slags from Hanroc (3(2)) and Hajkobile not only possess similar parageneses, but also exhibit highly overlapping olivine compositions. Data from sample 3(1) from Hanroc in contrast is significantly Fe-richer and similar to those from Voguçincë, Mirash and Mirash Novo as well as Marec.

9.2.2. Clinopyroxene [$(Ca,Fe^{2+},Mg,Mn,Zn,Al,Fe^{3+})_2(Si,Al,Fe^{3+})_2O_6$]

The presence of clinopyroxene is restricted to basin slags. It is a main component in clinopyroxene- and olivine + clinopyroxene-types, in which it precipitates early after Fe-rich oxides. Clinopyroxene-dominant slags are far less common than their olivine-rich analogues and have been retrieved from the sites at Mramor Proni Butoçit (samples 10024(2) and 10024(5)), Akllap (12016(2)) and Ostri Vrh (13030(1)). An olivine + clinopyroxene-type slag has been only sampled at Akllap (12016(1)). In some olivine-type slags (11027(1) and 11027(2) from Mirash, 11029(5) from Mirash Novo), clinopyroxene together with spinel *ss* crystallises late in the solidification sequence. Clinopyroxene occurs as typically sub- to euhedral prismatic or rhomboidal grains with a length ranging from a few micrometres for late to some hundred micrometres for early crystallised specimens. A close association with spinel *ss* rhombs, which often are the centre of star-shaped early to late formed clinopyroxene aggregates, is typical (Fig. 9.5b). In reflected light microscopy, the grains possess a rather dark grey colour similar to the shade of the surrounding glass and often exihibit slight zoning with a somewhat brigher coloured rim (Fig. 9.5a). Since early as well as late formed clinopyroxene often is very fine grained (width $<<$ 20 µm; Fig. 9.5b; 9.6b), quantitative in situ analysis (one-by-one mode, focused beam) has been a rather challenging task and contamination by surrounding glass is assumed due to determined elevated K and Pb contents. K_2O- (2.15 wt %) and PbO-bearing (7.33 wt %) clinopyroxenes also have been reported

by Ettler et al. (2009c) from medieval slags. Indeed, the siliceous melts of Pb-Ag metallurgy are marked by the excess presence of Pb and K mainly introduced by ore and charcoal ash as well as liquefying furnace lining, respectively. However, the ionic radii of octahedrally coordinated Pb^{2+} (1.19 Å) and K^{+} (1.38 Å) are significantly larger than those of Na^{+} (1.02 Å) and Ca^{2+} (1.00 Å) occupying the M2 site in the clinopyroxene's generalised $M1M2T_2O_6$ formula (Morimoto, 1988) and thus actually violate the substitution law. To test whether the elevated K and Pb contents represent true values, the data has been compared to analyses of the surrounding glass. Due to considerable compositional overlap, several measurements of particularly late formed fine grained clinopyroxene had to be omitted from the examination. However, based on petrography, general chemistry and XRD analyses, identification as Ca-rich clinopyroxene has always been possible. Sample 11029(3) from Mirash Novo, a finger-shaped glassy slag, contains besides firstly precipitated magnetite-rich spinel *ss* an unidentified silicate phase, whose SiO_2, FeO and Al_2O_3 contents are somewhat comparable to those of the examined clinopyroxenes. However, its elevated PbO abundances (median 22.36 wt %) in conjunction with the comparably low Pb contents of the surrounding glass (median 8.93 wt %; chapter 9.2.10) indicate that this phase presumably is a Pb silicate compound, whose detected Fe and Al abundances (mainly) derive from analytical contamination by the glass. With the exclusion of one wollastonite analysis from sample 10024(2) from Mramor Proni Butoçit, the clinopyroxenes can be classified as hedenbergite or augite. While the slags 10024(5) as well as 13030(1) and 12016(2) exclusively contain hedenbergite and augite, respectively, in 12016(1) both types have been found. In sample 10024(2), hedenbergite and rare wollastonite are present. All clinopyroxenes are, regardless of their classification, marked by a zincian (0.01 to 0.14 apfu) and aluminian composition (0.15 to 0.35 apfu) and in samples 10024(5) and 13030(1) and partially 12016(1) are subsilicic (i.e. < 1.75 apfu; Morimoto, 1988). The presence of tetrahedrally coordinated Al accounts for the negative correlation between SiO_2 and Al_2O_3 ($R^2 = -0.44$). The amount of Fe^{3+} has been calculated if necessary to fully occupy the tetrahedral position according to the method described by Droop (1987) and yielded contents between 5.00 and 12.26 wt % Fe_2O_3 (ferrian clinopyroxene; samples 10024(5) and 12016(2)). The abundances of Fe_2O_3 correlate positively with those of Al_2O_3 ($R^2 = 0.64$), thus indicating the elevated presence of an esseneite compound [$CaFe^{3+}AlSiO_6$] in the clinopyroxene's chemistry. Important minor elements include MnO (0.45 to 2.27 wt %), Na_2O (0.07 to 0.17 wt %) - which typically only is abundant in ferrian grains but does not correlate with Fe_2O_3 - and TiO_2 (0.08 to 0.84 wt %). The abundances of TiO_2 and Al_2O_3 in agreement with Kushiro (1960) and Le Bas (1962) show a positive correlation to ensure charge balance ($R^2 = 0.41$). NiO has only been detected in slags from Akllap with an overall median abundance of 0.10 wt % and a maximum of 0.36 wt % in sample 12016(2). The contents of K_2O (maximum 0.77 wt %) and PbO (up to 2.23 wt %) determined as already mentioned supposedly derive from contamination by adjacent glass.

The consistently elevated Al contents generally are similar to the chemistry of clinopyroxenes naturally occurring in alkaline rocks types and reflect the SiO_2-undersaturated nature of the slag melt (Kushiro, 1960; Le Bas, 1962) and indicate elevated formation temperatures when compared to that of stoichiometric phases (Hezarkhani-Zolgharnian, 1995; and references therein). Abundant Fe^{3+} also generally points to crystallisation of the pyroxenes at high temperatures

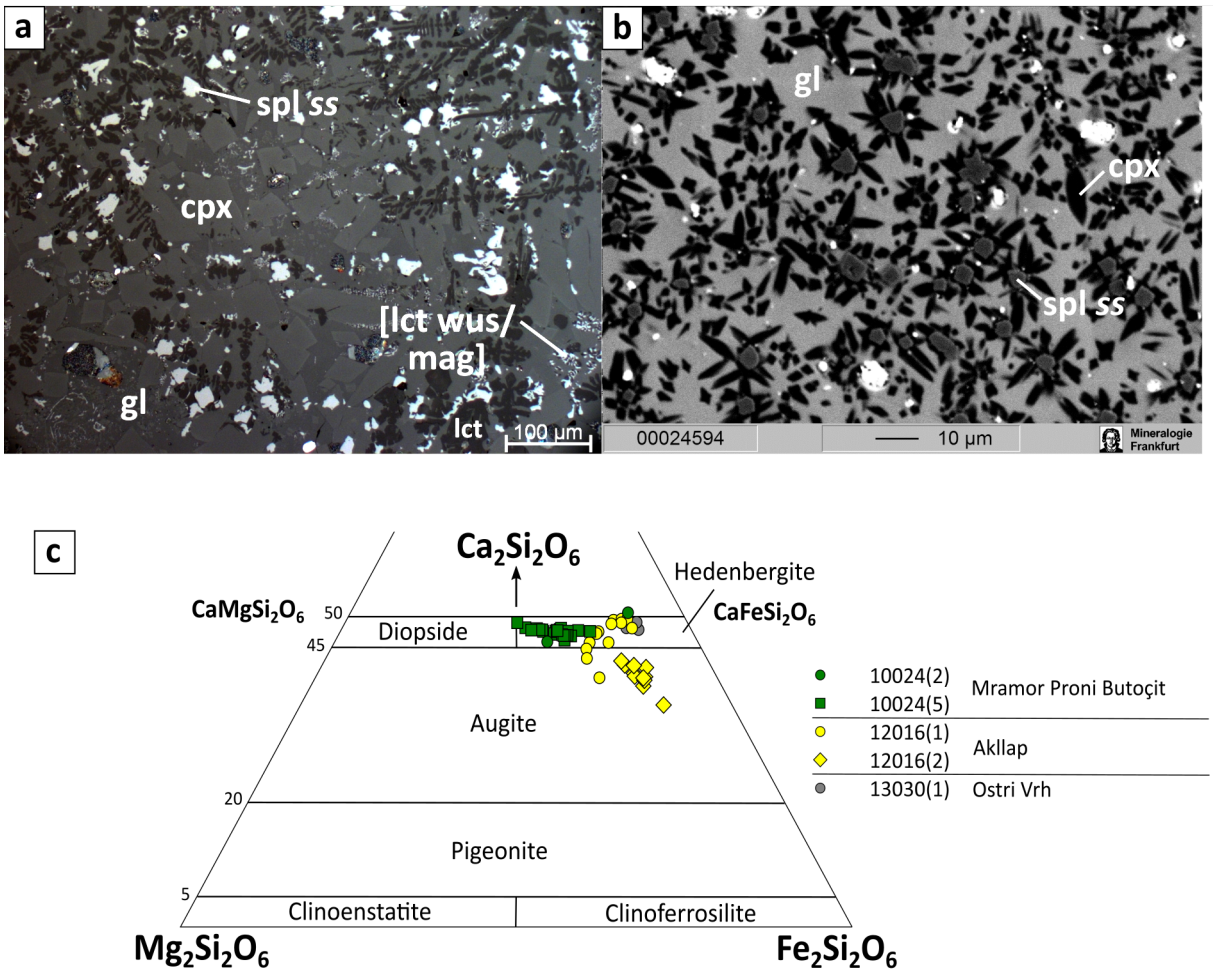

Figure 9.5.: a) Prismatic sub- to euhedral weakly zoned clinopyroxene grains are embedded in slightly darker glass, which furthermore contains skeletal spinel *ss* grains, dendritical leucite as well as a symplectite of leucite and an Fe-rich oxide phase, formerly probably wüstite, but now transformed to magnetite [sample 10024(5), Mramor Proni Butoçit, RL, PPL]. b) Prismatic clinopyroxenes are present as star-shaped aggregates centered on euhedral spinel *ss* rhombs [sample 13030(1), Ostri Vrh, BSE image]. c) Clinopyroxene compositions plotted in the quadrilateral $Mg_2Si_2O_6$ - $Fe_2Si_2O_6$ - $Ca_2Si_2O_6$.

and reflects rather oxidising conditions (Cosca & Peacor, 1987; Foit et al., 1987). The calculated tetrahedrally coordinated Fe^{3+} in samples 10024(5) and 12016(2) is similar to observations in artificially produced phases and points to rapid quenching (Cosca & Peacor, 1987).

9.2.3. Melilite [$(Ca,Na,K,Pb)_2(Al,Fe^{3+},Fe^{2+},Mg,Mn,Zn)(Si,Al)_2O_7$]

Melilite has been only observed in a sample from the Ostri Vrh site (13031(1)), where it occurs as rather broad (up to several ten micrometres wide) and large (up to a few hundred micrometres long) eu- to subhedral laths as the main phase together with kalsilite and spinel *ss.* Several grains typically are intergrown to form X- or star-shaped penetration aggregates (Fig. 9.6a). The melilite group phases chemically are approximately intermediate between hardystonite [$Ca_2ZnSi_2O_7$], gehlenite [$Ca_2Al_2SiO_7$] and impure (Fe-) åkermanite [$Ca_2(Fe,Mg)Si_2O_7$] with ZnO, Al_2O_3, MgO and FeO contents between 11.10 and 13.95 wt %, 3.04 and 5.45 wt %, 1.63 and 2.90 wt % and 2.26 and 4.03 wt %, respectively. Their SiO_2 and CaO abundances are in comparison to stoichiometric minerals notably depleted. Furthermore, the grains are marked by unusual Pb contents (8.97 to 15.91 wt %), thus yielding a median composition of $(Ca,Pb,Na,K)_{1.92}$ $(Mg,Mn,Fe^{2+},Zn,Al)_{1.03}(Si,Al)_2O_7$.
The determined high Pb abundances theoretically are not possible to substitute in the melilite structure due to largely differing ionic radii and, analogous to clinopyroxene, hence are thought to originate from contamination by nearby glass (cf. section 9.2.2). Additionally, the in comparison to the ideal chemistry depleted SiO_2 and CaO contents and the generally low calculated cation totals (4.91 to 4.97 apfu) indicate impairment of the measurements. Ettler et al. (2015) report Pb-bearing melilite (up to 7.00 wt % PbO) from slags associated with Ag refining which, however, are marked by cation sums exceeding 4.99 apfu. Since in contrast to clinopyroxenes the melilite phases actually possess grain sizes large enough for electron microprobe analysis, the poor quality of the data most likely is caused by insufficient thickness. Widening of the electron beam to a diameter of 5 µm and applying a beam current of 12 nA (analogous to the settings used for EMP measurements of foides and feldspars) proved to have no impact on the analyses. Therefore, the data could be only used to qualitatively identify the phase as a member of the melilite group.

9.2.4. Feldspar [$NaAlSi_3O_8$ - $CaAl_2Si_2O_8$ - $KAlSi_3O_8$]

Feldspar has been most prominently observed in a furnace slag sample from Mramor Samakove (10021(21)), where several laths are present in a glassy area together with leucite, olivine and droplets of base metal sulphide liquid. In basin slags in contrast, feldspar rarely occurs as a random accessory phase in samples from Voguçincë, Mirash Novo, Mramor Proni Butoçit, Akllap and Ostri Vrh (12015(7), 11029(5), 10024(2), 12016(1) and 13030(1)). It typically is present as fine needles and laths (several ten to less than ten micrometres wide; Fig. 9.6b) and more rarely as polyhedral grains, whose appearance then is somewhat similar to leucite.
In furnace slag, the analysed feldspars are classified as plagioclase possessing a composition intermediate between labradorite and bytownite (equivalent to $CaAl_2Si_2O_6$ contents between 66.4 and 87.3 mol %) with corresponding CaO and Na_2O abundances scattering between 13.65 and 17.62 wt % and 1.23 and 3.10 wt %, respectively. The K_2O contents do not exceed 1.10 wt %.

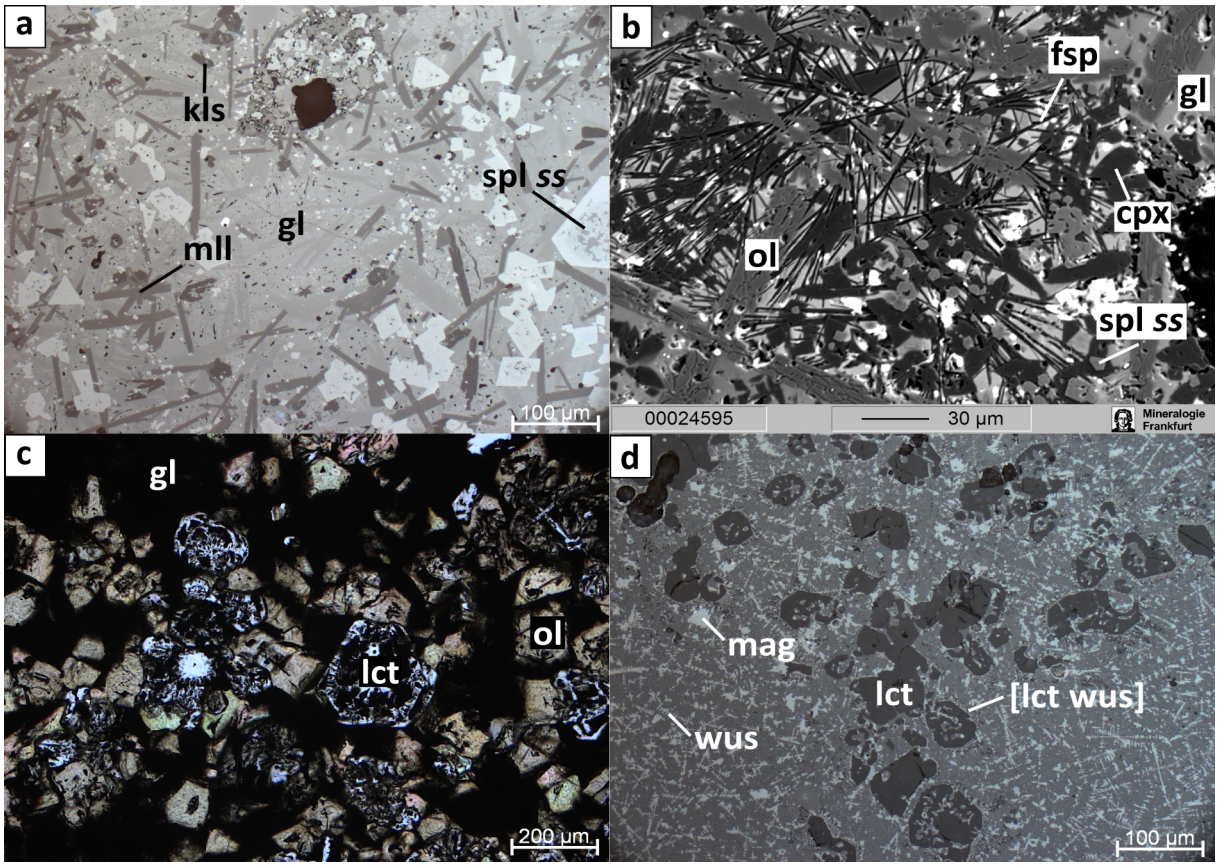

Figure 9.6.: a) Melilite laths (partially forming star-shaped aggregates) and kalsilite exhibiting granular or prismatic cross-sections as well as rhomboidal, often skeletal spinel *ss* are embedded in PbO-rich glass [sample 13031(1), Ostri Vrh, RL, PPL]. b) An area of a basin slag (sample 12016(1)) with a complex mineralogy comprises skeletal olivine, sub- to euhedral clinopyroxene, spinel *ss* grains and thin feldspar rods surrounded by PbO-rich glass (BSE image). c) Skeletal leucite grains and granular olivine are surrounded by glass [sample 12015(7), Voguçincë, TL, PPL]. d) Sub- to euhedral leucite grains, partially exhibiting skeletal growth, have presumably been generated by crystallisation of a segregated K-rich melt. Leucite also forms cotectoid intergrowths with wüstite, which mainly is present in dendritical form. Magnetite is slightly darker than wüstite and occurs subordinate. The matrix consists of fine-grained olivine and restitic glass [sample 3(2), Hanroc, RL, PPL].

Fe has been always detected and according to mineral formula recalculation substitutes for both Al and Si as Fe^{3+} with Fe_2O_3 contents between 2.67 and 3.53 wt %. In basin slags in contrast, only K-rich alkali feldspars have been observed, which exhibit K_2O and Na_2O abundances between 12.05 and 16.47 wt % and between 0.20 and 2.26 wt %, respectively. Ca only has been measured in one analysis which yielded 0.21 wt % CaO. Fe^{3+} is the only relevant impurity and substitutes Si and Al (see above) with Fe_2O_3 abundances ranging between 0.40 and 1.77 wt %.
The formation of feldspar in slags generally requires (locally) elevated Al contents in the partially inhomogenuous melt system. Liquefying furnace lining presumably has been the most important Al and potentially also Na source in furnace slags and hence offers an explanation for the increased abundance of plagioclase in these specimens. In basin slags in contrast, feldspar exclusively serves as a K carrier and thus partially replaces leucite.

9.2.5. Leucite [$KAlSi_2O_6$]

Leucite can be easily distinguished in the sections due to its characteristically low reflectivity. It always occurs as an- to subhedral grains commonly exhibiting skeletal growth (Fig. 9.6c). Leucite also has often been observed in symplectites with olivine or wüstite (e.g. Fig. 9.3f and 9.5a). The foid mostly apparently precipitates late in the solidification sequence of the slags. Some samples, however, indicate early crystallisation of this phase (Fig. 9.6d) and hence suggest silicate liquid immiscibility, which would also provide an explanation for the simultaneous occurrence of eutectoid intergrowths of leucite with olivine and wüstite (section 9.2.8), respectively. An extensive field of two coexisting melts is known from the thoroughly researched system leucite-SiO_2-fayalite (e.g. Visser & van Groos, 1976; Roedder, 1978) and, as Kronz (1997) already suggested, also must exist in leucite-fayalite-FeO space. The composition of leucite is almost stoichiometric, with Na_2O (0.07 to 1.44 wt %) and Fe_2O_3 (0.57 to 2.93 wt %) substituting K_2O and Al_2O_3, respectively, always being detected.

9.2.6. Kalsilite [$KAlSiO_4$]

Kalsilite has only been observed in a slag from Ostri Vrh, where it has been found together with a melilite-group phase (see above) and spinel *ss*. It is marked by a low reflectivity similar to that of leucite, but unlike the SiO_2-richer feldspathoid not only is present as typically subhedral grains with roughly hexagonal shape, but also as laths or with a prismatic cross-section often exhibiting skeletal growth. Similarly to leucite, the only impurities in kalsilite are Na_2O (0.22 to 0.44 wt %) and Fe_2O_3 (2.59 to 3.87 wt %). The width of the beam diameter and the beam current (i.e. 5 µm and 12 nA; analogous to the measurement setup used for leucite and feldspar) proved to have no detectable influence on the analysis of this phase.

9.2.7. Spinel *ss* [$(Fe^{2+},Mg,Mn,Ni,Zn)(Al,Fe^{3+},Cr,Ti)_2O_4$]

Spinel *ss* is, at least in accessory proportion, abundant in almost all slags investigated (Tab. 9.1). It is in some olivine- and all olivine + clinopyroxene-, clinopyroxene- and melilite-dominant types the first phase to crystallise and then typically has been observed as inclusions within olivine grains or in the centre of star-shaped clinopyroxene aggregates (see above). Some samples also

contain a second generation of extremely fine-grained (diameters of few micrometres) spinel *ss* in the glassy matrix. Close to the surface area of the slags, which usually consists exclusively of glass and Fe-rich oxides, the spinel *ss* grains typically exhibit skeletal growth or a 'surface tension' shape indicative of rapid cooling (Fig. 9.7b, d). Pseudomorphous replacement of dendritical wüstite by magnetite has been commonly observed in the uppermost slag areas (chapter 9.2.8; Fig. 9.7c). In lower slag areas, characteristic euhedral rhombs predominate. Pronounced zonation with a darker core and brighter rim has been regularly observed (Fig. 9.7a). Generally, the proportion of spinel *ss* increases from the surface to lower regions hence indicating gravitational segregation. Besides spinel *ss* formed during the smelting process, relictic grains, which are marked by a significantly larger size, smooth boundaries, reaction rim and a slightly different, i.e. brighter colour have been often observed (Fig. 9.7d). They are thought to originate from the serpentinite rocks partially hosting ore bodies in the study area and hence should be enriched in Cr and Mg. Presumably particularly magnetite-rich spinel *ss* also occurs in clusters with pyrrhotite (i.e. Fe oxide cluster; cf. chapter 10.1.3, Fig. 10.1h). The spinel *ss* compositions are enriched in Fe^{2+} (5.11 to 40.54 wt % FeO) and Zn (1.02 to 29.60 wt % ZnO) and can be mostly attributed to the magnetite (6.67 to 69.95 wt % Fe_2O_3) and spinel *ss* series (0.22 to 49.74 wt % Al_2O_3). The analyses thus have been plotted in an $Fe^{3+}/(Al+Fe^{3+})$ - $Zn/(Zn+Fe^{2+})$ binary (Fig. 9.8) with the end members $Fe^{2+}Al_2O_4$ (hercynite), $Fe^{2+}{Fe^{3+}}_2O_4$ (magnetite), $ZnAl_2O_4$ (gahnite) and $Zn{Fe^{3+}}_2O_4$ (franklinite). Magnetite typically predominates and is particularly abundant in clinopyroxene-type slags. Furthermore, spinel *ss* replacing wüstite due to elevated fO_2 (Fig. 9.7b, c) must be marked by a pure composition, but could be only scarcely analysed due to the small size of the grains.

Zoned spinel *ss* grains possess a darker core enriched in Al and Zn, while the brighter rim is marked by a higher abundance of Fe^{3+}. In the $Fe^{3+}/(Al+Fe^{3+})$ - $Zn/(Zn+Fe^{2+})$ diagram, these analyses hence compositionally trend from hercynite / gahnite towards magnetite (Fig. 9.7a; samples 10-1A, 12015(5) and (12)) due to limited solid solution between the spinel *ss* and magnetite series (Barnes & Roeder, 2001). The contents of ZnO and Al_2O_3 overall show a positive correlation ($R^2 = 0.43$). Samples containing particularly Zn-rich spinel *ss* (i.e. 12015(12), 10024(2), 12016(1) and 13031(1)) simultaneously comprise olivine and melilite, respectively, which are comparably enriched in Zn (cf. chapters 9.2.1 and 9.2.3). However, while data from the first-mentioned slags generally shows a trend towards higher Al and Zn proportions (see above), in the melilite-dominant sample 13031(1) the $Zn/(Zn+Fe^{2+})$ ratio is highly variable (0.3 to 0.8) in conjunction with rather consistent $Fe^{3+}/(Al+Fe^{3+})$ values (Fig. 9.8). Spinel *ss* analyses from the furnace slag sample 10021(2) are characterised by an elevated proportion of Al and Fe^{2+} and hence reflect the typically Al-richer composition thought to be related to liquefying furnace lining (cf. section 9.2.4) and the comparably low fO_2 under which these slags have been formed. Cr contents typically are low and rarely exceed 1 wt % in newly-formed spinel *ss*. Individual grains, however, may contain up to 24.27 wt % Cr_2O_3 (samples from Voguçincë, Mirash Novo, Mramor Proni Butoçit, Mramor Samakove, Akllap and Ostri Vrh). MgO always has been determined and scatters between 0.02 and 3.34 wt %. Ni has been detected in approximately half of the analyses (slags from Marec, Mramor Proni Butoçit, Mirash, Mirash Novo, Akllap, Voguçincë and Ostri Vrh) with a maximum content of 2.15 wt %. Cr and Mg, which both are highly compatible

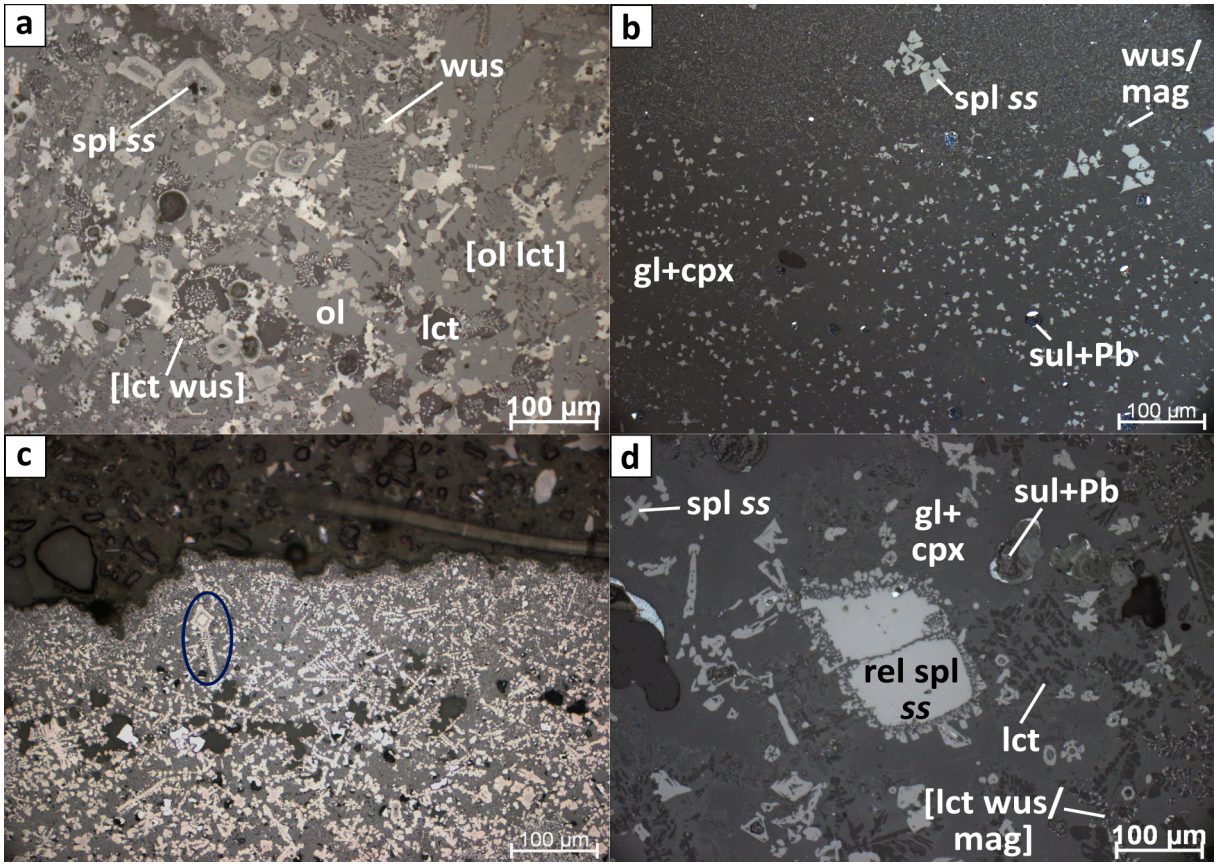

Figure 9.7.: a) Spinel *ss* rhombs show pronounced zoning with a darker, Al-richer core and a brighter coloured rim enriched in the magnetite component. Wüstite is present as interstitial dendrites with high reflectivity (significantly brighter than spinel *ss*) and also forms symplectites with leucite, which rarely also is seen in granular form. Olivine occurs as subhedral prismatic grains and as cotectoid intergrowths with leucite [sample 10-1A, Hajkobile, RL, PPL]. b) Early crystallised spinel *ss* grains mostly are euhedrally lozenge-shaped but often show prolonged tips (German 'Spitzenwachstum'), a phenomenon associated with rapid quenching. Small Fe oxide dendrites firstly have been precipitated as wüstite but now presumably have been completely transformed to magnetite due to increasing fO_2. The glass matrix hosts clinopyroxene grains and spherical droplets consisting of galena and native Pb [sample 10024(2), Mramor Proni Butoçit, RL, PPL]. c) Increasing fO_2 lead to transformation of initially precipitated wüstite (dendrites) to magnetite (typically lozenge-shaped grains). The encircled example shows replacement of wüstite by magnetite [sample 10-1A, Hajkobile, RL, PPL]. d) Relictic spinel *ss* is significantly larger and brighter-coloured than its newly-formed analogues, which often exhibit skeletal growth with the exception of euhedral rhombs nucleated at the rim of the older grains. Leucite is present as dendrites, partially containing symplectitic Fe-rich oxide (originally wüstite, now potentially transformed to magnetite). The slag matrix consists of minute, prismatic clinopyroxene grains and glass which often contains spherical droplets comprising base metal sulphide phases and native Pb [sample 10024(5), Mramor Proni Butoçit, RL, PPL].

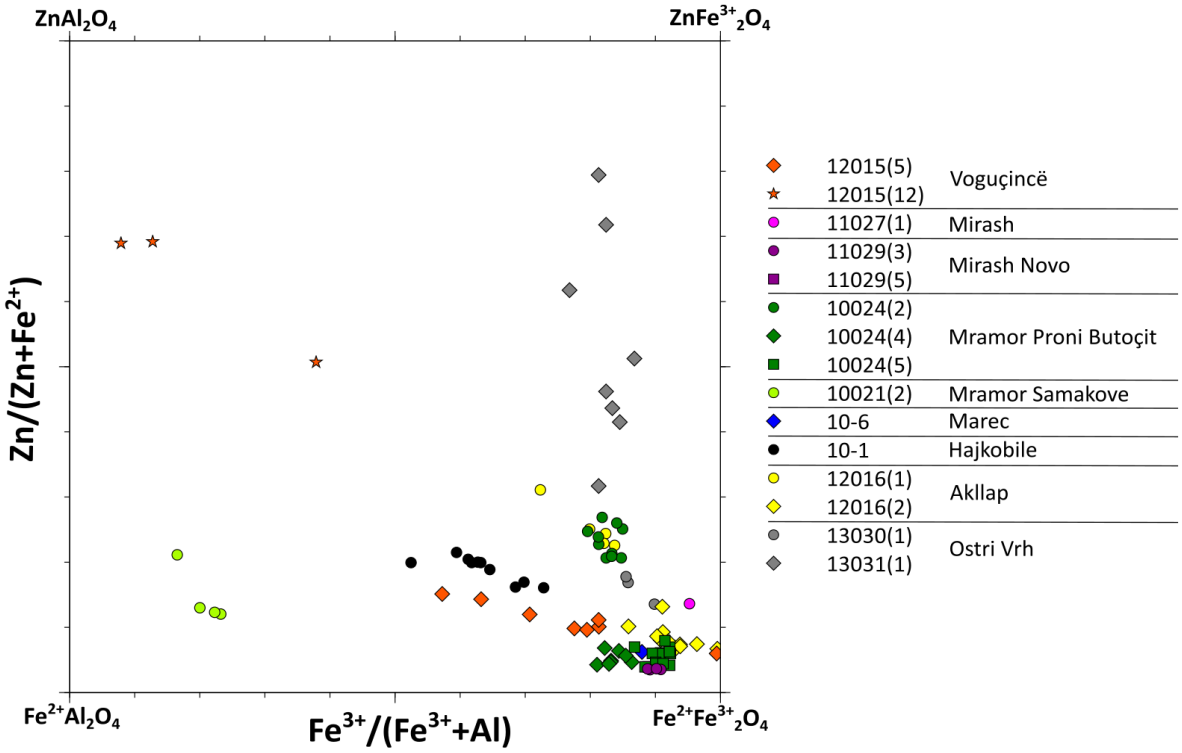

Figure 9.8.: Plot of spinel *ss* compositions in the $Fe^{3+}/(Fe^{3+}+Al)$ - $Zn/(Zn+Fe^{2+})$ binary diagram.

in spinel *ss*, in several samples (12015(5), 12015(12), 10021(2), 10-1A, 12016(1), 12016(2) and 13030(1)) from the sites at Voguçincë, Mramor Samakove, Hajkobile, Akllap and Ostri Vrh display a positive correlation (R^2 between 0.51 to 0.99), but rarely show any relation to Ni (with Mg in slags 12016(1) and 13031(1) and Cr in 12016(2), respectively). These observations are thought to be based on coupled introduction of Mg and Cr by relictic spinel *ss* derived from abundant serpentinite host rocks in the district of Shashkoc-Janjevo (discussed in detail in section 16.2). Spinel *ss* thus is a useful tool to document the influence of the deposit's barren rock and its contribution to the geochemical signature of the local mineralisation. Ni, although being typically enriched in ultrabasic rocks such as serpentinite, in contrast may also originate from the smelted ore (e.g. from pyrrhotite) and furthermore, unlike Mg and Cr, also partitions into speiss phases, e.g. NiSb abundant in sample 12016(2) from Akllap.

9.2.8. Wüstite [$Fe^{2+}_{1-x}O$]

Wüstite commonly occurs as dendrites or spheroids (Fig. 9.7a-c), which in basin slags mostly have been already replaced by magnetite (slightly darker and with a brownish tint under reflected light) due to increased fO_2. The diminished abundance of wüstite is reflected by XRD analyses, in which the phase only has been determined in the furnace slag 10021(2). However, in some samples wüstite has been microscopically observed to coexist with spinel *ss* (10024(2), 10021(2), 10-1A, 3(2)). Symplectitic intergrowths with leucite, particularly abundant in clinopyroxene-dominant slags, have been commonly observed (cf. Fig. 9.5a). Due to the different formation conditions – i.e. less oxidising compared to basin slags - wüstite generally is more abundant

in furnace slags, where the phase is present within symplectites with leucite or as interstitial spheroids (Fig. 9.9a).
FeO ranges between 84.50 and 98.55 wt % with corresponding apfu between 0.85 and 0.97, or, if the ZnO-rich analysis (see below) is excluded, between 94.62 and 98.55 wt % and 0.92 and 0.97 apfu, respectively, thus being in accordance with the non-stoichiometric compositional range ($0.12 < x < 0.04$) of the phase caused by its intermediate chemistry between pure FeO and magnetite (Hazen & Jeanloz, 1984). ZnO is an important constituent of the wüstite chemistry with abundances ranging from 0.46 to 13.08 wt % (median 1.03 wt %). Furthermore, MnO (0.18 to 0.36 wt %) and MgO (0.02 to 0.22 wt %) typically have been detected reflecting experimentally determined chemical variations (Degterov et al., 2001; Muan & Osborn, 1965). Al_2O_3 (0.20 to 1.82 wt %) and TiO_2 (0.06 to 1.31 wt %) are the most important impurities and are thought to derive from a non-exsolved spinel *ss* component, as proposed by Kronz (1997).

9.2.9. Iscorite [$Fe^{2+}{}_5Fe^{3+}{}_2SiO_{10}$]

Iscorite is an anthropogenic phase first described by Smuts et al. (1969) as a component of furnace material from a steel plant of the South African Iron and Steel Industrial Corporation (ISCOR). Due to its formation under conditions rarely found in nature - i.e. at high temperatures in Fe-rich, SiO_2-undersaturated oxidised melts – it only has been observed in metallurgical samples this far, where it is generated by reaction of wüstite and fayalite (Smuts, 1992) at fO_2 conditions of the magnetite stability field (Van Aken et al., 2005; cf. section 2.5.1). In accordance with its typical formation conditions, iscorite has been either observed close to the upper regions of slag layers, where it is present below a (former) wüstite-rich zone, or nearby vesicles and pores within the layers. It is a rather common phase, which occurs as euhedral, highly anisotropic thin (few micrometres wide) laths and needles forming a typical fabric (Fig. 9.9b, c). Due to its small width, iscorite has been difficult to analyse and data could be only obtained from two samples (10-1A and 3(2)). Several substitutions, mostly for Fe^{3+} and Fe^{2+}, have been found with ZnO, Al_2O_3 and MgO abundances ranging from 3.86 to 6.10 wt %, 2.61 to 3.04 wt % and 0.44 to 1.58 wt %, respectively. Elevated amounts of Zn apparently are typical for iscorites from Pb metallurgy and have also been described by Ströbele et al. (2010). Fe_2O_3 contents have been calculated (according to Droop, 1987) to scatter between 21.94 and 29.02 wt %. TiO_2, CaO and MnO are minor impurities with abundances typically being below 1 wt %.

9.2.10. Glass

Glass typically is opaque and of greyish to black colour due to the presence of fine interspersed metal and sulphide particulates as well as magnetite-dominant spinel *ss* phases. Only at slag areas which have reacted with the furnace lining and therefore are enriched in particularly SiO_2, the glass is translucent and appears brownish to ochre in transmitted light (Fig. 9.10a). Partially observed variations in reflectivity and colour, respectively, imply an inhomogeneous composition, which also might be influenced by interaction with abundant matte and speiss inclusions (Fig. 9.10b; cf. Rehren et al., 1999). Glass usually contains countless minute (dendritical) grains of olivine, spinel *ss* and late clinopyroxene (cf. Fig. 9.3b, d, f). The determined composition as already suspected on basis of microscopic examination is highly inhomogeneous and naturally

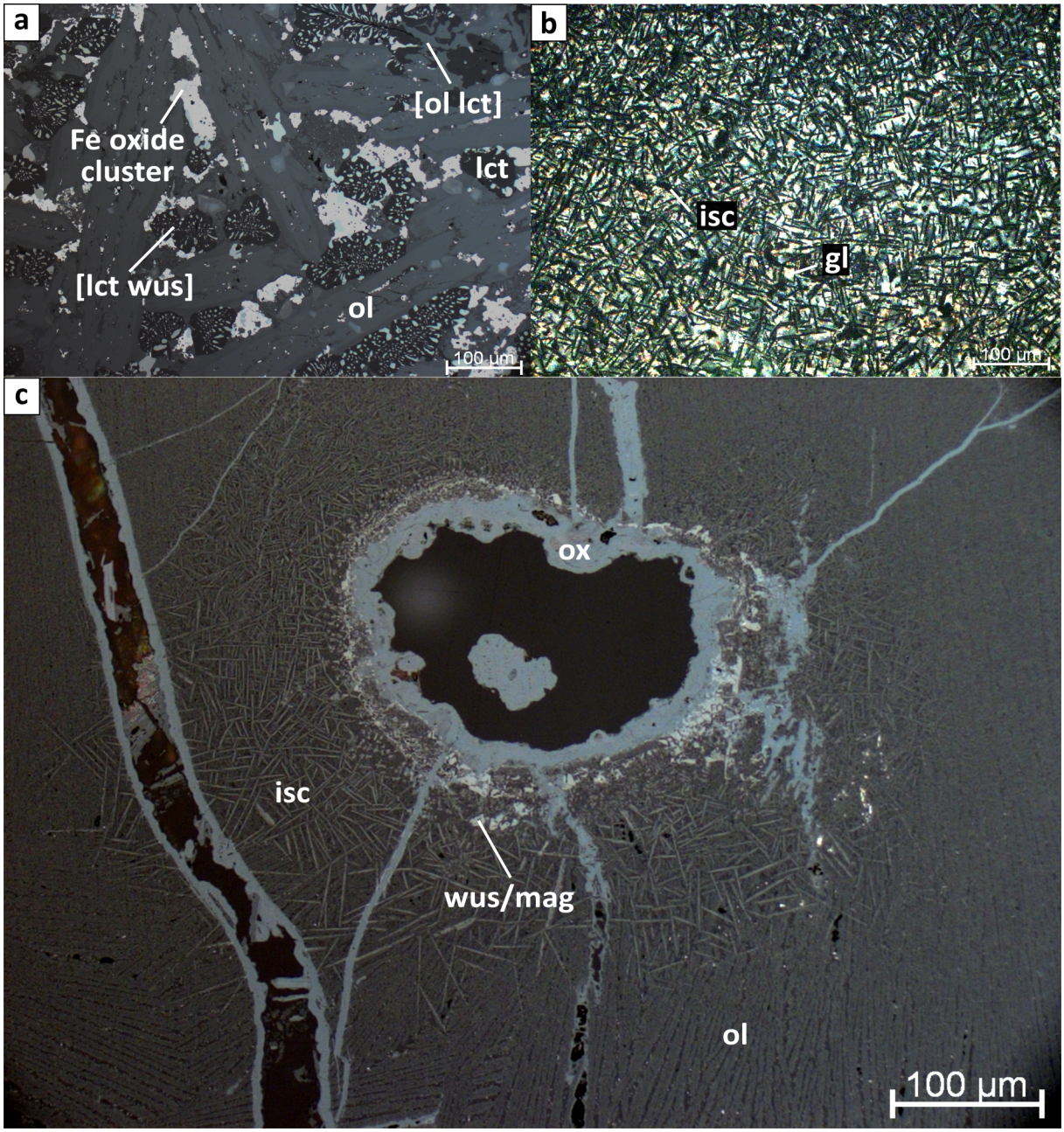

Figure 9.9.: a) Wüstite is present in symplectites with leucite, while Fe oxide cluster consist of magnetite-rich spinel *ss* and pyrrhotite. The sample furthermore comprises laths and prismatic grains of olivine, anhedral leucite and symplectites of olivine and leucite [sample 10021(2), RL, PPL]. b) Iscorite laths (black) forming a typical fabric are embedded in whitish glass [sample 10-1A, Hajkobile, RL, XPL]. c) A large vesicle in a basin slag is, as well as cracks within the slag matrix, rimmed by bluish-grey secondary Fe oxide and hydroxide phases. Close to the vesicle, a quenching layer comprising dendritic Fe-rich oxides (precipitated as wüstite, now presumably transformed to magnetite) and glass changes over to a zone with thin iscorite laths and glass. The iscorite zone passes into the olivine-dominant main zone of the slag [sample 11029(5), Mirash Novo, RL, PPL].

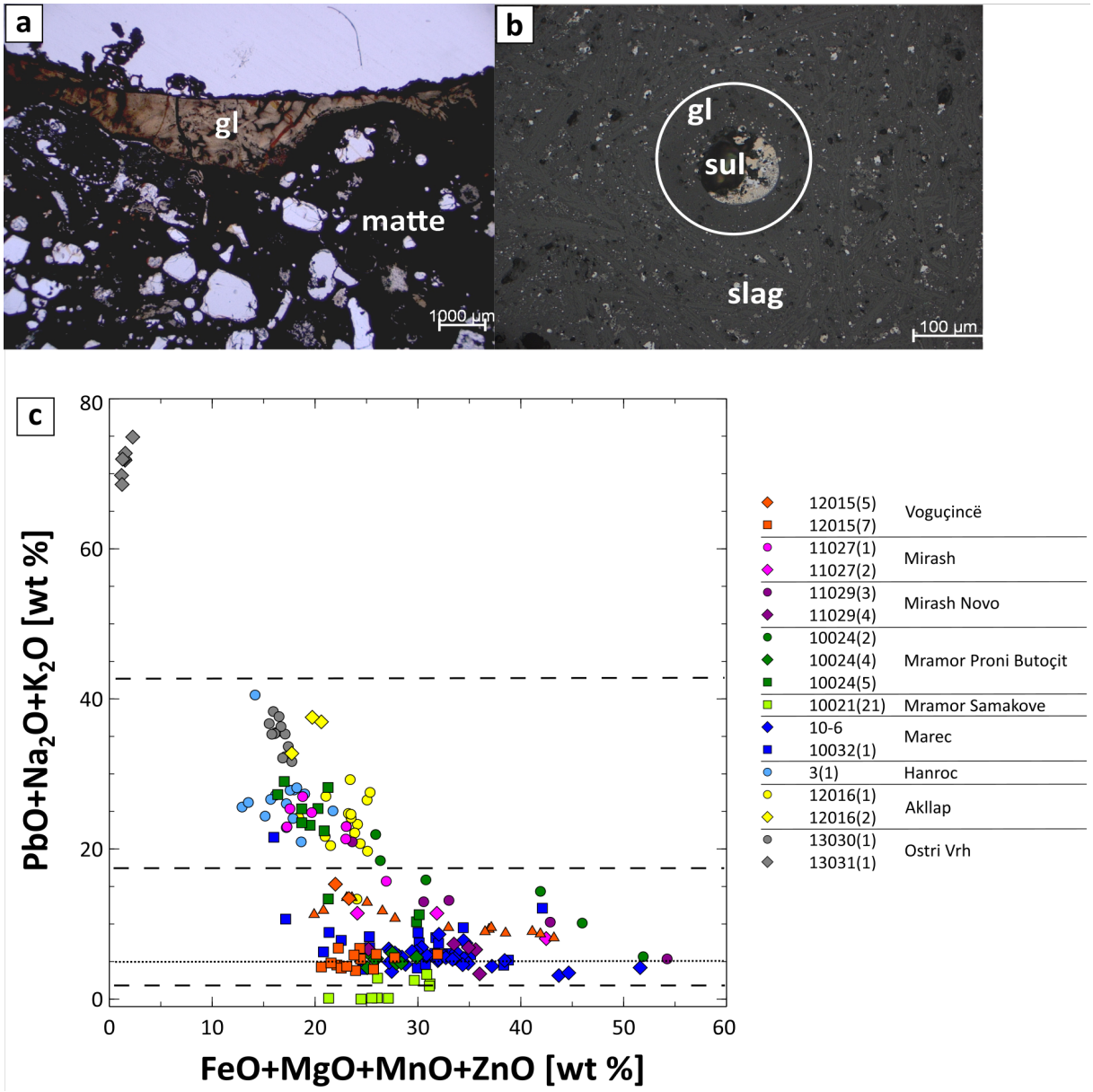

Figure 9.10.: a) Brownish, visibly inhomogeneous glass is present at the rim of a matte cake, presumably where the sulphide melt has been in contact with the furnace lining. The translucent phases below the glassy zone are silicates (mainly feldspar and SiO_2 phases, probably derived from furnace debris) surrounded by opaque matte sulphides [sample 10-1B, Hajkobile, TL, PPL]. b) A spherical inclusion of matte s.s. (comprising segregated pyrrhotite, (Zn,Fe)S, galena and symplectitic galena and bornite *ss*; cf. chapter 10.1) in slag is surrounded by a glass-rich halo [encircled; sample 12015(5), Voguçincë, RL, PPL]. c) Plot of $PbO + Na_2O + K_2O$ [wt %] versus $FeO + MgO + MnO + ZnO$ [wt %] abundances of glass analyses.

depends on the phase assemblage of the samples, which generally dictates the chemistry of the glass as restitic silicate liquid. External parameters such as furnace lining, but potentially also the presence of matte, speiss and Pb inclusions may further influence its composition (see above). Since the measurements necessarily must have been performed with focused beam due to the high abundance of small inclusions, possible artefacts such as Na and K evaporation (Siivola, 1969), but certainly also analytical contamination cannot be excluded and the data thus can only be used to state general trends.

The glass composition has been approached to characterise by comparison of the proportion of compatible and incompatible compounds, for which the abundances of FeO, MgO, MnO and ZnO and PbO, Na_2O and K_2O, respectively, have been utilised (Fig. 9.10c). Generally, olivine-dominant slags exhibit $PbO + Na_2O + K_2O$ contents below c. 17 wt % and form a cluster around approximately 5 wt %. Clinopyroxene-bearing samples typically possess $PbO + Na_2O + K_2O$ abundances between c. 17 and 42 wt %, while the melilite-dominant slag (13031(1)) is characterised by a significantly different and extremely PbO-rich composition ($>$ 65 wt %; see below). Data from sample 11029(3), a glassy slag, is characterised by comparably depleted $PbO + Na_2O + K_2O$ abundances, which are in accordance with the suspected exsolution of a Pb silicate phase from the glass (cf. section 9.2.2). Glass analysed in a furnace slag (10021(21)) not surprisingly is marked by very low $PbO + Na_2O + K_2O$ contents; most data points can be clearly distinguished from basin slag measurements.

The main components determined in glass are SiO_2 (27.79 to 50.18 wt %), CaO (1.67 to 29.50 wt %) and FeO (9.66 to 48.51 wt %). ZnO (0.61 to 14.17 wt %) and PbO (0.12 to 39.82 wt %) have been almost always detected. Additionally, glass typically concentrates incompatible elements such as Al_2O_3 (0.31 to 14.13 wt %), K_2O (0.02 to 4.40 wt %), Na_2O (0.07 to 4.68 wt %) and P_2O_5 (0.07 to 3.71 wt %). TiO_2, MnO and MgO typically are only minor impurities. The interstitial glass of the melilite-dominant slag (13031(1)) is marked by an unusually Pb-rich composition with PbO and SiO_2 contents ranging from 68.43 to 74.71 wt % and 14.85 and 18.95 wt %, respectively, and comparably low CaO (2.97 to 8.33 wt %) and FeO abundances (0.66 to 1.48 wt %).

9.3. Textures and phase assemblages of smithing slags

Unlike the two other sample groups (i.e. basin and furnace slags), smithing slags are not related to primary smelting and metal extraction, but indeed are waste material from the manufacturing and repairing of iron objects. Removed particles of the worked objects partially are visible in the slag matrix as hammerscale. Analogous to the other slag types, furnace lining and charcoal ash introduced mainly Al, Si, Ca and K into the melt system and lead to formation of e.g. leucite and feldspar phases. However, smithing slags can be clearly distinguished from their metallurgical analogues by the complete absence of sulphide compounds as well as metals with the exception of native Fe. It either is present in restitic form introduced by hammerscale or has been newly-formed by direct reduction of Fe oxides by charcoal. Generally, smithing slags possess a comparable silicate and oxide phase assemblage as metallurgical slags, but are marked by a particularly Fe-rich chemistry, which is expressed by the presence of fayalite-rich olivine, wüstite, magnetite-dominant spinel *ss* and native Fe as well as occasionally abundant

iscorite. All three analysed samples contain olivine, which occurs as skeletel laths or as eu- to subhedral grains in areas with a slowlier cooling regime. It has been identified by XRD as fayalite (Fig. 9.11c, d). Partially two generations of olivine are present. Later-formed grains typically possess a dendritical shape and exhibit a slightly darker colour in reflected light (Fig. 9.11d). In specimen 10041 from Shashkoc (the only one containing leucite) olivine forms symplectites with the feldspathoid, which in turn also occurs in eutectoid intergrowths with wüstite (Fig. 9.11b, c, d). Wüstite is highly common in all three smithing slags and occurs as spheroids and dendrites (Fig. 9.11a), which partially show evidence for the exsolution of spinel *ss* droplets. Hammerscale (Fig. 9.11b) is completely made up of the Fe oxide. Relictic droplets of primary Fe may be dispersed within these aggregates. The metal also has been observed enclosed in olivine or the glassy silicate matrix. Its abundance nearby charcoal points to formation due to direct reduction of Fe oxide phases. Magnetite-rich spinel *ss* is present in all investigated samples, but occurs subordinate compared to wüstite. The grains mostly possess a typical lozenge-shaped cross-section (Fig. 9.11a). Iscorite has only been observed in sample 12059(8) from Ulpiana, where it is present as lamellar laths closely associated with spinel *ss* (Fig. 9.11a). Silicate phases introduced by e.g. liquefying furnace construction material identified by XRD in an impure smithing slag (12059(4)) are anorthite, quartz and tetragonal cristobalite. Typical secondary phases are goethite and hematite.

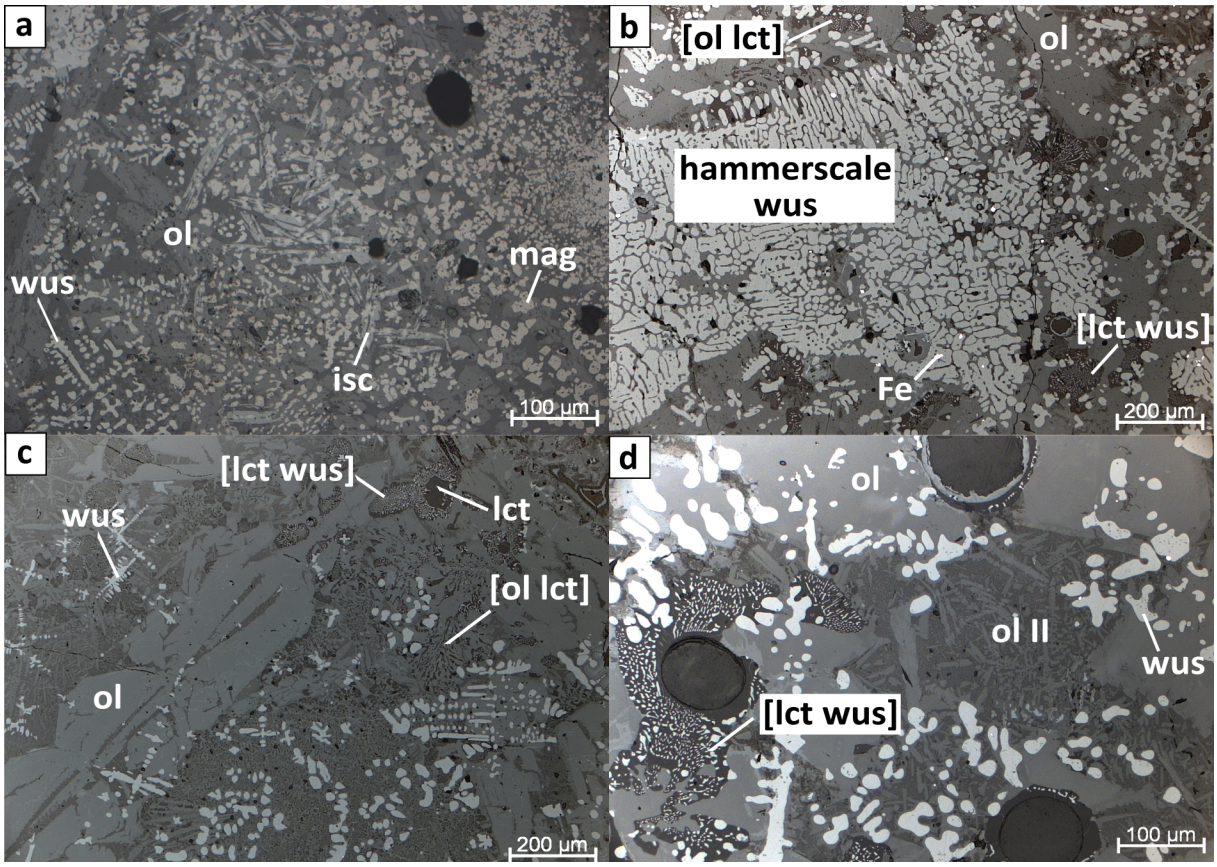

Figure 9.11.: a) A smithing slag comprises several Fe-bearing phases, namely dendritical wüstite, laths of iscorite, rhombs of magnetite-rich spinel *ss* and granular olivine [sample 12059(8), Ulpiana, RL, PPL]. b) A large aggregate of hammerscale consisting of dendritical wüstite besides few droplets of native Fe is seen in a smithing slag, which furthermore contains granular olivine and eutectoid intergrowths of olivine and leucite and leucite and wüstite, respectively [sample 10041, Shashkoc, RL, PPL]. c) H-chain laths of olivine partially are overgrown by dendrites of wüstite. Leucite is present in granular form, but also as symplectites with wüstite and olivine [sample 10041, Shashkoc, RL, PPL]. d) Olivine occurs as eu- to subhedral grains and as later-formed dendrites surrounded by glass. Wüstite is abundant as irregular-shaped spheroids and within eutectoid intergrowths with leucite [sample 10041, Shashkoc, RL, PPL].

10. Matte

Matte as sulphide melt is a typical metallurgical by-product in base metal smelting, which might have been deliberately produced in ancient treatment of polymetallic Pb ores in order to avoid the formation of Cu-bearing crude Pb, whose subsequent treatment (e.g. cupellation) would have been impeded by its notably raised liquidus temperature (cf. section 2.5.2). Matte consists of a mixture of base metal sulphides (mostly Cu, Fe, Pb and Zn compounds) and possesses a specific gravity between approximately 5 and 7 g/cm³. It hence accumulates between slag and speiss or crude Pb, respectively. In the investigated samples, it occurs as four different types: as spherical inclusions, interstitial clusters, Pb-Cu matte and matte sensu stricto (s.s.), the only type that has been sampled in the form of cakes.

10.1. Petrography of matte types

10.1.1. Smelting residues

The petrography and phase assemblage of smelting residues represents an intermediate stage between beneficiated ore submitted to the furnace and matte. It hence allows a direct glimpse of the type and composition of furnace feed. The most commonly observed type of smelting residue are grains of galena, often with cubic cross-section and smoothened grain boundaries due to the impact of heat applied during metallurgical treatment. A particularly large-sized (diameter of a few millimetres), roundish inclusion with a rather complex phase assemblage, which posseses a rim entirely composed of sphalerite and a core mainly made up of galena besides minor sphalerite, pyrrhotite and covellite (Fig. 10.1a, b), has been found in a basin slag from the site at Ostri Vrh (13030(1)).

10.1.2. Spherical inclusions in slag

Spherical sulphide inclusions are the most common type of matte and have been observed in all sampled slags. The droplets commonly possess a diameter between 10 and 50 µm and are particularly abundant in slag types, in which olivine is not the dominant silicate phase. The spheroids mostly are purely made up of galena (Fig. 10.1c); although droplets with segregated galena, or more rarely bornite *ss* embedded in a symplectite of galena and bornite *ss* are present as well (Fig. 10.1d). Segregated galena as well as bornite *ss* possess a round or oval shape. Particularly Cu-rich inclusions consisting of galena and Cu-(Fe) sulphides (e.g. chalcocite *ss*, bornite and chalcocite exsolved from bornite *ss*[1]) are petrographically analogous (Fig. 10.1e).(Zn,Fe)S[2] has

[1] Exsolutions are denoted as 'phase A : phase B' (cf. Kronz, 1997)

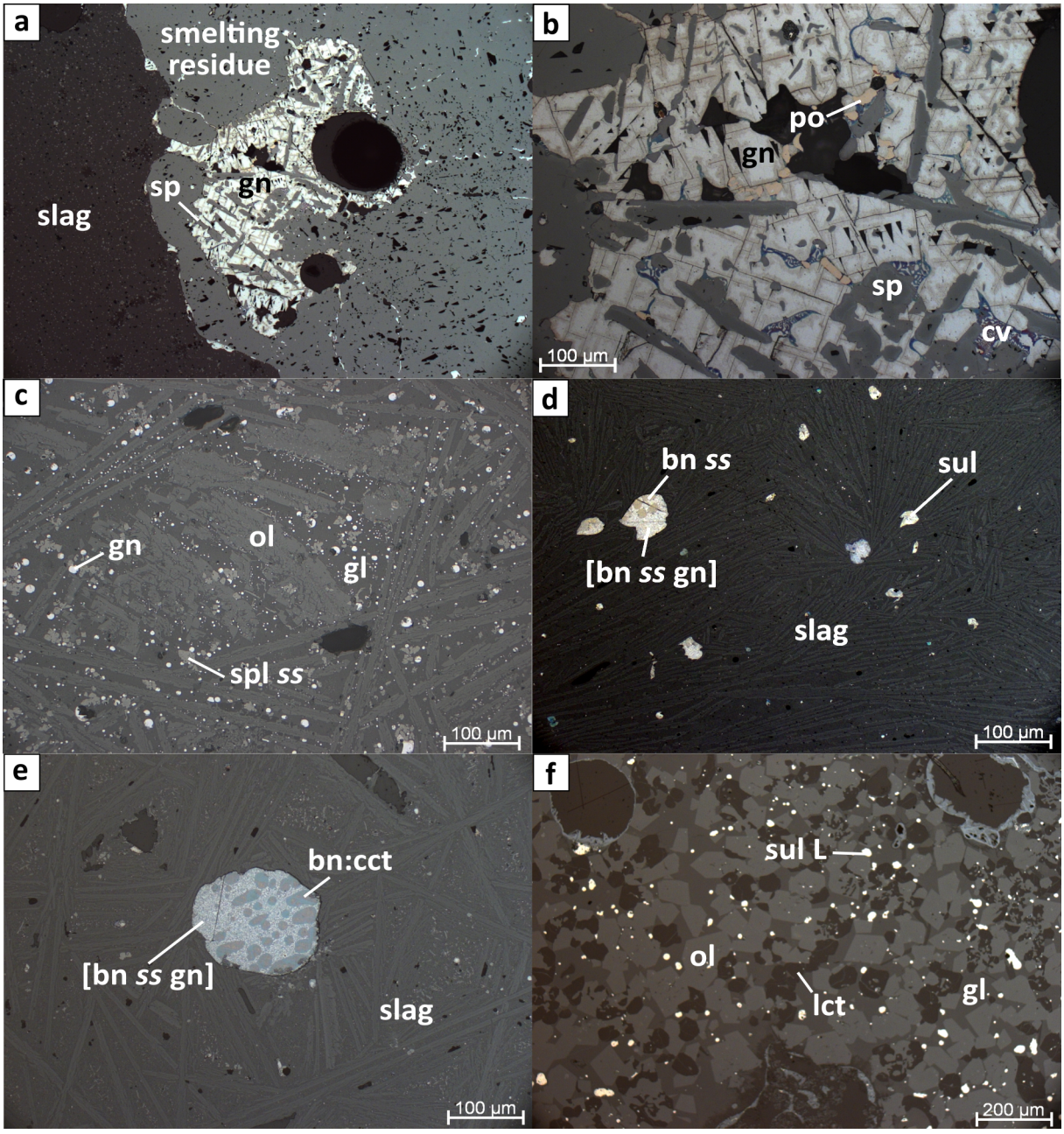
a
smelting residue
sp
gn
slag
b
po
gn
sp
cv
100 µm
c
gn
ol
gl
spl ss
100 µm
d
bn ss
sul
[bn ss gn]
slag
100 µm
e
bn:cct
[bn ss gn]
slag
100 µm
f
sul L
ol
lct
gl
200 µm

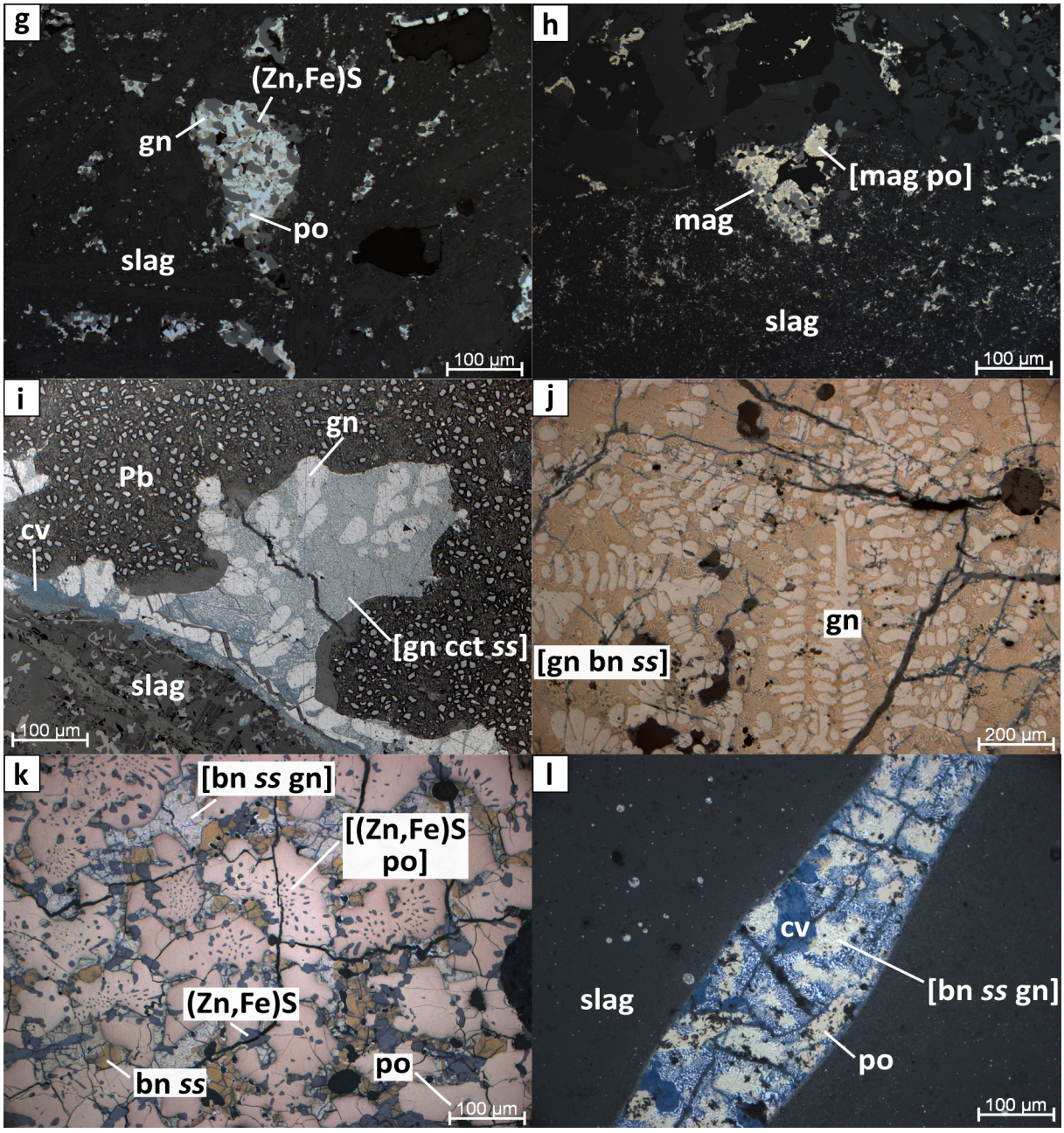
g
(Zn,Fe)S
gn
po
slag
100 µm
h
[mag po]
mag
slag
100 µm
i
gn
Pb
cv
[gn cct ss]
slag
100 µm
j
gn
[gn bn ss]
200 µm
k
[bn ss gn]
[(Zn,Fe)S po]
(Zn,Fe)S
bn ss
po
100 µm
l
cv
slag
[bn ss gn]
po
100 µm

Figure 10.1.: a) Overview of a large-sized smelting residue enclosed in a basin slag. The rim solely is made up of sphalerite, while the core area mostly consists of galena [sample 13030(1), Ostri Vrh, RL, PPL]. b) Detail of the core area of Fig. 10.1a comprising mainly galena besides sphalerite and subordinate pyrrhotite and covellite [sample 13030(1), Ostri Vrh, RL, PPL]. c) Numerous Pb sulphide blebs are enclosed in the glass matrix of a basin slag, which furthermore comprises olivine and spinel *ss* [sample 12015(5), Voguçincë, RL, PPL]. d) Multiphase sulphide droplets enclosed in the slag matrix are mainly made up of segregated bornite *ss*, which is surrounded by symplectitic bornite *ss* and galena [sample 11027(1), Mirash, RL, PPL]. e) A Cu-rich droplet consists of segregated Cu-(Fe) sulphides, i.e. chalcocite exsolved from bornite *ss* (optically similar to stoichiometric bornite), which are surrounded by a symplectite of exsolved Cu-(Fe) sulphides and galena [sample 11029(5), Mirash Novo, RL, PPL]. f) Numerous droplets of base metal sulphide liquid are trapped in the glassy matrix of a furnace slag, which furthermore comprises olivine and leucite [sample 10021(21), Mramor Samakove, RL, PPL]. g) An interstitial sulphide cluster comprises pyrrhotite and (Zn,Fe)S embedded in galena [sample 10032(1), Marec, RL, PPL]. h) An Fe oxide cluster contains segregated magnetite, which is surrounded by a symplectitic intergrowth of magnetite and pyrrhotite [sample 10021(2), Mramor Samakove, RL, PPL]. i) Pb-Cu matte is sharply separated from slag and consists of segregated galena embedded in a symplectitic intergrowth of galena and chalcocite *ss* (cf. Craig & Kullerud, 1968). Covellite is thought to be of secondary origin. The matte has exsolved from a huge droplet of native Pb, which is widely covered by polishing dust [sample 10024(5), Mramor Proni Butoçit, RL, PPL]. j) Matte s.s comprises segregated droplets and dendritical galena surrounded by a symplectitic intergrowth of galena and bornite *ss* with the latter being incipiently weathered to covellite (indigo blue) [sample 11029(3), Mirash Novo, RL, PPL]. k) Symplectitic intergrowths of pyrrhotite and (Zn,Fe)S as well as segregated grains of pyrrhotite, (Zn,Fe)S and bornite *ss* are embedded by a eutectoid of galena and bornite *ss* [sample 10-1B, Hajkobile, RL, PPL]. l) In a veinlet of matte s.s present within a slag layer, both segregated as well as symplectitic bornite *ss* (intergrown with galena) are severely weathered to covellite [sample 11027(1), Mirash, RL, PPL].

been observed to occur as monophase droplets, segregated in association with galena or embedded in a symplectitic intergrowth of galena and bornite *ss*. The Cu-Fe sulphide phase intermediate solid solution (iss; Cabri, 1973) has only been found in a multiphase droplet with galena, ferrous and base metal speiss (see chapter 11). Numerous spherical inclusions of pyrrhotite and base metal sulphide melt optically rather similar to the Fe sulphide are present in the glassy matrix of the two samples from Mramor Samakove (Fig. 10.1f).

10.1.3. Interstitial cluster

Sulphide cluster

Interstitial sulphide cluster possess a size from a few ten to several hundred micrometres and are abundant in basin slags from the sites at Voguçincë and Marec (samples 12015(5), 12015(7), 12015(12), 10-6 and 10032(1)). Their anhedral, roughly rectangular or ovoid shape is dictated by the interstice they occupy. The clusters always comprise galena and (Zn,Fe)S and - with one exception from Voguçincë (12015(12)) - also pyrrhotite (Fig. 10.1g). (Zn,Fe)S and pyrrhotite occur as anhedral vermicular grains or droplets with (Zn,Fe)S also often being present as small rods. Pyrrhotite and (Zn,Fe)S are partially or completely embedded within galena, which commonly is the main phase in these clusters. The Pb sulphide may be euhedral and often shows cubic cleavage typical for its naturally occurring analogue.

Fe oxide cluster

A slag sample from Mramor Samakove (10021(2)) contains besides droplets of base metal sulphide melt also a specific subtype of interstitial clusters, which comprise pyrrhotite and magnetite-rich spinel *ss*. Their size is comparable to those of sulphide clusters and scatters between a few ten to several hundred micrometres. The clusters comprise segregated droplets or anhedral grains of magnetite-rich spinel *ss* surrounded by a symplectitic intergrowth of pyrrhotite and magnetite (Fig. 10.1h; 9.9a).

10.1.4. Pb-Cu matte

Pb-Cu matte either is abundant as droplets within slag (diameters between 50 and 200 µm) or, most common, as rim (partially reaching sizes of several hundred micrometres) around native Pb. Due to its association with native Pb, Pb-Cu matte has been observed in several samples (12015(5), 11027(1), 11029(5), 10024(5), 12016(1), 13030(1) and 13031(1)). It contains droplets of segregated galena surrounded by a symplectitic intergrowth of galena and chalcocite *ss*; covellite is thought to be of secondary origin (Fig. 10.1i).

10.1.5. Matte sensu stricto (s.s.)

Matte s.s. occurs as veins and spherical inclusions (several hundred micrometres in size) within the slag matrix, as cakes (millimetre- to centimetre-scaled) between and beneath slag layers or

[2]Zn-Fe sulphides present in matte exhibit a wide range of compositions (Fig. 10.2) between almost pure ZnS and Fe-rich Zn sulphide, which is chemically similar to rudashevskyite described by Britvin et al. (2008). Therefore, the general denomination (Zn,Fe)S is used for these phases.

as small platy lumps (maximum width and height 5 and 3 cm, respectively). With the exception of Hajkobile (sample 10-1B) and the not yet dated site of Mramor Proni Butoçit (10024(4)), matte s.s. has only been retrieved from smelting sites with a preliminary Roman or late antique dating, i.e. Voguçincë (10-2B, 12015(5) and 14032), Mirash (11027(1) and 11027(2)) and Mirash Novo (11029(1), 11029(3) and 11029(5)). Inclusions of matte s.s. can be distinguished from spherical inclusions in slag (see above) by their considerably bigger size and more complex phase assemblage, which always comprises pyrrhotite and partially also (Zn,Fe)S and iss besides galena and bornite *ss*. In general, the proportions of Fe-Zn- (i.e. pyrrhotite and (Zn,Fe)S) and Pb-Cu-rich components (galena and bornite *ss*) seem to be negatively correlated (Fig. 10.1j, k).
All phases are present as rarely dendritical or vermicular grains or as spheroids, respectively, and are surrounded by a myrmecitic intergrowth of galena and bornite *ss*. Segregated galena and bornite *ss* do not occur together on microscale, but matte s.s. containing grains of galena or bornite *ss* have been found within one sample section. Besides its presence as anhedral grains or droplets, pyrrhotite with hexagonal cross-section has been rarely observed. Symplectites of pyrrhotite and subordinate (Zn,Fe)S are present in some of the investigated specimens of matte s.s. (Fig. 10.1k). (Zn,Fe)S often possesses a needle-like shape, similar to its occurrence within sulphide clusters (Fig. 10.1g). Rarely, the phase has been observed enclosed in pyrrhotite grains. Bornite *ss* and chalcocite *ss* can be partially or rarely even completely replaced by covellite, which is thought to be of secondary origin (Fig. 10.1i, j, l). The presence of bornite and chalcocite in symplectites with galena in contrast seems to be indicative of low-temperature breakdown of the Cu-Fe sulphide solid solution (Fig. 10.1e; see chapter 10.2.4). Segregated bornite *ss* often shows exsolution lamellae of an apparently metal-richer phase possessing a brighter colour in BSE images (cf. Fig. 10.3b; section 10.3). Iss has been scarcely observed as segregated grains within matte patches.

10.2. Geochemistry of matte phases

10.2.1. Pyrrhotite

The main element composition of pyrrhotite is rather consistent in the differing phase assemblages. Data from Fe oxide clusters unfortunately must have been excluded due to analytical contamination. Fe is slightly enriched in interstitial spherical droplets of a furnace slag (10021(21)) from Mramor Samakove (60.97 to 61.89 wt %; median 61.66 wt %) while the Fe abundances of pyrrhotite in sulphide clusters (59.00 to 62.16 wt %) and matte s.s. (58.76 to 62.12 wt %) typically are more variable, but exhibit virtually identical median contents (61.09 wt % and 61.07 wt %). Pyrrhotite always is cupriferous, with Cu abundances in sulphide clusters and spherical inclusions ranging from 0.43 to 1.00 wt % and 0.59 to 0.83 wt %, respectively. The highest contents (0.74 to 3.31 wt %), however, generally have been determined in matte s.s. Pyrrhotite is an important host for Co with median contents scattering around 0.11 wt % and to a lesser extent Ni, resulting in median abundances of 0.04 wt % and 0.09 wt % in sulphide cluster and matte s.s., respectively. In interstitial droplets in contrast, the Ni contents typically are below the detection limit (i.e. $<$ 140 ppm). Other elements detected include Mn, Cd and Sb.

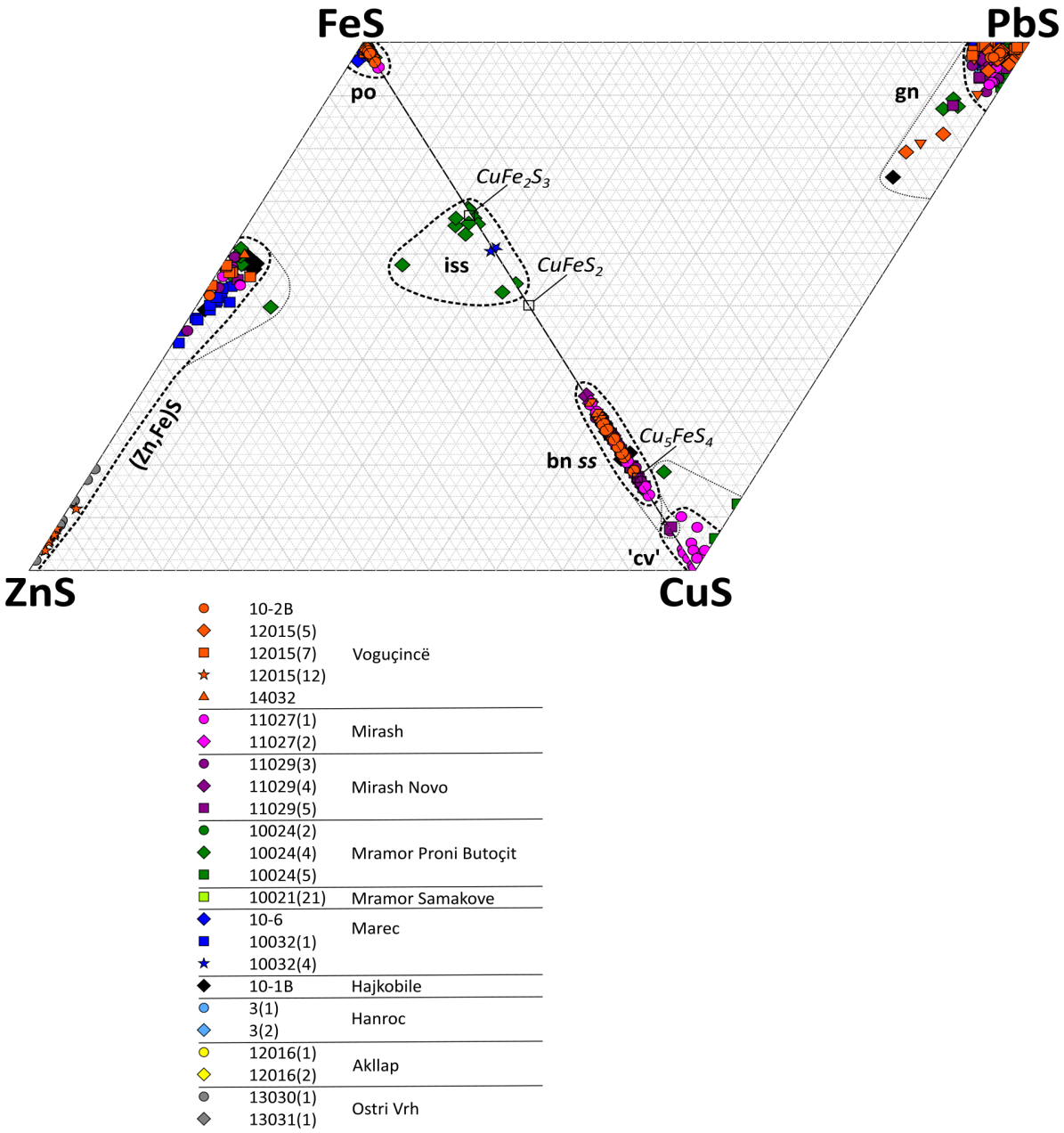

Figure 10.2.: Compositions of matte sulphides plotted in the ZnS - CuS - FeS and PbS - FeS - CuS ternary systems. 'Phase fields' including the majority of the data points are delineated boldly, while those also comprising outliers are drawn with thinner lines. Analyses of base metal sulphide melt have not been displayed since they typically cannot be compositionally distinguished from pyrrhotite in ZnS - CuS - FeS - PbS space. Stoichiometric compositions of cubanite ($CuFe_2S_3$), chalcopyrite ($CuFeS_2$) and bornite (Cu_5FeS_4) are indicated.

10.2.2. (Zn,Fe)S

(Zn,Fe)S is chemically highly variable and displays a wide range of Fe contents. In the ZnS - CuS - FeS ternary, the obtained analyses form two clusters (Fig. 10.2). Zn-rich compositions are characterised by FeS abundances below c. 20 mol % (1.9 to 19.2 mol % FeS) and thus overlap with data of sphalerite from the local ore (chapter 8.2.1). Zn-rich (Zn,Fe)S is abundant in a large-scaled inclusion of a smelting residue (sample 13030(1); see above) as well as spherical droplets and pyrrhotite-free sulphide cluster (both solely observed in sample 12015(12)). The cluster of Fe-rich (Zn,Fe)S extends from c. 43.1 to 61.1 mol % FeS and comprises significantly more analyses, which have been obtained from interstitial droplets, pyrrhotite-bearing cluster and matte s.s. The solubility limit of FeS in ZnS depends on the S fugacity and reaches a maximum extent of 52 mol % at conditions of the Fe/FeS buffer at 700 °C (Lepetit et al., 2003). The Fe-rich (Zn,Fe)S analyses thus partially exceed these experimentally determined solubilities, but agree very well with data of rudashevskyite (i.e. the Fe-rich analogue of (Zn,Fe)S, containing between 0.54 and 0.69 apfu Fe) given by Britvin et al. (2008). Rudashevskyite has been already described in slags of Pb-Zn metallurgy (Warchulski et al., 2015). Thus Zn-Fe sulphide, which precipitated from the solidifying matte melt and often cannot be unambiguously classified as Fe-rich sphalerite or rudashevskyite, is denominated as (Zn,Fe)S. Analyses from the smelting residue in contrast still preserve an ore-like composition (see above) and consequently have been identified as sphalerite.

Data from the rim of the smelting residue which consists of sphalerite and inclusions of galena shows a 'pristine', Zn-rich composition, which is marked by low Fe (1.07 to 4.94 wt %, corresponding FeS abundances between 1.9 and 8.8 mol %) and abundant Cd contents (0.18 to 0.26 wt %). Cu typically could not have been detected. Sphalerite from the core of the smelting residue, which also comprises a high proportion of galena accompanied by accessory pyrrhotite and covellite, exhibits elevated Cu (0.06 to 0.16 wt %) and Fe (4.83 to 10.73 wt %, corresponding FeS abundances between 8.6 and 19.2 mol %) as well as somewhat lower Cd contents (0.15 to 0.23 wt %). Hence, sphalerite analyses from the core are thought to record beginning geochemical effects of heat treatment due to metallurgical processing of the ore. This hypothesis is in accordance with the more versatile phase assemblage of the central area (galena, pyrrhotite and covellite), which allowed chemical exchange reactions between the different sulphide phases (cf. Fig. 10.1a, b).

(Zn,Fe)S precipitated from the solidifying matte melt and found to occur within droplets, sulphide clusters and matte s.s. generally is characterised by a different geochemical signature with strongly elevated Cu (and partially Fe) contents in conjunction with depleted Cd abundances. Mn is the only minor element which has been consistently determined in the different matte types. (Zn,Fe)S present in spherical inclusions within the slag matrix is chemically highly variable and partially distinctly cupriferous with Fe and Cu contents between 2.13 to 31.97 wt % and 0.04 to 7.38 wt %, respectively, and FeS abundances between 3.7 and 56.1 mol %. The composition of (Zn,Fe)S in sulphide clusters obviously is influenced by the fact whether pyrrhotite - which can be considered as a relative measure for the FeS activity of the sulphide melt (see above) - is present or not. (Zn,Fe)S from pyrrhotite-bearing sulphide clusters is significantly enriched in Fe (25.12 to 33.99 wt %; FeS contents between 43.1 and 57.9 mol %). Elevated Cu

abundances (0.22 to 3.55 wt %) are assumed to be related to the absence of a Cu-rich phase, thus leading to increased substitution in Fe-(Zn) sulphides. The composition of (Zn,Fe)S from pyrrhotite-free cluster in contrast is marked by notably lower Fe abundances (2.13 to 6.62 wt %, FeS between 3.7 and 11.7 mol %), which overlap with the range determined in natural analogues within the local ore, but is depleted in Cd ($\leq$ 770 ppm). The Cu contents generally are lower (0.05 to 0.78 wt %) when compared to other matte types. (Zn,Fe)S grains analysed in matte s.s. are significantly depleted in Zn with Fe contents ranging between 26.08 and 36.09 wt % (corresponding FeS between 45.5 and 61.1 mol %). Cu is strongly enriched and scatters between 0.65 and 3.51 wt %. Partially notable amounts of Mn have been detected (0.03 to 1.80 wt %).

10.2.3. Galena

Analysis of galena from matte phase assemblages has been impeded with elevated totals mostly scattering around 103 wt %. Unfortunately, this problem against all efforts could not be resolved and the data thus has been normalised to 100 wt % for better comparison. Cu as well as Fe have been detected in the vast majority of the analysed Pb sulphides. High Cu contents of up to 11.5 wt % have been described for natural galena formed at low temperatures under supergene conditions (Clark & Sillitoe, 1971). Fe in contrast actually is only slightly soluble in galena (Blackburn & Schwendeman, 1977). In galena artificially formed during metallurgical operations, however, Cu is the most common element substituting Pb; Fe as well has been frequently observed (e.g. Ettler et al., 2009a; b; c; Navarro et al., 2008; Piatak et al., 2004) with maximum abundances of 11.16 and 7.07 wt %, respectively. The highest Cu and Fe contents in this study have been observed nearby (Cu)-Fe-bearing phases (particularly pyrrhotite and bornite *ss*) in sulphide clusters and matte s.s. Consequently, although the determined abundances are far lower than the highest described in the literature, analytical contamination cannot be excluded. Zn contents may be prominent and at least partially might reflect mixed analyses. Common minor elements are Mn, Cd and Sb, whose abundances seem to be mostly unrelated to the petrographic occurrence. Ag regardless of the matte type typically is not detectable (i.e. $<$ 350 ppm). Exclusions are pyrrhotite-bearing sulphide clusters from sample 10032(1), in which partially abundances of 0.03 to 0.15 wt % have been determined; Ag similarly to late-ore stage galena (cf. chapter 8.2.1) correlates positively with Sb ($R^2 = 0.67$). In mostly monophase galena droplets of a slag from Hanroc (3(1)), Ag has always been detected (0.03 to 0.51 wt %) and exhibits a vaguely positive correlation with Cu ($R^2 = 0.45$). In sample 11029(5), Ag sporadically has been analysed in spherical inclusions in the slag matrix; no correlation though was observable.
Differences between the galena composition determined in analyses from the rim and core of smelting residues is not as conspicuous as those of (Zn,Fe)S. Cu and Fe contents in the rim scatter between 0.34 and 0.55 wt % and 0.05 and 0.19 wt % and range in the core from 0.28 to 1.17 wt % and 0.03 to 0.32 wt %, respectively. Comparably elevated Zn abundances determined in the exterior portion of the smelting residue (0.24 to 1.13 wt % versus 0.05 to 0.36 wt % in the core) might also be caused by the presence of sphalerite micro-inclusions. Minor amounts of Mn, Cd and Sb have been determined. Interestingly, Ag could not have been detected. Apart from Zn, no striking differences between core and rim are evident. However, both rim and core compositions are markedly different from ore galena analysed (i.e. higher Cu, not detectable Ag

and lowered Sb contents) and hence are, analogous to (Zn,Fe)S, assumed to reflect metallurgical processing rather than notable chemical variations of the Pb sulphide. Galena in spherical inclusions is marked by rather high Cu and Fe (0.03 to 2.04 wt % and 0.14 to 1.94 wt %, respectively) as well as abundant Zn contents (median 0.26 wt %, 0.04 to 1.27 wt %), generally thought to either record elevated Cu, Fe and Zn abundances of the sulphide melt or analytical contamination resulting from fine-grained intergrowths with other sulphide phases (see above). Pb sulphide in pyrrhotite-bearing sulphide clusters is marked by generally lower Cu and Zn in conjunction with higher Fe contents (0.06 to 0.71 wt %, 0.07 to 1.15 wt % and 0.04 to 1.94 wt %; median 0.21 wt %, 0.45 wt % and 1.38 wt %, respectively) compared to clusters without pyrrhotite being present (0.36 to 0.60 wt %, 0.59 to 1.22 wt % and 0.46 to 0.96 wt %; median 0.58 wt %, 1.09 wt % and 0.78 wt %, respectively). Galena segregates within Pb-Cu matte exsolved from a large droplet of native Pb could be only analysed in a slag sample from Mramor Proni Butoçit (10024(5)). They are characterised by elevated Cu contents ranging between 0.46 and 2.39 wt % and typically not detectable Fe and Zn abundances (i.e. $<$ 330 and $<$ 340 ppm, respectively). Since As virtually is insoluble in the galena structure, the determined values (0.02 to 0.14 wt %) probably result from the presence of minute speiss inclusions. Significant chemical differences exist between segregated and eutectoid galena from matte s.s. with the symplectites being marked by highly elevated Cu and Fe abundances (1.27 to 8.60 wt % and 0.31 to 2.32 wt %) in comparison to segregated grains (0.21 to 1.37 wt % and 0.08 to 0.82 wt %, respectively). Although these values are not exceedingly high (see above), they are due to the fine intergrowth suspected to have been most likely derived from contamination by adjacent bornite *ss*. The Zn contents are depleted and mostly below the detection limit, i.e. $<$ 390 ppm in segregated and $<$ 480 ppm in eutectoid galena.

10.2.4. Bornite *ss*

The composition of bornite *ss* from different matte types generally overlaps (Fig. 10.3a) with data mostly plotting in the field of $Cu_5FeS_4 + CuFeS_2$ (established at temperatures below 875 °C) or close to stoichiometric bornite, hence overall rendering it considerably Fe-richer than the naturally occurring mineral. Few analyses are marked by strongly elevated Cu abundances and attributed to the field of $Cu_5FeS_4 + Cu_2S$ appearing at temperatures below approximately 700 °C (Schlegel & Schüller, 1952). Low-temperature breakdown of bornite *ss*, as indicated by the two-phase fields bornite and chalcopyrite and bornite and chalcocite, respectively, being established with decreasing temperatures is recorded by XRD measurements, which determined chalcopyrite and bornite in matte cakes (samples 11029(3) and 10-2B) comprising optically homogeneous bornite *ss*. Segregated grains in matte s.s. exhibit the largest chemical variability with Cu and Fe contents scattering between 45.33 and 69.29 wt % (median 51.68 wt %) and 5.15 and 19.11 wt % (median 16.15 wt %), respectively. Furthermore, they are marked by a pronounced minor element signature with Mn, Co, As, Cd and Sb having been regularly detected. The Ag contents (0.04 to 0.50 wt %) show considerable scatter with a median abundance of 0.15 wt %. Elemental mapping of a segregated grain of Cu_5FeS_4 *ss* with abundant exsolution lamellae (Fig. 10.3b, c) revealed enrichment of Cu along with lower Fe and S contents in the lamellae, thus suggesting a composition closer to that of stoichiometric bornite. Symplectitic bornite *ss* is characterised by

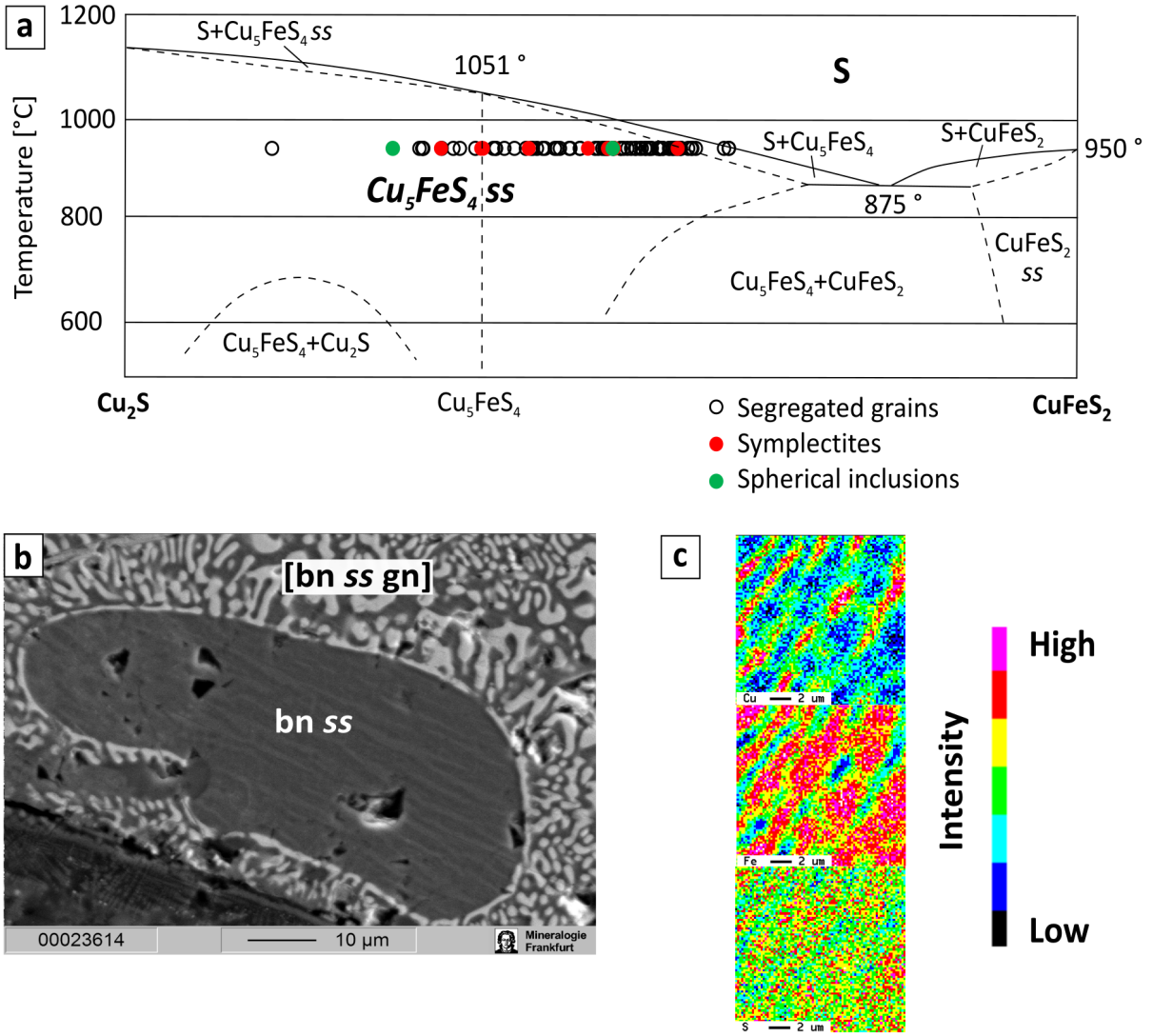

Figure 10.3.: a) Composition of spherical inclusions, segregated grains and symplectites of bornite *ss* plotted in the Cu_2S - $CuFeS_2$ binary diagram (redrawn after Schlegel & Schüller, 1952). b) A segregated droplet of bornite *ss* possesses subtle parallel exsolution lamellae of a Cu-richer phase (brighter grey) and is surrounded by a symplectite of bornite *ss* and galena [sample 11027(1), Mirash, RL, PPL]. c) Element maps display the relative abundances of Cu, Fe and S in a grain of bornite *ss* exhibiting exsolution lamellae, which are marked by higher Cu and lower Fe and S contents [sample 11027(1), Mirash].

higher median Cu (median 54.22 wt %; 50.08 to 60.49 wt %) and corresponding lower Fe contents (median 13.99 wt %; 10.61 to 17.99 wt %). The minor element signature overall is comparable to that of segregated grains. The Ag abundances exhibit a narrower range (0.04 to 0.25 wt %) and a higher median content of 0.19 wt %. The determined Pb abundances of up to 2.63 wt % partially are significantly higher than those of segregated bornite *ss* ($\leq$ 0.82 wt %) and are thought to be caused by contamination from intimately intergrown galena. Only two analyses of bornite *ss* in spherical inclusions have been possible. Their composition is marked by rather high Cu (52.46 and 63.75 wt %) and low Fe abundances (9.21 and 15.87 wt %). Ag (0.05 and 0.61 wt %) is the only significant impurity detected.

10.2.5. Intermediate solid solution (iss)

Iss grains in matte s.s. have been only observed in sample 10024(4) and exhibit Fe, Cu and Zn abundances between 31.29 and 40.07 wt %, 18.48 and 30.09 wt % and 0.82 and 10.62 wt %, respectively. Elevated Zn contents are permitted by the sphalerite-like structure of this phase (Cabri, 1973) and are highly positively correlated with Mn abundances (0.13 to 0.28 wt %; $R^2 = 0.96$). While Co and Ni have always been determined, two analyses revealed Ag contents of 0.15 wt % and 0.59 wt %, which otherwise are below the detection limit (i.e. $<$ 160 ppm). Only one analysis of iss segregated within a spherical inclusion in slag could be carried out, which yielded Fe, Cu and Zn contents of 35.60 wt %, 26.08 wt % and 0.36 wt %, respectively. Its minor element signature generally is depleted in comparison to iss in matte s.s., which could be explained by the fact that the droplet contains the speiss compounds FeAs and Cu_2Sb as well as galena preferentially incorporating e.g. Cd and Ni.

10.2.6. Covellite

Secondary CuS in Pb-Cu matte shows elevated Pb contents (11.49 wt % and 22.20 wt %) apparently resulting from contamination by adjacent galena and native Pb. In conjunction with the determined Cu (47.85 wt % and 57.28 wt %) and As abundances (0.50 wt % and 1.34 wt %), they yield a median composition of $Cu_{1.02}Pb_{0.10}As_{0.02}S$. Besides notable Ag contents (0.26 wt % and 0.28 wt %), Sb and Cd have always been detected.

The analyses of secondary CuS in matte s.s. apparently have been affected by the presence of nearby Fe- and Pb-bearing phases (i.e. particularly pyrrhotite, bornite *ss* and galena) resulting in Fe and Pb contents determined between 0.29 and 7.73 wt % and 2.59 and 9.05 wt %, respectively. The Cu abundances scatter between 50.89 and 64.84 wt %, resulting in a median composition of $Cu_{0.98}Fe_{0.03}Pb_{0.02}S$. With the exception of Ag, whose contents are remarkable with abundances between 0.14 and 0.37 wt %, covellite found in matte s.s. is rather devoid of minor elements, which seem to be irregularly distributed in this phase.

10.2.7. Base metal sulphide melt

Droplets of base metal sulphide melt have been solely observed within slags from Mramor Samakove (mainly in sample 10021(21), subordinate in 10021(2)) and generally are Fe-dominated with contents between 40.09 and 62.15 wt %. Other base metals present include Pb (2.41 to

13.11 wt %), Zn (0.05 to 20.79 wt %) and Cu (0.46 to 3.19 wt %). A broad array of minor elements has been determined, of which the elevated abundances of Sn (0.07 to 0.74 wt %) are most notable. Other impurities present are Mn and Co as well as in most analyses Cd and Sb.

10.2.8. Fe-rich oxide

Fe-rich oxide phases, presumably magnetite, have been observed within matte s.s. (samples 10-1B and 10024(4)) as well as in cluster with pyrrhotite (sample 10021(2)). Their composition is irrespective of the petrographic occurrence and rather pure with low MnO, ZnO and CuO contents (mostly $<<$ 1 wt %) as the most relevant minor elements. Al_2O_3 and MgO have not been analysed due to utilisation of the measurement setup Cuprico2 designed for sulphides, alloys and metals.

10.3. Solidification sequences of matte

The solidification sequences of the different matte types have been retraced based on petrography and experimentally determined phase equilibria. However, the composition of the cooling sulphide liquid might be far more complex than the binary, ternary or quaternary diagrams utilised to describe its crystallisation path. Due to the locally pronounced polymetallic character of the ore, the melt might also include minor components such as Ag, As and Sb, but potentially also e.g. Au, Bi, Hg, Se, Sn, Tl and Te. Minor compounds in the liquid such as this group of low-melting chalcophile elements (Frost et al., 2002), but also components of the fluid phase (e.g. CO_2, SO_2 and H_2O) as well as sulphur and oxygen fugacities (Tomkins et al., 2007) might (notably) influence the solidification behaviour of the sulphide melt. However, the impact of these factors could not have been fully comprehended yet and thus largely remains a speculative issue (Frost et al., 2002; Spry et al., 2008; Tomkins et al., 2007). Generally, the addition of components to a system typically will lower the melting point of the phase assemblage. The temperatures outlined below thus should be considered as conservative estimates.

10.3.1. Interstitial sulphide clusters

Petrographic evidence suggests that pyrrhotite and (Zn,Fe)S crystallised at similar temperatures (Fig. 10.1g), even though pure ZnS possesses a considerably higher melting point (1680 °C; Friedrich, 1907) than pyrrhotite (1190 °C for $Fe_{0.92}S$: Dutrizac, 1980; 1188 °C: Kullerud, 1953). However, the solidification temperature of (Zn,Fe)S potentially might be notably decreased by the presence of minor impurities and generally also is lowered with increasing Fe contents (Kullerud, 1953). Furthermore, furnace temperatures in ancient metallurgy typically are estimated to range between approximately 1150 and 1300 °C (e.g. Hauptmann, 2014; Manasse & Mellini, 2002a; b), hence allowing virtually simultaneous crystallisation of the two sulphide phases. This is followed by the precipitation of PbS, which occurs at 1115 °C in the pure Pb-S system (Dutrizac, 1980; Kullerud, 1969). However, abundant Cu contents (up to 0.71 wt %) potentially might lower its precipitation temperature, as proposed by Ettler et al. (2009b). The solidification of sulphide clusters theoretically ends at 1050° C with the binary eutectic of PbS and ZnS or at 850 °C, which is the temperature of the ternary eutectic in the system $Fe_{0.92}S$ - PbS - ZnS (Dutrizac, 1980).

The formation temperature of Fe oxide clusters consisting of myrmecitic intergrowths of magnetite and pyrrhotite (Fig. 10.1h) has been shown to depend on the Fe content of the sulphide phase and hence scatters between 934 and 1050 °C corresponding to 62.8 and 60.5 wt % Fe in pyrrhotite (Naldrett, 1969). Since analyses of pyrrhotite in Fe oxide clusters severely suffer from analytical contamination and thus had to be omitted from the examination, this temperature range cannot be narrowed down further.

10.3.2. Pb-Cu matte

Metal- (< 2 wt % S) and sulphide-rich liquids (containing 20 to 26 wt % S at the Cu - S and 9 to 27 wt % S at the Pb - S join) besides a S-rich melt are already established in the system Pb - Cu - S at 1130 °C (Craig & Kullerud, 1968) and thus allow early segregation of later Pb-Cu matte and native Pb (Fig. 10.1i). Cu_2S and PbS become stable at virtually identical temperatures, at 1129 and 1115 °C, respectively. Eutectoid intergrowths of galena and chalcocite-digenite *ss* are formed at 523 °C (Craig & Kullerud, 1968).

10.3.3. Matte s.s.

The solidification of matte s.s. begins analogous to interstitial sulphide clusters with the presumably nearly simultaneous crystallisation of pyrrhotite and (Zn,Fe)S around 1200 °C (see above; Dutrizac, 1980; Kullerud, 1953). Rarely observed inclusions of (Zn,Fe)S in pyrrhotite imply that (Zn,Fe)S at least partially segregated before the Fe sulphide. Symplectitic intergrowths of pyrrhotite and (Zn,Fe)S observed in some samples are interpreted as the product of eutectoid crystallisation which occurs at 1170 °C and 5 mol % ZnS in the system FeS - ZnS (Kullerud, 1953) and at 1178 °C and 10 mol % ZnS in the system $Fe_{0.92}S$ - ZnS (Dutrizac, 1980), respectively (cf. Fig. 10.1k). Their precipitation impoverishes the remaining melt in Zn and Fe, which hence becomes more enriched in Pb and Cu. Depending on the amount of Pb or Cu and Fe present in the restitic liquid, galena or the Cu-Fe sulphide bornite *ss* will precipitate from this melt (Fig. 10.1j).

Based on the composition of the segregated Cu_5FeS_4 *ss*, the formation temperatures are estimated to approximately range between 950 and 1100 °C (Fig. 10.3a), while PbS precipitates at 1115 °C (e.g. Craig & Kullerud, 1968; Dutrizac, 1980; Kullerud, 1969). The fact that matte s.s. with segregated PbS or Cu_5FeS_4 *ss*, respectively, has been observed within single samples points to a heterogeneous character of the sulphide liquid and thus suggests rapid cooling. At temperatures below 875 °C rather Cu-poor bornite *ss* breaks down to bornite and chalcopyrite (Schlegel & Schüller, 1952). X-ray diffractograms of samples containing optically homogeneous bornite showing reflexes of bornite and chalcopyrite prove this mechanism (cf. chapter 10.2.4). The determined CuS abundances, however, point to maximum decomposition temperatures slightly exceeding 800 °C and partially suggest significantly lower temperatures (Fig. 10.3a). The exsolution lamellae of a Cu-richer, but Fe- and S-poorer phase also are attributed to breakdown of bornite *ss* with decreasing temperatures and are interpreted to be chemically more similar to stoichiometric bornite, while the host phase should be compositionally closer to chalcopyrite (cf. Fig. 10.3b, c; chapter 10.2.4). Particularly Cu-rich bornite *ss* in contrast should disintegrate into bornite and chalcocite (cf. Fig. 10.1e) below temperatures of approximately 700 °C. The Cu

and Fe contents of several data points, however, analogous to the breakdown of Fe-richer bornite *ss* partially indicate notably lower temperatures. The rarely observed iss phase becomes stable at 960 °C (Kullerud et al. 1969). Its scarce occurrence might be attributed to the depletion of the sulphide melt in Fe as well as Cu and Zn after the precipitation of pyrrhotite, (Zn,Fe)S and bornite *ss*, thus largely impeding its formation. Simultaneous precipitation of galena and bornite *ss* (Fig. 10.1j) at the experimentally determined temperature of 609 °C (Craig & Kullerud, 1967) ends the solidification sequence of matte s.s.

11. Speiss and pig iron

11.1. Ferrous speiss

Ferrous speiss either has been sampled directly as heavily weathered lumps or indirectly within basin slags or scarcely matte s.s., particularly at the site at Mirash Novo, but also at Voguçincë and Marec. Sample 11029(7) from Mirash Novo is a platy piece of ferrous speiss, which consists of irregular, roundish segregated grains of Fe_9As embedded in a myrmecitic intergrowth of Fe_9As and Fe_2As (Fig. 11.1a). The speiss layer situated at the bottom of a layer of a slag sample (11029(4), Mirash Novo; Fig. 11.1b) comprises euhedral laths of Fe_2As surrounded by a heavily weathered symplectite of Fe_2As and presumably (arsenical) Fe. Furthermore, few exsolved grains of FeAs, a phase which has also been found to occur in a multiphase droplet (consisting of PbS, iss and Cu_2Sb) in a basin slag (10032(4)) as well as within matte s.s. (10-2B), are present.
The minor element inventory of these three phases (Fe_9As, Fe_2As and FeAs) is similar to that of pig iron, but generally is marked by higher Cu and partially also Ni contents. Furthermore, the As abundances of native Fe from ferrous speiss commonly exceed those of pig iron. Ferrous speiss itself can be excluded as Ag carrier (cf. section 2.5.3); the precious metal has only scantily been detected with the highest abundance (0.03 wt %) determined in FeAs within matte s.s.

11.1.1. Fe_9As

In contrast to native Fe analysed in pig iron, in ferrous speiss the phase exhibits elevated As and Cu in conjunction with not detectable Sb contents. The abundances of Sn and Co though are roughly similar. Segregated Fe_9As possesses Fe and As contents between 87.08 and 87.89 wt % and 9.13 and 9.96 wt %, respectively. The Cu abundances scatter between 0.82 and 0.92 wt % and thus yield the median composition $Fe_{9.1}As_{0.8}Cu_{0.1}$. The most common minor elements are Co, Ni and Sn. Symplectitic Fe_9As chemically virtually is indistinguishable from segregated Fe_9As in the same speiss sample investigated with Fe, As and Cu abundances ranging from 86.71 to 87.99 wt %, 9.79 to 10.12 wt % and 0.80 to 0.84 wt %, respectively, and an identical median composition. The minor element signature as well is strongly similar to that of segregated Fe_9As. Both varieties of Fe_9As contain only low to not detectable amounts of S ($\leq$ 0.02 wt %).

11.1.2. Fe_2As

Segregated Fe_2As is marked by Fe and As abundances between 53.44 and 56.03 wt % and 35.46 and 36.64 wt %, respectively, and possesses elevated Cu contents (5.35 to 7.68 wt %). Typical minor elements include Sb, Co, Ni and Sn; the S contents are low ($\leq$ 0.30 wt %). The median composition is $Fe_{1.9}As_{0.9}Cu_{0.2}$. Symplectitic Fe_2As in contrast shows higher Fe (56.32 to 64.63 wt %) in conjunction with decreased As and Cu contents (26.74 to 35.97 wt % and 2.78 to 3.74

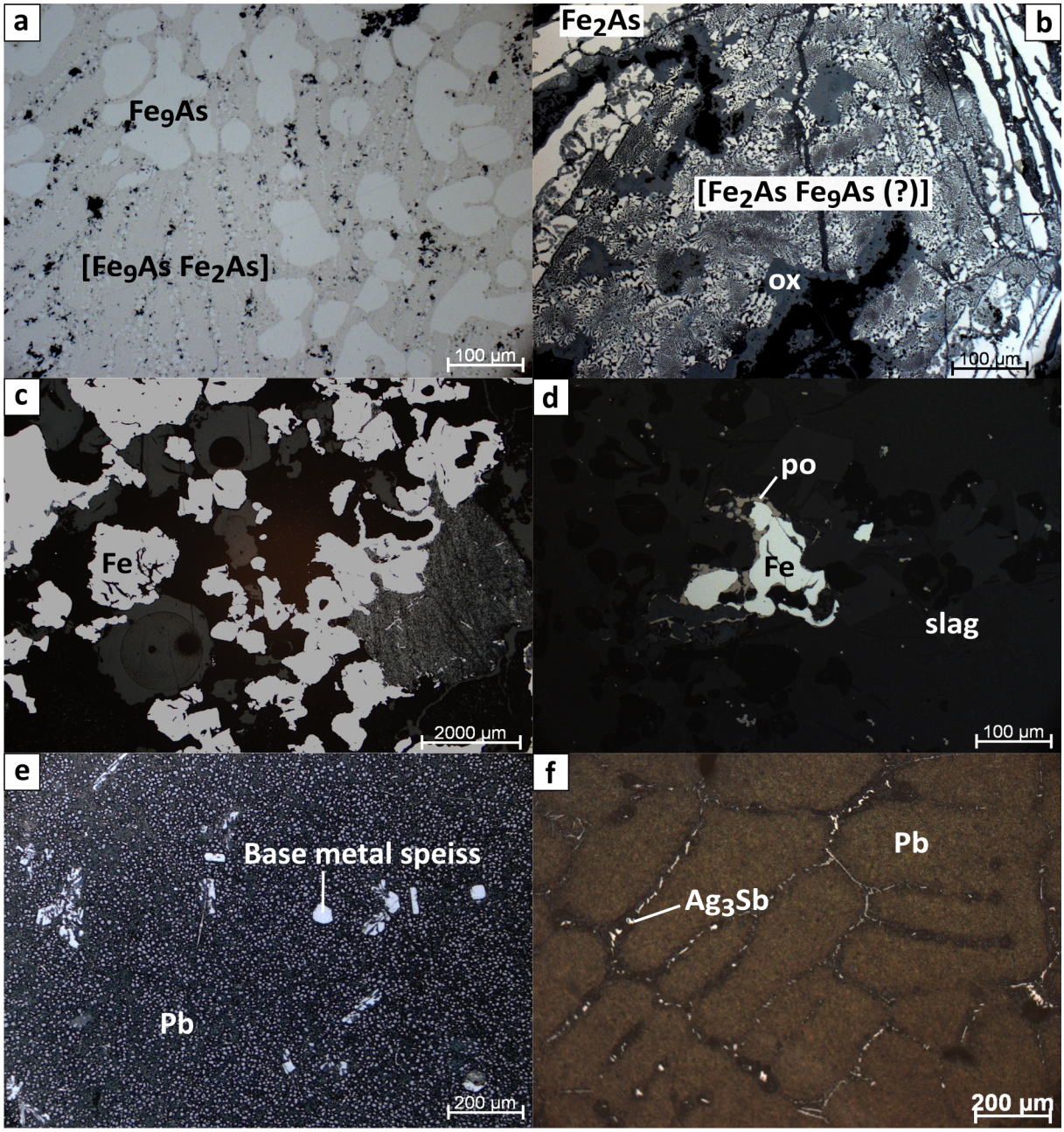

Figure 11.1.: a) Ferrous speiss: Roundish segregated grains of Fe_9As are embedded in a symplectitic intergrowth of Fe_9As and Fe_2As [sample 11029(7), Mirash Novo, RL, PPL]. b) Ferrous speiss: Euhedral laths of Fe_2As are surrounded by a symplectite of Fe_2As and a heavily weathered phase, potentially (As-bearing) Fe [sample 11029(4), Mirash Novo, RL, PPL]. c) Pig iron: Anhedral grains of arsenical Fe are surrounded by a matrix consisting of hydrosilicates and secondary Fe oxides and hydroxides [sample 10021(4), Mramor Samakove, RL, PPL]. d) Pig iron: An irregular shaped grain of native Fe in a furnace slag is rimmed by pyrrhotite [sample 10021(21), Mramor Samakove, RL, PPL]. e) Base metal speiss: Sb-As-bearing base metal speiss phases can be seen within a large droplet of native Pb [sample 10024(5), Mramor Proni Butoçit, RL, PPL]. f) Base metal speiss: Minute grains of base metal speiss (microscopically identified as dyscrasite) are present in native Pb [sample 11029(1), Mirash Novo, RL, PPL].

wt %). Cu correlates positively with As, Ni and Sb ($R^2 = 0.97$, 0.82 and 0.64). The abundances of Sb and Co are comparable to those of segregated grains while Ni is significantly depleted. High S contents (0.33 to 7.03 wt %) point to analytical contamination by base metal sulphides, e.g. by exsolved bornite *ss* as observed in FeAs (see below) or by FeS as described by Ströbele et al. (2010). The median composition is $Fe_{2.0}As_{0.7}Cu_{0.1}S_{0.1}$.

11.1.3. FeAs

FeAs exsolved in ferrous speiss (sample 11029(4)) possesses Fe and As contents of 46.51 wt % and 46.56 wt % and 32.07 wt % and 32.84 wt %, respectively. It is marked by elevated Cu (15.02 wt % and 15.35 wt %) and S abundances (1.26 wt % and 1.32 wt %) resulting in the median composition $Fe_{1.1}As_{0.6}Cu_{0.3}S_{0.1}$. Co (0.11 wt % and 0.12 wt %), Ni (0.25 wt % and 0.26 wt %) and Sn (0.03 wt % and 0.10 wt %) are the most abundant minor constituents of its chemistry. FeAs grains present in a lump of matte s.s. (sample 10-2B) are significantly enriched in Ni (18.23 to 23.15 wt %) and exhibit Fe and As contents scattering between 29.34 and 33.90 wt % and 33.28 and 36.05 wt %, respectively. Fe and As are partially substituted by Cu and Sb (6.40 to 7.40 wt % and 1.24 to 1.68 wt %). The median composition is $Fe_{0.7}As_{0.6}Ni_{0.4}Cu_{0.1}$. When compared to cupriferous FeAs in speiss, Sb as well as Co (0.43 to 0.63 wt %) are notably enriched, while Sn mostly could not be detected (i.e. $<$ 210 ppm). S is always present with abundances ranging between 1.14 and 1.91 wt %. FeAs analysed in a multiphase droplet consisting of galena, $(Cu,Ni)_2Sb$ and iss contains 37.57 wt % Fe and 47.16 wt % As. It shows elevated Ni and Sb along with low Cu abundances (2.97 wt %, 1.21 wt % and 0.14 wt %, respectively) and, similarly to FeAs in matte s.s., not detectable Sn contents. The high amount of Pb determined (5.49 wt %) presumably results from contamination by neighbouring Pb sulphide. The composition has been calculated as $Fe_{1.0}As_{0.9}Ni_{0.1}$.

11.2. Pig iron

The transition between pig iron and ferrous speiss generally is fluent. The analysed samples therefore have been distinguished on the basis of their occurrence and chemistry with 'true' pig iron due to its different formation conditions (cf. chapter 2.5.4) being defined as having (significantly) low(er) bulk As, Cu and Sb contents. While pig iron thus has been found to consist exclusively of (arsenical) native Fe, ferrous speiss always comprises an As-richer compound besides arsenical Fe (e.g. Fe_2As in the analysed samples; cf. Goldenberg, 1996; Ströbele et al., 2010). Due to its high melting point but also abundant impurities, pig iron could not have been processed in ancient times (cf. chapter 2.5.4). It therefore simply was discarded without further treatment and hence is typically found nearby furnace complexes of smelting sites, such as at the site at Mramor Samakove. Pig iron there is present as severely altered porous lumps and plates, in which pristine native Fe only is preserved in the inner areas. On micro-scale, it consists of irregularly shaped grains of native Fe surrounded by secondary oxides and hydroxides generated by atmospheric weathering as well as hydrous silicate phases (Fig. 11.1c). Pig iron also has been sampled indirectly as droplets locally generated due to reduction by charcoal, which often are surrounded by a thin rim of Fe sulphide within a furnace slag from the same site (Fig. 11.1d).

Grains of arsenical Fe from a lumpy sample (10021(4)) show Fe and As contents between 88.95 and 92.85 wt % and 5.59 and 8.52 wt %. Cu, Sb, Co, Ni and Sn are consistently detected minor elements, while small amounts of Mn, Zn and Cd have been mostly determined. The amount of S present is low, but detectable ($\leq$ 0.05 wt %). The median composition has been calculated as $Fe_{9.4}As_{0.5}$. Only two analyses of droplets of native Fe in a furnace slag sample (10021(21)) have been possible, which revealed Fe and As abundances of 95.38 wt % and 97.52 wt % and 0.33 wt % and 3.12 wt %, respectively. In contrast to the lumpy sample, the spherical inclusions are significantly depleted in Cu and Ni and somewhat enriched in Sb. The proportions of Co and Sn are rather constant. S abundances of 0.01 and 0.02 wt % have been detected. The median composition has been calculated as $Fe_{9.8}As_{0.1}$.

11.3. Base metal speiss

Base metal speiss either has been found - according to its specific gravity - exsolved in ferrous speiss or native Pb, but also as droplets within basin slags. Its typically close association with Pb bullion naturally accounts for the fact that it could be only scarcely analysed. Substitutions in base metal speiss compounds are highly common and a generalised formula thus can be given as $(Cu, Fe, Ni, Ag)_x(Sb, Sn, As)_y$.
Segregated droplets of native Pb in basin slag sample 10024(5) from Mramor Proni Butoçit (Fig. 11.1e) contain symplectites of a metal alloy phase, whose in situ analysis revealed the presence of Sb, As and Pb (the latter probably being caused by contamination from the surrounding Pb). A large segregated droplet of crude Pb (sample 11029(1)) comprises minute droplets of an alloy phase, which has been microscopically identified as dyscrasite (Fig. 11.1f). The Fe_2As-rich speiss layer within a basin slag (11029(4) from Mirash Novo) contains few grains of $(Cu,Fe)_3(Sn,Sb)$. While (Ni,Cu)(Sb,As) is present as monophase spherical inclusions in the glassy matrix of a basin slag (12016(2) from Akllap), $(Cu,Ni)_2Sb$ has been observed as part of multiphase droplets (either solely with bornite *ss* or galena, with both the Pb and Cu-Fe sulphide phase or associated with FeAs, iss and galena) within a basin slag (10032(4)).

11.3.1. (Ni,Cu)(Sb,As)

The Ni, Sb and As contents of (Ni,Cu)(Sb,As) range from 28.45 to 33.56 wt %, 30.46 to 59.86 wt % and 4.73 to 23.72 wt %, respectively. The substitution of Sb and As is in accordance with the naturally occurring solid solution series of breithauptite [NiSb] and nickeline [NiAs]. The most important minor constituents are Cu (2.46 to 5.13 wt %) and Fe (0.44 to 1.11 wt %) as well as Pb (0.81 to 6.61 wt %). The determined Pb content may be related to contamination of the analyses by adjacent Pb-bearing phases. The median composition has been calculated as $(Ni_{0.9}Cu_{0.1})(Sb_{0.7}As_{0.3})$. Sn, Zn and Cd are the most important minor elements. The ubiquitously determined comparably high S abundances (0.02 to 0.84 wt %) point to the presence of finely intergrown sulphide phases. The Ag contents often are below the detection limit (i.e. $<$ 250 ppm) with a maximum of 0.04 wt %.

11.3.2. $(Cu,Fe)_3(Sn,Sb)$

Due to the scarce presence of $(Cu,Fe)_3(Sn,Sb)$ only two analyses could be performed, which yielded Cu, Sn and Sb contents of 60.91 wt % and 61.53 wt %, 25.51 wt % and 26.48 wt % and 10.72 wt % and 11.33 wt %, respectively. Fe (1.30 wt % and 3.45 wt %), Ni (0.47 wt % and 0.48 wt %) and As (0.15 wt % and 0.30 wt %) are the most important minor elements. 0.06 wt % and 0.10 wt % Ag have been determined in this phase. The median composition has been calculated as $(Cu_{2.9}Fe_{0.1})(Sn_{0.7}Sb_{0.3})$.

11.3.3. $(Cu,Ni)_2Sb$

The Cu, Sb and Ni abundances of $(Cu,Ni)_2Sb$ scatter between 46.08 and 49.29 wt %, 49.51 and 50.30 wt % and 1.31 and 3.48 wt %, respectively. The resulting median composition of $(Cu_{1.9}Ni_{0.1})Sb$ is rather stoichiometric. Besides the remarkable Ag abundances (0.19 to 0.56 wt %), Fe, As and Sn have been consistently detected.

11.4. Temperature estimates

Precipitation temperatures of speiss and pig iron are estimated based on petrography and geochemistry of the phases. Analogous to the solidification sequences described for matte, the influence of factors such as e.g. fluid phases and chemical variation of the investigated components largely is unknown and hence the experimentally determined temperatures should be considered as upper limit. Particularly the widespread elemental substitutions render the temperatures provided by the thermodynamical database only approximate values. Therefore, with the exception of the rather stoichiometric arsenical Fe only data of pure compounds is given.

11.4.1. Ferrous speiss and pig iron

The composition of segregated Fe_9As of sample 11029(7), whose Fe contents range between 87.08 and 87.89 wt % yields maximum precipitation temperatures of approximately 1300 to 1320 °C, which approach the highest values typically estimated for ancient metallurgical processing (e.g. Hauptmann, 2014; Manasse & Mellini, 2002a; b; cf. chapter 10.3). The experimentally determined eutectoid temperature of Fe_9As and Fe_2As is 840 °C at a bulk Fe content of 70 mol %. The Fe abundances of both segregated and eutectoid Fe_9As varieties slightly exceed the solubility limit of As in α-Fe and plot in the two phase field of α-Fe and Fe_2As (Okamoto, 1991). Fe_2As, present as segregated laths and symplectite in sample 11029(4), ideally crystallises at 930 °C. Simultaneous precipitation of Fe_2As and arsenical Fe, as mentioned previously, occurs at 840 °C. Stoichiometric FeAs has been experimentally determined to solidify at 1030 °C (Okamoto, 1991).

Analyses of arsenical Fe classified as pig iron yield high temperature estimates between 1350 and 1420 °C for the lump sample and between 1460 and 1520 °C for the droplets observed in the furnace slag (Okamoto, 1991). However, the true formation temperatures are expected to have been markedly lower, particularly due to the presence of minor elements (e.g. Cu, Co, Ni and Sn).

11.4.2. Base metal speiss

(Ni,Cu)(Sb,As) abundant in sample 12016(2) is expected to have precipitated between the experimentally determined crystallisation temperatures of NiSb and NiAs (1153 °C and 970 °C, respectively; Hansen & Anderko, 1958). $(Cu,Fe)_2(Sn,Sb)$ exsolved in ferrous speiss is compositionally closer to Cu_3Sn, which forms at 676 °C; Cu_3Sb in contrast appears at the significantly lower temperature of 440 °C. $(Cu,Ni)_2Sb$ present in multiphase droplets within a basin slag sample is chemically dominated by Cu_2Sb, which ideally forms at 586 °C. Ag_3Sb, which has been microscopically identified in native Pb (Fig. 11.1f; sample 11029(1)), is generated by peritectic reaction at 559 °C (Hansen & Anderko, 1958).

12. Crude lead

Native Pb is present in the majority of the investigated basin slag samples while in matte and speiss in contrast it has not been observed. In slags, its abundance generally seems to be related to their paragenesis. Comparably elevated proportions of Pb droplets have been particularly found within slag types which do not contain olivine as dominant phase. Native Pb precipitated at the lower limit of slag layers often forms large-sized prills (partially reaching diameters of several hundred micrometres or few millimetres), which always contain segregated sulphide phases (Fig. 12.1a; cf. Fig. 9.3f, 9.7d and 10.1i). Droplets present within slag layers in contrast commonly are much smaller with diameters typically in the range of a few ten micrometres and commonly do not comprise exsolved Pb-Cu matte or galena. Besides indirectly sampled crude Pb within slag samples, a small, finger-shaped piece of native Pb has been found during the excavation at Mramor Samakove[1] (Fig. 12.1b; cf. chapter 15.1). The quantitative analysis of native Pb has been hampered by its poorly polishable surface, which is related to the low hardness and consequently differing mechanical properties of the metal [2]. Consequently, the totals of the Pb analyses often do not approach 100 wt %. Measurements with sums below 90 wt % have been omitted from the examination and the remaining data has been normalised to 100 wt % for better comparison. Furthermore, the presence of exsolved matte and speiss compounds apparently often contaminated the analyses with Fe, Cu, As and S, whose solubilities in Pb are lower than the determined values. The most important minor elements in the chemistry of native Pb are Sb (0.07 to 2.18 wt %) and As (0.02 to 1.27 wt %). Cd also has been commonly detected with contents between 0.04 and 0.58 wt %. Elevated Cu abundances particularly have been observed in matte-bearing basin slags (0.03 to 0.77 wt %). Fe (0.03 to 2.27 wt %) and S (0.04 to 1.50 wt %), as As reported to be virtually insoluble in native Pb (Hansen & Anderko, 1958), have been mostly detected and presumably indicate abundant matte and speiss micro-inclusions. Ag in contrast only could be determined in 2 analyses out of 40, which yielded abundances of 0.07 wt % and 0.67 wt %. Native Pb droplets in slags from the site of Mramor Samakove are markedly enriched in Sn (0.41 to 0.88 wt %), which in the other samples typically could not have been detected.

[1] This far, it has only been analysed for its isotope signature but further measurements are envisaged.

[2] Mohs hardness of Pb: 1.5; fay: 6.5 - 7; hd: 5.5 - 6.5; lct: 5.5 - 6; mag: 5.5 - 6.5; all values taken from Handbook of Mineralogy

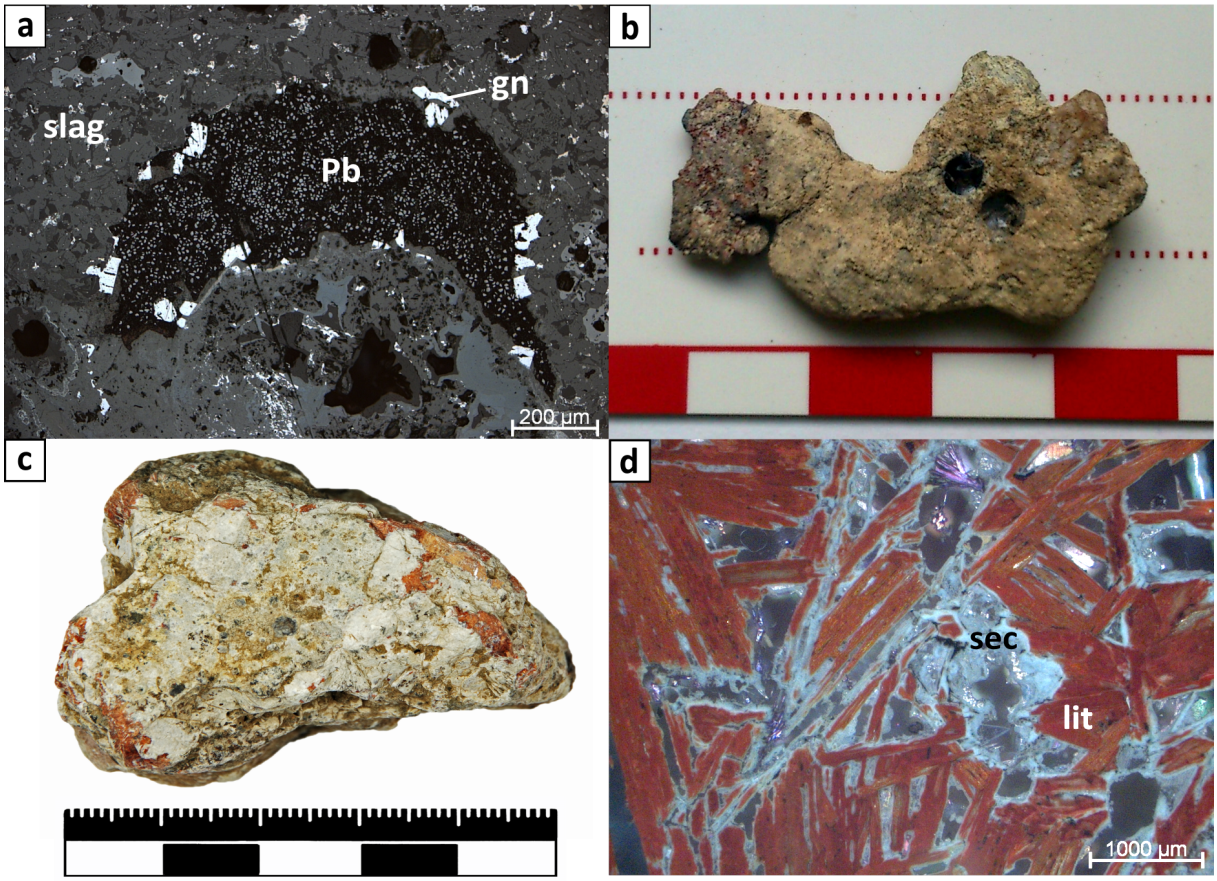

Figure 12.1.: *Crude Pb.* a) Eu- to subhedral galena grains are present at the rim of a large-sized droplet of native Pb [sample 12015(7), Voguçincë, RL, PPL]. b) Crude Pb retrieved from the excavation at Mramor Samakove. Drill holes have been caused by sampling for isotope analysis [sample MrS-Pb]. *Cupellation remains.* c) Fragment of a test cupel found at the smelting site of Marec [sample 10-5]. Photography taken by G. Gassmann. d) Entangled laths of brick-red litharge are rimmed by translucent secondary phases [sample 10-5, Marec, RL, XPL].

13. Cupellation remains

In the hand sample of the cupellation remain from Marec, red Pb oxide is clearly visible, which generally is heavily weathered to secondary oxidised Pb phases resulting in a thick whitish crust (Fig. 12.1c). On micro-scale, two different areas are discernible: yellowish-brown coloured technical ceramic and red Pb oxide (litharge), i.e. relictic oxidised crude Pb. Pb oxide is present as eu- to subhedral laths which form an interlocked texture (Fig. 12.1d). Litharge is the tetragonal low temperature form of the dimorphous Pb oxide, which transforms at 650 °C (Gavrichev et al., 2008) to the orthorombic high temperature variety (massicot). The laths often are rimmed by yellowish-green and colourless secondary phases (Fig. 12.1d), which have been identified by XRD as the jarosite-group phase beaverite, cerussite and lanarkite [$Pb_2(SO_4)O$]. Litharge is marked by a rather pure composition. The laths contain minor amounts of Sb_2O_3 (0.09 to 0.15 wt %), As_2O_3 (0.05 to 0.09 wt %) and SO_3 (0.07 to 0.16 wt %), which are thought to have been derived from base metal speiss cupelled along with Pb bullion and from exsolved sulphide phases, i.e. galena and other potentially present matte phases. Interestingly, CuO could not have been detected (i.e. abundances $<$ 750 ppm). This observation is in accordance with the Cu-poor nature of the Novobërdë mineralisation in the immediate vicinity. No metal or alloy phases, e.g. native Ag or Au are present in the cupellation remains.

14. Metal artefacts

Lead (Fig. 14.1 a-c) as well as copper-rich artefacts (Fig. 14.1d, e) discovered in Ulpiana or - as it is the case for one bronze coin - at the smelting site of Voguçincë, could be sampled and hence complete the investigation of the local *chaîne opératoire*.

14.1. Lead objects

Similar to native Pb in the investigated sections of slag samples, the mounted drilling chips taken from the four lead artefacts could not have been polished adequately due to the low hardness of the metal. This resulted in a porous spongy surface, which has rendered in situ measurements difficult. All analyses with totals below 90 wt % therefore alike to the previous approach utilised for crude Pb in slag (cf. chapter 12) have been omitted from the examination and the remaining data has been normalised to 100 wt % for better comparison.
Generally, the composition of repeatedly sampled artefacts - i.e. the sarcophagi, cf. chapter 7 - agrees very well and no significant discrepancies could be observed (this is confirmed by Pb isotope analysis; cf. chapter 15.1). All impurities are due to refining treatment significantly diminished when compared to the elemental signature of crude Pb present in slag samples. Low Ag contents, which only have been detected in two analyses of specimen I.3 (0.03 and 0.30 wt %, respectively), demonstrate that the metal has been desilverated previous to its manufacture. Significantly lower amounts of S than in crude Pb (cf. chapter 12) have always been detected (0.05 to 0.23 wt %) and consequently indicate that all artefacts have been produced from (predominantly) sulphidic ores. As mentioned previously, the analysed S contents should derive from the presence of sulphide micro-inclusions. Due to their in comparison to native Pb notably better polishing properties, areas of impure metal unwittingly might have been preferentially selected for analysis. Sb as well always has been detected (0.04 to 0.19 wt %). As, Mn and Cd are further typically present minor elements, whose abundances range between 0.02 to 0.18 wt %, 0.02 and 0.04 wt % and 0.04 and 0.16 wt %, respectively. Cu has been randomly determined, with rather low contents particularly detected in samples II (0.03 to 0.06 wt %) and IV (0.03 to 0.04 wt %).

14.2. Copper-rich objects

The two coins are chance finds retrieved from the smelting site at Voguçincë (sample III) and from Ulpiana (sample VI). Due to imprintings of Probus (276 - 282 CE) and Aurelian (270 - 275 CE; cf. Fig. 14.1d and e), respectively, a late antique dating can be clearly assigned to both. Based on their Sn content, which ranges from 5.36 to 6.67 wt % and from 0.22 to 0.83 wt % in the samples from Voguçincë and Ulpiana, the first mentioned is according to Stech (1999)

Figure 14.1.: The metal artefacts investigated in this study. a) Two children's lead sarcophagi (samples I and II). b) Small lead block with 'III' carved in it, possibly a weight (sample IV). c) Fragment of an ornamentally decorated lead platelet (sample V). d) Bronze coin from the smelting site at Voguçincë, showing an imprinting of Emperor Probus (276 - 282 CE; sample III). e) Copper coin from Ulpiana, attributed to the reign of Aurelian (270 - 275 CE; M. Berisha & E. Shala, pers. comm.; sample VI). The total lenght of the scale is 10 cm.

classified as bronze and the second as an impure copper coin. The bronze furthermore is marked by higher Ag abundances (1.92 to 3.03 wt %) than the copper coin (1.19 to 2.41 wt %). Sb and As are important minor elements, which always have been detected in both the sample from Voguçincë (0.10 to 0.14 wt % and 0.08 to 0.12 wt %, respectively) and Ulpiana (0.06 to 0.14 wt % and 0.04 to 0.11 wt %, respectively). As and Sb, As and Sn as well as Sn and Sb are positively correlated in specimen VI ($R^2 = 0.65$, 0.64 and 0.87; Fig. 14.2). These relations either could be due to the fact that the three elements are concentrated in heterogeneities or a distinct phase within the native Cu or that they were introduced together, i.e. by the same raw material from which the coin was produced. In the latter case, the correlation either could be of primary origin and hence reflect the geochemical signature of the ore type smelted to gain the desired metal(s) or of artificial character, i.e. caused by metallurgical processing. A likely explanation for this relationship would be the introduction of As, Sb and Sn by addition of a small quantity of bronze-like material - e.g. due to recycling of scrap metal - to the metal melt from which the impure Cu coin was cast. The sample from Voguçincë in contrast does not exhibit any correlations between these elements. While Fe (0.06 to 0.11 wt %) and S (0.01 to 0.04 wt %) have always been determined in the bronze sample, S has never and Fe has been randomly detected within the impure copper material. Cd in contrast is comparably enriched in the latter (0.03 to 0.07 wt %) and depleted in the bronze coin with abundances typically being below the detection limit (i.e. < 280 ppm). Pb in both coins is inordinately distributed and varies between 0.05 and 2.57 wt % and 0.03 and 7.49 wt % (median contents: 0.06 and 0.07 wt %) in the samples from Voguçincë and Ulpiana, respectively. These large discrepancies are thought to be caused by exsolved Pb inclusions within the Cu-(Sn) groundmass. In the bronze coin from Voguçincë, Pb and Ag show a positive correlation ($R^2 = 0.77$), while in the copper sample no distinct relation between the two elements is discernible ($R^2 = 0.35$). Generally, a correlation between Pb and Ag can be explained in two ways: The elements either are present within the same phase in the metal objects (e.g. in exsolved native Pb) or originate from a concurrent material source, e.g. from deliberately added Ag containing restitic Pb from cupellation or primary smelted Pb-Ag ores. Narrowing down the source(s) of the determined Pb content within the coins virtually is impossible since the metal might not only have been haphazardly introduced in relation with Ag or other raw materials, but native Pb might also have been deliberately added to debase the coinage. The bulk Pb content of both coins, however, is clearly high enough to ensure that Pb isotope analysis solely will retrace possible Pb (and potential Ag) ore mining districts, but that no conclusion can be drawn on the provenance of Cu and Sn raw materials. When interpreting the Pb isotope data, it also has to be considered that the mints surely were supplied with raw material from various regions of the Empire - which subsequently was most likely mixed during coin production - and to a certain extent also relied on the recycling of scrap metal.

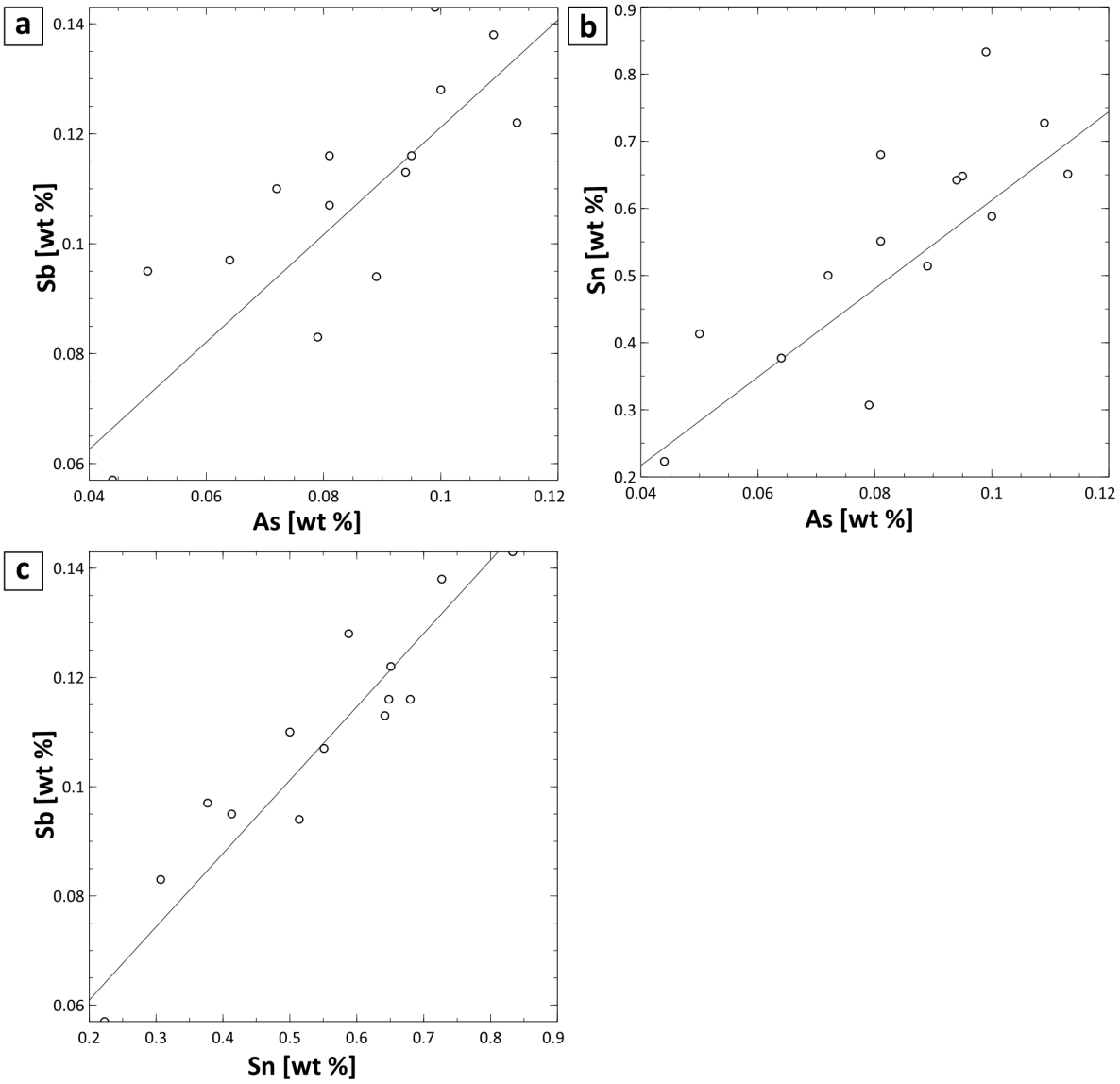

Figure 14.2.: Correlation plots of the copper coin (sample VI). a) Sb versus As contents ($R^2 = 0.65$). b) Sn versus As contents ($R^2 = 0.64$). c) Sb versus Sn contents ($R^2 = 0.87$).

15. Isotope analyses

15.1. Lead isotopes

The Pb isotope data gained in this study closes an analytical gap since Kosovo's resources generally are insufficiently characterised. Only few datasets of the Pb-Zn-Ag mineralisations of the Kopaonik Mountains in the vicinity of Municipium DD, which include the world-class skarn deposit of Stan Tërg besides Crnac and Bellobërdë, are currently available (Gale, 1990, pers. comm.; Pernicka et al., 1993; Veselinović-Williams, 2011). The resources of the Zhegovc Mountains in the hinterland of Ulpiana, which are mined today at Kishnica, Badovc, Novobërdë and Hajvali, this far have been barely investigated with state-of-the-art geochemical analytical techniques at all. This lack of data is in stark contrast to the current and historic relevance of the region's mineral wealth. Indeed, the Balkan Peninsula in general possesses an outstanding mining tradition and apparently is one of the cradles of metallurgy (cf. section 3.1). The isotope analyses carried out in this project thus are of high importance for research projects focusing on the (local) economic geology of Pb-Zn-Ag mineralisations as well as mining history / archaeology and archaeometallurgy and help to clear one of the last remaining white spots of the European Pb isotope literature database.

15.1.1. Ore

Ten ore samples from the mining district of Shashkoc-Janjevo, which also have been studied by means of petrography and in situ geochemistry (cf. chapter 8) have been analysed. The variability of the mineralisation - i.e. primary ore from differing precipitation stages, secondary sulphide and oxidised ore – has been assessed by the selected specimens. The ratios of $^{206}Pb/^{204}Pb$, $^{207}Pb/^{204}Pb$ and $^{208}Pb/^{204}Pb$ scatter between 18.781 and 18.793, 15.665 and 15.675 and 38.950 and 39.004, while those of $^{207}Pb/^{206}Pb$ and $^{208}Pb/^{206}Pb$ range between 0.83382 and 0.83433 and 2.07268 and 2.07595 (Fig. 15.1), respectively. The ore data yields a narrow, sharply defined field in which the $^{206}Pb/^{204}Pb$ and $^{207}Pb/^{204}Pb$ values completely overlap within the error range, thus indicating that the local mineralisation has been formed by one single continuous ore forming event whose three precipitation stages (cf. section 8.1.1) cannot be distinguished based on this data. The Pb isotope ratios of a piece of restitic galena ore (MrS-gn) from the excavation at Mramor Samakove are in excellent agreement with ore data of the Shashkoc-Janjevo district.
The characterisation of the local mineral resources has been further expanded by three analyses each of ores from the deposits of Novobërdë and Melenica. Generally, the Pb isotope signature of a deposit or even mining district should not be based on only three samples, as is the case for the pilot study undertaken on these two deposits. The attribution of the metallurgical remains in the following therefore obviously must be considered tentatively. However, it is hoped that

the ore Pb isotope data gathered during this project will be complemented by future investigations. The data of Novobërdë is important with regard to geographical considerations since the northern smelting sites studied (particularly Marec) are closer to this deposit than the district of Shashkoc-Janjevo. Furthermore, the mine's high historical and current relevance – its resources were exploited on a large scale since at least medieval times and potentially also already under Roman rule (cf. chapter 4.1) – strongly argue for a more thorough geochemical characterisation of this mineralisation. Pb-Zn-Ag ore sampled at Melenica close to the renowned Stan Tërg deposit in northern Kosovo (cf. section 3.2.3) has been investigated to gather additional data from resources in the vicinity of Municipium DD, particularly in light of the *MET DARD* inscriptions found on lead objects (section 4.2), and to use the opportunity to generate additional isotope data of the ancient Balkan ore districts.

Novobërdë possesses the oldest isotope signature of the Pb-Zn-Ag deposits of the Šumadija-Kopaonik district ($^{206}Pb/^{204}Pb$ = 18.617 - 18.625; $^{207}Pb/^{204}Pb$ = 15.656 - 15.659; $^{208}Pb/^{204}Pb$ = 38.788 - 38.789; $^{207}Pb/^{206}Pb$ = 0.84076 - 0.84096; $^{208}Pb/^{206}Pb$ = 2.08308 - 2.08350). The isotope ratios fully overlap in a narrow field (Fig. 15.1). Data from Melenica also completely overlaps and possesses Pb isotope ratios intermediate between Novobërdë and Shashkoc-Janjevo ($^{206}Pb/^{204}Pb$ = 18.732 - 18.735; $^{207}Pb/^{204}Pb$ = 15.666 - 15.669; $^{208}Pb/^{204}Pb$ = 38.892 - 38.901; $^{207}Pb/^{206}Pb$ = 0.83637 - 0.83645; $^{208}Pb/^{206}Pb$ = 2.07622 - 2.07650). The isotope signature of Melenica agrees very well with analyses of other mineralisations of the Kopaonik Mountains (Gale, 1990, pers. comm.; Pernicka et al., 1993; Veselinović-Williams, 2011), not surprisingly particularly with the isotope field of the adjacent, apparently genetically related Stan Tërg deposit. Data from the Rudnik deposit of the Šumadija district (Pernicka et al., 1993) in comparison is marked by somewhat lower Pb isotope ratios (Fig. 15.1).

Due to their virtually identical formation ages, the isotope signature of the Pb-Zn-Ag mineralisations of the Šumadija-Kopaonik district largely overlaps with data of other deposits of the Serbomacedonian-Rhodope belt stretching throughout Greece, Bulgaria and Macedonia, but also with analyses of ore bodies located in Romania's Inner Carpathian-Alpine belt and southeast Spain. However, the ancient mining district of Shaskoc-Janjevo can be well distinguished in the ^{206}Pb-normalised diagram due to its comparably low $^{207}Pb/^{206}Pb$ and elevated $^{208}Pb/^{206}Pb$ ratios. The deposit of Novobërdë - even though the number of samples examined so far only allows preliminary conclusions – is marked by a rather unique signature which stands out in the ^{204}Pb- and ^{206}Pb-normalised plots and extends the known isotope field of the Šumadija-Kopaonik district. Given the economic relevance of the mine for the Serbian and Ottoman Empires (and potential earlier Roman / late antique activities; cf. chapter 4.1), which also is reflected by the presence of numerous, often particularly large-scaled ancient smelting sites in the immediate vicinity (Fig. 6.1), a thorough isotopic characterisation of its according to preliminary data specific pattern is deemed to be highly important.

15.1.2. Metallurgical by-products

The Pb isotope ratios of the metallurgical by-products from the smelting sites investigated possess $^{206}Pb/^{204}Pb$, $^{207}Pb/^{204}Pb$, $^{208}Pb/^{204}Pb$, $^{207}Pb/^{206}Pb$ and $^{208}Pb/^{206}Pb$ values ranging between 18.616 and 18.792, 15.655 and 15.675, 38.780 and 39.010, 0.83393 and 0.84132 and 2.07426 and

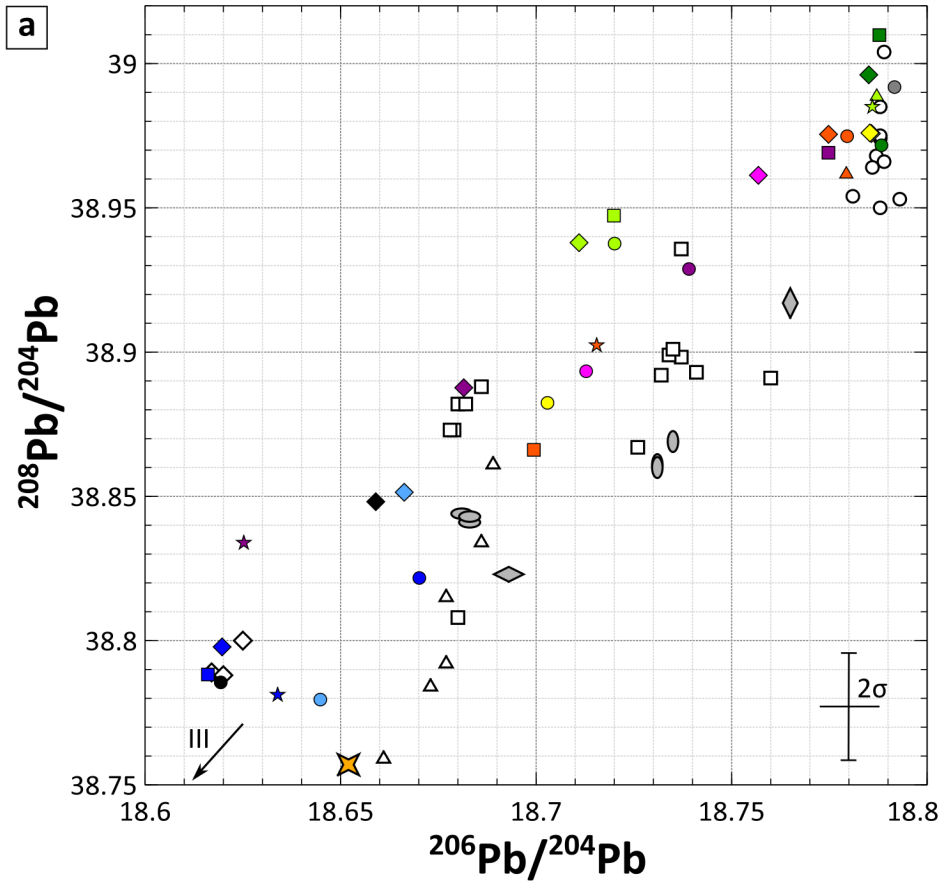
a
39
38.95
38.9
38.85
38.8
38.75
18.6
18.65
18.7
18.75
18.8
$^{208}Pb/^{204}Pb$
$^{206}Pb/^{204}Pb$
2σ
III

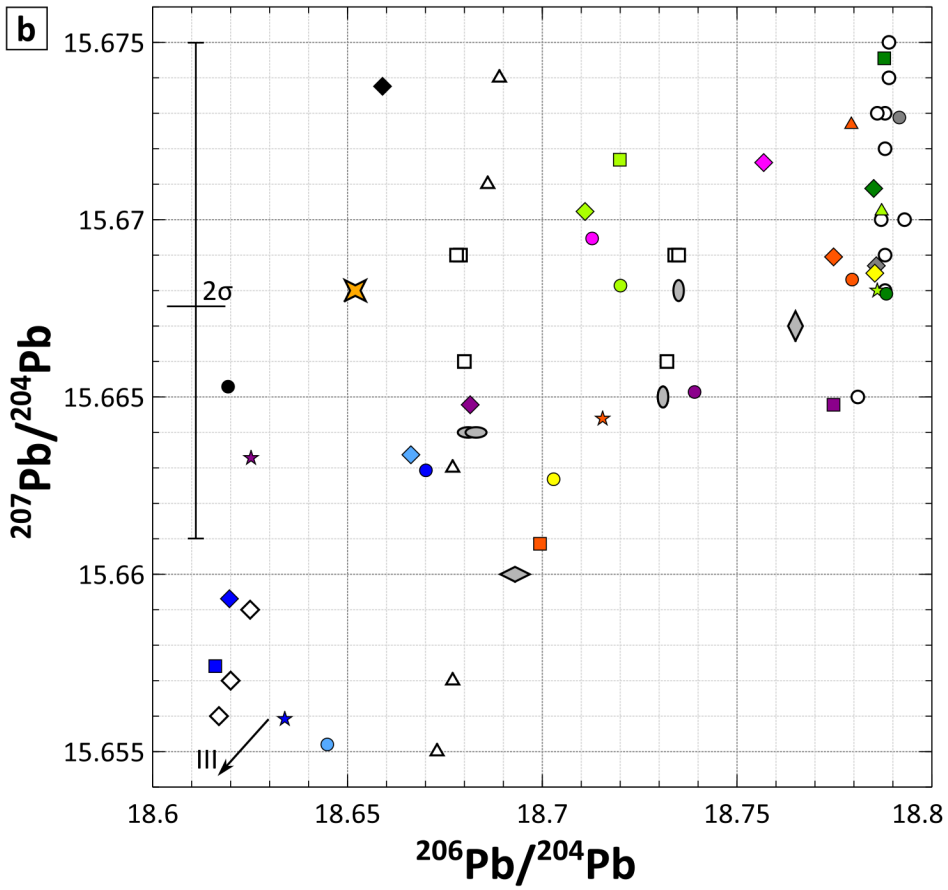
b
15.675
15.67
15.665
15.66
15.655
18.6
18.65
18.7
18.75
18.8
$^{207}Pb/^{204}Pb$
$^{206}Pb/^{204}Pb$
2σ
III

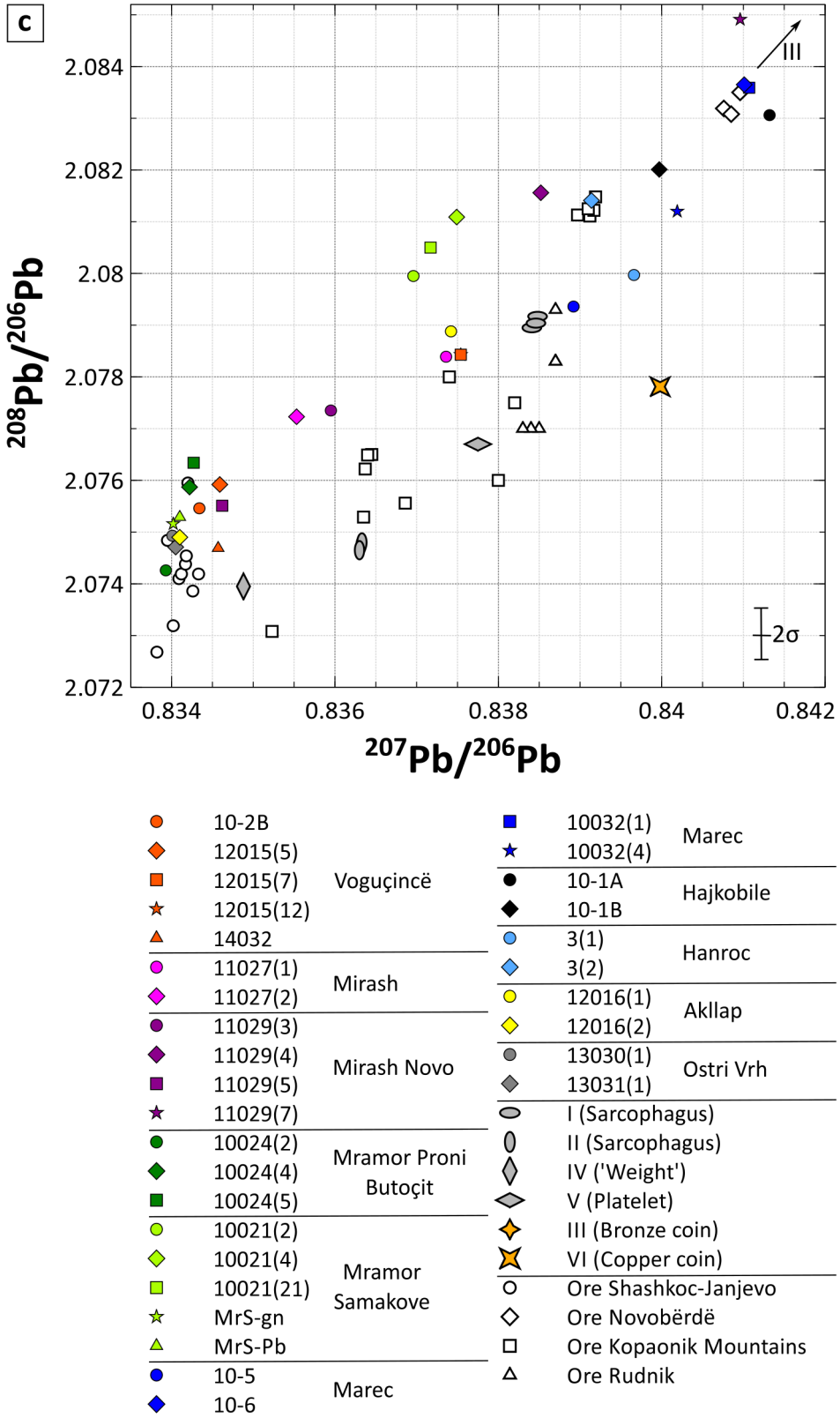
c
2.084
2.082
2.08
2.078
2.076
2.074
2.072
0.834
0.836
0.838
0.84
0.842
$^{208}Pb/^{206}Pb$
$^{207}Pb/^{206}Pb$
III
2σ
10-2B
12015(5)
12015(7)
12015(12)
14032
Voguçincë
11027(1)
11027(2)
Mirash
11029(3)
11029(4)
11029(5)
11029(7)
Mirash Novo
10024(2)
10024(4)
10024(5)
Mramor Proni
Butoçit
10021(2)
10021(4)
10021(21)
MrS-gn
MrS-Pb
Mramor
Samakove
10-5
10-6
Marec
10032(1)
10032(4)
Marec
10-1A
10-1B
Hajkobile
3(1)
3(2)
Hanroc
12016(1)
12016(2)
Akllap
13030(1)
13031(1)
Ostri Vrh
I (Sarcophagus)
II (Sarcophagus)
IV ('Weight')
V (Platelet)
III (Bronze coin)
VI (Copper coin)
Ore Shashkoc-Janjevo
Ore Novobërdë
Ore Kopaonik Mountains
Ore Rudnik

Figure 15.1.: Biplots of Pb isotope ratios of analysed ores, metallurgical by-products and metal artefacts in comparison with literature data of the Kopaonik and Šumadija districts (Gale, 1990, pers. comm.; Pernicka et al., 1993; Veselinović-Williams, 2011). Due to its significantly differing (i.e. older) isotope signature as indicated by the arrows in the diagrams, the bronze coin (III) has not been included in these plots to ensure better readability; the Pb isotope signatures of the investigated metal artefacts are discussed in detail in chapter 15.1.3. The error bars depict the average 2σ values (two times standard deviation) of all analysed samples. a) $^{208}Pb/^{204}Pb$ versus $^{206}Pb/^{204}Pb$. b) $^{207}Pb/^{204}Pb$ versus $^{206}Pb/^{204}Pb$. c) $^{208}Pb/^{206}Pb$ versus $^{207}Pb/^{206}Pb$.

2.08491, respectively, which form a cloud roughly extending between the ore fields of Shashkoc-Janjevo as the youngest and Novobërdë as the oldest data. They hence generally can be clearly related to production from local ores (Fig. 15.1). Samples from Voguçincë (10-2B, 12015(5), 14032), Mirash Novo (11029(5)), Mramor Samakove (MrS-gn, MrS-Pb), Akllap (12016(2)) and all specimens from Mramor Proni Butoçit and Ostri Vrh can be unambiguously assigned to resources from the Shashkoc-Janjevo district. Slags from Marec (10-6, 10032(1)) partially agree with ore from the Novobërdë deposit. The Pb isotope signatures of the metallurgical by-products which cannot be unambiguously attributed to either the Shashkoc-Janjevo or Novobërdë ores, might result from smelting of not yet characterised raw material or from mixing of several, isotopically slightly differing mineralisations (this aspect is discussed in detail in chapter 16.3).

Voguçincë

The samples 10-2B (matte cake) and 12015(5) and 14032 (slags with adhering matte layers) match each other and the Shashkoc-Janjevo ores. The basin slags 12015(7) and 12015(12) possess an overlapping, but significantly differing older Pb isotope signature and plot between the Shashkoc-Janjevo and Novobërdë data. They both coincide with the samples 11027(1) from Mirash and 12016(1) from Akllap.

Mirash

The two matte-bearing basin slags from Mirash (11027(1), 11027(2)) can be clearly distinguished on basis of their differing Pb isotope ratios with the latter being slightly closer to the Shashkoc-Janjevo ore data. Sample 11027(1) in contrast overlaps with basin slags from Voguçincë (12015(7) and 12015(12)) and Akllap (12016(1)).

Mirash Novo

Metallurgical remains from Mirash Novo exhibit the most versatile signature of all sites investigated so far with the four samples not matching each other. The matte-bearing basin slag 11029(5) overlaps with the signature of Shashkoc-Janjevo ore and consequently also matching metallurgical products, e.g. samples 10-2B, 12015(5) and 14032 from Voguçincë. The specimens 11029(3), 11029(4) and 11029(7), ordered according to increasing age, are marked by older Pb isotope ratios with the lump of ferrous speiss (11029(7)) even plotting close to Novobërdë's

resource data.

Mramor Proni Butoçit

The isotope ratios of all samples (10024(2), 10024(4), 10024(5)) from this smelting complex perfectly overlap with each other, restitic galena ore (MrS-gn) and crude Pb (MrS-Pb) from the neighbouring Mramor Samakove and the Shashkoc-Janjevo ore data.

Mramor Samakove

The furnace slags 10021(2) and 10021(21) possess extremely similar isotope ratios overlapping with pig iron (10021(4)) from the same site within the error range. They all, however, are not in accordance with neither the Shashkoc-Janjevo nor Novobërdë ores. Restitic galena ore excavated at this site (MrS-gn) in contrast agrees very well with native Pb (MrS-Pb) from Mramor Samakove and the Shashkoc-Janjevo ore signature.

Marec

The basin slags 10-6 and 10032(1) perfectly overlap with each other and, as it already has been suspected based on geographic considerations, the Novobërdë ores (Fig. 6.1). Sample 10032(4) plots close to data of this deposit, but does not match them within the error range. The cupel (10-5) exhibits a younger signature and neither overlaps with the three slags nor the resources of Novobërdë.

Hajkobile

The two samples from Hajkobile (i.e. basin slag and matte cake) do no overlap within their error range. While the slag (10-1A) plots close to ore data from Novobërdë, the matte signature is younger.

Hanroc

The two slags from Hanroc do not show any overlap in their Pb isotope signatures. Both samples cannot be attributed to a distinct mineralisation in the study area. Sample 3(1), however, plots closer to data of ores from the Novobërdë deposit than 3(2).

Akllap

The Pb isotope data determined of slags from Akllap generally is comparable to that of the nearby Voguçincë complex and extends over an identical range. Sample 12016(1) is similar to the basin slags 12015(7) and 12015(12) from Voguçincë and 11027(1) from Mirash and consequently does not overlap with Shashkoc-Janjevo's signature. Specimen 12016(2), however, agrees very well with this district and is isotopically highly similar to samples 10-2B and 12015(5) from Voguçincë and particularly 13031(1) from the site at Ostri Vrh amidst the investigated mining district.

Ostri Vrh

Both slags from Ostri Vrh, as the location of the site in the very heart of the ancient mining district already implies, perfectly overlap with each other and the local ore from Shashkoc-Janjevo. Sample 13031(1) isotopically is almost identical to the basin slag sample 12016(2) from Akllap.

15.1.3. Lead metal artefacts

The artefacts plot amidst data of mining districts located within the Serbomacedonian-Rhodope belt extending across the Balkan region (i.e. Bulgaria, Kosovo / Serbia, Romania, Greece, Macedonia) and partially overlap with Pb isotope ratios of ore occurrences of the Inner Carpathian-Alpine metallogenetic belt in modern-day Romania and Tertiary mineralisations hosted by mountain massifs of the Betic Cordillera (Sierra Almagrera, Sierra del Cabo de Gata and Sierra de Cartagena) situated in southeast Spain (Fig. 15.2)[1]. Although exploitation of the Sierra de Cartagena and Sierra de Almagrera has been proven until (late) imperial times (cf. section 5.2.1), the everyday character of the lead metal objects in conjunction with the abundant rich ore resources of the region render a local origin of the raw material highly plausible.
With the exception of specimens I and V, the samples possess significantly differing Pb isotope ratios with $^{206}Pb/^{204}Pb$, $^{207}Pb/^{204}Pb$, $^{208}Pb/^{204}Pb$, $^{207}Pb/^{206}Pb$ and $^{208}Pb/^{206}Pb$ scattering from 18.681 to 18.765, 15.660 to 15.668, 38.823 to 38.917, 0.83488 and 0.83848 and 2.07395 and 2.07904, respectively. The three individual samples taken from the sarcophagi (I and II) cannot be distinguished isotopically and hence are interpreted to have been completely manufactured from the same raw material, as it already has been assumed on basis of in situ geochemical analysis (cf. chapter 14.1). These two objects overlap with data of ore from the Rudnik deposit in the Šumadija district (sample I) and of mineralisations of the Kopaonik Mountains (sample II). The lead block and platelet, however, do not unambiguously match Pb isotope ratios of local ores (Fig. 15.1). The first-mentioned is the only metal artefact which overlaps with resources from the Shashkoc-Janjevo district in the plots normalised to ^{204}Pb. Similarly to data of the metallurgical by-products (see above), the Pb isotope signature of the artefacts as well could result from mixing of ore from several, isotopically slightly differing mineralisations for metallurgical processing (discussed in detail in section 16.3). Mixing also could have occurred after primary ore smelting. Merkel (2007) assumes that cupellation of the crude Pb was carried out by the Romans at central points within the mining districts under greater administrative control than the primary Pb extraction. Pb bullion produced at several smelting sites thus might have been collected and subsequently treated in bulk (discussed more detailed in section 19.1).

[1] The following references have been utilised to compile the database: Amov (1974; 1979; 1983; 1993) reported in Gale et al. (2000); Arribas & Tosdal (1994); Baron et al. (2006); Bode (2008); Bode et al. (2009); Boni et al. (1985); Brevart et al. (1982); Chalkias et al. (1988); Durali-Müller (2005); Gale (1990, pers. comm); Graeser & Friedrich (1970); Harms et al. (2012); Kalogeropoulos et al. (1989); Krahn & Baumann (1996); Large et al. (1983); Le Guen et al. (1991); Lescuyer et al. (1998); Lillo (1992); Lippolt et al. (1983); Ludwig et al. (1989); Marcoux (1997); Marcoux et al. (2002); Orgeval et al. (2000); Pernicka et al. (1993); Pomiès et al. (1998); Santos Zalduegui et al. (2004); Scaife et al. (2001); Schneider (1998); Stos-Gale et al. (1996); Stos-Gale et al. (1998); Swainbank et al. (1982); Tornos & Chiaradia (2004); Trincherini et al. (2001); Valera et al. (2005); Veselinović-Williams (2011); Wagner & Schneider (2002); own data.

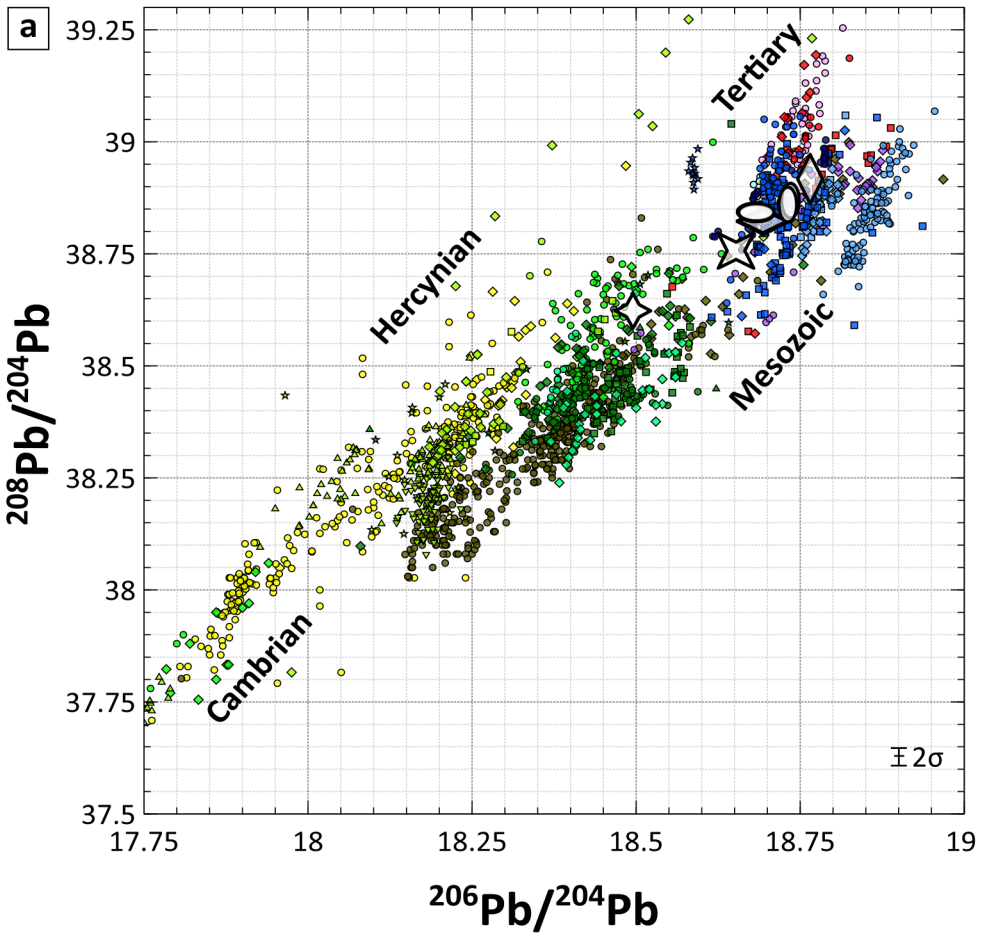
a
39.25
39
38.75
38.5
38.25
38
37.75
37.5
17.75
18
18.25
18.5
18.75
19
$^{208}Pb/^{204}Pb$
$^{206}Pb/^{204}Pb$
Tertiary
Hercynian
Mesozoic
Cambrian
±2σ

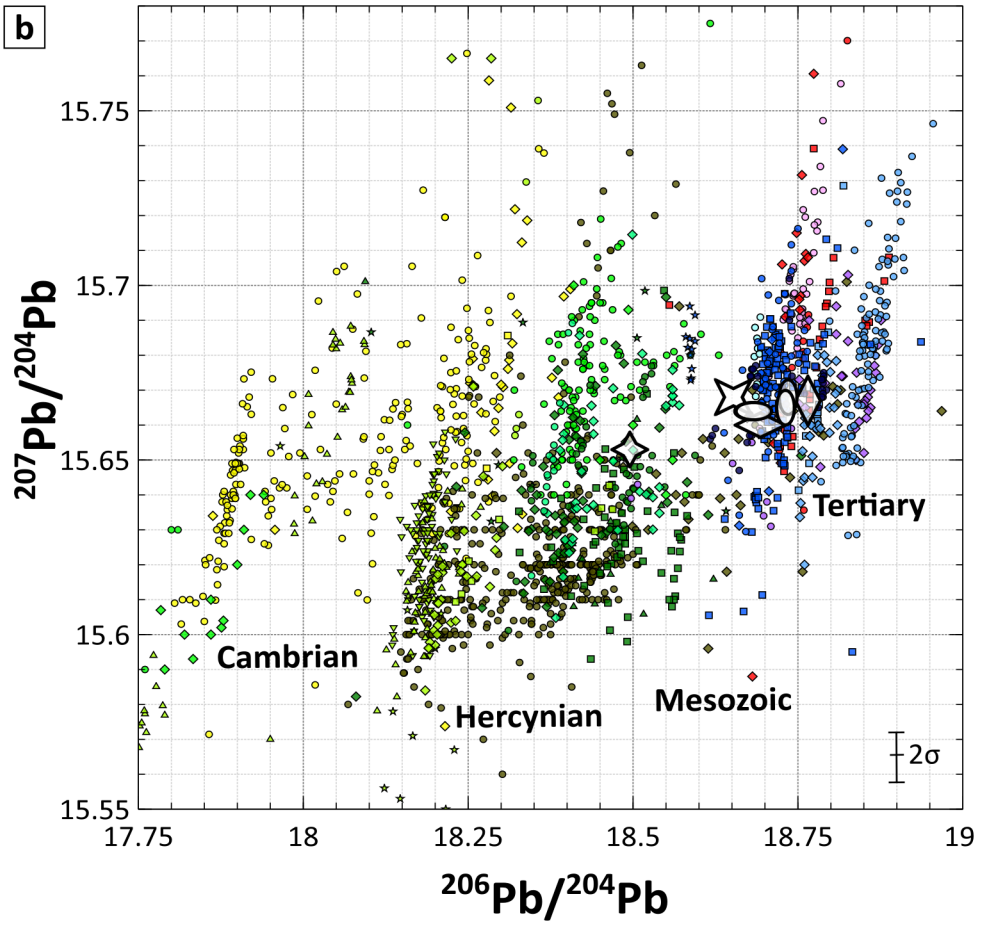
b
15.75
15.7
15.65
15.6
15.55
17.75
18
18.25
18.5
18.75
19
$^{207}Pb/^{204}Pb$
$^{206}Pb/^{204}Pb$
Tertiary
Cambrian
Hercynian
Mesozoic
2σ

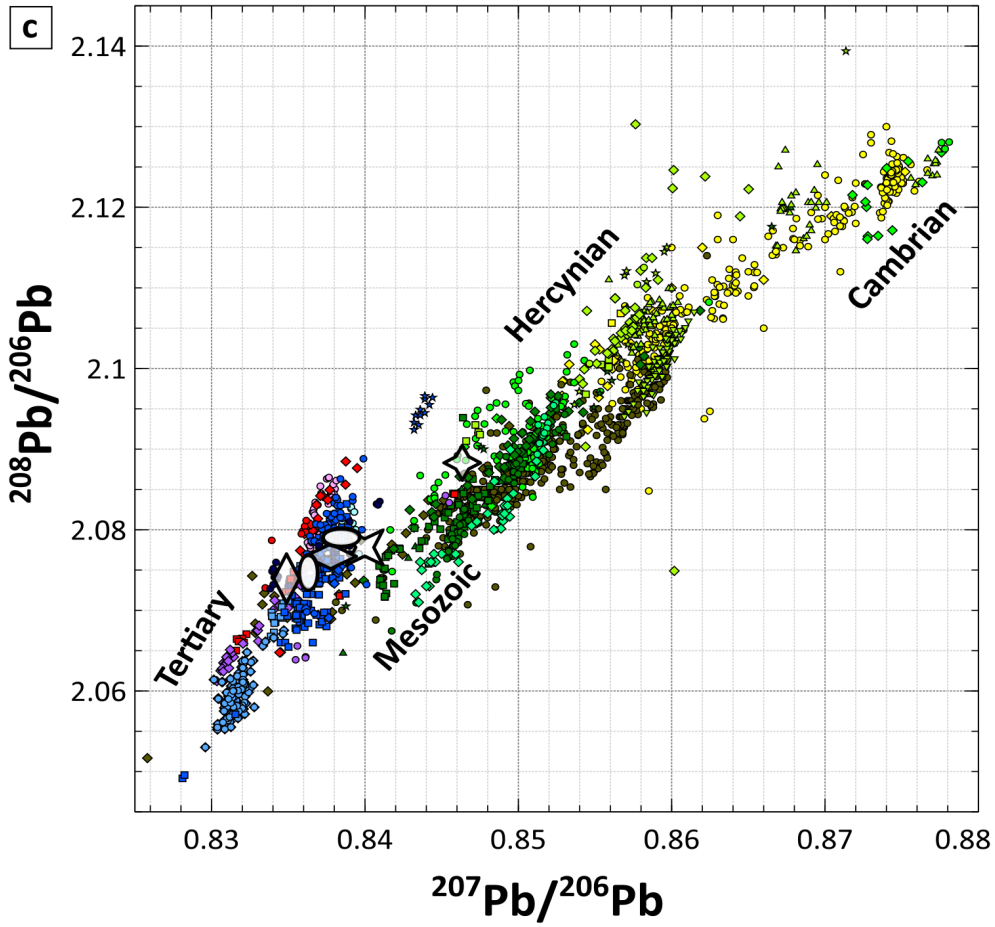
c
2.14
2.12
2.1
2.08
2.06
208Pb/206Pb
Cambrian
Hercynian
Mesozoic
Tertiary
0.83
0.84
0.85
0.86
0.87
0.88
207Pb/206Pb

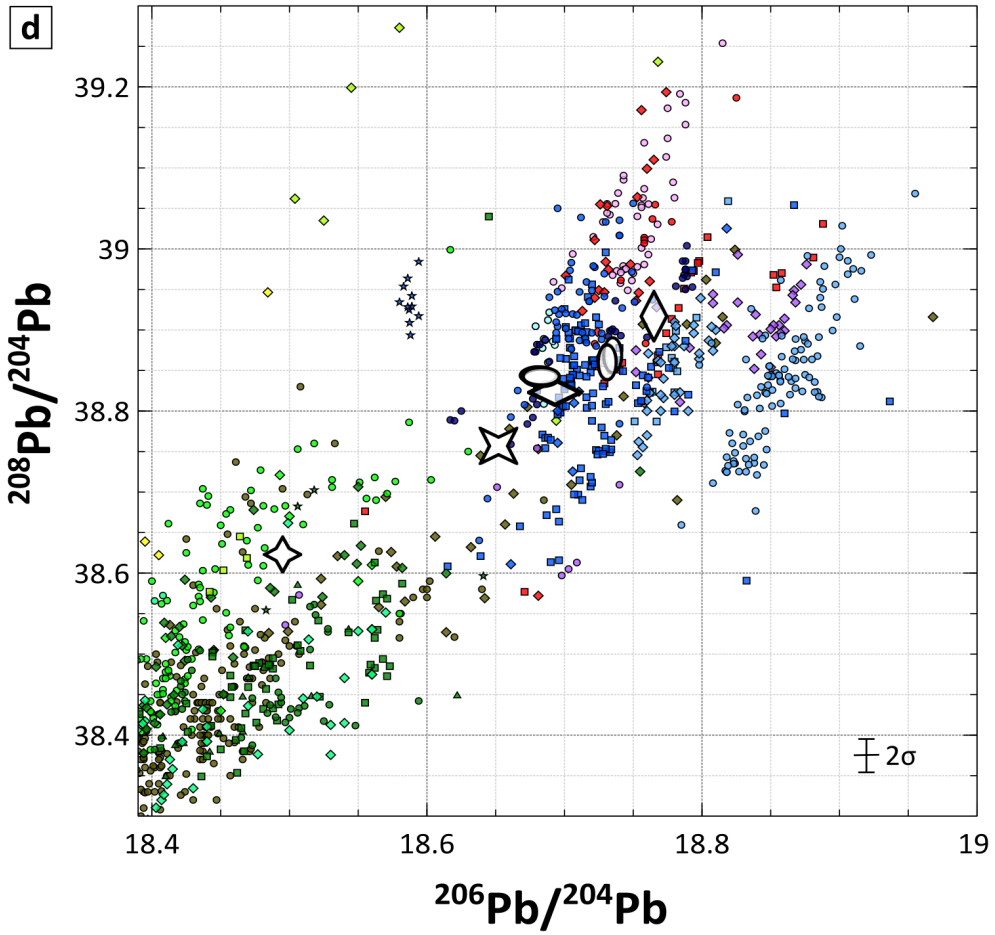
d
39.2
39
38.8
38.6
38.4
208Pb/204Pb
2σ
18.4
18.6
18.8
19
206Pb/204Pb

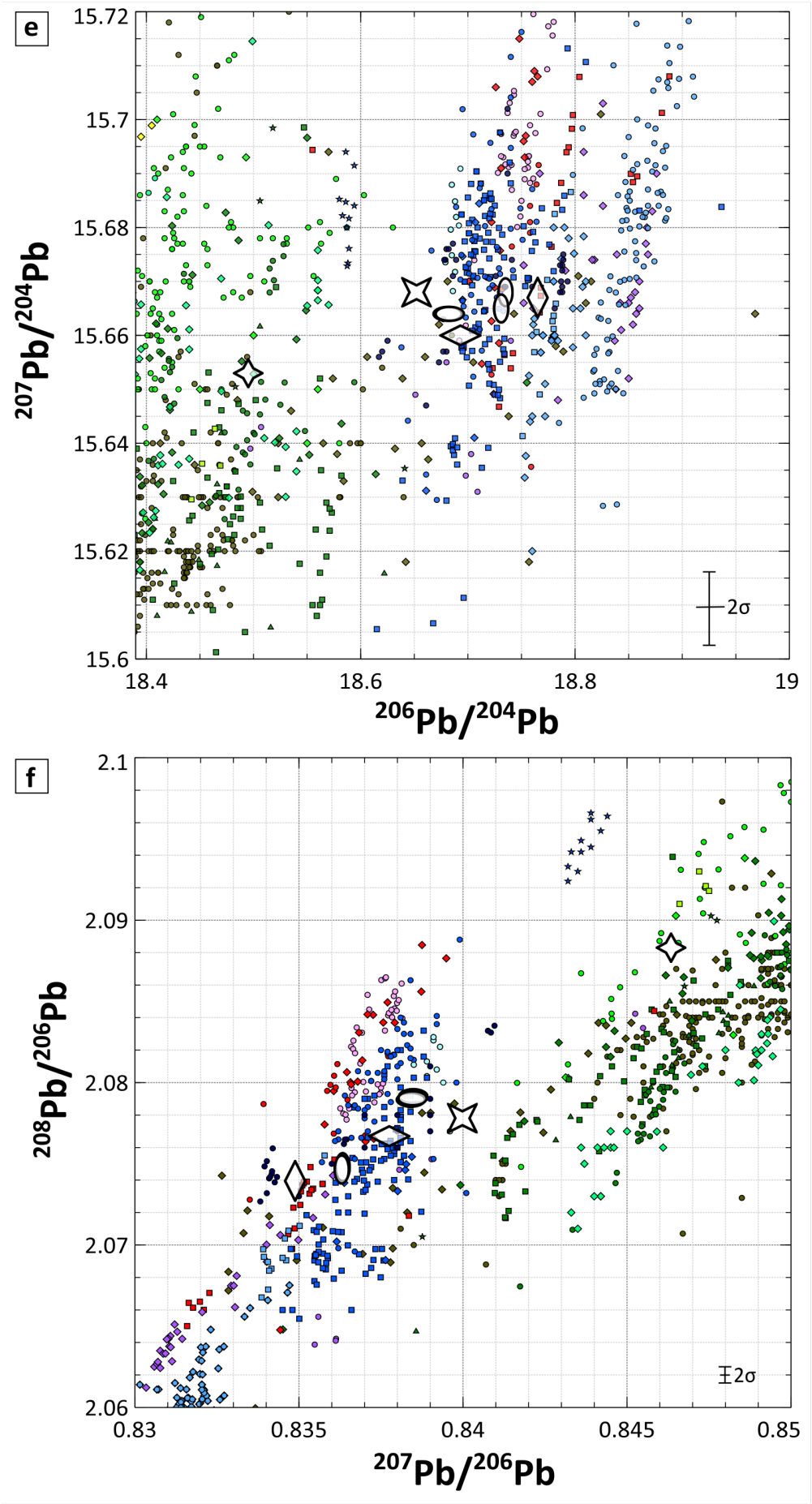
e
15.72
15.7
15.68
15.66
15.64
15.62
15.6
18.4
18.6
18.8
19
$^{207}Pb/^{204}Pb$
$^{206}Pb/^{204}Pb$
2σ
f
2.1
2.09
2.08
2.07
2.06
0.83
0.835
0.84
0.845
0.85
$^{208}Pb/^{206}Pb$
$^{207}Pb/^{206}Pb$
2σ

Figure 15.2.: Pb isotope data of analysed metal artefacts in comparison with literature data of Roman imperial Pb-(Ag) mining districts. 2σ represents two times the average standard deviation of the isotope ratios; in Fig. c) the error bars are smaller than the size of the literature data points. In Fig. a to c, the corresponding geological periods are indicated at their approximate position. a) $^{208}Pb/^{204}Pb$ versus $^{206}Pb/^{204}Pb$, overview of the compiled data. b) $^{207}Pb/^{204}Pb$ versus $^{206}Pb/^{204}Pb$, overview of the compiled data. c) $^{208}Pb/^{206}Pb$ versus $^{207}Pb/^{206}Pb$, overview of the compiled data. d) $^{208}Pb/^{204}Pb$ versus $^{206}Pb/^{204}Pb$, detailed view. e) $^{207}Pb/^{204}Pb$ versus $^{206}Pb/^{204}Pb$, detailed view. f) $^{208}Pb/^{206}Pb$ versus $^{207}Pb/^{206}Pb$, detailed view.

15.1.4. Copper-rich artefacts

As mentioned in chapter 14.2, the Pb isotope data only allows drawing conclusions about the source region of the Pb and, in case of the bronze sample due to the correlation of the two elements, potentially the Ag content of the coins, but not on the provenance of the Cu or even Sn metal sources. Furthermore, due to the production volume of the mints, mixing of raw material as well as recycling have to be considered as potential factors largely impeding provenance analysis.
Both coins can be isotopically clearly distinguished and do not overlap with each other within the error range. The impure copper coin generally agress with ores of a Mesozoic / Tertiary formation age ($^{206}Pb/^{204}Pb$ = 18.652; $^{207}Pb/^{204}Pb$ = 15.668; $^{208}Pb/^{204}Pb$ = 38.757; $^{207}Pb/^{206}Pb$ = 0.83998; $^{208}Pb/^{206}Pb$ = 2.07781). The bronze coin in contrast possesses a significantly older signature ($^{206}Pb/^{204}Pb$ = 18.495; $^{207}Pb/^{204}Pb$ = 15.653; $^{208}Pb/^{204}Pb$ = 38.623; $^{207}Pb/^{206}Pb$ = 0.84634; $^{208}Pb/^{206}Pb$ = 2.08831) and plots within the transitional area between Hercynian and Mesozoic mineralisations (Fig. 15.2). Both samples, however, rather plot at the rims of Pb isotope 'fields', overlap with literature data from different districts depending on which ratios are examined or, within the error range, do not match any data at all (sample III in the $^{208}Pb/^{204}Pb$ versus $^{206}Pb/^{204}Pb$, VI in the $^{207}Pb/^{204}Pb$ versus $^{206}Pb/^{204}Pb$ and $^{208}Pb/^{206}Pb$ versus $^{207}Pb/^{206}Pb$ diagram). This observation further argues for on the basis of electron microprobe data (cf. chapter 14.2) already suspected mixed isotope signature caused by utilisation of raw material with differing provenance and / or recycling of scrap metal. Furthermore, as has been suggested for metallurgical by-products and lead artefacts (see above; cf. chapter 16.3), mixing of ore resources already on a local scale bears the potential to notably influence the Pb isotope signature.
The bronze coin's $^{207}Pb/^{204}Pb$-$^{206}Pb/^{204}Pb$ signature (Fig. 15.2b, e) matches ore data points of Bulgaria's Stara Planina range, Britain (Mendips, Pennines and Northern district; OXALID; Scaife et al., 2001) and the Rheinisches Schiefergebirge (Bode, 2008; Durali-Müller, 2005; Harms et al., 2012; Krahn & Baumann, 1996; Large et al., 1983; Schneider, 1998; Wagner & Schneider, 2002). Its $^{208}Pb/^{206}Pb$-$^{207}Pb/^{206}Pb$ ratios (Fig. 15.2c, f) overlap with literature values reported for the Cévennes (Baron et al., 2006; Bode et al., 2009; Brevart et al., 1982; Le Guen et al., 1991; Orgeval et al., 2000), a subunit of the French Massif Central, within the error range of the sample. In the $^{208}Pb/^{204}Pb$-$^{206}Pb/^{204}Pb$ diagram (Fig. 15.2a, d), the copper sample agrees with ore analyses of the Rudnik deposit (Šumadija district; Pernicka et al., 1993) and the Schwarzwald (Bode, 2008; Lippolt et al., 1983). It is not possible to exclude distinct mining districts as ore source regions since the mixing ratios of the utilised raw materials cannot be comprehended. Consequently, the provenance of potential Pb (and possibe Ag) sources of the two coins could not have been reconstructed.

15.2. Copper isotopes

Cu isotope data might serve as an additional tool to further characterise the raw material sources of metal artefacts (i.e. primary sulphides, phases associated with supergene processes and oxidation). However, a multitude of both geological, but possibly also metallurgical and archaeological

factors potentially controlls and affects the element's isotope signature. Since their possible impact has not yet been fully deciphered and awaits further research, Cu isotope data only provides tentative conclusions on this subject (cf. section 3.3.2).
Only local ores and metal artefacts have been analysed for their Cu isotope signature. No measurements of metallurgical by-products have been carried out since the presence of numerous sulphide inclusions or even restitic smelting remains already clearly indicates the (predominantly) primary sulphide nature of the smelter feed. The ore samples have been characterised in order to contribute to the literature database of Cu isotope values and to obtain data from raw material potentially utilised for the manufacturing of the metal artefacts investigated.

15.2.1. Ore

The δ^{65}Cu values of the investigated ores cover a wide range which extends between -4.29 and 11.90 ‰ (Fig. 15.3). Utilisation of data of sample 14018 has not been possible, since the elevated Ni content of the specimen hosted by particularly marcasite conflicted with the application of Ni as internal standard to correct for mass fractionation (cf. chapter 7.5). The rather low bulk Cu content of sample 11043(3), which consists almost exclusively of arsenopyrite, resulted in high analytical uncertainties.
Generally, the δ^{65}Cu values of the ores correspond to the known fractionation behaviour (cf. chapter 3.3.2) with samples containing phases related to supergene enrichment (i.e. secondary sulphides and carbonates) being marked by comparably enriched δ^{65}Cu and primary sulphides typically plotting in a δ^{65}Cu range between -1 and +1 ‰. Samples 13099(2) and 11015, however, which possess δ^{65}Cu values below -1 ‰ typically assigned to oxidation and leaching processes, based on their phase assemblage have been, as well as 11043(3), classified as primary ore. Bacterial activity, though, has been experimentally demonstrated to significantly affect or even reverse the Cu isotope signature of ores (cf. section 3.3.2) and hence might provide a possible explanation for these observations. The high δ^{65}Cu values of the samples 11043(2) and 13020(1), which consist of secondary sulphides (particularly covellite, chalcocite, digenite) and especially in the case of 13020(1), oxidised carbonate phases, are interpreted to result from extreme weathering conditions on the waste heaps which in combination with the large surface area of the ore specimens highly influenced the isotope signature.

15.2.2. Metal artefacts

All metal artefacts, regardless of their composition (i.e. lead, bronze or copper objects) possess δ^{65}Cu values between -0.75 and 0.44 ‰, hence suggesting that they were produced from primary sulphide ore. This hypothesis generally matches the analytical determined restitic S content of the artefacts and the fact that Pb was almost always and Cu in Roman times mostly - due to the exhaustion of oxidised mineralisations located at or near the surface particularly mined in earlier times - was extracted from primary sulphide ore. Crude Pb excavated at Mramor Samakove (sample MrS-Pb) in contrast possesses a δ^{65}Cu value of 1.43 ‰, which slightly exceeds the range of -1 to +1 ‰ typically attributed to primary sulphides (cf. chapter 3.3.2). However, due to the fact that this sample only has been analysed for its Pb and Cu isotope data, but not by means of petrography and in situ geochemistry, this δ^{65}Cu value only can be tentatively interpreted. A

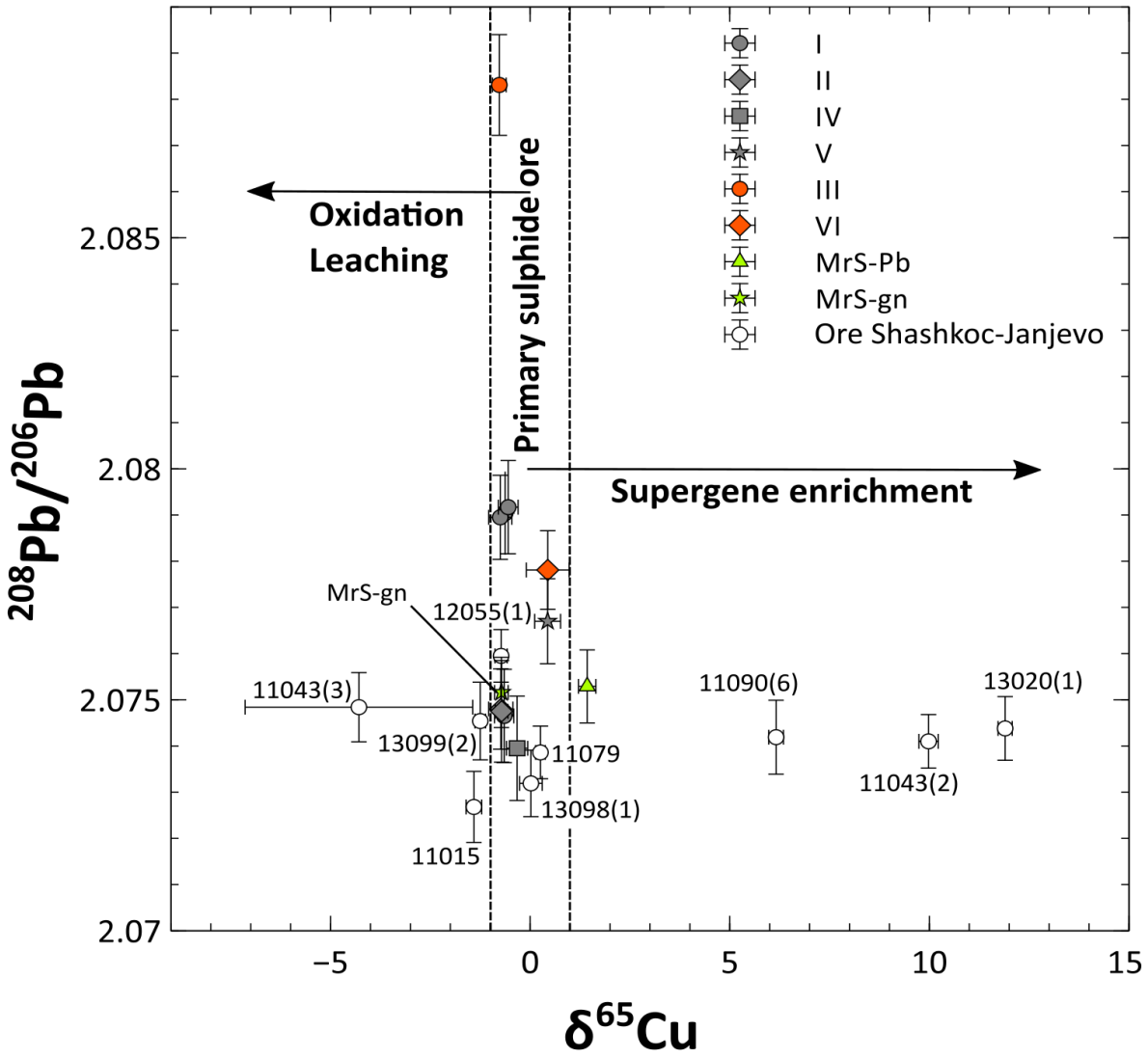

Figure 15.3.: Plot of $^{208}Pb/^{206}Pb$ versus $\delta^{65}Cu$ of the investigated ore and metal artefact samples. The range of $\delta^{65}Cu$ typically attributed to primary sulphides (i.e. -1 to +1 ‰) is indicated, as well as the general influence of supergene enrichment and oxidation / leaching processes, which increase and decrease $\delta^{65}Cu$, respectively.

possible explanation for this observation could be that the determined Cu content is present in the form of matte inclusions comprehending Cu-(Fe) sulphides, which due to supergene weathering and enrichment processes might account for the observed positive δ^{65}Cu value.

Part III.

Discussion and interpretation

16. Reconstruction of archaeometallurgical processes: I. The ore basis

16.1. The local ore mineralisation and extracted metal(s)

The ubiquitous presence of Pb sulphide and metal in the investigated samples as well as findings of native Pb and cupellation remains at several smelting sites (Mramor Samakove, Hanroc and Marec) clearly indicate that the metallurgical process focused on the extraction of Pb and Ag and potentially Au. Abundant sulphide phases in slags or matte prove the predominantly primary character of the smelted ore. This observation is in agreement with the fact that Pb was typically won from sulphide ores with galena as the principal source of the metal (cf. chapter 2.1). Oxidised Pb ores (e.g. cerussite, anglesite) generally are thought to have been exploited in the early stages of mining activities. Their occurrences therefore most likely were typically already exhausted in the era of the Roman Empire. Indeed, findings of Bronze Age stone tools nearby ancient workings in the Shaskoc-Janjevo district (cf. section 6.1) indicate a significantly earlier beginning of local mining activities, which initially might aimed mainly for locally present Cu ores (cf. chapter 8.1.2).
The omnipresence of Pb sulphide and metal in the investigated metallurgical by-products agrees with the mineralogy of the local mineralisation. It can be generally addressed as Pb-Ag ore, even though it locally shows a pronounced polymetallic character (cf. chapter 8, also see chapter 18.2). However, the ubiquitous presence of galena, which comprises noteworthy Ag contents (all analyses: median 895 ppm) renders the local mineralisation an excellent source for Pb and Ag - commodities, which still are extracted from the local ore today. Other Ag carriers, particularly fahlore and locally secondary Cu phases, contributed to its precious metal grade. The occurrence of secondary Cu sulphides and oxidised phases in the Shashkoc-Janjevo district apparently is restricted to certain ore bodies. Due to its impure character with elevated Pb, Zn, Fe and As abundances it is assumed to have been smelted together with Pb-richer ore and mainly treated for its precious metal content. It is not clear whether Cu was also extracted from this ore type. In the Iberian Pyrite Belt, however, Rothenberg & Blanco-Freijeiro (1981) assume that the Romans smelted the secondary Cu sulphide chalcocite for both its Ag and Cu content.

16.2. The geochemical signature of the Shashkoc-Janjevo district

Geochemical patterns observed in metallurgical remains may be linked to distinct mineralisation styles and thus may add to the characterisation of the smelted raw material. Consequently, different ore types may be retraced within the investigated *chaîne opératoire* by their elemental signature. Grains of restitic spinel *ss* observed in the examined smelting remains (cf. chapter

9.2.7) mirror the local abundance of serpentinite within the Shashkoc-Janjevo district (cf. section 8). The skarn-type replacement deposit of Novobërdë in contrast is associated with marble, andesite and amphibolite. Pb-Zn- and Cu-bearing ore at the Zhegovcë occurrence in the vicinity of the smelting sites Voguçincë, Mirash, Mirash Novo and Akllap mainly is present within trachyte and basalt, gabbro, tectonic mélange and only subordinate serpentinite, respectively (cf. sections 3.2.1 & 6.1). Consequently, a characteristic 'serpentinite signature' (i.e. elevated abundances of Mg, Cr and Ni; these elements partially also correlate in their host phases - cf. chapter 9.2.7) in addition to Pb isotope data may provide further local provenance information on the (dominant) source region of the furnace feed processed at the investigated smelting sites (section 16.3). In order to assess a potential relation of the sampled metallurgical remains with ultramafic rocks, the abundances of the index elements Mg, Cr and Ni in their main carrier phases (i.e. olivine, clinopyroxene and spinel *ss*) have been evaluated with regard to the Pb isotope ratios of the specimens (Fig. 16.1).

In the specimens 12015(5) from Voguçincë, 11029(5) from Mirash Novo, 12016(2) from Akllap and 13030(1) from Ostri Vrh, spinel *ss* with comparably elevated Cr contents is present (Fig. 16.1a). Enriched Ni abundances in spinel *ss* are observable in the samples 10024(2) from Mramor Proni Butoçit, 12016(1) from Akllap as well as 13030(1) and 13031(1) from Ostri Vrh (Fig. 16.1b). A slag sample from Akllap (12016(2)) and a matte cake from Voguçincë (sample 10-2B) comprise (Ni,Cu)(Sb,As) and Ni-rich FeAs, respectively (cf. chapters 11.1.3 and 11.3.1). Olivine analyses of the specimens 10024(2), 10024(4) and 10024(5) from Mramor Proni Butoçit as well as 10021(21) from Mramor Samakove and 12016(1) from Akllap are marked by significantly elevated Mg #[1]. Of the clinopyroxene data, only sample 10024(5) shows an above-average value (Fig. 16.1c). Altogether, the serpentinite signature expressed by elevated Mg, Cr and Ni abundances in olivine, clinopyroxene and spinel *ss* grains from metallurgical remains thus can be retraced to the sites of Mramor Proni Butoçit, Akllap and Ostri Vrh as well as partially to the complexes of Voguçincë (10-2B, 12015(5)), Mirash Novo (11029(5)) and Mramor Samakove (10021(21)). The often pronounced correlation of enriched Cr, Ni and Mg contents with the Pb isotope ratios of the Shashkoc-Janjevo district implies that the ultramafic signature is related to locally abundant serpentinite. This interpretation is further confirmed by the fact that the Pb isotope data of samples, which display the strongest signature at the investigated smelting sites (i.e. 10-2B and 12015(5) at Voguçincë, 11029(5) at Mirash Novo, 12016(2) at Akllap), overlap with those of the Shashkoc-Janjevo ores. Serpentinite generally could have been potentially introduced into the smelting system by restitic gangue material, which was not completely removed during beneficiation, as deliberately added siliceous fluxing agent or, if the ultramafic rock was utilised as furnace building material, by liquefaction. The furnace debris discovered so far, however, solely comprises quartzite or igneous rocks (mainly andesite and dacite) which have been won in open quarries, e.g. nearby Shashkoc (cf. Fig. 6.1). Utilisation of serpentinite as furnace construction material furthermore appears due to its thermal instability caused by the heat-induced breakdown of hydrous secondary minerals rather unlikely. An association due to the usage of clays derived from weathered serpentinite for the lining of the furnace seems more plausible. Indeed, phyllosilicate minerals (smectites, illites and chlorites) generated by weathering

[1] $\mathrm{Mg\#} = \mathrm{Mg}/(\mathrm{Mg}+\mathrm{Fe})\times 100$

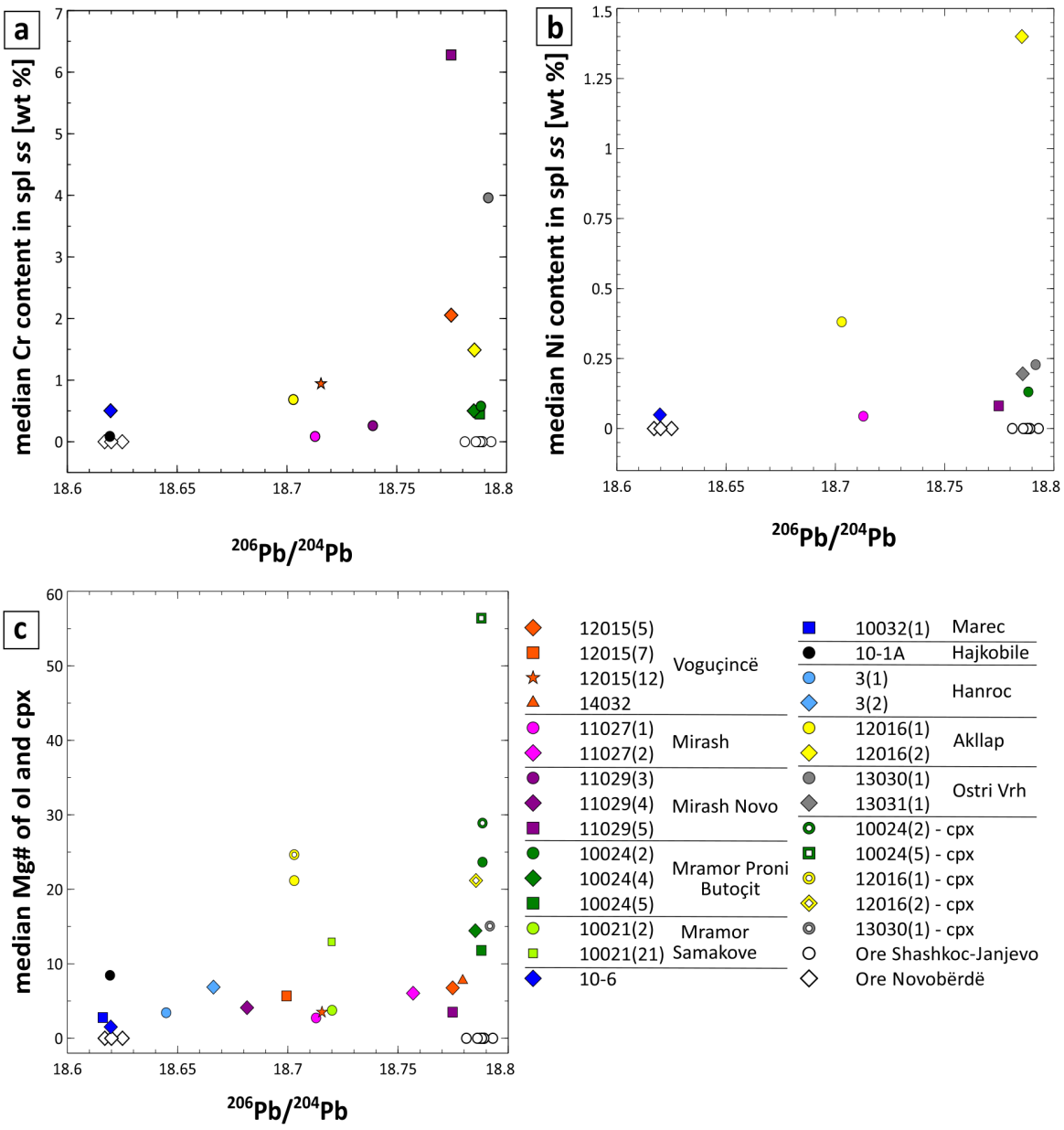

Figure 16.1.: Biplots of serpentinite index elements in slag phases related to the Pb isotope signature of the specimens. a) Median Cr content [wt %] in spinel *ss* versus $^{206}Pb/^{204}Pb$. b) Median Ni content [wt %] in spinel *ss* versus $^{206}Pb/^{204}Pb$. c) Median Mg# of olivine and clinopyroxene versus $^{206}Pb/^{204}Pb$.

of the ultramafic rock have been identified in the Kishnica area (Dangić, 1989). However, these clays are not available in the immediate vicinity of smelting sites other than Ostri Vrh, which is located c. 1.5 km southeast of the Kishnica mine in the very heart of the Shashkoc-Janjevo district. Since it is highly likely that the ancient metallurgists if possibly relied on locally abundant materials for the construction of the furnaces, the observed serpentinite signature most probably is directly linked to the smelter feed. In this case, Ni, Mg and Cr were introduced either due to the utilisation of serpentinite barren rock, which accumulated during ore beneficiation, as silica source for the slag melt or by unintentional adding due to incomplete separation of the gangue material from the ore.
Consequently, the observed serpentinite signature in addition to matching Pb isotope ratios implies that the smelting sites of Voguçincë, Mirash Novo, Mramor Proni Butoçit, Mramor Samakove, Akllap and Ostri Vrh were to a certain extent supplied with ore from the Shashkoc-Janjevo district. No unambiguous association to the Shashkoc-Janjevo district, neither by Pb isotope data nor enrichment of serpentinite index elements, could be found for the sites of Mirash, Marec, Hajkobile and Hanroc. The first three localities mentioned are relatively far away from the district ($>$ 15 km distance; cf. Fig. 6.1) and thus might have been (predominantly) supplied from other mineralisations located closer to them. This is most likely for samples from Marec (10-6 and 10032(1)), which isotopically match ore data from the nearby Novobërdë deposit situated approximately 16 km northeast of the Shashkoc-Janjevo district. Hanroc, which is situated within eyeshot to the workings of the mining district of Shashkoc-Janjevo though could not be geochemically linked to the local resources. It either has been, as the Pb isotope ratios of its two samples indicate, mainly supplied by ore from Novobërdë or by another, not yet investigated occurrence in its vicinity, which also possesses a slightly older formation age than the mineralisation at Shashkoc-Janjevo.

16.3. Ore supply of the smelting sites

Several samples of the investigated metallurgical by-products could be isotopically matched to either the ore data of Shashkoc-Janjevo or Novobërdë (cf. Fig. 15.1). The examined specimens from Mramor Proni Butoçit and Ostri Vrh could be completely related to ores from the Shashkoc-Janjevo district. The sites of Voguçincë (10-2B, 12015(5), 14032), Mirash Novo (11029(5)), Mramor Samakove (MrS-gn, MrS-Pb) and Akllap (12016(2)) could be partially attributed to supply from this mineralisation (cf. chapter 15.1.2). The samples linked to raw material from the Shashkoc-Janjevo district furthermore are marked by elevated abundances of Cr, Ni and Mg, which presumably were introduced by locally abundant serpentinite rocks (chapter 16.2). Two basin slag samples from Marec (10-6, 10032(1)) overlap with ore data of the nearby Novobërdë mineralisation (cf. chapter 15.1.2).
Several of the examined metallurgical remains, however, also plot between the Pb isotope datasets of the two deposits (cf. Fig. 15.1). This implies that the ancient metallurgists either processed ore with a Pb isotope signature intermediate between those of Shashkoc-Janjevo and Novobërdë or it has to be assumed that the smelting sites were supplied with 'mixed' raw material from several, isotopically slightly differing mineralisations. The latter hypothesis offers a likely explanation particularly for the origin of the Pb content of metallurgical by-products, which plot

close to ore data of the two deposits but do not overlap with them in all three Pb isotope diagrams. The corresponding samples are 11027(1) from Mirash with the Shashkoc-Janjevo data and 10032(4), 10-1A and 3(1) from Marec, Hajkobile and Hanroc with Novobërdë, respectively. Among the samples which do not match the isotope signatures of the Novobërdë deposit and the Shashkoc-Janjevo district, the specimens 12015(7) and 12015(12) from Voguçincë, 11027(1) from Mirash and 12016(1) from Akllap overlap in their Pb isotope ratios. All three sites are located south of the Shashkoc-Janjevo district (Fig. 6.1). However, while Voguçincë and Akllap are located relatively close to each other (c. 4 km), the distance between these two sites and Mirash is with approximately 15 km significantly larger. The samples not only are isotopically similar. 12015(12) and 12016(1) are marked by comparably elevated Zn contents in olivine and spinel *ss* (cf. chapters 9.2.1 and 9.2.7) while 11027(1) comprises layers and veins of matte s.s. with a significant proportion of (Zn,Fe)S. Specimen 12015(7) does not follow this pattern and does not contain particularly Zn-enriched phases. However, Zn can be easily volatilised during metallurgical treatment and thus is introduced in varying proportions into the slag melt. Hence, it is reasonable to assume that the three sites were at least partially supplied with ore from the same mineralisation. Occurrences of Pb-Zn-Cu-Sb and Cu ore have been reported from Zhegovcë (ICMM, 2011; cf section 3.2.2), which is located between the three sites and only a few kilometres away from Voguçincë and Akllap and hence constitutes a very likely source of raw material. The fact that the $^{208}Pb/^{204}Pb$, $^{207}Pb/^{204}Pb$, $^{206}Pb/^{204}Pb$, $^{208}Pb/^{206}Pb$ and $^{207}Pb/^{206}Pb$ ratios of the four slag samples completely overlap within their error ranges renders it highly probable that this data cluster corresponds to the isotope signature of the ore mineralisation exploited and finally smelted at these sites. Isotopic characterisation of ore occurrences south of the Shashkoc-Janjevo district, particularly of Zhegovcë, thus should be envisaged to investigate in future research projects (cf. section 20).

The cupellation remains collected at Marec (10-5), despite the vicinity of the smelting site to the Novobërdë deposit, exhibit a significantly different isotope signature than the ores from this mineralisation. This observation either could be due to the fact that raw material from several, isotopically slightly different ores was treated or that the relatively high Pb losses during the cupellation process led to fractionation of the isotopes. When considering that ^{204}Pb as the lightest isotope theoretically should be easier volatilised, the sample signature should be more 'pristine' in the ^{206}Pb-normalised diagram. However, this is not the case (Fig. 15.1) and therefore, in accordance with experimental studies (cf. section 3.3.1), fractionation processes apparently did not affect the Pb isotope ratios of this specimen. Slags from Hanroc, even though the site is located within eyeshot to workings of the Shashkoc-Janjevo district, surprisingly do not overlap with this Pb isotope ore data but in fact plot closer to analyses from the Novobërdë deposit. Samples from Hajkobile as well do not match the Pb isotope signature of raw material from the study area. However, since this site is located rather distant to the deposits of Shashkoc-Janjevo and Novobërdë (c. 15 km northeast of the latter; Fig. 6.1), this observation is not unexpected and potentially implies that in Hajkobile (mainly) ore derived from mineralisations outside the study area was treated. Particularly Pb-rich samples from Mramor Samakove (restitic galena ore and crude Pb) agree very well with isotope data of Shashkoc-Janjevo, while furnace slags and pig iron from this site in contrast exhibit significantly different Pb isotope ratios. Analytical

artefacts due to an insufficient Pb content can be excluded; however, potential isotope fractionation processes might at least be theoretically relevant. Analogous to the investigated cupellation remains (sample 10-5; see above), the furnace slags and pig iron show a comparable pattern in the ^{206}Pb - normalised isotope ratio plot (Fig. 15.1). Consequently, fractionation processes apparently did not (significantly) influence the Pb isotope ratios of these samples.
In sum, it can be stated that at most smelting sites, irrespective of their preliminary dating, isotopically heterogeneous raw material was treated, consequently implying in most cases a decentralised organisational structure. Due to the rich and abundant mineral resources in the study area and the apparently often large-scaled operations, it seems highly likely that the metallurgical sites were supplied with ore from different workings. Furthermore, the smelter feed composition also might have been deliberately selected from differing ore types by the metalworkers to ensure and maintain a rather consistent raw material basis and thus optimum process conditions for the extraction of Pb, Ag and potentially Au. Particularly the contents of Cu, As and Sb in the furnace charge, which might lead to formation of the by-products matte and speiss (cf. sections 2.5.2 and 2.5.3), could be balanced by deliberate selection of raw material, i.e. mixing of different ore types. Ferrous speiss is generated due to abundant As contents introduced by e.g. fahlore and arsenopyrite and apparently was considered an unwanted by-product (cf. section 2.5.3; discussed in detail in chapter 18.3.1). The formation of matte depends on the availability of Cu and S in the melt system and thus can be, similarly to ferrous speiss, partially controlled by roasting during which S and As are volatilised. The proportion of matte generated generally should be kept low since it may incorporate notable amounts of Ag. However, if Cu-bearing ores are treated, the formation of a certain amount of matte is desirable since it effectively binds Cu contents, which would otherwise partition into crude Pb and drastically rise its melting point, thus impeding subsequent treatment (cf. chapter 2.5.2). Considering the commonly polymetallic, Cu-Sb-As-bearing character of the mineralisation at Shashkoc-Janjevo (and also at Zhegovcë) as well as the fact that Ag grades of the ore often are coupled to Cu-Sb-As-rich phases (i.e. fahlore, secondary Cu phases), a carefully selected raw material basis must have been highly relevant for the efficiency of the metallurgical process.

16.4. Preparation of the ore charges

16.4.1. Beneficiation

Generally, Pb-rich ore should be rather easily beneficiated due to the high specific gravity of the main phase galena, which significantly differs from that of the gangue minerals (i.e. particularly quartz and carbonates). Mining archaeological surveys in the study area indicate that the mined ore was roughly sorted by weight and colour and crushed on-site, potentially at terraces in the immediate vicinity of the workings (cf. chapter 6.1). Troughs, which might potentially have been used for wet-mechanical beneficiation, were discovered nearby the hamlet of Shashkoc. Compared to the extent of the ancient mining remains, the number and capacity of the troughs though is very small. No other wet-mechanical beneficiation installations were found in the study area so far and hence indicate that the ore - in contrast to e.g. Laurion where widely similar ore was mined and elaborately beneficiated (cf. section 5.1.1) - mainly was concentrated with 'dry'

techniques. However, formerly potentially present facilities also might have been destroyed by later activities, particularly by modern mining and housing development. Since it is known from historical transcripts that at least precious metal-bearing ore was finely ground and sieved (cf. chapter 2.2), appropriate beneficiation installations also are to be expected in the study area. Archaeological evidence to substantiate this assumption though is still lacking. The myriads of mill stone negatives - if these were de facto used for the grinding of ores (cf. chapter 6.1) - besides the troughs this far are the only potential signs for the application of more lavish beneficiation techniques.

Several pieces of restitic pristine galena ore (i.e. not roasted or otherwise treated with heat) retrieved from the excavation at Mramor Samakove nearby the furnace complex possess dimensions of approximately 1cm × 1cm × 1cm. The finding situation does not provide any indications whether the ore was further treated - i.e. crushed and ground or roasted - before it was charged into the furnaces. However, it can be noted that the ore was delivered to at least the site of Mramor Samakove as approximately pea-sized pieces (cf. chapter 2.2). The typically remote and spacious location of all presumably Roman / late antique and some potentially medieval / early modern sites would have provided the necessary space for beneficiation facilities. Additionally, the location of the smelting complexes nearby rivulets could also be due to the application of wet-mechanical techniques to further concentrate the ore. However, as mentioned earlier, to date neither in the mining district nor in the vicinity of the smelting sites preserved beneficiation installations could be discovered yet.

The efficiency of wet-mechanical beneficiation methods strongly depends on the mineralisation style (e.g. disseminated, veins or massive ore bodies) and the phase assemblage of the raw material. Galena possesses a significantly higher specific density than other minerals typically abundant in the local deposits[2] and, if the ore is finely ground, should have been possible to separate relatively effectively from the barren host material (i.e. mainly quartz and carbonate gangue or siliceous host rocks). However, the other commonly intimately intergrown ore phases typically possess similar specific gravities (see above) and hence are difficult to separate. Due to their role as Ag carriers, particularly fahlore and secondary Cu sulphides also surely were not intended to remove from the charge. Thus, especially if ore bodies with a pronounced polymetallic character were exploited, a chemically diverse mixture of base metal sulphides is assumed to have been subjected to metallurgical processing.

16.4.2. Roasting

While rich galena concentrates can be efficiently processed by the single-step roast-reaction process, polymetallic ore charges comprising elevated proportions of pyrite, chalcopyrite, sphalerite and As- and Sb-bearing phases in modern metallurgy are roasted prior to the actual smelting process carried out under reducing conditions (cf. chapter 2.3). Rivalling advantageous and detrimental effects - the volatilisation of undesired (e.g. As, Sb, Zn), but also desired elements (Pb, potentially precious metals) as well as the possible retention of a certain S content to generate matte, which effectively binds the Cu abundances of the ore - necessitate a carefully

[2]Specific gravities of locally relevant ore and gangue minerals (all values taken from Handbook of Mineralogy): gn: 7.7; sp: 4.1; py: 5.0; apy: 6.2; ccp: 4.3; tnt: 4.6; ttr: 5.0; cct: 5.8; dg: 5.7; cv: 4.6; mlc: 4.0; qz: 2.7; cal: 2.7; sd: 3.9; rds: 3.7.

balanced roasting step. A certain amount of restitic pyrite in the smelted furnace charge is even favourable since it lowers the fuel demand due to the heat resulting from the combustion of its S content (Gowland, 1914); pyritic smelting, i.e. the deliberate utilisation of this advantageous effect, has been applied in metallurgical processing since medieval times (e.g. Heimbruch, 1990; Laub, 1980).
However, although roasting partially is suspected on basis of geophysical measurements of smelting sites, this far no definite proof for appropriate installations could be found. If roasting was performed at all, it definitely was not carried out completely as the ubiquitously present newly-formed sulphide inclusions within the slags clearly demonstrate. The fact that restitic ore minerals commonly present in the slag samples always are sulphide phases further argues for a rather low degree of roasting or that the raw material was not roasted at all.

16.4.3. Dressing

Due to the ubiquitous presence of Fe-bearing sulphides (particularly pyrite, but also sphalerite, chalcopyrite, arsenopyrite and fahlore) within the local ore, no Fe had to be externally added to the furnace charge to adjust the slag melt (cf. chapter 2.5.1). SiO_2 to ensure the formation of slag and potentially CaO[3], however, would have to be deliberately added to the furnace charge. Silica is provided by the quartz gangue as well as by the igneous and metamorphic rocks partially hosting the ore bodies (i.e. andesite, dacite and serpentinite; cf. chapter 8), by the leached cap of the mineralisations (prominently at the 'Mondlandschaft' close to Shashkoc) but also as sand from the creeks the smelting sites are located at. Liquefying furnace material as well introduces notable amounts of SiO_2 into the slag melt (cf. Kronz, 1997; Ströbele et al., 2010). CaO-bearing material mainly could be obtained from the often Fe- and Mn-rich carbonate gangue of the mineralisations and partially also as marble, e.g. in the vicinity of Novobërdë. Gangue and host rock material automatically accumulates during the beneficiation of the ores. Restitic base and precious metal-bearing compounds (particularly the reportedly auriferous gangue quartz gangue; Hyseni & Alliu, 1999) furthermore contribute to the amount of metal extractable from the furnace charge. In contrast to sand from the creeks, however, the barren rock gained during beneficiation potentially must have been further crushed or ground before its grain size was sufficiently small to ensure efficient metallurgical processing.

[3]The potential addition of calcareous fluxes is discussed in detail in the following chapter.

17. Reconstruction of archaeometallurgical processes: II. Smelting of ores

17.1. Deciphering of the process type indicated by the investigated slags

The often observed restitic ore grains (particularly galena) and smelting remains as well as the generally high proportion of sulphide phases indicate that the investigated basin slags all are related to primary smelting. The only sample with a slightly ambiguous character is a Pb-rich slag (13031(1)) from the Ostri Vrh site, which is made up of melilite and kalsilite. Kalsilite has been mainly described in particularly PbO-rich metallurgical material such as cupellation remains and associated slags (Eckstein et al., 1994; Ettler et al., 2015; Rehren & Hauptmann, 1995), i.e. in metallurgical debris related to metal refining. It therefore has to be questioned whether the examined specimen truly is related to primary treatment of ore. However, the presence of base metal sulphides often associated with droplets of native Pb as well as the absence of metal oxide phases (i.e. particularly PbO and CuO) typically described in raffination slags (Eckstein et al., 1994; Ettler et al., 2015; Rehren & Hauptmann, 1995), strongly argues for the interpretation of the specimen as smelting slag. Besides, no evidence for cupellation this far has been discovered at Ostri Vrh. Furthermore, in a slag sample (13030(1)) from the same site, a large inclusion of a smelting residue (intermediate between primary ore and matte; cf. section 10.1.1) has been observed. Consequently, Ostri Vrh as well has been interpreted as a site where (mainly) primary ore smelting was carried out.

From Mramor Samakove, this far only furnace slags have been investigated in detail, i.e. by means of petrography, in situ phase analysis and Pb isotope characterisation. However, during the latest excavation campaign basin slags, restitic galena ore and a small piece of crude Pb have been collected. The examined furnace slags are comparably Pb-poor and contain droplets of typically Fe-dominant base metal sulphide melt and, in one sample, Fe oxide cluster comprising pyrrhotite and magnetite. Even though these slags are not directly indicative of a relation to primary Pb-dominant metallurgy, the overall unambiguous relation of the site to Pb-(Ag) production by native Pb and galena ore exclude a different interpretation. Noteworthy elevated Sn abundances (up to 0.95 wt %), which have been determined in Pb droplets of the samples 10021(2) and 10021(21) from Mramor Samakove, could be either introduced by smelting of comparably Sn-rich ore or addition of Sn-bearing compounds for recycling, e.g. solder. Slag specimens collected at the 'Mondlandschaft' nearby Shashkoc and Ulpiana's workshop complex (chapters 9.1.3 and 9.3) could be unambiguously identified as smithing slags.

17.2. Classification of slags

Slags are the most important tool to reconstruct metallurgical process schemes. While their morphology mirrors the furnace construction, the differing chemistry of the siliceous slag melt is expressed by the varying phase assemblages of the investigated samples. They record the composition of the smelted charges (i.e. the proportion and type of fluxes applied), the process parameters (i.e. the furnace atmosphere and temperature) and potential interaction of the slag melt with charcoal ash and furnace material (Keesmann et al., 1984; cf. chapter 2.5.1). As proposed by Keesmann et al. (1984), a first approach to classify the investigated basin slags has been done on the basis of their dominant silicate phases (cf. section 9.2). Ordered according to increasing CaO and SiO_2 contents of the main phases, five different types can be distinguished :

Olivine-type: Particularly early precipitated olivine is typically Fe-rich and compositionally close to fayalite [$2\,FeO \cdot SiO_2$], later crystallised grains often are Ca-richer and chemically more similar to kirschsteinite [$FeO \cdot CaO \cdot SiO_2$]

Olivine + clinopyroxene-type: Only one sample (12016(1) from Akllap) could be attributed to this subtype, which contains comparably Fe-poor olivine and clinopyroxene (hedenbergite / augite) in approximately equal proportions

Clinopyroxene-type: The main phase is Fe-dominant clinopyroxene, whose composition typically ranges between hedenbergite [$FeO \cdot CaO \cdot 2\,SiO_2$] and augite

Melilite-type: The melilite chemistry is predominated by Zn-, Fe- and Mg-bearing endmembers and can be generally given as $(FeO,ZnO,MgO) \cdot 2\,CaO \cdot 2\,SiO_2$

Glassy type: Besides glass, which makes up the biggest part of this type, these slags comprise spinel *ss* and potentially Pb-bearing silicates

While the silicate phases effectively record variations of the bulk chemistry of the slag melt (and thus document changes of the furnace composition), information on the fO_2 conditions is provided by the presence or absence of Fe^{2+} / Fe^{3+}-bearing oxides (i.e. spinel *ss* and wüstite) and their precipitation within the crystallisation sequence. Thus further subtypes can be established (Fig. 17.1). The formation of alkali carriers (i.e. foids and feldspars) is related to interaction of the slag liquid mainly with charcoal ash, but also the furnace material and hence generally records the impact of these two influences on the chemistry of the smelting system. Since these factors only to a limited extent could be controlled by the ancient metallurgists, they are not included in the classification scheme.

17.2.1. Olivine-type

Subtype a: Olivine (I), low to absent spinel *ss*

Olivine-dominant slags with accessory or absent spinel *ss* have been retrieved from Marec (where all investigated samples can be attributed to this subtype), Hanroc and Voguçincë. The preliminary dating of these smelting sites ranges from Roman / late antique to medieval / early modern. The phase assemblage of the samples is rather simply and comprises olivine, of which partially

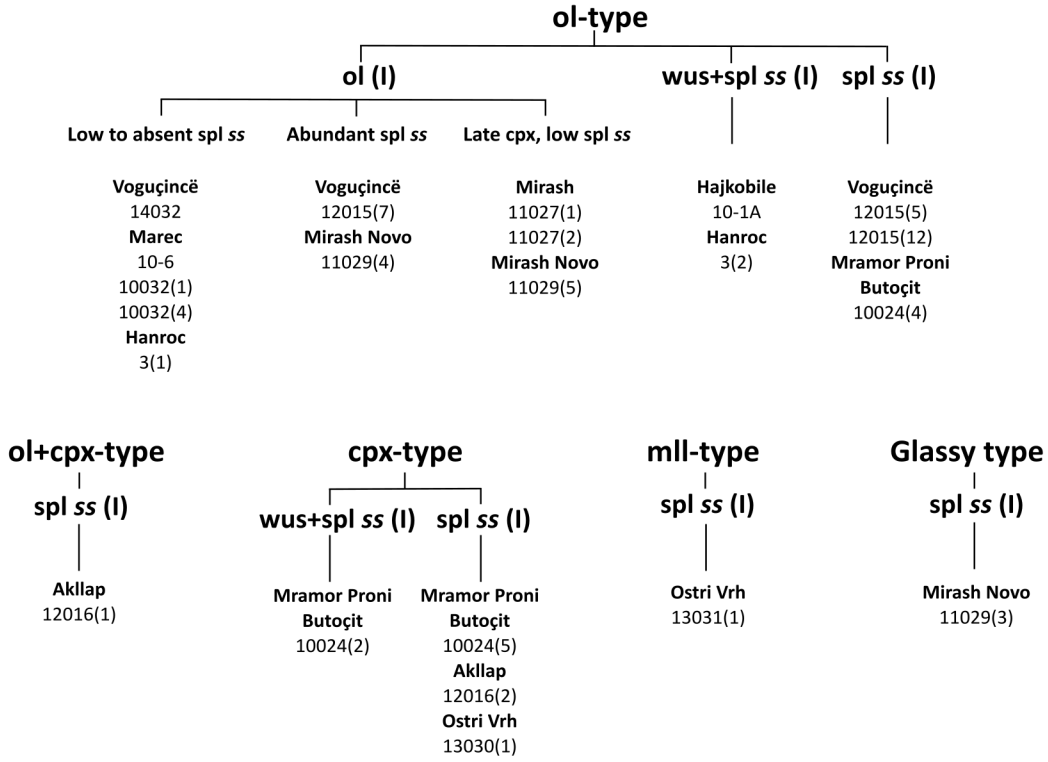

Figure 17.1.: Classification scheme of metallurgical slags according to the dominant silicate compounds. Subtypes are established on basis of the presence or absence of Fe^{2+} / Fe^{3+}-bearing oxide phases (spinel *ss* and wüstite), late clinopyroxene (only in olivine-type slags) and the general solidification sequence of the specimens. '(I)' denotes the firstly precipitated phase(s).

two generations are present, in most slags accessory Fe-rich oxides (particularly spinel *ss*) and, solely in sample 14032, leucite. Frequently present feathery olivines record particularly high cooling rates (c. 1450 °C/hour; Donaldson, 1976; cf. Fig. 9.3a). Zoning of olivine grains has been commonly observed and is particularly developed in samples 10032(1) and 10-6 (cf. Fig. 9.3e). It points to comparably rapid cooling under non-equilibrium conditions. The samples 10-6 and 10032(4) from Marec do not contain a late generation of olivine. While the olivine data of the samples from Marec and Hanroc generally is Fe-rich and plots in a relatively narrow field, the analyses from sample 14032 (Voguçincë) are somewhat enriched in Ca (cf. Fig. 9.4). In sample 14032, leucite precipitated from a K-rich siliceous melt, which apparently crystallised parallel to the Fe-richer main liquid (cf. chapter 9.2.5). Symplectitic crystallisation of olivine and leucite ended the solidification of this specimen. Due to the typically rapid cooling of the slags, influence of atmospheric oxygen which may lead to e.g. formation of iscorite, is not observable. Generally, the small proportion of Fe^{2+} / Fe^{3+}-bearing phases (i.e. spinel *ss* and wüstite) abundant in these samples records comparably low fO_2. Sulphides are present as matte s.s. (sample 14032) and interstitial cluster, respectively, and as ubiquitous spherical inclusions.

Subtype b: Olivine (I), abundant spinel *ss*

Olivine-type slags with lately precipitated, subordinate spinel *ss* have been collected at the sites of Voguçincë and Mirash Novo. The corresponding preliminary dating of these sites is Roman / late antique. The two samples both contain a second generation of olivine. The chemistry of this phase generally is dominated by the fayalite component. While the Fe abundances are rather constant, the Ca content exhibits notable variation (cf. Fig. 9.4). In 12015(7) relatively high amounts of leucite are present, which forms symplectites with olivine. Sulphide phases occur as interstitial cluster (12015(7)) and spherical droplets. Sample 11029(4) contains a layer of ferrous speiss (cf. chapter 11.1).

Subtype c: Olivine (I), late clinopyroxene and low spinel *ss*

This subtype as well is exclusively linked with smelting sites of a potentially Roman / late antique dating and has been found at Mirash and Mirash Novo. Both spinel *ss* and clinopyroxene are formed late in the solidification sequence of this type and occur as star-shaped aggregates centered on grains of magnetite-rich spinel *ss* (cf. Fig. 9.5b). All samples also contain a second generation of lately precipitated olivine grains. Olivine generally possesses a Fe-rich composition with low Ca, Mg and Zn contents (cf. Fig. 9.4). Leucite only has been observed in accessory proportions. Sulphides are present as widespread veinlets and layers of matte s.s. and spherical droplets.

Subtype d: Wüstite + spinel *ss* (I)

This subtype has been observed at the presumably medieval / early modern sites of Hajkobile and Hanroc. The two samples (10-1A and 3(2)) both solely contain a first generation of olivine, which is marked by notably enriched and variable Ca contents in conjunction with rather constant Fe abundances. The solidification of this subtype begins with the simultaneous precipitation of spinel *ss* and wüstite dendrites (cf. Fig. 9.7a, c), which, however, have been already largely

transformed to spinel *ss* due to rising fO_2 after the slags came in contact with atmospheric oxygen. The common presence of iscorite in both samples (cf. Fig. 9.9b) as well records increasing fO_2 and consequently stability conditions outside the wüstite field. The pronounced zoning of spinel *ss* grains with an Al-richer core and Fe^{3+}-richer rim is expressed in the spinel *ss* classification diagram as mixing line between hercynite- and magnetite-richer compositions (Fig. 9.8). Both samples are comparably coarse-grained and only contain a low amount of interstitial glass. The increased presence of leucite – which forms symplectites with olivine and (former) wüstite (cf. Fig. 9.6d) – as well as the spinel *ss* compositions determined indicate elevated bulk Al contents. Sulphides only are present as droplets.

Subtype e: Spinel *ss* (I)

Samples attributed to this subtype have been retrieved from the sites at Voguçincë (preliminary Roman / late antique dating; 12015(5) and 12015(12)) and Mramor Proni Butoçit (not dated yet; 10024(4)). All samples contain two generations of olivine. The olivine data of the three slags is chemically clearly distinguishable. Particularly analyses of grains from sample 10024(4) are significantly different and marked by comparably low Fe in conjunction with elevated and highly variable Ca contents (cf. Fig. 9.4). Spinel *ss* grains from samples 12015(5) and 12015(12) exhibit a slight zoning with an Al-richer core and Fe^{3+}-richer rim (cf. Fig. 9.8). Analyses of spinel *ss* and olivine from sample 12015(12) are particularly Zn-rich. 10024(4) comprises particularly magnetite-rich spinel *ss*. Iscorite occurs accessory in the two samples from Voguçincë (i.e. 12015(5) and 12015(12)). All slags contain comparably high proportions of leucite, which forms eutectoid intergrowths with olivine (cf. Fig. 9.3f). Sulphide phases are present as layers of matte s.s. (samples 12015(5) and 10024(4)), interstitial cluster (12015(5), 12015(12)) and spheroids.

17.2.2. Olivine + clinopyroxene-type

This subtype has been only assigned to sample 12016(1) from the presumably medieval / early modern site of Akllap. It is marked by approximately equal proportions of olivine and clinopyroxene (cf. Fig. 9.6b). Relatively Zn-rich, magnetite-dominant spinel *ss* is the first phase which crystallised (cf. Fig. 9.8). Olivine is relatively Fe- and Ca-poor, but comparably enriched in Zn and Mg (cf. Fig. 9.4). Clinopyroxene is marked by a hedenbergitic to augitic composition and, according to recalculation procedures, does not contain Fe^{3+}(cf. Fig. 9.5c). Abundant leucite forms symplectites with olivine. The glass possesses an elevated PbO content (cf. Fig. 9.10c). Sulphides are only present as droplets.

17.2.3. Clinopyroxene-type

Subtype a: Wüstite + spinel *ss* (I)

Only sample 10024(2) from the not yet dated site of Mramor Proni Butoçit could be attributed to this subtype. The composition of the clinopyroxene ranges between hedenbergite and rather Ca-poor wollastonite; no Fe^{3+} has been calculated (cf. Fig. 9.5c). Spinel *ss* data overlaps with analyses of 12016(1) and similarly is marked by elevated contents of Zn and Fe^{3+} (cf. Fig. 9.8).

Spinel *ss* is significantly more abundant than wüstite (cf. Fig. 9.7b). Olivine is present as accessory phase. One analysis yielded an Fe-poor composition with elevated Zn and Mg contents (cf. Fig. 9.4), which is highly similar to data of sample 12016(1) from Akllap. Leucite occurs in symplectites with both olivine and wüstite. Sulphides are only present as droplets.

Subtype b: Spinel *ss* (I)

The subtype of clinopyroxene-dominant slags solely containing spinel *ss* as Fe^{2+} / Fe^{3+}-bearing oxide phase has been considerably more often observed. Associated samples have been collected from the not yet dated complex of Mramor Proni Butoçit and the presumably medieval / early modern sites of Akllap and Ostri Vrh. Clinopyroxene is present as prismatic sub- to euhedral grains, which partially are centered on spinel *ss* rhombs (cf. Fig. 9.5a, b). The composition is hedenbergitic to augitic (cf. Fig. 9.5c). Fe^{3+} has been calculated for analyses of samples 12016(2) and 10024(5). Clinopyroxenes of the samples 10024(5) and 13030(1) are subsilicic (cf. chapter 9.2.2). Spinel *ss* is significantly enriched in the magnetite component. Data of sample 13030(1) exhibits considerable Zn contents (cf. Fig. 9.8). One analysis of lately precipitated olivine from sample 10024(5) yielded a Fe-depleted, notably Ca-rich composition (cf. Fig. 9.4). Sulphides are solely present as droplets, but a significant amount of Pb also is present as native metal.

17.2.4. Melilite-type

The only melilite-type slag has been collected at the potentially medieval / early modern site of Ostri Vrh. The sample shows an uncommon slag chemistry, which is characterised by a comparably low bulk SiO_2 content leading to the formation of kalsilite instead of leucite. Magnetite-dominated spinel *ss* is the main phase (cf. Fig. 9.6a and 9.8). The slag apparently is particularly Zn-rich with the element being mainly hosted by melilite and spinel *ss*. The interstitial glass possesses extraordinary high PbO contents, which hence significantly differs from analyses of other samples (cf. Fig. 9.10c).

17.2.5. Glassy type

The only sample of the glassy slag type investigated by in situ analysis is 11029(3) from the presumably Roman / late antique site of Mirash Novo. Similar specimens, however, have also been collected at Voguçincë. Analogous to the melilite-type slag, sample 11029(3) is characterised by a high proportion of magnetite-rich spinel *ss*, which possesses skeletal grain shapes indicative of rapid cooling. The glass contains an unidentified Pb-bearing silicate phase (cf. section 9.2.2) whose abundance corresponds to the rather low PbO contents determined in the glass (cf. Fig. 9.10c). The sample consists to equal proportions of slag and a layer of matte s.s. (cf. Fig. 10.1j), thus indicating that it was one of the last portions of slag to be tapped from the furnace.

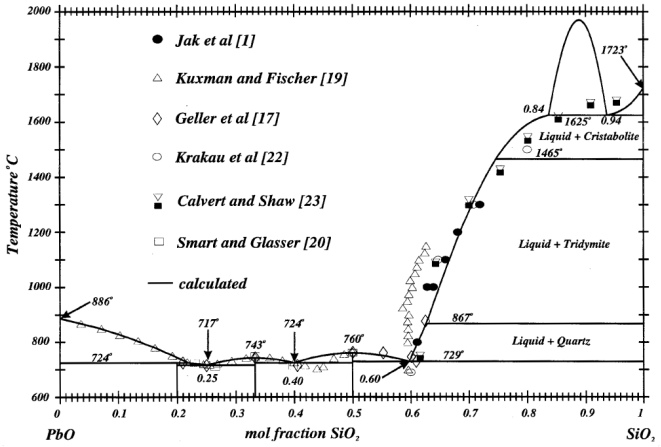

Figure 17.2.: Binary diagram PbO - SiO_2 (Jak et al., 1997).

17.3. Relation of slag types to process parameters

17.3.1. Temperature

The temperature under which the furnaces were worked generally can be assumed to must have exceeded the melting point of galena (1115 °C; Dutrizac, 1980; Kullerud, 1969), which irrespective of the fact whether the ores were partially roasted before smelting surely was one of the main compounds of the smelter feed. To ensure the complete liquefaction of the furnace charge, the temperature thus must have been significantly higher than 1100 °C and potentially at least approximated 1200 °C. Maximum temperatures, in accordance with previous estimates by e.g. Hauptmann (2014) and Manasse & Mellini (2002a; b), are assessed to have been around 1400 °C. Typically, the temperatures are assumed to have ranged between 1200 and 1300 °C and potentially were higher only in the vicinity of the tuyeres. The liquidus temperature of the slags, however, potentially may have been effectively lowered by K and Pb. Kronz (1997) estimated that elevated bulk K contents may have decreased the temperature to less than 1100 °C. Similarly, high PbO abundances in the slag melt also drastically lower the liquidus temperature, as can be deduced by phase relations in the PbO - SiO_2 system (Fig. 17.2; Jak et al., 1997). Olivine-type slags record beginning solidification at temperatures around 1200 °C. The liquidus temperatures of pure fayalite and kirschsteinite are 1205 and 1208 °C, respectively (Bowen et al., 1935). The highest melting point of Ca-Fe olivines (1230 °C) corresponds to a composition of 41 % Fe_2SiO_4, which also marks the limit of solid solution in the Fe_2SiO_4 - Ca_2SiO_4 binary. The minimum temperature of the Ca-Fe olivine solid solution is 1117 °C at a proportion of 81 % Fe_2SiO_4 (Bowen et al., 1935). Incorporation of Zn into the fayalite structure does not significantly influence the liquidus temperature (Jak et al., 2001). Pyroxenes with a hedenbergitic composition are precipitated as ferriferous wollastonite *ss* from the liquid at c. 1240 °C and upon cooling are transformed to hedenbergite *ss* (Lindsley & Munoz, 1969). The Ca-Mg melilite phase åkermanite melts at 1454 °C (Osborn & Muan, 1960). The melting points of Fe^{2+} / Fe^{3+}-bearing oxides (i.e. wüstite and spinel *ss*) are significantly higher than 1400 °C (Muan & Osborn, 1965) and surely do not correspond to realistic liquidus temperatures. In fact, slags in which oxide phases precipitated first are assumed to possess approximately similar liquidus temperatures

than specimens whose solidification sequence begins with the crystallisation of olivine.
Generally, the working temperatures employed in the furnaces seem to have been sufficient to ensure complete liquefaction of the furnace charge. Partially restitic galena, often with cubic cross-section, is abundant. Sample 13030(1), a clinopyroxene slag from the Ostri Vrh site, contains a particularly large-scaled sulphide inclusion of a smelting remain (cf. chapter 10.1.1). Besides relictic ore, also siliceous or oxidic phases derived from the added fluxes or from gangue material, which was not completely removed during beneficiation, have been observed in some of the examined slags. The most prominent relictic mineral certainly is spinel *ss*, which is interpreted to have been introduced into the furnace charge by serpentinite rocks (cf. chapters 9.2.7 and 16.2). Since the generally high melting points of spinel-group phases (cf. Muan & Osborn, 1965) could not have been reached by the ancient metallurgists, these minerals are preserved in the slag. However, typically only few single grains of restitic ore, gangue and host rock or fluxes are abundant. They thus are assumed to rather record local inhomogeneities of the charges and fluctuating temperatures within the furnace than a significant degree of incomplete liquefaction of the smelter feed. Overall, the compositions of the slags consequently record temperatures high enough to ensure a completely molten charge.

17.3.2. Furnace atmosphere

The furnace atmosphere conditions during slag formation can be roughly assessed on the basis of the mineral redox buffer equilibria. The breakdown of fayalite with increasing fO_2 to magnetite and SiO_2 (FMQ redox buffer; cf. section 2.5.1) is the main reaction accounting for the differing phase assemblages of the investigated slags and explains the formation of olivine-dominated specimens and SiO_2-richer slags, i.e. clinopyroxene- and melilite- as well as glassy types. Generally, slags containing a main silicate phase other than olivine as well as glassy types testify to a more oxidising furnace atmosphere. The –log pO_2 values of the differing slag types have been estimated at extreme temperature ranges between 1100 and 1400 °C. The PbO - Pb buffer equilibrium has been taken as upper pO_2 limit in the Pb extraction process. Thus, the –log pO_2 values of the differing slag types can be delimited as c. between 12 and 7 for the phase assemblage fayalite + magnetite and as c. between 10 and 5 for non-olivine slag types comprising either clinopyroxene, melilite or glass as main SiO_2-bearing compound besides magnetite (Fig.17.3). While the furnace atmosphere hence was reducing enough for the extraction of Pb as well as Cu, it was too oxidising for the formation of native Fe.
The actual, realistic process conditions leading to formation of clinopyroxene-type slags often presumably were relatively close to the FMQ buffer equilibrium, as is indicated by the presence of accessory olivine in the samples 10024(2) and 10024(5) from Mramor Proni Butoçit. The phase assemblage fayalite + wüstite has not been observed in the investigated basin, but only in smithing slag samples. Indeed, since accessory relictic wüstite always occurs together with spinel *ss* in the examined basin slags, the furnace atmosphere must have been in accordance with the stability conditions of magnetite.

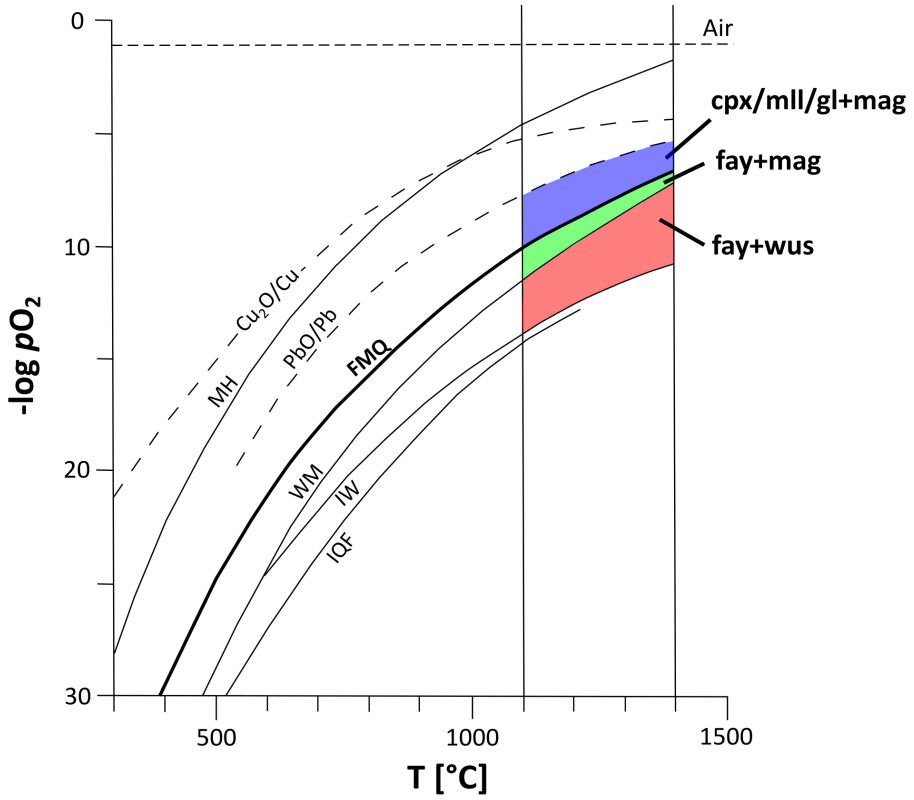

Figure 17.3.: Stability fields of the phase assemblages fayalite + wüstite, fayalite + magnetite and non-olivine, SiO_2-richer slag types in the $-\log pO_2$ versus temperature diagram (redrawn from Bode, 2008). Abbreviations of the buffer equilibria are as in Fig. 2.2.

Slag type	Representative phase	Chemistry	FeO	CaO	SiO_2
Olivine-type	Fayalite	Fe_2SiO_4	2	0	1
	Kirschsteinite	$CaFeSiO_4$	1	1	1
Clinopyroxene-type	Hedenbergite	$CaFeSi_2O_6$	1	1	2
Melilite-type	Fe-åkermanite	$Ca_2FeSi_2O_7$	1	2	2

Table 17.1.: Main silicate phases of olivine-, clinopyroxene- and melilite-type slags and FeO, CaO and SiO_2 contents of representative compounds.

17.3.3. Correlation of furnace atmosphere and bulk chemistry of the slag melt

As outlined above, the relation between the fO_2 conditions during smelting and the formation of olivine- and non-olivine slag types is established by the FMQ buffer equilibrium. This reaction generates freed silica incorporated by clinopyroxene- and melilite-group phases and glass or Pb silicates, respectively. The (main) silicate phases of olivine-, clinopyroxene- and melilite-slag types are marked by different CaO, FeO and SiO_2 abundances (Tab. 17.1). Both clinopyroxene- and melilite-group phases possess an in comparison to olivine higher SiO_2 content (two parts SiO_2 in clinopyroxene and melilite in comparison to only one part in olivine). Melilite-group phases and clinopyroxene differ in their CaO abundances, which are lower in the latter (Tab. 17.1). It thus can be noted that the main silicate phases of the respective slag types, i.e. fayalite, hedenbergite and Fe-åkermanite (kirschsteinite chemically only represents late crystallised olivine in olivine-type basin slags, but not the grains precipitated during the early and main phases of slag solidification) are marked by increasing SiO_2, but also CaO proportions. In fact, the formation of both clinopyroxene- and melilite-group phases requires Ca since both hypothetical Fe endmembers ($Fe_2Si_2O_6$, 'clinoferrosilite', and $Fe_3Si_2O_7$, respectively) are not stable. Ca, however, as well as silica had to be externally added to the furnace charge; Fe in contrast is already supplied in sufficient amounts by the ore (cf. chapter 16.4). The simplest slag system comprises olivine as main phase and is generated by smelting of Fe-bearing ore with added silica to ensure removal of impurities by slagging. Addition of Ca and a comparably higher amount of silica, leads to the formation of clinopyroxene- and melilite-group phases, which are in contrast to olivine stable at higher fO_2 conditions.

A rather oxidising furnace atmosphere (i.e. in the magnetite + SiO_2 stability field; Fig. 17.3) in conjunction with too low Ca contents in the slag melt, which are insufficient for the generation of clinopyroxene- and melilite-dominant slags, yields glassy types. These either contain glass with a high proportion of PbO or glass with relatively low PbO contents and precipitated Pb silicates. Adequate CaO abundances in the slag melts from which clinopyroxene- and melilite-types were formed effectively drive off PbO from silicate compounds and allow it to be reduced to its native state (cf. chapter 2.5.1). In glassy types, however, the amount of Ca in the slag melt, due to a too low or no proportion of Ca fluxed, was largely insufficient for this reaction. Consequently, a relatively high amount of Pb was slagged as PbO and hence yielded viscous slags with a comparably high specific gravity.

The subtypes of olivine- and clinopyroxene-type slags, which have been defined on basis of the occurrence of Fe^{2+} / $^{3+}$-bearing oxides and precipitation sequence of the phases (Fig. 17.1), are directly related to differing fO_2 conditions. These variations of the phase assemblage and

crystallisation sequence within the main slag types caused differing partition behaviour of the elements, which should be recorded by varying phase compositions. Olivine occurs in almost all slag types as main silicate phase or accessory compound and is, due to the FMQ buffer reaction, the most relevant fO_2 index phase. It incorporates only divalent cations in notable amounts and hence possesses a rather restricted composition. These characteristics render it ideal to examine possible correlations between chemical variations and fO_2 conditions, but also to decipher potential Ca addition to the furnace charges.

The olivine chemistry is strongly controlled by the partitioning behaviour of Fe, which typically is one of the main elements in slag and is most sensitive to variations of the redox conditions. A more oxidising furnace atmosphere corresponds to increasing formation of Fe^{3+}, which almost exclusively is hosted by Fe-rich oxide phases, i.e. spinel *ss* and wüstite and does not enter the olivine structure in significant amounts. Other early precipitating Fe^{3+} carriers (i.e. alumosilicates such as leucite, in which Al^{3+} partially is substituted by Fe^{3+}) are due to their in comparison to the oxide phases significantly lower Fe contents irrelevant for the bulk $Fe^{2+}:Fe^{3+}$ ratio of the solidifying slag melt.

Generally, the under more oxidising furnace conditions higher bulk Fe^{3+} content of the idealised slag melt leads to precipitation of Fe-rich oxides (mainly spinel *ss*, more rarely spinel *ss* + wüstite; cf. Fig. 17.1) before olivine. Since particularly spinel *ss* readily incorporates a wide range of elements (Zn^{2+}, Mn^{2+}, Mg^{2+} and Ni^{2+} as well as Al^{3+} and Cr^{3+}), but only trace amounts of Ca^{2+} and Si^{4+}, these two elements with progressing precipitation of Fe-rich oxides become more and more enriched in the restitic slag melt. Consequently, the composition of olivines of slags in which Fe-rich oxides precipitated first should be marked by a comparably (slightly) elevated Ca content (Fig. 17.4). Comparison of the Ca_2SiO_4 and Fe_2SiO_4 contents of olivine analyses attributed to the differing slag types yields several defined fields, which exhibit considerable overlap at Fe-rich olivine compositions. The similarity of the fields can be explained by the overall small differences between the subtypes. However, a general trend to Ca-richer olivine compositions with increasing proportions of Fe^{3+}-bearing spinel *ss* is discernible for data of preliminary Roman / late antique dated sites. Olivines from olivine-type slags of the sites of Mramor Proni Butoçit, Hajkobile and Hanroc, in which spinel *ss* or wüstite + spinel *ss* precipitated first, in contrast are marked by significantly Ca-richer compositions. Olivines measured in olivine + clinopyroxene- and clinopyroxene-type slags from specimens of Mramor Proni Butoçit and Akllap possess a comparably Fe-poor and partially notably Ca-rich composition. Data from olivines of the individual samples from the sites of Mramor Proni Butoçit and Hajkobile are heterogeneous and marked by highly different Fe_2SiO_4 and Ca_2SiO_4 abundances. However, the samples also have been attributed to different slag types.

Analyses from olivine-type slags, subtype a (low to absent spinel *ss*) form two separate fields. Extremely Fe-rich data originates from specimens from the preliminary medieval / early modern dated sites of Marec and Hanroc, while sample 14032 from Voguçincë is considerably Ca-richer. The elevated Ca content of the olivines is not assumed to be necessarily caused by a different composition of the furnace charge, but instead thought to be linked to the high proportion of leucite abundant in this specimen. The formation of leucite particularly depends on the availability of K, which can be introduced by charcoal ash and liquefying furnace lining. Both materials also

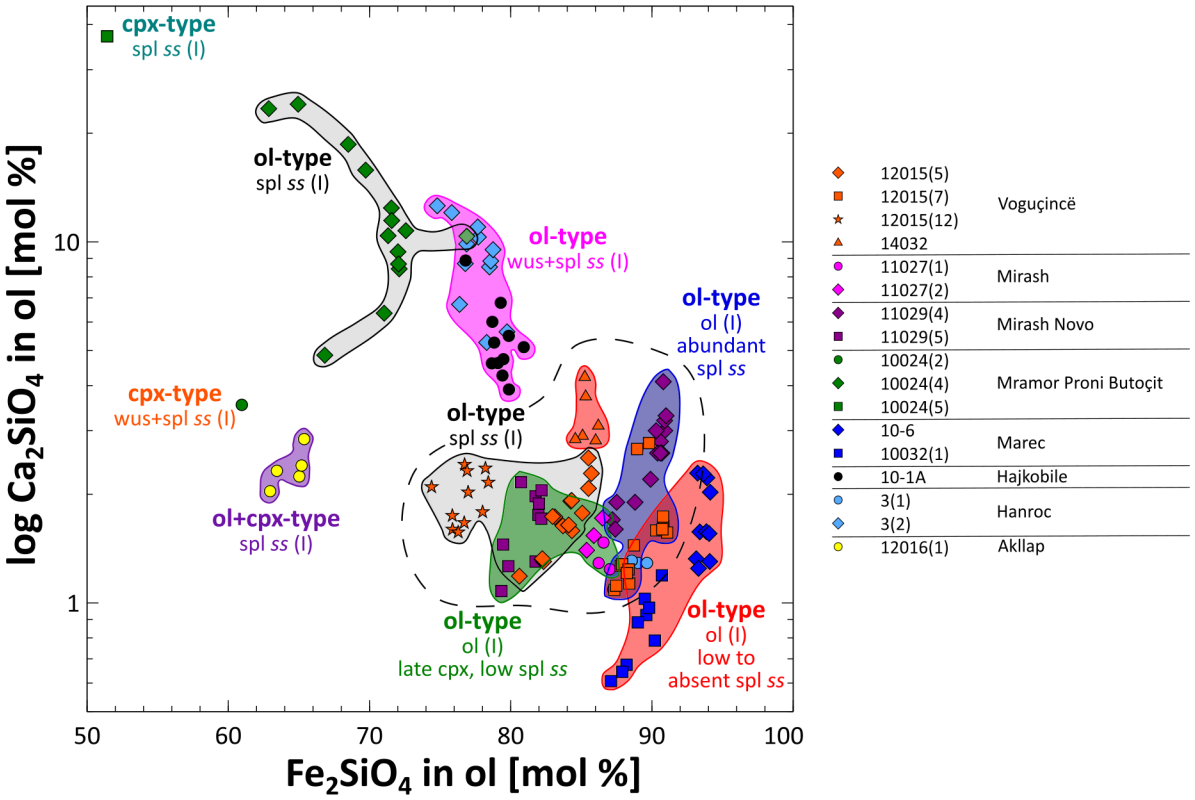

Figure 17.4.: Plot of log Ca_2SiO_4 versus Fe_2SiO_4 contents of olivine analyses sorted according to the defined slag types. Olivine data from preliminary Roman / late antique dated smelting sites (i.e. Voguçincë, Mirash and Mirash Novo) is encircled (dotted line).

contain high amounts of Ca (the composition of charcoal strongly depends on the type of wood used and hence can be highly variable; cf. chapter 2.5.1) and thus may significantly influence the composition of the slag melt and consequently the chemistry of olivine.
Data of olivine from olivine-type slags, subtype b (abundant spinel *ss*) are marked by a rather constant Fe_2SiO_4 content and considerably varying Ca_2SiO_4 proportions. It plots between the fields of subtype a and c (late clinopyroxene, low spinel *ss*) of olivine-type slags.
Olivine analyses from olivine-type slags with lately precipitated clinopyroxene (subtype c; all samples contain matte s.s.) slightly coincide with the field of subtype b, but significantly overlap with data of preliminary Roman / late antique data of olivine-dominant slags in which spinel *ss* precipitated first (subtype e). The Ca_2SiO_4 abundances are in comparison with data from other preliminary Roman / late antique dated sites rather low, which can be ascribed to the fact that Ca was preferentially incorporated in late clinopyroxene. The formation of late clinopyroxene (and magnetite-rich spinel *ss*) instead of Ca-rich olivine is favoured by elevated fO_2 and a comparably high availability of SiO_2 in the restitic melt.
Analyses of olivine-type slags in which spinel *ss* precipitated first (subtype e) form two different fields. While data of samples from the potentially Roman / late antique dated site Voguçincë (12015(5) and 12015(12)) are distinguishable on basis of their Fe_2SiO_4 contents, their Ca_2SiO_4 abundances are highly similar. Olivines from a slag sampled at Mramor Proni Butoçit (10024(4)) in comparison generally are strongly enriched in the Ca_2SiO_4 component and somewhat Fe-poorer than the analyses of grains of the samples from Voguçincë of this group. The extremely high Ca contents, which are markedly different from the two other slags of this group, are assumed to be related to addition of Ca to the furnace charge. This hypothesis also is in accordance with the abundance of clinopyroxene-type specimens at this site (i.e. samples 10024(2) and 10024(5)), which must have been generated by employment of a calcareous flux. The wide range of Fe_2SiO_4 and Ca_2SiO_4 contents covered by the analyses from sample 10024(4) potentially depict pronounced elemental variation of different olivine generations (i.e. grains precipitated during the main phase of slag solidification and lately crystallised ones).
The field of analyses from olivine-dominant slags, in which wüstite and spinel *ss* crystallised first (subtype d), comprises one sample from Hajkobile (10-1A) and Hanroc (3(2)) each. It is characterised by highly elevated, rather variable Ca_2SiO_4 abundances, which are comparable to likewise scattering data of sample 10024(2). Similarly, they are interpreted to have been potentially generated by utilisation of a Ca-bearing flux. The high proportion of leucite present in both slags suggests that the Ca_2SiO_4 contents of the olivines additionally might have been influenced by interaction of the slag melt with charcoal ash or furnace material. The rather homogeneous Fe_2SiO_4 contents overlap with olivine analyses from presumably Roman / late antique dated sites.
Olivine data from clinopyroxene-rich slag types naturally is scarce since this phase occurs only accessory. The few analyses yielded generally Fe-poor compositions with varying Ca contents. The abundance of clinopyroxene precipitated during the main stage of slag solidification generally is thought to be related to Ca fluxing (see above). The occurrence of late clinopyroxene (in olivine-type slags, subtype c) in contrast does not reflect deliberate fluxing, but can be explained by fractional crystallisation of the slag melt and slightly elevated fO_2 conditions at the end of

the slag solidification (see above).
Data of olivines from olivine + clinopyroxene-type slags forms a small field at rather low Fe_2SiO_4 contents and Ca_2SiO_4 abundances in the range of typical analyses from potentially Roman / late antique dated sites. The in comparison to other olivine datasets from clinopyroxene-bearing slag types rather low Ca contents can be explained by the fact that Ca mainly entered clinopyroxene. Olivine, however, preferentially incorporated Mg and Zn (median Mg_2SiO_4 and Zn_2SiO_4 17.5 and 10.9 mol %, respectively; cf. Fig. 9.4), which to a considerable extent substituted Fe.
Only one analysis each of olivine from clinopyroxene-dominant slag types could be carried out. They exhibit the lowest Fe_2SiO_4 abundances determined. While the dataset of subtype a (in which wüstite + spinel *ss* precipitated first; sample 10024(2)) shows unremarkable Ca_2SiO_4 contents, the analysis of subtype b (in which spinel *ss* crystallised first; sample 10024(5)) is highly enriched in Ca. The comparably low Ca abundances of olivine from sample 10024(2) similarly to data from olivine + clinopyroxene-type slag (see above) can be explained by preferential incorporation of Mg and Zn in olivine (18.9 mol % Mg_2SiO_4, 9.4 mol % Zn_2SiO_4) and of Ca in clinopyroxene, respectively. The high proportion of leucite present in sample 10024(5) as an index phase for particularly pronounced interaction of the slag melt with K- and Ca-bearing substances (i.e. charcoal ash and furnace lining; see above) presumably also partially accounts for the high Ca_2SiO_4 content of olivine. The fact that leucite only occurs accessory in specimen 10024(2) likewise offers an additional explanation for the comparably low Ca content of the olivine dataset.
Relative estimates on the furnace atmosphere during formation of clinopyroxene-dominated slag types can be done on basis of the presence of Fe^{3+} in this phase, which has been calculated if necessary to fully occupy the tetrahedral position (cf. section 9.2.2). At comparably oxidising conditions, which generate elevated amounts of Fe^{3+}, it should not only partition into spinel *ss* as the main host phase, but to a certain extent also in clinopyroxene. According to this approach, the samples 12016(2) from Akllap and particularly 10024(5) from Mramor Proni Butoçit for which ferrian clinopyroxene compositions have been calculated, testify to the comparably most oxidising furnace atmosphere of clinopyroxene-type slags. The extremely high PbO contents in glass of the a melilite-dominant slag 13031(1) from the Ostri Vrh site in conjunction with the elevated SiO_2 and CaO contents of the main silicate phase are interpreted as the result of comparably strongly oxidising conditions, whose fO_2 probably exceeded those recorded by clinopyroxene-type specimens. In general, the PbO content of the glass could be used to draw conclusions on the furnace atmosphere since under more oxidising conditions a higher proportion of Pb should be retained in oxidic form in the slag melt. However, analytical artefacts (evaporation of light elements due to necessary measuring with focused beam, potential analytical contamination), but also the interaction with Pb-bearing sulphide inclusions possibly influence the composition of the glass determined (cf. chapter 9.2.10). Furthermore, precipitation of Pb silicates deprives the restitic melt of Pb and thus yields comparably Pb-poor glass compositions contradicting the actual bulk slag chemistry. Exsolution of Pb-bearing silicate phases is assumed for the glassy type slag sample 11029(3) and would explain the notably Pb-poor composition of its glass (cf. Fig. 9.10c). As discussed above, glassy slag types are thought to have been formed under comparably high fO_2 and solidified from melts with insufficient Ca content, i.e since no

or too low Ca was added.

17.3.4. The smelting sites and the chemistry of the slags

As outlined in the previous chapter, several slag samples apparently document the addition of a calcareous fluxing agent. Besides Ca, however, no other commonly applied fluxes could be proven at the smelting sites of the study area. Ba, which effectively decreases the liquidus temperatures of slags and effectively drives PbO out of its silicate compounds (cf. chapter 2.5.1), has been described by e.g. Eckstein et al. (1994) and Goldenberg (1996) to have been utilised at German medieval Pb-Ag smelting sites. Even though Ba would have been accessible as baryte, which is one of the host phases of the local ore mineralisation in the Shashkoc-Janjevo district (Monthel et al., 2002), Ba abundances this far could not have been determined in the investigated slags. Due to its high specific gravity, baryte is difficult to remove with wet-mechanical beneficiation techniques, but could be effectively separated from the ore due to its light colour.

Preliminary Roman / late antique dated sites: Voguçincë, Mirash and Mirash Novo

Slags from the preliminary Roman / late antique dated sites of Voguçincë, Mirash and Mirash Novo all can be classified as olivine-dominant or glassy type. The specimens always contain at least accessory proportions of spinel *ss*, which partially crystallised before olivine. Increasing abundances of spinel *ss* as the most relevant Fe^{3+} carrier phase in the different slag types testify to higher fO_2. Wüstite has not been observed in these samples. The Fe_2SiO_4 and Ca_2SiO_4 proportions of the olivine analyses attributed to the different subtypes gradually merge into each other and widely overlap. A general trend of increasing Ca abundances in olivine with rising fO_2 (expressed by the elevated presence of Fe^{3+}-bearing spinel *ss*) is discernible and can be explained by fractional crystallisation of the slag melt and relative enrichment of Ca in the restitic liquid due to previous precipitation of spinel *ss*. Olivine-type slags as the most simple slag system (see above) imply that the furnace charges at the potentially Roman / late antique sites solely consisted of (partially roasted) ore, charcoal and silica. Variations of the Ca content of olivines attributed to the same subtype correlate with the proportion of leucite present and can be related to different degrees of interaction of the slag melt with charcoal ash or furnace lining. However, Ca surely also is introduced by carbonate gangue material not completely removed during beneficiation of the ore. Glassy slags are generated at comparably oxidising conditions outside the fayalite stability field and, due to an insufficient bulk Ca content of the charge related to no or too low addition of Ca fluxing, solidified in a predominantly glassy state. Analogous to the olivine-type slags, it is assumed that probably no Ca at all has been externally added to the furnace charges.

Preliminary medieval / early modern dated sites, Ca-poor type: Marec and Hanroc

All slags retrieved from Marec as well as one sample from Hanroc (3(1)) could be attributed to the same type, i.e. olivine-dominated with low to absent spinel *ss*. The olivines are particularly Fe-rich, but exhibit some scatter in their Ca_2SiO_4 contents which are thought to be related to fractional crystallisation with slight Ca enrichment in latter precipitated grains. Analogous to the

preliminary Roman / late antique dated sites (see above), the formation of the phase assemblage of these slags can be fully explained by smelting of (partially roasted) ore with a siliceous fluxing agent and charcoal. When compared to olivine-type slags with higher proportions of spinel *ss* present, these samples indicate relatively low fO_2 conditions due to minor Fe^{3+} contents in their bulk chemistry.

Preliminary medieval / early modern dated sites, Ca-rich type: Hanroc, Hajkobile, Akllap and Ostri Vrh

The second group of potentially medieval / early modern dated sites comprises a broad spectrum of different slag types, i.e. olivine-, olivine + clinopyroxene-, clinopyroxene- and melilite-types. Olivine analyses, if possible, commonly exhibit a comparably Ca-rich composition with the exclusion of the samples 10024(2) and 12016(2), which correspond to clinopyroxene-type, subtype a and olivine + clinopyroxene-type, respectively. Their differing chemistry, however, can be explained by preferential incorporation of Mg and Zn into olivine in conjunction with favoured partitioning of Ca into clinopyroxene. While the previously discussed slag types all are interpreted to have been generated by a simple metallurgical setup in which only silica was added to (partially roasted) ore and charcoal, the pronounced Ca-enriched phase assemblages of this group are assumed to have been formed by employment of a calcareous fluxing agent. Subtle differences of the furnace atmosphere during the smelting process dictated the type and proportion of Fe^{2+} / Fe^{3+}-bearing oxides in the slags, which are a measure for the prevailing fO_2 conditions. Generally, the phase assemblage wüstite + spinel *ss* indicates somewhat lower fO_2 than if solely spinel *ss* is present. Increased interaction of charcoal ash and furnace lining, respectively, with the slag melt is suspected on basis of significant leucite abundances and is assumed to have influenced the composition of samples 3(2) from Hanroc and 10-1A from Hajkobile. The specimens 12016(2) from Akllap and 13030(1) from Ostri Vrh both are clinopyroxene-type slags, which do not contain olivine and hence clearly indicate the addition of a calcareous fluxing agent. The melilite-type slag (sample 13031(1)) from the latter site further confirms the previous hypothesis. The chemistry of slags from several sites indicates variations of the metallurgical setup and varying composition of the furnace charges. While sample 3(2) from Hanroc is assumed to have resulted from addition of a calcareous flux to the furnace charge, the phase assemblage of 3(1) can be fully explained by smelting of (partially roasted) ore with silica and charcoal. The two specimens retrieved from Akllap are classified as olivine + clinopyroxene-type and clinopyroxene-type, respectively, and point to varying amounts of calcareous flux added to the furnace charge as well as differing fO_2 conditions. Slags from Ostri Vrh (clinopyroxene- and melilite-type) similarly document heterogeneous smelter charges with differing Ca contents.
An interpretation of these findings based on only two samples from each site is difficult, since the observed differences also could have come about by chance. However, the fact that obviously varying furnace charges are recorded by slags from three smelting sites with an overlapping preliminary dating renders it more likely that particular factors account for these variations. It could be explained by e.g. the discovery of the advantageous effects of calcareous fluxes, which, however, were added to the charge in varying proportions at each smelting site due to the lack of knowledge which amount would be most appropriate for the efficiency of the process. Another

possible reason would be that the proportion of calcareous flux added was rather constant (at least at each of the smelting sites), but that the control over the smelting charge was limited due to the type of furnace employed. The latter hypothesis is rather unlikely since no particular evidence for inhomogeneous smelting conditions (e.g. varying proportions of unreacted flux) has been discovered in the investigated samples. Thus, deliberately added, varying proportions of flux certainly are the main reason for the observed differences of the phase assemblages and chemistry of these slags.

The not yet dated site of Mramor Proni Butoçit

The site of Mramor Proni Butoçit could not be dated yet. However, the phase assemblages of the investigated samples and consequently recorded bulk slag melt chemistry and furnace atmosphere group them together with other Ca-rich, non-olivine slags from smelting sites with a preliminary medieval / early modern dating (i.e. Hajkobile, Akllap, Ostri Vrh; partially Hanroc). Further mining archaeological investigations are envisaged for Mramor Proni Butoçit and are expected to yield datable material to test this hypothesis. Analogous to slags from the preliminary medieval / early modern dated sites of Hanroc, Akllap and Ostri Vrh, the specimens from Mramor Proni Butoçit, which are classified as olivine- and clinopyroxene-types, respectively, as well record differing Ca contents and fO_2 conditions. The samples from Mramor Proni Butoçit similarly are most likely to result from varying proportions of calcareous flux charged to the furnace.

Résumé

- All slag samples from preliminary Roman / late antique dated sites imply solely the addition of silica to the furnace charge to ensure slagging. Variations of the phase assemblage and geochemistry can be fully explained by slightly differing fO_2, interaction of the slag melt with charcoal ash and furnace lining as well as by introduction of restitic calcareous gangue material with the beneficiated ore.
- The potentially medieval / early samples from Marec as well as one sample from Hanroc similarly document a simple metallurgical setup, in which only silica has been added to the furnace charge.
- Slags retrieved from the other preliminary medieval / early modern dated sites of Hajkobile, Akllap, Ostri Vrh as well as one sample from Hanroc testify to employment of a calcareous fluxing agent and a significantly more oxidising furnace atmosphere. Samples from the not yet dated site of Mramor Proni Butoçit exhibit similar characteristics and thus are hypothesised to also have been generated during medieval / early modern activities.

17.4. Type and construction of the smelting furnaces

The morphology of the slag samples allows only general conclusions about their chemistry, but directly relates to the furnace construction. Generally, significant differences relate to the presence or absence, respectively, of flow structures (cf. section 9.1.1).

17.4.1. Slags with flow structures

The most characteristic feature of this slag type are the surficially present finger-like structures which typically are between 1 and 3 cm wide. They were generated due to flowing of the siliceous melt and unambiguously prove that the slag was removed from the furnace by tapping. The width of these flow structures corresponds to the diameter of the tap hole. The shape and size of the specimens is rather variable and includes thin platy types as well as larger, relatively thick slag cakes. These two parameters relate to the amount of slag being tapped. All olivine-type slags possess finger-like flow structures. However, also glassy types[1]in fact represent a finger-like flow structure indicative of tapping (cf. Fig. 9.1d). Specimens from Mramor Proni Butoçit (i.e. olivine- as well as clinopyroxene-dominant slags) as well possess finger-like flow structures, which may be up to 5 cm wide and often exhibit pronounced parallel wrinkles (cf. Fig. 9.1c). These wrinkles, not observed in any other of the investigated slags with finger-like flow structures, are thought to be related to the elevated bulk Ca content of the slags from Mramor Proni Butoçit (cf. section 17.3.3). Several specimens show marks of tuyeres, which were used to adjust and establish a suitable working temperature of the furnace.

The fact that slags with finger-like flow structures always possess multiple tap layers clearly indicates that the tap hole of the furnace was opened intermittently to allow for discharging of the slag and was sealed in-between two tapping events. The marks observed at some of the specimens are related to the basin outside the furnace in which the slags solidified or to the tapping channel connecting the furnace and the reservoir. The bottom sides of all handsamples are coarse and sandy, partially with a knotty structure, and result from reaction of the glowing hot slags with the substrate, thus clearly representing the base layers of slags emptied from the furnace. The flow structures on their upper sides possess a glassy surface due to comparably rapid cooling after tapping. The phase assemblage of the individual tap layers shows evidence for gravitational separation with e.g. matte or crude Pb, but also spinel *ss* accumulated in the lowest zones. The upper margins of the tap layers commonly are rimmed by a layer mainly consisting of Fe oxide and glass, which turns into an iscorite-rich layer with increasing distance from the slag surface. Both zones result from reaction of the slag melt with atmospheric oxygen after tapping. Overall, these observations imply that each tap layer represents a temporally restricted tapping event and that a certain time elapsed between each of these events. In situ analysis revealed that the phases from the differing tap layers cannot be distinguished chemically and thus are interpreted to have been precipitated from an overall well-homogenised furnace charge. Due to several imponderable factors influencing the chemistry of the smelting process (e.g. composition of ores and fluxes, differing furnace atmosphere and temperatures due to variations of the draught, liquefying furnace lining and charcoal ash), the accuracy and reproducibility of ancient process schemes should not be overestimated. Consequently, based on the properties of surface and bottom sides of the slags and the tap layers as well as the phase chemistry, each slag sample is interpreted to represent one furnace charge treated.

[1]Olivine-type slags have been sampled at the potentially Roman / late antique sites Voguçincë (12015(5), 12015(7), 12015(12), 14032), Mirash (11027(1), 11027(2)) and Mirash Novo (11029(4), 11029(5)) as well as the presumably medieval / early modern workshops of Marec (10-6, 10032(1), 10032(4)), Hajkobile (10-1A) and Hanroc (3(1), 3(2)). Glassy types have been collected at Voguçincë (not analysed) and Mirash Novo (11029(3)).

17.4.2. Slags without flow structures

Slags without distinct, i.e. finger-like flow structures, exhibit either only few wrinkles on their upper surface (Akllap: 12016(1), 12016(2)) or do not show any structures at all (Ostri Vrh: 13030(1), 13031(1)). The shape and size of the specimens is comparably uniform. All investigated samples possess only one tap layer. The upper surfaces of these slags appear comparably less glassy than those of specimens with flow structures and consequently testify to a lower grade of chilling. The bottom sides of the slags are coarse and sandy, but in contrast to some samples with flow structures show no evidence for pronounced reaction of the slag liquid with the substrate. While top and bottom sides of these slags partially are difficult to distinguish in the handsample, gradual increase of grain sizes and elevated abundances of phases with a higher specific gravity (i.e. particularly spinel *ss*) can be observed in the lower regions of the specimens. Reaction zones of the slags with atmospheric oxygen (marked by the presence of e.g. iscorite layers; see above) could be rarely observed and, if present, are only weakly developed.
In sum, these findings altogether unambiguously indicate that these slags did not have been generated by tapping through a hole, but instead apparently were collected in a basin located within the furnace. Thus the slags do not show pronounced flow or movement structures in general. Due to the overall comparably oxidising furnace atmosphere recorded by the slag types abundant at these sites (i.e. olivine-clinopyroxene-, clinopyroxene- and melilite-types), the furnaces either must have been worked with rather high air supply (e.g. caused by utilisation of more tuyeres) or must have possessed a relatively large diameter. The different furnace constructions observed at the investigated smelting sites either could be related to spatial or temporal factors. Large differences of the metallurgical knowledge in consideration of the rather small distances between the sites appear rather unrealistic. It seems clearly more likely that the furnace constructions can be attributed to varying operating periods. This hypothesis, however, has yet to be confirmed by unambiguously datable material.

18. Technological changes and developments in relation to chronology

18.1. The choice of the slag system: Addition of calcareous material as fluxing agent

One of the most significant questions arising from the examination of the different slag types is why an apparently chronologically related change of the process scheme occurred, which is based on the deliberate addition of calcareous material as fluxing agent. As discussed in detail before, more oxidising furnace conditions (i.e. exceeding the stability field of fayalite limited by the FMQ buffer equilibrium) necessitate a higher bulk Ca content of the furnace charge to avoid the formation of PbO-rich glassy slag types, which possess a high viscosity and specific gravity and have been exclusively observed at preliminary Roman / late antique dated sites. According to experimental studies by Bachmann (1980), increasing CaO contents even more than elevated FeO and MnO abundances in slags lower their viscosity. Consequently, from temperatures of approximately 1230 °C on, clinopyroxene slags are less viscuous than their fayalite-dominated analogues (Bachmann, 1980). Furthermore, CaO-richer slags possess a lower specific gravity and thus facilitate the separation of the different melts (i.e. siliceous slag and liquid Pb besides potentially present matte and speiss melts). Generally, slags with an elevated CaO content also possess a lower ability to retain metal sulphides. In Pb metallurgy, a higher CaO content of the slag melt advantageously drives Pb off of its silicate phases (cf. section 2.5.1; e.g. Gowland, 1914). The furnace atmosphere at higher CaO abundances, however, has to be kept at a sufficiently oxidising level since Ca also pushes Fe out of its silicate compounds; Fe consequently may be reduced to its native state and accumulate as impure pig iron, a generally unwanted by-product (cf. section 2.5.4). Lumps of pig iron have been found at the smelting site of Mramor Samakove, where the ancient metallurgists apparently also employed comparably Ca-rich furnace charges[1]. Increasingly oxidising furnace conditions furthermore lead to elevated rates of Pb being slagged as PbO. Consequently, a smaller amount of Pb bullion accumulates below the slag, which hence is comparably enriched in precious metals. If the metallurgical process scheme focused particularly on the Ag and potentially present Au contents of the local ore and considered Pb as a by-product of the operations, this factor as well might be relevant for the adjustment of a Ca-rich slag chemistry in later times. In the Roman era in contrast, Pb was a valuable commodity applied for numerous purposes and also was smelted from its ores in its own right (cf. the notoriously Ag-poor British Pb mines; chapter 5.3.1). Pb losses during metallurgical processing surely were

[1] This far, from Mramor Samakove solely furnace slags, pig iron, restitic galena ore and a piece of crude Pb have been analysed. The excavation campaign in 2015 also yielded tap slags, which are optically similar to Ca-rich specimens collected at the neighbouring site of Mramor Proni Butoçit.

accepted, but overall are assumed to have been kept below a certain level.

18.2. Variations of the raw material: Evidence from the metallurgical by-products matte and speiss

Besides slag and crude Pb, also the metallurgical by-products matte[2] and speiss have been sampled at some of the investigated smelting sites. Both materials indicate a polymetallic character of the smelted ore, which apparently contained elevated abundances of particularly Cu, As and Sb.

In Pb metallurgy, matte is generated due to abundant Cu and S contents of the furnace charge. It furthermore also contains other base metals from the ore, i.e. particularly Pb, Fe and Zn. Matte as sulphide melt is insoluble in the siliceous slag liquid as well as in the metal melts of speiss and crude Pb. It hence forms a segregated layer in the smelting furnace, which due to its specific gravity accumulates between slag and speiss (if abundant) and crude Pb. The formation of a certain amount of matte in Pb metallurgy in principle is desirable since it effectively collects the Cu contents of the furnace charge. These would otherwise partition into the crude Pb and drastically raise its melting point, hence impeding further treatment of the metal bullion, particularly cupellation. Although the main part of Ag is incorporated into the Pb melt, the Cu-(Fe) sulphides of matte also host notable amounts of Ag (Fig. 18.1; cf. chapters 10 for in situ analyses of the investigated samples and 2.5.2 for a recapitulation of literature data).

Matte s.s. until now has been retrieved from the preliminary Roman / late antique dated smelting sites of Voguçincë (samples 10-2B, 12015(5) and 14032), Mirash (11027(1) and 11027(2)) and Mirash Novo (11029(3) and 11029(5)), from the not yet dated workshop of Mramor Proni Butoçit (10024(4)) and the potentially medieval / early modern metallurgical complex of Hajkobile (10-1B). All specimens from Voguçincë and one sample from Mirash Novo (11029(5)) and Mramor Proni Butoçit each could be, based on their Pb isotope ratios and geochemical signature (chapters 8.2.1 and 16.2), unambiguously related to production of ores from the Shashkoc-Janjevo district. Matte from sample 11029(3) apparently was generated by smelting of ores which completely or partially were won at a not yet characterised occurrence, possibly at Zhegovcë (cf. chapter 16.3). The matte cake from Hajkobile could not have been assigned to a particular raw material source. However, due to the fact that the smelting site is located rather distant from the examined ore deposits, this observation is not surprising and suggests that the site might have been supplied by mineralisations outside of the study area.

Speiss occurs as ferrous or base metal variety which, due to its immiscibility in the other melts potentially generated in Pb metallurgy, accumulates between slag or matte (if present), respectively, and crude Pb. Ferrous speiss consists of Fe-As compounds, i.e. particularly FeAs, Fe_2As and arsenical Fe. Base metal speiss is chemically more versatile and is made up of antimonides, arsenides and stannides of mainly Cu, Ni, Fe and Ag. While in situ analyses of ferrous speiss have not detected notable Ag contents, base metal speiss may be an effective collector of the

[2] Although the term matte can be used to collectively refer to the sulphide compounds generated during metallurgical treatment of base metal ores, it commonly is understood as a segregated melt phase always comprising a certain amount of Cu. Therefore, the following discussion solely addresses matte s.s., which is the only type to occur as cakes or lumps being indicative of liquid segregation during the smelting process.

precious metal (Fig. 18.1; cf. chapters 11 for in situ analyses of the investigated samples and 2.5.3 for a recapitulation of literature data).

Significant amounts of speiss, i.e. abundant as cakes or layers, until now solely have been observed at the preliminary Roman / late antique dated site of Mirash Novo. Both specimens represent ferrous speiss and comprise Fe_2As and a weathered Fe-rich phase (sample 11029(4)) or Fe_9As and Fe_2As (11029(7)), respectively. Base metal speiss is abundant as dispersed droplets in slag (samples 10032(4) from Marec and 12016(2) from Akllap), within ferrous speiss (11029(4)) or exsolved in crude Pb (samples 11029(1) from Mirash Novo and 10024(5) from Mramor Proni Butoçit). The fact that notable amounts of speiss only have been collected from one smelting site (i.e. Mirash Novo) can be explained by the behaviour of the involved elements during metallurgical processing and their presence within the smelted ore (Fig. 18.1). As and Sb both are easily volatilised and hence largely removed during metallurgical treatment; the ores from which the samples 11029(4) and 11029(7) were produced thus must have been particularly As-rich. Cu as a main element of base metal speiss compounds presumably rather partitions into sulphide phases and becomes enriched in matte. The contents of Ni and Sn in the ore and gangue material only are locally enriched (cf. chapter ii). Ag mainly is collected by native Pb (Tafel, 1929).

The two samples comprising notable amounts of ferrous speiss from Mirash Novo could not have been attributed to one of the investigated mineralisations. Analogous to the matte-bearing specimen 11029(3) from the same site, they are assumed to have been formed by treatment of ores which completely or partially were won at a not yet characterised occurrence, potentially the Cu-As-Sb-rich mineralisation of Zhegovcë. When considering the smelting sites where significant amounts of matte and speiss have been found, a chronological trend is clearly discernible. With the exception of Mramor Proni Butoçit - which could not have been dated yet but is suspected to have been worked in medieval / early modern times (chapter 17.3.4) – and the potentially medieval / early modern complex of Hajkobile, a preliminary Roman / late antique dating has been attributed to all smelting sites at which matte and speiss have been sampled. At potentially medieval / early modern sites in contrast, the array of metallurgical by-products found with few exclusions (see above) solely comprises slag and crude Pb. This observation can be used to draw general conclusions about the type of ore smelted. In medieval / early modern times, the smelted ore apparently was rather homogeneous and essentially consisted of Pb-Zn-Fe phases. At Roman / late antique sites a trend to rather polymetallic ore charges, which must have contained elevated levels of particularly Cu and As, is discernible. On a local scale matte-rich samples, which could be attributed to smelting of ores from the Shashkoc-Janjevo district, must have been generated by smelting of furnace charges containing significant amounts of Cu-As-Sb-enriched early- and main-stage ore. Its phase assemblage mainly is made up of galena, sphalerite, pyrite, arsenopyrite, chalcopyrite and fahlore or secondary Cu phases, i.e. chalcocite, digenite, covellite and malachite (cf. chapter 8). Besides elevated Cu, As and Sb abundances, this ore type also is characterised by in comparison to late-stage ore typically higher Ag contents, which are mainly hosted by Cu-, As- and Sb-bearing fahlore minerals and secondary Cu phases. Additionally, the quartz gangue of main-stage ore reportedly is auriferous (Hyseni & Alliu, 1999). The elevated precious metal contents of this ore type – if known to the ancient miners – thus render its preferential exploitation in earlier times highly likely. Main- and early-stage predominated ore

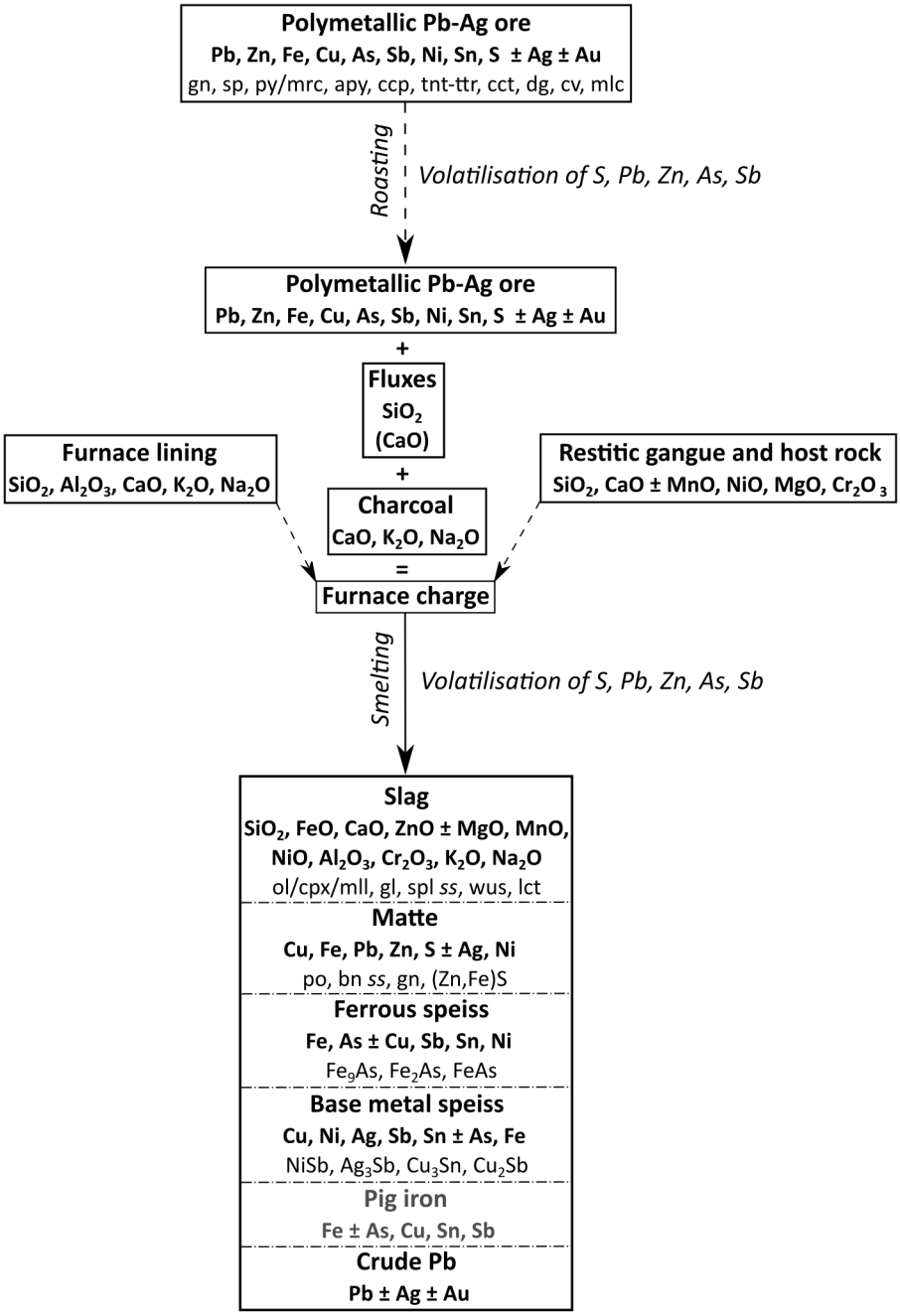

Figure 18.1.: Generalised distribution scheme of major and minor elements between slag, matte, speiss, crude Pb and potentially generated pig iron during smelting of complex polymetallic ore.

rather is abundant in the southern part of the mining district of Shashkoc-Janjevo and e.g. could be sampled at old workings immediately uphill Janjevo (see appendix, chapter ii). The apparently Pb-Zn-Fe-rich ore smelted at presumably medieval / early modern dated sites, which are linked to the Shashkoc-Janjevo district by matching Pb isotope ratios, corresponds to the phase assemblage of late-stage ore mainly comprising galena, sphalerite and pyrite / marcasite. This ore type is particularly abundant in the northern and western part of the district and has been e.g. collected in the vicinity of ancient workings at the 'Mondlandschaft' nearby Shashkoc (see appendix, chapter ii) and close to the modern mines of Kishnica and Badovc. These observations match the descriptions of Davies (1935), who noted:

> "At Janjevo are ancient workings for gold and silver. The hamlet of Šaškovac and their characteristic pitting indicate the presence of Saxons..."

18.3. Reconstruction of metallurgical process schemes

18.3.1. Potential re-use and treatment of metallurgical (by-) products

Smelting of complex polymetallic ores generated not only slag as metallurgical by-product, but also matte and speiss. Furthermore, under certain conditions also pig iron, which has been observed at Mramor Samakove, may be formed. The presence of these by-products, whose phases partially host noteworthy Ag contents (cf. sections 10 and 11.3 on matte and base metal speiss, respectively), naturally rises the question whether these materials simply were discarded or were treated to extract certain metal(s) and / or were used for other applications.

Slag

Slag is the ubiquitous by-product of metallurgical processes, which accumulates in large quantities during these operations. Generally, in Pb-Ag metallurgy slags related to primary smelting and those linked to refining treatment of crude metal can be distinguished. Primary smelting slags take up undesired elements of the furnace charge (introduced by ore, restitic host rock, fluxes, charcoal ash and liquefying furnace lining) to produce crude Pb, which except for potentially collected precious metal contents should be as pure as possible. Due to slagging of Pb as PbO, but also due to the presence of newly-formed sulphide inclusions trapped within the silicate matrix, slags may contain relatively high amounts of Pb. Bode (2008) and Ettler et al. (2009c) report up to 27.1 wt % PbO in Roman slags from the Lüderich (Germany) and a maximum of 34.4 wt % PbO in medieval material from Příbram, respectively. However, the Pb abundances in slag as well may be in the range of only a few wt %, particularly if oxidised ores were smelted (e.g. Anguilano, 2012; Manasse & Mellini, 2002a; Ströbele et al., 2010). Refining slags accumulate during refining or purification treatment of the crude metal, particularly cupellation. They typically are marked by Pb contents scattering in the range of several ten wt % (Ettler et al., 2015; Rehren & Hauptmann, 1995).
Generally, slags provide particularly SiO_2 and PbO and thus could be used as a fluxing agent by re-submitting them to the furnace. However, the huge dimensions of the waste heaps described from large-scaled smelting sites in the most productive ancient districts (e.g. Rio Tinto, Laurion)

rather imply that at least primary smelting slags simply were discarded without further use. Indeed, the volume of the slag heaps piled up at the investigated sites of the study area is thought to have been diminished by re-smelting only in modern times (cf. chapter 6.2). This finding probably is related to the fact that the Pb content of the slags was not high enough to render re-smelting profitable in earlier periods. Furthermore, sandy sediments from creeks nearby the smelting sites or siliceous gangue material accumulating during ore beneficiation constituted a more readily available source of SiO_2-rich material (with no or less need for further preparation, i.e. crushing) to be added for metallurgical treatment. The refining slags due to their significantly higher Pb content (almost exclusively present as PbO) are assumed to have been more likely recycled and, along with the oxidised Pb metal generated during cupellation, re-submitted to the furnaces. This hypothesis is in accordance with the fact that until now only one cupel (sample 10-5, Marec) has been found in the study area, even though the precious metal content of the local ore certainly justifies its extraction.

Matte

Matte, as discussed detailed in the previous chapter, as potentially deliberately generated by-product of metallurgical treatment of relatively Cu-rich Pb-Ag ores has been collected at several, mostly preliminary Roman / late antique dated sites. In situ phase analysis of the examined samples revealed noteworthy Ag contents hosted by Cu-(Fe) sulphides, i.e. median abundances of 1530 and 2880 ppm and and maximum contents of 6080 and 3690 ppm Ag in bornite *ss* and covellite, respectively. Interestingly, also chalcocite *ss* abundant in Pb-Cu matte rimming droplets of native Pb is significantly enriched in the precious metal (median 2675 ppm). Rarely any Ag in contrast could be detected in droplets of native Pb - which actually should serve as a collector of the Ag and Au contents of the furnace charge - in slags. This observation is in accordance with the chalcophile behaviour of Ag, which hence preferentially partitions into the sulphide melt. In the base zone of the furnace where the Pb bullion settles, the lower fS_2 and Cu and S contents of the melt ensure that Ag is concentrated in native Pb or base metal speiss compounds, respectively (see below).

In order to avoid Ag losses to Cu-bearing sulphide phases and to effectively extract the precious metal along with crude Pb, both the S and Cu contents of the furnace charge hence should be rather low. However, as mentioned in the previous section, increased Cu in conjunction with depleted S abundances (e.g. due to roasting) rise the potential that Cu partitions into crude Pb. This reaction should be avoided since Cu enhances the melting point of Pb and thus impedes refining of the metal. These reciprocal effects again confirm that roasting should be carefully balanced due to battling positive and negative consequences influencing the efficiency of metallurgical processing.

Whether the process scheme was deliberately adjusted to generate matte and avoid unfavourable ramifications, the Ag contents determined in matte phases raise the question if this material might have been treated in some way to extract its precious metal content. Bachmann (1993) suggested roasting and re-submitting of matte to the smelting process to have been practised in ancient times at least for particularly Ag-rich material. Written records prove re-smelting of matte from Pb-Ag metallurgy for medieval Germany (Goldenberg, 1996).

Generally, if rather Ag-rich Cu-bearing ores were smelted, a considerable share of the precious metal also was incorporated into matte, which hence is assumed to easily have reached ore grade Ag contents. Re-submitting of matte cakes to the furnace charge, i.e. (roasting and) smelting along with the primary ore thus should be considered a likely possibility. This scenario matches the low abundance of matte cakes at the investigated smelting sites, which contrast the presumably higher amounts of matte generated due to the partially particularly Cu-rich nature of the local ore.

Ferrous speiss

Notable amounts of ferrous speiss this far solely have been found at the presumably Roman / late antique site of Mirash Novo (section 18.2). A potential usage of this material, particularly on basis of potential Ag contents, has been discussed controversially in the past (cf. chapter 2.5.3). However, at least in Roman times ferrous speiss apparently was neither utilised directly nor further processed. Ag typically could not be detected by in situ EMP analysis of speiss phases. As already suggested by Photos et al. (1989) and as evidenced by the finding situation at the smelting sites, it thus most likely simply was discarded. Potentially determinable bulk Ag contents are assumed to derive from inclusions of argentiferous crude Pb and / or base metal speiss.

Base metal speiss

Base metal speiss, unlike its ferrous analogue, is marked by a more versatile chemistry and consists of Cu, Fe, Ni, Ag, Sn, Sb and As compounds. Ag is particularly enriched in antimonides, probably due to existent solid solution between Cu and Ag antimonide. Due to similar specific gravities, base metal speiss typically is closely associated with crude Pb (cf. section 11.3). Keesmann (1993) on basis of geochemical signatures has proposed 'automatic' cupellation of base metal speiss along with crude Pb. Its partially significant Ag contents (up to e.g. 5570 ppm in $(Cu,Ni)_2Sb$) therefore typically were not lost. This far, only one sample of a cupellation remain from the site at Marec could be investigated. Its Cu and Sb contents - elements which typically are indicative of the (former) presence of base metal speiss - are low to not detectable and hence in this case do not imply cupellation of this material. This observation, however, is in agreement with the mineralogy of the local mineralisation mined until today at the carbonate replacement type deposit of Novobërdë (Monthel et al., 2002; cf. section 3.2.1), whose massive ore essentially consists of galena, sphalerite and pyrite with commonly only accessory present Cu- and Sb-bearing phases leading to speiss formation.

Pig iron

Pig iron may be unintentionally produced if the furnace conditions were too reducing and Fe, further promoted by relatively high Ca contents in slag (cf. section 2.5.4) was transformed to its native state. This material until now solely has been discovered at the site of Marmor Samakove, where the finding situation implies that it simply was discarded. Indeed, pig iron, due its impure composition and high melting point, typically is assumed to could not have been further processed (cf. section 11.2).

Crude Pb and cupellation remains

Even though only one sample of cupellations remains has béen discovered in the study area this far (sample 10-5; Marec), the Ag (and potentially Au) content of the local ore (cf. chapters 3.2.1, 4.1.1 and 8.2) definitely justifies its extraction[3]. This also is in accordance with Roman precious metal extraction evidenced by the mentioning of a *procurator metallorum Dardanicorum* (cf. chapter 4.2) and the rich evidence for local Pb, Ag and Au mining in medieval and early modern times (e.g. Ćirković, 1981; Mrkobrad, 1994). Furthermore, the unambiguous isotope signature of the investigated Pb objects found in Ulpiana could be explained by bulk cupellation of Pb bullion produced at several smelting sites (cf. chapter 15.1.3). After the Ag metal was removed, the oxidised Pb was reduced to its native state again. If the Ag contained an amount of Au worth to be recovered, the two precious metals were subsequently separated from each other.

18.3.2. Metallurgical process schemes in relation to the ore type smelted

Variations of the design of the metallurgical process scheme are to a large extent related to differences in the mineralogy of the ore smelted. While slags serve as excellent indicators for process parameters (particularly furnace conditions and working temperature, addition of fluxes, influence of charcoal and liquefying furnace lining), matte and speiss as well as crude metal directly relate to the raw material basis. These by-products hence allow to reconstruct potential variations of the treated ore which in the study area apparently are related to a chronological context, i.e. from often comparably polymetallic raw material smelted at presumably Roman / late antique to typically less complex ore processed at potentially medieval / early modern sites (chapter 18.2). Formation of matte and speiss naturally raises the question whether these materials were treated or re-used in ancient times, as has been discussed in chapter 18.3.1. In the following, these findings are summed up to exemplarily reconstruct process schemes for rather 'pure' and complex Pb-Ag ores with elevated contents of particularly Cu, As and Sb. Pig iron has not been displayed since it is not a metallurgical by-product sensu stricto, but is generated unwittingly due to concurrence of comparably Ca-rich smelter charges and too reducing furnace conditions (cf. chapter 2.5.4).

Process scheme for rather 'pure' Pb-Ag ore

Smelting of rather 'pure' Pb-Ag ore, which - analogous to late-stage ore in the Shashkoc-Janjevo district (cf. chapter 8) - consists mainly of galena, sphalerite and pyrite / marcasite corresponds to a particularly simple process scheme. The ore potentially was roasted before smelting under reducing conditions ('roast-reduction process') or was submitted without previous treatment to the smelter, where the sulphide components were oxidised in the uppermost and reduced in the lower zones of the furnace ('roast-reaction process'; cf. chapter 2.3). Smelting generated siliceous slag, which either was used as SiO_2- and PbO-bearing fluxing agent or simply discarded, and precious metal-bearing Pb bullion. The crude Pb was cupelled to separate (auriferous) Ag, which also contained other metals from the furnace charge, e.g. Cu. The extracted Ag was further refined and, if it comprised a recoverable amount of Au, the two precious metals were separated

[3] Also see chapter 19.1 for a discussion on the refining of the produced raw metal.

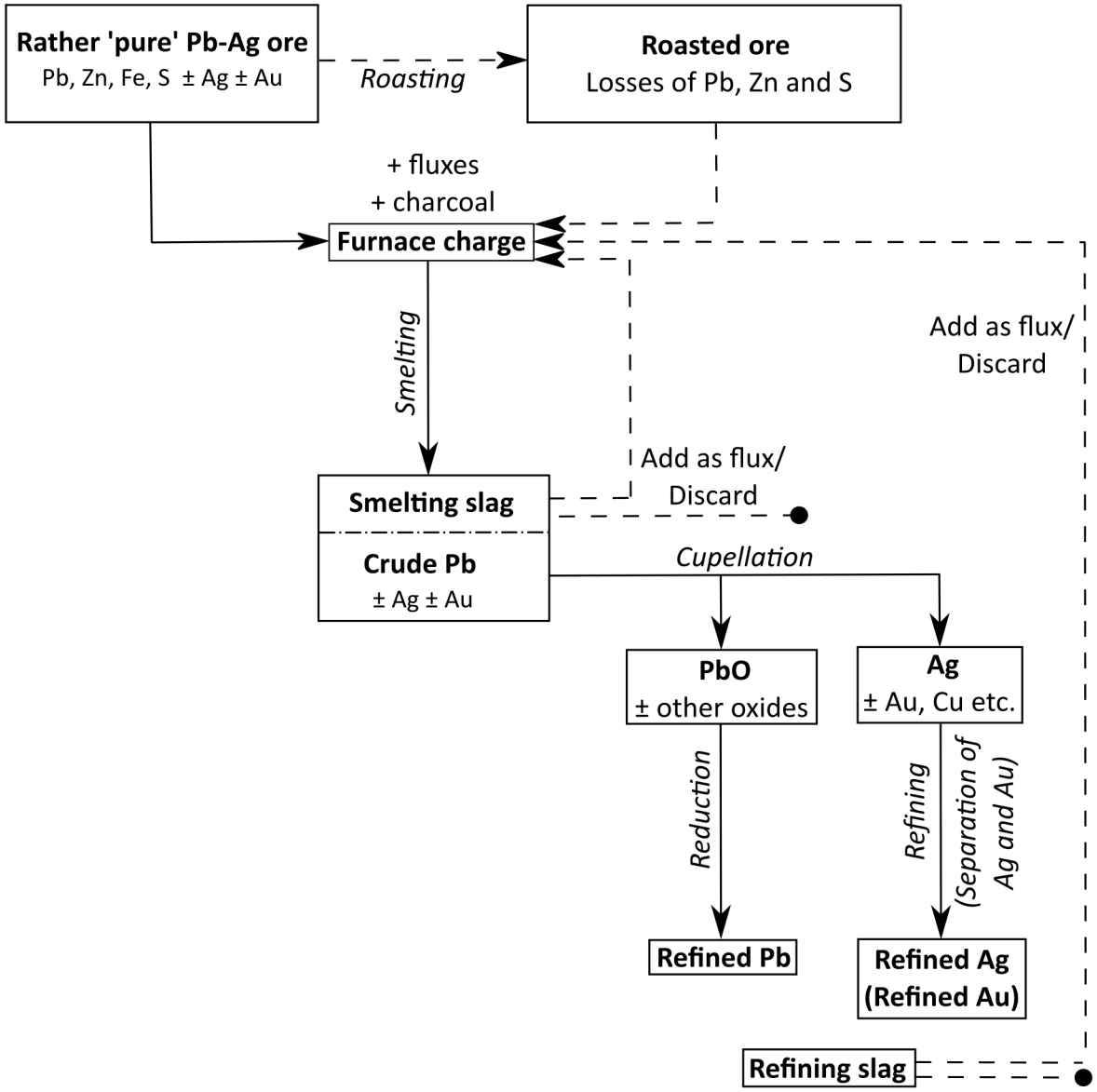

Figure 18.2.: Metallurgical process scheme for rather 'pure' Pb-Ag ore.

from each other. The oxidised Pb was reduced to its native state ('refined Pb'). These metal-refining processes also produced slags, which due to their high metal content presumably were re-smelted as fluxing agent.

Process scheme for polymetallic Pb-Ag ore

Polymetallic Pb-Ag ore, which corresponds to early- and main-stage mineralisations of the Shashkoc-Janjevo district and hence mainly comprises galena, sphalerite, pyrite, arsenopyrite, chalcopyrite, sulphosalt minerals (e.g. fahlore) as well as potentially secondary Cu phases (cf. chapter 8), may generate up to four different liquids in the furnace. Matte, a mixture of base metal sulphides, may host appreciable amounts of Ag and therefore might have been mixed with ore and re-submitted to the furnace. Ferrous speiss apparently simply was discarded. Base metal speiss, which is due to its similar specific gravity closely associated with crude Pb, is assumed to have been automatically cupelled with Pb bullion (cf. Keesmann, 1993). The (potential) treat-

ment or re-use of smelting and refining slags as well as crude Pb and (auriferous) Ag corresponds to the descriptions in the previous section.

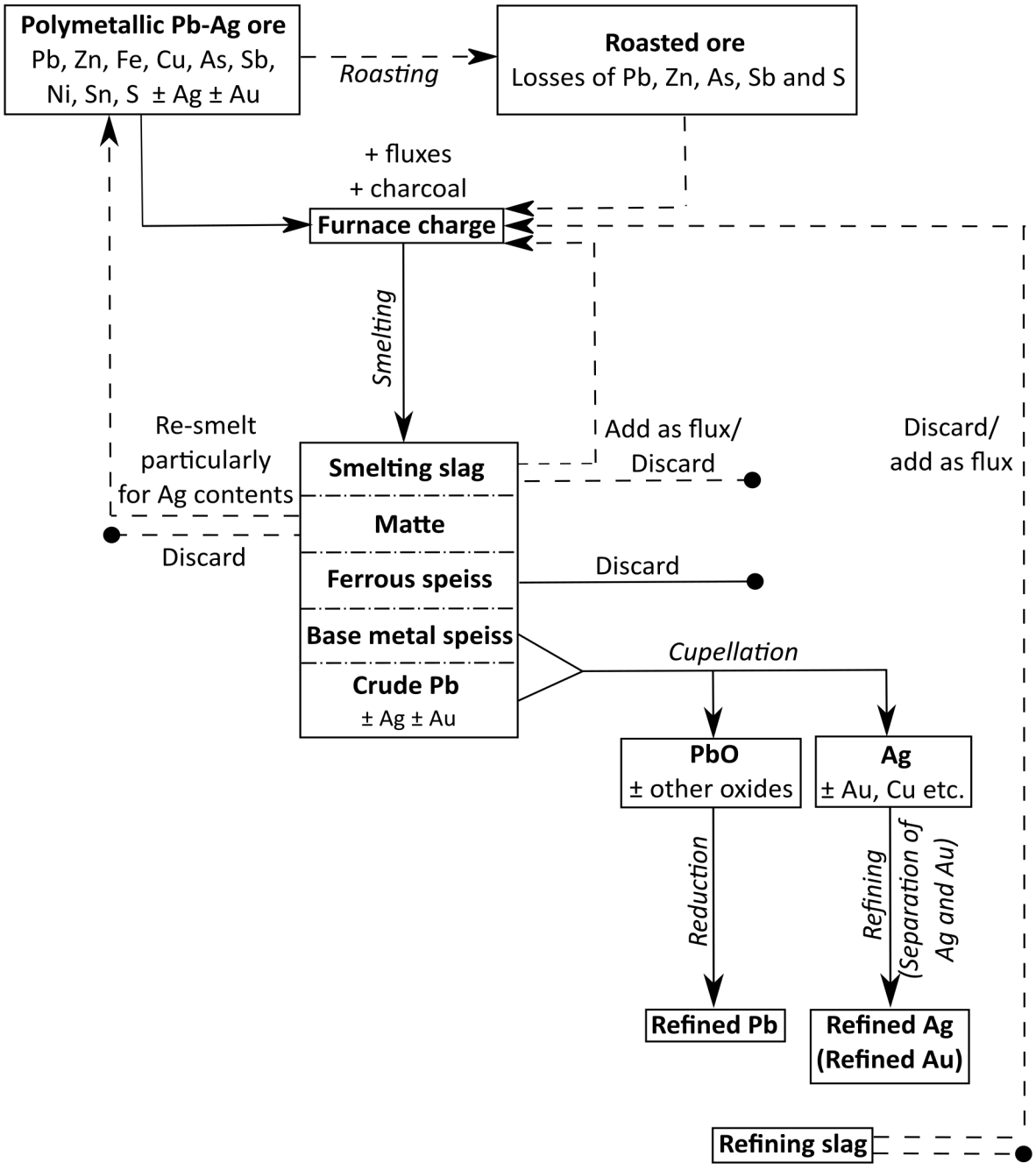

Figure 18.3.: Metallurgical process scheme for polymetallic Pb-Ag ore.

19. Economic relevance of the local metal production in Roman times

19.1. Processing of the raw metal and trade in relation to Ulpiana

With the exception of the cupellation remains discovered at Marec, there is no evidence for refining of crude Pb at the investigated smelting sites. The examined slags all record the processing of (predominantly) sulphidic furnace charges (chapter 16.1). The Ag content of the ore mineralisation in the study area (cf. chapters 8 and 3.2.1) certainly justifies its recovery by cupellation. Merkel (2007), who studied Roman Pb-Ag production in the Mt. Kosmaj region (northern Moesia Superior), has suggested that the precious metal content of crude Pb was extracted under greater administrative control and not at the often rather remotely located smelting sites. This argumentation would explain the lack of by-products related to metal refining at the investigated preliminary Roman / late antique dated sites. The discovery of a mould potentially used for the production of Ag ingots and a lump of Pb adhering to a furnace (cf. chapter 4.1.2) points to (at least temporary) precious metal extraction within the city limits of Ulpiana and correlates with Merkel's (2007) hypothesis. The mineralogy of the local ore (Hyseni & Alliu, 1999) and the medieval production of 'argentum de glama' (cf. chapter 4.1.1) implies that the extracted silver was auriferous. If the Romans were aware of the potentially present Au contents, the two precious metals undoubtedly were separated under control of the state, possibly also within Ulpiana. Parović-Pešikan & Stojković (1995) reported findings of ore, slags, native Pb and partially related the furnaces excavated in the workshop complex of Ulpiana to processing of Pb-Ag ores. Primary smelting, however, even at the increasingly troubled times of the later Empire, is highly unlikely to have been carried out within the *municipium*. Several reasons contradict this hypothesis:

- There is not sufficient space within the city limits, neither for the metallurgical processes themselves nor for the thousands of tons of waste material - for Mount Kosmaj in the Šumadija district, Laurion and the Rio Tinto region 1,000,000 t, 1,500,000 t and 15,000,000 t of smelting remains have been described in the literature (Merkel, 2007; Rehren et al., 2002; and references therein) - which accumulate during the operations.

- The ore ought to have been elaborately transported from the workings in the hinterland to Ulpiana. Considering the plentifulness of Pb ores at the Balkan Peninsula and generally the Roman Empire in conjunction with the consequently rather low price of the metal (Boulakia, 1972), it cannot have been worth the effort.

- Supplies employed in large quantities for the smelting process (i.e. charcoal, fluxes, furnace construction material) ought to have been elaborately delivered to the city as well.

Additionally, the slags sampled at Ulpiana unambiguously have been related to smithing activities (cf. sections 9.1.3 and 9.3). Indeed, while, as outlined above, primary smelting operations in the city seem highly unlikely, the presence of a blacksmith's workshop is to be expected. Thus, the other metallurgical findings retrieved from Ulpiana (i.e. a mould for Ag ingots, a furnace with adhering Pb metal, tuyeres and slags) are interpreted to be linked to cupellation of precious metal-bearing crude Pb, which was produced by metallurgical processing at sites in the hinterland of the *municipium* in the vicinity of the Pb-Ag deposits. Collecting of Pb bullion from several smelting sites - which all processed isotopically slightly different ore - and subsequent bulk treatment of the raw metal at a central point also would fit to the unambiguous isotope signature of the Pb objects retrieved from Ulpiana (cf. chapter 15.1.3). The cupellation remains accumulating in the city either might have been traded from Ulpiana (see below) in their oxidised state or re-reduced back to native Pb. The mill stone fragments discovered in the workshop complex hence are unlikely to have been used for the beneficiation of the raw ore. Instead, they might as well be related to metal refining processes. The desilverated lead ingots and the extracted, potentially auriferous silver subsequently due to the advantageous location of Ulpiana (cf. Fig. 4.1) could be easily distributed within the Empire. Towards the northeast, the city is connected with Municipium DD and Naissus, from which roads lead to Singidunum in the north and to the provinces Dacia and Thracia in the northeast and east, respectively. South of Ulpiana, the main road passed Scupi. Sea transport was possible from the port of Lissus, which as well was linked with the *municipium*. Due to its advantageous location close to main roads of the Empire connecting it in all geographic directions and amid a prosperous mining and smelting district, Ulpiana might have been a highly relevant regional trade centre for metal.

19.2. Case study on the provenance of Roman imperial lead-based objects

The Balkan Peninsula is considered to have been one of the most important Pb-Ag producers in late Roman imperial times (cf. sections 4 and 5). Large-scaled ancient mining districts are known to have been operated in the Kopaonik Mountains and Šumadija region of the province Moesia Superior (cf. chapter 4). The historical and current relevance of the region's mineral wealth, however, is in stark contrast to the scarcity of the previously available ore Pb isotope values. Due to the data produced in this study, there now is an array of analyses at hand which allows establishing a more significant isotope 'field' for Moesia Superior's Kopaonik-Šumadija district. This ore isotope signature offers the opportunity to test a relation of Roman imperial lead (-bearing) objects, which based on epigraphy or finding location potentially might have been produced from ore resources of the Balkan Peninsula. For this purpose, two datasets have been selected: 1) a shipwreck cargo discovered nearby the harbour of Caesarea (Israel) comprising lead ingots, which partially are stamped with '*MET DARD*' (Raban, 1999) and 2) Pb-glazed pottery (dating from the 1st to the 5th century CE) from Roman settlements in Serbia and Romania (Walton & Tite, 2010). Unlike the Cu-rich coins (cf. chapter 15.1.4), provenance analysis in

these cases is more likely to be successful. Both the shipwreck cargo as well as the Pb glaze are expected to possess a rather pristine Pb isotope signature not (significantly) influenced by e.g. mixing, later processing and recycling. Furthermore, everyday goods (such as the investigated pottery) are thought to typically have been manufactured from local raw material, as proposed by Merkel (2007). Re-evaluation of these datasets also allows drawing further conclusions whether the Romans also in this case might have relied on the local ore resources of the conquered provinces, as has been described for e.g. Germany (cf. chapter 5.3.3).

19.2.1. The *MET DARD* shipwreck cargo

The shipwreck cargo was discovered in 1993 at the K8 area of the harbour of Caesarea (Raban, 1999), a settlement which was located approximately halfway between the modern cities of Haifa and Tel Aviv. A total of six lead ingots could be retrieved from the site, of which only the four best preserved have been further examined. Based on inscriptions at the ingots, their casting could be narrowed down to the time range between 83 and 96 CE. They are stamped with the mine name *MET (alla) DARD (anica)*. Pb isotope analysis has been performed on one of the ingots and two pieces of lead sheathing. The three samples possess a similar isotopic signature and have been related to ores from the Eastern Rhodopes, where they match data of galena from Kirki and Essimi in Greece and Madjarovo and Zvezdel in Bulgaria (Raban, 1999). Interestingly, the author states that several other lead objects from Roman shipwrecks discovered at Israeli territorium show a similar isotopic composition. In this case study, it shall be tested whether the objects from this cargo, which can be epigraphically related to local mining districts in Serbia and Kosovo (cf. section 4.2), can also be attributed to this region by means of their Pb isotope signatures. It is not the aim to disprove the provenance of the objects proposed by Raban (1999). However, by combining the new isotope data with previously published literature values (Gale, 1990, pers. comm.; Pernicka et al., 1993; Veselinović-Williams, 2011), it shall be tried to assess whether Dardania's mines in their entity or specific districts can be correlated with the Pb isotope signature of these metal objects.

Generally, all three artefacts plot within the data cloud of the Kopaonik-Šumadija district (Fig. 19.1). While they cannot be distinguished isotopically in the $^{208}Pb/^{206}Pb$ versus $^{206}Pb/^{204}Pb$ diagram, the metal objects signficiantly differ in $^{208}Pb/^{206}Pb$- $^{207}Pb/^{206}Pb$ space. One of the lead sheathing analyses overlaps with the platelet retrieved from Ulpiana (sample V) in the $^{208}Pb/^{206}Pb$- $^{206}Pb/^{204}Pb$ plot. Both sheathings, however, do not directly match ore data points. The ingot overlaps with an outlier of the Šumadija dataset (i.e. the Rudnik mine; Pernicka et al., 1993) in the $^{208}Pb/^{206}Pb$ versus $^{206}Pb/^{204}Pb$ diagram (Fig. 19.1a) and plots close to a data point of the Kopaonik Mountains (Karadak prospect; Veselinović-Williams, 2011) in the $^{208}Pb/^{206}Pb$- $^{207}Pb/^{206}Pb$ graphic (Fig. 19.1b). Altogether, none of the three analyses of the *MET DARD* shipwreck cargo directly matches local ores from Kosovo and Serbia. The objects, however, can be unambiguously related to the data cloud of the Kopaonik-Šumadija district. As has been demonstrated by the investigation of smelting sites near Ulpiana, the hypothesised mixing of raw material already on a local scale has the potential to generate a blurred isotope signature (chapter 16.3). This resulted in a data cloud extending between the uttermost values of the local ore, i.e. between Shashkoc-Janjevo as the youngest and Novobërdë as the oldest

deposits (cf. Fig. 15.1).
In summary, the Pb isotope data generally allows an attribution of the three objects to mineralisations of the Kopaonik-Šumadija district. In conjunction with the inscription *MET DARD*, a production from Kosovarian / Serbian ores seems most likely. Thus, the existence of a '*Metalla Dardanica*' district - which until now solely has been suspected on basis of epigraphic considerations - could be established due to the availability of matching geochemical data. However, it could not be resolved based on geochemical data alone whether *MET DARD* specifically refers to the ancient workings nearby Municipium DD or all mines of the region Dardania.

19.2.2. Lead-glazed pottery

Walton & Tite (2010) investigated Pb-glazed pottery dating from the 1st to the 5th century CE to assess the applied production technology and to estimate the locations of workshops. Furthermore, they carried out Pb isotope analyses of the glazes to reconstruct the possible provenance of the raw material used for their production. They sampled ceramic from excavations in Italy, France, England as well as from Serbia (Singidunum / Belgrade and Diana, a fortress in the easternmost part of the country, close to the border to Romania) and Romania (Apulum Partos / Alba Iulia in Transylvania). While pottery from the Diana fortress has been dated from the 1st to the 4th century CE, all samples from Apulum Partos and Singidunum have been assigned to the 2nd century CE. Interestingly, the Romanian sample location is situated c. 50 km northeast of Sarmizegetusa (Roman Ulpia Traiana), the capital of the province Dacia where a lead ingot with the inscription *MET ULP* has been found (cf. chapter 4.1.2). Based on Pb isotope provenance analysis, Walton & Tite (2010) assumed most investigated samples to have been produced from regional ore resources. They have matched pottery from Romania and Serbia with ores from the Central and Eastern Rhodopes. Due to the abundant rich Pb mineralisations in the region, however, it is aimed to test whether raw material for production of the glaze might as well have been derived from deposits located closer to the three finding sites. Immediately south of Belgrade, the mines of the Šumadija district (e.g. Avala, Kosmaj Babe, Rudnik; cf. chapter 4.3) are located. In the vicinity of the Diana Fortress, literature on regional economic geology only lists Cu-rich base metal deposits of the Cretaceous Timoc Magmatic Complex district, but no Pb-dominant mineralisations (Monthel et al., 2002). The base metal occurrences of the Apuseni district (cf. chapter 5.1.2) are approximately 55 km to the southwest of Alba Iulia.
Overall, the data of the sherds plotting in the range of local ores forms two larger clusters (Fig. 19.1). Pottery from Diana, Singidunum and Apulum Partos (1st to 4th century CE) concentrates at $^{206}Pb/^{204}Pb$, $^{207}Pb/^{206}Pb$ and $^{208}Pb/^{206}Pb$ values of 18.695, 0.8385 and 2.0780, while early imperial (1st to 2nd century CE) ceramic from Diana and Singidunum clusters around $^{206}Pb/^{204}Pb$, $^{207}Pb/^{206}Pb$ and $^{208}Pb/^{206}Pb$ ratios of 18.635, 0.8410 and 2.0835. An outlier data point of a sample from Apulum Partos possesses $^{206}Pb/^{204}Pb$, $^{207}Pb/^{206}Pb$ and $^{208}Pb/^{206}Pb$ values of 18.678, 0.8396 and 2.0788. Analyses of one of the sarcophagi from Ulpiana (sample I) partially match the Pb glazing (Fig. 19.1). The sherds retrieved from the Serbian settlements, besides the proposed origin from ores of the Rhodope Mountains (Walton & Tite, 2010), can be generally related to the Pb isotope cloud of the Kopaonik-Šumadija district. While the

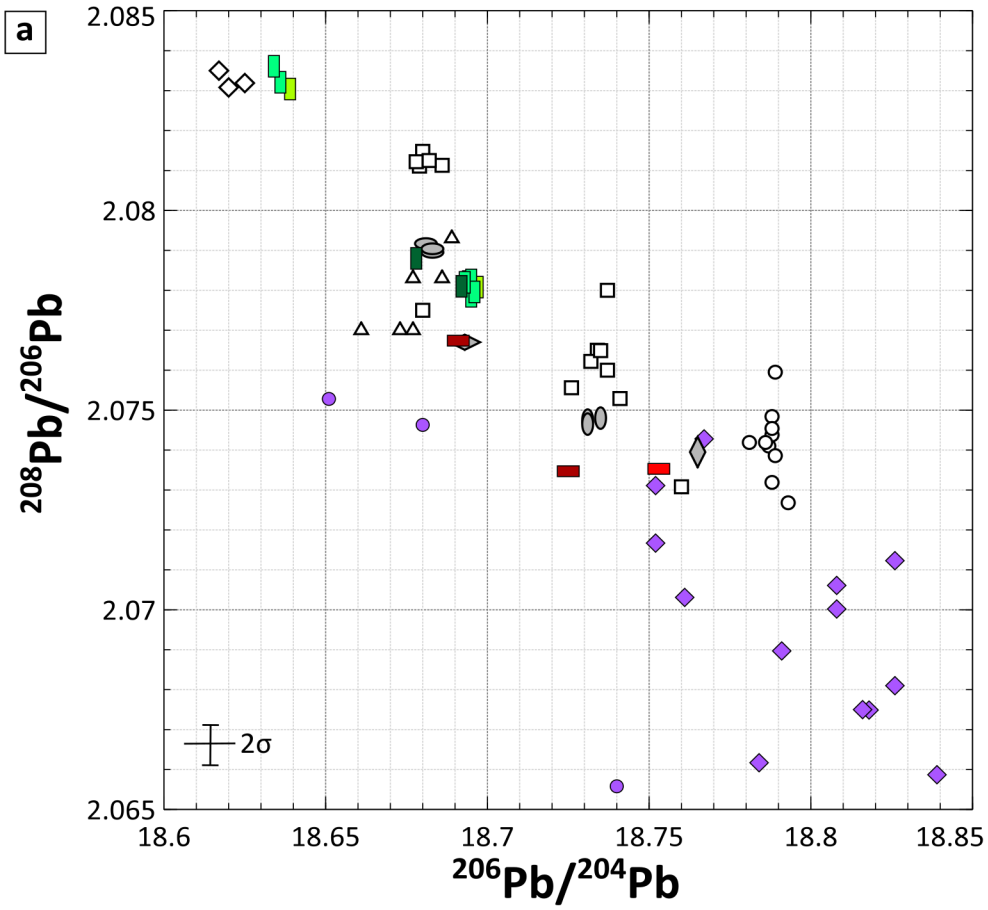
a
2.085
2.08
2.075
2.07
2.065
208Pb/206Pb
2σ
18.6
18.65
18.7
18.75
18.8
18.85
206Pb/204Pb

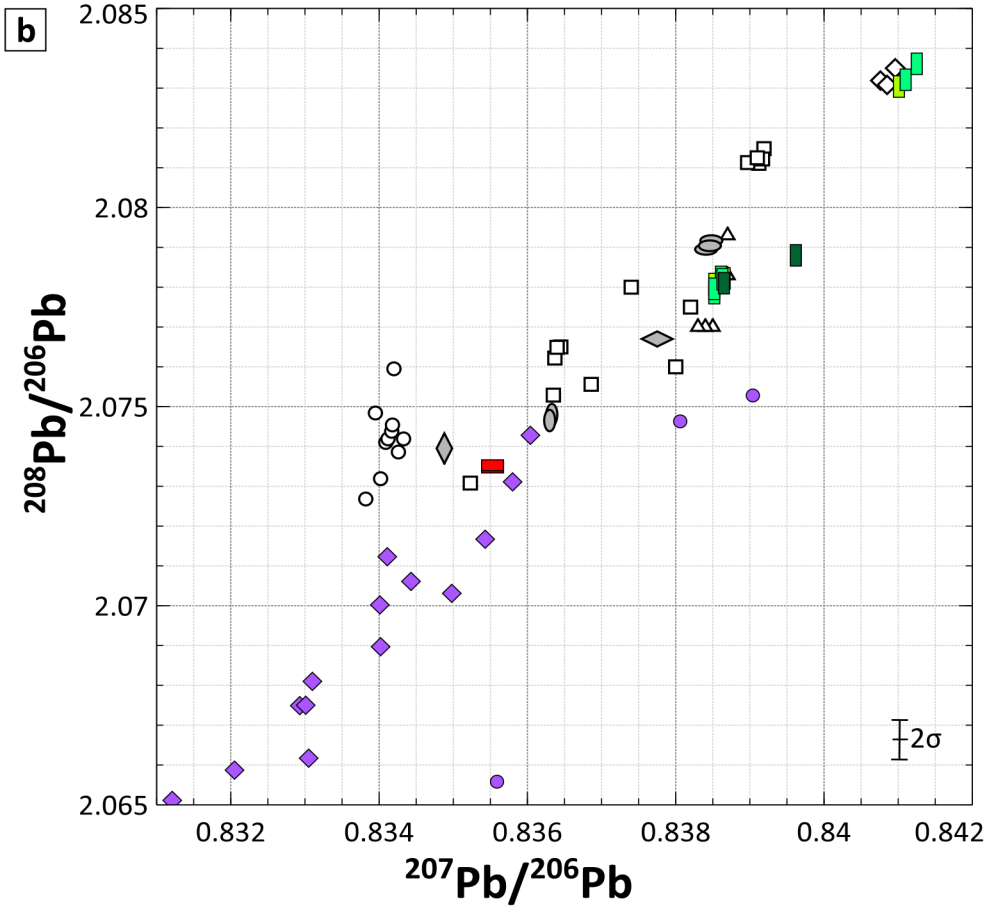
b
2.085
2.08
2.075
2.07
2.065
208Pb/206Pb
2σ
0.832
0.834
0.836
0.838
0.84
0.842
207Pb/206Pb

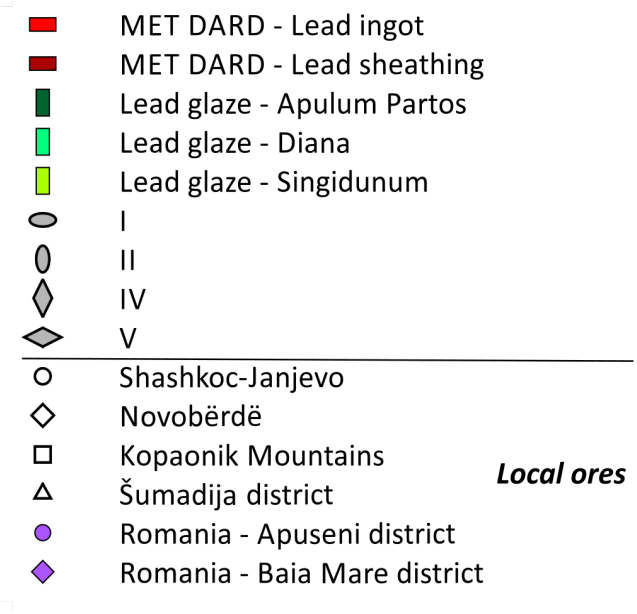

Figure 19.1.: Biplots of Pb isotope ratios of Roman lead (-bearing) objects retrieved from Ulpiana, Israel (*MET DARD*) as well as Serbia and Romania (lead glaze) in comparison with local ores from Kosovo, Serbia and Romania (Kosovo and Serbia: Gale, 1990, pers. comm.; Pernicka et al., 1993; Veselinović-Williams, 2011; own data; Romania: Marcoux et al., 2002). The error bars depict the average 2σ values (two times standard deviation) of the ore and lead object samples analysed in Frankfurt. a) $^{208}Pb/^{206}Pb$ versus $^{206}Pb/^{204}Pb$. b) $^{208}Pb/^{206}Pb$ versus $^{207}Pb/^{206}Pb$.

isotopically younger cluster plots closest to data of the Šumadija district (i.e. the Rudnik deposit) and partially the Kopaonik Mountains, the older one overlaps with Pb ratios determined for ore from the Novobërdë deposit. The glazing from the Romanian Alba Iulia in contrast shows no direct relation with local ores from the Apuseni and Baia Mare districts (Marcoux et al., 2002) and instead could have been produced from ores of the Kopaonik-Šumadija district (Fig. 19.1). Roman mining in Romania apparently focused on the country's rich Au occurences (cf. chapter 5.1.2). The finding of the *MET ULP* ingot in Ulpia Traiana (see above) as well as the fact that the Pb isotope signature of a litharge roll retrived from Roman workings at Roşia Montană is significantly different from the local ore (Baron et al., 2011) implies that Pb at least partially was imported, e.g. for utilisation in Au-Ag metallurgy.

In summary, comparison of Pb isotope ratios of glazed pottery retrieved from settlements in Serbia with those of mineralisations of the Kopaonik-Šumadija district justifies considering a local origin of the raw material utilised for its manufacture. The Pb glazing of the investigated Romanian sherds, however, doubtlessly has not been produced from local ores. Indeed, as has been suggested by the finding of a *MET ULP* ingot in Ulpia Traiana, located few ten kilometres northeast of the finding location of the ceramic, lead metal might have been regularly imported from mines in Moesia Superior.

20. Further implications for research

Ore

The suspected preferential exploitation of main-stage ore in Roman / late antique times and assumed increasing focus on late-stage ore in the medieval / early modern period in the Shashkoc-Janjevo district (chapter 18.2) should be substantiated by mining archaeological investigations, e.g. excavations of suitable workings. Jarosite-group minerals locally have been observed associated with early- and main-stage dominated mineralisations (cf. chapter 8). It should be assessed whether these secondary phases, analogous to Rio Tinto (cf. chapter 5.2.1), might have been used as a source for Ag. Furthermore, the Au content of the ore (Féraud & Deschamps, 2009; Hießleitner, 1927; Hyseni & Alliu, 1999; Monthel et al., 2002) which significantly contributed to the relevance of the medieval workings at Janjevo and Novobërdë (Ćirković, 1981) and still is won from these mineralisations today, should be located in its host phases and analysed. Besides the district of Shashkoc-Janjevo, further ores from the deposit of Novobërdë should be petrographically and geochemically characterised. This far, only three samples have been analysed for their Pb isotope signature (cf. chapter 15.1.1), even though the smelting sites in the immediate vicinity (e.g. Marec) presumably were mainly supplied with raw material from Novobërdë. The poor analytical characterisation of this mineralisation furthermore is in stark contrast to its high relevance in medieval as well as Ottoman and potentially also Roman times (cf. section 4.1.1). Ore from the occurrence at Zhegovcë to date has not been investigated at all. Considering that ore from this mineralisation might have been treated particularly at the sites of Voguçincë, Mirash and Akllap (chapter 16.3) and in order to thoroughly characterise the local resources, this analytical gap should be closed.

Beneficiation

As has been discussed in chapter 16.4, it could not have been assessed how the ore was beneficiated, i.e. whether it was only crushed or also finely ground and potentially concentrated with wet-mechanical techniques. Furthermore, it could not have been satisfyingly resolved by analytical methods alone whether the raw material was partially roasted before the smelting process. It is thus desirable that these questions are tried to be clarified by mining archaeological investigations.

Smelting sites

Besides the already investigated Marec, further metallurgical sites have been discovered at the rivulet Kriva. Their different dating ranging from Roman / late antique to medieval / early modern eras offers the possibility to study potential organisational and technological changes at a very narrow scale at a time period of several centuries. Due to their location in the immediate

vicinity of the Novobërdë deposit, it is assumed that they have been mainly supplied by this mineralisation, which since at least medieval times is a highly relevant Pb-Zn-Ag-Au mine. The site of Trubuhoc / Trbuvce is located south of Voguçincë and according to the latest survey in 2016 similarly possesses a preliminary Roman / late antique dating. Investigation of Trubuhoc also is rendered interesting by the fact that the distance to the occurrence of Zhegovcë - which is suspected to have partially provided the furnace feed for the sites of Voguçincë, Mirash and Akllap (see above) - is less than 3 km.

Metal artefacts

More sampling of lead and silver objects, which were excavated in Ulpiana or possess a regional context (e.g. the *MET ULP* ingot; cf. section 4.1.2), is strongly desired to further assess trade routes and to draw conclusions about the relevance of local metal production. Due to the flourishing medieval / early modern mining and smelting activities proven in the hinterland of the *municipium*, analysis of artefacts from the region with a later dating is a desideratum for possible future investigations.

Conclusions

- Ore from the Shashkoc-Janjevo district could be identified by Pb isotope analysis to have (partially) supplied the raw material basis for six of the ten investigated smelting sites, including the preliminary Roman / late antique dated complexes of Voguçincë and Mirash Novo as well as the potentially medieval / early modern sites of Mramor Samakove, Akllap and Ostri Vrh. Pb isotope signatures of metallurgical remains from the not yet dated site of Mramor Proni Butoçit also overlap with the ore data. The geochemical signature of the serpentinite rocks (i.e. elevated Mg, Cr and Ni abundances) partially hosting mineralisations in the district as well is reflected within the smelting (by-) products and further confirm the observed correlation.

- The mineralisation of the Shashkoc-Janjevo district can be generally classified as Pb-Ag ore. These two commodities clearly were the focus of the archaeometallurgical activities. Precipitation of the ore occurred in three stages (not distinguishable by Pb isotope analysis), which are marked by a slightly differing mineralogy. Ore from the first two stages overall possesses a more polymetallic character with comparably enriched Cu, As and Sb contents due to the elevated presence of tennantite-tetrahedrite minerals, chalcopyrite and arsenopyrite and chalcocite, digenite, covellite, malachite and jarosite-group phases in primary and secondary parageneses, respectively. The more complex composition of these ore types is mirrored by the metallurgical by-products matte and speiss, which until now almost exclusively have been observed at sites with a preliminary Roman / late antiqe dating. The generally higher Ag content of the polymetallic ore bodies offers an explanation for their assumed preferential exploitation in the earlier stages of local mining. Since these ores were formed at comparably higher temperatures and consequently are more abundant in the vicinity of genetically related Tertiary igneous rocks, the district is slightly zoned with respect to its Ag-Cu-As-Sb grades. While at workings nearby Shashkoc later precipitated, relatively 'pure' Pb-Ag ore essentially consisting of galena, sphalerite and pyrite / marcasite predominates, in the vicinity of Janjevo polymetallic parageneses are comparably enriched. This observation in conjunction with the suspected chronology of ancient mining activities in the district matches the hypothesis of Davies (1935), who believes the workings nearby Shashkoc to be of medieval age and those in the vicinity of Janjevo to be Roman.

- Notable Ag abundances in matte might have been extracted by re-submitting the material to the furnace with added native Pb to collect the freed Ag. The precious metal content of base metal speiss due to its close association with crude Pb presumably has been automatically won by cupellation of the metal bullion. Both ferrous speiss and partially generated pig iron are assumed to have been discarded without further treatment.

- Metallurgical remains from the site of Marec located in the immediate vicinity of the deposit of Novobërdë partially overlap with the Pb isotope signature of these ores. Samples which could not be unambiguously assigned to one of the two mineralisations form a cloud extending between the data of Shashkoc-Janjevo as the youngest and Novobërdë as the oldest Pb isotope ratios on local scale. Their Pb isotope signatures could have been generated by smelting of ores from several, isotopically slightly different occurrences, by treatment of raw material from a not yet characterised mineralisation or a combination of both effects.

- Besides hypothesised differences of the smelter feed, partially also variations of the metallurgical installations and process scheme have been identified. The slags were typically discharged by intermittently opening a tap hole and subsequently cooled in a basin outside the furnace. At the sites of Akllap and Ostri Vrh, a different construction was utilised, in which the slags accumulated in a reservoir within the furnace.

- At all presumably Roman / late antique and the potentially medieval / early modern sites of Marec and partially Hanroc olivine-dominant smelting slags have been sampled. These were generated by smelting of (partially roasted) ore with charcoal and silica, which ensured sufficient slag formation and thus removal of impurities from the charge. The only small differences between the parageneses and crystallisation sequence and the overlapping phase compositions indicate widely similar process conditions. From the other presumably medieval / early modern sites, slags with a Ca-richer composition containing calcio-olivine, olivine + clinopyroxene or melilite as main phase(s) have been retrieved. These types were generated by addition of a calcareous flux besides silica to the charge consisting of (partially roasted) ore and charcoal. The furnace atmosphere was more oxidising and outside the fayalite stability field. Glassy slags rarely sampled at preliminary Roman / late antique sites as well were formed at higher fO_2, but presumably without utilisation of a Ca-rich fluxing agent.

- Roman objects excavated in Ulpiana could not be directly assigned by Pb isotope provenance studies to resources of the Shashkoc-Janjevo and Novobërdë mineralisations, but analogous to some of the studied metallurgical by-products plot in the data cloud extending between the two deposits. The data of two of the four metal artefacts could be matched with ores from the Kopaonik Mountains and the Šumadija district. Even though the Pb isotope signatures of the objects are in a similar range than other Tertiary mineralisations of the Balkan Peninsula and Betic Cordillera, due to their everyday character a production from local resources is most likely. Blurring of the isotope signatures could already be established during primary smelting of ores from different mineralisations (see above), but also during refining treatment if Pb bullion from several metallurgical sites was collected and subsequently refined (e.g. cupelled) in bulk.

- Pb isotope data of imperial lead ingots with *'MET DARD'* imprinting (Raban, 1999) and Pb-glazed pottery dating from the 1st to the 5th century CE from Serbia and Romania (Walton & Tite, 2010) generally match those of Kosovarian / Serbian ores. Together with the data of lead objects from Ulpiana collected during this study (see above), these provenance studies a) confirm the existence of a *Metalla Dardanica* district, b) indicate that

the Romans as in other regions of the Empire if possibly utilised local resources for metal production and c) document flourishing trade of locally produced metal and testify to the relevance of the Balkan regions' mineral wealth for the metal supply of the (late) Empire.

References

Agricola, G. (1950). *De Re Metallica* (H. C. Hoover & L. H. Hoover, Trans.). New York: Dover Publications (Original work published 1556).

Allègre, C. J. (2008). *Isotope geology.* Cambridge: Cambridge University Press.

Anguilano, L. (2012). *Roman lead silver smelting at Rio Tinto: The case study of Corta Lago* (Doctoral thesis, University College London, United Kingdom).

Anguilano, L., Rehren, Th., Müller, W., & Rothenberg, B. (2010). The importance of lead in the silver production at Riotinto (Spain). *Revue d'archéométrie, 34*, 269-276.

Arribas, A., & Tosdal, R. M. (1994). Isotopic composition of Pb in ore deposits of the Betic Cordillera, Spain; origin and relationship to other European deposits. *Economic Geology, 89*(5), 1074-1093.

Artioli, G., Baumgarten, B., Marelli, M., Giussani, B., Recchia, S., Nimis, P., Giunti, I., Angelini, I., & Omenetto, P. (2008). Chemical and isotopic tracers in Alpine copper deposits: Geochemical links between mines and metal. *Geo. Alp, 5*, 139-148.

Asael, D., Matthews, A., Bar-Matthews, M., Harlavan, Y., & Segal, I. (2012). Tracking redox controls and sources of sedimentary mineralization using copper and lead isotopes. *Chemical Geology, 310-311*, 23-35.

Avrupa Minerals. *Slivovo Gossan.* Retrieved from http://www.avrupaminerals.com/projects/kosovo/slivovo_gossan/; 6 June 2016.

Bachmann, H.-G. (1980). Early copper smelting techniques in Sinai and in the Negev as deduced from slag investigations. In P. T. Craddock (Ed.), *Scientific studies in early mining and extractive metallurgy* (103-134). British Museum Occasional Paper 20. London: British Museum.

Bachmann, H.-G. (1993). Zur frühen Blei- und Silbergewinnung in Europa. In H. Steuer & U. Zimmermann (Eds.), *Montanarchäologie in Europa: Berichte zum Kolloquium "Frühe Erzgewinnung und Verhüttung in Europa" in Freiburg im Breisgau vom 4. bis 7. Oktober 1990* (29-36). Sigmaringen: Jan Thorbecke.

Baker, J., Stos, S., & Waight, T. (2006). Lead isotope analysis of archaeological metals by multiple-collector inductively coupled plasma mass spectrometry. *Archaeometry, 48*(1), 45-56.

Barnes, S. J., & Roeder, P. L. (2001). The range of spinel compositions in terrestrial mafic and ultramafic rocks. *Journal of Petrology, 42*(12), 2279-2302.

Baron, S., Carignan, J., Laurent, S., & Ploquin, A. (2006). Medieval lead making on Mont-Lozère Massif (Cévennes-France): Tracing ore sources using Pb isotopes. *Applied Geochemistry, 21*(2), 241-252.

Baron, S., Le-Carlier, C., Carignan, J., & Ploquin, A. (2009). Archaeological reconstruction of medieval lead production: Implications for ancient metal provenance studies and paleopollu-

tion tracing by Pb isotopes. *Applied Geochemistry, 24*(11), 2093-2101.

Baron, S., Tămaş, C. G., Cauuet, B., & Munoz, M. (2011). Lead isotope analyses of gold–silver ores from Roşia Montană (Romania): a first step of a metal provenance study of Roman mining activity in Alburnus Maior (Roman Dacia). *Journal of Archaeological Science, 38*(5), 1090-1100.

Baron, S., Tămaş, C. G., & Le Carlier, C. (2014). How mineralogy and geochemistry can improve the significance of Pb isotopes in metal provenance studies. *Archaeometry, 56*(4), 665-680.

Bartels, C. (2014). Bleiglanz als hauptsächliches Silbererz des Mittelalters und der frühen Neuzeit? - Zur Entstehung und Geschichte eines grundlegenden Irrtums. *Der Anschnitt, 66*(4), 190-213.

Barth, A., Kühne, H., & Legler, C. (2005). *Report - Description of the map compilation.* Beak Consultants GmbH, project-no. 20040156.

Bau, M., Romer, R. L., Lüders, V., & Dulski, P. (2003). Tracing element sources of hydrothermal mineral deposits: REE and Y distribution and Sr-Nd-Pb isotopes in fluorite from MVT deposits in the Pennine Orefield, England. *Mineralium Deposita, 38*(8), 992-1008.

Berisha, M., Drafehn, A., Gashi, S., Gauß, R., Helfert, M., Luci, K., Lüth. F., Mertl, P., Reichler, S., Schafferer, G., Teichner, F., Wendling, H. (2012). Archäologisch-geophysikalische Prospektion im Kosovo – Erste Resultate einer bilateralen Forschungskooperation. *Archäologischer Anzeiger, 2*, 65-92.

Blackburn, W. H., & Schwendeman, J. F. (1977). Trace-element substitution in galena. *The Canadian Mineralogist, 15*(3), 365-373.

Bode, M. (2008). *Archäometallurgische Untersuchungen zur Blei-/Silbergewinnung im Germanien der frühen Römischen Kaiserzeit* (Doctoral thesis, Westfälische Wilhelms-Universität Münster, Germany).

Bode, M., Hauptmann, A., & Mezger, K. (2009). Tracing Roman lead sources using lead isotope analyses in conjunction with archaeological and epigraphic evidence - a case study from Augustan / Tiberian Germania. *Archaeological and Anthropological Sciences, 1*(3), 177-194.

Bogosavljević, D. (1994). Medieval mining tools from the Belgrade National Museum collection. In P. Petrović & S. Đurđekanović (Eds.), *Ancient mining and metallurgy in southeast Europe: International Symposium Donji Milanovac, May 20-25, 1990* (251-264). Belgrade: Archaeological Institute, Belgrade; Museum of Mining and Metallurgy, Bor.

Bogosavljević-Petrović, V. (2006). Continuity of metallurgy in the Ibar valley. *Metalurgija, 12*(2-3), 129-144.

Boni, M., Di Maio, G., Frei, R., & Villa, I. M. (2000). Lead isotopic evidence for a mixed provenance for Roman water pipes from Pompeii. *Archaeometry, 42*(1), 201-208

Boni, M., & Koeppel, V. (1985). Ore-lead isotope pattern from the Iglesiente-Sulcis area (SW Sardinia) and the problem of remobilization of metals. *Mineralium Deposita, 20*(3), 185-193.

Borojević Šoštarić, S., Palinkaš, L. A., Topa, D., Spangenberg, J. E., & Prochaska, W. (2011). Silver-base metal epithermal vein and listwaenite types of deposit Crnac, Rogozna Mts., Kosovo. Part I: Ore mineral geochemistry and sulfur isotope study. *Ore Geology Reviews, 40*(1), 65-80.

Borojević Šoštarić, S., Cvetković, V., Neubauer, F., Palinkaš, L. A., Bernroider, M., & Genser, J.

(2012). Oligocene shoshonitic rocks of the Rogozna Mts. (Central Balkan Peninsula): Evidence of petrogenetic links to the formation of Pb-Zn-Ag ore deposits. *Lithos, 148*, 176-195.

Borojević Šoštarić, S., Palinkaš, L. A., Neubauer, F., Hurai, V., Cvetković, V., Roller-Lutz, Z., Mandić, M., & Genser, J. (2013). Silver-base metal epithermal vein and listwanite hosted deposit Crnac, Rogozna Mts., Kosovo, part II: A link between magmatic rocks and epithermal mineralization. *Ore Geology Reviews, 50*, 98-117.

Bouch, J. E., Naden, J., Shepherd, T. J., McKervey, J. A., Young, B., Benham, A. J., & Sloane, H. J. (2006). Direct evidence of fluid mixing in the formation of stratabound Pb–Zn–Ba–F mineralisation in the Alston Block, North Pennine Orefield (England). *Mineralium Deposita, 41*(8), 821-835.

Boulakia, J. D. C. (1972). Lead in the Roman world. *American Journal of Archaeology, 76*(2), 139-144.

Bowen, N. L., & Schairer, J. F. (1935). The system MgO-FeO-SiO_2. *American Journal of Science, 29*(170), 151-217.

Bowen, N. L., Schairer, J. F., & Posnjak, E. (1935). The system Ca_2SiO_4-Fe_2SiO_4. *American Journal of Science, 25*(148), 273-297.

Braxton, D., & Mathur, R. (2011). Exploration applications of copper isotopes in the supergene environment: A case study of the Bayugo porphyry copper-gold deposit, southern Philippines. *Economic Geology, 106*(8), 1447-1463.

Brevart, O., Dupré, B., & Allegre, C. J. (1982). Metallogenic provinces and the remobilization process studied by lead isotopes; lead-zinc ore deposits from the southern Massif Central, France. *Economic Geology, 77*(3), 564-575.

Brill, R. H., & Wampler, J. M. (1967). Isotope studies of ancient lead. *American Journal of Archaeology, 71*(1), 63-77.

Britvin, S. N., Bogdanova, A. N., Boldyreva, M. M., & Aksenova, G. Y. (2008). Rudashevskyite, the Fe-dominant analogue of sphalerite, a new mineral: Description and crystal structure. *American Mineralogist, 93*(5-6), 902-909.

Brown, G. E. (1982). Olivines and silicate spinels. In P. H. Ribbe (Ed.), *Orthosilicates* (275-381). Reviews in Mineralogy, 5. Washington: Mineralogical Society of America.

Budd, P., Pollard, A. M., Scaife, B., & Thomas, R. G. (1995). The possible fractionation of lead isotopes in ancient metallurgical processes. *Archaeometry, 37*(1), 143-150.

Cabri, L. J. (1973). New data on phase relations in the Cu-Fe-S system. *Economic Geology, 68*(4), 443-454.

Cattin, F., Guénette-Beck, B., Besse, M., & Serneels, V. (2009). Lead isotopes and archaeometallurgy. *Archaeological and Anthropological Sciences, 1*(3), 137-148.

Chalkias G., Vavelidis M., Schmitt-Strecker S., & Begemann F. (1988). Geologische Interpretation der Blei-Isotopen-Verhältnisse von Erzen der Insel Thasos, der Ägäis und Nordgriechenlands. In G. A. Wagner & G. Weisgerber (Eds.), *Antike Edel- und Buntmetallgewinnung auf Thasos* (59-74). Der Anschnitt: Beiheft 6. Bochum: Deutsches Bergbau-Museum.

Charef, A., & Sheppard, S. M. F. (1988). The Malines Cambrian carbonate-shale-hosted Pb-Zn deposit, France: Thermometric and isotopic (H, O) evidence for pulsating hydrothermal mineralization. *Mineralium Deposita, 23*(2), 86-95.

Chiarantini, L., Benvenuti, M., Costagliola, P., Fedi, M. E., Guideri, S., & Romualdi, A. (2009). Copper production at Baratti (Populonia, southern Tuscany) in the early Etruscan period (9th–8th centuries BC). *Journal of Archaeological Science, 36*(7), 1626-1636.

Chutas, N. I., Kress, V. C., Ghiorso, M. S., & Sack, R. O. (2008). A solution model for high-temperature PbS-$AgSbS_2$-$AgBiS_2$ galena. *American Mineralogist, 93*(10), 1630-1640.

Ćirković, S. (1981). The production of gold, silver and copper in the central parts of the Balkans from the 13th to the 16th century. In H. Kellenbenz (Ed.), *Precious metals in the age of expansion: Papers of the XIVth International Congress of the Historical Sciences* (41-69). Stuttgart: Franz Steiner Verlag.

Clark, A. H., & Sillitoe, R. H. (1971). Cuprian galena solid solutions, Zapallar mining district, Atacama, Chile. *American Mineralogist, 56*(11-12), 2142-2144.

Clark, A. H., & Ullrich, T. D. (2004). ^{40}Ar-^{39}Ar age data for andesitic magmatism and hydrothermal activity in the Timok Massif, eastern Serbia: implications for metallogenetic relationships in the Bor copper-gold subprovince. *Mineralium Deposita, 39*(2), 256-262.

Cook, N. J., Ciobanu, C. L., Pring, A., Skinner, W., Shimizu, M., Danyushevsky, L., Saini-Eidukat, B., & Melcher, F. (2009). Trace and minor elements in sphalerite: A LA-ICPMS study. *Geochimica et Cosmochimica Acta, 73*(16), 4761-4791.

Cook, N. J., Ciobanu, C. L., Danyushevsky, L. V., & Gilbert, S. (2011). Minor and trace elements in bornite and associated Cu-(Fe)-sulfides: A LA-ICP-MS study. *Geochimica et Cosmochimica Acta, 75*(21), 6473-6496.

Cosca, M.A., & Peacor, D. R. (1987). Chemistry and structure of esseneite ($CaFe^{3+}AlSiO_6$), a new pyroxene produced by pyrometamorphism. *American Mineralogist, 72*, 148-156.

Craddock, P. T., Freestone, I. C., & Ortiz, M. H. (1987). Recovery of silver from speiss at Rio Tinto (SW Spain). *iams Newsletter, 10-11*, 8-11.

Craig, J. R., & Kullerud, G. (1967). The Cu-Fe-Pb-S system. *Carnegie Institution of Washington Yearbook, 65*, 344-352.

Craig, J. R., & Kullerud, G. (1968). Phase relations and mineral assemblages in the copper-lead-sulfur system. *American Mineralogist, 53*(1-2), 145-161.

Cui, J., & Wu, X. (2011). An experimental investigation on lead isotopic fractionation during metallurgical processes. *Archaeometry, 53*(1), 205-214.

Cvetković, V., Prelević, D., Downes, H., Jovanović, M., Vaselli, O., & Pécskay, Z. (2004). Origin and geodynamic significance of Tertiary postcollisional basaltic magmatism in Serbia (central Balkan Peninsula). *Lithos, 73*(3), 161-186.

Dangić, A. (1985). Minor element distribution between galena and sphalerite as a geothermometer - application to two lead-zinc areas in Yugoslavia. *Economic Geology, 80*(1), 180-183.

Dangić, A. (1989). Alteracioni filosilikati - chidrotermalna alteracija intermedijarnich vulkanita i ultramafita oko Pb-Zn ruda [Alteration phyllosilicates – wall rock alternation of intermediate volcanics and ultramafic rocks around Pb-Zn sulphide ores]. *Geološki anali Balkanskoga poluostrva (= Annales géologiques de la péninsule Balkanique), 53*, 429-444 [in Serbian with English summary].

Davies, O. (1935). *Roman mines in Europe.* Oxford: Arno Press.

Davies, O. (1938). Ancient mining in the central Balkans. *Revue Internationale des Études*

Balkaniques, 3, 405-418.

De Andrade Lima, L. R. P., & Bernardez, L. A. (2011). Characterization of the lead smelter slag in Santo Amaro, Bahia, Brazil. *Journal of Hazardous Materials, 189*(3), 692-699.

De Bièvre, P., & Taylor, P. D. P. (1993). Table of the isotopic compositions of the elements. *International Journal of Mass Spectrometry and Ion Processes, 123*(2), 149-166.

De Boorder, H., Spakman, W., White, S. H., & Wortel, M. J. R. (1998). Late Cenozoic mineralization, orogenic collapse and slab detachment in the European Alpine Belt. *Earth and Planetary Science Letters, 164*(3), 569-575.

Degterov, S. A., Jak, E., Hayes, P. C., & Pelton, A. D. (2001). Experimental study of phase equilibria and thermodynamic optimization of the Fe-Zn-O system. *Metallurgical and Materials Transactions B, 32*(4), 643-657.

Desaulty, A. M., Telouk, P., Albalat, E., & Albarède, F. (2011). Isotopic Ag–Cu–Pb record of silver circulation through 16th–18th century Spain. *Proceedings of the National Academy of Sciences, 108*(22), 9002-9007.

De Vivo, B., Boni, M., & Costabile, S. (1998). Formational anomalies versus mining pollution: geochemical risk maps of Sardinia, Italy. *Journal of Geochemical Exploration, 64*(1), 321-337.

Dill, H. G. (2015). Supergene alteration of ore deposits: From nature to humans. *Elements, 11*(5), 311-316.

Dimitrijević, M. D. (2001). Dinarides and the Vardar Zone: a short review of the geology. *Acta Vulcanologica, 13*(1-2), 1000-1008.

Domergue, C. (2008). *Les mines antiques: La production des métaux aux époques grecque et romaine* [The ancient mines: Production of metals in Greek and Roman times]. Paris: Éditions A&J Picard [in French].

Donaldson, C. H. (1976). An experimental investigation of olivine morphology. *Contributions to Mineralogy and Petrology, 57*(2), 187-213.

Droop, G. T. R. (1987). A general equation for estimating Fe^{3+} concentrations in ferromagnesian silicates and oxides from microprobe analyses, using stoichiometric criteria. *Mineralogical Magazine, 51*(361), 431-435.

Dube, R. K. (2006). The extraction of lead from its ores by the iron-reduction process: A historical perspective. *JOM, 58*(10), 18-23.

Durali-Müller, S. (2005). *Roman lead and copper mining in Germany: their origin and development through time, deduced from lead and copper isotope provenance studies* (Doctoral thesis, Johann Wolfgang Goethe-Universität Frankfurt am Main, Germany).

Durali-Mueller, S., Brey, G. P., Wigg-Wolf, D., & Lahaye, Y. (2007). Roman lead mining in Germany: its origin and development through time deduced from lead isotope provenance studies. *Journal of Archaeological Science, 34*(10), 1555-1567.

Dušanić (1977). Aspects of Roman mining in Noricum, Pannonia, Dalmatia, and Moesia Superior. In H. Temporini (Ed.), *Aufstieg und Niedergang der römischen Welt, II. 6* (52-94). Berlin: Walter de Gruyter.

Dušanić, S. (2000). Army and mining in Moesia Superior. In G. Alföldy, B. Dobson, & W. Eck (Eds.), *Kaiser, Heer und Gesellschaft in der römischen Kaiserzeit: Gedenkschrift für Eric Birley* (343–363). Stuttgart: Franz Steiner.

Dušanić, S. (2004). Roman mining in Illyrikum: Historical aspects. In: G. Urso (Ed.), *Dall'Adriatico al Danubio: L'Illirico nell'età greca e romana: Atti del convegno internazionale, Cividale del Friuli, 25-27 settembre 2003, Pisa* (247-270). Pisa: Edizioni ETS.

Dutrizac, J. E. (1980). The $Fe_{1-x}S$-PbS-ZnS phase system. *Canadian Journal of Chemistry, 58*, 739-743.

Dvorani, S., Kozmaqi, K., Bejta, S., & Bajraktari, N. (2012). *Pb-Zn-Cu mineralization deposits and occurrences in the territory of the Republic of Kosovo.* Prishtina, Kosovo: Republic of Kosovo - Government, Ministry of Economic Development; Geological Institute of Kosovo.

Eckstein, K., Rehren, Th., & Hauptmann, A. (1994). Hochmittelalterliches Montanwesen im sächsischen Erzgebirge und seinem Vorland - Die Gewinnung von Blei und Silber. *Der Anschnitt, 46*(4-5), 122-132.

Einaudi, M. T., Hedenquist, J. W., & Inan, E. E. (2003). Sulfidation state of fluids in active and extinct hydrothermal systems: transitions from porphyry to epithermal environments. In S. F. Simmons & I. Graham (Eds.), *Volcanic, geothermal, and ore-forming fluids: Rulers and witnesses of processes within the Earths* (285-314). Special Publications of the Society of Economic Geologists Volume 10. Littleton: Society of Economic Geologists.

Eliopoulos, D. G., & Kilias, S. P. (2011). Marble-hosted submicroscopic gold mineralization at Asimotrypes area, Mount Pangeon, southern Rhodope core complex, Greece. *Economic Geology, 106*(5), 751-780.

Ericsson, E., & Filippidis, A. (1986). Cation ordering in the limited solid solution Fe_2SiO_4-Zn_2SiO_4. *American Mineralogist, 71*(11), 1502-1509.

Ettler, V., Johan, Z., Kříbek, B., Šebek, O., & Mihaljevič, M. (2009a). Mineralogy and environmental stability of slags from the Tsumeb smelter, Namibia. *Applied Geochemistry, 24*(1), 1-15.

Ettler, V., Johan, Z., Bezdička, P., Drábek, M., & Šebek, O. (2009b). Crystallization sequences in matte and speiss from primary lead metallurgy. *European Journal of Mineralogy, 21*(4), 837-854.

Ettler, V., Červinka, R., & Johan, Z. (2009c). Mineralogy of medieval slags from lead and silver smelting (Bohutin, Příbram district, Czech Republic): Towards estimation of historical smelting conditions. *Archaeometry, 51*(6), 987-1007.

Ettler, V., Johan, Z., Zavřel, J., Wallisová, M. S., Mihaljevič, M., & Šebek, O. (2015). Slag remains from the Na Slupi site (Prague, Czech Republic): evidence for early medieval non-ferrous metal smelting. *Journal of Archaeological Science, 53*, 72-83.

Ettler, V., Legendre, O., Bodénan, F., & Touray, J. C. (2001). Primary phases and natural weathering of old lead–zinc pyrometallurgical slag from Příbram, Czech Republic. *The Canadian Mineralogist, 39*(3), 873-888.

Evans, J. A. S. (1996). *The age of Justinian: The circumstances of imperial power.* London: Routledge.

Féraud, J., & Deschamps, Y. (2009). *French scientific cooperation 2007-2008 on the Trepča lead-zinc-silver mine and the gold potential of Novo Brdo / Artana tailings (Kosovo).* BRGM report No. RP-57204-FR.

Fernandez, A., & Borrok, D. M. (2009). Fractionation of Cu, Fe, and Zn isotopes during the

oxidative weathering of sulfide-rich rocks. *Chemical Geology, 264*(1), 1-12.

Foit Jr., F. F., Rosenberg, P. E., & Hooper, R. L. (1987). An unusual pyroxene, melilite, and iron oxide mineral assemblage in a coal-fire buchite from Buffalo, Wyoming. *American Mineralogist, 72*, 137-147.

Friedrich, K. (1907). Die Schmelzdiagramme der binären Systeme Schwefelsilber-Kupfersulfur und Bleiglanz-Kupfersulfur. *Metallurgie, 4*, 671-673.

Frost, B. R., Mavrogenes, J. A., & Tomkins, A. G. (2002). Partial melting of sulfide ore deposits during medium-and high-grade metamorphism. *The Canadian Mineralogist, 40*(1), 1-18.

Gale, N. H., Stos-Gale, Z., Radouncheva, A., Ivanov, I., Lilov, P., Todorov, T., & Panayotov, I. (2000). Early metallurgy in Bulgaria. *Annuary of Department of Archaeology, 4-5*, 102-168.

Gale, N. H., Woodhead, A. P., Stos-Gale, Z. A., Walder, A., & Bowen, I. (1999). Natural variations detected in the isotopic composition of copper: possible applications to archaeology and geochemistry. *International Journal of Mass Spectrometry, 184*(1), 1-9.

Gardiner, V. (2001). An analysis of Romano-British lead pigs. *iams, 21*, 11-13.

Gassmann, G., Körlin, G., & Klein, S. (2011). Römischer Erzbergbau im Umfeld der antiken Stadt Ulpiana bei Priština (Kosovo). *Der Anschnitt, 63*(4-5), 157-167.

Gassmann, G., Klein, S., & Körlin, G. (2015). The Roman mines near Ulpiana, Kosovo. In: A. Hauptmann & D. Modarressi-Tehrani (Eds.), *Archaeometallurgy in Europe III: Proceedings of the 3rd International Conference. Deutsches Bergbau-Museum Bochum, June 29 - July 1* (33-43). Der Anschnitt Beiheft 26. Bochum: Deutsches Bergbau-Museum.

Gassmann, G., & Rehren, Th. (1998). Die mittelalterlichen Bleischlacken von der 'Wilden Wiese' bei Müsen. In C. Dahm, U. Lobbedey & G. Weisgerber (Eds.), *Der Altenberg. Bergwerk und Siedlung aus dem 13. Jahrhundert im Siegerland. Band 2 – Die Funde* (216-228). Bonn: Dr. Rudolf Habelt.

Gavrichev, K., Bolshakov, A., Kondakov, D., Khoroshilov, A., & Denisov, S. (2008). Thermal transformations of lead oxides. *Journal of Thermal Analysis and Calorimetry, 92*(3), 857-863.

Glasser, F. P. (1961). The system Ca_2SiO_4-Mn_2SiO_4. *American Journal of Science, 259*(1), 46-59.

Glasser, F. P., & Osborn, E. F. (1960). The ternary system MgO-MnO-SiO_2. *Journal of the American Ceramic Society, 43*, 132-140.

Goldenberg, G. (1996). Archäometallurgische Untersuchungen zur Entwicklung des Metallhüttenwesens im Schwarzwald: Blei-, Silber- und Kupfergewinnung von der Frühgeschichte bis zum 19. Jahrhundert. In G. Goldenberg, J. Otto & H. Steuer (Eds.), *Archäometallurgische Untersuchungen zum Metallhüttenwesen im Schwarzwald* (9-274). Sigmaringen: Jan Thorbecke.

Golubović, S. (2002). Decorated lead sarcophagi in Moesia Superior. In P. Freeman, J. Bennett, Z. T. Fiema & B. Hoffmann, *Limes XVIII: Proceedings of the XVIIIth International Congress of Roman Frontier Studies held in Amman, Jordan (September 2000)* (629-640). BAR International Series 1084 (II). Oxford: Archaeopress.

Gordus, A. A., & Metcalf, D. M. (1969). The metal contents of the early Serbian coinage. *Revue Belge de Numismatique et de Sigillographie, 65*, 57-82.

Gottschalk, R., & Baumann, A. (2001). Material provenance of late-Roman lead coffins in the

Rheinland, Germany. *European Journal of Mineralogy, 13*(1), 197-205.

Gowland, W. (1901). XXI. – The early metallurgy of silver and lead: Part I., lead. *Archaeologia, 57*(2), 359-422.

Gowland, W. (1914). *The metallurgy of the non-ferrous metals.* London: Charles Griffin and Company.

Graeser, S., & Friedrich, G. (1970). Zur Frage der Altersstellung und Genese der Blei-Zink-Vorkommen der Sierra de Cartagena in Spanien. *Mineralium Deposita, 5*(4), 365-374.

Grafenauer, S., Gorenc, B., Marinković, V., Strmole, D., & Maksimović, Z. (1969). Physical properties and the chemical composition of sphalerites from Yugoslavia. *Mineralium Deposita, 4*(3), 275-282.

Grögler, N., Geiss, J., Grünenfelder, M., & Houtermans, F. G. (1966). Isotopenuntersuchungen zur Bestimmung der Herkunft römischer Bleirohre und Bleibarren. *Zeitschrift für Naturforschung, 21a*(7), 1167-1172.

Guénette-Beck, B. & Furger, A. R. (2004). Blei für Augusta Raurica. *Jahresberichte aus Augst und Kaiseraugst, 25*, 245–272.

Guilbert, J. M., & Park Jr, C. F. (1986). *The geology of ore deposits.* Long Grove: Waveland Press.

Gulson, B. L. (1986). *Lead isotopes in mineral exploration.* Philadelphia: Elsevier.

Gulson, B. L., & Mizon, K. J. (1979). Lead isotopes as a tool for gossan assessment in base metal exploration. *Journal of Geochemical Exploration, 11*(3), 299-320.

Hansen, M., & Anderko, K. (1958). *The constitution of binary alloys.* New York: McGraw-Hill Book Company.

Harms, U., Heckmann, H., Weyer, S., & Mali, H. (2012). Galenit-Mineralchemie und Blei-Isotopengeochemie der postvariszischen Gangvererzungen des Niederbergischen Landes, Deutschland. *Zeitschrift der Deutschen Gesellschaft für Geowissenschaften, 163*(1), 69-90.

Hauptmann, A. (2014). The investigation of archaeometallurgical slag. In B. W. Roberts & C. P. Thornton (Eds.), *Archaeometallurgy in global perspective: Methods and syntheses* (91-105). New York: Springer.

Hauptmann, A., Begemann, F., Heitkemper, E., Pernicka, E., & Schmitt-Strecker, S. (1992). Early copper produced at Feinan, Wadi Araba, Jordan: The composition of ores and copper. *Archeomaterials, 6*(1), 1-33.

Hauptmann, A., Rehren, T., & Pernicka, E. (1995). The composition of gold from the ancient mining district of Verespatak / Roşia Montană, Romania. In G. Morteani & J. P. Northover (Eds.), *Prehistoric gold in Europe: Mines, metallurgy and manufacture* (369-381). Dordrecht: Springer Netherlands.

Hazen, R. M., & Jeanloz, R. (1984). Wüstite ($Fe_{1-x}O$): A review of its defect structure and physical properties. *Reviews of Geophysics and Space Physics, 22*(1), 37-46.

Healy, J. F. (1978). *Mining and metallurgy in the Greek and Roman world.* London: Thames and Hudson.

Heimbruch, G. (1990). *Archäometrie an Verhüttungsrelikten der Harzregion* (Doctoral thesis, Technische Universität Clausthal, Germany).

Heinrich, C. A., & Neubauer, F. (2002). Cu-Au-Pb-Zn-Ag metallogeny of the Alpine-Balkan-

Carpathian-Dinaride geodynamic province. *Mineralium Deposita, 37*(6), 533-540.

Hezarkhani-Zolgharnian, Z. (1995). *Archäometallurgische Untersuchungen zur Buntmetallurgie im Zentraliran: Posht-e-Badam-Saghand* (Doctoral thesis, Johannes-Gutenberg-Universität Mainz, Germany).

Hießleitner, G. (1927): Das Bergbaugebiet (Pb, Zn, S, Au, Ag) von Janjevo am Amselfeld in Nordmazedonien / SHS. *Berg- und Hüttenmännisches Jahrbuch, 75*(3), 106-114.

Hirata, T. (1996). Lead isotopic analyses of NIST standard reference materials using multiple collector inductively coupled plasma mass spectrometry coupled with a modified external correction method for mass discrimination effect. *The Analyst, 121*(10), 1407-1411.

Hirt, A. M. (2010). *Imperial mines and quarries in the Roman world: Organizational aspects 27 BC - 330 AD*. Oxford: Oxford University Press.

Hofman, H. O. (1899). *The metallurgy of lead and the desilverization of base bullion*. New York and London: The Scientific Publishing Company.

Hong, S., Candelone, J.-P., Patterson, C. C., & Boutron, C. F. (1994). Greenland ice evidence of hemispheric lead pollution two millennia ago by Greek and Roman civilizations. *Science, 265*(5180), 1841-1843.

Horner, J., Neubauer, F., Paar, W. H., Hansmann, W., Koeppel, V., & Robl, K. (1997). Structure, mineralogy, and Pb isotopic composition of the As-Au-Ag deposit Rotgülden, Eastern Alps (Austria): Significance for formation of epigenetic ore deposits within metamorphic domes. *Mineralium Deposita, 32*(6), 555-568.

Hruby, P., Hejhal, P., & Malý, K. (2007). Montanarchäologische Untersuchungen in Jihlava-Staré Hory (Iglau-Altenberg, Tschechien). *Zeitschrift für Archäologie des Mittelalters, 35*, 17-60.

Hyseni, S., & Alliu, I. (1999). Veçorite gjeologjike dhe metalogjenike te fushes xeherore Hajvali-Badovc-Kishnice (Kosove) [Geological and metallogenic features of the Hajvali-Badovc-Kishnica ore field (Kosovo)]. *Buletini i Shkencave Gjeologjike, 1*, 59-66 [in Albanian with English summary].

ICMM (2011). *Zhegovcë: Mineral site passport*. Prishtina, Kosovo: Independent Commission for Mines and Minerals in Kosovo.

Iles, M. W. (1904). *Lead-smelting: the construction, equipment, and operation of lead blast furnaces, and observations on the influence of metallic elements on slags and the scientific handling of smoke*. New York: John Wiley and Sons.

Ivanišević, V., & Špehar, P. (2005). Early Byzantine finds from Čečan and Gornji Streoc (Kosovo). *Starinar, 55*, 133-159.

Ixer, R. A., & Vaughan, D. J. (1982). The primary ore mineralogy of the Alderley Edge deposit, Cheshire. *Mineralogical Magazine, 46*(341), 485-492.

Jak, E., Degterov, S., Wu, P., Hayes, P. C., & Pelton, A. D. (1997). Thermodynamic optimization of the systems PbO-SiO_2, PbO-ZnO, ZnO-SiO_2 and PbO-ZnO-SiO_2. *Metallurgical and Materials Transactions B, 28*(6), 1011-1018.

Jak, E., Hayes, P. C., Degterov, S., & Peiton, A. D. (2001). Coupled experimental and thermodynamic study of the Zn-Fe-Si-O system. *Metallurgical and Materials Transactions B, 32*(5), 793-800.

Janković, S. (1990). Types of copper deposits related to volcanic environment in the Bor district,

Yugoslavia. *Geologische Rundschau, 79*(2), 467-478.

Janković, S. (1997). The Carpatho-Balkanides and adjacent area: a sector of the Tethyan Eurasian metallogenic belt. *Mineralium Deposita, 32*(5), 426-433.

Jireček, C. J. (1879). *Die Handelsstrassen und Bergwerke von Serbien und Bosnien während des Mittelalters: Historisch-geographische Studien.* Prag: Verlag der Königlich Böhmischen Gesellschaft der Wissenschaften.

Jones, G. D. B. (1980). The Roman mines at Riotinto. *The Journal of Roman Studies, 70*, 146-165.

Jovanović, B. (2009). Beginning of the metal age in the central Balkans according to the results of the archeometallurgy. *Journal of Mining and Metallurgy, 45*(2), B, 143-148.

Jovanović, V. S. (2003). Utvrđeno naselje Veletin [Fortified settlement Veletin]. *Starinar, 53-54*, 139-161 [in Serbian with English summary].

Kalogeropoulos, S. I., Kilias, S. P., Bitzios, D. C., Nicolaou, M., & Both, R. A. (1989). Genesis of the Olympias carbonate-hosted Pb-Zn (Au, Ag) sulfide ore deposit, eastern Chalkidiki Peninsula, northern Greece. *Economic Geology, 84*(5), 1210-1234.

Karamata, S., Knežević, V., Memović, E. & Popević, A (1994). The evolution of the northern part of the Vardar Zone in Mesozoic. *Bulletin of the Geological Society of Greece, 30*(2), 479-486.

Kassianidou, V. (1998). Was silver actually recovered from speiss in antiquity? In Th. Rehren, A. Hauptmann & J. D. Muhly (Eds.), *Metallurgica Antiqua: In honour of Hans-Gert Bachmann and Robert Maddin* (69-76). Der Anschnitt, Beiheft 8. Bochum: Deutsches Bergbau-Museums.

Kassianidou, V. (2003). Early extraction of silver from complex polymetallic ores. In P. T. Craddock & J. Lang (Eds.), Mining and metal production through the Ages (198-206). London: British Museum.

Keesmann, I. (1993). Naturwissenschaftliche Untersuchungen zur antiken Kupfer- und Silberverhüttung in Südwestspanien. In H. Steuer & U. Zimmermann (Eds.), *Montanarchäologie in Europa: Berichte zum Kolloquium "Frühe Erzgewinnung und Verhüttung in Europa" in Freiburg im Breisgau vom 4. bis 7. Oktober 1990* (105-122). Sigmaringen: Jan Thorbecke.

Keesmann, I., Bachmann, H. G., & Hauptmann, A. (1984). Klassifikation eisenreicher Schlacken nach dem Phasenbestand. *Fortschritte der Mineralogie 62, Beiheft 1*, 114-116.

Kimball, B. E., Mathur, R., Dohnalkova, A. C., Wall, A. J., Runkel, R. L., & Brantley, S. L. (2009). Copper isotope fractionation in acid mine drainage. *Geochimica et Cosmochimica Acta, 73*(5), 1247-1263.

Klein, S., Brey, G. P., Durali-Müller, S., & Lahaye, Y. (2010). Characterisation of the raw metal sources used for the production of copper and copper-based objects with copper isotopes. *Archaeological and Anthropological Sciences, 2*(1), 45-56.

Klein, S., Domergue, C., Lahaye, Y., Brey, G. P., & von Kaenel, H. M. (2009). The lead and copper isotopic composition of copper ores from the Sierra Morena (Spain). *Journal of Iberian Geology, 35*(1), 59-68.

Klein, S., Lahaye, Y., Brey, G. P., & Von Kaenel, H. M. (2004). The early Roman imperial AES coinage II: Tracing the copper sources by analysis of lead and copper isotopes - copper coins of Augustus and Tiberius. *Archaeometry, 46*(3), 469-480.

Klemm, D. D., & Klemm, R. (1989). Antike Goldgewinnung in der Ostwüste Ägyptens. In A. Hauptmann, E. Pernicka & G. A. Wagner (Eds.), *Archäometallurgie der Alten Welt: Beiträge zum internationalen Symposium "Old World Archaeometallurgy" Heidelberg 1987* (227-234). Der Anschnitt, Beiheft 7. Bochum: Deutsches Bergbau-Museum.

Körlin, G., & Gassmann, G. (2016). Der römische Bergbau und die Metallverarbeitung im Hinterland der antiken Stadt Ulpiana (Kosovo). Ein Zwischenbericht. In: G. Körlin, M. Prange, Th. Stöllner & Ü. Yalçin (Eds.), *From Bright Ores to Shiny Metals: Festschrift for Andreas Hauptmann on the Occasion of 40 Years Research in Archaeometallurgy and Archaeometry* (187-204). Der Anschnitt, Beiheft 29. Bochum: Deutsches Bergbau-Museum.

Körlin, G., & Gechter, M. (2003). Römischer Bergbau auf dem Lüderich – Vorbericht über die Grabungen 2000-2002. In Th. Stöllner, G. Körlin, G. Steffens & J. Cierny (Eds.), *Man and Mining: Studies in honour of Gerd Weisgerber* (237-248). Der Anschnitt, Beiheft 16. Bochum: Deutsches Bergbau-Museum.

Krahn, L., & Baumann, A. (1996). Lead isotope systematics of epigenetic lead-zinc mineralization in the western part of the Rheinisches Schiefergebirge, Germany. *Mineralium Deposita, 31*(3), 225-237.

Kretschmar, U., & Scott, S. D. (1976). Phase relations involving arsenopyrite in the system Fe-As-S and their application. *Canadian Mineralogist, 14*(3), 364-386.

Kronz, A. (1997). *Phasenbeziehungen und Kristallisationsmechanismen in fayalitischen Schmelzsystemen – Untersuchungen an Eisen- und Buntmetallschlacken* (Doctoral thesis, Johannes Gutenberg-Universität Mainz, Germany).

Kronz, A. (2005). Erzbergbau, Buntmetallmineralisationen und Silber-Metallurgie im Bereich der mittleren Mosel. *Zeitschrift zur Geschichte des Berg- und Hüttenwesens – Fischbacher Hefte, 11*(1), 4-33.

Kudrnáč, J., & Michálek, J. (1993). Urgeschichtliche und mittelalterliche Goldgewinnung in Südböhmen. In H. Steuer & U. Zimmermann (Eds.), *Montanarchäologie in Europa: Berichte zum Kolloquium "Frühe Erzgewinnung und Verhüttung in Europa" in Freiburg im Breisgau vom 4. bis 7. Oktober 1990* (401-408). Sigmaringen: Jan Thorbecke.

Kuleff, I., Iliev, I., Pernicka, E., & Gergova, D. (2006). Chemical and lead isotope compositions of lead artefacts from ancient Thracia (Bulgaria). *Journal of Cultural Heritage, 7*(4), 244-256.

Kullerud, G. (1953). The FeS-ZnS system, a geological thermometer. *Norsk Geologisk Tidsskrift, 32*(2-4), 61-147.

Kullerud, G. (1969). The lead-sulfur system. *American Journal of Science, 267-A*, 233-256.

Kullerud, G., Yund, R. A., & Moh, G. H. (1969). Phase relations in the Cu-Fe-S, Cu-Ni-S and Fe-Ni-S systems. In: H. D. B. Wilson (Ed.), *Magmatic Ore Deposits* (323-343). Economic Geology Monograph 4. Littleton: Society of Economic Geologists.

Kushiro, I. (1960). Si-Al relation in clinopyroxenes from igneous rocks. *American Journal of Science, 258*(7), 548-554.

Large, D., Schaeffer, R., & Höhndorf, A. (1983). Lead isotope data from selected galena occurrences in the North Eifel and North Sauerland, Germany. *Mineralium Deposita, 18*(2), 235-243.

Larson, P. B., Maher, K., Ramos, F. C., Chang, Z., Gaspar, M., & Meinert, L. D. (2003). Copper

isotope ratios in magmatic and hydrothermal ore-forming environments. *Chemical Geology, 201*(3), 337-350.

Laub, G. (1980). Zur Technologie der Kupfergewinnung aus Rammelsberger Erzen im Mittelalter. *Harz-Zeitschrift, 32*, 15-76.

Le Bas, M. J. (1962). The role of aluminum in igneous clinopyroxenes with relation to their parentage. *American Journal of Science, 260*(22), 267-288.

Le Guen, M., Lescuyer, J. L., & Marcoux, E. (1992). Lead-isotope evidence for a Hercynian origin of the Salsigne gold deposit (Southern Massif Central, France). *Mineralium Deposita, 27*(2), 129-136.

Leistel, J. M., Marcoux, E., Thiéblemont, D., Quesada, C., Sánchez, A., Almodóvar, G. R., Pascual, E., & Sáez, R. (1997). The volcanic-hosted massive sulphide deposits of the Iberian Pyrite Belt: Review and preface to the Thematic Issue. *Mineralium Deposita, 33*(1-2), 2-30.

Lepetit, P., Bente, K., Doering, T., & Luckhaus, S. (2003). Crystal chemistry of Fe-containing sphalerites. *Physics and Chemistry of Minerals, 30*(4), 185-191.

Lescuyer, J. L., Leistel, J. M., Marcoux, E., Milési, J. P., & Thiéblemont, D. (1997). Late Devonian-Early Carboniferous peak sulphide mineralization in the Western Hercynides. *Mineralium Deposita, 33*(1-2), 208-220.

Lewis, P. R., & Jones, G. D. B. (1970). Roman gold-mining in north-west Spain. *Journal of Roman Studies, 60*, 169-185.

Lillo, J. (1992). Vein-type base-metal ores in Linares-La Carolina (Spain): ore-lead isotopic constrains. *European Journal of Mineralogy, 4*(2), 337-343.

Lindsley, D. H. (1976). Experimental studies of oxide minerals. In D. Rumble, III (Ed.), *Oxide minerals* (61-88). Reviews in Mineralogy, Volume 3. Washington, DC: Mineralogical Society of America.

Lindsley, D. H., & Munoz, J. L. (1969). Subsolidus relations along the join hedenbergite-ferrosilite. *American Journal of Science, 267-A*, 295-324.

Lippolt, H. J., Schorn, U., & Pidgeon, R. T. (1983). Genetic implications of new lead isotope measurements on Schwarzwald vein and Upper Triassic sediment galenas. *Geologische Rundschau, 72*(1), 77-104.

Liu, S., Rehren, Th., Chen, J., Xu, C., Venunan, P., Larreina-Garcia, D., & Martinón-Torres, M. (2015). Bullion production in imperial China and its significance for sulphide ore smelting world-wide. *Journal of Archaeological Science, 55*, 151-165.

Ludwig, K. R., Vollmer, R., Turi, B., Simmons, K. R., & Perna, G. (1989). Isotopic constraints on the genesis of base-metal ores in southern and central Sardinia. *European Journal of Mineralogy, 1*(5), 657-666.

lupa = F. und O. Harl, www.ubi-erat-lupa.org (photography database of antique stone artefacts).

Manasse, A., & Mellini, M. (2002a). Chemical and textural characterisation of medieval slags from the Massa Marittima smelting sites (Tuscany, Italy). *Journal of Cultural Heritage, 3*(3), 187-198.

Manasse, A., & Mellini M. (2002b). Archaeometallurgic slags from Kutná Hora. *Neues Jahrbuch für Mineralogie, Monatshefte, 8*, 369-384.

Mankov, S. (2006). The ore belt "Osogovo - Besna Kobila" (ore formations, morphogenetic types

of deposits and physico-chemical conditions of forming). *Annual of the University of Mining and Geology "St. Ivan Rilski", 49*(1), 119-130.

Marchev, P., Kaiser-Rohrmeier, M., Heinrich, C., Ovtcharova, M., von Quadt, A., & Raicheva, R. (2005). 2: Hydrothermal ore deposits related to post-orogenic extensional magmatism and core complex formation: The Rhodope Massif of Bulgaria and Greece. *Ore Geology Reviews, 27*(1), 53-89.

Marcoux, E. (1997). Lead isotope systematics of the giant massive sulphide deposits in the Iberian Pyrite Belt. *Mineralium Deposita, 33*(1-2), 45-58.

Marcoux, E., Grancea, L., Lupulescu, M., & Milési, J. (2002). Lead isotope signatures of epithermal and porphyry-type ore deposits from the Romanian Carpathian Mountains. *Mineralium Deposita, 37*(2), 173-184.

Maréchal, C. N., Télouk, P., & Albarède, F. (1999). Precise analysis of copper and zinc isotopic compositions by plasma-source mass spectrometry. *Chemical Geology, 156*(1), 251-273.

Markl, G., Lahaye, Y., & Schwinn, G. (2006). Copper isotopes as monitors of redox processes in hydrothermal mineralization. *Geochimica et Cosmochimica Acta, 70*(16), 4215-4228.

Mathur, R., Ruiz, J., Titley, S., Liermann, L., Buss, H., & Brantley, S. (2005). Cu isotopic fractionation in the supergene environment with and without bacteria. *Geochimica et Cosmochimica Acta, 69*(22), 5233-5246.

Mathur, R., Titley, S., Barra, F., Brantley, S., Wilson, M., Phillips, A., Munizaga, F., Maksaev, V., Vervoort, J., & Hart, G. (2009). Exploration potential of Cu isotope fractionation in porphyry copper deposits. *Journal of Geochemical Exploration, 102*(1), 1-6.

Meier, S. W. (1995). *Blei in der Antike: Bergbau, Verhüttung, Fernhandel* (Doctoral thesis, Universität Zürich, Switzerland).

Mellaart, J. (1967). *Çatal Hüyük: A neolithic town in Anatolia.* New York: McGraw-Hill Book Company.

Merkel, J. F. (1990). Experimental reconstruction of Bronze Age copper smelting based on archaeological evidence from Timna. In B. Rothenberg (Ed.), *The ancient metallurgy of copper: archaeology-experiment-theory* (78-120). London: Institute for Archaeo-Metallurgical Studies.

Merkel, J. F. (2007). Imperial Roman production of lead and silver in the northern part of Upper Moesia (Mt. Kosmaj area). *Journal of the Serbian Archaeological Society, 23*, 39-78.

Mirdita, Z. (1978). Eine Inschrift aus Ulpianum. *Zeitschrift für Papyrologie und Epigraphik, 29*, 161-166.

Misra, M. K., Ragland, K. W., & Baker, A. J. (1993). Wood ash composition as a function of furnace temperature. *Biomass and Bioenergy, 4*(2), 103-116.

Mócsy, A. (1970). *Gesellschaft und Romanisation in der römischen Provinz Moesia Superior.* Amsterdam: Adolf M. Hakkert.

Monthel J., Vadala P., Leistel J. M., Cottard F., Ilic M., Strumberger A., Tosovic R., & Stepanovic A. (2002). *Mineral deposits and mining districts of Serbia: Compilation map and GIS databases.* BRGM/RC-51448-FR.

Moorbath, S. (1962). Lead isotope abundance studies on mineral occurrences in the British Isles and their geological significance. *Philosophical Transactions of the Royal Society of London A: Mathematical, Physical and Engineering Sciences, 254*(1042), 295-360.

Morimoto, N. (1988). Nomenclature of pyroxenes. *Mineralogy and Petrology, 39*(1), 55-76.

Morimoto, N., & Clark, L. A. (1961). Arsenopyrite crystal-chemical relations. *American Mineralogist, 46*(11-12), 1448-1469.

Mrkobrad, D. (1994). Research of the medieval mining and metallurgy in the Rudnik Mountain. In P. Petrović & S. Đurđekanović (Eds.), *Ancient mining and metallurgy in southeast Europe: International Symposium Donji Milanovac, May 20-25, 1990* (241-250). Belgrade: Archaeological Institute, Belgrade; Museum of Mining and Metallurgy, Bor.

Muan, A., & Osborn, E. F. (1965). *Phase equilibria among oxides in steelmaking.* Reading: Addison-Wesley.

Muhly, J. D. (1989). Çayönü Tepesi and the beginnings of metallurgy in The Old World. In A. Hauptmann, E. Pernicka & G. A. Wagner (Eds.), *Archäometallurgie der Alten Welt: Beiträge zum internationalen Symposium "Old World Archaeometallurgy" Heidelberg 1987* (1-12). Der Anschnitt, Beiheft 7. Bochum: Deutsches Bergbau-Museum.

Müller, R., Brey, G. P., Seitz, H.-M., & Klein, S. (2015). Lead isotope analyses on Late Republican sling bullets. *Archaeological and Anthropological Sciences, 7*(4), 473-485.

Naldrett, A. J. (1969). A portion of the system Fe–S–O between 900 and 1080 °C and its application to sulfide ore magmas. *Journal of Petrology, 10*(2), 171-201.

Navarro, A., Cardellach, E., Mendoza, J. L., Corbella, M., & Domènech, L. M. (2008). Metal mobilization from base-metal smelting slag dumps in Sierra Almagrera (Almería, Spain). *Applied Geochemistry, 23*(4), 895-913.

Nesbitt, R. W., Billett, M. F., Ashworth, K.L., Deniel, Constantinides, C. D., Demetriades, A., Katirtzoglou, C., Michael, C., Mposkos, E., Zachos, S., Sanderson, D. (1988). The geological setting of base metal mineralisation in the Rhodope region, northern Hellas. In J. Boissonas & P. Omenetto (Eds.), *Mineral Deposits within the European Community* (499-514). Special Publication No. 6 of the Society for Geology Applied to Mineral Deposits. Berlin & Heidelberg: Springer.

Neubauer, F. (2002). Contrasting Late Cretaceous with Neogene ore provinces in the Alpine-Balkan-Carpathian-Dinaride collision belt. In D. J. Blundell, F. Neubauer & A. von Quadt (Eds.), *The timing and location of major ore deposits in an evolving orogeny* (81-102). Special Publications, 204. London: Geological Society.

Neubauer, F., Lips, A., Kouzmanov, K., Lexa, J., & Ivăşcanu, P. (2005). 1: Subduction, slab detachment and mineralization: The Neogene in the Apuseni Mountains and Carpathians. *Ore Geology Reviews, 27*(1), 13-44.

Nickel, E. H. (1995). The definition of a mineral. *Mineralogical Journal, 17*(7), 346-349.

Nriagu, J. O. (1983). Lead resources of the ancient world. In J. O. Nriagu (Ed.), *Lead and lead poisoning in antiquity* (103-199). New York: John Wiley and Sons.

Nriagu, J. O. (1985). Cupellation: The oldest quantitative chemical process. *Journal of Chemical Education, 62*(8), 668-674.

Oen, I. S., Windt, C. J., Winnubst, T. G. M., & Kager, P. (1975). Epigenetic lead-zinc mineralization in Miocene pebbly mudstones, Sierra de Cartagena, Spain. *Mineralium Deposita, 10*(4), 362-373.

Okamoto, H. (1991). The As-Fe (arsenic-iron) system. *Journal of Phase Equilibria, 12*(4),

457-461.

Orgeval, J.-J., Caron, C., Lancelot, J., & Omenetto, P. (2000). Genesis of polymetallic and precious-metal ores in the Western Mediterranean (Cevennes, France-Sardinis, Italy). *Transactions of the Institution of Mining and Metallurgy B, 109*, 77-180.

Osborn, E. F., & Muan, A. (1960). *Phase equilibrium diagrams of oxide systems.* Columbus: American Ceramic Society.

Palinkaš, L. A., Borojević Šoštarić, S., & Palinkaš, S. S. (2008). Metallogeny of the northwestern and central Dinarides and southern Tisia. *Ore Geology Reviews, 34*(3), 501-520.

Palinkaš, S. S., Palinkaš, L. A., Renac, C., Spangenberg, J. E., Lüders, V., Molnar, F., & Maliqi, G. (2013). Metallogenic model of the Trepča Pb-Zn-Ag skarn deposit, Kosovo: Evidence from fluid inclusions, rare earth elements, and stable isotope data. *Economic Geology, 108*(1), 135-162.

Pamić, J., Gušić, I., & Jelaska, V. (1998). Geodynamic evolution of the Central Dinarides. *Tectonophysics, 297*(1), 251-268.

Pamuk, S. (2000). *A monetary history of the Ottoman Empire.* New York: Cambridge University Press.

Parović-Pešikan, M. & Stojković, S. (1995). Groupe des fours metallurgiques a Ulpiana [Group of metallurgical furnaces in Ulpiana]. In P. Petrović & S. Đurđekanović (Eds.), *Ancient mining and metallurgy in southeast Europe: International Symposium Donji Milanovac, May 20-25, 1990* (213-217). Belgrade: Archaeological Institute, Belgrade; Museum of Mining and Metallurgy, Bor.

Pelton, A., Stamatakis, M. G., Kelepertzis, E., & Panagou, T. (2015). The origin and archaeometallurgy of a mixed sulphide ore for copper production on the island of Kea, Aegean Sea, Greece. *Archaeometry, 57*(2), 318-343.

Pérez-García, L. C., Sánchez-Palencia, F. J., & Torres-Ruiz, J. (2000). Tertiary and Quaternary alluvial gold deposits of Northwest Spain and Roman mining (NW of Duero and Bierzo Basins). *Journal of Geochemical Exploration, 71*(2), 225-240.

Pernicka, E. (2014). Provenance determination of archaeological metal objects. In B. W. Roberts & C. P. Thornton (Eds.), *Archaeometallurgy in global perspective: Methods and syntheses* (239-268). New York: Springer.

Pernicka, E., & Bachmann, H.-G. (1983). Archäometallurgische Untersuchungen zur antiken Silbergewinnung in Laurion: III. Das Verhalten einiger Spurenelemente beim Abtreiben des Bleis. *Erzmetall, 12*, 592-597.

Pernicka, E., Begemann, F., Schmitt-Strecker, S., & Wagner, G. A. (1993). Eneolithic and Early Bronze Age copper artefacts from the Balkans and their relation to Serbian copper ores. *Prähistorische Zeitschrift, 68*(1), 1-54.

Pernicka, E., Gentner, W., Wagner, G. A., Vavelidis, M., & Gale, N. H. (1981). Ancient lead and silver production on Thasos (Greece). *Revue d'Archéométrie, 1*(1), 227-237.

Pernicka, E., Lutz, C., Bachmann, H.-G., Wagner, G. A., Elitzsch, C., & Klein, E. (1985). Alte Blei-Silber-Verhüttung auf Sifnos. In G. A. Wagner & G. Weisgerber (Eds.), *Silber, Blei und Gold auf Sifnos: Prähistorische und antike Metallproduktion* (185-199). Der Anschnitt, Beiheft 3. Bochum: Deutsches Bergbau-Museum.

Pernicka, E., Rehren, Th., & Schmitt-Strecker, S. (1998). Late Uruk silver production by cupellation at Habuba Kabira, Syria. In Th. Rehren, A. Hauptmann & J. D. Muhly (Eds.), *Metallurgica Antiqua: In honour of Hans-Gert Bachmann and Robert Maddin* (123-134). Der Anschnitt, Beiheft 8. Bochum: Deutsches Bergbau-Museums.

Petković, S. (2003). Roman fibulae from Ulpiana: Archaeological investigations 1981-87. *Starinar, 53/54*, 241-253.

Petrović, V. P. (2007). Pre-Roman and Roman Dardania: Historical and geographical considerations. *Balcanica, 37*, 7-23.

Photos, E., Koukouli-Chrysanthaki, C., Tylecote, R. F., & Gialoglou, G. (1989). Precious metals extraction in Palaia Kavala, N. E. Greece. An archaeometallurgical attempt to locate Skapte Hyle. In A. Hauptmann, E. Pernicka, & G. A. Wagner (Eds.), *Archäometallurgie der Alten Welt: Beiträge zum internationalen Symposium "Old World Archaeometallurgy" Heidelberg 1987* (179-190). Der Anschnitt, Beiheft 7. Bochum: Deutsches Bergbau-Museum.

Piatak, N. M., Seal, R. R., & Hammarstrom, J. M. (2004). Mineralogical and geochemical controls on the release of trace elements from slag produced by base-and precious-metal smelting at abandoned mine sites. *Applied Geochemistry, 19*(7), 1039-1064.

Plumlee, G. S., Montour, M., Taylor, C. D., Wallace, A. R., & Klein, D.P. (1995). Polymetallic vein and replacement deposits. In: E. A. du Bray (Ed.), *Preliminary compilation of descriptive geoenvironmental mineral deposit models* (121-129). US Geological Survey Open-File Book 95-831.

Pomiès, C., Cocherie, A., Guerrot, C., Marcoux, E., & Lancelot, J. (1998). Assessment of the precision and accuracy of lead-isotope ratios measured by TIMS for geochemical applications: example of massive sulphide deposits (Rio Tinto, Spain). *Chemical Geology, 144*(1), 137-149.

Popović, I. (Ed.). (1994). *Antičko srebro u Srbiji. Antique silver from Serbia.* Belgrade: Narodni Muzej.

Popović, Lj. & Čerškov, E. (1956). Ulpiana: Prethodni izveštaj o arheološkim istraživanjima od 1954 do 1956 god [Ulpiana: A preliminary report on archaeological researches from 1954 until 1956)]. *Glasnik Muzeja Kosova i Metohije, 1*, 319-327 [in Serbian with English summary].

Raban, A. (1999). The lead ingots from the wreck site (area K8). *Journal of Roman Archaeology, Supplementary Series, 35*, 179-188.

Radivojević, M., Rehren, Th., Pernicka, E., Šljivar, D., Brauns, M., & Borić, D. (2010). On the origins of extractive metallurgy: new evidence from Europe. *Journal of Archaeological Science, 37*(11), 2775-2787.

Rehren, Th., Boscher, L., & Pernicka, E. (2012). Large scale smelting of speiss and arsenical copper at Early Bronze Age Arisman, Iran. *Journal of Archaeological Science, 39*(6), 1717-1727.

Rehren, Th., & Hauptmann, A. (1995). Silberraffinations-Schlacken aus der CUT (Xanten), Insula 39: Mineralogische Untersuchung und archäometallurgische Interpretation. *Xantener Berichte, 6*, 119-137.

Rehren, Th., & Klappauf, L. (1995). ... ut oleum aquis: Vom Schwimmen des Silbers auf Bleiglätte. *Metalla, 2*, 19-28.

Rehren, Th., & Prange, M. (1998). Lead metal and patina: a comparison. In Th. Rehren,

A. Hauptmann & J. D. Muhly (Eds.), *Metallurgica Antiqua: In honour of Hans-Gert Bachmann and Robert Maddin* (183-196). Der Anschnitt, Beiheft 8. Bochum: Deutsches Bergbau-Museum.

Rehren, Th., Schneider, J., & Bartels, C. (1999). Medieval lead-silver smelting in the Siegerland, West Germany. *Historical Metallurgy, 33*(2), 73-84.

Rehren, Th., Vanhove, D., & Mussche, H. (2002). Ores from the ore washeries in the Lavriotiki. *Metalla, 9*(1), 27-46.

Reich, M., Chryssoulis, S. L., Deditius, A., Palacios, C., Zuñiga, A., Weldt, M., & Alvear, M. (2010). "Invisible" silver and gold in supergene digenite ($Cu_{1.8}S$). *Geochimica et Cosmochimica Acta, 74*(21), 6157-6173.

Robertson, A. H. F., & Karamata, S. (1994). The role of subduction-accretion processes in the tectonic evolution of the Mesozoic Tethys in Serbia. *Tectonophysics, 234*(1), 73-94.

Robertson, A. H., Trivić, B., Đerić, N., & Bucur, I. I. (2013). Tectonic development of the Vardar ocean and its margins: Evidence from the Republic of Macedonia and Greek Macedonia. *Tectonophysics, 595-596*, 25-54.

Roedder, E. (1978). Silicate liquid immiscibility in magmas and in the system K_2O-FeO-Al_2O_3-SiO_2: an example of serendipity. *Geochimica et Cosmochimica Acta, 42*(11), 1597-1617.

Rohl, B. M. (1996). Lead isotope data from the Isotrace Laboratory, Oxford: Archaeometry data base 2, galena from Britain and Ireland. *Archaeometry, 38*(1), 165-180.

Rosman, K. J., Chisholm, W., Hong, S., Candelone, J. P., & Boutron, C. F. (1997). Lead from Carthaginian and Roman Spanish mines isotopically identified in Greenland ice dated from 600 BC to 300 AD. *Environmental Science & Technology, 31*(12), 3413-3416.

Rothenberg, B., & Blanco-Freijeiro, A. (1981). *Ancient mining and metallurgy in south-west Spain.* London: Institute for Archaeo-Metallurgical Studies.

Rothenhoefer, P., & Hanel, N. (2013). The Romans and their lead – tracing innovations in the production, distribution, and secondary processing of an ancient metal. In S. Burmeister, S. Hansen, M. Kunst & N. Müller-Scheeßel (Eds.), *Metal matters. Innovative technologies and social change in prehistory and antiquity* (273-282). Rahden: Marie Leidorf.

Ryndina, N., Indenbaum, G., & Kolosova, V. (1999). Copper production from polymetallic sulphide ores in the northeastern Balkan Eneolithic culture. *Journal of Archaeological Science, 26*(8), 1059-1068.

Sáez, R., Pascual, E., Toscano, M., & Almodóvar, G. R. (1999). The Iberian type of volcano-sedimentary massive sulphide deposits. *Mineralium Deposita, 34*(5-6), 549-570.

Salkield, L. U. (1987). *A technical history of the Rio Tinto mines: some notes on exploitation from pre-Phoenician times to the 1950s.* Dordrecht: Springer Netherlands.

Santos Zalduegui, J. F., García de Madinabeitia, S., Gil Ibarguchi, J. I., & Palero, F. (2004). A lead isotope database: The Los Pedroches-Alcudia area (Spain); implications for archaeometallurgical connections across southwestern and southeastern Iberia. *Archaeometry, 46*(4), 625-634.

Sarver, J. F., & Hummel, F. A. (1962). Solid solubility and eutectic temperature in the system Zn_2SiO_4 - Mg_2SiO_4. *Journal of the American Ceramic Society, 45*(6), 304.

Scaife, B., Barreiro, B. A., McDonnell, J. G., & Pollard, A. M. (2001). Lead isotope ratios of 36

galenas from the Northern Pennines. Retrieved from http://www.brettscaife.net/lead/npennine/npennine.html; 28 February, 2016.

Schefer, S., Cvetković, V., Fügenschuh, B., Kounov, A., Ovtcharova, M., Schaltegger, U., & Schmid, S. M. (2011). Cenozoic granitoids in the Dinarides of southern Serbia: age of intrusion, isotope geochemistry, exhumation history and significance for the geodynamic evolution of the Balkan Peninsula. *International Journal of Earth Sciences, 100*(5), 1181-1206.

Schlegel, H., & Schüller, A. (1952). Das Zustandsbild Kupfer-Eisen-Schwefel. *Zeitschrift für Metallkunde, 43*, 421-427.

Schmid, S. M., Bernoulli, D., Fügenschuh, B., Matenco, L., Schefer, S., Schuster, R., Tischler, M., & Ustaszewski, K. (2008). The Alpine-Carpathian-Dinaridic orogenic system: correlation and evolution of tectonic units. *Swiss Journal of Geosciences, 101*(1), 139-183.

Schmitt-Strecker, S., & Begemann, F. (2005). Kupfer-und bronzezeitliche Metallartefakte vom Westbalkan: Zur Frage nach den Quellen ihres Kupfers. *Praehistorische Zeitschrift, 80*(1), 49-64.

Schneider, J. (1998). Die Herkunft des Siegerländer Münzsilbers. In C. Dahm, U. Lobbedey, G. Weisgerber (Eds.), *Der Altenberg: Bergwerk und Siedlung aus dem 13. Jahrhundert im Siegerland. Band 2 - Die Funde* (202-215). Bonn: Dr. Rudolf Habelt.

Schumacher, F. (1950). *Die Lagerstätte der Trepça und ihre Umgebung.* Belgrade: Izdavačko preduzeće saveta za energetiku i ekstraktivnu industriju vlade FNRJ.

Schumacher, F. (1954). The ore deposits of Jugoslavia and the development of its mining industry. *Economic Geology, 49*(5), 451-492.

Shepherd, R. (1993). *Ancient mining.* London and New York: Institution of Mining and Metallurgy by Elsevier Applied Science.

Shields, W. R., Murphy, T. J., & Garner, E. L. (1964). Absolute isotopic abundance ratio and the atomic weight of a reference sample of copper. *Journal of Research of the National Bureau of Standards, 68A*(6), 589-592.

Siivola, J. (1969). On the evaporation of some alkali metals during the electron microprobe analysis. *Bulletin of the Geological Society of Finland, 41*, 85-91.

Sillitoe, R. H., Folk, R. L., & Saric, N. (1996). Bacteria as mediators of copper sulfide enrichment during weathering. *Science, 272*(5265), 1153-1155.

Skarpelis, N. (2007). The Lavrion deposit (SE Attica, Greece): geology, mineralogy and minor elements chemistry. *Neues Jahrbuch für Mineralogie - Abhandlungen, 183*(3), 227-249.

Smuts J. (1992). Formation and morphology of iron silicate 'iscorite'. *Ironmaking and Steelmaking, 19*(2), 111–119.

Smuts, J., Steyn, J. G. D., & Boeyens, J. C. A. (1969). The crystal structure of an iron silicate, iscorite. *Acta Crystallographica B, 25*(7), 1251-1255.

Snoek, W., Plimer, I. R., & Reeves, S. (1999). Application of Pb isotope geochemistry to the study of the corrosion products of archaeological artefacts to constrain provenance. *Journal of Geochemical Exploration, 66*(1), 421-425.

Spry, P. G., Plimer, I. R., & Teale, G. S. (2008). Did the giant Broken Hill (Australia) Zn–Pb–Ag deposit melt? *Ore Geology Reviews, 34*(3), 223-241.

Stanton, W. I. (1991). The habitat and origin of lead ore in Grebe Swallet Mine, Charterhouse-

on-Mendip, Somerset. *Proceedings of the University of Bristol Speleological Society, 19*(1), 43-65.

Stech, T. (1999). Aspects of early metallurgy in Mesopotamia and Anatolia. In: V. C. Pigott (Ed.), *The archaeometallurgy of the Asian old world* (59-71). Philadelphia: University Museum; University of Pennsylvania.

Stoianovich, T. (1994). *Balkan worlds: The first and last Europe.* New York and London: M.E. Sharpe.

Stos-Gale, Z. A. (1993). Lead isotope provenance studies - do they work? *Archaeologia Polona, 31*, 149-180.

Stos-Gale, Z. A., & Gale, N. H. (2009). Metal provenancing using isotopes and the Oxford archaeological lead isotope database (OXALID). *Archaeological and Anthropological Sciences, 1*(3), 195-213.

Stos-Gale, Z. A., Gale, N. H., & Annetts, N. (1996). Lead isotope data from the Isotrace Laboratory, Oxford: Archaeometry data base 3, ores from the Aegean, part 1. *Archaeometry, 38*(2), 381-390.

Stos-Gale, Z. A., Gale, N. H., Annetts, N., Todorov, T., Lilov, P., Raduncheva, A., & Panayotov, I. (1998). Lead isotope data from the Isotrace Laboratory, Oxford: Archaeometry data base 5, ores from Bulgaria. *Archaeometry, 40*(1), 217-226.

Stos-Gale Z. A., Gale N. H., Houghton J., & Speakman R. (1995). Lead isotope data from the Isotrace Laboratory, Oxford: Archaeometry data base 1, ores from the western mediterranean. *Archaeometry, 37*(2), 407–415.

Stos-Gale, Z. A., Maliotis, G., Gale, N. H., & Annetts, N. (1997). Lead isotope characteristics of the Cyprus copper ore deposits applied to provenance studies of copper oxhide ingots. *Archaeometry, 39*(1), 83-123.

Ströbele, F., Hildebrandt, L. H., Baumann, A., Pernicka, E., & Markl, G. (2014). Pb isotope data of Roman and medieval objects from Wiesloch near Heidelberg, Germany. *Archaeological and Anthropological Sciences, 7*(4), 465-472.

Ströbele, F., Staude, S., Pfaff, K., Premo, W. R., Hildebrandt, L. H., Baumann, A., Pernicka, E., & Markl, G. (2012). Pb isotope constraints on fluid flow and mineralization processes in SW Germany. *Neues Jahrbuch für Mineralogie - Abhandlungen, 189*(3), 287-309.

Ströbele, F., Wenzel, T., Kronz, A., Hildebrandt, L. H., & Markl, G. (2010). Mineralogical and geochemical characterization of high-medieval lead–silver smelting slags from Wiesloch near Heidelberg (Germany) - an approach to process reconstruction. *Archaeological and Anthropological Sciences, 2*(3), 191-215.

Swainbank, I. G., Shepherd, T. J., Caboi, R., & Massoli-Novelli, R. (1982). Lead isotopic composition of some galena ores from Sardinia. *Periodico di Mineralogia, 51*(3), 275-286.

Tafel, V. (1929). *Lehrbuch der Metallhüttenkunde (Wismut, Blei, Zinn, Antimon, Zink, Quecksilber, Nickel, Aluminium).* Leipzig: S. Hirzel.

Teichner, F. (2015). Ulpiana – Iustiniana Secunda (Kosovo): Das urbane Zentrum des dardanischen Bergbaubezirkes. *Ephemeris Napocensis, 25*, 81-93.

Thornton, C. P., Rehren, T., & Pigott, V. C. (2009). The production of speiss (iron arsenide) during the Early Bronze Age in Iran. *Journal of Archaeological Science, 36*(2), 308-316.

Tomkins, A. G., Pattison, D. R., & Frost, B. R. (2007). On the initiation of metamorphic sulfide anatexis. *Journal of Petrology, 48*(3), 511-535.

Tomović, M. (1994). Roman mines and mining in the mountain of Kosmaj. In P. Petrović & S. Đurđekanović (Eds.), *Ancient mining and metallurgy in southeast Europe: International Symposium Donji Milanovac, May 20-25, 1990* (203-212). Belgrade: Archaeological Institute, Belgrade; Museum of Mining and Metallurgy, Bor.

Tornos, F. (2006). Environment of formation and styles of volcanogenic massive sulfides: The Iberian Pyrite Belt. *Ore Geology Reviews, 28*(3), 259-307.

Tornos, F., & Chiaradia, M. (2004). Plumbotectonic evolution of the Ossa Morena zone, Iberian Peninsula: Tracing the influence of mantle-crust interaction in ore-forming processes. *Economic Geology, 99*(5), 965-985.

Trepca Kosovo under UNMIK administration (Eds.) (2005). Summary description of the lead zinc silver resources and the Trepca Mines in Kosovo.

Trincherini, P. R., Barbero, P., Quarati, P., Domergue, C., & Long, L. (2001). Where do the lead ingots of the Saintes-maries-de-la-mer Wreck come from? Archaeology compared with physics. *Archaeometry, 43*(3), 393-406.

Trincherini, P. R., Domergue, C., Manteca, I., Nesta, A., & Quarati, P. (2009). The identification of lead ingots from the Roman mines of Cartagena: the role of lead isotope analysis. *Journal of Roman Archaeology, 22*, 123-145.

Tsaimou, C., Tsakiridis, P. E., & Oustadakis, P. (2015). Analytical and technological evaluation of ancient lead slags from Lavrion, Attika, Greece. *Mediterranean Archaeology and Archaeometry, 15*(2), 113-127.

Tunningley, A. J. (2011). *Independent Technical Report on the Parlozi Property, Serbia: NI43-101 Technical Report*. Prepared for Reservoir Minerals Inc. and for Reservoir Capital Corp. Exploration Alliance Ltd.

Tylecote, R. F. (1962). *Metallurgy in archaeology: A prehistory of metallurgy in the British Isles*. London: Edward Arnold.

Tylecote, R. F. (1964). Roman lead working in Britain. *The British Journal for the History of Science, 2*, 25-43.

Tylecote, R. F., Ghaznavi, H. A., & Boydell, P. J. (1977). Partitioning of trace elements between the ores, fluxes, slags and metal during the smelting of copper. *Journal of Archaeological Science, 4*(4), 305-333.

Ujes, D. (2002). Recherche sur la localisation de Damastion et ses mines [Research on the location of Damastion and its mines]. *Revue numismatique, 6*(158), 103-129 [in French with English summary].

Valera, P. G., & Valera, R. G. (2005). Outline of geology and mineral deposits of Sardinia. In F. Lo Schiavo, A. Giumlia-Mair, U. Sanna & R. Valera (Eds.), *Archaeometallurgy in Sardinia: From the origins to the beginning of the Early Iron Age* (35-42). Montagnac: Éditions Monique Mergoil.

Valera, R. G., Valera, P. G., & Rivoldini, A. (2005). Sardinian ore deposits and metals in the Bronze Age. In F. Lo Schiavo, A. Giumlia-Mair, U. Sanna & R. Valera (Eds.), *Archaeometallurgy in Sardinia: From the origins to the beginning of the Early Iron Age* (43-88). Montagnac:

Éditions Monique Mergoil.

Van Aken, P. A., Miehe, G., Woodland, A. B., & Angel, R. J. (2005). Crystal structure and cation distribution in Fe_7SiO_{10} ("Iscorite"). *European Journal of Mineralogy, 17*(5), 723-731.

Van Hook, H. J. (1960). The ternary system Ag_2S-Bi_2S_3-PbS. *Economic Geology 55*(4), 759-788.

Vasić, R. (1990). The early Iron Age in southern Serbia and Kosovo. In J. Jevtović (Ed.), *Gospodari srebra: Gvozdeno doba na tlu Srbije. Masters of silver: The Iron Age in Serbia* (119-138). Belgrade: Narodni Muzej.

Veselinović-Williams (2011). *Characteristics and origin of polymetallic mineralisation in the Kopaonik region of Serbia and Kosovo, with particular reference to the Belo Brdo Pb-Zn (Ag) deposit* (Doctoral thesis, Kingston University London, United Kingdom).

Villa, I. M. (2009). Lead isotopic measurements in archaeological objects. *Archaeological and Anthropological Sciences, 1*(3), 149-153.

Visser, W., & van Groos, A. F. K. (1976). Liquid immiscibility in K_2O–FeO–Al_2O_3–SiO_2. *Nature, 264*, 426-427.

Voudouris, P., Melfos, V., Spry, P. G., Bonsall, T., Tarkian, M., & Economou-Eliopoulos, M. (2008a). Mineralogical and fluid inclusion constraints on the evolution of the Plaka intrusion-related ore system, Lavrion, Greece. *Mineralogy and Petrology, 93*(1-2), 79-110.

Voudouris, P., Melfos, V., Spry, P. G., Bonsall, T. A., Tarkian, M., & Solomos, Ch. (2008b). Carbonate-replacement Pb-Zn-Ag±Au mineralization in the Kamariza area, Lavrion, Greece: Mineralogy and thermochemical conditions of formation. *Mineralogy and Petrology, 94*(1-2), 85-106.

Vryonis, S. (1962). The question of the Byzantine mines. *Speculum, 37*(1), 1-17.

Wagner, G. A., & Pernicka, E. (1982). Blei und Silber im Altertum: Ein Beitrag der Archäometrie. *Chemie in unserer Zeit, 16*(2), 45-56.

Wagner, G. A., Pernicka, E., Gialoglou, G., & Vavelidis, M. (1981). Ancient gold mines on Thasos. *Naturwissenschaften, 68*(5), 263-264.

Wagner, T., & Schneider, J. (2002). Lead isotope systematics of vein-type antimony mineralization, Rheinisches Schiefergebirge, Germany: a case history of complex reaction and remobilization processes. *Mineralium Deposita, 37*(2), 185-197.

Wahl, J. (1993). Três Minas. Vorbericht über die archäologischen Ausgrabungen im Bereich des römischen Goldbergwerks 1986 / 87. In H. Steuer & U. Zimmermann (Eds.), *Montanarchäologie in Europa: Berichte zum Kolloquium "Frühe Erzgewinnung und Verhüttung in Europa" in Freiburg im Breisgau vom 4. bis 7. Oktober 1990* (123-152). Sigmaringen: Jan Thorbecke.

Walker, E. C., Cuttitta, F., & Senftle, F. E. (1958). Some natural variations in the relative abundance of copper isotopes. *Geochimica et Cosmochimica Acta, 15*(3), 183-194.

Wall, A. J., Mathur, R., Post, +J. E., & Heaney, P. J. (2011). Cu isotope fractionation during bornite dissolution: An in situ X-ray diffraction analysis. *Ore Geology Reviews, 42*(1), 62-70.

Walton, M. S., & Tite, M. S. (2010). Production technology of Roman lead-glazed pottery and its continuance into late antiquity. *Archaeometry, 52*(5), 733-759.

Warchulski, R., Gawęda, A., Kądziołka-Gaweł, M., & Szopa, K. (2015). Composition and element mobilization in pyrometallurgical slags from the Orzeł Biały smelting plant in the Bytom–Piekary Śląskie area, Poland. *Mineralogical Magazine, 79*(2), 459-483.

Warner, R. D., & Luth, W. C. (1973). Two-phase data for the join monticellite ($CaMgSiO_4$)-forsterite ($Mg2SiO_4$): experimental results and numerical analysis. *American Mineralogist, 58*(11-12), 998-1008.

Whitney, D. L., & Evans, B. W. (2010). Abbreviations for names of rock-forming minerals. *American Mineralogist, 95*(1), 185-187.

Wortel, M. J. R., & Spakman, W. (2000). Subduction and slab detachment in the Mediterranean-Carpathian region. *Science, 290*(5498), 1910-1917.

Wyttenbach, A., & Schubiger, P. A. (1973). Trace element content of Roman lead by neutron activation analysis. *Archaeometry, 15*(2), 199-207.

Yazawa, A. (1980). Distribution of various elements between copper, matte and slag. *Erzmetall, 33*, 377-382.

Yesares, L., Sáez, R., Nieto, J. M., De Almodovar, G. R., Gómez, C., & Escobar, J. M. (2015). The Las Cruces deposit, Iberian Pyrite Belt, Spain. *Ore Geology Reviews, 66*, 25-46.

Zhu, X. K., O'Nions, R. K., Guo, Y., Belshaw, N. S., & Rickard, D. (2000). Determination of natural Cu-isotope variation by plasma-source mass spectrometry: implications for use as geochemical tracers. *Chemical Geology, 163*(1), 139-149.

Danksagung

Diese Dissertation wäre ohne die Unterstützung folgender Personen und Institutionen nicht möglich gewesen. Ihnen allen möchte ich herzlich danken:

apl. Prof. dr. Sabine Klein für die Vergabe des Projektes und die Betreuung der Dissertation.

Prof. Dr. Gerhard Brey, auch für die kurzfristige Zusage diese Arbeit zu begutachten.

Dr. Guntram Gassmann (ARGUs) und Dr. Gabriele Körlin (Deutsches Bergbau-Museum Bochum) für die Unterstützung sowie die hilfreichen Kommentare, Anregungen und Diskussionen.

Der Deutschen Forschungsgemeinschaft für die Förderung dieses Projektes.

Dr. Heidi Höfer für die Erstellung der Messprogramme für die Mikrosondenanalysen.

Dr. Hans-Michael Seitz, Linda Marko und Janina Schastok für die Unterstützung bei den Massenspektrometer-Analysen bzw. im Labor.

Dr. Rainer Petschick für die Unterstützung bei der Durchführung der Röntgenanalysen und der Auswertung der Daten sowie Alfred Schaub für die Unterstützung bei der Aufbereitung der Proben.

Maria Bladt, Nils Prawitz und Jennifer Steppler sowie Andreas Ludwig und Sandra Morszeck (Deutsches Bergbau-Museum Bochum) für die Präparation der Proben.

Der Arbeitsgruppe Archäometrie: Dr. Thomas Birch, Thomas Rose, Eveline Salzmann und Hendrick Wick.

Allen weiteren Mitarbeitern der Mineralogie.

Den Mitarbeitern des Archäologischen Institutes des Kosovo: Premtim Alaj, Milot Berisha, Kemal Luci und Elvis Shala.

Babsi, Beate, Bernd, Izet, Judith, Otto und Peter für die Zeit im Gelände.

Meinen Eltern möchte ich für ihre fortwährende Unterstützung während des Studiums und der Promotion danken.

Part IV.

Appendix

i. Abbreviations

Abbreviation	Mineral/phase name	Chemistry
apy	Arsenopyrite	FeAsS
bn	Bornite	Cu_5FeS_4
cal	Calcite	$CaCO_3$
cb	Carbonate mineral [group]	$(Ca,Fe,Mn)CO_3$
ccp	Chalcopyrite	$CuFeS_2$
cct	Chalcocite	Cu_2S
cpx	Clinopyroxene [group]	$(Ca,Fe^{2+},Mg,Mn,Zn,Al,Fe^{3+})_2(Si,Al,Fe^{3+})_2O_6$
cv	Covellite	CuS
dg	Digenite	$Cu_{1.8}S$
fay	Fayalite	Fe_2SiO_4
fsp	Feldspar [group]	$NaAlSi_3O_8$ - $CaAl_2Si_2O_8$ - $KAlSi_3O_8$
gl	Glass	-
gn	Galena	PbS
hd	Hedenbergite	$CaFe^{2+}Si_2O_6$
isc	Iscorite	$Fe^{2+}{}_5Fe^{3+}{}_2SiO_{10}$
iss	Intermediate solid solution	$Cu_xFe_yS_z$
kls	Kalsilite	$KAlSiO_4$
lct	Leucite	$KAlSi_2O_6$
lit	Litharge	PbO
mag	Magnetite	$Fe^{2+}Fe^{3+}{}_2O_4$
mlc	Malachite	$Cu_2(CO_3)(OH)_2$
mll	Melilite [group]	$(Ca,Na,K,Pb)_2(Al,Fe^{3+},Fe^{2+},Mg,Mn,Zn)(Si,Al)_2O_7$
mrc	Marcasite	FeS_2
ol	Olivine [group]	$(Fe,Zn,Mg,Mn,Ca)_2SiO_4$
po	Pyrrhotite	$Fe_{1-x}S$
py	Pyrite	FeS_2
qz	Quartz	SiO_2
rds	Rhodochrosite	$MnCO_3$
rud	Rudashevskyite	(Zn,Fe)S
sd	Siderite	$FeCO_3$
sp	Sphalerite	(Zn,Fe)S
spl	Spinel *ss* [group]	$(Fe^{2+},Mg,Mn,Ni,Zn)(Al,Fe^{3+},Cr,Ti)_2O_4$
tnt	Tennantite	$(Cu,Ag,Zn,Fe)_{12}As_4S_{13}$
ttr	Tetrahedrite	$(Cu,Ag,Zn,Fe)_{12}Sb_4S_{13}$
wo	Wolframite	$(Fe,Mn)WO_4$
wus	Wüstite	$Fe^{2+}{}_{1-x}O$

Table i.1.: Abbreviations for minerals and phases. If available, abbreviations have been taken from Whitney & Evans (2010).

Abbreviation/symbol	Meaning
acc	Accessory phase
apfu	Atoms per formula unit
BSE	Back-scatter electrons
CIA	Copper isotope analysis
LIA	Lead isotope analysis
ox	Oxidised phase
PPL	Plain-polarised light
rel	Relictic phase
RL	Reflected light
sec	Secondary phase
ss	solid solution
s.s.	sensu stricto
sul	Sulphide phase
TL	Transmitted light
XPL	Cross-polarised light
X:Y	Phases X and Y are products of an exsolution reaction
[X Y]	Phases X and Y occur in a symplectitic intergrowth

Table i.2.: Other abbreviations and symbols. Symbols 'X:Y' and '[X Y]' have been taken from Kronz (1997).

ii. Samples and sampling locations

Sample	OM	XRD	EMP	LIA	CIA
11015	x	na	x	x	x
11043(2)	x	na	x	x	x
11043(3)	x	na	x	x	x
11043(4)	x	na	na	na	na
11079	x	na	x	x	x
11090(6)	x	na	x	x	x
12025	x	na	na	na	na
12055(1)	x	na	x	x	x
13020(1)	x	na	x	x	x
13098(1)	x	na	x	x	x
13099(2)	x	na	x	x	x
13099(4)	x	na	na	na	na
13099(5)	x	na	na	na	na
14018	x	na	x	x	na
13105(1)	na	na	na	x	na
13105(2)	na	na	na	x	na
13105(3)	na	na	na	x	na
13130(1)	na	na	na	x	na
13130(2)	na	na	na	x	na
13130(3)	na	na	na	x	na

Table ii.1.: Analytical techniques applied for the ores.

Sample	OM	XRD	EMP	LIA	CIA
10-2A	x	x	na	na	na
10-2B	x	x	x	x	na
12015(5)	x	x	x	x	na
12015(7)	x	x	x	x	na
12015(12)	x	x	x	x	na
14032	x	na	x	x	na
11027(1)	x	x	x	x	na
11027(2)	x	x	x	x	na
11029(1)	x	x	na	na	na
11029(2)	x	x	na	na	na
11029(3)	x	x	x	x	na
11029(4)	x	x	x	x	na
11029(5)	x	x	x	x	na
11029(7)	x	x	x	x	na
10024(2)	x	x	x	x	na
10024(4)	x	x	x	x	na
10024(5)	x	x	x	x	na
10021(2)	x	x	x	x	na
10021(4)	x	na	x	x	na
10021(21)	x	x	x	x	na
MrS_gn	na	na	na	x	x
MrS_Pb	na	na	na	x	x
10-5	x	x	x	x	na
10-6	x	x	x	x	na
10032(1)	x	x	x	x	na
10032(2)	x	x	na	na	na
10032(4)	x	x	x	x	na
10-1A	x	x	x	x	na
10-1B	x	x	x	x	na
3(1)	x	na	x	x	na
3(2)	x	na	x	x	na
12016(1)	x	x	x	x	na
12016(2)	x	x	x	x	na
13030(1)	x	na	x	x	na
13031(1)	x	na	x	x	na

Table ii.2.: Analytical techniques applied for the metallurgical (by-) products.

Sample	OM	XRD	EMP	LIA	CIA
I.1	x	na	x	x	x
I.2	x	na	x	x	x
I.3	x	na	x	x	x
II.1	x	na	x	x	x
II.2	x	na	x	x	x
II.3	x	na	x	x	x
IV	x	na	x	x	x
V	x	na	x	x	x
III	x	na	x	x	x
VI	x	na	x	x	x

Table ii.3.: Analytical techniques applied for the metal artefacts.

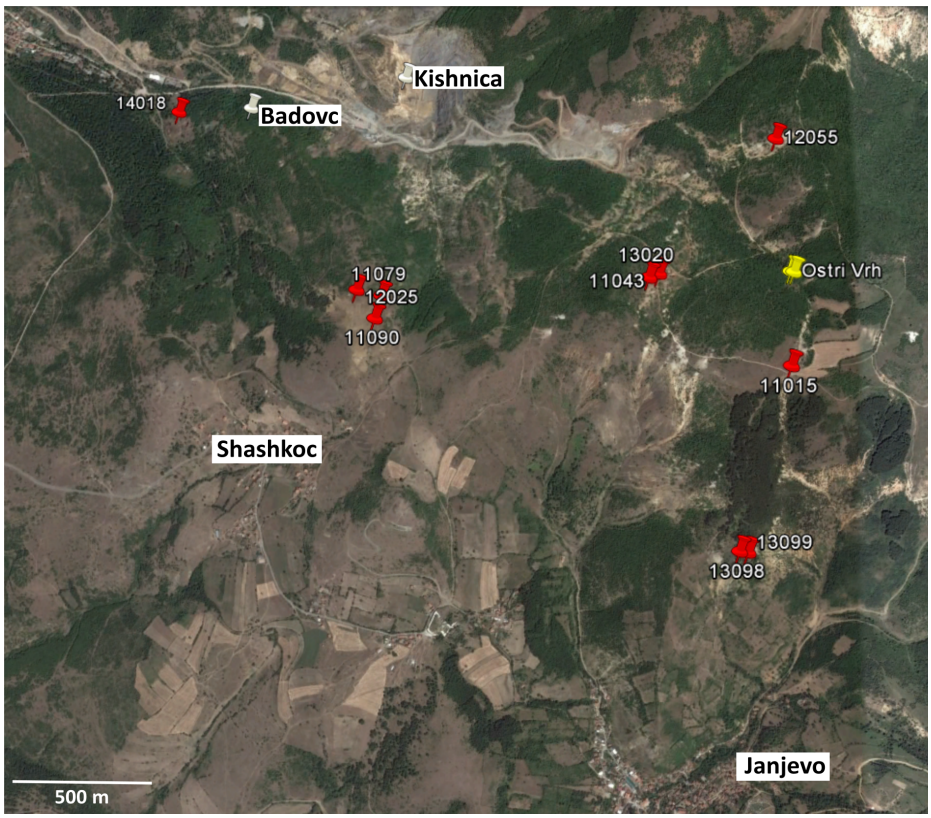

Figure ii.1.: Sampling locations of the investigated ores in the Shashkoc-Janjevo district. The smelting site of Ostri Vrh as well as the modern mines of Badovc and Kishnica are indicated as well.

Sample	Ore formation stages	gn	sp	py	mrc	po	apy	ccp	tnt-ttr	Other sulphosalts	wo	Sec Cu sul	Sec ox Cu phases	Gangue
11015	**Early** to main	xx	x	xxx			x	xx	x	acc				qz, subordinate cb
11043(2)	Main	acc	acc	acc				x	acc			xxx	xx	-
11043(3)	**Early** to main	acc		x			xxx	acc						qz
11043(4)	**Early** to main	acc		x			xxx	acc						qz
11079	Main to **late**	x	x	xxx				xx	acc			acc		cb, subordinate qz
11090(6)	Main to **late**	xxx	x	x	acc	acc	acc	x				acc		qz[a]
12025	Main to **late**	xxx		x				x						cb
12055(1)	Main to **late**	xxx	x	xxx			xx	x	x					cb, subordinate qz
13020(1)	Main			x				acc				xx	xxx	-
13098(1)	Early to **main**	x		xxx			xx	xx	xx			acc		qz, subordinate cb
13099(2)	Early to **main**	xxx	x	xx			x	x	xx					cb (Fe-rich), subordinate qz
13099(4)	**Early** to main	acc		xx			xxx	acc						qz
13099(5)	Early to **main**	x		xxx			xx	xxx	xx	acc	xx	acc		cb, subordinate qz
14018	Main to **late**	xxx	xxx		xx	acc		x						cb (Fe-rich)

Table ii.4.: Formation stages (dominant paragenesis is bold) and phase assemblages of the investigated ore samples from the Shashkoc-Janjevo district.

[a] Newly-formed during secondary weathering processes

Sample	Ore formation stages	median FeS in sp [mol %]	As in apy [at %]	T [°C] apy thermometry
11015	**Early** to main	-	32.41	450
11043(2)	Main	0.8	-	-
11043(3)	**Early** to main	-	29.81 - 32.41	345 - 450
11043(4)	**Early** to main	-	-	-
11079	Main to **late**	14.7	-	-
11090(6)	Main to **late**	3.5	-	-
12025	Main to **late**	-	-	-
12055(1)	Main to **late**	-	29.61	330
13020(1)	Main	-	-	-
13098(1)	Early to **main**	-	-	-
13099(2)	Early to **main**	-	29.77 - 32.54	345 - 475
13099(4)	**Early** to main	-	-	-
13099(5)	Early to **main**	-	-	-
14018	Main to **late**	18.3	-	-

Table ii.5.: Median FeS abundances of sp [mol %], As contents in apy [at %] and corresponding estimated temperatures of the investigated ore samples from the Shashkoc-Janjevo district.

Slag type	Subtype	Smelting site	Sample	Preliminary dating	ol	ol II	cpx	mll	fsp	lct	kls	spl *ss*	wus	isc	Symplectite
ol	ol (I); low or absent spl *ss*	Voguçincë	14032	R/la	xxx	x				xx		acc			[ol lct]
ol	ol (I); low or absent spl *ss*	Marec	10-6	M/em	xxx							acc			
ol	ol (I); low or absent spl *ss*	Marec	10032(1)	M/em	xxx	x						acc			
ol	ol (I); low or absent spl *ss*	Marec	10032(4)	M/em	xxx										
ol	ol (I),; low or absent spl *ss*	Hanroc	3(1)	M/em	xxx	x							acc		
ol	ol (I); abundant spl *ss*	Voguçincë	12015(7)	R/la	xxx	x			acc	xx		x			[ol lct]
ol	ol (I); abundant spl *ss*	Mirash Novo	11029(4)	R/la	xxx	x	acc			acc		x		acc	
ol	ol (I); late cpx, low spl *ss*	Mirash	11027(1)	R/la	xxx	x	x			acc		acc			
ol	ol (I); late cpx, low spl *ss*	Mirash	11027(2)	R/la	xxx	x	x					acc			
ol	ol (I); late cpx, low spl *ss*	Mirash Novo	11029(5)	R/la	xxx	x	x		acc	acc		acc			
ol	wus+spl *ss* (I)	Hajkobile	10-1A	M/em	xxx					xx		xx	xx	x	[ol lct], [lc wus]
ol	wus+spl *ss* (I)	Hanroc	3(2)	M/em	xxx					xx		x	xx	xx	[lc wus]
ol	spl *ss* (I)	Voguçincë	12015(5)	R/la	xxx	x				x		xx		acc	[ol lct]
ol	spl *ss* (I)	Voguçincë	12015(12)	R/la	xxx	x				x		xx		acc	[ol lct]
ol	spl *ss* (I)	Mramor Proni Butoçit	10024(4)	-	xxx	x	acc			x		xx			[ol lct]
ol+cpx	spl *ss* (I)	Akllap	12016(1)	M/em	xx		xx		acc	x		xx			[ol lct]
cpx	wus+spl *ss* (I)	Mramor Proni Butoçit	10024(2)	-	x		xxx		acc	x		xx	x	acc	[ol lct], [lc wus]
cpx	spl *ss* (I)	Mramor Proni Butoçit	10024(5)	-	acc		xxx			xx		xx	x		[lc wus]
cpx	spl *ss* (I)	Akllap	12016(2)	M/em	acc		xxx					xx			
cpx	spl *ss* (I)	Ostri Vrh	13030(1)	M/em			xxx		acc	x		xx		acc	
mll	spl *ss* (I)	Ostri Vrh	13031(1)	M/em				xx			x	xxx			
gl	spl *ss* (I)	Mirash Novo	11029(3)	R/la								xx			
Furnace	ol (I)	Mramor Samakove	10021(2)	M/em	xxx	xx				xx		x	xx		[lc wus]
slags	ol(I)	Mramor Samakove	10021(21)	M/em	xxx	xx			xx	xx					

Table ii.6.: Classification and phase assemblages of the investigated basin and furnace slags.

iii. X-ray diffractograms

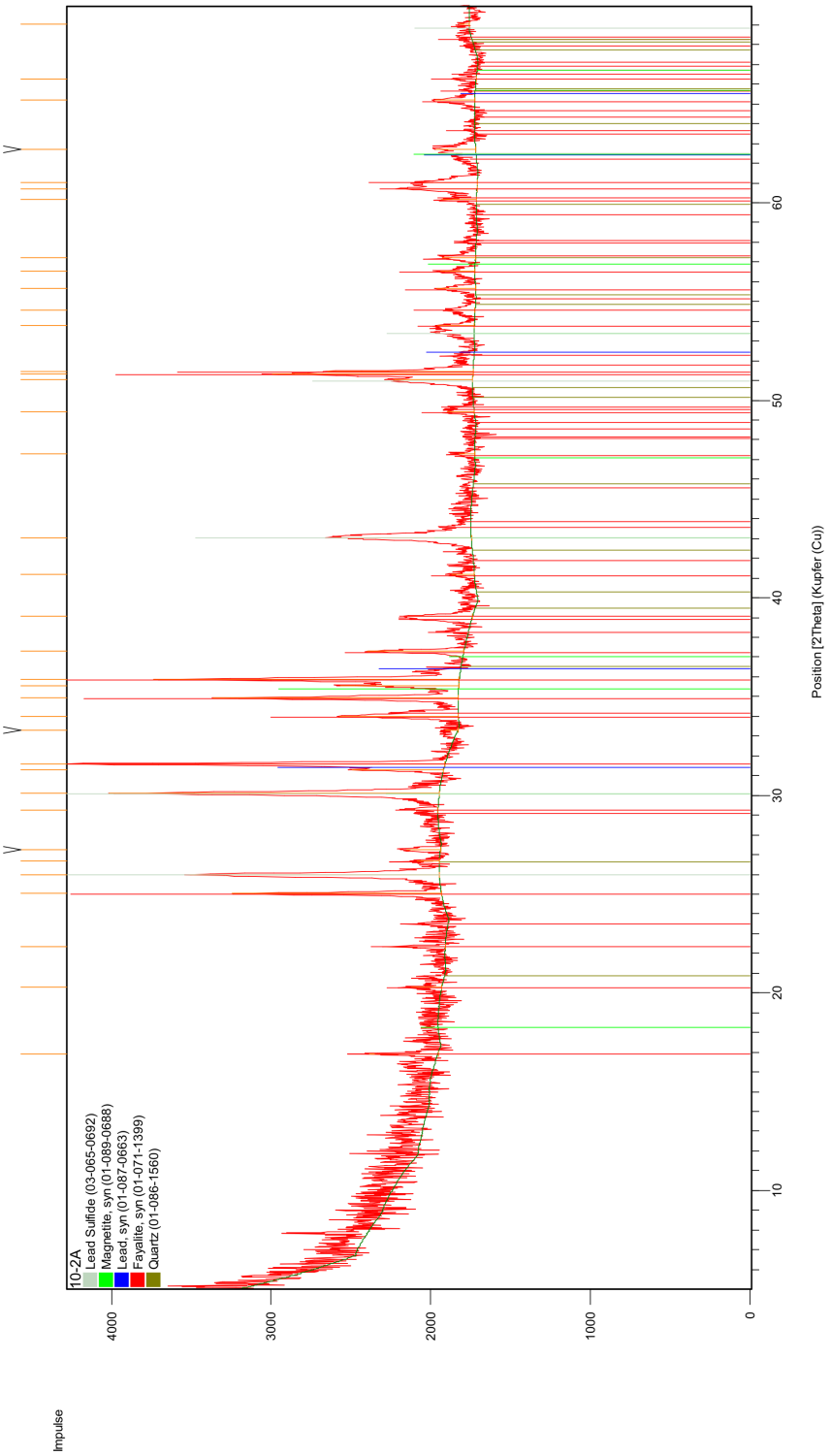

Figure iii.1.: XRD analysis of sample 10-2A. The following phases have been furthermore determined by by OM and EMP: Leucite, iscorite; pyrrhotite, (Zn,Fe)S, bornite *ss.* Quartz has not been observed in the section.

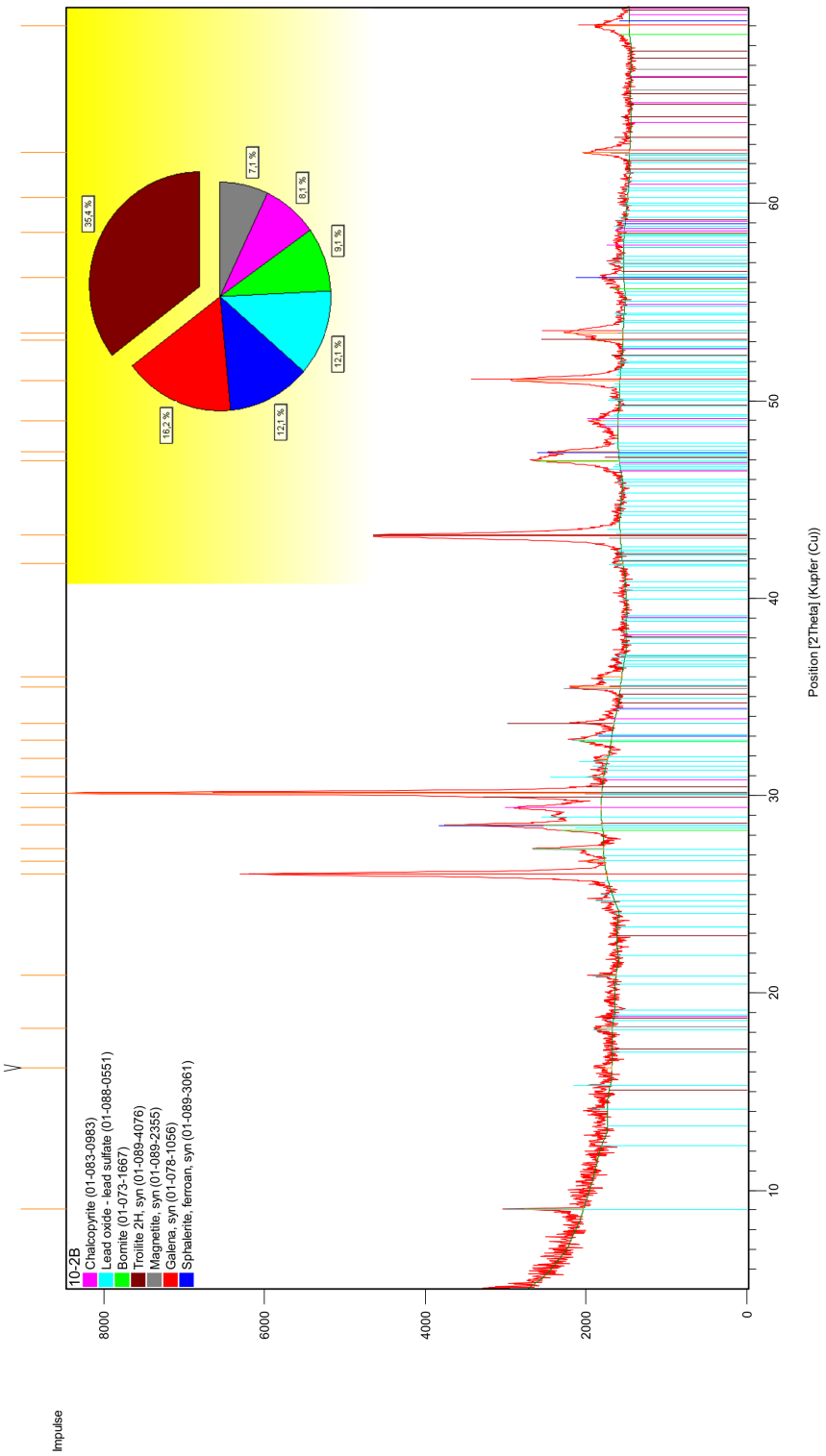

Figure iii.2.: XRD analysis of sample 10-2B. The following phases have been furthermore determined by OM and EMP: iss. A slag inclusion contains olivine, leucite and spinel *ss*.

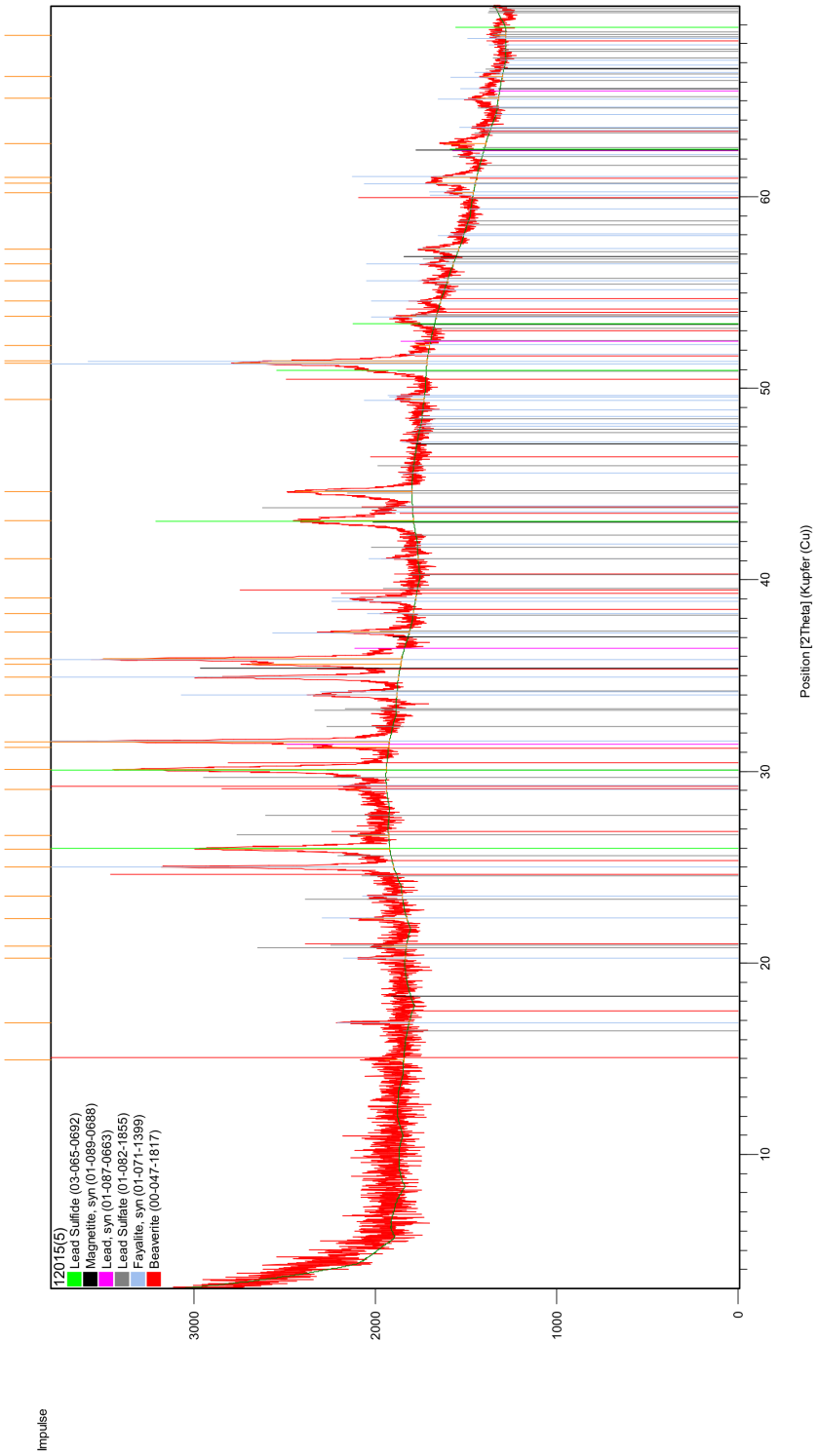

Figure iii.3.: XRD analysis of sample 12015(5). The following phases have been furthermore determined by OM and EMP: Leucite, iscorite; pyrrhotite, (Zn,Fe)S, bornite *ss*, covellite.

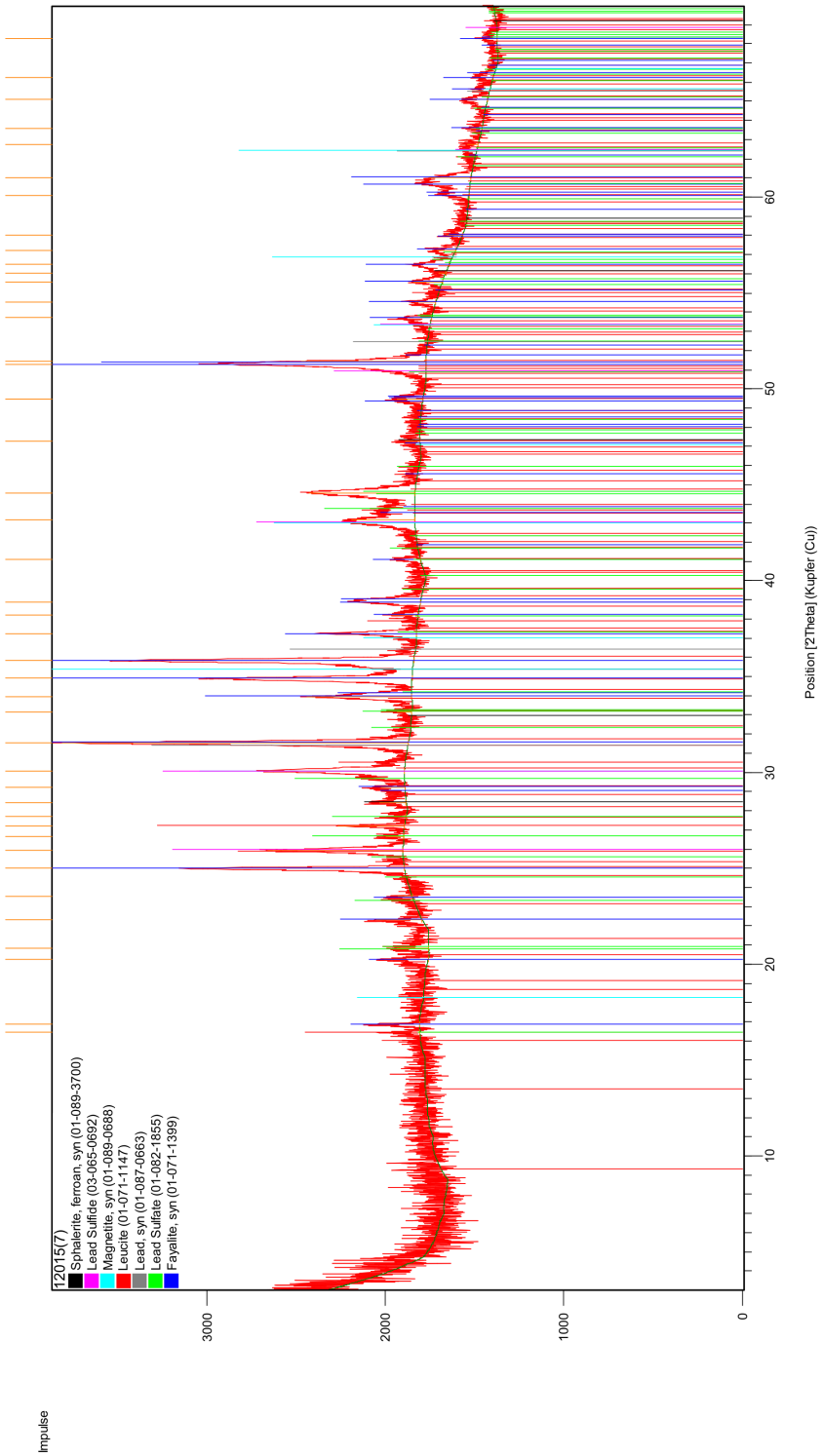

Figure iii.4.: XRD analysis of sample 12015(7). The following phases have been furthermore determined by OM and EMP: Alkali feldspar; pyrrhotite.

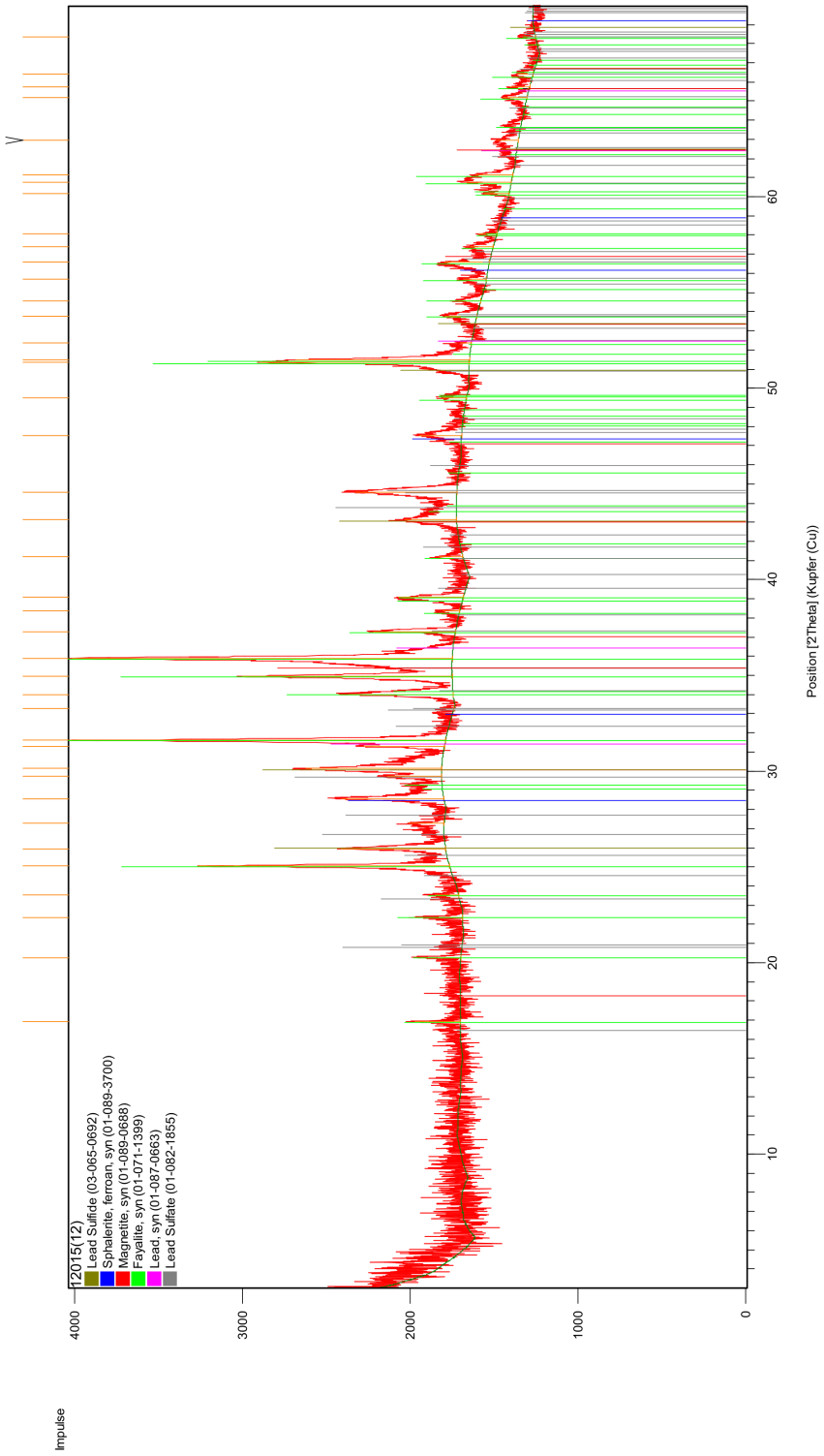

Figure iii.5.: XRD analysis of sample 12015(12).The following phases have been furthermore determined by OM and EMP: Leucite, iscorite; covellite.

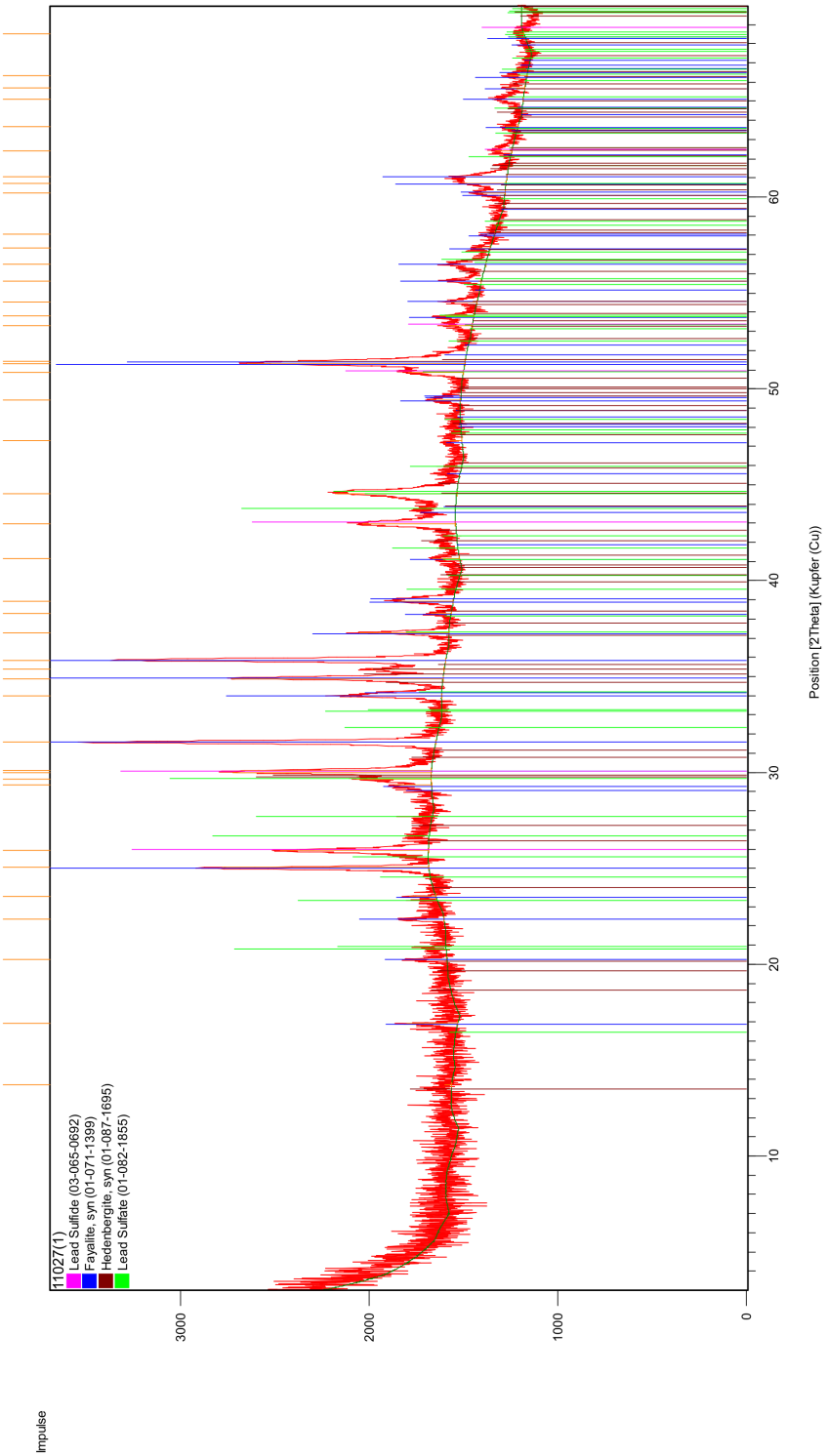

Figure iii.6.: XRD analysis of sample 11027(1). The following phases have been furthermore determined by OM and EMP: Leucite, spinel *ss*; pyrrhotite, (Zn,Fe)S, bornite *ss*, covellite, lead.

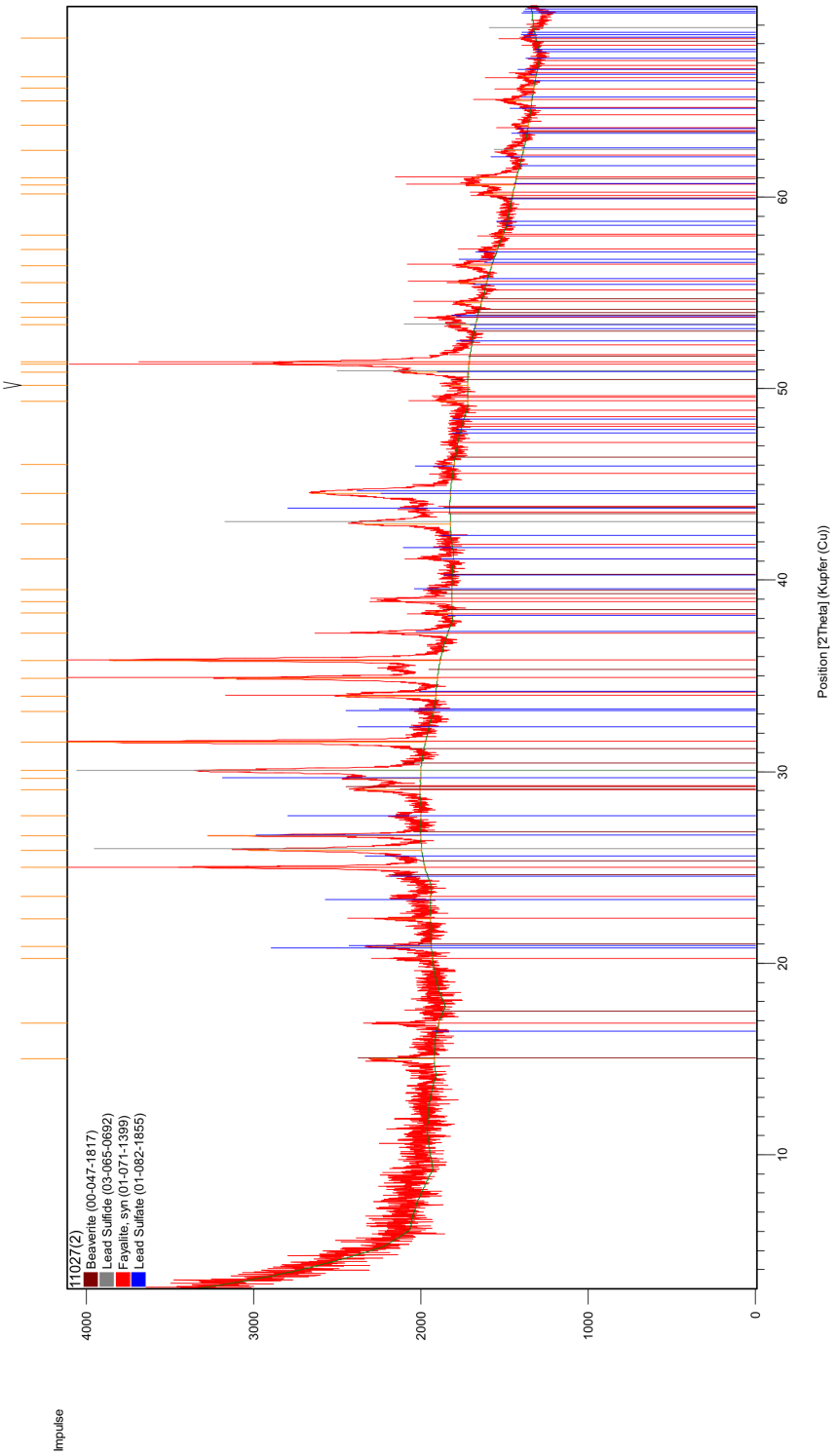

Figure iii.7.: XRD analysis of sample 11027(2). The following phases have been furthermore determined by OM and EMP: Clinopyroxene, spinel *ss*; pyrrhotite, bornite *ss*, lead.

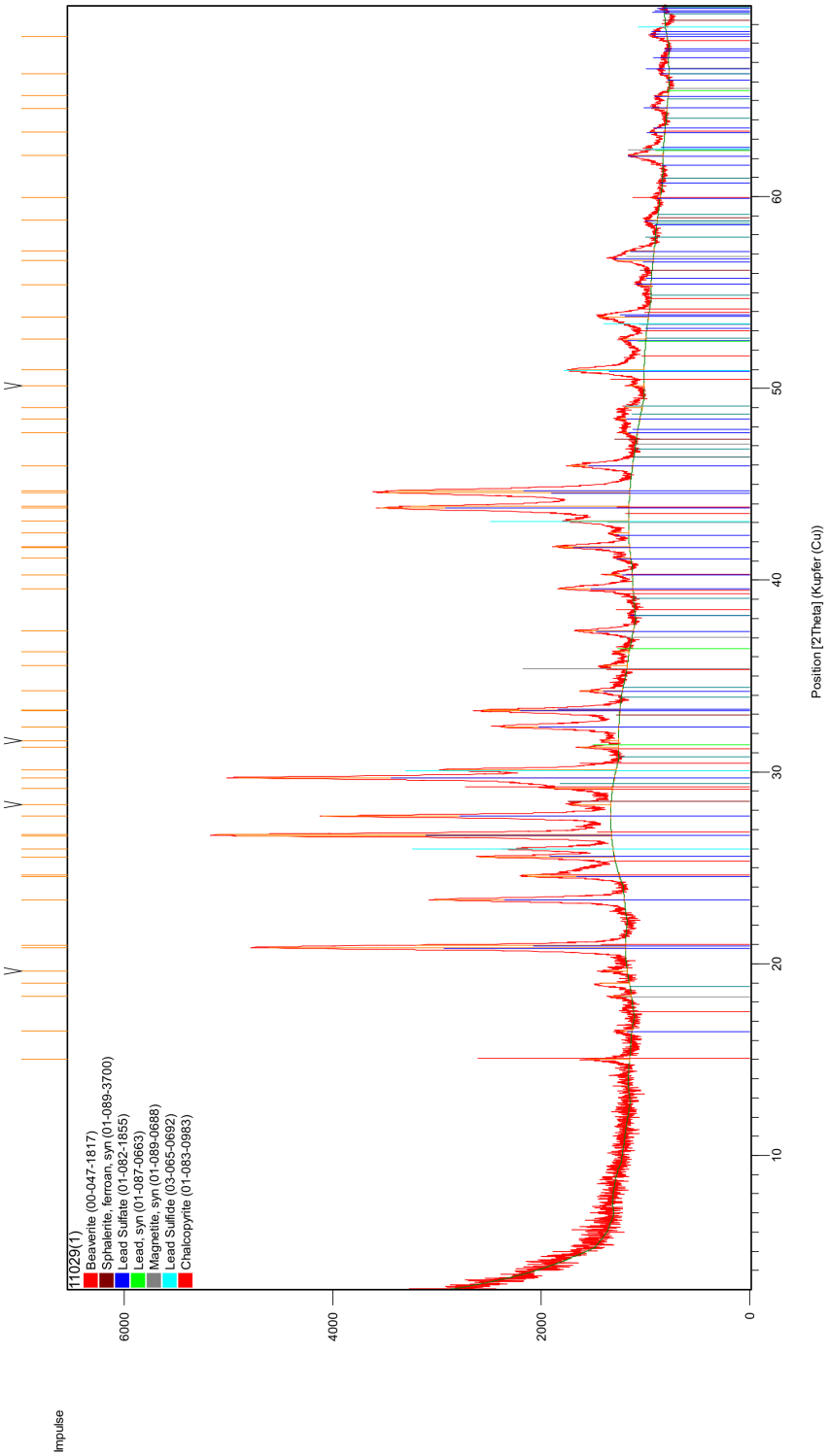

Figure iii.8.: XRD analysis of sample 11029(1). The following phases have been furthermore determined by OM and EMP: Dyscrasite. A slag inclusion contains olivine and spinel *ss*.

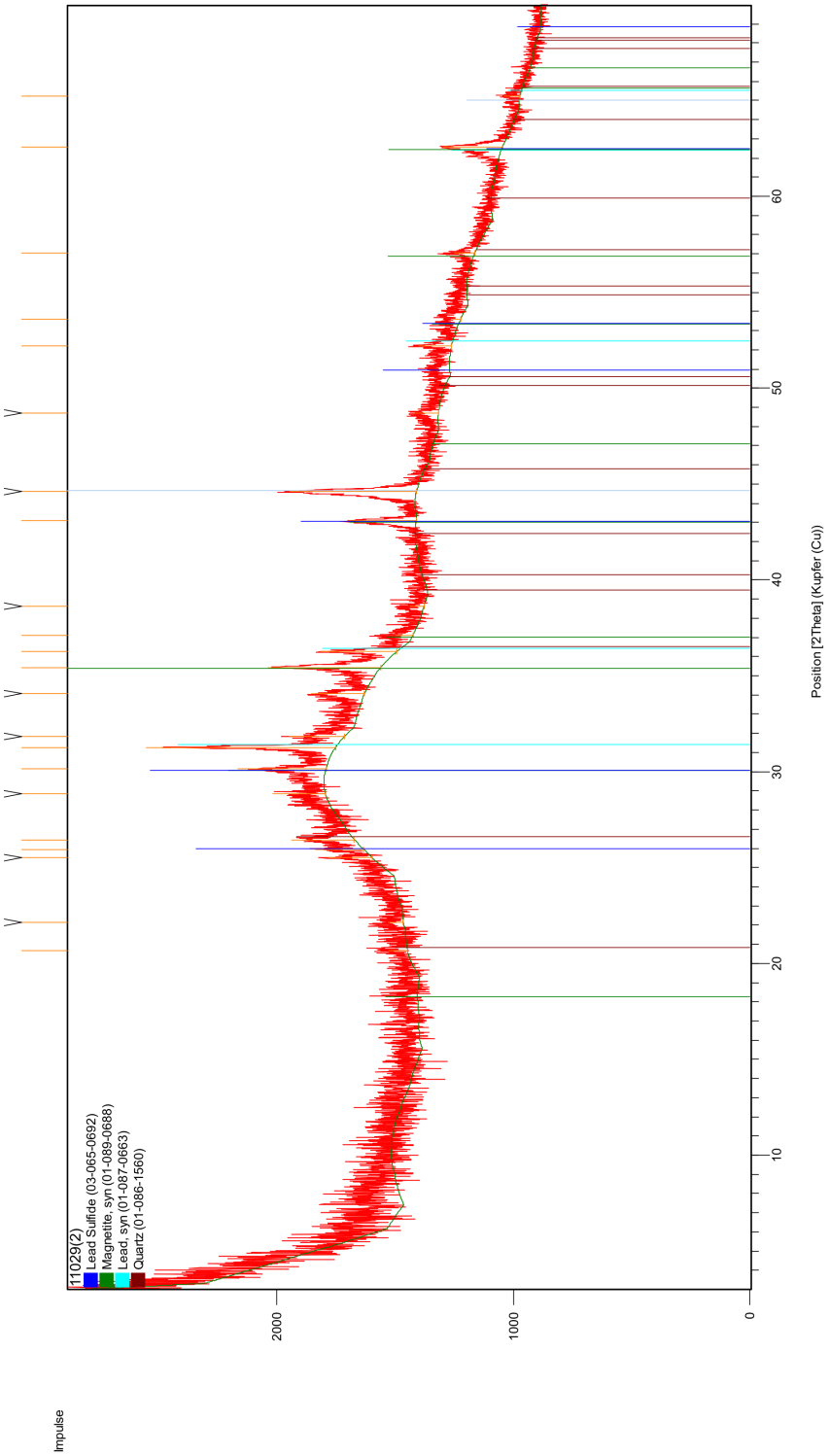

Figure iii.9.: XRD analysis of sample 11029(2). Quartz has not been observed in the section.

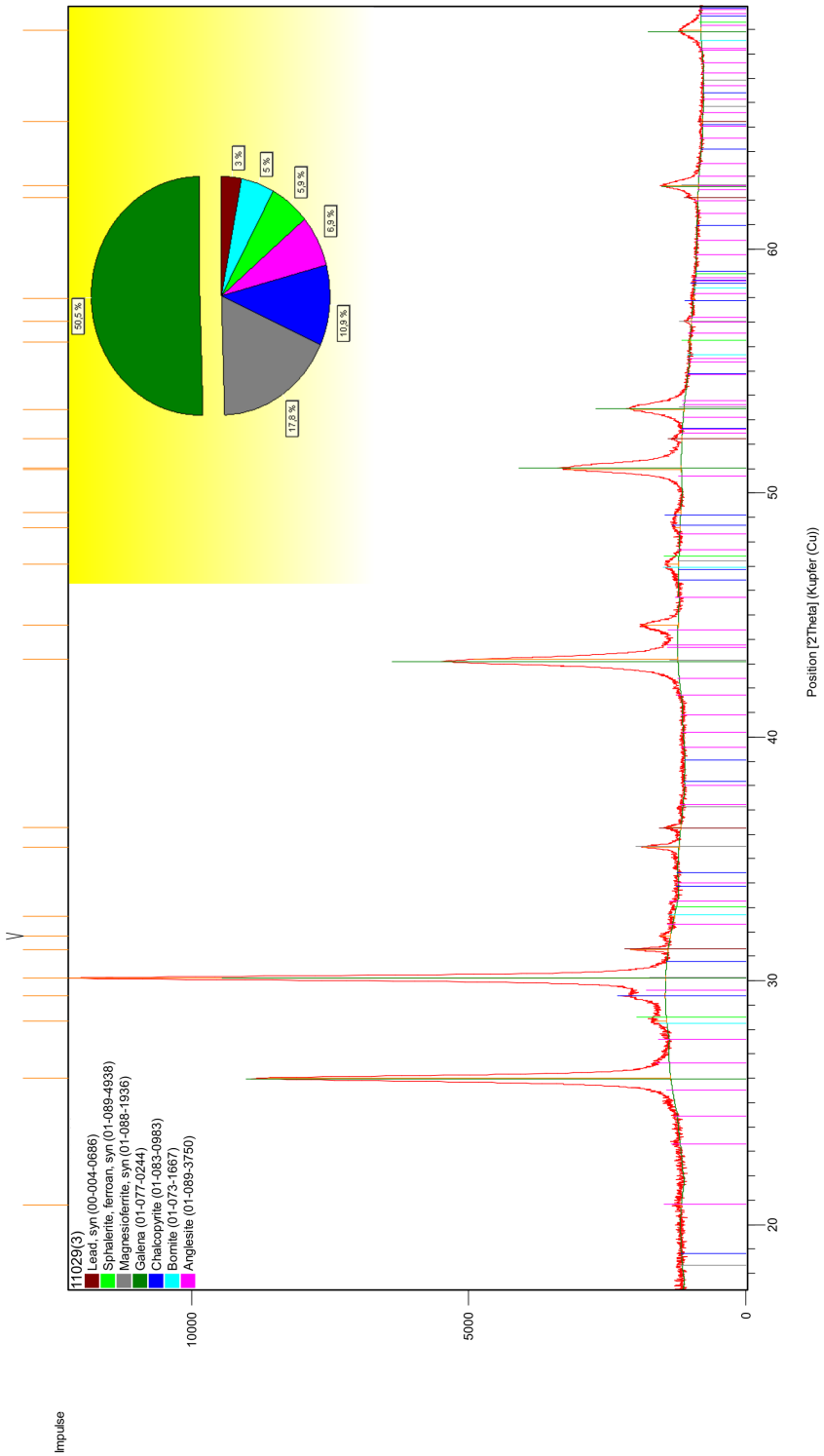

Figure iii.10.: XRD analysis of sample 11029(3). The following phases have been furthermore determined by OM and EMP: Pyrrhotite, covellite.

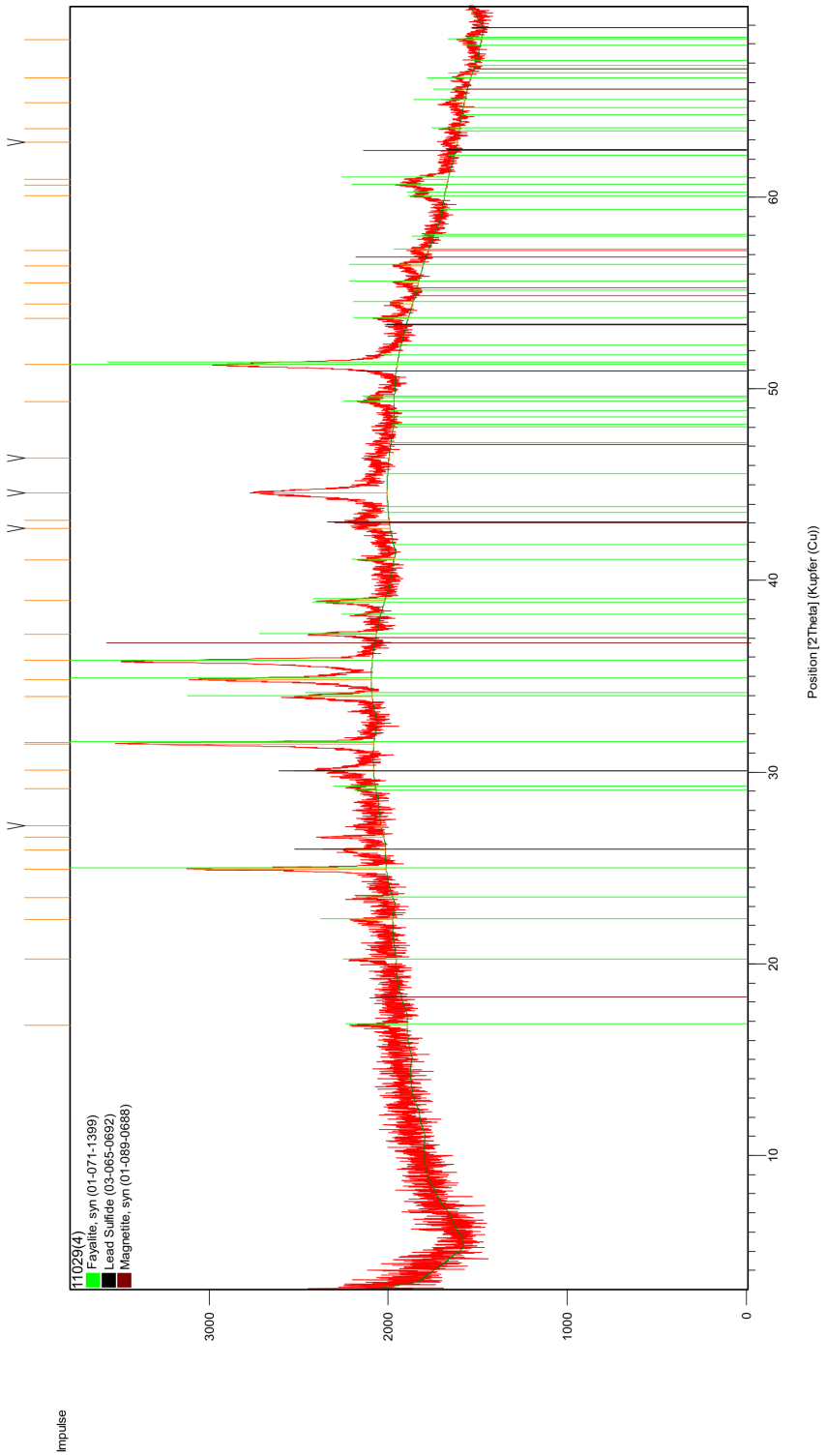

Figure iii.11.: XRD analysis of sample 11029(4). The following phases have been furthermore determined by OM and EMP: Clinopyroxene, leucite, iscorite; bornite *ss*, lead, Fe_2As, FeAs, $(Cu,Fe)_3(Sn,Sb)$.

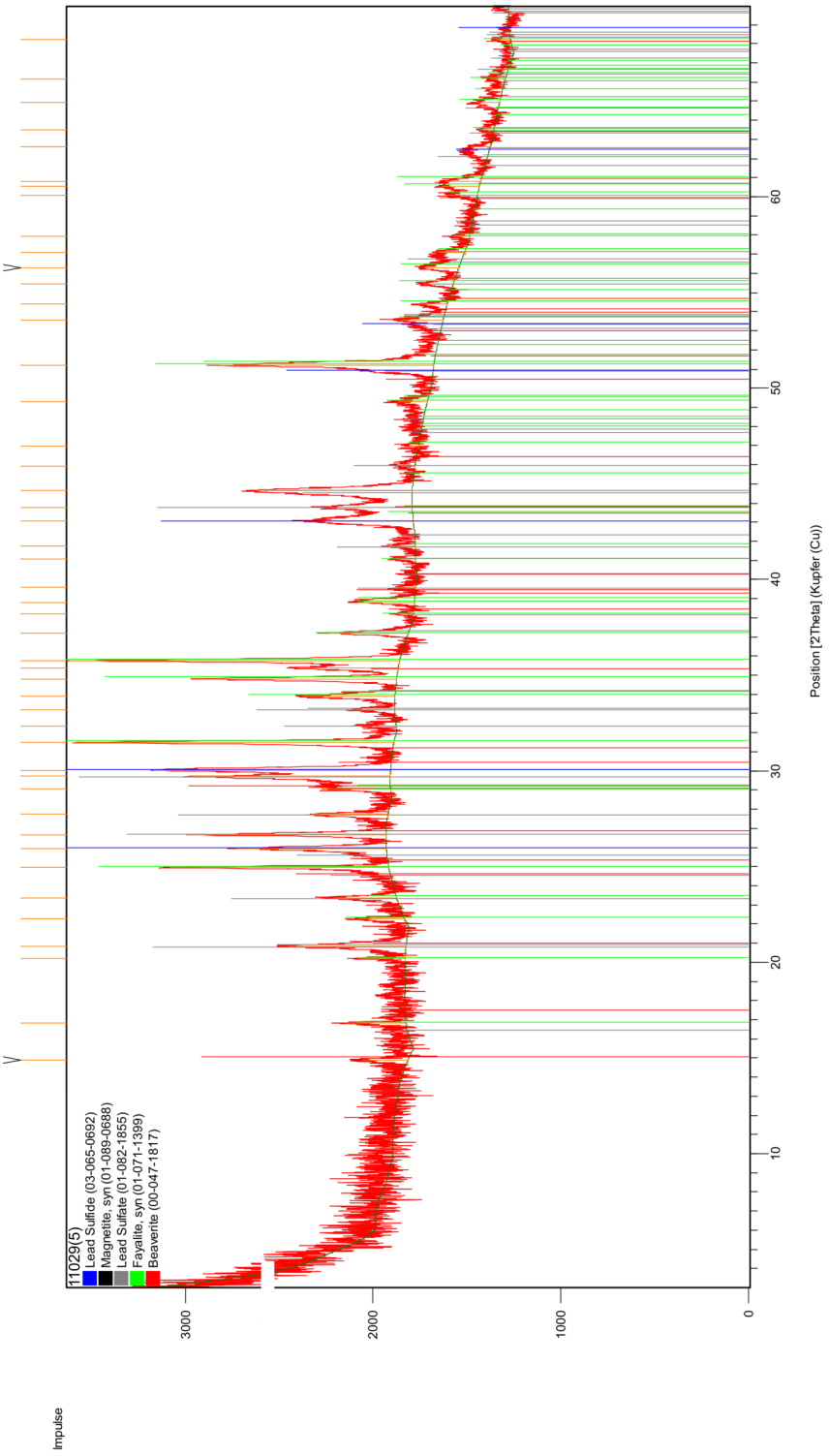

Figure iii.12.: XRD analysis of sample 11029(5). The following phases have been furthermore determined by OM and EMP: Clinopyroxene, alkali feldspar, leucite; pyrrhotite, (Zn,Fe)S, bornite *ss*, covellite.

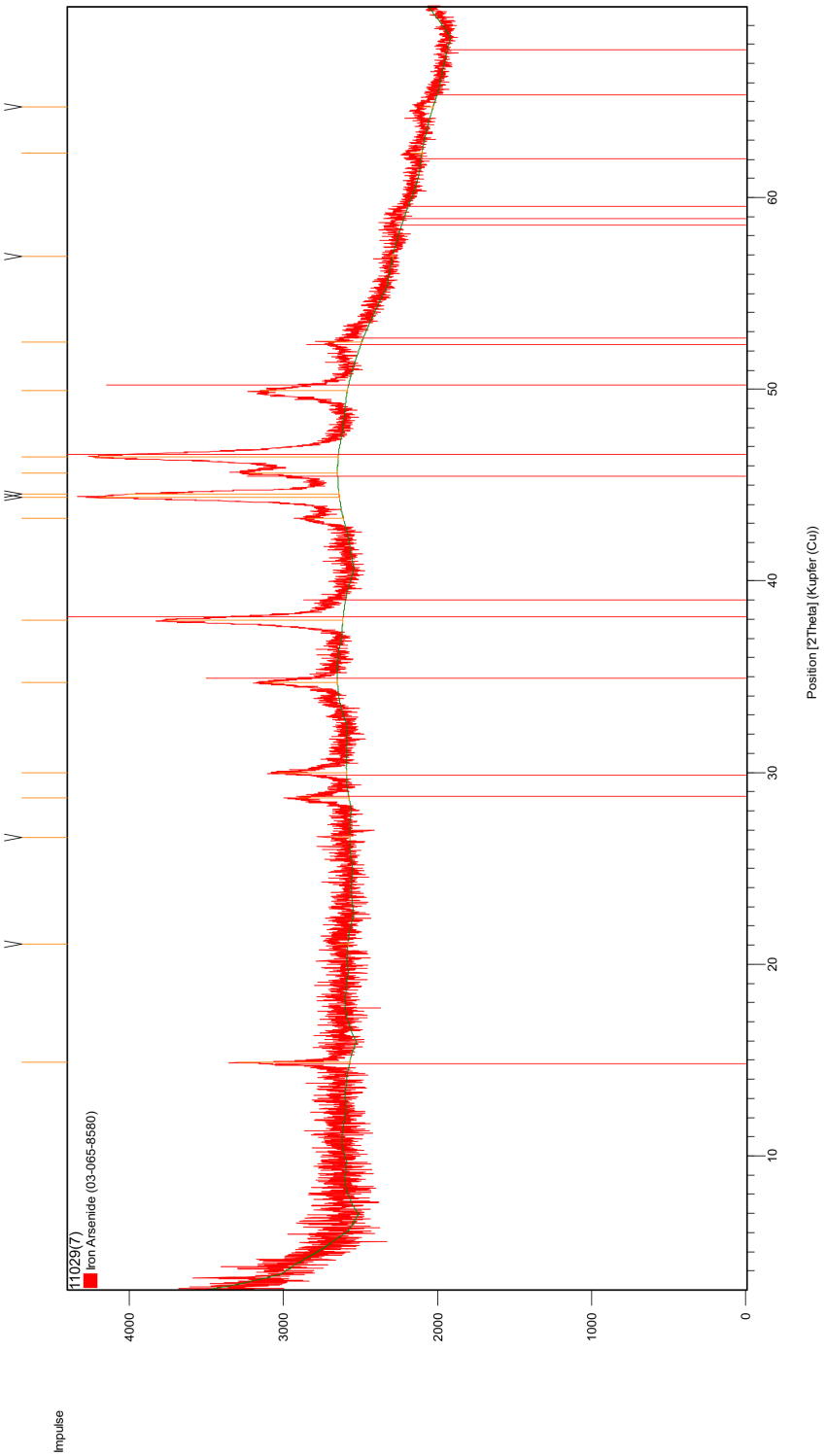

Figure iii.13.: XRD analysis of sample 11029(7). The following phases have been furthermore determined by OM and EMP: Fe_9As.

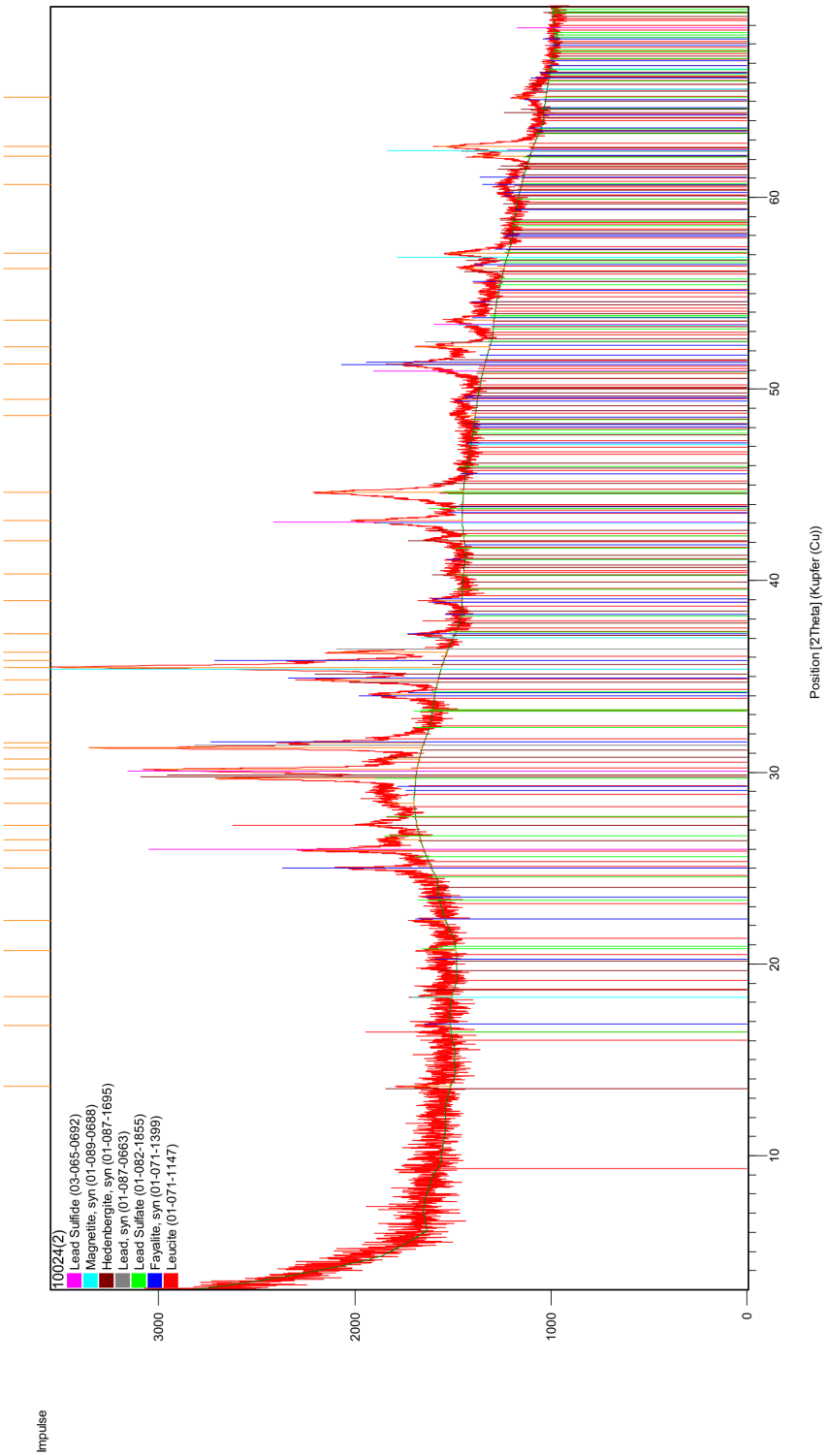

Figure iii.14.: XRD analysis of sample 10024(2). The following phases have been furthermore determined by OM and EMP: Wüstite, iscorite, alkali feldspar, leucite.

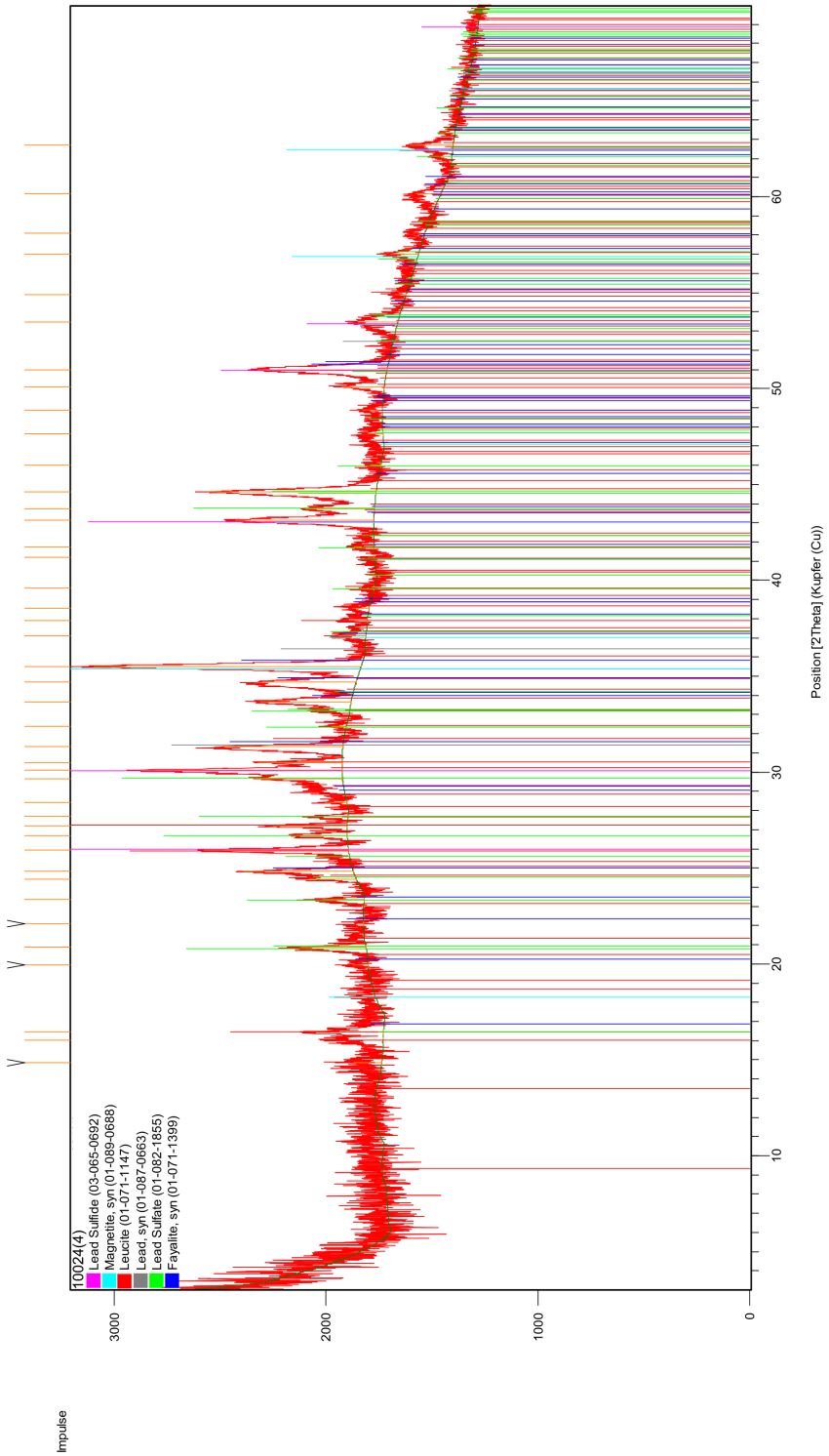

Figure iii.15.: XRD analysis of sample 10024(4). The following phases have been furthermore determined by OM and EMP: Clinopyroxene; pyrrhotite, (Zn,Fe)S, iss, bornite *ss*, covellite.

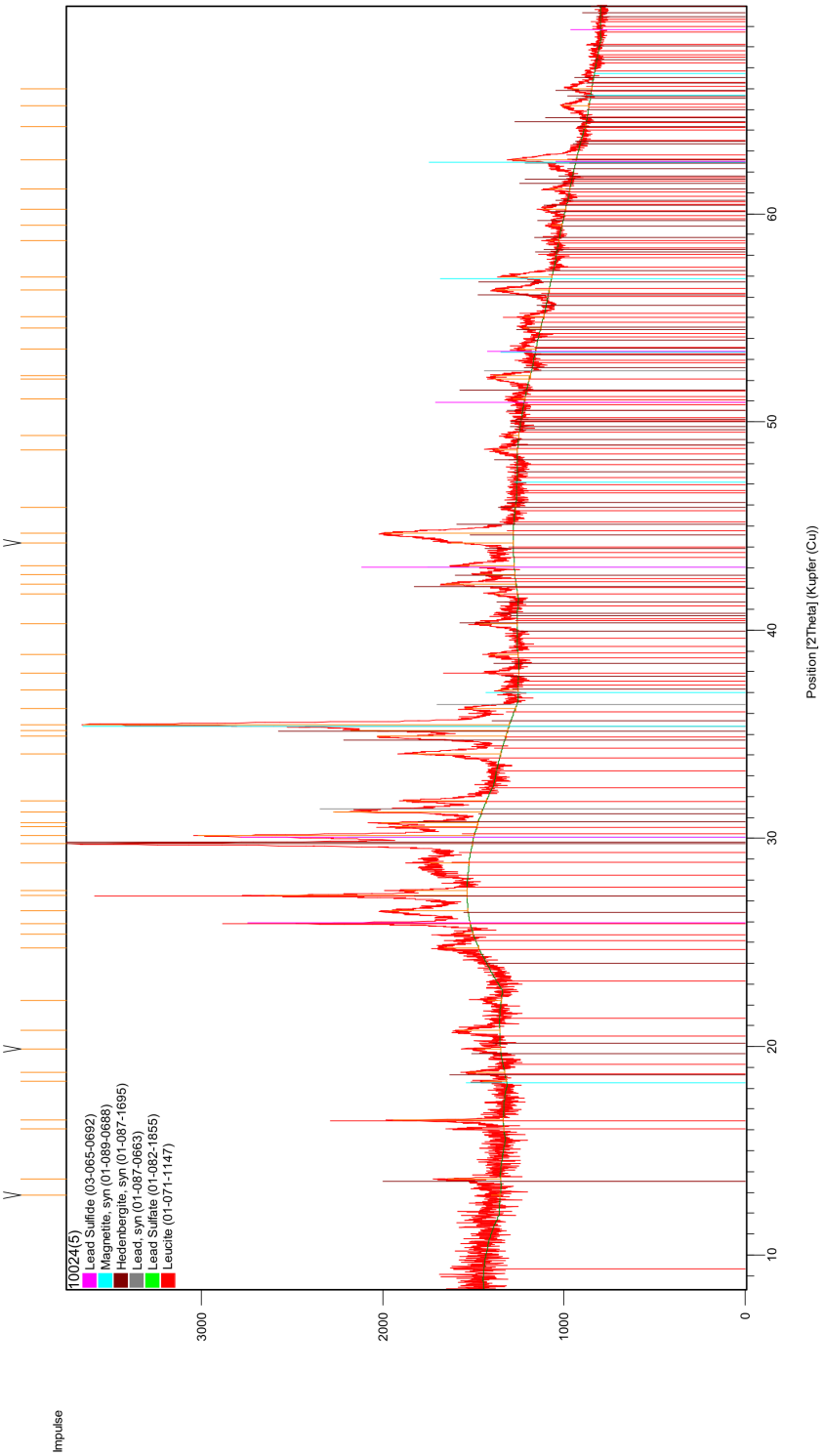

Figure iii.16.: XRD analysis of sample 10024(5). The following phases have been furthermore determined by OM and EMP: Olivine, wüstite; pyrrhotite, chalcocite *ss*, covellite.

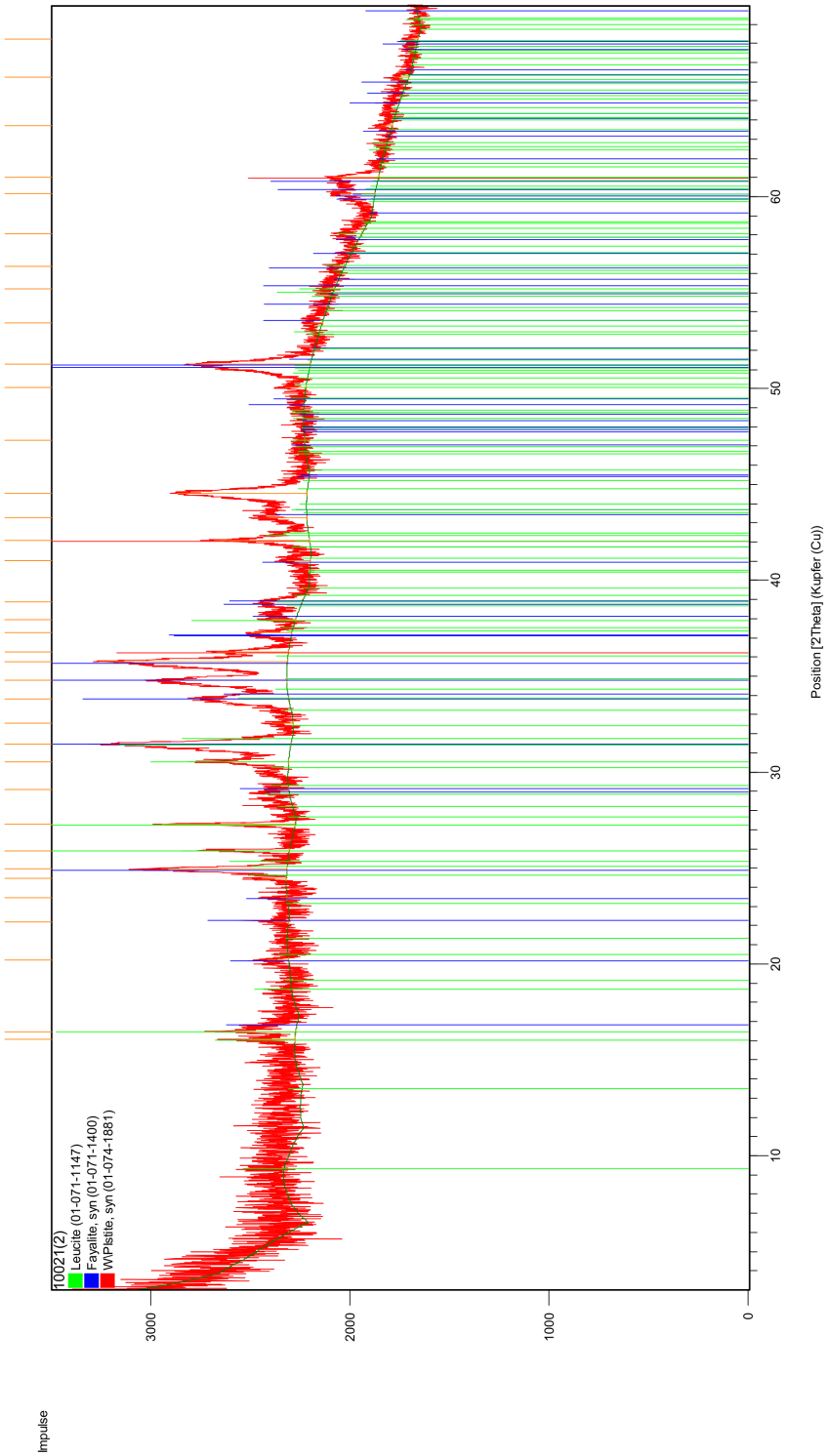

Figure iii.17.: XRD analysis of sample 10021(2). The following phases have been furthermore determined by OM and EMP: spinel *ss*; base metal sulphide melt, lead.

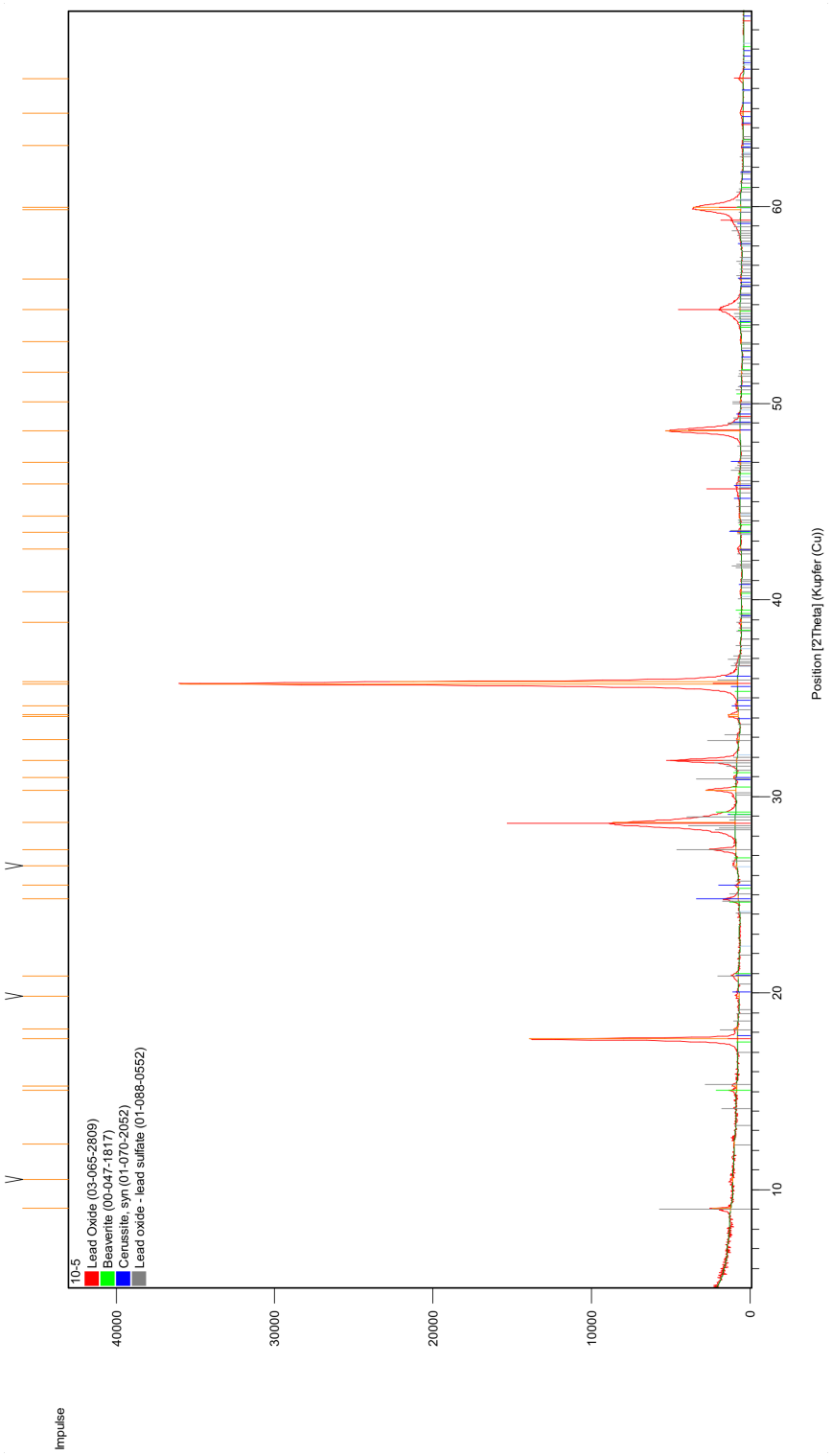

Figure iii.18.: XRD analysis of sample 10-5.

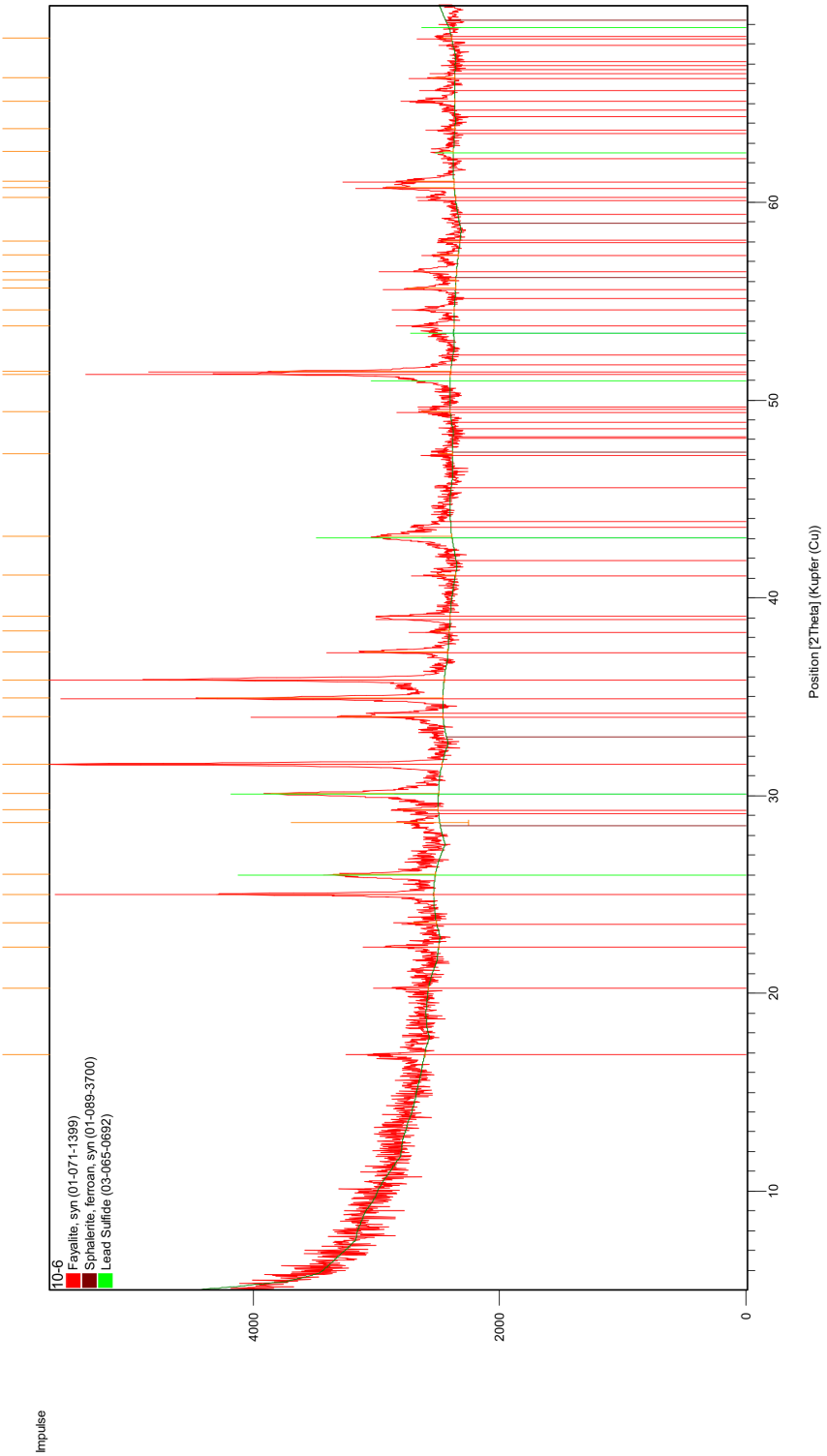

Figure iii.19.: XRD analysis of sample 10-6. The following phases have been furthermore determined by OM and EMP: Spinel *ss*; pyrrhotite.

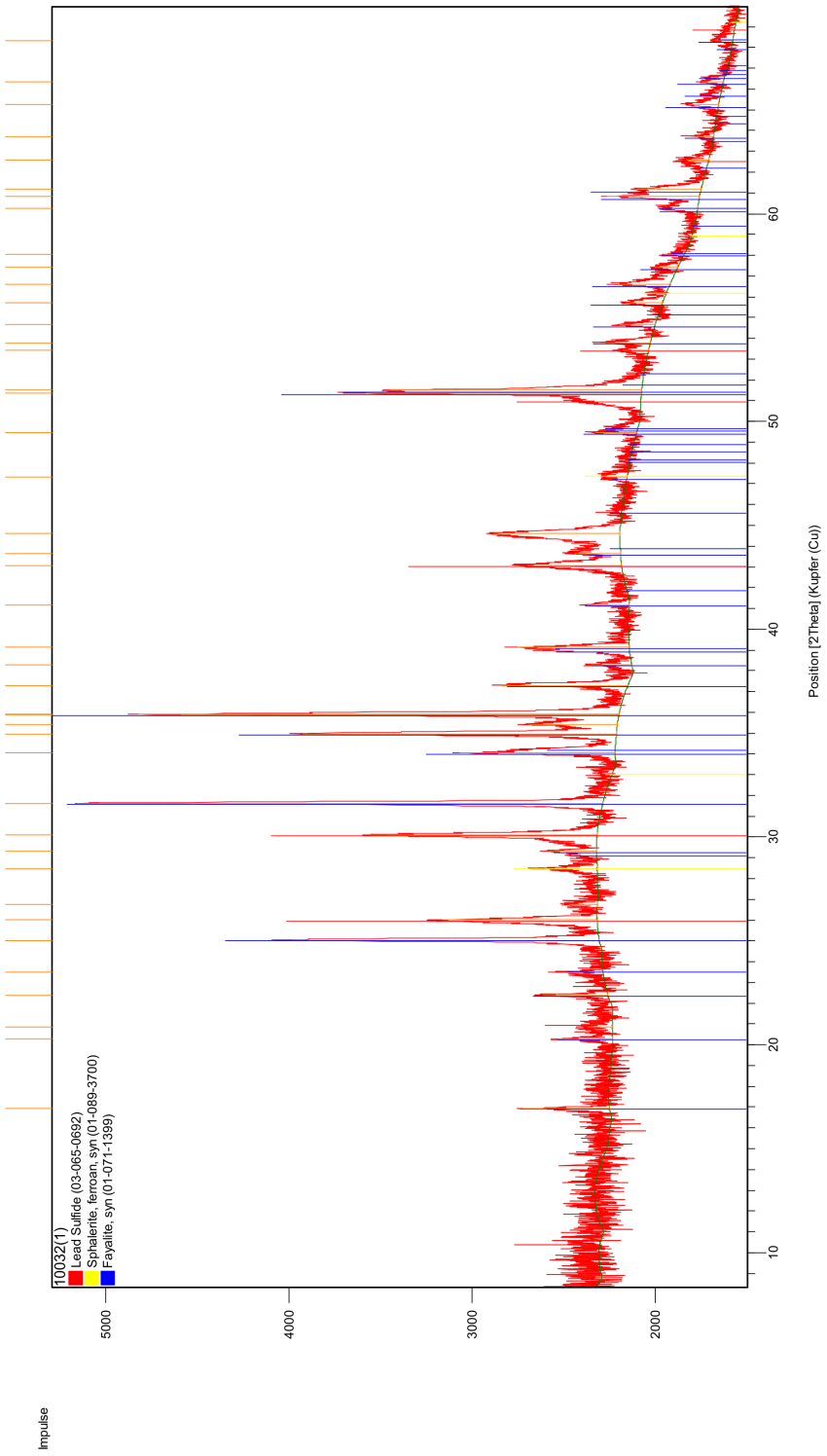

Figure iii.20.: XRD analysis of sample 10032(1). The following phases have been furthermore determined by OM and EMP: Spinel *ss*; pyrrhotite.

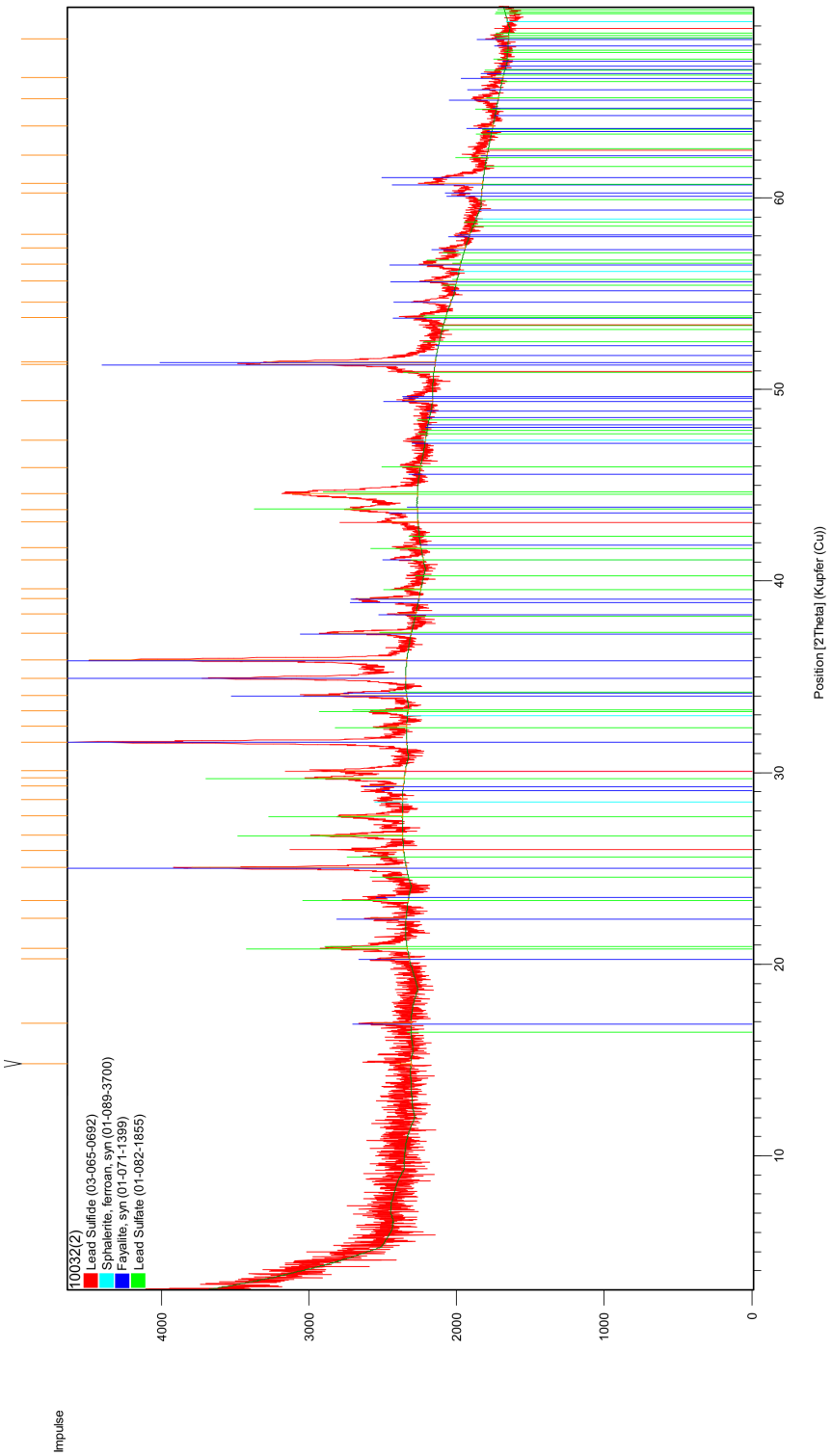

Figure iii.21.: XRD analysis of sample 10032(2). The following phases have been furthermore determined by OM and EMP: Leucite; pyrrhotite.

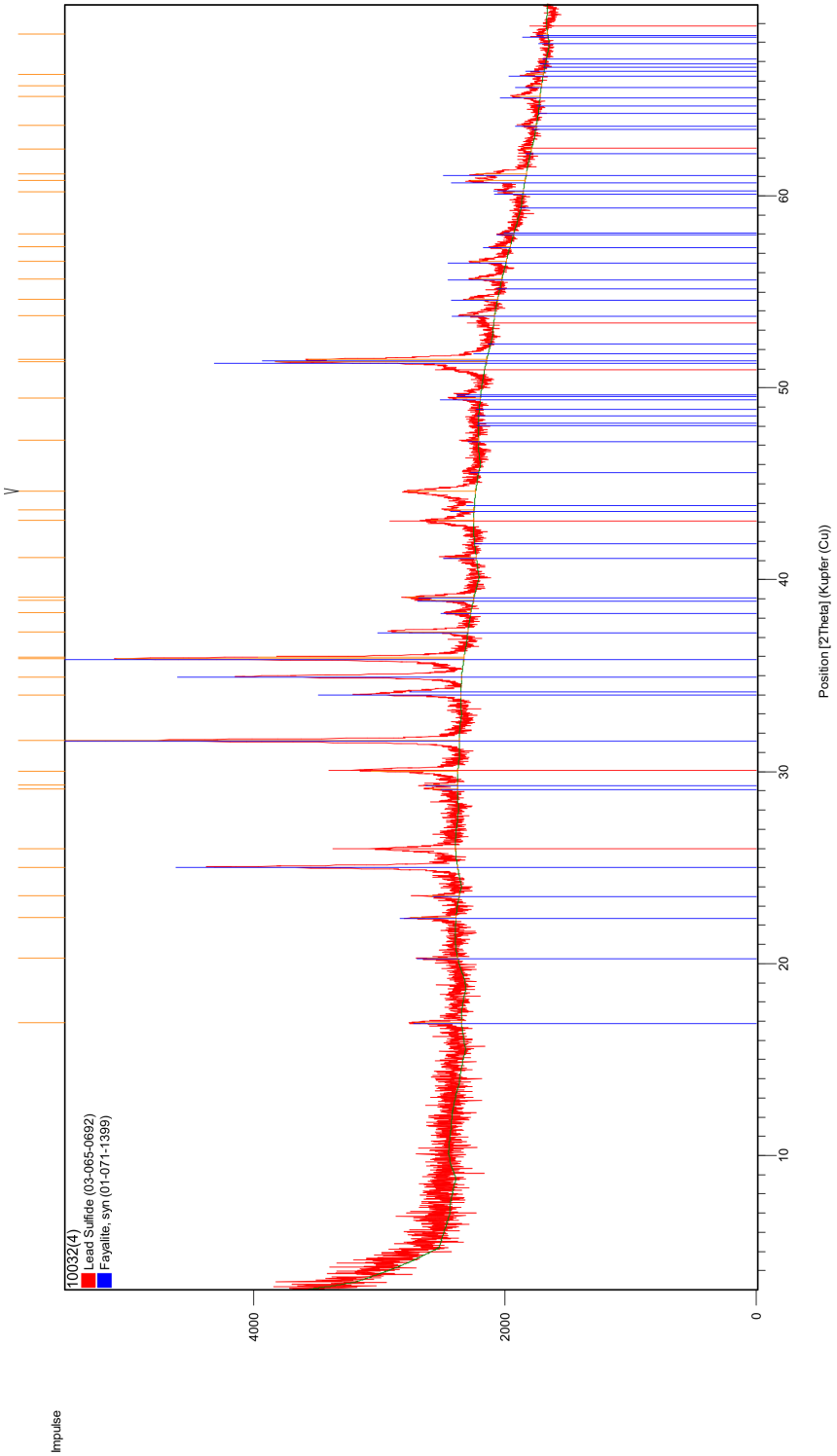

Figure iii.22.: XRD analysis of sample 10032(4). The following phases have been furthermore determined by OM and EMP: Leucite; iss, bornite *ss*, FeAs, $(Cu,Ni)_2Sb$.

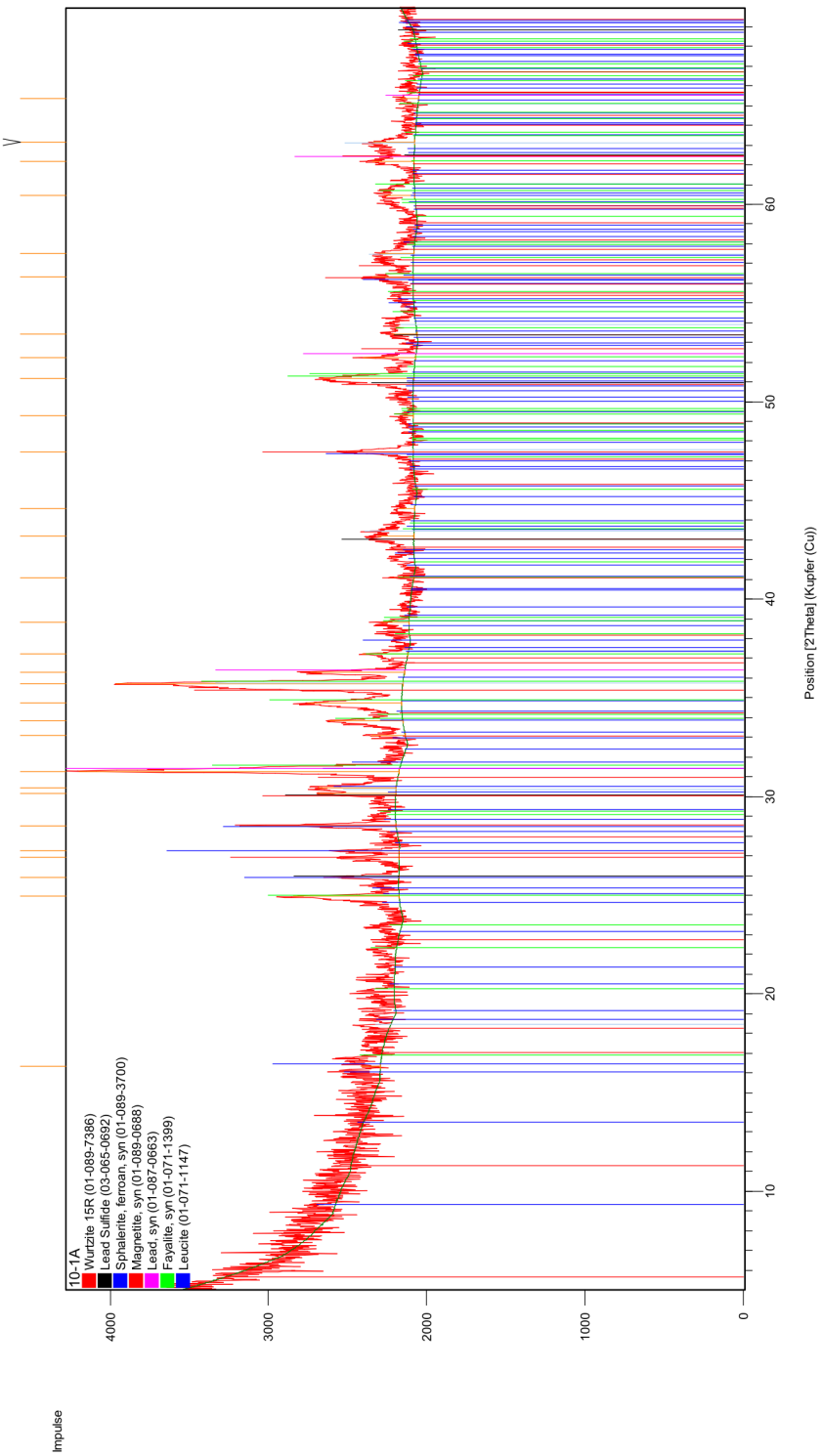

Figure iii.23.: XRD analysis of sample 10-1A. The following phases have been furthermore determined by OM and EMP: Wüstite, iscorite.

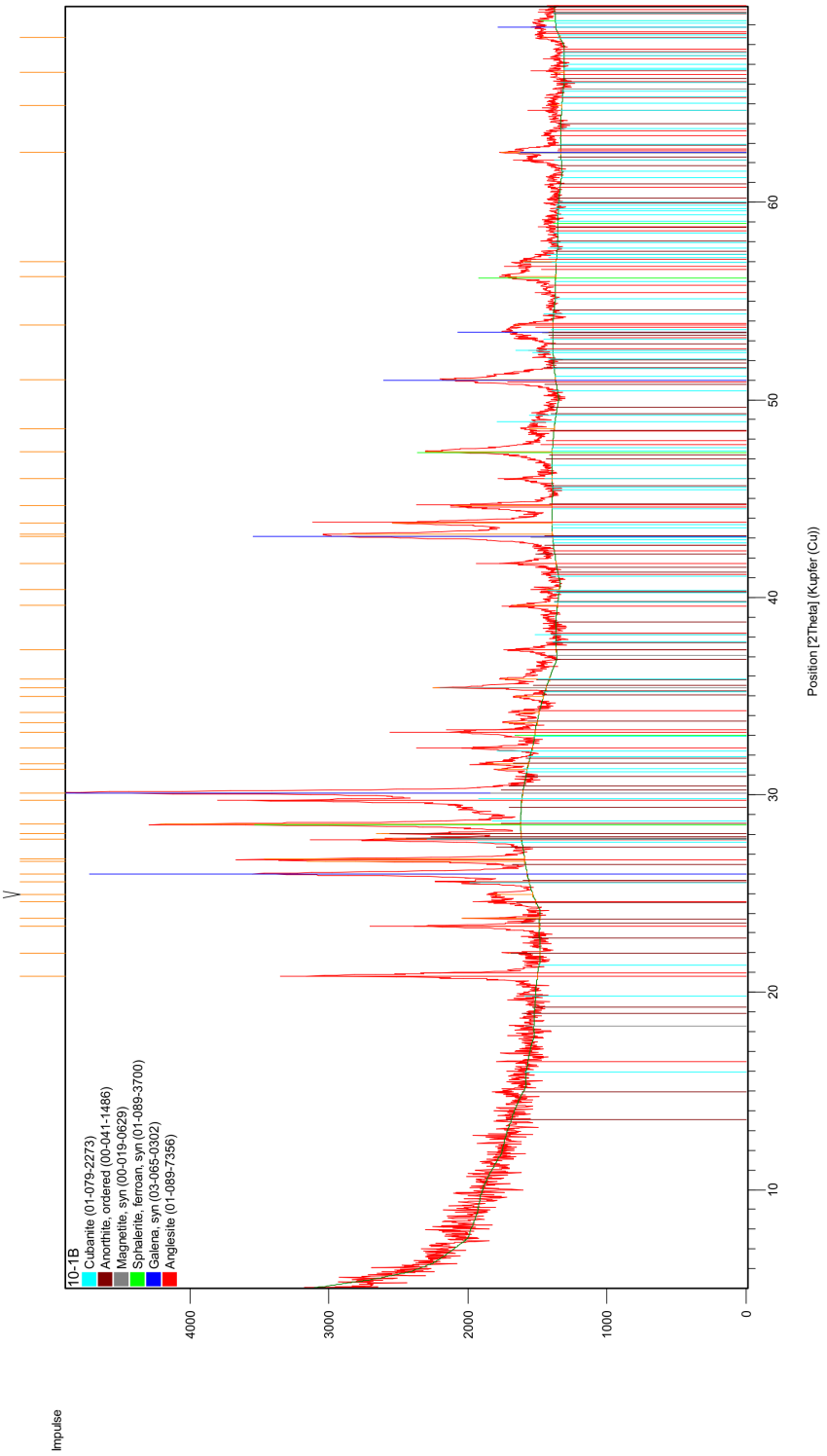

Figure iii.24.: XRD analysis of sample 10-1B. The following phases have been furthermore determined by OM and EMP: Pyrrhotite, bornite *ss*.

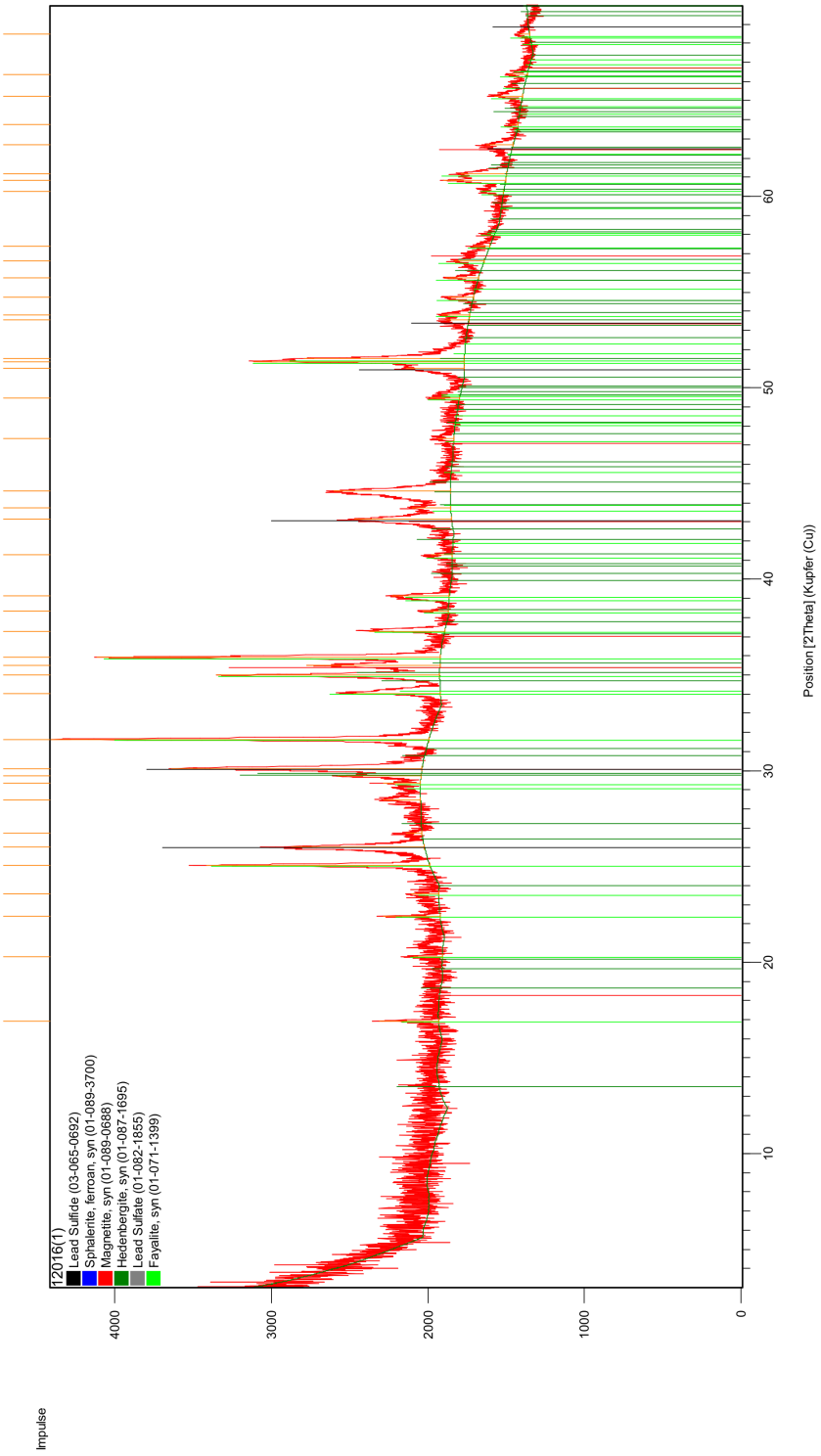

Figure iii.25.: XRD analysis of sample 12016(1). The following phases have been furthermore determined by OM and EMP: Alkali feldspar, leucite; chalcocite *ss*, lead.

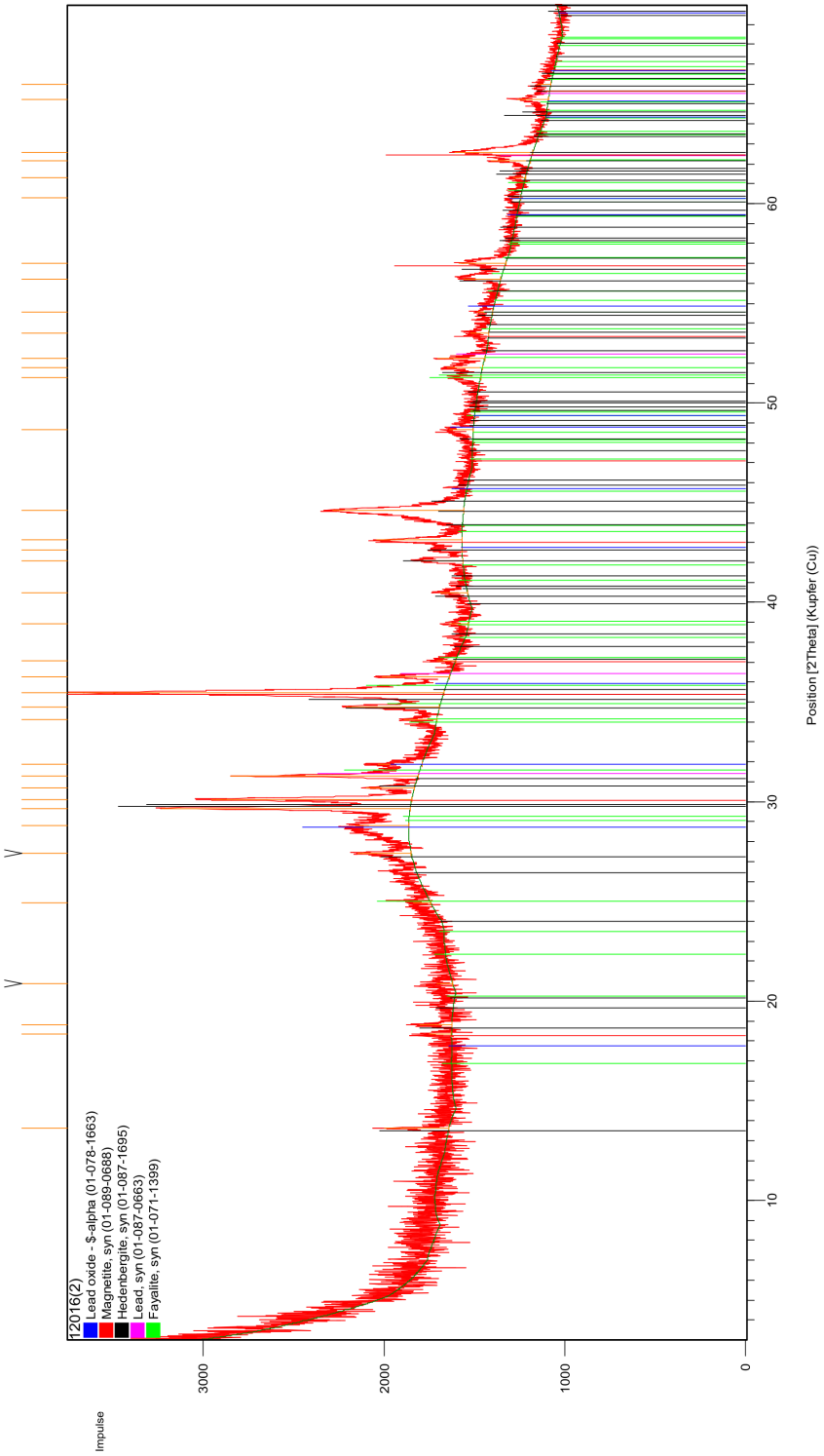

Figure iii.26.: XRD analysis of sample 12016(2). The following phases have been furthermore determined by OM and EMP: Galena, $(Cu,Ni)_2Sb$. Olivine has only been observed accessory.

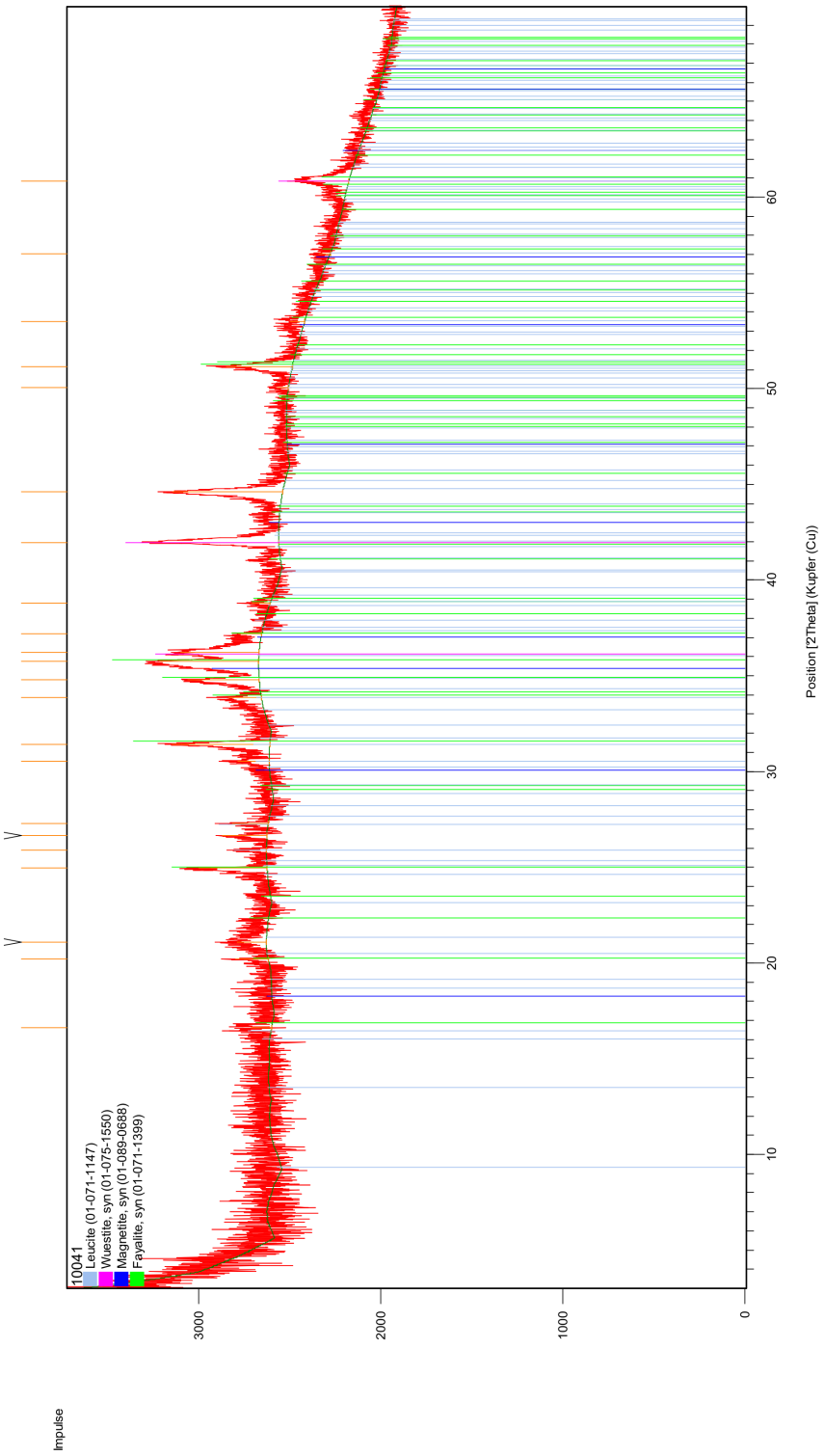

Figure iii.27.: XRD analysis of sample 10041.

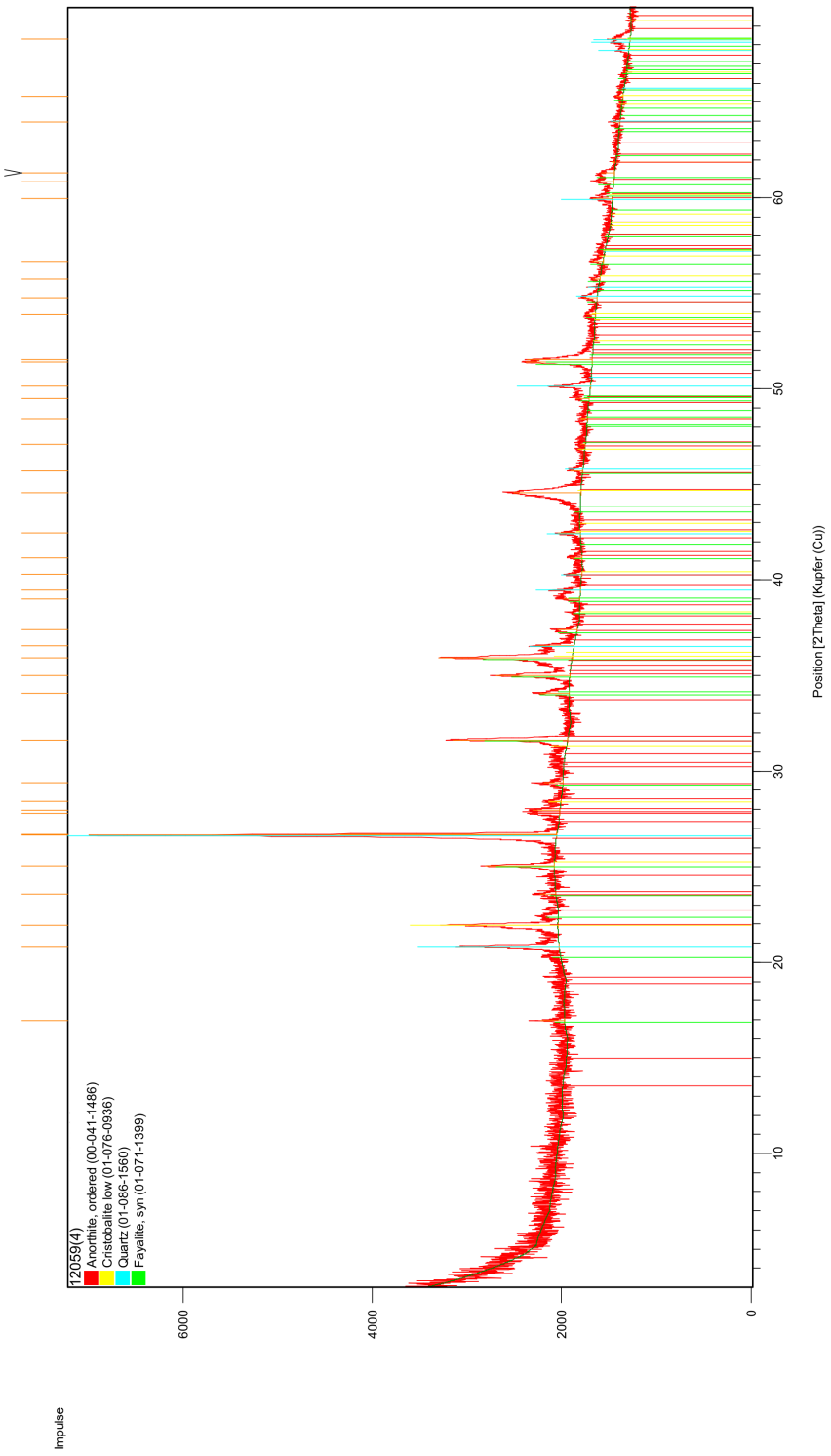

Figure iii.28.: XRD analysis of sample 12059(4).

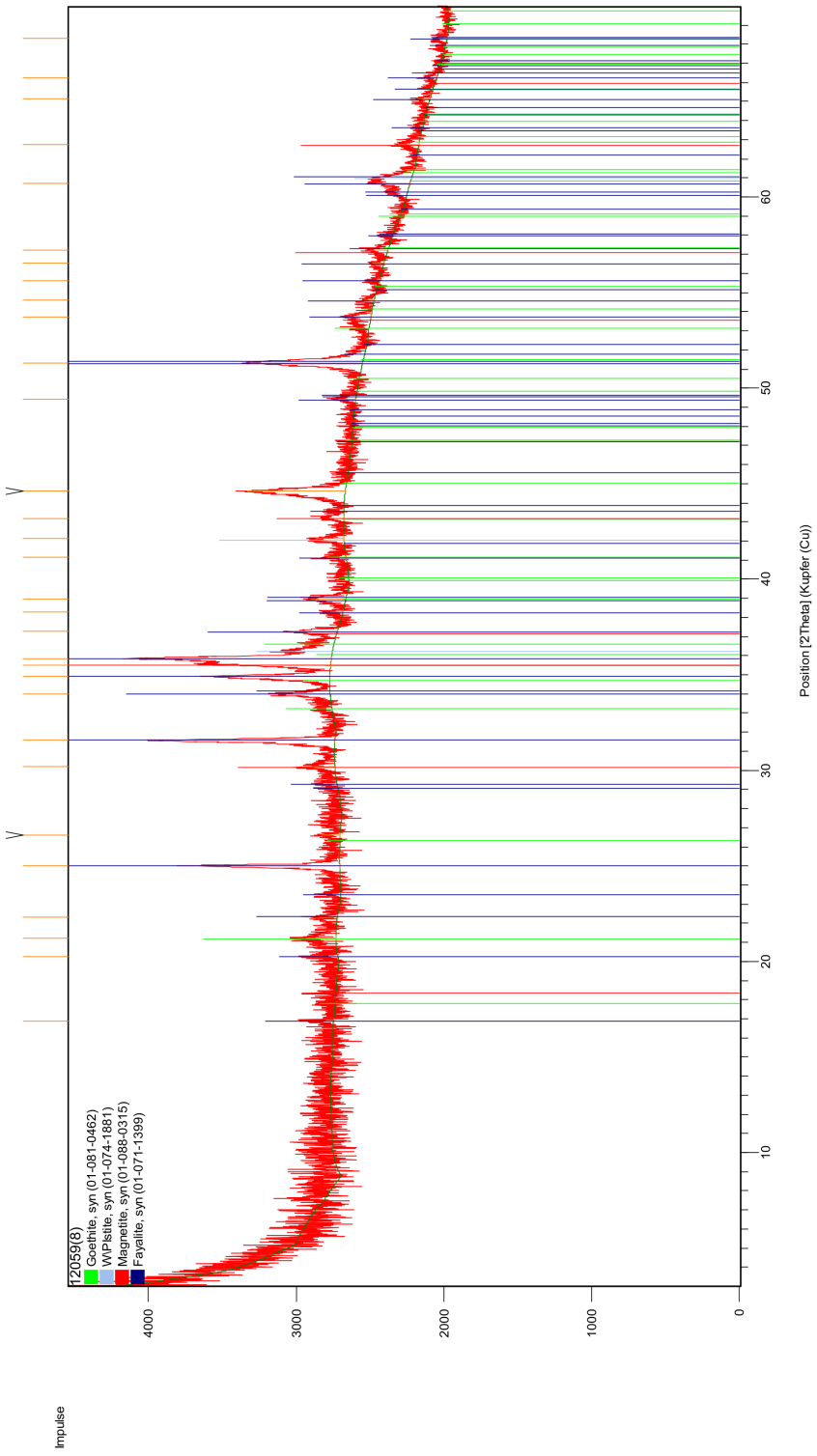

Figure iii.29.: XRD analysis of sample 12059(8).

iv. Electron microprobe analyses

Sample	**11015**	**11015**	**11015**	**11015**	**11015**	**11015**	**11015**	**11015**	**11015**	**11043(3)**	**11043(3)**
No.	**#7**	**#9**	**#21**	**#22**	**#23**	**#24**	**#26**	**#27**	**#28**	**#33**	**#49**
Pb	86.069	86.585	85.659	86.097	85.934	85.741	86.273	86.414	85.707	86.309	86.042
Sb	0.067	< 0.043	< 0.039	0.040	0.097	0.056	0.056	< 0.039	0.122	0.179	0.119
Ag	0.024	< 0	< 0	< 0.025	0.033	0.041	0.025	< 0.024	0.100	0.063	< 0
Mn	0.08	0.049	0.025	0.027	0.016	0.067	< 0.015	0.025	0.028	0.018	0.020
Cu	0.036	0.075	< 0.028	< 0	< 0.028	0.041	< 0.029	< 0.028	< 0.029	< 0	< 0
Cd	< 0.055	0.063	0.055	< 0.055	< 0.053	< 0.053	< 0.054	< 0.054	0.065	< 0.034	0.041
S	13.614	13.511	13.640	13.829	13.963	13.800	13.729	13.690	13.642	13.481	13.547
Total	**99.890**	**100.283**	**99.379**	**99.993**	**100.043**	**99.746**	**100.083**	**100.129**	**99.664**	**100.050**	**99.769**
					Atom-%						
Pb	49.289	49.637	49.231	49.022	48.702	48.862	49.262	49.388	49.120	49.627	49.468
Sb	0.065	0.000	0.000	0.039	0.094	0.054	0.054	0.000	0.119	0.175	0.116
Ag	0.026	0.000	0.000	0.000	0.036	0.045	0.027	0.000	0.110	0.070	0.000
Mn	0.173	0.106	0.054	0.058	0.034	0.144	0.000	0.054	0.061	0.039	0.043
Cu	0.067	0.140	0.000	0.000	0.000	0.076	0.000	0.000	0.000	0.000	0.000
Cd	0.000	0.067	0.058	0.000	0.000	0.000	0.000	0.000	0.069	0.000	0.043
S	50.379	50.050	50.657	50.881	51.135	50.818	50.656	50.559	50.522	50.089	50.329
Total	**100.000**	**100.000**	**100.000**	**100.000**	**100.000**	**100.000**	**100.000**	**100.000**	**100.000**	**100.000**	**100.000**
					Normalised to 1 S atom						
Pb	0.978	0.992	0.972	0.963	0.952	0.962	0.972	0.977	0.972	0.991	0.983
Sb	0.001	0.000	0.000	0.001	0.002	0.001	0.001	0.000	0.002	0.003	0.002
Ag	0.001	0.000	0.000	0.000	0.001	0.001	0.001	0.000	0.002	0.001	0.000
Mn	0.003	0.002	0.001	0.001	0.001	0.003	0.000	0.001	0.001	0.001	0.001
Cu	0.001	0.003	0.000	0.000	0.000	0.001	0.000	0.000	0.000	0.000	0.000
Cd	0.000	0.001	0.001	0.000	0.000	0.000	0.000	0.000	0.001	0.000	0.001
S	1.000	1.000	1.000	1.000	1.000	1.000	1.000	1.000	1.000	1.000	1.000
Total	**1.985**	**1.998**	**1.974**	**1.965**	**1.956**	**1.968**	**1.974**	**1.978**	**1.979**	**1.996**	**1.987**

Table iv.1.: EMP analyses of galena from early ore stage-dominated samples.

Sample	**11043(2)**	**13098(1)**	**13098(1)**	**13098(1)**	**13098(1)**	**13098(1)**	**13098(1)**	**13098(1)**	**13098(1)**	**13099(2)**	**13099(2)**	**13099(2)**	**13099(2)**
No.	**#90**	**#37**	**#43**	**#49**	**#52**	**#54**	**#60**	**#63**	**#64**	**#37**	**#38**	**#40**	**#41**
Pb	85.890	79.916	82.413	85.059	84.207	85.265	87.681	82.329	81.002	86.005	85.822	85.146	85.521
Sb	0.127	0.048	0.080	0.069	0.040	0.114	0.099	0.084	0.058	0.107	0.079	0.342	0.083
Ag	0.156	2.231	1.372	0.753	0.900	0.614	0.117	1.535	1.729	0.047	0.024	0.051	0.043
Mn	0.031	0.022	0.025	0.019	0.023	0.031	< 0.015	< 0.016	0.027	0.033	0.039	0.062	< 0.014
Cu	0.369	0.534	0.382	0.672	0.057	1.144	< 0.028	1.578	0.817	< 0.027	0.032	0.113	< 0
Cd	0.044	0.053	0.038	0.039	0.046	0.043	0.060	0.081	< 0.034	< 0.054	0.082	0.060	< 0.053
S	13.679	14.060	13.933	13.813	13.984	13.886	13.761	14.034	14.002	13.743	13.747	13.718	13.693
Total	**100.296**	**96.864**	**98.243**	**100.424**	**99.257**	**101.097**	**101.718**	**99.641**	**97.635**	**99.935**	**99.825**	**99.492**	**99.340**
						Atom-%							
Pb	48.746	44.887	46.659	47.728	47.649	47.292	49.507	45.385	45.412	49.088	48.975	48.604	49.086
Sb	0.123	0.046	0.077	0.066	0.039	0.108	0.095	0.079	0.055	0.104	0.077	0.332	0.081
Ag	0.170	2.407	1.492	0.812	0.978	0.654	0.127	1.625	1.862	0.052	0.026	0.056	0.047
Mn	0.066	0.047	0.053	0.040	0.049	0.065	0.000	0.000	0.057	0.071	0.084	0.133	0.000
Cu	0.683	0.978	0.705	1.229	0.105	2.069	0.000	2.836	1.493	0.000	0.060	0.210	0.000
Cd	0.046	0.055	0.040	0.040	0.048	0.044	0.062	0.082	0.000	0.000	0.086	0.063	0.000
S	50.166	51.031	50.973	50.084	51.132	49.768	50.208	49.992	50.725	50.686	50.692	50.601	50.786
Total	**100.000**	**100.000**	**100.000**	**100.000**	**100.000**	**100.000**	**100.000**	**100.000**	**100.000**	**100.000**	**100.000**	**100.000**	**100.000**
						Normalised to 1 S atom							
Pb	0.972	0.880	0.915	0.953	0.932	0.950	0.986	0.908	0.895	0.968	0.966	0.961	0.967
Sb	0.002	0.001	0.002	0.001	0.001	0.002	0.002	0.002	0.001	0.002	0.002	0.007	0.002
Ag	0.003	0.047	0.029	0.016	0.019	0.013	0.003	0.033	0.037	0.001	0.001	0.001	0.001
Mn	0.001	0.001	0.001	0.001	0.001	0.001	0.000	0.000	0.001	0.001	0.002	0.003	0.000
Cu	0.014	0.019	0.014	0.025	0.002	0.042	0.000	0.057	0.029	0.000	0.001	0.004	0.000
Cd	0.001	0.001	0.001	0.001	0.001	0.001	0.001	0.002	0.000	0.000	0.002	0.001	0.000
S	1.000	1.000	1.000	1.000	1.000	1.000	1.000	1.000	1.000	1.000	1.000	1.000	1.000
Total	**1.993**	**1.960**	**1.962**	**1.997**	**1.956**	**2.009**	**1.992**	**2.000**	**1.971**	**1.973**	**1.973**	**1.976**	**1.969**

Sample	13099(2)	13099(2)	13099(2)	13099(2)	13099(2)	13099(2)
No.	**#42**	**#46**	**#48**	**#49**	**#66**	**#73**
Pb	85.993	85.372	85.374	85.194	84.428	85.667
Sb	0.046	0.095	0.176	0.289	0.921	0.075
Ag	< 0.022	0.035	0.099	< 0.025	0.036	0.027
Mn	< 0.014	0.024	0.019	0.018	0.019	0.015
Cu	0.037	< 0.03	0.037	0.115	0.444	< 0
Cd	< 0.054	< 0.054	0.074	< 0.054	0.059	0.071
S	13.824	13.765	13.710	13.879	14.071	13.745
Total	**99.900**	**99.291**	**99.489**	**99.495**	**99.978**	**99.600**
			Atom-%			
Pb	48.993	48.885	48.845	48.457	47.267	48.994
Sb	0.045	0.093	0.171	0.280	0.877	0.073
Ag	0.000	0.038	0.109	0.000	0.039	0.030
Mn	0.000	0.052	0.041	0.039	0.040	0.032
Cu	0.069	0.000	0.069	0.213	0.811	0.000
Cd	0.000	0.000	0.078	0.000	0.061	0.075
S	50.894	50.932	50.687	51.011	50.905	50.796
Total	**100.000**	**100.000**	**100.000**	**100.000**	**100.000**	**100.000**
			Normalised to 1 S atom			
Pb	0.963	0.960	0.964	0.950	0.929	0.965
Sb	0.001	0.002	0.003	0.005	0.017	0.001
Ag	0.000	0.001	0.002	0.000	0.001	0.001
Mn	0.000	0.001	0.001	0.001	0.001	0.001
Cu	0.001	0.000	0.001	0.004	0.016	0.000
Cd	0.000	0.000	0.002	0.000	0.001	0.001
S	1.000	1.000	1.000	1.000	1.000	1.000
Total	**1.965**	**1.963**	**1.973**	**1.960**	**1.964**	**1.969**

Table iv.2.: EMP analyses of galena from main ore stage-dominated samples.

Sample	**11079**	**11079**	**11079**	**11090(6)**	**11090(6)**	**11090(6)**	**11090(6)**	**11090(6)**	**11090(6)**	**11090(6)**	**11090(6)**	**11090(6)**	**11090(6)**	**11090(6)**	**11090(6)**	**12055(1)**
No.	**#3**	**#6**	**#29**	**#6**	**#7**	**#8**	**#9**	**#11**	**#14**	**#16**	**#19**	**#22**	**#34**	**#35**	**#37**	**#38**
Pb	87.452	87.896	87.449	86.173	85.989	86.001	85.807	86.677	85.692	87.211	86.542	86.593	86.522	86.504	86.642	86.626
Sb	0.080	0.076	0.080	0.203	0.157	0.164	0.207	0.215	0.237	0.093	0.154	0.202	0.136	0.206	0.119	0.140
Ag	0.031	0.042	< 0.025	0.136	0.105	0.120	0.126	0.119	0.133	0.025	0.118	0.150	0.079	0.171	0.073	0.123
Mn	0.044	0.024	0.030	0.025	0.015	0.019	< 0.015	0.016	0.019	0.038	< 0.015	0.026	0.028	0.022	< 0.015	0.024
Cu	< 0.028	< 0.029	< 0.027	< 0.025	< 0.027	< 0.027	< 0.028	< 0	< 0.028	< 0.026	< 0.028	0.050	0.030	< 0.03	< 0	< 0.03
Cd	< 0	< 0	< 0.04	0.052	0.076	0.066	0.076	0.081	0.053	0.083	0.042	0.056	0.026	0.060	0.046	0.066
S	13.269	13.453	13.506	13.381	13.331	13.383	13.329	13.321	13.301	13.525	13.572	13.538	13.490	13.683	13.570	13.686
Total	**100.876**	**101.491**	**101.065**	**99.970**	**99.673**	**99.753**	**99.545**	**100.429**	**99.435**	**100.975**	**100.428**	**100.615**	**100.311**	**100.646**	**100.450**	**100.665**
								Atom-%								
Pb	50.388	50.190	49.979	49.686	49.763	49.659	49.694	49.941	49.685	49.803	49.507	49.462	49.632	49.207	49.579	49.289
Sb	0.078	0.074	0.078	0.199	0.155	0.161	0.204	0.211	0.234	0.090	0.150	0.196	0.133	0.199	0.116	0.136
Ag	0.034	0.046	0.000	0.151	0.117	0.133	0.140	0.132	0.148	0.027	0.130	0.165	0.087	0.187	0.080	0.134
Mn	0.096	0.052	0.065	0.054	0.033	0.041	0.000	0.035	0.042	0.082	0.000	0.056	0.061	0.047	0.000	0.052
Cu	0.000	0.000	0.000	0.000	0.000	0.000	0.000	0.000	0.000	0.000	0.000	0.093	0.056	0.000	0.000	0.000
Cd	0.000	0.000	0.000	0.055	0.081	0.070	0.081	0.086	0.057	0.087	0.044	0.059	0.027	0.063	0.049	0.069
S	49.403	49.639	49.879	49.855	49.852	49.935	49.881	49.596	49.835	49.910	50.169	49.969	50.004	50.296	50.177	50.320
Total	**100.000**	**100.000**	**100.000**	**100.000**	**100.000**	**100.000**	**100.000**	**100.000**	**100.000**	**100.000**	**100.000**	**100.000**	**100.000**	**100.000**	**100.000**	**100.000**
								Normalised to 1 S atom								
Pb	1.020	1.011	1.002	0.997	0.998	0.994	0.996	1.007	0.997	0.998	0.987	0.990	0.993	0.978	0.988	0.980
Sb	0.002	0.001	0.002	0.004	0.003	0.003	0.004	0.004	0.005	0.002	0.003	0.004	0.003	0.004	0.002	0.003
Ag	0.001	0.001	0.000	0.003	0.002	0.003	0.003	0.003	0.003	0.001	0.003	0.003	0.002	0.004	0.002	0.003
Mn	0.002	0.001	0.001	0.001	0.001	0.001	0.000	0.001	0.001	0.002	0.000	0.001	0.001	0.001	0.000	0.001
Cu	0.000	0.000	0.000	0.000	0.000	0.000	0.000	0.000	0.000	0.000	0.000	0.002	0.001	0.000	0.000	0.000
Cd	0.000	0.000	0.000	0.001	0.002	0.001	0.002	0.002	0.001	0.002	0.001	0.001	0.001	0.001	0.001	0.001
S	1.000	1.000	1.000	1.000	1.000	1.000	1.000	1.000	1.000	1.000	1.000	1.000	1.000	1.000	1.000	1.000
Total	**2.024**	**2.015**	**2.005**	**2.006**	**2.006**	**2.003**	**2.005**	**2.016**	**2.007**	**2.004**	**1.993**	**2.001**	**2.000**	**1.988**	**1.993**	**1.987**

Sample	**12055(1)**	**12055(1)**	**12055(1)**	**12055(1)**	**12055(1)**	**12055(1)**	**14018**	**14018**	**14018**	**14018**	**14018**	**14018**	**14018**	**14018**	**14018**
No.	**#39**	**#43**	**#45**	**#46**	**#51**	**#56**	**#1**	**#2**	**#3**	**#4**	**#14**	**#15**	**#16**	**#17**	**#18**
Pb	86.074	87.016	86.298	86.452	84.686	86.216	86.845	86.880	87.265	87.440	87.199	87.073	86.938	87.196	87.326
Sb	0.506	< 0.041	0.115	0.116	0.739	0.147	0.172	0.188	0.145	0.153	0.179	0.132	0.117	0.233	0.098
Ag	0.392	< 0.025	0.068	0.089	0.559	0.084	0.084	0.070	0.079	0.090	0.095	0.040	0.047	0.143	0.035
Mn	0.018	0.026	0.016	< 0.015	0.020	0.019	< 0.015	< 0.015	< 0.015	0.026	< 0.015	< 0.015	0.016	0.016	0.027
Cu	< 0.028	< 0	< 0.027	< 0	0.629	0.029	< 0	< 0	< 0.024	< 0.027	0.032	< 0.027	< 0	< 0	< 0.028
Cd	0.067	0.049	0.054	0.031	0.058	0.065	0.043	< 0.034	0.066	0.045	0.040	< 0.035	0.050	0.072	0.082
S	13.882	13.607	13.755	13.541	13.780	13.575	13.679	13.747	13.660	13.688	13.827	13.815	13.770	13.809	13.782
Total	**100.939**	**100.698**	**100.306**	**100.229**	**100.471**	**100.135**	**100.823**	**100.885**	**101.215**	**101.442**	**101.372**	**101.060**	**100.938**	**101.469**	**101.350**
							Atom-%								
Pb	48.470	49.686	49.126	49.577	47.498	49.370	49.408	49.317	49.567	49.540	49.206	49.293	49.296	49.182	49.373
Sb	0.485	0.000	0.111	0.113	0.705	0.143	0.167	0.182	0.140	0.148	0.172	0.127	0.113	0.224	0.094
Ag	0.424	0.000	0.074	0.098	0.602	0.092	0.092	0.076	0.086	0.098	0.103	0.043	0.051	0.155	0.038
Mn	0.038	0.056	0.034	0.000	0.042	0.041	0.000	0.000	0.000	0.056	0.000	0.000	0.034	0.034	0.058
Cu	0.000	0.000	0.000	0.000	1.150	0.054	0.000	0.000	0.000	0.000	0.059	0.000	0.000	0.000	0.000
Cd	0.070	0.052	0.057	0.033	0.060	0.069	0.045	0.000	0.069	0.047	0.042	0.000	0.052	0.075	0.085
S	50.514	50.206	50.597	50.179	49.942	50.231	50.288	50.425	50.137	50.112	50.419	50.537	50.454	50.330	50.352
Total	**100.000**	**100.000**	**100.000**	**100.000**	**100.000**	**100.000**	**100.000**	**100.000**	**100.000**	**100.000**	**100.000**	**100.000**	**100.000**	**100.000**	**100.000**
							Normalised to 1 S atom								
Pb	0.960	0.990	0.971	0.988	0.951	0.983	0.982	0.978	0.989	0.989	0.976	0.975	0.977	0.977	0.981
Sb	0.010	0.000	0.002	0.002	0.014	0.003	0.003	0.004	0.003	0.003	0.003	0.003	0.002	0.004	0.002
Ag	0.008	0.000	0.001	0.002	0.012	0.002	0.002	0.002	0.002	0.002	0.002	0.001	0.001	0.003	0.001
Mn	0.001	0.001	0.001	0.000	0.001	0.001	0.000	0.000	0.000	0.001	0.000	0.000	0.001	0.001	0.001
Cu	0.000	0.000	0.000	0.000	0.023	0.001	0.000	0.000	0.000	0.000	0.001	0.000	0.000	0.000	0.000
Cd	0.001	0.001	0.001	0.001	0.001	0.001	0.001	0.000	0.001	0.001	0.001	0.000	0.001	0.001	0.002
S	1.000	1.000	1.000	1.000	1.000	1.000	1.000	1.000	1.000	1.000	1.000	1.000	1.000	1.000	1.000
Total	**1.980**	**1.992**	**1.976**	**1.993**	**2.002**	**1.991**	**1.989**	**1.983**	**1.995**	**1.996**	**1.983**	**1.979**	**1.982**	**1.987**	**1.986**

Table iv.3.: EMP analyses of galena from late ore stage-dominated samples.

Sample	**11043(2)**	**11043(2)**	**11043(2)**
No.	**#89**	**#94**	**#95**
Zn	66.225	65.955	66.283
Fe	0.450	0.617	0.268
Co	< 0	< 0.012	< 0.012
Mn	0.014	< 0.011	< 0.011
Cu	0.146	0.229	0.475
Cd	0.094	0.033	< 0.021
Sb	< 0.039	< 0.028	< 0.031
S	34.024	33.929	34.049
Total	**100.953**	**100.763**	**101.075**
	Atom-%		
Zn	48.560	48.445	48.544
Fe	0.386	0.531	0.230
Co	0.000	0.000	0.000
Mn	0.012	0.000	0.000
Cu	0.110	0.173	0.358
Cd	0.040	0.014	0.000
Sb	0.000	0.000	0.000
S	50.891	50.837	50.868
Total	**100.000**	**100.000**	**100.000**
	Normalised to 1 S atom		
Zn	0.954	0.953	0.954
Fe	0.008	0.010	0.005
Co	0.000	0.000	0.000
Mn	0.000	0.000	0.000
Cu	0.002	0.003	0.007
Cd	0.001	0.000	0.000
Sb	0.000	0.000	0.000
S	1.000	1.000	1.000
Total	**1.965**	**1.967**	**1.966**
mol % FeS	0.8	1.1	0.5
mol % CuS	0.2	0.4	0.73
mole % ZnS	99.0	98.6	98.8

Table iv.4.: EMP analyses of sphalerite from main ore stage-dominated samples.

Sample	**11079**	**11090(6)**	**14018**	**14018**	**14018**	**14018**	**14018**
No.	**#19**	**#25**	**#9**	**#10**	**#11**	**#21**	**#22**
Zn	57.129	62.116	58.184	53.723	54.799	56.954	54.108
Fe	8.505	1.949	6.969	11.110	10.511	8.880	10.798
Co	< 0	< 0	0.021	0.015	0.021	0.014	0.022
Mn	< 0.007	0.020	0.166	0.107	0.102	0.120	0.189
Cu	0.396	0.521	0.031	0.167	< 0.022	< 0.021	< 0.022
Cd	0.118	0.192	0.233	< 0	0.202	0.167	0.230
Sb	< 0.020	0.045	0.048	< 0	0.036	0.024	0.027
S	33.683	33.729	34.023	34.198	34.165	34.075	34.132
Total	**99.831**	**98.572**	**99.675**	**99.320**	**99.836**	**100.234**	**99.506**
			Atom-%				
Zn	41.921	46.390	42.731	39.268	39.975	41.532	39.559
Fe	7.310	1.705	5.995	9.511	8.981	7.584	9.247
Co	0.000	0.000	0.017	0.012	0.017	0.011	0.018
Mn	0.000	0.018	0.145	0.093	0.089	0.104	0.165
Cu	0.299	0.401	0.023	0.126	0.000	0.000	0.000
Cd	0.050	0.083	0.100	0.000	0.086	0.071	0.098
Sb	0.000	0.018	0.019	0.000	0.014	0.009	0.011
S	50.419	51.385	50.970	50.990	50.839	50.688	50.904
Total	**100.000**	**100.000**	**100.000**	**100.000**	**100.000**	**100.000**	**100.000**
			Normalised to 1 S atom				
Zn	0.831	0.903	0.838	0.770	0.786	0.819	0.777
Fe	0.145	0.033	0.118	0.187	0.177	0.150	0.182
Co	0.000	0.000	0.000	0.000	0.000	0.000	0.000
Mn	0.000	0.000	0.003	0.002	0.002	0.002	0.003
Cu	0.006	0.008	0.000	0.002	0.000	0.000	0.000
Cd	0.001	0.002	0.002	0.000	0.002	0.001	0.002
Sb	0.000	0.000	0.000	0.000	0.000	0.000	0.000
S	1.000	1.000	1.000	1.000	1.000	1.000	1.000
Total	**1.983**	**1.946**	**1.962**	**1.961**	**1.967**	**1.973**	**1.964**
mol % FeS	14.8	3.5	12.3	19.4	18.3	15.4	18.9
mol % CuS	0.6	0.8	0.0	0.3	0.0	0.0	0.0
mole % ZnS	84.6	95.7	87.7	80.3	81.7	84.6	81.1

Table iv.5.: EMP analyses of sphalerite from late ore stage-dominated samples.

Sample	**11015**	**11015**	**11015**	**11015**	**11015**	**11015**	**11015**	**11015**	**11015**	**11015**	**11043(3)**	**11043(3)**	**11043(3)**	**11043(3)**
No.	**#1**	**#3**	**#8**	**#12**	**#13**	**#15**	**#16**	**#25**	**#29**	**#32**	**#35**	**#36**	**#38**	**#39**
Fe	46.468	46.587	46.281	46.495	46.360	46.365	46.564	46.213	46.306	46.517	46.754	46.620	46.745	46.453
As	< 0	< 0	0.062	0.712	< 0	0.813	0.964	0.754	0.167	0.189	< 0	< 0	< 0	0.020
Mn	< 0.010	< 0.011	0.020	0.020	0.022	< 0.008	0.023	0.026	0.011	< 0.010	0.300	0.230	0.019	0.250
Co	0.062	0.083	0.073	0.078	0.080	0.068	0.080	0.078	0.086	0.091	0.068	0.072	0.071	0.067
Cu	< 0.021	0.026	0.037	0.024	< 0.021	< 0.021	0.030	0.030	0.024	< 0	< 0.02	< 0	0.021	< 0.021
Cd	0.111	< 0.039	0.061	< 0.039	0.298	0.318	0.203	0.614	0.046	0.063	0.056	0.043	< 0.025	0.035
S	53.875	53.866	53.140	53.459	53.924	53.692	53.808	53.668	54.155	54.560	54.094	54.301	54.159	54.023
Total	**100.516**	**100.562**	**99.674**	**100.788**	**100.684**	**101.256**	**101.672**	**101.383**	**100.795**	**101.420**	**101.272**	**101.266**	**101.015**	**100.848**
							Atom-%							
Fe	33.081	33.142	33.271	33.143	32.978	32.942	32.966	32.841	32.856	32.798	33.065	32.929	33.097	32.957
As	0.000	0.000	0.033	0.378	0.000	0.431	0.509	0.399	0.088	0.099	0.000	0.000	0.000	0.011
Mn	0.000	0.000	0.015	0.014	0.016	0.000	0.017	0.019	0.008	0.000	0.216	0.165	0.014	0.180
Co	0.042	0.056	0.050	0.053	0.054	0.046	0.054	0.053	0.058	0.061	0.046	0.048	0.048	0.045
Cu	0.000	0.016	0.023	0.015	0.000	0.000	0.019	0.019	0.015	0.000	0.000	0.000	0.013	0.000
Cd	0.039	0.000	0.022	0.000	0.105	0.112	0.071	0.217	0.016	0.022	0.020	0.015	0.000	0.012
S	66.798	66.740	66.532	66.369	66.807	66.439	66.346	66.423	66.922	66.998	66.628	66.798	66.785	66.753
Total	**100.000**	**100.000**	**100.000**	**100.000**	**100.000**	**100.000**	**100.000**	**100.000**	**100.000**	**100.000**	**100.000**	**100.000**	**100.000**	**100.000**
							Normalised to 2 S atoms							
Fe	0.990	0.993	1.000	0.999	0.987	0.992	0.994	0.989	0.982	0.979	0.993	0.986	0.991	0.987
As	0.000	0.000	0.001	0.011	0.000	0.013	0.015	0.012	0.003	0.003	0.000	0.000	0.000	0.000
Mn	0.000	0.000	0.000	0.000	0.000	0.000	0.000	0.001	0.000	0.000	0.006	0.005	0.000	0.005
Co	0.001	0.002	0.001	0.002	0.002	0.001	0.002	0.002	0.002	0.002	0.001	0.001	0.001	0.001
Cu	0.000	0.000	0.001	0.000	0.000	0.000	0.001	0.001	0.000	0.000	0.000	0.000	0.000	0.000
Cd	0.001	0.000	0.001	0.000	0.003	0.003	0.002	0.007	0.000	0.001	0.001	0.000	0.000	0.000
S	2.000	2.000	2.000	2.000	2.000	2.000	2.000	2.000	2.000	2.000	2.000	2.000	2.000	2.000
Total	**2.993**	**2.995**	**3.004**	**3.013**	**2.993**	**3.009**	**3.014**	**3.010**	**2.987**	**2.985**	**3.001**	**2.993**	**2.993**	**2.995**

Table iv.6.: EMP analyses of pyrite from early ore stage-dominated samples.

Sample	**11043(2)**	**11043(2)**	**11043(2)**	**11043(2)**	**11043(2)**	**13098(1)**	**13098(1)**	**13098(1)**	**13098(1)**	**13098(1)**	**13098(1)**	**13098(1)**	**13098(1)**	**13099(2)**	**13099(2)**	**13099(2)**
No.	**#67**	**#84**	**#85**	**#86**	**#98**	**#33**	**#46**	**#56**	**#59**	**#61**	**#69**	**#70**	**#71**	**#47**	**#50**	**#65**
Fe	46.798	46.416	46.471	46.238	46.183	46.659	46.587	46.689	46.662	46.901	46.830	46.916	46.711	46.462	46.852	46.602
As	0.037	< 0	0.115	0.126	1.117	1.198	1.618	< 0	0.297	0.949	0.919	0.285	1.049	< 0	< 0	< 0
Mn	< 0.011	0.021	0.013	0.024	< 0.011	0.025	0.026	< 0.01	0.012	< 0.011	0.018	0.013	< 0.011	< 0.011	< 0.011	0.037
Co	0.074	0.074	0.073	0.078	0.082	0.092	0.069	0.080	0.077	0.072	0.066	0.067	0.067	0.075	0.080	0.086
Cu	0.673	0.187	0.266	0.310	0.059	< 0.02	< 0.022	< 0	< 0	< 0.024	0.035	0.043	< 0.021	< 0	< 0.023	< 0
Cd	0.032	0.074	0.045	0.035	0.020	< 0.025	< 0.025	0.033	< 0.024	< 0.025	< 0.024	0.040	< 0.028	< 0.039	< 0	< 0.036
S	53.420	53.914	53.548	53.632	52.855	53.221	52.802	53.534	53.209	53.264	53.499	54.073	53.483	54.430	54.018	54.457
Total	**101.034**	**100.686**	**100.531**	**100.443**	**100.316**	**101.195**	**101.102**	**100.336**	**100.257**	**101.186**	**101.367**	**101.437**	**101.310**	**100.967**	**100.950**	**101.182**
								Atom-%								
Fe	33.282	33.003	33.137	32.968	33.169	33.232	33.301	33.332	33.409	33.384	33.251	33.159	33.186	32.868	33.217	32.910
As	0.020	0.000	0.061	0.067	0.598	0.636	0.862	0.000	0.158	0.503	0.486	0.150	0.556	0.000	0.000	0.000
Mn	0.000	0.015	0.009	0.017	0.000	0.018	0.019	0.000	0.009	0.000	0.013	0.009	0.000	0.000	0.000	0.027
Co	0.050	0.050	0.049	0.053	0.056	0.062	0.047	0.054	0.052	0.049	0.044	0.045	0.045	0.050	0.054	0.058
Cu	0.421	0.117	0.167	0.194	0.037	0.000	0.000	0.000	0.000	0.000	0.022	0.027	0.000	0.000	0.000	0.000
Cd	0.011	0.026	0.016	0.012	0.007	0.000	0.000	0.012	0.000	0.000	0.000	0.014	0.000	0.000	0.000	0.000
S	66.167	66.764	66.500	66.600	66.113	66.017	65.735	66.562	66.349	66.029	66.157	66.559	66.176	67.061	66.699	66.977
Total	**100.000**	**100.000**	**100.000**	**100.000**	**100.000**	**100.000**	**100.000**	**100.000**	**100.000**	**100.000**	**100.000**	**100.000**	**100.000**	**100.000**	**100.000**	**100.000**
								Normalised to 2 S atoms								
Fe	1.006	0.989	0.997	0.990	1.003	1.007	1.013	1.002	1.007	1.011	1.005	0.996	1.003	0.980	0.996	0.983
As	0.001	0.000	0.002	0.002	0.018	0.019	0.026	0.000	0.005	0.015	0.015	0.005	0.017	0.000	0.000	0.000
Mn	0.000	0.000	0.000	0.001	0.000	0.001	0.001	0.000	0.000	0.000	0.000	0.000	0.000	0.000	0.000	0.001
Co	0.002	0.001	0.001	0.002	0.002	0.002	0.001	0.002	0.002	0.001	0.001	0.001	0.001	0.001	0.002	0.002
Cu	0.013	0.004	0.005	0.006	0.001	0.000	0.000	0.000	0.000	0.000	0.001	0.001	0.000	0.000	0.000	0.000
Cd	0.000	0.001	0.000	0.000	0.000	0.000	0.000	0.000	0.000	0.000	0.000	0.000	0.000	0.000	0.000	0.000
S	2.000	2.000	2.000	2.000	2.000	2.000	2.000	2.000	2.000	2.000	2.000	2.000	2.000	2.000	2.000	2.000
Total	**3.021**	**2.995**	**3.006**	**3.000**	**3.025**	**3.028**	**3.041**	**3.004**	**3.014**	**3.028**	**3.022**	**3.004**	**3.021**	**2.982**	**2.998**	**2.985**

Sample	**13099(2)**
No.	**#74**
Fe	46.423
As	1.253
Mn	0.012
Co	0.075
Cu	< 0
Cd	< 0.038
S	53.561
Total	**101.324**
	Atom-%
Fe	32.982
As	0.664
Mn	0.009
Co	0.050
Cu	0.000
Cd	0.000
S	66.275
Total	**100.000**
	Normalised to 2 S atoms
Fe	0.995
As	0.020
Mn	0.000
Co	0.002
Cu	0.000
Cd	0.000
S	2.000
Total	**3.017**

Table iv.7.: EMP analyses of pyrite from main ore stage-dominated samples.

Sample	**11079**	**11079**	**11079**	**11079**	**11079**	**11079**	**11079**	**11079**	**11079**	**11079**	**11079**	**11079**	**11079**	**11090(6)**	**11090(6)**	**11090(6)**
No.	**#1**	**#2**	**#9**	**#10**	**#12**	**#15**	**#21**	**#24**	**#26**	**#27**	**#28**	**#31**	**#32**	**#12**	**#20**	**#24**
Fe	45.681	46.232	46.006	46.348	46.071	46.245	46.038	45.625	45.823	45.536	45.558	45.607	45.983	46.501	45.675	46.422
As	< 0	0.022	0.843	< 0	< 0	< 0.014	< 0	< 0	< 0.015	0.821	0.062	0.071	0.059	< 0.011	< 0.019	1.516
Mn	0.023	< 0.008	0.016	0.021	0.019	0.015	0.017	0.021	0.022	< 0.007	< 0.007	0.013	0.018	0.022	0.016	< 0.011
Co	< 0	< 0	< 0	< 0	< 0	< 0	< 0	< 0	< 0	< 0	< 0	< 0	< 0	0.092	0.079	0.071
Cu	< 0.019	0.350	0.191	0.064	0.140	0.049	0.148	0.205	0.301	< 0.024	0.386	0.031	< 0.021	< 0.020	0.590	< 0.024
Cd	< 0.029	0.161	< 0.029	< 0.028	0.096	0.076	< 0.029	< 0.028	0.090	0.032	< 0.03	0.046	0.050	0.034	< 0.017	0.050
S	52.684	52.765	51.398	52.394	53.215	52.612	52.944	53.018	53.084	52.982	52.998	52.990	52.970	51.896	51.641	50.782
Total	**98.388**	**99.530**	**98.454**	**98.827**	**99.541**	**98.997**	**99.147**	**98.869**	**99.320**	**99.371**	**99.004**	**98.758**	**99.080**	**98.545**	**98.001**	**98.841**
								Atom-%								
Fe	33.224	33.347	33.733	33.656	33.124	33.503	33.216	33.002	33.038	32.882	32.942	33.036	33.230	33.940	33.529	34.112
As	0.000	0.012	0.461	0.000	0.000	0.000	0.000	0.000	0.000	0.442	0.033	0.038	0.032	0.000	0.000	0.830
Mn	0.017	0.000	0.012	0.016	0.014	0.011	0.012	0.015	0.016	0.000	0.000	0.010	0.013	0.016	0.012	0.000
Co	0.000	0.000	0.000	0.000	0.000	0.000	0.000	0.000	0.000	0.000	0.000	0.000	0.000	0.064	0.055	0.049
Cu	0.000	0.222	0.123	0.041	0.088	0.031	0.094	0.130	0.191	0.000	0.245	0.020	0.000	0.000	0.381	0.000
Cd	0.000	0.058	0.000	0.000	0.034	0.027	0.000	0.000	0.032	0.011	0.000	0.017	0.018	0.012	0.000	0.018
S	66.734	66.285	65.635	66.262	66.634	66.382	66.528	66.789	66.657	66.632	66.741	66.850	66.668	65.968	66.023	64.990
Total	**100.000**	**100.000**	**100.000**	**100.000**	**100.000**	**100.000**	**100.000**	**100.000**	**100.000**	**100.000**	**100.000**	**100.000**	**100.000**	**100.000**	**100.000**	**100.000**
								Normalised to 2 S atoms								
Fe	0.996	1.006	1.028	1.016	0.994	1.009	0.999	0.988	0.991	0.987	0.987	0.988	0.997	1.029	1.016	1.050
As	0.000	0.000	0.014	0.000	0.000	0.000	0.000	0.000	0.000	0.013	0.001	0.001	0.001	0.000	0.000	0.026
Mn	0.001	0.000	0.000	0.000	0.000	0.000	0.000	0.000	0.000	0.000	0.000	0.000	0.000	0.000	0.000	0.000
Co	0.000	0.000	0.000	0.000	0.000	0.000	0.000	0.000	0.000	0.000	0.000	0.000	0.000	0.002	0.002	0.002
Cu	0.000	0.007	0.004	0.001	0.003	0.001	0.003	0.004	0.006	0.000	0.007	0.001	0.000	0.000	0.012	0.000
Cd	0.000	0.002	0.000	0.000	0.001	0.001	0.000	0.000	0.001	0.000	0.000	0.000	0.001	0.000	0.000	0.001
S	2.000	2.000	2.000	2.000	2.000	2.000	2.000	2.000	2.000	2.000	2.000	2.000	2.000	2.000	2.000	2.000
Total	**2.996**	**3.015**	**3.046**	**3.018**	**2.998**	**3.011**	**3.002**	**2.993**	**2.998**	**3.001**	**2.995**	**2.991**	**2.999**	**3.032**	**3.029**	**3.077**

Sample	**11090(6)**	**11090(6)**	**11090(6)**	**11090(6)**	**12055(1)**	**12055(1)**	**12055(1)**	**12055(1)**	**12055(1)**	**12055(1)**
No.	**#27**	**#28**	**#30**	**#33**	**#40**	**#41**	**#42**	**#44**	**#50**	**#57**
Fe	46.180	46.445	46.566	46.453	46.490	46.571	46.002	46.019	46.094	46.241
As	< 0	< 0.017	< 0	0.720	0.040	< 0.020	0.979	1.453	1.611	0.201
Mn	0.027	< 0.01	< 0.010	< 0.010	0.011	0.012	0.014	0.016	< 0.010	< 0.011
Co	0.067	0.080	0.078	0.080	0.077	0.073	0.070	0.072	0.076	0.071
Cu	0.097	0.030	< 0.020	< 0.019	< 0.020	0.035	0.094	< 0.022	< 0	0.495
Cd	0.030	< 0	0.110	0.049	0.113	0.082	0.040	0.423	0.435	0.170
S	53.369	52.897	52.202	52.043	53.544	52.722	52.935	52.415	51.236	53.491
Total	**99.770**	**99.452**	**98.956**	**99.345**	**100.275**	**99.495**	**100.134**	**100.398**	**99.452**	**100.669**
					Atom-%					
Fe	33.147	33.492	33.839	33.728	33.215	33.600	33.053	33.172	33.679	32.983
As	0.000	0.000	0.000	0.390	0.021	0.000	0.524	0.781	0.877	0.107
Mn	0.020	0.000	0.000	0.000	0.008	0.009	0.010	0.012	0.000	0.000
Co	0.046	0.055	0.054	0.055	0.052	0.050	0.048	0.049	0.053	0.048
Cu	0.061	0.019	0.000	0.000	0.000	0.022	0.059	0.000	0.000	0.310
Cd	0.011	0.000	0.040	0.018	0.040	0.029	0.014	0.151	0.158	0.060
S	66.716	66.434	66.068	65.810	66.626	66.247	66.242	65.803	65.200	66.451
Total	**100.000**	**100.000**	**100.000**	**100.000**	**100.000**	**100.000**	**100.000**	**100.000**	**100.000**	**100.000**
					Normalised to 2 S atoms					
Fe	0.994	1.008	1.024	1.025	0.997	1.014	0.998	1.008	1.033	0.993
As	0.000	0.000	0.000	0.012	0.001	0.000	0.016	0.024	0.027	0.003
Mn	0.001	0.000	0.000	0.000	0.000	0.000	0.000	0.000	0.000	0.000
Co	0.001	0.002	0.002	0.002	0.002	0.002	0.001	0.001	0.002	0.001
Cu	0.002	0.001	0.000	0.000	0.000	0.001	0.002	0.000	0.000	0.009
Cd	0.000	0.000	0.001	0.001	0.001	0.001	0.000	0.005	0.005	0.002
S	2.000	2.000	2.000	2.000	2.000	2.000	2.000	2.000	2.000	2.000
Total	**2.998**	**3.011**	**3.027**	**3.039**	**3.001**	**3.018**	**3.018**	**3.038**	**3.066**	**3.009**

Table iv.8.: EMP analyses of pyrite from late ore stage-dominated samples.

Sample	**14018**	**14018**	**14018**	**14018**	**14018**	**14018**	**14018**
No.	**#6**	**#8**	**#13**	**#19**	**#20**	**#23**	**#24**
Fe	47.070	46.885	47.159	46.606	46.710	45.902	46.923
As	0.450	1.386	0.496	1.903	0.967	0.351	0.504
Mn	0.104	0.126	0.040	0.296	0.013	0.038	0.139
Co	0.122	0.078	0.092	0.070	0.084	0.196	0.097
Ni	0.141	0.017	< 0.014	0.177	0.190	1.111	0.125
S	54.271	53.316	53.798	52.797	53.370	54.246	54.152
Total	**102.158**	**101.808**	**101.585**	**101.849**	**101.334**	**101.844**	**101.940**
			Atom-%				
Fe	33.083	33.254	33.363	33.169	33.209	32.343	33.053
As	0.236	0.733	0.262	1.009	0.512	0.184	0.265
Mn	0.074	0.091	0.029	0.214	0.009	0.027	0.100
Co	0.081	0.052	0.062	0.047	0.057	0.131	0.065
Ni	0.094	0.011	0.000	0.120	0.129	0.745	0.084
S	66.432	65.859	66.285	65.441	66.084	66.569	66.434
Total	**100.000**	**100.000**	**100.000**	**100.000**	**100.000**	**100.000**	**100.000**
			Normalised to 2 S atoms				
Fe	0.996	1.010	1.007	1.014	1.005	0.972	0.995
As	0.007	0.022	0.008	0.031	0.016	0.006	0.008
Mn	0.002	0.003	0.001	0.007	0.000	0.001	0.003
Co	0.002	0.002	0.002	0.001	0.002	0.004	0.002
Ni	0.003	0.000	0.000	0.004	0.004	0.022	0.003
S	2.000	2.000	2.000	2.000	2.000	2.000	2.000
Total	**3.011**	**3.037**	**3.017**	**3.056**	**3.026**	**3.004**	**3.010**

Table iv.9.: EMP analyses of marcasite from late ore stage-dominated sample 14018.

Sample	**14018**
No.	**#30**
Fe	59.603
Mn	0.293
Co	0.095
Sb	0.034
S	39.991
Total	**100.016**
Atom-%	
Fe	45.970
Mn	0.230
Co	0.069
Sb	0.012
S	53.719
Total	**100.000**
Normalised to 1 S atom	
Fe	0.856
Mn	0.004
Co	0.001
Sb	0.000
S	1.000
Total	**1.862**

Table iv.10.: EMP analysis of pyrrhotite from late ore stage-dominated sample 14018.

Sample	11015	11043(3)	11043(3)	11043(3)	11043(3)	11043(3)	11043(3)	11043(3)	11043(3)	11043(3)
No.	**#5**	**#29**	**#31**	**#40**	**#41**	**#43**	**#45**	**#46**	**#52**	**#53**
Fe	35.036	35.935	35.976	35.833	35.867	35.856	35.849	35.866	35.990	35.889
As	44.192	42.637	41.986	41.098	41.175	41.383	41.846	41.448	41.311	41.845
Mn	0.129	0.027	0.024	0.024	0.031	0.039	0.031	0.029	0.030	0.018
Co	0.063	0.063	0.055	0.052	0.049	0.056	0.055	0.059	0.059	0.050
Ni	< 0	< 0.021	0.021	< 0.013	< 0.014	0.015	< 0	< 0.014	< 0.014	< 0.011
Cu	0.104	0.025	0.076	0.025	< 0	< 0.020	0.037	< 0.021	< 0.021	0.027
Sb	0.211	0.301	0.094	0.323	0.330	0.290	0.133	0.213	0.199	0.227
S	19.114	20.108	20.527	20.600	20.740	20.561	20.538	20.806	20.840	20.349
Total	**98.849**	**99.096**	**98.759**	**97.955**	**98.192**	**98.200**	**98.489**	**98.421**	**98.429**	**98.405**
					Atom-%					
Fe	34.477	34.884	34.844	34.921	34.842	34.896	34.805	34.757	34.855	34.934
As	32.414	30.851	30.311	29.854	29.814	30.020	30.283	29.939	29.822	30.361
Mn	0.129	0.027	0.024	0.024	0.031	0.039	0.031	0.029	0.030	0.018
Co	0.059	0.058	0.050	0.048	0.045	0.052	0.051	0.054	0.054	0.046
Ni	0.000	0.000	0.019	0.000	0.000	0.014	0.000	0.000	0.000	0.000
Cu	0.068	0.016	0.049	0.016	0.000	0.000	0.024	0.000	0.000	0.018
Sb	0.095	0.134	0.042	0.144	0.147	0.129	0.059	0.095	0.088	0.101
S	32.758	33.996	34.625	34.964	35.089	34.850	34.728	35.115	35.151	34.497
Total	**100.000**	**100.000**	**100.000**	**100.000**	**100.000**	**100.000**	**100.000**	**100.000**	**100.000**	**100.000**
					Normalised to 1 S atom					
Fe	1.052	1.026	1.006	0.999	0.993	1.001	1.002	0.990	0.992	1.013
As	0.990	0.907	0.875	0.854	0.850	0.861	0.872	0.853	0.848	0.880
Mn	0.004	0.001	0.001	0.001	0.001	0.001	0.001	0.001	0.001	0.001
Co	0.002	0.002	0.001	0.001	0.001	0.001	0.001	0.002	0.002	0.001
Ni	0.000	0.000	0.001	0.000	0.000	0.000	0.000	0.000	0.000	0.000
Cu	0.002	0.000	0.001	0.000	0.000	0.000	0.001	0.000	0.000	0.001
Sb	0.003	0.004	0.001	0.004	0.004	0.004	0.002	0.003	0.003	0.003
S	1.000	1.000	1.000	1.000	1.000	1.000	1.000	1.000	1.000	1.000
Total	**3.053**	**2.941**	**2.887**	**2.859**	**2.849**	**2.869**	**2.879**	**2.847**	**2.845**	**2.898**

Table iv.11.: EMP analyses of arsenopyrite from early stage-dominated samples.

Sample	13099(2)	13099(2)	13099(2)	13099(2)	13099(2)	12055(1)
No.	**#34**	**#35**	**#45**	**#69**	**#71**	**#62**
Fe	34.228	34.171	34.064	34.988	35.535	35.297
As	43.533	43.903	42.903	42.127	41.451	40.902
Mn	0.044	0.056	0.199	0.018	0.031	0.029
Co	0.053	0.060	0.060	0.073	0.086	0.057
Ni	< 0.015	< 0	0.042	0.138	0.033	< 0
Cu	0.047	0.024	0.026	0.814	0.325	0.173
Sb	0.041	0.044	< 0.029	0.054	0.174	0.130
S	19.777	19.254	20.152	21.065	21.193	21.191
Total	**97.723**	**97.512**	**97.446**	**99.277**	**98.828**	**97.779**
			Atom-%			
Fe	33.800	33.974	33.575	33.686	34.240	34.286
As	32.043	32.536	31.520	30.233	29.771	29.614
Mn	0.044	0.057	0.199	0.018	0.030	0.029
Co	0.050	0.057	0.056	0.067	0.079	0.052
Ni	0.000	0.000	0.039	0.126	0.030	0.000
Cu	0.031	0.016	0.017	0.524	0.209	0.112
Sb	0.019	0.020	0.000	0.024	0.077	0.058
S	34.013	33.340	34.593	35.322	35.565	35.849
Total	**100.000**	**100.000**	**100.000**	**100.000**	**100.000**	**100.000**
			Normalised to 1 S atom			
Fe	0.994	1.019	0.971	0.954	0.963	0.956
As	0.942	0.976	0.911	0.856	0.837	0.826
Mn	0.001	0.002	0.006	0.000	0.001	0.001
Co	0.001	0.002	0.002	0.002	0.002	0.001
Ni	0.000	0.000	0.001	0.004	0.001	0.000
Cu	0.001	0.000	0.000	0.015	0.006	0.003
Sb	0.001	0.001	0.000	0.001	0.002	0.002
S	1.000	1.000	1.000	1.000	1.000	1.000
Total	**2.940**	**2.999**	**2.891**	**2.831**	**2.812**	**2.789**

Table iv.12.: EMP analyses of arsenopyrite from main [13099(2)] and late ore stage-dominated samples [12055(1)].

Sample	**11015**	**11015**
No.	**#10**	**#14**
Cu	34.848	34.716
Fe	30.183	29.776
Mn	0.023	0.021
Co	0.045	0.051
Sn	< 0	< 0.026
S	35.741	35.412
Total	**100.840**	**99.976**
	Atom-%	
Cu	24.868	24.995
Fe	24.509	24.394
Mn	0.019	0.017
Co	0.035	0.040
Sn	0.000	0.000
S	50.545	50.527
Total	**100.000**	**100.000**
	Normalised to 2 S atoms	
Cu	0.984	0.989
Fe	0.970	0.966
Mn	0.001	0.001
Co	0.001	0.002
Sn	0.000	0.000
S	2.000	2.000
Total	**3.956**	**3.957**

Table iv.13.: EMP analyses of chalcopyrite from early ore stage-dominated sample 11015.

Sample	**11043(2)**	**11043(2)**	**11043(2)**	**13098(1)**	**13098(1)**	**13098(1)**	**13098(1)**	**13099(2)**	**13099(2)**	**13099(2)**	**13099(2)**	**13099(2)**	**13099(2)**
No.	**#80**	**#82**	**#83**	**#35**	**#36**	**#47**	**#51**	**#52**	**#54**	**#55**	**#57**	**#58**	**#59**
Cu	35.607	34.776	35.214	33.439	33.913	33.678	33.524	34.649	34.284	34.183	34.171	34.432	34.424
Fe	29.238	29.706	29.474	30.290	30.404	30.315	30.451	29.937	29.949	30.149	29.573	29.981	30.150
Mn	0.014	0.013	0.012	0.039	0.012	0.011	0.011	0.018	< 0.011	0.012	0.019	0.031	0.012
Co	0.046	0.038	0.046	0.039	0.038	0.056	0.044	0.051	0.041	0.043	0.049	0.049	0.051
Sn	0.224	0.315	0.119	< 0.030	< 0.030	0.032	< 0	< 0	< 0.030	< 0.027	0.087	< 0	< 0.027
S	35.333	35.274	35.282	35.290	35.362	35.320	35.049	35.842	35.585	35.631	35.603	35.754	35.877
Total	**100.462**	**100.122**	**100.147**	**99.097**	**99.729**	**99.412**	**99.079**	**100.497**	**99.859**	**100.018**	**99.502**	**100.247**	**100.514**
						Atom-%							
Cu	25.568	25.045	25.344	24.243	24.460	24.358	24.347	24.776	24.669	24.560	24.656	24.679	24.602
Fe	23.890	24.344	24.138	24.989	24.954	24.950	25.165	24.359	24.522	24.649	24.281	24.452	24.519
Mn	0.012	0.011	0.010	0.033	0.010	0.009	0.009	0.015	0.000	0.010	0.016	0.026	0.010
Co	0.036	0.030	0.036	0.030	0.030	0.044	0.034	0.039	0.032	0.033	0.038	0.038	0.039
Sn	0.086	0.121	0.046	0.000	0.000	0.012	0.000	0.000	0.000	0.000	0.034	0.000	0.000
S	50.280	50.345	50.324	50.705	50.547	50.627	50.445	50.791	50.744	50.734	50.911	50.786	50.813
Total	**100.000**	**100.000**	**100.000**	**100.000**	**100.000**	**100.000**	**100.000**	**100.000**	**100.000**	**100.000**	**100.000**	**100.000**	**100.000**
						Normalised to 2 S atoms							
Cu	1.017	0.995	1.007	0.956	0.968	0.962	0.965	0.976	0.972	0.968	0.969	0.972	0.968
Fe	0.950	0.967	0.959	0.986	0.987	0.986	0.998	0.959	0.966	0.972	0.954	0.963	0.965
Mn	0.000	0.000	0.000	0.001	0.000	0.000	0.000	0.001	0.000	0.000	0.001	0.001	0.000
Co	0.001	0.001	0.001	0.001	0.001	0.002	0.001	0.002	0.001	0.001	0.001	0.001	0.002
Sn	0.003	0.005	0.002	0.000	0.000	0.000	0.000	0.000	0.000	0.000	0.001	0.000	0.000
S	2.000	2.000	2.000	2.000	2.000	2.000	2.000	2.000	2.000	2.000	2.000	2.000	2.000
Total	**3.973**	**3.968**	**3.970**	**3.944**	**3.957**	**3.950**	**3.965**	**3.937**	**3.940**	**3.942**	**3.926**	**3.937**	**3.935**

Sample	**13099(2)**	**13099(2)**	**13099(2)**	**13099(2)**	**13099(2)**
No.	**#60**	**#61**	**#64**	**#67**	**#72**
Cu	34.324	34.385	34.471	34.125	34.284
Fe	29.725	29.795	30.152	29.902	29.492
Mn	0.030	< 0.011	< 0.010	0.065	< 0.010
Co	0.043	0.051	0.056	0.042	0.048
Sn	< 0.026	< 0.026	< 0.027	< 0.032	< 0
S	35.769	35.781	35.562	35.611	35.654
Total	**99.891**	**100.012**	**100.241**	**99.745**	**99.478**
			Atom-%		
Cu	24.670	24.688	24.738	24.570	24.739
Fe	24.310	24.342	24.622	24.499	24.215
Mn	0.025	0.000	0.000	0.054	0.000
Co	0.033	0.039	0.043	0.033	0.037
Sn	0.000	0.000	0.000	0.000	0.000
S	50.948	50.912	50.577	50.814	50.986
Total	**100.000**	**100.000**	**100.000**	**100.000**	**100.000**
			Normalised to 2 S atoms		
Cu	0.968	0.970	0.978	0.967	0.970
Fe	0.954	0.956	0.974	0.964	0.950
Mn	0.001	0.000	0.000	0.002	0.000
Co	0.001	0.002	0.002	0.001	0.001
Sn	0.000	0.000	0.000	0.000	0.000
S	2.000	2.000	2.000	2.000	2.000
Total	**3.925**	**3.928**	**3.954**	**3.935**	**3.922**

Table iv.14.: EMP analyses of chalcopyrite from main ore stage-dominated samples.

Sample	**11079**	**11079**	**11079**	**11079**	**11079**	**11079**	**11079**	**11090(6)**	**11090(6)**	**11090(6)**	**11090(6)**	**11090(6)**	**14018**	**14018**	**14018**	**14018**
No.	**#7**	**#8**	**#11**	**#13**	**#14**	**#18**	**#23**	**#10**	**#17**	**#21**	**#23**	**#36**	**#5**	**#12**	**#26**	**#27**
Cu	34.847	34.645	34.617	34.287	34.595	34.573	34.8	34.154	34.244	34.2	34.161	33.941	33.026	33.699	33.15	33.514
Fe	29.736	30.191	30.219	29.76	30.129	30.631	30.054	29.537	29.343	29.377	29.21	29.092	30.998	30.986	31.305	30.768
Mn	< 0.008	0.022	0.016	< 0.008	0.016	0.026	0.022	< 0.009	0.013	< 0.010	0.013	< 0.011	1.005	0.423	1.064	0.751
Co	< 0	< 0	< 0	< 0	< 0	< 0	< 0	0.047	0.044	0.056	0.043	0.046	0.04	0.048	0.048	0.045
Sn	0.028	0.093	< 0.025	0.075	0.045	0.227	< 0.026	< 0	0.043	< 0.031	< 0.026	< 0.021	0.198	0.028	0.098	0.099
S	35.086	34.602	34.945	34.919	34.69	34.536	35.074	34.181	34.396	34.862	34.506	34.683	35.339	35.373	35.289	35.466
Total	**99.697**	**99.553**	**99.797**	**99.041**	**99.475**	**99.993**	**99.95**	**97.919**	**98.083**	**98.495**	**97.933**	**97.762**	**100.606**	**100.557**	**100.954**	**100.643**
								Atom-%								
Cu	25.179	25.126	25.024	24.794	25.105	24.984	25.100	25.196	25.201	25.004	25.147	24.988	23.650	24.137	23.671	23.976
Fe	24.449	24.916	24.857	24.488	24.879	25.188	24.666	24.795	24.572	24.440	24.468	24.372	25.259	25.254	25.437	25.047
Mn	0.000	0.018	0.013	0.000	0.013	0.022	0.018	0.000	0.011	0.000	0.011	0.000	0.832	0.350	0.879	0.621
Co	0.000	0.000	0.000	0.000	0.000	0.000	0.000	0.037	0.035	0.044	0.034	0.037	0.031	0.037	0.037	0.035
Sn	0.011	0.036	0.000	0.029	0.017	0.088	0.000	0.000	0.017	0.000	0.000	0.000	0.076	0.011	0.037	0.038
S	50.242	49.733	50.061	50.042	49.889	49.460	50.135	49.972	50.164	50.512	50.340	50.604	50.152	50.210	49.939	50.283
Total	**100.000**	**100.000**	**100.000**	**100.000**	**100.000**	**100.000**	**100.000**	**100.000**	**100.000**	**100.000**	**100.000**	**100.000**	**100.000**	**100.000**	**100.000**	**100.000**
								Normalised to 2 S atoms								
Cu	1.002	1.010	1.000	0.991	1.006	1.010	1.001	1.008	1.005	0.990	0.999	0.988	0.943	0.961	0.948	0.954
Fe	0.973	1.002	0.993	0.979	0.997	1.019	0.984	0.992	0.980	0.968	0.972	0.963	1.007	1.006	1.019	0.996
Mn	0.000	0.001	0.001	0.000	0.001	0.001	0.001	0.000	0.000	0.000	0.000	0.000	0.033	0.014	0.035	0.025
Co	0.000	0.000	0.000	0.000	0.000	0.000	0.000	0.001	0.001	0.002	0.001	0.001	0.001	0.001	0.001	0.001
Sn	0.000	0.001	0.000	0.001	0.001	0.004	0.000	0.000	0.001	0.000	0.000	0.000	0.003	0.000	0.002	0.002
S	2.000	2.000	2.000	2.000	2.000	2.000	2.000	2.000	2.000	2.000	2.000	2.000	2.000	2.000	2.000	2.000
Total	**3.976**	**4.015**	**3.993**	**3.971**	**4.005**	**4.033**	**3.986**	**4.002**	**3.987**	**3.959**	**3.973**	**3.952**	**3.988**	**3.983**	**4.005**	**3.977**

Sample	**14018**	**14018**
No.	**#28**	**#29**
Cu	32.917	33.081
Fe	31.133	31.126
Mn	1.387	0.429
Co	0.045	0.043
Sn	0.035	< 0.031
S	34.873	35.868
Total	**100.39**	**100.547**
	Atom-%	
Cu	23.660	23.608
Fe	25.463	25.276
Mn	1.153	0.354
Co	0.035	0.033
Sn	0.013	0.000
S	49.675	50.728
Total	**100.000**	**100.000**
	Normalised to 2 S atoms	
Cu	0.953	0.931
Fe	1.025	0.997
Mn	0.046	0.014
Co	0.001	0.001
Sn	0.001	0.000
S	2.000	2.000
Total	**4.026**	**3.943**

Table iv.15.: EMP analyses of chalcopyrite from late ore stage-dominated samples.

Sample	11015	13098(1)	13098(1)	13098(1)	13098(1)	13098(1)	13098(1)	13098(1)	13098(1)
No.	#11	#39	#40	#48	#50	#53	#58	#62	#66
Cu	36.633	36.346	32.500	36.280	41.589	35.797	36.093	36.719	37.031
Fe	5.880	5.265	4.729	3.536	5.297	5.400	6.236	4.701	6.355
Zn	3.361	2.902	2.518	4.054	3.388	1.799	0.574	2.426	0.535
Sb	26.159	22.924	28.506	21.458	0.198	22.710	23.418	24.545	21.666
As	0.392	3.950	0.141	4.734	18.795	3.928	3.683	2.913	4.872
Ag	2.728	4.020	7.935	3.828	0.983	4.636	4.303	3.029	3.337
Mn	0.016	0.058	0.022	0.063	0.014	0.053	0.026	< 0.011	0.017
Cd	0.107	0.065	0.065	0.071	0.050	0.075	0.055	< 0.028	0.045
Sn	0.132	0.063	0.140	0.104	< 0	0.093	0.093	0.096	0.109
S	25.514	26.013	24.911	26.219	28.974	26.151	25.855	25.739	26.048
Total	**100.922**	**101.606**	**101.467**	**100.347**	**99.288**	**100.642**	**100.336**	**100.168**	**100.015**
				Atom-%					
Cu	32.449	31.735	29.679	31.869	33.272	31.516	31.947	32.624	32.508
Fe	5.927	5.231	4.914	3.534	4.822	5.410	6.281	4.753	6.348
Zn	2.892	2.462	2.234	3.460	2.633	1.539	0.494	2.094	0.456
Sb	12.093	10.446	13.586	9.837	0.083	10.435	10.818	11.381	9.926
As	0.295	2.925	0.109	3.527	12.753	2.933	2.765	2.195	3.628
Ag	1.424	2.068	4.269	1.981	0.463	2.404	2.244	1.585	1.726
Mn	0.016	0.059	0.023	0.064	0.013	0.054	0.027	0.000	0.017
Cd	0.054	0.032	0.034	0.035	0.023	0.037	0.028	0.000	0.022
Sn	0.063	0.029	0.068	0.049	0.000	0.044	0.044	0.046	0.051
S	44.788	45.013	45.084	45.643	45.938	45.628	45.354	45.321	45.317
Total	**100.000**	**100.000**	**100.000**	**100.000**	**100.000**	**100.000**	**100.000**	**100.000**	**100.000**
				Normalised to 13 S atoms					
Cu	9.418	9.165	8.558	9.077	9.416	8.979	9.157	9.358	9.326
Fe	1.720	1.511	1.417	1.007	1.365	1.541	1.800	1.363	1.821
Zn	0.840	0.711	0.644	0.985	0.745	0.438	0.141	0.601	0.131
Sb	3.510	3.017	3.918	2.802	0.023	2.973	3.101	3.265	2.848
As	0.085	0.845	0.031	1.005	3.609	0.836	0.793	0.630	1.041
Ag	0.413	0.597	1.231	0.564	0.131	0.685	0.643	0.455	0.495
Mn	0.005	0.017	0.007	0.018	0.004	0.015	0.008	0.000	0.005
Cd	0.016	0.009	0.010	0.010	0.006	0.011	0.008	0.000	0.006
Sn	0.018	0.009	0.020	0.014	0.000	0.012	0.013	0.013	0.015
S	13.000	13.000	13.000	13.000	13.000	13.000	13.000	13.000	13.000
Total	**29.025**	**28.881**	**28.835**	**28.482**	**28.299**	**28.491**	**28.664**	**28.684**	**28.687**

Table iv.16.: EMP analyses of tennantite-tetrahedrite minerals from early- [11015] and main [13098(1)] ore stage-dominated samples.

Sample	13098(1)	13098(1)	13099(2)	13099(2)	11079	12055(1)	12055(1)
No.	**#67**	**#68**	**#53**	**#62**	**#20**	**#55**	**#58**
Cu	37.538	37.616	38.505	38.923	39.502	39.855	41.870
Fe	6.185	5.153	5.998	5.264	0.908	2.999	3.424
Zn	0.737	2.375	0.881	2.187	7.570	4.586	4.517
Sb	21.767	22.583	22.111	21.041	27.812	20.915	11.724
As	4.594	4.099	4.343	5.077	0.173	5.468	11.227
Ag	2.961	2.521	2.665	1.833	< 0.017	0.623	0.201
Mn	< 0.012	0.138	< 0.011	0.022	< 0.011	0.013	0.015
Cd	0.045	0.035	0.050	< 0.041	0.391	0.070	0.059
Sn	0.103	0.097	0.092	0.089	0.149	0.105	0.065
S	26.267	26.220	26.513	26.445	25.156	26.481	27.882
Total	**100.197**	**100.837**	**101.158**	**100.881**	**101.661**	**101.115**	**100.984**
			Atom-%				
Cu	32.805	32.787	33.309	33.587	35.049	34.289	34.530
Fe	6.150	5.111	5.904	5.169	0.917	2.936	3.213
Zn	0.626	2.011	0.740	1.833	6.525	3.833	3.619
Sb	9.928	10.273	9.982	9.476	12.879	9.391	5.046
As	3.405	3.030	3.187	3.716	0.130	3.990	7.853
Ag	1.524	1.294	1.358	0.932	0.000	0.316	0.098
Mn	0.000	0.139	0.000	0.022	0.000	0.013	0.014
Cd	0.022	0.017	0.024	0.000	0.196	0.034	0.028
Sn	0.048	0.045	0.043	0.041	0.071	0.048	0.029
S	45.492	45.292	45.453	45.224	44.234	45.150	45.570
Total	**100.000**	**100.000**	**100.000**	**100.000**	**100.000**	**100.000**	**100.000**
			Normalised to 13 S atoms				
Cu	9.374	9.411	9.527	9.655	10.301	9.873	9.851
Fe	1.758	1.467	1.689	1.486	0.269	0.845	0.917
Zn	0.179	0.577	0.212	0.527	1.918	1.104	1.032
Sb	2.837	2.949	2.855	2.724	3.785	2.704	1.440
As	0.973	0.870	0.911	1.068	0.038	1.149	2.240
Ag	0.436	0.372	0.388	0.268	0.000	0.091	0.028
Mn	0.000	0.040	0.000	0.006	0.000	0.004	0.004
Cd	0.006	0.005	0.007	0.000	0.058	0.010	0.008
Sn	0.014	0.013	0.012	0.012	0.021	0.014	0.008
S	13.000	13.000	13.000	13.000	13.000	13.000	13.000
Total	**28.577**	**28.703**	**28.601**	**28.746**	**29.389**	**28.793**	**28.528**

Table iv.17.: EMP analyses of tennantite-tetrahedrite minerals from main [13098(1), 13099(2)] and late ore stage-dominated samples [11079, 12055(1)].

Sample	11015	11015
No.	#2	#6
Pb	42.104	42.752
Sb	22.693	23.807
Cu	13.817	13.758
Mn	0.026	0.035
Fe	0.052	0.095
Zn	0.040	< 0.036
As	0.520	0.618
Ag	0.032	< 0
Sn	0.079	0.110
S	20.361	20.354
Total	**99.724**	**101.529**
	Atom-%	
Pb	16.231	16.315
Sb	14.887	15.461
Cu	17.368	17.120
Mn	0.038	0.050
Fe	0.074	0.135
Zn	0.049	0.000
As	0.554	0.652
Ag	0.024	0.000
Sn	0.053	0.073
S	50.721	50.194
Total	**100.000**	**100.000**
	Normalised to 3 S atoms	
Pb	0.960	0.975
Sb	0.881	0.924
Cu	1.027	1.023
Mn	0.002	0.003
Fe	0.004	0.008
Zn	0.003	0.000
As	0.033	0.039
Ag	0.001	0.000
Sn	0.003	0.004
S	3.000	3.000
Total	**5.915**	**5.977**

Table iv.18.: EMP analyses of bournonite from early ore stage-dominated sample 11015.

Sample	**11043(2)**	**11043(2)**	**11043(2)**	**11043(2)**	**11043(2)**	**11043(2)**	**11043(2)**	**11043(2)**
No.	**#66**	**#71**	**#76**	**#92**	**#93**	**#96**	**#102**	**#103**
Cu	75.348	79.577	78.548	79.646	79.075	79.753	80.182	79.654
Fe	0.014	0.019	0.035	0.01	0.12	0.029	0.04	0.06
Ag	1.158	0.421	0.463	0.562	0.235	0.387	0.153	0.078
Cd	0.122	0.038	0.057	0.026	0.035	0.037	0.03	0.028
Sb	0.036	0.092	0.284	0.099	0.107	0.148	0.029	0.053
S	20.893	19.814	20.238	20.879	21.234	20.872	20.789	21.595
Total	**97.571**	**99.961**	**99.625**	**101.222**	**100.806**	**101.226**	**101.223**	**101.468**
				Atom-%				
Cu	64.104	66.769	65.924	65.589	65.079	65.653	65.967	64.966
Fe	0.014	0.018	0.033	0.009	0.112	0.027	0.037	0.056
Ag	0.580	0.208	0.229	0.273	0.114	0.188	0.074	0.037
Cd	0.059	0.018	0.027	0.012	0.016	0.017	0.014	0.013
Sb	0.016	0.040	0.124	0.043	0.046	0.064	0.012	0.023
S	35.227	32.947	33.662	34.075	34.633	34.051	33.895	34.905
Total	**100.000**	**100.000**	**100.000**	**100.000**	**100.000**	**100.000**	**100.000**	**100.000**
				Normalised to 1 S atom				
Cu	1.820	2.027	1.958	1.925	1.879	1.928	1.946	1.861
Fe	0.000	0.001	0.001	0.000	0.003	0.001	0.001	0.002
Ag	0.016	0.006	0.007	0.008	0.003	0.006	0.002	0.001
Cd	0.002	0.001	0.001	0.000	0.000	0.001	0.000	0.000
Sb	0.000	0.001	0.004	0.001	0.001	0.002	0.000	0.001
S	1.000	1.000	1.000	1.000	1.000	1.000	1.000	1.000
Total	**2.839**	**3.035**	**2.971**	**2.935**	**2.887**	**2.937**	**2.950**	**2.865**

Table iv.19.: EMP analyses of supergene Cu sulphides from main ore stage-dominated sample 11043(2).

Sample	**11043(2)**	**11043(2)**	**11043(2)**	**13020(1)**	**13020(1)**	**13020(1)**	**13020(1)**	**13020(1)**	**13020(1)**	**13020(1)**
No.	**#78**	**#79**	**#101**	**#1**	**#2**	**#3**	**#4**	**#5**	**#9**	**#10**
Cu	56.039	55.869	56.460	54.196	52.210	52.167	58.736	56.226	55.093	52.348
Ag	0.057	0.052	0.628	0.060	0.863	0.151	0.024	0.069	0.058	0.024
Fe	0.175	0.216	0.209	0.035	0.051	0.022	0.090	0.029	0.034	0.029
As	0.084	0.078	0.800	<0.027	0.027	<0.027	<0.026	0.038	<0.027	<0.027
Sb	0.058	0.157	< 0.023	0.024	0.079	0.030	<0.023	<0.023	<0.023	0.025
S	1.536	1.282	0.454	0.013	0.266	0.033	0.072	0.018	0.829	0.286
Total	**57.949**	**57.654**	**58.551**	**54.328**	**53.496**	**52.403**	**58.922**	**56.380**	**56.014**	**52.712**

Table iv.20.: EMP analyses of oxidised Cu minerals from main ore stage-dominated samples.

Sample	**12015(5)**	**12015(5)**	**12015(5)**	**12015(5)**	**12015(5)**	**12015(5)**	**12015(5)**	**12015(5)**	**12015(5)**	**12015(5)**	**12015(5)**	**12015(5)**	**12015(5)**	**12015(5)**	**12015(5)**
No.	**#56**	**#59**	**#60**	**#62**	**#66**	**#67**	**#70**	**#71**	**#74**	**#75**	**#78**	**#80**	**#82**	**#84**	**#86**
SiO_2	29.650	30.140	30.020	29.850	29.810	30.330	29.830	30.180	29.720	29.730	29.690	30.010	29.690	29.980	29.950
FeO	61.630	61.410	60.670	61.640	60.540	60.460	60.710	61.150	61.250	61.090	61.070	60.880	59.880	59.640	60.830
MnO	2.370	2.420	2.380	2.410	2.410	2.760	2.240	2.690	2.290	2.730	2.470	2.160	2.440	2.510	2.300
MgO	2.250	2.160	3.750	1.416	3.770	2.570	1.193	2.130	2.440	2.490	2.590	3.240	3.710	4.520	1.334
CaO	1.003	1.089	0.749	1.168	0.758	0.983	1.397	0.897	1.090	0.931	0.932	0.994	0.754	0.685	1.265
ZnO	3.540	4.290	3.370	4.520	3.340	4.120	4.660	4.180	3.770	3.970	3.660	3.700	3.270	3.250	4.320
NiO	<0.042	<0.044	<0	<0	0.065	<0	<0.044	<0.044	<0.040	<0.042	<0.043	<0.044	<0.040	<0	<0
Total	**100.443**	**101.509**	**100.939**	**101.004**	**100.693**	**101.223**	**100.030**	**101.227**	**100.560**	**100.941**	**100.412**	**100.984**	**99.744**	**100.585**	**99.999**
							Atoms per formula unit								
Si	0.989	0.994	0.987	0.995	0.983	0.999	1.002	0.998	0.989	0.987	0.989	0.989	0.987	0.984	1.005
Fe	1.720	1.694	1.668	1.718	1.670	1.665	1.706	1.691	1.705	1.696	1.701	1.678	1.665	1.638	1.706
Mn	0.067	0.068	0.066	0.068	0.067	0.077	0.064	0.075	0.065	0.077	0.070	0.060	0.069	0.070	0.065
Mg	0.112	0.106	0.184	0.070	0.185	0.126	0.060	0.105	0.121	0.123	0.129	0.159	0.184	0.221	0.067
Ca	0.036	0.038	0.026	0.042	0.027	0.035	0.050	0.032	0.039	0.033	0.033	0.035	0.027	0.024	0.045
Zn	0.087	0.104	0.082	0.111	0.081	0.100	0.116	0.102	0.093	0.097	0.090	0.090	0.080	0.079	0.107
Ni	0.000	0.000	0.000	0.000	0.002	0.000	0.000	0.000	0.000	0.000	0.000	0.000	0.000	0.000	0.000
Total	**3.011**	**3.006**	**3.013**	**3.005**	**3.017**	**3.001**	**2.998**	**3.002**	**3.011**	**3.013**	**3.011**	**3.011**	**3.013**	**3.016**	**2.995**
Mg_2SiO_4	5.79	5.57	9.45	3.71	9.51	6.63	3.18	5.52	6.27	6.39	6.65	8.24	9.46	11.33	3.54
Ca_2SiO_4	1.85	2.02	1.36	2.20	1.37	1.82	2.68	1.67	2.01	1.72	1.72	1.82	1.38	1.23	2.41
$(Fe,Mn)SiO_4$	92.36	92.41	89.19	94.10	89.12	91.55	94.15	92.81	91.71	91.90	91.62	89.95	89.16	87.44	94.05
Zn_2SiO_4	4.56	5.48	4.44	5.73	4.41	5.34	5.97	5.37	4.87	5.11	4.75	4.83	4.36	4.35	5.56
$(Fe,Mn)SiO_4$	93.56	92.50	94.13	92.11	94.14	92.82	91.43	92.96	93.08	93.15	93.49	93.29	94.18	94.32	92.08
Ca_2SiO_4	1.88	2.02	1.43	2.15	1.45	1.85	2.60	1.67	2.04	1.74	1.76	1.88	1.46	1.33	2.36
Mg #	6.11	5.90	9.92	3.93	9.99	7.04	3.38	5.85	6.63	6.77	7.03	8.66	9.95	11.90	3.76

Table iv.21: EMP analyses of olivine from sample 12015(5) [Voguçincë].

Sample	**12015(7)**	**12015(7)**	**12015(7)**	**12015(7)**	**12015(7)**	**12015(7)**	**12015(7)**	**12015(7)**	**12015(7)**	**12015(7)**	**12015(7)**	**12015(7)**	**12015(7)**	**12015(7)**	**12015(7)**
No.	**#107**	**#25**	**#28**	**#31**	**#34**	**#37**	**#40**	**#44**	**#46**	**#49**	**#52**	**#55**	**#59**	**#64**	**#66**
SiO2	30.370	29.830	30.020	30.360	30.410	30.280	30.350	30.550	30.170	30.450	30.300	30.240	30.480	30.430	30.060
FeO	63.200	64.320	65.640	63.820	64.800	65.290	64.630	64.200	65.560	64.480	65.100	64.460	65.840	65.030	65.830
MnO	1.281	1.245	1.350	1.340	1.340	1.310	1.340	1.258	1.220	1.330	1.320	1.380	1.262	1.380	1.273
MgO	1.196	1.065	1.153	2.730	2.190	1.081	2.490	2.720	1.455	3.050	2.500	2.910	1.063	2.580	1.182
CaO	1.480	1.550	0.921	0.719	0.823	0.974	0.646	0.730	0.900	0.626	0.712	0.642	0.884	0.696	0.906
ZnO	2.860	2.450	2.310	1.970	2.180	2.410	2.120	2.030	2.340	2.000	2.130	2.070	2.430	2.030	2.450
NiO	<0.042	<0	<0.041	<0	<0	<0.042	<0.043	<0	<0		<0.043	<0	<0	<0.043	<0
Total	**100.387**	**100.460**	**101.394**	**100.939**	**101.743**	**101.345**	**101.576**	**101.488**	**101.645**	**101.936**	**102.062**	**101.702**	**101.959**	**102.146**	**101.701**
							Atoms per formula unit								
Si	1.011	0.998	0.997	0.999	0.998	1.003	0.996	1.000	0.997	0.993	0.992	0.991	1.004	0.994	0.995
Fe	1.759	1.800	1.822	1.757	1.778	1.809	1.774	1.758	1.812	1.759	1.782	1.766	1.814	1.776	1.823
Mn	0.036	0.035	0.038	0.037	0.037	0.037	0.037	0.035	0.034	0.037	0.037	0.038	0.035	0.038	0.036
Mg	0.059	0.053	0.057	0.134	0.107	0.053	0.122	0.133	0.072	0.148	0.122	0.142	0.052	0.126	0.058
Ca	0.053	0.056	0.033	0.025	0.029	0.035	0.023	0.026	0.032	0.022	0.025	0.023	0.031	0.024	0.032
Zn	0.070	0.060	0.057	0.048	0.053	0.059	0.051	0.049	0.057	0.048	0.051	0.050	0.059	0.049	0.060
Ni	0.000	0.000	0.000	0.000	0.000	0.000	0.000	0.000	0.000	0.000	0.000	0.000	0.000	0.000	0.000
Total	**2.989**	**3.002**	**3.003**	**3.001**	**3.002**	**2.997**	**3.004**	**3.000**	**3.003**	**3.007**	**3.008**	**3.009**	**2.996**	**3.006**	**3.005**
Mg_2SiO_4	3.11	2.73	2.93	6.86	5.49	2.76	6.23	6.80	3.68	7.54	6.21	7.22	2.70	6.39	2.99
Ca_2SiO_4	2.77	2.86	1.68	1.30	1.48	1.79	1.16	1.31	1.63	1.11	1.27	1.14	1.61	1.24	1.65
(Fe,Mn)SiO_4	94.12	94.41	95.39	91.84	93.03	95.45	92.61	91.88	94.69	91.34	92.52	91.64	95.68	92.37	95.36
Zn_2SiO_4	3.66	3.10	2.90	2.56	2.78	3.04	2.72	2.63	2.95	2.58	2.72	2.67	3.05	2.59	3.07
(Fe,Mn)SiO_4	93.59	94.05	95.42	96.08	95.69	95.18	96.07	96.00	95.40	96.25	95.97	96.13	95.34	96.12	95.28
Ca_2SiO_4	2.75	2.85	1.68	1.36	1.53	1.78	1.20	1.37	1.65	1.17	1.32	1.20	1.61	1.29	1.65
Mg #	3.26	2.87	3.04	7.08	5.68	2.87	6.43	7.02	3.81	7.78	6.41	7.45	2.80	6.60	3.10

Table iv.22: EMP analyses of olivine from sample 12015(7) [Voguçincë].

Sample	**12015(12)**	**12015(12)**	**12015(12)**	**12015(12)**	**12015(12)**	**12015(12)**	**12015(12)**	**12015(12)**	**12015(12)**	**12015(12)**	**12015(12)**
No.	**#36**	**#37**	**#39**	**#41**	**#44**	**#46**	**#48**	**#51**	**#53**	**#54**	**#55**
SiO2	29.050	29.920	29.800	29.580	30.180	28.390	29.100	29.490	29.550	29.910	29.960
FeO	54.580	55.150	54.920	55.320	54.670	52.300	54.350	55.840	56.040	56.240	54.910
MnO	2.130	2.310	2.330	2.360	2.310	2.150	2.190	2.170	2.260	2.220	2.370
MgO	0.604	1.549	2.010	1.690	0.902	1.535	0.906	0.733	1.145	0.774	2.140
CaO	1.342	0.936	0.903	0.889	1.123	1.150	1.281	1.316	1.002	1.208	0.986
ZnO	13.140	11.840	11.740	12.080	12.420	13.160	12.290	11.750	11.540	11.680	11.320
NiO	<0.043	<0	0.046	<0	<0	<0	<0.041	<0.044	<0.044	<0	<0
Total	**100.846**	**101.705**	**101.749**	**101.919**	**101.605**	**98.685**	**100.117**	**101.299**	**101.537**	**102.032**	**101.686**
					Atoms per formula unit						
Si	0.988	0.998	0.992	0.988	1.008	0.983	0.992	0.994	0.992	0.999	0.995
Fe	1.553	1.538	1.529	1.545	1.527	1.514	1.550	1.574	1.573	1.570	1.525
Mn	0.061	0.065	0.066	0.067	0.065	0.063	0.063	0.062	0.064	0.063	0.067
Mg	0.031	0.077	0.100	0.084	0.045	0.079	0.046	0.037	0.057	0.039	0.106
Ca	0.049	0.033	0.032	0.032	0.040	0.043	0.047	0.048	0.036	0.043	0.035
Zn	0.330	0.291	0.288	0.298	0.306	0.336	0.309	0.292	0.286	0.288	0.277
Ni	0.000	0.000	0.001	0.000	0.000	0.000	0.000	0.000	0.000	0.000	0.000
Total	**3.012**	**3.002**	**3.008**	**3.012**	**2.992**	**3.017**	**3.008**	**3.006**	**3.008**	**3.001**	**3.005**
Mg_2SiO_4	1.81	4.49	5.78	4.87	2.68	4.66	2.70	2.14	3.31	2.25	6.11
Ca_2SiO_4	2.89	1.95	1.87	1.84	2.40	2.51	2.74	2.76	2.08	2.52	2.02
(Fe,Mn)SiO_4	95.30	93.56	92.36	93.29	94.93	92.83	94.56	95.10	94.61	95.23	91.86
Zn_2SiO_4	16.55	15.11	15.06	15.34	15.79	17.19	15.71	14.79	14.59	14.65	14.57
(Fe,Mn)SiO_4	80.99	83.15	83.26	83.02	82.14	80.63	81.92	82.80	83.57	83.15	83.59
Ca_2SiO_4	2.45	1.73	1.68	1.64	2.07	2.18	2.38	2.41	1.84	2.20	1.84
Mg #	1.93	4.77	6.12	5.16	2.86	4.97	2.89	2.29	3.51	2.39	6.50

Table iv.23: EMP analyses of olivine from sample 12015(12) [Voguçincë].

Sample	**14032**	**14032**	**14032**	**14032**	**14032**	**14032**
No.	**#9**	**#13**	**#15**	**#19**	**#21**	**#23**
SiO_2	30.310	30.580	29.880	30.270	30.760	30.570
FeO	62.080	63.110	62.130	63.750	63.510	62.530
MnO	1.217	1.230	1.166	1.206	1.164	1.202
MgO	2.580	3.410	2.860	3.080	2.830	3.690
CaO	2.400	1.680	2.120	1.630	1.780	1.640
ZnO	2.080	1.790	1.930	1.770	1.880	1.710
NiO	<0.043	<0	<0.042	<0.043	<0.073	<0.042
Total	**100.667**	**101.800**	**100.086**	**101.706**	**101.924**	**101.342**
			Atoms per formula unit			
Si	0.998	0.993	0.990	0.988	0.999	0.994
Fe	1.709	1.714	1.722	1.741	1.725	1.701
Mn	0.034	0.034	0.033	0.033	0.032	0.033
Mg	0.127	0.165	0.141	0.150	0.137	0.179
Ca	0.085	0.058	0.075	0.057	0.062	0.057
Zn	0.051	0.043	0.047	0.043	0.045	0.041
Ni	0.000	0.000	0.000	0.000	0.000	0.000
Total	**3.002**	**3.007**	**3.010**	**3.012**	**3.001**	**3.006**
Mg_2SiO_4	6.48	8.37	7.17	7.57	7.01	9.08
Ca_2SiO_4	4.33	2.97	3.82	2.88	3.17	2.90
$(Fe,Mn)SiO_4$	89.19	88.66	89.01	89.55	89.83	88.02
Zn_2SiO_4	2.69	2.32	2.51	2.28	2.42	2.24
$(Fe,Mn)SiO_4$	92.80	94.52	93.48	94.68	94.26	94.64
Ca_2SiO_4	4.51	3.16	4.01	3.04	3.32	3.12
Mg #	6.90	8.79	7.58	7.93	7.36	9.52

Table iv.24: EMP analyses of olivine from sample 14032 [Voguçincë].

Sample	**11027(1)**	**11027(1)**	**11027(1)**	**11027(1)**	**11027(2)**	**11027(2)**	**11027(2)**
No.	**#26**	**#27**	**#32**	**#184**	**#77**	**#78**	**#93**
SiO_2	30.620	30.600	30.280	30.110	30.590	30.900	30.380
FeO	61.730	60.940	62.660	62.740	61.590	61.490	62.000
MnO	1.028	1.050	0.953	1.034	1.470	1.490	1.480
MgO	0.728	0.939	1.004	1.092	2.550	2.220	1.586
CaO	0.816	0.714	0.696	0.611	0.788	0.859	0.961
ZnO	7.020	6.890	6.460	6.110	3.970	4.010	4.670
NiO	<0.047	<0.043	<0	<0.043	<0.043	<0	<0.043
Total	**101.942**	**101.133**	**102.053**	**101.697**	**100.958**	**100.969**	**101.077**
			Atoms per formula unit				
Si	1.013	1.017	1.003	1.001	1.007	1.016	1.007
Fe	1.708	1.695	1.735	1.744	1.696	1.691	1.718
Mn	0.029	0.030	0.027	0.029	0.041	0.041	0.042
Mg	0.036	0.047	0.050	0.054	0.125	0.109	0.078
Ca	0.029	0.025	0.025	0.022	0.028	0.030	0.034
Zn	0.171	0.169	0.158	0.150	0.096	0.097	0.114
Ni	0.000	0.000	0.000	0.000	0.000	0.000	0.000
Total	**2.987**	**2.983**	**2.997**	**2.999**	**2.993**	**2.984**	**2.993**
Mg_2SiO_4	1.99	2.59	2.70	2.93	6.62	5.81	4.18
Ca_2SiO_4	1.61	1.42	1.34	1.18	1.47	1.62	1.82
(Fe,Mn)SiO_4	96.40	95.99	95.96	95.90	91.91	92.57	93.99
Zn_2SiO_4	8.85	8.81	8.12	7.71	5.18	5.23	5.99
(Fe,Mn)SiO_4	89.66	89.86	90.61	91.17	93.32	93.14	92.23
Ca_2SiO_4	1.49	1.33	1.27	1.12	1.49	1.63	1.79
Mg #	2.06	2.67	2.78	3.01	6.87	6.05	4.36

Table iv.25: EMP analyses of olivine from samples 11027(1) and 11027(2) [Mirash].

Sample	**11029(4)**	**11029(4)**	**11029(4)**	**11029(4)**	**11029(4)**	**11029(4)**	**11029(4)**	**11029(4)**	**11029(4)**	**11029(4)**	**11029(4)**	**11029(4)**	**11029(4)**	**11029(4)**
No.	**#16**	**#17**	**#19**	**#20**	**#22**	**#23**	**#24**	**#25**	**#27**	**#28**	**#29**	**#30**	**#31**	**#32**
SiO_2	31.100	31.110	31.300	31.100	30.850	30.630	30.590	31.100	30.820	30.830	30.500	30.950	30.900	30.800
FeO	65.240	64.690	64.720	64.650	65.440	65.940	66.130	65.450	65.660	66.330	65.890	66.100	66.340	65.570
MnO	1.278	1.310	1.310	1.380	1.115	1.113	1.028	1.050	1.210	1.166	1.083	1.144	1.125	1.077
MgO	2.640	3.210	3.460	3.340	2.050	1.265	1.260	0.826	1.486	1.552	1.730	1.097	1.615	1.556
CaO	1.104	1.090	0.982	0.927	1.235	1.680	1.800	2.310	1.610	1.470	1.490	1.880	1.490	1.690
ZnO	0.900	0.874	0.884	0.910	1.076	1.212	1.169	1.260	0.979	1.085	1.008	1.160	1.104	1.104
NiO	<0	<0	<0	<0.041	<0	<0	<0	<0.046	<0	<0.045	<0.044	<0	<0	<0
Total	**102.262**	**102.284**	**102.656**	**102.307**	**101.766**	**101.840**	**101.977**	**101.996**	**101.765**	**102.433**	**101.701**	**102.331**	**102.574**	**101.797**
						Atoms per formula unit								
Si	1.006	1.003	1.004	1.003	1.007	1.005	1.003	1.016	1.009	1.004	1.000	1.009	1.004	1.007
Fe	1.765	1.745	1.736	1.743	1.786	1.809	1.813	1.788	1.797	1.807	1.808	1.803	1.803	1.794
Mn	0.035	0.036	0.036	0.038	0.031	0.031	0.029	0.029	0.034	0.032	0.030	0.032	0.031	0.030
Mg	0.127	0.154	0.165	0.161	0.100	0.062	0.062	0.040	0.072	0.075	0.085	0.053	0.078	0.076
Ca	0.038	0.038	0.034	0.032	0.043	0.059	0.063	0.081	0.056	0.051	0.052	0.066	0.052	0.059
Zn	0.021	0.021	0.021	0.022	0.026	0.029	0.028	0.030	0.024	0.026	0.024	0.028	0.026	0.027
Ni	0.000	0.000	0.000	0.000	0.000	0.000	0.000	0.000	0.000	0.000	0.000	0.000	0.000	0.000
Total	**2.994**	**2.997**	**2.996**	**2.997**	**2.993**	**2.995**	**2.997**	**2.984**	**2.991**	**2.996**	**3.000**	**2.991**	**2.996**	**2.993**
Mg_2SiO_4	6.48	7.82	8.39	8.13	5.09	3.15	3.13	2.08	3.70	3.83	4.28	2.73	3.98	3.87
Ca_2SiO_4	1.95	1.91	1.71	1.62	2.20	3.01	3.22	4.17	2.88	2.61	2.65	3.36	2.64	3.02
(Fe,Mn)SiO_4	91.58	90.27	89.89	90.24	92.71	93.83	93.65	93.75	93.42	93.56	93.06	93.91	93.37	93.10
Zn_2SiO_4	1.16	1.13	1.15	1.18	1.37	1.52	1.46	1.58	1.24	1.36	1.27	1.45	1.38	1.40
(Fe,Mn)SiO_4	96.79	96.82	97.01	97.07	96.34	95.42	95.27	94.23	95.81	95.96	95.99	95.14	95.90	95.50
Ca_2SiO_4	2.06	2.05	1.85	1.75	2.29	3.06	3.27	4.19	2.95	2.68	2.74	3.41	2.71	3.10
Mg #	6.73	8.13	8.70	8.43	5.29	3.31	3.28	2.20	3.88	4.00	4.47	2.87	4.16	4.06

Table iv.26: EMP analyses of olivine from sample 11029(4) [Mirash Novo].

Sample	**11029(5)**	**11029(5)**	**11029(5)**	**11029(5)**	**11029(5)**	**11029(5)**	**11029(5)**	**11029(5)**	**11029(5)**	**11029(5)**
No.	**#3**	**#6**	**#7**	**#10**	**#11**	**#14**	**#15**	**#16**	**#19**	**#22**
SiO_2	30.880	30.450	31.030	30.260	30.900	30.340	30.780	30.680	30.830	30.410
FeO	58.290	59.340	58.830	57.680	58.020	59.120	58.520	57.800	59.910	58.240
MnO	6.660	7.220	6.940	6.650	7.200	7.120	7.420	6.920	7.460	7.150
MgO	2.010	1.920	1.800	2.100	3.260	1.770	3.140	1.700	2.270	3.430
CaO	0.973	1.118	1.146	1.204	0.827	0.961	0.723	1.037	0.745	0.618
ZnO	1.420	1.218	1.190	1.970	0.951	1.400	0.846	1.500	0.918	1.152
NiO	<0.038	<0	<0.039	<0.043	<0.044	<0.042	<0.044	<0.041	<0.042	0.064
Total	**100.233**	**101.266**	**100.936**	**99.864**	**101.158**	**100.711**	**101.429**	**99.637**	**102.133**	**101.064**
					Atoms per formula unit					
Si	1.019	1.002	1.018	1.006	1.006	1.004	1.002	1.020	1.003	0.995
Fe	1.608	1.632	1.614	1.604	1.580	1.636	1.593	1.607	1.630	1.594
Mn	0.186	0.201	0.193	0.187	0.199	0.200	0.205	0.195	0.206	0.198
Mg	0.099	0.094	0.088	0.104	0.158	0.087	0.152	0.084	0.110	0.167
Ca	0.034	0.039	0.040	0.043	0.029	0.034	0.025	0.037	0.026	0.022
Zn	0.035	0.030	0.029	0.048	0.023	0.034	0.020	0.037	0.022	0.028
Ni	0.000	0.000	0.000	0.000	0.000	0.000	0.000	0.000	0.000	0.002
Total	**2.981**	**2.998**	**2.982**	**2.994**	**2.994**	**2.996**	**2.998**	**2.980**	**2.997**	**3.005**
Mg_2SiO_4	5.13	4.79	4.55	5.37	8.05	4.46	7.71	4.38	5.58	8.45
Ca_2SiO_4	1.78	2.00	2.08	2.21	1.47	1.74	1.28	1.92	1.32	1.09
(Fe,Mn)SiO_4	93.09	93.21	93.37	92.42	90.48	93.80	91.01	93.70	93.10	90.46
Zn_2SiO_4	1.86	1.55	1.54	2.57	1.25	1.80	1.10	1.96	1.17	1.51
(Fe,Mn)SiO_4	96.30	96.37	96.32	95.15	97.17	96.41	97.53	96.07	97.45	97.31
Ca_2SiO_4	1.85	2.07	2.15	2.28	1.58	1.79	1.37	1.97	1.38	1.18
Mg #	5.79	5.45	5.17	6.09	9.10	5.07	8.73	4.98	6.33	9.50

Table iv.27: EMP analyses of olivine from sample 11029(5) [Mirash Novo].

Sample	**10021(2)**	**10021(2)**	**10021(2)**	**10021(2)**	**10021(2)**	**10021(2)**	**10021(2)**	**10021(2)**	**10021(2)**	**10021(2)**	**10021(2)**	**10021(2)**
No.	**#34**	**#35**	**#36**	**#38**	**#39**	**#42**	**#44**	**#45**	**#46**	**#47**	**#48**	**#49**
SiO_2	30.940	30.630	31.250	31.540	30.710	30.870	31.680	31.580	31.300	30.950	30.690	30.960
FeO	59.360	59.180	60.790	46.360	52.540	58.830	60.290	58.770	61.180	55.480	54.290	53.050
MnO	1.132	1.132	1.176	0.793	0.755	1.050	1.235	1.210	1.176	1.004	0.916	0.881
MgO	1.880	1.780	2.970	0.301	0.110	1.910	5.290	2.640	3.620	0.610	0.321	0.381
CaO	6.830	7.740	4.920	20.780	14.810	7.220	2.710	6.200	3.860	11.870	12.530	13.920
ZnO	1.420	1.480	1.320	1.450	1.760	1.570	1.243	1.360	1.350	1.710	1.810	1.790
NiO	<0.042	<0	<0.041	<0	<0	<0.042	<0	<0	<0.043	<0.044	<0.042	<0.073
Total	**101.562**	**101.942**	**102.426**	**101.224**	**100.685**	**101.450**	**102.448**	**101.760**	**102.486**	**101.624**	**100.557**	**100.982**
					Atoms per formula unit							
Si	1.001	0.990	1.000	0.999	0.996	0.999	1.001	1.011	0.999	0.998	1.000	1.000
Fe	1.606	1.600	1.627	1.228	1.425	1.593	1.594	1.574	1.634	1.496	1.479	1.433
Mn	0.031	0.031	0.032	0.021	0.021	0.029	0.033	0.033	0.032	0.027	0.025	0.024
Mg	0.091	0.086	0.142	0.014	0.005	0.092	0.249	0.126	0.172	0.029	0.016	0.018
Ca	0.237	0.268	0.169	0.705	0.515	0.250	0.092	0.213	0.132	0.410	0.437	0.482
Zn	0.034	0.035	0.031	0.034	0.042	0.038	0.029	0.032	0.032	0.041	0.044	0.043
Ni	0.000	0.000	0.000	0.000	0.000	0.000	0.000	0.000	0.000	0.000	0.000	0.000
Total	**2.999**	**3.010**	**3.000**	**3.001**	**3.004**	**3.001**	**2.999**	**2.989**	**3.001**	**3.002**	**3.000**	**3.000**
Mg_2SiO_4	4.62	4.32	7.20	0.72	0.27	4.69	12.67	6.48	8.75	1.49	0.80	0.94
Ca_2SiO_4	12.05	13.51	8.57	35.82	26.18	12.75	4.66	10.93	6.70	20.89	22.34	24.61
(Fe,Mn)SiO_4	83.33	82.17	84.24	63.46	73.55	82.56	82.67	82.59	84.55	77.61	76.86	74.45
Zn_2SiO_4	1.78	1.83	1.68	1.70	2.10	1.96	1.66	1.74	1.74	2.06	2.19	2.15
(Fe,Mn)SiO_4	85.81	84.32	89.25	62.83	72.20	84.92	93.09	86.78	91.04	77.17	75.78	73.54
Ca_2SiO_4	12.41	13.86	9.08	35.47	25.70	13.12	5.25	11.49	7.22	20.77	22.03	24.31
Mg #	5.34	5.09	8.01	1.14	0.37	5.47	13.53	7.41	9.54	1.92	1.04	1.26

Sample	**10021(2)**	**10021(2)**	**10021(2)**	**10021(2)**	**10021(2)**	**10021(2)**	**10021(2)**	**10021(2)**	**10021(2)**	**10021(2)**	**10021(2)**	**10021(2)**
No.	**#50**	**#52**	**#55**	**#56**	**#59**	**#61**	**#62**	**#63**	**#64**	**#65**	**#67**	**#69**
SiO_2	30.610	30.850	31.470	31.340	31.020	30.670	31.820	31.090	31.370	30.930	30.910	30.850
FeO	56.890	58.440	56.110	60.690	56.090	57.750	60.810	55.010	61.600	59.690	58.490	58.160
MnO	1.162	1.060	1.022	1.203	0.927	1.108	1.254	0.975	1.214	1.179	1.030	1.215
MgO	0.825	0.310	1.413	3.360	0.403	1.081	4.950	0.686	3.720	1.870	0.190	1.071
CaO	9.790	9.540	10.600	4.350	11.110	9.090	2.830	11.630	3.540	7.110	9.460	9.320
ZnO	1.600	1.760	1.790	1.229	1.970	1.540	1.135	1.700	1.190	1.370	1.840	1.430
NiO	<0.043	<0	<0.044	<0.042	<0	<0	<0	<0	<0	<0	<0	0.050
Total	**100.877**	**101.960**	**102.405**	**102.172**	**101.520**	**101.239**	**102.799**	**101.091**	**102.634**	**102.149**	**101.920**	**102.096**
					Atoms per formula unit							
Si	0.998	1.000	1.003	1.003	1.003	0.997	1.004	1.005	1.000	0.996	1.002	0.995
Fe	1.551	1.584	1.495	1.624	1.517	1.570	1.604	1.487	1.642	1.608	1.586	1.568
Mn	0.032	0.029	0.028	0.033	0.025	0.031	0.034	0.027	0.033	0.032	0.028	0.033
Mg	0.040	0.015	0.067	0.160	0.019	0.052	0.233	0.033	0.177	0.090	0.009	0.051
Ca	0.342	0.331	0.362	0.149	0.385	0.317	0.096	0.403	0.121	0.245	0.329	0.322
Zn	0.039	0.042	0.042	0.029	0.047	0.037	0.026	0.041	0.028	0.033	0.044	0.034
Ni	0.000	0.000	0.000	0.000	0.000	0.000	0.000	0.000	0.000	0.000	0.000	0.001
Total	**3.002**	**3.000**	**2.997**	**2.997**	**2.997**	**3.003**	**2.996**	**2.995**	**3.000**	**3.004**	**2.998**	**3.005**
Mg_2SiO_4	2.04	0.76	3.44	8.15	1.00	2.66	11.84	1.70	8.96	4.55	0.47	2.61
Ca_2SiO_4	17.40	16.91	18.54	7.59	19.77	16.08	4.86	20.66	6.13	12.42	16.84	16.30
$(Fe,Mn)SiO_4$	80.56	82.33	78.02	84.26	79.23	81.26	83.30	77.64	84.91	83.03	82.69	81.09
Zn_2SiO_4	1.96	2.12	2.18	1.58	2.38	1.89	1.50	2.07	1.54	1.70	2.22	1.74
$(Fe,Mn)SiO_4$	80.62	81.20	79.03	90.29	78.12	81.91	93.06	77.35	91.84	85.51	81.24	81.81
Ca_2SiO_4	17.42	16.68	18.78	8.13	19.50	16.20	5.44	20.58	6.63	12.79	16.54	16.45
Mg #	2.52	0.94	4.30	8.98	1.26	3.23	12.67	2.17	9.72	5.29	0.58	3.18

Table iv.28: EMP analyses of olivine from sample 10021(2) [Mramor Samakove].

Sample	**10021(21)**	**10021(21)**	**10021(21)**	**10021(21)**	**10021(21)**	**10021(21)**	**10021(21)**
No.	**#73**	**#74**	**#82**	**#84**	**#85**	**#86**	**#93**
SiO_2	31.930	30.710	31.330	31.900	30.550	31.690	31.910
FeO	58.130	54.690	60.210	58.550	58.470	58.210	57.860
MnO	1.340	1.470	1.790	1.960	1.720	1.630	1.990
MgO	7.330	1.308	3.930	5.750	0.971	6.920	4.460
CaO	2.260	9.690	3.090	2.720	7.040	2.660	4.050
ZnO	1.310	2.340	1.660	1.740	2.220	1.370	2.280
NiO	<0	<0	<0	<0.046	<0.043	<0	<0.041
Total	**102.300**	**100.208**	**102.010**	**102.620**	**100.971**	**102.480**	**102.550**
			Atoms per formula unit				
Si	0.998	1.003	1.003	1.003	1.001	0.993	1.008
Fe	1.520	1.494	1.612	1.540	1.602	1.526	1.529
Mn	0.035	0.041	0.049	0.052	0.048	0.043	0.053
Mg	0.342	0.064	0.188	0.270	0.047	0.323	0.210
Ca	0.076	0.339	0.106	0.092	0.247	0.089	0.137
Zn	0.030	0.056	0.039	0.040	0.054	0.032	0.053
Ni	0.000	0.000	0.000	0.000	0.000	0.000	0.000
Total	**3.002**	**2.997**	**2.997**	**2.997**	**2.999**	**3.007**	**2.992**
Mg_2SiO_4	17.32	3.29	9.60	13.80	2.44	16.32	10.89
Ca_2SiO_4	3.84	17.50	5.42	4.69	12.71	4.51	7.11
(Fe,Mn)SiO_4	78.84	79.21	84.98	81.51	84.85	79.18	82.01
Zn_2SiO_4	1.82	2.92	2.17	2.34	2.75	1.88	3.00
(Fe,Mn)SiO_4	93.62	79.51	91.96	92.34	84.58	92.84	89.26
Ca_2SiO_4	4.56	17.57	5.87	5.32	12.67	5.29	7.74
Mg #	18.35	4.09	10.42	14.90	2.88	17.49	12.08

Sample	**10021(21)**	**10021(21)**	**10021(21)**	**10021(21)**	**10021(21)**	**10021(21)**
No.	**#94**	**#96**	**#97**	**#100**	**#102**	**#104**
SiO_2	31.720	31.440	32.340	31.800	31.230	31.620
FeO	58.030	58.110	57.080	59.680	59.870	60.240
MnO	1.340	1.400	1.440	1.510	1.550	1.680
MgO	7.090	7.330	8.330	5.370	2.670	4.000
CaO	2.840	2.440	2.140	2.780	4.830	3.230
ZnO	1.205	1.340	1.195	1.530	1.850	1.770
NiO	<0.042	<0.04	<0	<0	<0	<0.042
Total	**102.225**	**102.060**	**102.525**	**102.670**	**102.000**	**102.540**
			Atoms per formula unit			
Si	0.994	0.989	1.001	1.002	1.004	1.006
Fe	1.521	1.528	1.478	1.573	1.610	1.602
Mn	0.036	0.037	0.038	0.040	0.042	0.045
Mg	0.331	0.344	0.384	0.252	0.128	0.190
Ca	0.095	0.082	0.071	0.094	0.166	0.110
Zn	0.028	0.031	0.027	0.036	0.044	0.042
Ni	0.000	0.000	0.000	0.000	0.000	0.000
Total	**3.006**	**3.011**	**2.999**	**2.998**	**2.996**	**2.994**
Mg_2SiO_4	16.70	17.26	19.50	12.88	6.57	9.74
Ca_2SiO_4	4.81	4.13	3.60	4.79	8.55	5.65
(Fe,Mn)SiO_4	78.49	78.62	76.89	82.33	84.88	84.61
Zn_2SiO_4	1.66	1.85	1.69	2.04	2.36	2.31
(Fe,Mn)SiO_4	92.66	93.25	93.91	92.57	88.71	91.57
Ca_2SiO_4	5.68	4.90	4.40	5.39	8.93	6.12
Mg #	17.88	18.36	20.64	13.82	7.36	10.58

Table iv.29: EMP analyses of olivine from sample 10021(21) [Mramor Samakove].

Sample	**10024(2)**	**10024(4)**	**10024(4)**	**10024(4)**	**10024(4)**	**10024(4)**	**10024(4)**	**10024(4)**	**10024(4)**
No.	**#13**	**#30**	**#31**	**#34**	**#37**	**#39**	**#41**	**#44**	**#46**
SiO_2	31.350	31.330	31.540	31.420	31.400	31.820	31.300	32.130	32.260
FeO	46.150	54.450	54.870	53.850	55.290	54.930	51.890	55.050	52.740
MnO	5.430	2.240	2.180	1.910	2.230	2.250	1.830	2.240	2.210
MgO	8.020	5.760	5.110	5.660	6.210	7.760	3.350	6.200	10.560
CaO	2.090	6.200	6.340	5.480	5.040	3.830	11.020	5.180	2.990
ZnO	8.030	1.610	1.470	2.130	1.820	1.560	2.180	1.580	1.450
NiO	0.056	<0.042	<0.042	<0.042	<0	<0.042	<0	<0.042	<0.041
Total	**101.126**	**101.590**	**101.510**	**100.450**	**101.990**	**102.150**	**101.570**	**102.380**	**102.210**
				Atoms per formula unit					
Si	0.995	0.991	0.999	1.002	0.990	0.992	0.994	1.003	0.989
Fe	1.225	1.440	1.453	1.437	1.457	1.432	1.378	1.437	1.352
Mn	0.146	0.060	0.058	0.052	0.060	0.059	0.049	0.059	0.057
Mg	0.379	0.271	0.241	0.269	0.292	0.361	0.159	0.288	0.482
Ca	0.071	0.210	0.215	0.187	0.170	0.128	0.375	0.173	0.098
Zn	0.188	0.038	0.034	0.050	0.042	0.036	0.051	0.036	0.033
Ni	0.001	0.000	0.000	0.000	0.000	0.000	0.000	0.000	0.000
Total	**3.005**	**3.009**	**3.001**	**2.998**	**3.010**	**3.008**	**3.006**	**2.997**	**3.011**
Mg_2SiO_4	20.83	13.70	12.26	13.84	14.74	18.21	8.09	14.73	24.25
Ca_2SiO_4	3.90	10.60	10.93	9.63	8.60	6.46	19.12	8.85	4.93
(Fe,Mn)SiO_4	75.27	75.70	76.81	76.53	76.65	75.33	72.79	76.42	70.82
Zn_2SiO_4	11.54	2.15	1.95	2.91	2.45	2.17	2.76	2.13	2.13
(Fe,Mn)SiO_4	84.10	85.83	85.83	86.24	87.71	90.10	77.01	87.71	91.50
Ca_2SiO_4	4.36	12.02	12.21	10.85	9.84	7.73	20.23	10.16	6.38
Mg #	23.65	15.87	14.24	15.78	16.68	20.12	10.32	16.72	26.30

Table iv.30: EMP analyses of olivine from samples 10024(2) and 10024(4) [Mramor Proni Butoçit].

Sample	**10024(4)**	**10024(4)**	**10024(4)**	**10024(4)**	**10024(4)**	**10024(4)**	**10024(5)**
No.	**#51**	**#53**	**#55**	**#57**	**#61**	**#63**	**#119**
SiO_2	30.930	31.560	31.560	31.600	31.620	31.340	31.230
FeO	57.520	54.180	53.930	52.890	47.360	48.710	39.180
MnO	2.130	2.020	2.050	2.140	1.970	1.850	2.170
MgO	3.170	4.770	5.190	4.130	4.060	2.770	2.940
CaO	6.060	7.340	6.740	9.360	13.760	14.090	22.070
ZnO	1.950	1.800	1.650	1.630	1.260	1.620	1.470
NiO	<0	<0	<0	<0	<0	<0	<0
Total	**101.760**	**101.670**	**101.120**	**101.750**	**100.030**	**100.380**	**99.060**
			Atoms per formula unit				
Si	0.994	0.998	1.001	0.998	1.002	1.000	0.990
Fe	1.546	1.433	1.430	1.397	1.255	1.299	1.039
Mn	0.058	0.054	0.055	0.057	0.053	0.050	0.058
Mg	0.152	0.225	0.245	0.194	0.192	0.132	0.139
Ca	0.209	0.249	0.229	0.317	0.467	0.482	0.750
Zn	0.046	0.042	0.039	0.038	0.029	0.038	0.034
Ni	0.000	0.000	0.000	0.000	0.000	0.000	0.000
Total	**3.006**	**3.002**	**2.999**	**3.002**	**2.998**	**3.000**	**3.010**
Mg_2SiO_4	7.73	11.47	12.52	9.89	9.75	6.71	7.00
Ca_2SiO_4	10.62	12.69	11.69	16.12	23.75	24.54	37.75
(Fe,Mn)SiO_4	81.65	75.85	75.79	73.99	66.50	68.75	55.25
Zn_2SiO_4	2.49	2.36	2.20	2.10	1.63	2.04	1.83
(Fe,Mn)SiO_4	86.29	83.65	84.73	80.39	72.48	72.20	58.32
Ca_2SiO_4	11.23	13.99	13.06	17.51	25.89	25.76	39.85
Mg #	8.95	13.56	14.64	12.22	13.26	9.20	11.80

Table iv.31: EMP analyses of olivine from samples 10024(4) and 10024(5) [Mramor Proni Butoçit].

Sample	**10-6**	**10-6**	**10-6**	**10-6**	**10-6**	**10-6**	**10-6**	**10-6**	**10-6**	**10-6**
No.	**#112**	**#116**	**#118**	**#132**	**#191**	**#148**	**#158**	**#193**	**#167**	**#195**
SiO_2	30.420	29.580	29.370	30.210	30.640	29.240	30.790	30.510	30.460	30.140
FeO	67.150	67.630	67.840	67.450	67.870	66.920	66.940	66.550	67.880	67.290
MnO	0.190	0.203	0.158	0.158	0.191	0.136	0.183	0.120	0.162	0.150
MgO	0.171	1.285	0.661	0.867	0.670	0.375	1.127	0.294	0.514	0.387
CaO	1.240	0.751	0.733	0.887	0.889	1.282	0.698	1.118	0.877	1.278
ZnO	2.590	1.730	2.250	2.190	2.170	2.730	1.950	2.350	2.370	2.380
NiO	<0	<0.046	<0		<0	<0	<0	<0	<0	0.013
Total	**101.761**	**101.179**	**101.012**	**101.762**	**102.430**	**100.683**	**101.688**	**100.942**	**102.263**	**101.638**
					Atoms per formula unit					
Si	1.009	0.987	0.987	1.000	1.007	0.987	1.013	1.016	1.005	1.001
Fe	1.862	1.887	1.906	1.868	1.865	1.889	1.842	1.853	1.872	1.870
Mn	0.005	0.006	0.004	0.004	0.005	0.004	0.005	0.003	0.005	0.004
Mg	0.008	0.064	0.033	0.043	0.033	0.019	0.055	0.015	0.025	0.019
Ca	0.044	0.027	0.026	0.031	0.031	0.046	0.025	0.040	0.031	0.045
Zn	0.063	0.043	0.056	0.054	0.053	0.068	0.047	0.058	0.058	0.058
Ni	0.000	0.000	0.000	0.000	0.000	0.000	0.000	0.000	0.000	0.000
Total	**2.991**	**3.013**	**3.013**	**3.000**	**2.993**	**3.013**	**2.987**	**2.984**	**2.995**	**2.999**
Mg_2SiO_4	0.44	3.22	1.68	2.20	1.70	0.96	2.87	0.76	1.31	0.99
Ca_2SiO_4	2.29	1.35	1.34	1.62	1.62	2.37	1.28	2.09	1.60	2.35
$(Fe,Mn)SiO_4$	97.27	95.42	96.98	96.18	96.69	96.67	95.85	97.15	97.09	96.66
Zn_2SiO_4	3.21	2.17	2.80	2.73	2.69	3.39	2.47	2.96	2.94	2.95
$(Fe,Mn)SiO_4$	94.56	96.46	95.88	95.66	95.71	94.30	96.25	95.00	95.49	94.75
Ca_2SiO_4	2.23	1.37	1.32	1.61	1.60	2.31	1.28	2.04	1.58	2.30
Mg #	0.45	3.28	1.71	2.24	1.73	0.99	2.91	0.78	1.33	1.01

Table iv.32: EMP analyses of olivine from sample 10-6 [Marec].

Sample	**10032(1)**	**10032(1)**	**10032(1)**	**10032(1)**	**10032(1)**	**10032(1)**	**10032(1)**	**10032(1)**	**10032(1)**
No.	**#187**	**#79**	**#81**	**#83**	**#85**	**#88**	**#90**	**#97**	**#99**
SiO_2	29.770	30.220	29.410	29.630	29.800	30.090	30.280	29.940	30.440
FeO	63.740	64.010	64.900	64.910	63.490	64.510	64.430	63.810	63.970
MnO	0.281	0.279	0.261	0.258	0.254	0.219	0.222	0.302	0.235
MgO	0.601	2.160	0.036	1.042	0.784	0.709	1.515	2.740	2.420
CaO	0.514	0.382	0.666	0.442	0.568	0.544	0.499	0.347	0.366
ZnO	6.090	4.510	6.220	4.990	5.700	5.850	4.940	4.290	4.290
NiO	<0.044	<0	<0	<0	<0	<0.043	<0	<0	<0
Total	**100.996**	**101.561**	**101.493**	**101.272**	**100.596**	**101.922**	**101.886**	**101.429**	**101.721**
				Atoms per formula unit					
Si	1.000	0.998	0.991	0.992	1.003	1.001	1.000	0.989	1.000
Fe	1.791	1.767	1.829	1.817	1.786	1.794	1.780	1.762	1.758
Mn	0.008	0.008	0.007	0.007	0.007	0.006	0.006	0.008	0.007
Mg	0.030	0.106	0.002	0.052	0.039	0.035	0.075	0.135	0.119
Ca	0.019	0.014	0.024	0.016	0.020	0.019	0.018	0.012	0.013
Zn	0.151	0.110	0.155	0.123	0.142	0.144	0.120	0.105	0.104
Ni	0.000	0.000	0.000	0.000	0.000	0.000	0.000	0.000	0.000
Total	**3.000**	**3.002**	**3.009**	**3.008**	**2.997**	**2.999**	**3.000**	**3.011**	**3.000**
Mg_2SiO_4	1.63	5.61	0.10	2.75	2.12	1.90	3.97	7.03	6.25
Ca_2SiO_4	1.00	0.71	1.29	0.84	1.10	1.05	0.94	0.64	0.68
$(Fe,Mn)SiO_4$	97.37	93.68	98.61	96.41	96.77	97.06	95.09	92.33	93.07
Zn_2SiO_4	7.67	5.79	7.68	6.28	7.24	7.31	6.26	5.54	5.53
$(Fe,Mn)SiO_4$	91.39	93.50	91.13	92.91	91.72	91.70	92.82	93.81	93.79
Ca_2SiO_4	0.94	0.71	1.19	0.81	1.05	0.99	0.92	0.65	0.68
Mg #	1.65	5.67	0.10	2.78	2.15	1.92	4.02	7.11	6.32

Table iv.33: EMP analyses of olivine from sample 10032(1) [Marec].

Sample	**10-1A**	**10-1A**	**10-1A**	**10-1A**	**10-1A**	**10-1A**	**10-1A**	**10-1A**	**10-1A**	**10-1A**	**10-1A**
No.	**#5**	**#7**	**#10**	**#12**	**#15**	**#19**	**#23**	**#25**	**#27**	**#33**	**#36**
SiO_2	30.970	31.230	30.280	30.620	29.980	30.780	31.010	30.010	30.760	30.390	30.270
FeO	58.720	57.820	58.330	59.000	59.630	58.150	58.070	56.370	58.680	58.370	58.800
MnO	1.500	1.470	1.440	1.420	1.410	1.480	1.440	1.380	1.500	1.530	1.480
MgO	3.120	2.000	2.490	3.650	2.600	3.010	2.730	2.370	3.270	3.550	3.330
CaO	2.730	3.860	3.130	2.250	2.940	3.030	3.460	5.090	2.460	2.670	2.680
ZnO	5.190	5.780	5.440	4.580	4.790	5.520	5.620	5.530	5.340	5.140	5.300
NiO	<0.041	<0	<0	<0.047	<0.041	<0.043	<0	<0	<0.041	<0.042	0.042
Total	**102.230**	**102.160**	**101.110**	**101.520**	**101.350**	**101.970**	**102.330**	**100.750**	**102.010**	**101.650**	**101.902**
					Atoms per formula unit						
Si	1.001	1.012	0.996	0.996	0.986	0.999	1.003	0.989	0.998	0.990	0.986
Fe	1.588	1.567	1.604	1.604	1.641	1.578	1.570	1.553	1.592	1.590	1.602
Mn	0.041	0.040	0.040	0.039	0.039	0.041	0.039	0.039	0.041	0.042	0.041
Mg	0.150	0.097	0.122	0.177	0.128	0.146	0.132	0.116	0.158	0.172	0.162
Ca	0.095	0.134	0.110	0.078	0.104	0.105	0.120	0.180	0.085	0.093	0.094
Zn	0.124	0.138	0.132	0.110	0.116	0.132	0.134	0.134	0.128	0.124	0.127
Ni	0.000	0.000	0.000	0.000	0.000	0.000	0.000	0.000	0.000	0.000	0.001
Total	**2.999**	**2.988**	**3.004**	**3.004**	**3.014**	**3.001**	**2.997**	**3.011**	**3.002**	**3.010**	**3.014**
Mg_2SiO_4	8.03	5.26	6.50	9.32	6.67	7.79	7.07	6.17	8.43	9.08	8.52
Ca_2SiO_4	5.05	7.29	5.88	4.13	5.42	5.63	6.44	9.52	4.56	4.91	4.93
(Fe,Mn)SiO_4	86.93	87.45	87.62	86.55	87.90	86.58	86.49	84.32	87.02	86.01	86.55
Zn_2SiO_4	6.70	7.35	7.00	6.00	6.12	7.12	7.20	7.06	6.92	6.68	6.84
(Fe,Mn)SiO_4	88.18	85.51	87.16	89.72	88.42	87.20	86.37	83.52	88.45	88.28	88.14
Ca_2SiO_4	5.12	7.13	5.85	4.28	5.45	5.68	6.43	9.43	4.63	5.04	5.02
Mg #	8.65	5.81	7.07	9.93	7.21	8.45	7.73	6.97	9.04	9.78	9.17

Table iv.34: EMP analyses of olivine from sample 10-1A [Hajkobile].

Sample	**3(1)**	**3(1)**	**3(1)**	**3(2)**	**3(2)**	**3(2)**	**3(2)**	**3(2)**	**3(2)**	**3(2)**	**3(2)**	**3(2)**	**3(2)**	**3(2)**	**3(2)**
No.	**#116**	**#134**	**#135**	**#2**	**#120**	**#6**	**#8**	**#11**	**#12**	**#14**	**#16**	**#18**	**#20**	**#22**	**#28**
SiO_2	30.110	29.780	30.290	30.570	30.470	31.230	30.800	30.610	31.100	31.040	30.830	30.810	30.870	30.560	30.850
FeO	62.570	63.850	62.950	58.170	57.220	57.420	55.820	57.550	57.090	55.400	57.050	58.870	59.470	57.430	58.190
MnO	2.210	2.190	2.190	0.986	1.003	0.989	0.989	1.013	0.985	0.975	1.051	1.055	1.023	1.039	1.017
MgO	1.246	1.064	1.333	2.440	2.270	4.550	2.160	2.120	2.500	2.260	3.090	4.200	3.500	1.860	2.040
CaO	0.708	0.719	0.726	4.930	5.030	3.940	6.930	5.960	5.720	7.280	5.050	3.090	3.280	6.350	5.490
ZnO	2.670	2.650	2.950	4.840	4.630	4.080	4.610	4.610	4.970	4.900	4.770	4.310	4.120	4.550	4.540
NiO	<0	<0.042	<0	<0.042	<0	<0	<0	<0.041	<0	<0	<0	<0	<0.073	<0.043	<0
Total	**99.514**	**100.253**	**100.439**	**101.936**	**100.623**	**102.209**	**101.309**	**101.863**	**102.365**	**101.855**	**101.841**	**102.335**	**102.263**	**101.789**	**102.127**
							Atoms per formula unit								
Si	1.012	1.000	1.009	0.993	1.000	0.997	1.000	0.994	1.001	1.001	0.996	0.990	0.995	0.994	0.999
Fe	1.759	1.793	1.755	1.581	1.571	1.533	1.516	1.563	1.536	1.494	1.542	1.582	1.603	1.562	1.576
Mn	0.063	0.062	0.062	0.027	0.028	0.027	0.027	0.028	0.027	0.027	0.029	0.029	0.028	0.029	0.028
Mg	0.062	0.053	0.066	0.118	0.111	0.216	0.105	0.103	0.120	0.109	0.149	0.201	0.168	0.090	0.098
Ca	0.025	0.026	0.026	0.172	0.177	0.135	0.241	0.207	0.197	0.252	0.175	0.106	0.113	0.221	0.191
Zn	0.066	0.066	0.073	0.116	0.112	0.096	0.110	0.111	0.118	0.117	0.114	0.102	0.098	0.109	0.109
Ni	0.000	0.000	0.000	0.000	0.000	0.000	0.000	0.000	0.000	0.000	0.000	0.000	0.000	0.000	0.000
Total	**2.988**	**3.000**	**2.991**	**3.007**	**3.000**	**3.003**	**3.000**	**3.006**	**2.999**	**2.999**	**3.004**	**3.010**	**3.005**	**3.006**	**3.001**
Mg_2SiO_4	3.27	2.75	3.47	6.23	5.89	11.33	5.54	5.40	6.38	5.78	7.86	10.49	8.79	4.74	5.20
Ca_2SiO_4	1.34	1.34	1.36	9.04	9.38	7.05	12.77	10.91	10.49	13.37	9.23	5.55	5.92	11.63	10.06
(Fe,Mn)SiO_4	95.40	95.91	95.17	84.73	84.74	81.62	81.70	83.69	83.13	80.85	82.91	83.97	85.28	83.63	84.73
Zn_2SiO_4	3.46	3.37	3.79	6.12	5.94	5.37	5.83	5.79	6.28	6.17	6.12	5.62	5.32	5.68	5.70
(Fe,Mn)SiO_4	95.21	95.30	94.86	84.82	84.69	87.11	81.44	83.35	83.22	80.51	84.48	88.53	88.53	82.80	84.29
Ca_2SiO_4	1.33	1.33	1.35	9.05	9.37	7.53	12.73	10.86	10.50	13.32	9.40	5.85	6.15	11.52	10.01
Mg #	3.43	2.88	3.64	6.96	6.60	12.38	6.45	6.16	7.24	6.78	8.80	11.28	9.49	5.46	5.88

Table iv.35: EMP analyses of olivine from samples 3(1) and 3(2) [Hanroc].

Sample	**12016(1)**	**12016(1)**	**12016(1)**	**12016(1)**	**12016(1)**
No.	**#32**	**#44**	**#51**	**#58**	**#64**
SiO_2	31.100	31.140	31.730	31.550	31.770
FeO	47.610	48.890	48.020	48.220	49.710
MnO	4.440	4.060	3.530	3.740	3.750
MgO	5.410	6.340	8.620	7.840	7.490
CaO	1.281	1.660	1.214	1.378	1.430
ZnO	11.130	9.470	8.790	9.360	8.570
NiO	0.063	0.054	0.159	0.117	<0.043
Total	**101.034**	**101.614**	**102.063**	**102.205**	**102.720**
			Atoms per formula unit		
Si	1.007	0.998	0.996	0.996	0.998
Fe	1.290	1.310	1.261	1.273	1.306
Mn	0.122	0.110	0.094	0.100	0.100
Mg	0.261	0.303	0.404	0.369	0.351
Ca	0.044	0.057	0.041	0.047	0.048
Zn	0.266	0.224	0.204	0.218	0.199
Ni	0.002	0.001	0.004	0.003	0.000
Total	**2.993**	**3.002**	**3.004**	**3.004**	**3.002**
Mg_2SiO_4	15.21	17.01	22.43	20.63	19.44
Ca_2SiO_4	2.59	3.20	2.27	2.61	2.67
(Fe,Mn)SiO_4	82.20	79.79	75.30	76.77	77.90
Zn_2SiO_4	15.45	13.16	12.74	13.32	12.02
(Fe,Mn)SiO_4	81.97	83.49	84.71	83.84	85.06
Ca_2SiO_4	2.58	3.35	2.55	2.85	2.91
Mg #	16.84	18.78	24.24	22.47	21.17

Table iv.36: EMP analyses of olivine from sample 12016(1) [Akllap].

Sample	**10024(2)**	**10024(2)**
No.	**#4**	**#14**
SiO_2	46.170	44.210
TiO_2	0.079	0.221
Al_2O_3	4.370	4.110
MgO	6.930	2.320
CaO	19.760	20.280
MnO	2.050	1.710
FeO	17.440	21.210
Fe_2O_3	0.000	0.000
NiO	<0	<0
ZnO	3.150	4.590
PbO	0.271	0.345
Na_2O	<0	<0
K_2O	0.031	0.016
P_2O_5	0.837	0.526
Total	**101.088**	**99.538**
Atoms per formula unit		
Si	1.820	1.829
Ti	0.002	0.007
Al	0.203	0.200
Mg	0.407	0.143
Ca	0.835	0.899
Mn	0.068	0.060
Fe^{2+}	0.575	0.734
Fe^{3+}	0.000	0.000
Ni	0.000	0.000
Zn	0.092	0.140
Pb	0.003	0.004
Na	0.000	0.000
K	0.002	0.001
Pb	0.028	0.018
Total	**4.035**	**4.036**
$\mathbf{Ca_2Si_2O_6}$	45.94	50.62
$\mathbf{Fe_2Si_2O_6}$	31.65	41.32
$\mathbf{Mg_2Si_2O_6}$	22.42	8.06
Mg #	41.46	16.32

Table iv.37: EMP analyses of clinopyroxene from sample 10024(2) [Mramor Proni Butoçit].

Sample	**10024(5)**	**10024(5)**	**10024(5)**	**10024(5)**	**10024(5)**	**10024(5)**	**10024(5)**	**10024(5)**
No.	**#67**	**#69**	**#71**	**#72**	**#76**	**#77**	**#80**	**#81**
SiO_2	41.450	40.430	41.100	41.380	41.070	42.830	41.020	40.550
TiO_2	0.395	0.480	0.322	0.452	0.532	0.275	0.372	0.387
Al_2O_3	6.360	5.920	5.680	5.540	5.650	3.850	6.840	6.680
MgO	6.530	6.850	5.610	7.740	7.300	7.520	6.610	6.290
CaO	22.250	22.340	22.050	22.610	22.240	22.430	21.890	21.850
MnO	0.575	0.578	0.806	0.536	0.541	0.680	0.597	0.584
FeO	10.114	8.848	10.677	8.189	8.957	9.960	8.769	8.631
Fe_2O_3	10.264	11.515	11.372	10.358	10.939	9.179	11.214	11.479
NiO	<0.043	<0	<0	0.000	<0	<0	<0.041	<0.040
ZnO	0.725	0.677	0.876	0.620	0.595	0.930	0.700	0.658
PbO	0.496	0.490	0.406	0.390	0.423	0.471	0.710	0.750
Na_2O	0.122	0.074	0.108	0.095	0.076	0.106	0.092	0.154
K_2O	0.020	0.060	0.046	<0	0.024	<0	0.271	0.257
P_2O_5	1.161	1.369	0.945	1.369	1.240	1.380	0.947	0.945
Total	**100.462**	**99.631**	**99.998**	**99.279**	**99.587**	**99.611**	**100.032**	**99.215**
			Atoms per formula unit					
Si	1.635	1.609	1.643	1.638	1.630	1.699	1.625	1.623
Ti	0.012	0.014	0.010	0.013	0.016	0.008	0.011	0.012
Al	0.296	0.278	0.268	0.258	0.264	0.180	0.319	0.315
Mg	0.384	0.407	0.334	0.457	0.432	0.445	0.390	0.375
Ca	0.940	0.953	0.944	0.959	0.946	0.954	0.929	0.937
Mn	0.019	0.019	0.027	0.018	0.018	0.023	0.020	0.020
Fe^{2+}	0.334	0.295	0.357	0.271	0.297	0.330	0.290	0.289
Fe^{3+}	0.305	0.345	0.342	0.309	0.327	0.274	0.334	0.346
Ni	0.000	0.000	0.000	0.000	0.000	0.000	0.000	0.000
Zn	0.021	0.020	0.026	0.018	0.017	0.027	0.020	0.019
Pb	0.005	0.005	0.004	0.004	0.005	0.005	0.008	0.008
Na	0.009	0.006	0.008	0.007	0.006	0.008	0.007	0.012
K	0.001	0.003	0.002	0.000	0.001	0.000	0.014	0.013
Pb	0.039	0.046	0.032	0.046	0.042	0.046	0.032	0.032
Total	**4.000**	**4.000**	**4.000**	**4.000**	**4.000**	**4.000**	**4.000**	**4.000**
$Ca_2Si_2O_6$	47.91	47.67	47.75	48.06	47.25	47.61	47.79	48.13
$Fe_2Si_2O_6$	32.52	31.99	35.34	29.05	31.17	30.18	32.14	32.60
$Mg_2Si_2O_6$	19.56	20.34	16.90	22.89	21.58	22.21	20.08	19.28
Mg #	53.51	57.98	48.36	62.75	59.23	57.37	57.33	56.51

Sample	**10024(5)**	**10024(5)**	**10024(5)**	**10024(5)**	**10024(5)**	**10024(5)**	**10024(5)**	**10024(5)**
No.	**#84**	**#88**	**#89**	**#92**	**#93**	**#95**	**#97**	**#100**
SiO_2	40.860	43.530	41.080	42.900	42.390	40.030	41.520	43.700
TiO_2	0.484	0.335	0.515	0.481	0.396	0.656	0.582	0.308
Al_2O_3	5.980	4.600	4.650	4.750	4.350	7.190	5.970	3.870
MgO	7.000	8.310	6.270	6.210	4.980	6.770	7.480	7.630
CaO	22.510	22.710	22.210	22.210	21.710	22.310	22.440	22.470
MnO	0.569	0.613	0.697	0.693	0.846	0.516	0.531	0.670
FeO	8.841	9.761	10.470	12.529	14.283	8.499	8.991	10.563
Fe_2O_3	12.256	7.434	11.791	8.524	8.265	12.181	10.001	7.986
NiO	<0.038	<0.038	<0	<0	<0	<0.039	<0.039	<0.039
ZnO	0.711	0.785	0.887	0.669	0.814	0.426	0.521	0.709
PbO	0.496	0.530	0.676	0.389	0.759	0.273	0.357	0.386
Na_2O	0.083	0.108	0.107	0.147	0.170	0.109	0.149	0.133
K_2O	<0.014	0.032	0.060	<0	0.018	0.038	0.032	0.037
P_2O_5	1.291	1.708	1.434	1.197	1.321	1.137	1.416	1.301
Total	**101.081**	**100.456**	**100.847**	**100.700**	**100.302**	**100.135**	**99.990**	**99.764**
			Atoms per formula unit					
Si	1.605	1.696	1.633	1.694	1.700	1.580	1.632	1.723
Ti	0.014	0.010	0.015	0.014	0.012	0.019	0.017	0.009
Al	0.277	0.211	0.218	0.221	0.206	0.334	0.277	0.180
Mg	0.410	0.483	0.371	0.366	0.298	0.398	0.438	0.449
Ca	0.947	0.948	0.946	0.940	0.933	0.943	0.945	0.949
Mn	0.019	0.020	0.023	0.023	0.029	0.017	0.018	0.022
Fe^{2+}	0.290	0.318	0.348	0.414	0.479	0.280	0.295	0.348
Fe^{3+}	0.362	0.218	0.353	0.253	0.249	0.362	0.296	0.237
Ni	0.000	0.000	0.000	0.000	0.000	0.000	0.000	0.000
Zn	0.021	0.023	0.026	0.019	0.024	0.012	0.015	0.021
Pb	0.005	0.006	0.007	0.004	0.008	0.003	0.004	0.004
Na	0.006	0.008	0.008	0.011	0.013	0.008	0.011	0.010
K	0.000	0.002	0.003	0.000	0.001	0.002	0.002	0.002
Pb	0.043	0.056	0.048	0.040	0.045	0.038	0.047	0.043
Total	**4.000**	**4.000**	**4.000**	**4.000**	**4.000**	**4.000**	**4.000**	**4.000**
$Ca_2Si_2O_6$	47.13	48.20	46.87	47.64	47.62	47.55	47.86	47.87
$Fe_2Si_2O_6$	32.47	27.25	34.72	33.82	37.18	32.37	29.95	29.52
$Mg_2Si_2O_6$	20.39	24.54	18.41	18.53	15.20	20.08	22.20	22.62
Mg #	58.53	60.28	51.63	46.91	38.33	58.68	59.73	56.28

Sample	**10024(5)**	**10024(5)**	**10024(5)**	**10024(5)**	**10024(5)**	**10024(5)**	**10024(5)**	**10024(5)**
No.	**#101**	**#102**	**#105**	**#108**	**#111**	**#112**	**#114**	**#118**
SiO_2	41.680	41.610	41.730	41.760	41.330	40.330	42.360	43.630
TiO_2	0.403	0.663	0.761	0.696	0.618	0.578	0.550	0.621
Al_2O_3	4.830	5.440	5.460	5.170	6.060	6.340	5.590	6.080
MgO	8.040	6.350	6.690	6.450	6.560	6.540	6.620	8.410
CaO	22.420	21.920	21.820	21.970	21.880	21.920	21.980	22.620
MnO	0.550	0.594	0.597	0.584	0.598	0.612	0.638	0.454
FeO	8.067	11.859	11.527	11.774	10.831	9.497	12.243	8.521
Fe_2O_3	9.938	9.525	10.105	9.442	9.978	11.761	7.553	7.378
NiO	0.000	<0	<0.040	<0	<0	<0	<0.041	<0.039
ZnO	0.664	0.473	0.481	0.526	0.462	0.612	0.544	0.302
PbO	0.468	0.200	0.220	0.206	0.253	0.376	0.142	<0.065
Na_2O	0.105	0.127	0.117	0.137	0.142	0.132	0.136	0.092
K_2O	0.016	<0	0.034	0.035	0.043	0.069	<0.014	0.038
P_2O_5	1.359	1.276	1.270	1.345	1.218	1.283	1.413	0.510
Total	**98.540**	**100.037**	**100.812**	**100.095**	**99.973**	**100.050**	**99.769**	**98.656**
				Atoms per formula unit				
Si	1.661	1.651	1.642	1.655	1.636	1.600	1.674	1.709
Ti	0.012	0.020	0.023	0.021	0.018	0.017	0.016	0.018
Al	0.227	0.254	0.253	0.242	0.283	0.296	0.260	0.281
Mg	0.478	0.376	0.392	0.381	0.387	0.387	0.390	0.491
Ca	0.957	0.932	0.920	0.933	0.928	0.932	0.931	0.949
Mn	0.019	0.020	0.020	0.020	0.020	0.021	0.021	0.015
Fe^{2+}	0.269	0.394	0.379	0.390	0.359	0.315	0.405	0.279
Fe^{3+}	0.298	0.284	0.299	0.282	0.297	0.351	0.225	0.218
Ni	0.000	0.000	0.000	0.000	0.000	0.000	0.000	0.000
Zn	0.020	0.014	0.014	0.015	0.014	0.018	0.016	0.009
Pb	0.005	0.002	0.002	0.002	0.003	0.004	0.002	0.000
Na	0.008	0.010	0.009	0.011	0.011	0.010	0.010	0.007
K	0.001	0.000	0.002	0.002	0.002	0.003	0.000	0.002
Pb	0.046	0.043	0.042	0.045	0.041	0.043	0.047	0.017
Total	**4.000**	**4.000**	**4.000**	**4.000**	**4.000**	**4.000**	**4.000**	**4.000**
$\mathbf{Ca_2Si_2O_6}$	47.82	46.94	46.21	46.98	47.08	46.95	47.73	49.01
$\mathbf{Fe_2Si_2O_6}$	28.32	34.15	34.08	33.83	33.27	33.57	32.27	25.64
$\mathbf{Mg_2Si_2O_6}$	23.86	18.92	19.71	19.19	19.64	19.49	20.00	25.35
Mg #	63.98	48.83	50.85	49.41	51.91	55.11	49.08	63.76

Table iv.38: EMP analyses of clinopyroxene from sample 10024(5) [Mramor Proni Butoçit].

Sample	**12016(1)**	**12016(1)**	**12016(1)**	**12016(1)**	**12016(1)**	**12016(1)**	**12016(1)**
No.	**#27**	**#29**	**#35**	**#38**	**#39**	**#42**	**#46**
SiO_2	43.860	45.320	45.730	44.710	45.610	45.110	45.070
TiO_2	0.244	0.272	0.187	0.256	0.380	0.379	0.226
Al_2O_3	5.990	4.600	3.790	5.110	4.300	4.550	5.400
MgO	3.140	4.900	5.140	5.170	4.210	5.380	4.350
CaO	19.970	19.310	16.360	18.760	19.950	18.130	19.840
MnO	1.350	1.600	2.270	1.550	1.430	1.650	1.490
FeO	20.590	20.530	22.090	20.430	20.660	20.870	20.610
Fe_2O_3	0.000	0.000	0.000	0.000	0.000	0.000	0.000
NiO	<0.041	<0.039	<0.040	0.041	0.058	0.087	0.050
ZnO	3.970	3.610	4.450	3.320	3.750	3.300	3.550
PbO	0.530	0.257	0.220	0.340	0.336	0.351	0.267
Na_2O	<0.076	<0	<0	<0.066	<0.071	<0	<0.069
K_2O	0.146	0.021	0.043	<0	0.029	0.018	<0.013
P_2O_5	0.504	0.538	0.398	0.559	0.684	0.524	0.485
Total	**100.294**	**100.958**	**100.678**	**100.246**	**101.397**	**100.349**	**101.338**
			Atoms per formula unit				
Si	1.786	1.818	1.851	1.803	1.826	1.818	1.802
Ti	0.007	0.008	0.006	0.008	0.011	0.011	0.007
Al	0.287	0.217	0.181	0.243	0.203	0.216	0.255
Mg	0.191	0.293	0.310	0.311	0.251	0.323	0.259
Ca	0.871	0.830	0.709	0.810	0.856	0.783	0.850
Mn	0.047	0.054	0.078	0.053	0.048	0.056	0.050
Fe^{2+}	0.701	0.689	0.748	0.689	0.692	0.704	0.689
Fe^{3+}	0.000	0.000	0.000	0.000	0.000	0.000	0.000
Ni	0.000	0.000	0.000	0.001	0.002	0.003	0.002
Zn	0.119	0.107	0.133	0.099	0.111	0.098	0.105
Pb	0.006	0.003	0.002	0.004	0.004	0.004	0.003
Na	0.000	0.000	0.000	0.000	0.000	0.000	0.000
K	0.008	0.001	0.002	0.000	0.001	0.001	0.000
Pb	0.017	0.018	0.014	0.019	0.023	0.018	0.016
Total	**4.041**	**4.038**	**4.034**	**4.039**	**4.028**	**4.036**	**4.039**
$Ca_2Si_2O_6$	49.42	45.81	40.14	44.77	47.58	43.26	47.26
$Fe_2Si_2O_6$	39.77	38.02	42.31	38.06	38.46	38.87	38.32
$Mg_2Si_2O_6$	10.81	16.17	17.55	17.17	13.97	17.86	14.42
Mg #	21.37	29.85	29.32	31.09	26.65	31.48	27.34

Sample	**12016(1)**	**12016(1)**	**12016(1)**	**12016(1)**	**12016(1)**	**12016(1)**
No.	**#48**	**#49**	**#54**	**#57**	**#59**	**#62**
SiO_2	43.610	43.950	41.970	43.980	43.270	43.120
TiO_2	0.308	0.406	0.837	0.343	0.578	0.335
Al_2O_3	5.380	5.020	6.200	5.450	6.030	5.640
MgO	2.830	4.010	2.540	2.910	3.410	2.550
CaO	20.470	19.140	20.210	20.100	20.260	19.650
MnO	1.239	1.450	1.135	1.310	1.181	1.400
FeO	21.630	21.850	21.770	21.620	21.130	22.570
Fe_2O_3	0.000	0.000	0.000	0.000	0.000	0.000
NiO	<0.041	<0.041	0.058	0.051	<0.040	<0.039
ZnO	3.790	3.650	3.770	3.820	3.510	3.980
PbO	0.288	0.313	0.345	0.132	0.259	0.491
Na_2O	<0	<0.067	<0	<0	<0.066	<0
K_2O	0.025	0.018	0.052	0.020	0.047	0.142
P_2O_5	0.724	0.579	0.640	0.438	0.647	0.476
Total	**100.294**	**100.386**	**99.527**	**100.174**	**100.322**	**100.354**
			Atoms per formula unit			
Si	1.781	1.789	1.736	1.795	1.759	1.774
Ti	0.009	0.012	0.026	0.011	0.018	0.010
Al	0.259	0.241	0.302	0.262	0.289	0.274
Mg	0.172	0.243	0.157	0.177	0.207	0.156
Ca	0.896	0.835	0.896	0.879	0.882	0.866
Mn	0.043	0.050	0.040	0.045	0.041	0.049
Fe^{2+}	0.739	0.744	0.753	0.738	0.718	0.777
Fe^{3+}	0.000	0.000	0.000	0.000	0.000	0.000
Ni	0.000	0.000	0.002	0.002	0.000	0.000
Zn	0.114	0.110	0.115	0.115	0.105	0.121
Pb	0.003	0.003	0.004	0.001	0.003	0.005
Na	0.000	0.000	0.000	0.000	0.000	0.000
K	0.001	0.001	0.003	0.001	0.002	0.007
Pb	0.025	0.020	0.022	0.015	0.022	0.017
Total	**4.043**	**4.049**	**4.055**	**4.041**	**4.047**	**4.057**
$\mathbf{Ca_2Si_2O_6}$	49.58	45.82	49.61	49.00	48.82	48.14
$\mathbf{Fe_2Si_2O_6}$	40.89	40.83	41.71	41.13	39.74	43.16
$\mathbf{Mg_2Si_2O_6}$	9.54	13.36	8.68	9.87	11.43	8.69
Mg #	18.91	24.65	17.22	19.35	22.34	16.76

Table iv.39: EMP analyses of clinopyroxene from sample 12016(1) [Akllap].

Sample	**12016(2)**	**12016(2)**	**12016(2)**	**12016(2)**	**12016(2)**	**12016(2)**
No.	**#67**	**#72**	**#75**	**#77**	**#82**	**#83**
SiO_2	44.23	43.050	43.800	44.09	43.390	42.890
TiO_2	0.221	0.280	0.260	0.183	0.142	0.291
Al_2O_3	3.64	3.380	3.190	3.76	3.280	4.080
MgO	3.15	3.390	3.810	3.67	3.030	3.870
CaO	15.38	17.830	17.950	16.96	17.990	17.890
MnO	1.071	0.798	0.820	0.871	0.906	0.770
FeO	29.79	21.072	21.306	27.72	21.214	20.448
Fe_2O_3	0.000	7.477	5.806	0.000	6.108	7.181
NiO	0.097	0.228	0.168	0.214	0.067	0.225
ZnO	1.63	1.340	1.420	1.42	1.870	1.146
PbO	0.422	0.995	0.672	0.518	1.250	0.707
Na_2O	0.084	0.082	0.057	<0.056	0.108	0.059
K_2O	0.029	0.025	0.017	0.058	0.059	0.081
P_2O_5	0.46	0.601	0.625	0.427	0.676	0.729
Total	**100.204**	**100.548**	**99.900**	**99.891**	**100.090**	**100.367**
			Atoms per formula unit			
Si	1.834	1.766	1.796	1.825	1.791	1.749
Ti	0.007	0.009	0.008	0.006	0.004	0.009
Al	0.178	0.163	0.154	0.183	0.160	0.196
Mg	0.195	0.207	0.233	0.226	0.186	0.235
Ca	0.683	0.784	0.788	0.752	0.796	0.782
Mn	0.038	0.028	0.028	0.031	0.032	0.027
Fe^{2+}	1.033	0.723	0.730	0.960	0.732	0.698
Fe^{3+}	0.000	0.231	0.179	0.000	0.190	0.220
Ni	0.003	0.008	0.006	0.007	0.002	0.007
Zn	0.050	0.041	0.043	0.043	0.057	0.035
Pb	0.005	0.011	0.007	0.006	0.014	0.008
Na	0.007	0.007	0.005	0.000	0.009	0.005
K	0.002	0.001	0.001	0.003	0.003	0.004
Pb	0.016	0.021	0.022	0.015	0.024	0.025
Total	**4.050**	**3.999**	**4.000**	**4.057**	**4.000**	**4.000**
$\mathbf{Ca_2Si_2O_6}$	35.75	40.30	40.83	38.81	41.78	40.40
$\mathbf{Fe_2Si_2O_6}$	54.06	49.04	47.11	49.51	48.42	47.44
$\mathbf{Mg_2Si_2O_6}$	10.19	10.66	12.06	11.68	9.79	12.16
Mg #	15.86	22.29	24.17	19.09	20.29	25.23

Sample	**12016(2)**	**12016(2)**	**12016(2)**	**12016(2)**	**12016(2)**
No.	**#86**	**#89**	**#94**	**#96**	**#100**
SiO_2	43.670	45.13	44.140	44.1	44.85
TiO_2	0.183	0.179	0.279	0.208	0.163
Al_2O_3	3.230	3.57	3.080	3.89	3.52
MgO	4.050	4.01	3.470	3.47	3.59
CaO	18.660	18.48	17.350	17.58	18.39
MnO	0.776	0.783	0.768	0.84	0.843
FeO	19.794	24.44	23.018	27.43	25.99
Fe_2O_3	6.374	0.000	5.003	0.000	0.000
NiO	0.147	0.359	0.209	0.097	0.108
ZnO	1.520	1.163	1.470	1.34	1.68
PbO	0.854	0.766	0.888	0.48	0.886
Na_2O	0.057	0.171	0.083	0.057	<0.056
K_2O	0.036	0.26	0.020	0.093	0.06
P_2O_5	0.719	0.532	0.696	0.684	0.557
Total	**100.070**	**99.843**	**100.474**	**100.269**	**100.637**
		Atoms per formula unit			
Si	1.784	1.847	1.808	1.815	1.837
Ti	0.006	0.006	0.009	0.006	0.005
Al	0.156	0.172	0.149	0.189	0.170
Mg	0.247	0.245	0.212	0.213	0.219
Ca	0.817	0.810	0.761	0.775	0.807
Mn	0.027	0.027	0.027	0.029	0.029
Fe^{2+}	0.676	0.836	0.788	0.944	0.890
Fe^{3+}	0.196	0.000	0.154	0.000	0.000
Ni	0.005	0.012	0.007	0.003	0.004
Zn	0.046	0.035	0.044	0.041	0.051
Pb	0.009	0.008	0.010	0.005	0.010
Na	0.005	0.014	0.007	0.005	0.000
K	0.002	0.014	0.001	0.005	0.003
Pb	0.025	0.018	0.024	0.024	0.019
Total	**4.000**	**4.044**	**4.000**	**4.054**	**4.045**
$Ca_2Si_2O_6$	42.20	42.84	39.74	40.12	42.11
$Fe_2Si_2O_6$	45.06	44.22	49.20	48.86	46.45
$Mg_2Si_2O_6$	12.74	12.93	11.06	11.02	11.44
Mg #	26.73	22.63	21.18	18.40	19.76

Table iv.40: EMP analyses of clinopyroxene from sample 12016(2) [Akllap].

Sample	**13030(1)**	**13030(1)**	**13030(1)**
No.	**#50**	**#56**	**#60**
SiO_2	41.420	41.790	41.220
TiO_2	0.450	0.443	0.391
Al_2O_3	6.870	6.690	6.520
MgO	2.240	2.810	2.230
CaO	19.010	19.810	20.150
MnO	1.400	1.360	1.450
FeO	22.500	22.280	22.810
Fe_2O_3	0.000	0.000	0.000
NiO	<0.040	<0.043	<0
ZnO	1.860	1.810	1.980
PbO	1.840	1.400	2.230
Na_2O	<0	<0	<0
K_2O	0.771	0.574	0.509
P_2O_5	0.675	0.773	0.734
Total	**99.036**	**99.740**	**100.224**
	Atoms per formula unit		
Si	1.736	1.729	1.721
Ti	0.014	0.014	0.012
Al	0.339	0.326	0.321
Mg	0.140	0.173	0.139
Ca	0.854	0.878	0.901
Mn	0.050	0.048	0.051
Fe^{2+}	0.789	0.771	0.796
Fe^{3+}	0.000	0.000	0.000
Ni	0.000	0.000	0.000
Zn	0.058	0.055	0.061
Pb	0.021	0.016	0.025
Na	0.000	0.000	0.000
K	0.041	0.030	0.027
Pb	0.024	0.027	0.026
Total	4.065	4.068	4.081
$\mathbf{Ca_2Si_2O_6}$	47.90	48.19	49.08
$\mathbf{Fe_2Si_2O_6}$	44.25	42.30	43.36
$\mathbf{Mg_2Si_2O_6}$	7.85	9.51	7.56
Mg #	15.07	18.36	14.84

Table iv.41: EMP analyses of clinopyroxene from sample 13030(1) [Ostri Vrh].

Sample	**13031(1)**	**13031(1)**	**13031(1)**	**13031(1)**	**13031(1)**	**13031(1)**	**13031(1)**	**13031(1)**	**13031(1)**	**13031(1)**
No.	**#6**	**#10**	**#14**	**#15**	**#29**	**#34**	**#39**	**#46**	**#11**	**#14**
SiO_2	35.920	36.040	36.560	36.150	35.430	35.170	34.170	35.620	35.910	36.690
Al_2O_3	4.530	3.360	3.180	3.090	3.040	3.170	3.980	3.650	5.450	3.290
MgO	1.790	1.740	1.910	1.920	1.780	1.632	1.700	1.710	2.900	1.900
CaO	27.240	28.420	28.930	28.940	27.590	26.110	28.050	28.580	30.560	28.240
MnO	0.329	0.393	0.396	0.361	0.490	0.418	0.368	0.371	0.293	0.378
FeO	2.280	2.260	2.560	2.530	4.030	2.360	3.070	2.870	2.650	2.340
ZnO	13.410	13.080	13.480	13.700	13.590	12.660	12.860	13.340	11.100	13.950
PbO	11.160	11.950	11.750	11.880	13.350	15.910	13.400	11.810	8.970	10.670
K_2O	2.090	0.696	0.684	0.646	0.606	0.600	0.479	0.666	0.504	0.657
P_2O_5	<0.025	<0.027	0.052	0.060	<0.029	0.047	0.056	0.079	0.054	<0.025
Total	**98.749**	**98.218**	**99.502**	**99.277**	**99.906**	**98.077**	**98.133**	**98.696**	**98.391**	**98.115**
				Atoms per formula unit						
Si	1.962	1.988	1.988	1.978	1.965	2.005	1.923	1.960	1.904	2.004
Al	0.292	0.218	0.204	0.199	0.199	0.213	0.264	0.237	0.341	0.212
Mg	0.146	0.143	0.155	0.157	0.147	0.139	0.143	0.140	0.229	0.155
Ca	1.595	1.680	1.686	1.697	1.639	1.595	1.692	1.685	1.736	1.653
Mn	0.015	0.018	0.018	0.017	0.023	0.020	0.018	0.017	0.013	0.017
Fe^{2+}	0.104	0.104	0.116	0.116	0.187	0.113	0.145	0.132	0.118	0.107
Zn	0.541	0.533	0.541	0.553	0.556	0.533	0.534	0.542	0.434	0.562
Pb	0.164	0.177	0.172	0.175	0.199	0.244	0.203	0.175	0.128	0.157
K	0.146	0.049	0.047	0.045	0.043	0.044	0.034	0.047	0.034	0.046
P	0.000	0.000	0.002	0.003	0.000	0.002	0.003	0.004	0.002	0.000
Total	**4.965**	**4.942**	**4.930**	**4.940**	**4.958**	**4.907**	**4.958**	**4.939**	**4.939**	**4.913**

Table iv.42: EMP analyses of melilite from sample 13031(1) [Ostri Vrh].

Sample	**12015(7)**	**11029(5)**	**10024(2)**	**10021(21)**	**10021(21)**	**10021(21)**	**10021(21)**	**10021(21)**	**13030(1)**
No.	**#22**	**#1**	**#1**	**#106**	**#108**	**#111**	**#112**	**#113**	**#13**
SiO_2	64.280	63.130	64.140	51.700	51.610	46.710	47.110	49.730	63.820
Al_2O_3	18.910	18.350	22.670	29.520	29.820	33.010	33.020	31.250	18.070
Fe_2O_3	1.774	0.520	1.100	3.534	3.023	2.667	3.090	2.736	0.396
CaO	0.213	na	na	13.650	14.020	17.620	17.470	15.360	na
Na_2O	2.260	0.974	9.510	3.100	3.100	1.230	1.410	2.510	0.201
K_2O	12.050	14.880	0.269	1.097	0.856	0.285	0.332	0.539	16.470
Total	**99.487**	**97.854**	**97.689**	**102.601**	**102.429**	**101.522**	**102.432**	**102.125**	**98.957**
				Atoms per formula unit					
Si	2.954	2.976	2.867	2.325	2.321	2.135	2.137	2.247	2.990
Al	1.024	1.019	1.194	1.564	1.580	1.778	1.765	1.664	0.998
Fe^{3+}	0.061	0.018	0.037	0.120	0.102	0.092	0.105	0.093	0.014
Ca	0.010	0.000	0.000	0.658	0.675	0.863	0.849	0.744	0.000
Na	0.201	0.089	0.824	0.270	0.270	0.109	0.124	0.220	0.018
K	0.706	0.895	0.015	0.063	0.049	0.017	0.019	0.031	0.985
Total	**4.957**	**4.997**	**4.937**	**5.000**	**4.998**	**4.993**	**5.000**	**4.999**	**5.005**
$CaAl_2Si_2O_8$	1.14	0.00	0.00	66.37	67.90	87.29	85.57	74.77	0.00
$NaAlSi_3O_8$	21.93	9.05	98.17	27.28	27.17	11.03	12.50	22.11	1.82
$KAlSi_3O_8$	76.93	90.95	1.83	6.35	4.94	1.68	1.94	3.12	98.18

Table iv.43: EMP analyses of feldspar.

Sample	**12015(5)**	**12015(5)**	**12015(5)**	**12015(5)**	**12015(5)**	**12015(5)**
No.	**#32**	**#33**	**#36**	**#40**	**#42**	**#43**
SiO_2	54.780	55.160	54.390	55.980	54.750	54.840
Al_2O_3	21.900	21.470	21.710	21.530	21.610	21.990
Fe_2O_3	2.476	2.934	2.890	2.394	2.407	2.014
Na_2O	0.476	0.400	0.411	0.264	0.383	0.452
K_2O	19.920	19.840	19.820	19.740	19.950	20.110
Total	**99.552**	**99.804**	**99.221**	**99.908**	**99.100**	**99.406**
			Atoms per formula unit			
Si	2.020	2.033	2.019	2.047	2.027	2.021
Al	0.952	0.933	0.950	0.928	0.943	0.955
Fe^{3+}	0.031	0.037	0.036	0.030	0.030	0.025
Na	0.034	0.029	0.030	0.019	0.027	0.032
K	0.937	0.933	0.938	0.921	0.942	0.945
Total	**3.974**	**3.963**	**3.972**	**3.944**	**3.971**	**3.978**

Table iv.44: EMP analyses of leucite from sample 12015(5) [Voguçincë].

Sample	**12015(7)**	**12015(7)**	**12015(7)**	**12015(7)**	**12015(7)**	**12015(7)**	**12015(7)**	**12015(7)**	**12015(7)**	**12015(7)**
No.	**#103**	**#33**	**#36**	**#45**	**#48**	**#51**	**#54**	**#58**	**#63**	**#68**
SiO_2	56.210	55.860	55.980	55.470	56.870	55.920	56.220	55.870	55.840	55.520
Al_2O_3	21.600	21.970	21.910	21.320	21.530	21.990	21.860	21.790	21.550	21.590
Fe_2O_3	2.112	1.389	1.280	3.023	1.389	1.418	2.043	1.149	2.054	2.436
Na_2O	0.424	0.512	0.557	0.705	0.575	0.588	0.715	0.593	0.614	0.679
K_2O	20.470	20.470	20.320	19.490	19.880	20.320	19.990	20.230	20.220	20.050
Total	**100.816**	**100.201**	**100.047**	**100.008**	**100.244**	**100.236**	**100.828**	**99.632**	**100.278**	**100.275**
				Atoms per formula unit						
Si	2.042	2.034	2.038	2.038	2.059	2.034	2.037	2.040	2.039	2.033
Al	0.925	0.943	0.940	0.923	0.919	0.943	0.934	0.938	0.927	0.932
Fe^{3+}	0.026	0.017	0.016	0.038	0.017	0.017	0.025	0.014	0.025	0.030
Na	0.030	0.036	0.039	0.050	0.040	0.041	0.050	0.042	0.043	0.048
K	0.949	0.951	0.944	0.914	0.918	0.943	0.924	0.942	0.942	0.936
Total	**3.972**	**3.980**	**3.976**	**3.963**	**3.953**	**3.978**	**3.970**	**3.976**	**3.977**	**3.979**

Table iv.45: EMP analyses of leucite from sample 12015(7) [Voguçincë].

Sample	**12015(12)**	**12015(12)**	**12015(12)**	**12015(12)**	**12015(12)**	**12015(12)**	**12015(12)**	**12015(12)**	**12015(12)**	**12015(12)**	**12015(12)**	**12015(12)**	**12015(12)**
No.	**#16**	**#18**	**#19**	**#20**	**#21**	**#22**	**#23**	**#24**	**#26**	**#27**	**#28**	**#29**	**#30**
SiO_2	54.630	54.220	54.400	54.930	54.520	54.500	55.120	54.940	54.620	54.800	54.930	55.670	54.390
Al_2O_3	22.510	22.450	22.080	21.920	22.330	22.190	21.810	21.840	21.940	21.970	22.010	21.860	22.210
Fe_2O_3	2.447	2.850	2.314	2.092	2.258	2.501	2.638	2.283	1.556	2.298	2.127	1.703	1.903
Na_2O	0.216	0.703	0.168	0.214	0.466	0.327	0.579	0.453	0.478	0.172	0.457	0.229	0.382
K_2O	20.720	19.860	20.510	20.670	20.170	20.410	19.930	20.100	20.460	20.800	20.280	20.400	20.470
Total	**100.523**	**100.083**	**99.472**	**99.826**	**99.744**	**99.928**	**100.077**	**99.616**	**99.054**	**100.040**	**99.804**	**99.862**	**99.355**
						Atoms per formula unit							
Si	2.002	1.997	2.012	2.021	2.007	2.008	2.024	2.023	2.019	2.017	2.019	2.036	2.009
Al	0.972	0.974	0.962	0.951	0.969	0.964	0.944	0.948	0.956	0.953	0.954	0.942	0.967
Fe^{3+}	0.030	0.036	0.029	0.026	0.028	0.031	0.033	0.028	0.019	0.029	0.026	0.021	0.024
Na	0.015	0.050	0.012	0.015	0.033	0.023	0.041	0.032	0.034	0.012	0.033	0.016	0.027
K	0.969	0.933	0.968	0.970	0.947	0.959	0.934	0.944	0.965	0.977	0.951	0.952	0.965
Total	**3.989**	**3.990**	**3.983**	**3.983**	**3.985**	**3.986**	**3.975**	**3.977**	**3.993**	**3.987**	**3.983**	**3.967**	**3.992**

Table iv.46: EMP analyses of leucite from sample 12015(12) [Voguçincë].

Sample	**14032**	**14032**	**14032**	**14032**	**14032**	**14032**	**14032**	**14032**	**14032**	**14032**	**14032**
No.	**#2**	**#3**	**#5**	**#6**	**#8**	**#9**	**#10**	**#12**	**#13**	**#14**	**#15**
SiO_2	55.470	55.830	55.900	55.460	54.920	55.660	55.700	55.000	55.540	55.700	55.400
Al_2O_3	22.230	21.890	21.580	21.790	21.970	21.810	22.070	21.860	21.840	22.100	21.850
Fe_2O_3	1.689	1.769	2.458	2.372	2.481	2.049	2.145	2.807	1.903	2.345	2.229
Na_2O	0.244	0.192	0.150	0.169	0.358	0.479	0.500	0.310	0.363	0.508	0.434
K_2O	20.370	20.270	20.270	20.310	20.090	19.880	19.950	20.110	20.060	19.910	20.050
Total	**100.003**	**99.951**	**100.358**	**100.101**	**99.819**	**99.878**	**100.365**	**100.087**	**99.706**	**100.563**	**99.963**
					Atoms per formula unit						
Si	2.025	2.038	2.042	2.032	2.020	2.036	2.029	2.022	2.034	2.027	2.030
Al	0.957	0.942	0.929	0.941	0.953	0.940	0.947	0.947	0.943	0.948	0.943
Fe^{3+}	0.021	0.022	0.030	0.029	0.031	0.025	0.026	0.035	0.024	0.029	0.028
Na	0.017	0.014	0.011	0.012	0.026	0.034	0.035	0.022	0.026	0.036	0.031
K	0.949	0.944	0.944	0.949	0.943	0.927	0.927	0.943	0.937	0.924	0.937
Total	**3.969**	**3.959**	**3.956**	**3.964**	**3.972**	**3.962**	**3.965**	**3.970**	**3.964**	**3.964**	**3.969**

Table iv.47: EMP analyses of leucite from sample 14032 [Voguçincë].

Sample	**11029(5)**	**11029(5)**	**10024(4)**	**10024(4)**	**10024(4)**	**10024(4)**	**10024(4)**	**10024(4)**	**10024(4)**	**10024(5)**	**10024(5)**	**10024(5)**	**10024(5)**	**10024(5)**
No.	**#5**	**#6**	**#14**	**#15**	**#16**	**#18**	**#20**	**#21**	**#22**	**#23**	**#24**	**#25**	**#26**	**#27**
SiO_2	55.650	55.570	54.020	54.100	54.910	54.030	54.040	54.350	54.660	54.040	54.140	54.310	55.350	54.660
Al_2O_3	21.540	21.600	22.750	22.850	22.430	22.480	22.550	22.690	22.500	22.050	22.590	22.470	22.520	22.690
Fe_2O_3	2.234	2.367	2.890	2.509	1.229	2.756	2.734	2.069	1.391	2.703	1.240	1.398	0.567	1.214
Na_2O	0.178	0.241	0.703	0.748	0.781	1.029	0.779	0.839	0.649	0.298	0.846	0.715	1.086	1.440
K_2O	19.750	19.670	20.510	20.420	20.260	19.930	20.120	20.180	20.280	21.200	20.200	20.340	19.880	19.670
Total	**99.352**	**99.448**	**100.873**	**100.627**	**99.610**	**100.225**	**100.223**	**100.128**	**99.480**	**100.291**	**99.016**	**99.233**	**99.403**	**99.674**
						Atoms per formula unit								
Si	2.045	2.042	1.983	1.984	2.012	1.990	1.990	1.994	2.007	1.998	1.998	2.003	2.018	2.000
Al	0.933	0.935	0.984	0.988	0.968	0.976	0.979	0.981	0.974	0.961	0.983	0.976	0.968	0.978
Fe^{3+}	0.028	0.029	0.036	0.031	0.015	0.034	0.034	0.026	0.017	0.034	0.015	0.017	0.007	0.015
Na	0.013	0.017	0.050	0.053	0.055	0.073	0.056	0.060	0.046	0.021	0.061	0.051	0.077	0.102
K	0.926	0.922	0.960	0.955	0.947	0.936	0.945	0.944	0.950	1.000	0.951	0.957	0.925	0.918
Total	**3.944**	**3.946**	**4.013**	**4.011**	**3.998**	**4.010**	**4.004**	**4.005**	**3.995**	**4.015**	**4.008**	**4.004**	**3.995**	**4.014**

Table iv.48: EMP analyses of leucite from samples 11029(5) [Mirash Novo] and 10024(4) and 10024(5) [Mramor Proni Butoçit].

Sample	**10021(2)**	**10021(2)**	**10021(2)**	**10021(21)**	**10021(21)**	**10021(21)**	**10021(21)**	**10021(21)**	**10021(21)**	**10021(21)**	**10021(21)**	**10021(21)**	**10021(21)**
No.	**#4**	**#12**	**#15**	**#16**	**#17**	**#18**	**#19**	**#20**	**#24**	**#27**	**#28**	**#29**	**#30**
SiO_2	54.450	54.270	54.540	54.610	54.810	54.220	54.060	54.090	54.110	54.550	54.310	53.540	54.830
Al_2O_3	22.690	22.930	23.140	23.190	22.930	23.110	23.180	23.190	23.240	23.170	23.110	23.070	22.710
Fe_2O_3	1.703	1.894	1.174	1.062	1.171	1.334	2.072	1.331	1.754	1.185	1.676	1.938	1.460
Na_2O	0.521	0.459	0.448	0.543	0.508	0.698	0.672	0.645	0.670	0.734	0.603	0.653	0.957
K_2O	21.150	21.330	21.680	21.340	21.060	20.910	20.680	20.880	20.910	20.800	21.040	20.510	20.410
Total	**100.514**	**100.883**	**100.982**	**100.745**	**100.479**	**100.272**	**100.664**	**100.136**	**100.684**	**100.439**	**100.739**	**99.711**	**100.367**
						Atoms per formula unit							
Si	1.994	1.984	1.985	1.987	1.997	1.984	1.978	1.981	1.977	1.988	1.983	1.976	2.000
Al	0.979	0.988	0.993	0.994	0.985	0.997	1.000	1.001	1.001	0.995	0.994	1.004	0.976
Fe^{3+}	0.021	0.023	0.014	0.013	0.014	0.017	0.026	0.017	0.022	0.015	0.021	0.024	0.018
Na	0.037	0.033	0.032	0.038	0.036	0.050	0.048	0.046	0.047	0.052	0.043	0.047	0.068
K	0.988	0.995	1.007	0.991	0.979	0.976	0.965	0.976	0.975	0.967	0.980	0.966	0.950
Total	**4.019**	**4.024**	**4.030**	**4.024**	**4.011**	**4.022**	**4.016**	**4.021**	**4.022**	**4.017**	**4.021**	**4.016**	**4.012**

Table iv.49: EMP analyses of leucite from samples 10021(2) and 10021(21) [Mramor Samakove].

Sample	**10-1A**	**10-1A**	**10-1A**	**10-1A**	**10-1A**	**10-1A**	**10-1A**	**10-1A**	**3(2)**	**3(2)**	**3(2)**	**3(2)**	**3(2)**	**3(2)**	**3(2)**	**3(2)**
No.	**#1**	**#2**	**#3**	**#4**	**#5**	**#6**	**#8**	**#9**	**#1**	**#3**	**#2**	**#4**	**#6**	**#7**	**#11**	**#12**
SiO_2	53.830	53.860	54.350	54.370	54.010	53.300	53.710	54.180	53.860	53.570	54.020	53.960	53.810	54.000	53.860	53.560
Al_2O_3	22.790	22.760	22.830	22.750	22.830	22.750	22.860	22.790	23.180	23.240	23.070	23.090	23.150	23.140	22.860	23.050
Fe_2O_3	2.850	2.514	2.534	2.114	2.569	2.723	2.643	2.723	1.491	2.143	2.036	1.405	2.509	1.845	2.683	1.818
Na_2O	1.020	1.220	1.099	0.549	1.006	0.870	0.915	1.054	0.273	0.233	0.439	0.563	0.535	0.702	0.716	0.554
K_2O	19.760	19.690	19.900	20.680	20.140	20.360	20.060	19.990	20.990	21.240	20.820	20.750	20.540	20.520	20.180	20.640
Total	**100.250**	**100.044**	**100.713**	**100.463**	**100.555**	**100.003**	**100.188**	**100.737**	**99.794**	**100.426**	**100.385**	**99.768**	**100.544**	**100.207**	**100.299**	**99.622**
							Atoms per formula unit									
Si	1.982	1.983	1.987	1.992	1.982	1.974	1.979	1.985	1.981	1.971	1.982	1.983	1.975	1.980	1.982	1.978
Al	0.989	0.988	0.984	0.982	0.987	0.993	0.993	0.984	1.005	1.008	0.997	1.000	1.002	1.000	0.991	1.003
Fe^{3+}	0.036	0.031	0.031	0.026	0.032	0.034	0.033	0.034	0.019	0.027	0.025	0.017	0.031	0.023	0.033	0.023
Na	0.073	0.087	0.078	0.039	0.072	0.062	0.065	0.075	0.019	0.017	0.031	0.040	0.038	0.050	0.051	0.040
K	0.928	0.925	0.928	0.967	0.943	0.962	0.943	0.934	0.985	0.997	0.974	0.973	0.962	0.960	0.947	0.972
Total	**4.007**	**4.014**	**4.008**	**4.006**	**4.016**	**4.025**	**4.013**	**4.011**	**4.009**	**4.019**	**4.010**	**4.014**	**4.008**	**4.013**	**4.005**	**4.015**

Table iv.50: EMP analyses of leucite from samples 10-1A [Hajkobile] and 3(2) [Hanroc].

Sample	**13030(1)**	**13030(1)**	**13030(1)**	**13030(1)**
No.	**#10**	**#11**	**#12**	**#14**
SiO_2	55.430	54.860	55.160	54.760
Al_2O_3	21.910	21.940	21.830	21.970
Fe_2O_3	1.967	2.292	2.154	2.387
Na_2O	0.070	0.067	0.068	0.082
K_2O	20.510	20.790	20.620	20.960
Total	**99.887**	**99.949**	**99.832**	**100.159**
		Atoms per formula unit		
Si	2.031	2.019	2.028	2.015
Al	0.946	0.952	0.946	0.953
Fe^{3+}	0.024	0.029	0.027	0.030
Na	0.005	0.005	0.005	0.006
K	0.959	0.976	0.967	0.984
Total	**3.965**	**3.981**	**3.972**	**3.988**

Table iv.51: EMP analyses of leucite from sample 13030(1) [Ostri Vrh].

Sample	**13031(1)**	**13031(1)**	**13031(1)**	**13031(1)**	**13031(1)**	**13031(1)**	**13031(1)**	**13031(1)**	**13031(1)**	**13031(1)**	**13031(1)**	**13031(1)**	**13031(1)**	**13031(1)**	**13031(1)**	**13031(1)**
No.	**#15**	**#17**	**#23**	**#26**	**#27**	**#29**	**#32**	**#34**	**#11**	**#16**	**#21**	**#26**	**#30**	**#31**	**#35**	**#36**
SiO_2	37.480	37.510	37.310	37.320	37.450	37.270	37.410	37.460	37.460	37.460	37.460	37.460	37.460	37.460	37.460	37.460
Al_2O_3	30.090	30.020	30.330	30.110	30.430	29.880	30.510	30.250	30.250	30.250	30.250	30.250	30.250	30.250	30.250	30.250
Fe_2O_3	2.818	3.868	3.445	3.512	2.594	3.645	2.774	3.179	3.467	2.890	3.290	3.090	2.810	3.179	3.445	3.490
Na_2O	0.439	0.223	0.347	0.254	0.343	0.234	0.387	0.290	0.290	0.290	0.290	0.290	0.290	0.290	0.290	0.290
K_2O	28.470	28.630	28.300	28.380	28.460	28.450	28.230	28.280	28.280	28.280	28.280	28.280	28.280	28.280	28.280	28.280
Total	**99.297**	**100.251**	**99.732**	**99.576**	**99.277**	**99.479**	**99.311**	**99.459**	**99.747**	**99.170**	**99.570**	**99.370**	**99.090**	**99.459**	**99.725**	**99.770**
							Atoms per formula unit									
Si	1.000	0.994	0.992	0.994	0.998	0.995	0.996	0.997	0.995	0.999	0.996	0.998	1.000	0.997	0.995	0.995
Al	0.946	0.938	0.950	0.945	0.956	0.940	0.957	0.949	0.947	0.951	0.948	0.949	0.951	0.949	0.947	0.947
Fe^{3+}	0.057	0.077	0.069	0.070	0.052	0.073	0.056	0.064	0.069	0.058	0.066	0.062	0.056	0.064	0.069	0.070
Na	0.023	0.011	0.018	0.013	0.018	0.012	0.020	0.015	0.015	0.015	0.015	0.015	0.015	0.015	0.015	0.015
K	0.969	0.968	0.959	0.964	0.967	0.969	0.959	0.960	0.958	0.962	0.959	0.961	0.963	0.960	0.958	0.958
Total	**2.994**	**2.988**	**2.988**	**2.987**	**2.991**	**2.989**	**2.987**	**2.984**	**2.984**	**2.985**	**2.984**	**2.985**	**2.985**	**2.984**	**2.984**	**2.984**

Sample	**13031(1)**	**13031(1)**	**13031(1)**	**13031(1)**	**13031(1)**	**13031(1)**
No.	**#40**	**#41**	**#43**	**#48**	**#49**	**#50**
SiO_2	37.460	37.460	37.460	37.460	37.460	37.460
Al_2O_3	30.250	30.250	30.250	30.250	30.250	30.250
Fe_2O_3	2.956	2.770	3.090	3.356	3.401	3.423
Na_2O	0.290	0.290	0.290	0.290	0.290	0.290
K_2O	28.280	28.280	28.280	28.280	28.280	28.280
Total	**99.236**	**99.050**	**99.370**	**99.636**	**99.681**	**99.703**
			Atoms per formula unit			
Si	0.999	1.000	0.998	0.996	0.995	0.995
Al	0.950	0.952	0.949	0.948	0.947	0.947
Fe^{3+}	0.059	0.056	0.062	0.067	0.068	0.068
Na	0.015	0.015	0.015	0.015	0.015	0.015
K	0.962	0.963	0.961	0.959	0.959	0.958
Total	**2.985**	**2.985**	**2.985**	**2.984**	**2.984**	**2.984**

Table iv.52: EMP analyses of kalsilite from sample 13031(1) [Ostri Vrh].

Sample	**12015(5)**	**12015(5)**	**12015(5)**	**12015(5)**	**12015(5)**	**12015(5)**	**12015(5)**	**12015(5)**	**12015(12)**	**12015(12)**	**12015(12)**
No.	**#65**	**#68**	**#72**	**#73**	**#76**	**#77**	**#81**	**#83**	**#35**	**#38**	**#40**
TiO_2	3.170	2.880	2.060	2.800	2.060	2.880	2.410	0.058	0.196	0.283	1.840
Al_2O_3	11.920	9.530	8.130	16.470	8.190	14.510	8.840	0.263	49.740	47.560	30.450
Cr_2O_3	3.280	0.830	0.227	9.140	<0.026	6.200	0.614	<0.024	2.850	0.942	0.077
FeO	30.217	30.750	29.937	29.479	29.933	29.312	30.332	28.709	11.765	11.613	17.960
Fe_2O_3	45.011	51.553	55.391	34.540	55.683	39.071	53.618	69.557	6.673	10.898	29.071
MgO	0.528	0.457	0.343	0.623	0.189	0.582	0.469	0.308	0.915	0.786	0.605
MnO	0.626	0.558	0.546	0.655	0.503	0.659	0.574	0.424	0.229	0.265	0.377
NiO	<0.043	<0.044	<0.041	<0	<0	<0.044	<0.079	0.073	<0.039	<0	<0.042
ZnO	4.660	3.800	3.810	5.950	4.250	5.550	3.660	2.070	29.600	29.560	20.920
Total	**99.412**	**100.358**	**100.444**	**99.657**	**100.809**	**98.764**	**100.517**	**101.462**	**101.968**	**101.907**	**101.301**
					Atoms per formula unit						
Ti	0.086	0.079	0.057	0.074	0.057	0.078	0.066	0.002	0.004	0.007	0.046
Al	0.508	0.408	0.351	0.683	0.353	0.614	0.380	0.012	1.771	1.714	1.185
Cr	0.094	0.024	0.007	0.254	0.000	0.176	0.018	0.000	0.068	0.023	0.002
Fe^{2+}	0.914	0.935	0.918	0.867	0.916	0.880	0.924	0.910	0.297	0.297	0.496
Fe^{3+}	1.225	1.410	1.528	0.915	1.533	1.055	1.470	1.985	0.152	0.251	0.722
Mg	0.028	0.025	0.019	0.033	0.010	0.031	0.025	0.017	0.041	0.036	0.030
Mn	0.019	0.017	0.017	0.020	0.016	0.020	0.018	0.014	0.006	0.007	0.011
Ni	0.000	0.000	0.000	0.000	0.000	0.000	0.000	0.002	0.000	0.000	0.000
Zn	0.124	0.102	0.103	0.155	0.115	0.147	0.098	0.058	0.660	0.667	0.510
Total	**3.000**	**3.000**	**3.000**	**3.000**	**3.000**	**3.000**	**3.000**	**3.000**	**3.000**	**3.000**	**3.000**
Fe^{3+}/(Fe^{3+}+Al)	0.71	0.78	0.81	0.57	0.81	0.63	0.79	0.99	0.08	0.13	0.38
Zn/(Zn+Fe^{2+})	0.12	0.10	0.10	0.15	0.11	0.14	0.10	0.06	0.69	0.69	0.51

Table iv.53: EMP analyses of spinel *ss* from samples 12015(5) and 12015(12) [Voguçincë].

Sample	**11027(1)**	**11029(3)**	**11029(3)**	**11029(3)**	**11029(3)**	**11029(5)**	**11029(5)**
No.	**#183**	**#1**	**#11**	**#14**	**#20**	**#9**	**#20**
TiO_2	1.870	1.860	1.920	2.140	1.680	1.097	3.590
Al_2O_3	1.980	4.700	3.940	4.770	4.250	5.460	4.460
Cr_2O_3	0.086	0.333	0.097	0.723	0.189	6.070	6.490
FeO	27.972	31.683	31.557	31.827	31.205	29.130	31.212
Fe_2O_3	61.964	60.541	61.158	59.213	61.016	53.076	49.095
MgO	0.040	0.556	0.477	0.516	0.511	0.349	0.257
MnO	0.179	0.230	0.227	0.244	0.258	1.790	1.830
NiO	0.044	<0.044	<0	<0	<0.045	0.107	0.054
ZnO	5.000	1.300	1.310	1.360	1.340	1.023	1.340
Total	**99.135**	**101.202**	**100.686**	**100.793**	**100.449**	**98.102**	**98.328**
			Atoms per formula unit				
Ti	0.054	0.052	0.054	0.060	0.047	0.031	0.102
Al	0.090	0.205	0.173	0.208	0.187	0.244	0.199
Cr	0.003	0.010	0.003	0.021	0.006	0.182	0.195
Fe^{2+}	0.902	0.978	0.984	0.986	0.974	0.922	0.990
Fe^{3+}	1.799	1.682	1.716	1.651	1.713	1.512	1.401
Mg	0.002	0.031	0.027	0.029	0.028	0.020	0.015
Mn	0.006	0.007	0.007	0.008	0.008	0.057	0.059
Ni	0.001	0.000	0.000	0.000	0.000	0.003	0.002
Zn	0.142	0.035	0.036	0.037	0.037	0.029	0.038
Total	**3.000**	**3.000**	**3.000**	**3.000**	**3.000**	**3.000**	**3.000**
$Fe^{3+}/(Fe^{3+}+Al)$	0.95	0.89	0.91	0.89	0.90	0.86	0.88
$Zn/(Zn+Fe^{2+})$	0.14	0.03	0.04	0.04	0.04	0.03	0.04

Table iv.54: EMP analyses of spinel *ss* from samples 11027(1) [Mirash] and 11029(3) and 11029(5) [Mirash Novo].

Sample	**10024(2)**	**10024(2)**	**10024(2)**	**10024(2)**	**10024(2)**	**10024(2)**	**10024(2)**	**10024(2)**	**10024(2)**	**10024(2)**
No.	**#1**	**#6**	**#11**	**#12**	**#16**	**#18**	**#19**	**#20**	**#21**	**#24**
TiO_2	2.560	1.730	2.430	2.260	1.690	1.800	2.040	1.412	2.480	2.880
Al_2O_3	6.360	7.690	7.090	8.000	6.520	6.800	8.820	8.290	7.420	6.990
Cr_2O_3	0.675	1.340	0.480	0.910	0.252	0.326	1.174	1.059	0.343	0.411
FeO	24.672	22.313	24.577	24.141	22.837	22.466	24.134	23.134	24.854	24.981
Fe_2O_3	55.396	54.206	55.435	54.453	57.702	56.181	53.838	56.239	54.527	54.508
MgO	1.071	0.967	1.079	1.097	1.034	0.986	0.803	1.323	1.016	1.080
MnO	1.139	1.154	1.222	1.286	1.221	1.251	1.105	1.300	1.142	1.189
NiO	0.177	0.155	0.140	0.135	0.153	0.075	0.055	0.127	0.099	0.118
ZnO	7.280	9.290	7.550	8.050	8.670	8.950	8.980	8.220	7.330	7.480
Total	**99.330**	**98.845**	**100.003**	**100.332**	**100.079**	**98.835**	**100.949**	**101.103**	**99.211**	**99.637**
				Atoms per formula unit						
Ti	0.072	0.049	0.068	0.062	0.047	0.051	0.056	0.039	0.069	0.080
Al	0.280	0.339	0.309	0.346	0.285	0.301	0.379	0.355	0.325	0.306
Cr	0.020	0.040	0.014	0.026	0.007	0.010	0.034	0.030	0.010	0.012
Fe^{2+}	0.770	0.697	0.760	0.741	0.709	0.706	0.735	0.703	0.773	0.775
Fe^{3+}	1.556	1.524	1.542	1.503	1.613	1.588	1.476	1.537	1.526	1.522
Mg	0.060	0.054	0.059	0.060	0.057	0.055	0.044	0.072	0.056	0.060
Mn	0.036	0.037	0.038	0.040	0.038	0.040	0.034	0.040	0.036	0.037
Ni	0.005	0.005	0.004	0.004	0.005	0.002	0.002	0.004	0.003	0.004
Zn	0.201	0.256	0.206	0.218	0.238	0.248	0.241	0.220	0.201	0.205
Total	**3.000**	**3.000**	**3.000**	**3.000**	**3.000**	**3.000**	**3.000**	**3.000**	**3.000**	**3.000**
Fe^{3+}/(Fe^{3+}+Al)	0.85	0.82	0.83	0.81	0.85	0.84	0.80	0.81	0.82	0.83
Zn/(Zn+Fe^{2+})	0.21	0.27	0.21	0.23	0.25	0.26	0.25	0.24	0.21	0.21

Table iv.55: EMP analyses of spinel *ss* from sample 10024(2) [Mramor Proni Butoçit].

Sample	**10024(4)**	**10024(4)**	**10024(4)**	**10024(4)**	**10024(4)**	**10024(4)**	**10024(4)**	**10024(4)**
No.	**#32**	**#36**	**#40**	**#42**	**#45**	**#50**	**#56**	**#65**
TiO_2	3.100	2.910	2.580	2.180	3.470	2.830	2.230	2.690
Al_2O_3	8.090	7.170	7.250	5.930	7.420	6.690	6.310	7.350
Cr_2O_3	0.573	0.699	0.386	0.721	0.210	<0.026	0.233	0.502
FeO	31.917	31.801	31.248	30.828	32.405	32.213	31.377	31.530
Fe_2O_3	54.124	55.553	56.034	58.812	53.692	56.662	58.058	55.676
MgO	1.128	0.906	1.038	1.122	0.300	0.262	0.550	1.014
MnO	0.545	0.557	0.504	0.558	0.409	0.416	0.447	0.515
NiO	<0.043	<0.042	<0	<0.043	0.000	<0	<0.042	<0.076
ZnO	1.610	1.850	1.740	1.710	2.690	2.490	2.130	1.640
Total	**101.087**	**101.446**	**100.780**	**101.861**	**100.596**	**101.563**	**101.335**	**100.917**
			Atoms per formula unit					
Ti	0.084	0.079	0.071	0.060	0.096	0.078	0.061	0.074
Al	0.344	0.306	0.311	0.254	0.321	0.288	0.272	0.315
Cr	0.016	0.020	0.011	0.021	0.006	0.000	0.007	0.014
Fe^{2+}	0.964	0.964	0.952	0.936	0.994	0.984	0.960	0.959
Fe^{3+}	1.471	1.515	1.536	1.607	1.482	1.557	1.598	1.523
Mg	0.061	0.049	0.056	0.061	0.016	0.014	0.030	0.055
Mn	0.017	0.017	0.016	0.017	0.013	0.013	0.014	0.016
Ni	0.000	0.000	0.000	0.000	0.000	0.000	0.000	0.000
Zn	0.043	0.049	0.047	0.046	0.073	0.067	0.058	0.044
Total	**3.000**	**3.000**	**3.000**	**3.000**	**3.000**	**3.000**	**3.000**	**3.000**
Fe^{3+}/(Fe^{3+}+Al)	0.81	0.83	0.83	0.86	0.82	0.84	0.85	0.83
Zn/(Zn+Fe^{2+})	0.04	0.05	0.05	0.05	0.07	0.06	0.06	0.04

Table iv.56: EMP analyses of spinel *ss* from sample 10024(4) [Mramor Proni Butoçit].

Sample	**10024(5)**	**10024(5)**	**10024(5)**	**10024(5)**	**10024(5)**	**10024(5)**	**10024(5)**	**10024(5)**	**10024(5)**	**10024(5)**	**10024(5)**	**10024(5)**	**10024(5)**	**10024(5)**
No.	**#68**	**#73**	**#75**	**#79**	**#83**	**#87**	**#91**	**#96**	**#99**	**#104**	**#106**	**#109**	**#113**	**#116**
TiO_2	1.537	1.545	1.381	1.386	1.172	1.167	2.120	1.830	1.840	2.640	2.820	2.680	1.605	1.790
Al_2O_3	4.060	4.180	4.660	3.390	3.410	5.660	4.330	4.830	5.090	4.210	3.290	3.720	3.410	3.690
Cr_2O_3	0.281	0.170	0.597	0.104	0.050	3.580	0.637	0.770	0.481	0.810	0.423	1.028	0.106	0.062
FeO	28.499	28.560	28.323	28.195	27.043	27.455	29.640	28.865	29.104	30.192	29.939	30.086	28.544	29.290
Fe_2O_3	62.712	62.766	62.397	63.705	63.107	58.271	61.321	60.616	60.794	59.686	60.722	60.203	62.795	61.877
MgO	1.680	1.690	1.820	1.641	1.770	2.090	1.730	2.050	1.980	1.532	1.690	1.640	1.351	0.598
MnO	0.628	0.597	0.636	0.596	0.700	0.667	0.586	0.622	0.563	0.619	0.646	0.604	0.725	0.799
NiO	<0.045	0.061	0.108	0.072	<0.046	0.088	<0.043	<0.045	0.085	<0.044	<0	<0	<0.044	<0.043
ZnO	2.090	2.050	2.050	2.040	2.290	2.330	1.630	1.340	1.350	1.590	1.480	1.580	2.160	2.860
Total	**101.487**	**101.619**	**101.971**	**101.129**	**99.542**	**101.308**	**101.995**	**100.923**	**101.288**	**101.279**	**101.011**	**101.542**	**100.696**	**100.966**
						Atoms per formula unit								
Ti	0.042	0.043	0.038	0.039	0.033	0.032	0.058	0.050	0.050	0.073	0.078	0.074	0.045	0.050
Al	0.176	0.180	0.200	0.148	0.151	0.242	0.186	0.208	0.219	0.182	0.143	0.161	0.149	0.162
Cr	0.008	0.005	0.017	0.003	0.001	0.103	0.018	0.022	0.014	0.024	0.012	0.030	0.003	0.002
Fe^{2+}	0.874	0.875	0.861	0.872	0.848	0.833	0.902	0.883	0.887	0.927	0.925	0.923	0.888	0.913
Fe^{3+}	1.731	1.730	1.708	1.772	1.782	1.591	1.680	1.669	1.667	1.649	1.688	1.662	1.758	1.736
Mg	0.092	0.092	0.099	0.090	0.099	0.113	0.094	0.112	0.108	0.084	0.093	0.090	0.075	0.033
Mn	0.020	0.019	0.020	0.019	0.022	0.021	0.018	0.019	0.017	0.019	0.020	0.019	0.023	0.025
Ni	0.000	0.002	0.003	0.002	0.000	0.003	0.000	0.000	0.002	0.000	0.000	0.000	0.000	0.000
Zn	0.057	0.055	0.055	0.056	0.063	0.062	0.044	0.036	0.036	0.043	0.040	0.043	0.059	0.079
Total	**3.000**	**3.000**	**3.000**	**3.000**	**3.000**	**3.000**	**3.000**	**3.000**	**3.000**	**3.000**	**3.000**	**3.000**	**3.000**	**3.000**
Fe^{3+}/(Fe^{3+}+Al)	0.91	0.91	0.90	0.92	0.92	0.87	0.90	0.89	0.88	0.90	0.92	0.91	0.92	0.91
Zn/(Zn+Fe^{2+})	0.06	0.06	0.06	0.06	0.07	0.07	0.05	0.04	0.04	0.04	0.04	0.04	0.06	0.08

Table iv.57: EMP analyses of spinel *ss* from sample 10024(5) [Mramor Proni Butoçit].

Sample	**10021(2)**	**10021(2)**	**10021(2)**	**10021(2)**	**10-6**	**10-1A**	**10-1A**	**10-1A**	**10-1A**	**10-1A**	**10-1A**	**10-1A**	**10-1A**	**10-1A**	**10-1A**
No.	**#41**	**#43**	**#54**	**#57**	**#165**	**#11**	**#13**	**#14**	**#16**	**#18**	**#26**	**#28**	**#32**	**#35**	**#37**
TiO_2	0.996	1.475	1.135	3.450	12.55	1.990	2.330	2.130	1.890	1.820	1.730	1.970	1.970	1.780	1.880
Al_2O_3	30.060	27.320	26.750	42.160	3.520	16.940	22.180	14.190	18.100	13.900	17.460	16.440	12.330	17.950	19.140
Cr_2O_3	21.180	22.540	24.270	0.113	0.504	0.156	0.413	0.073	0.356	0.079	0.056	0.062	0.071	0.100	0.095
FeO	29.228	29.935	29.310	32.480	40.542	27.224	28.044	28.436	27.341	28.184	27.391	27.898	28.435	27.538	27.138
Fe_2O_3	11.782	12.941	12.013	13.080	40.171	45.514	38.324	48.324	44.773	50.326	46.007	46.900	51.770	45.432	43.943
MgO	2.390	2.210	2.190	0.221	0.022	0.971	1.055	0.761	0.967	0.825	0.868	0.862	0.746	0.901	0.989
MnO	0.423	0.406	0.436	0.274	0.051	0.331	0.349	0.322	0.373	0.345	0.350	0.334	0.344	0.333	0.348
NiO	<0	<0	<0	<0	0.049	<0.043	<0.043	<0.043	<0	<0.043	<0	<0	<0.043	<0	<0.045
ZnO	4.950	4.640	4.660	9.860	3.050	7.680	7.910	6.220	7.960	6.510	7.760	7.350	6.170	7.770	8.420
Total	**101.009**	**101.467**	**100.764**	**101.638**	**100.459**	**100.806**	**100.605**	**100.456**	**101.760**	**101.989**	**101.622**	**101.815**	**101.836**	**101.804**	**101.953**
						Atoms per formula unit									
Ti	0.024	0.036	0.028	0.080	0.352	0.052	0.060	0.057	0.049	0.048	0.045	0.051	0.052	0.046	0.048
Al	1.133	1.039	1.026	1.533	0.155	0.696	0.889	0.594	0.734	0.574	0.711	0.672	0.514	0.728	0.771
Cr	0.536	0.575	0.624	0.003	0.015	0.004	0.011	0.002	0.010	0.002	0.002	0.002	0.002	0.003	0.003
Fe^{2+}	0.782	0.808	0.798	0.838	1.264	0.794	0.798	0.844	0.786	0.826	0.792	0.809	0.842	0.793	0.776
Fe^{3+}	0.284	0.314	0.294	0.304	1.127	1.195	0.981	1.291	1.159	1.328	1.197	1.224	1.379	1.177	1.130
Mg	0.114	0.106	0.106	0.010	0.001	0.050	0.053	0.040	0.050	0.043	0.045	0.045	0.039	0.046	0.050
Mn	0.011	0.011	0.012	0.007	0.002	0.010	0.010	0.010	0.011	0.010	0.010	0.010	0.010	0.010	0.010
Ni	0.000	0.000	0.000	0.000	0.001	0.000	0.000	0.000	0.000	0.000	0.000	0.000	0.000	0.000	0.000
Zn	0.117	0.111	0.112	0.225	0.084	0.198	0.199	0.163	0.202	0.168	0.198	0.188	0.161	0.197	0.212
Total	**3.000**	**3.000**	**3.000**	**3.000**	**3.000**	**3.000**	**3.000**	**3.000**	**3.000**	**3.000**	**3.000**	**3.000**	**3.000**	**3.000**	**3.000**
$Fe^{3+}/(Fe^{3+}+Al)$	0.20	0.23	0.22	0.17	0.88	0.63	0.52	0.68	0.61	0.70	0.63	0.65	0.73	0.62	0.59
$Zn/(Zn+Fe^{2+})$	0.13	0.12	0.12	0.21	0.06	0.20	0.20	0.16	0.20	0.17	0.20	0.19	0.16	0.20	0.21

Table iv.58: EMP analyses of spinel *ss* from samples 10021(2) [Mramor Samakove], 10-6 [Marec] and 10-1A [Hajkobile].

Sample	**12016(1)**	**12016(1)**	**12016(1)**	**12016(1)**	**12016(1)**
No.	**#30**	**#36**	**#45**	**#52**	**#63**
TiO_2	4.260	3.200	1.840	4.100	3.940
Al_2O_3	7.070	7.490	7.130	10.700	8.250
Cr_2O_3	0.838	0.685	0.260	4.440	0.337
FeO	25.091	25.058	24.403	23.036	25.191
Fe_2O_3	51.708	53.744	57.462	43.789	51.319
MgO	0.995	0.941	0.910	1.140	0.837
MnO	0.874	0.985	0.847	0.810	0.860
NiO	0.483	0.381	0.327	0.449	0.175
ZnO	9.170	8.430	8.060	11.780	9.550
Total	**100.489**	**100.915**	**101.239**	**100.245**	**100.459**
		Atoms per formula unit			
Ti	0.118	0.088	0.051	0.112	0.109
Al	0.307	0.323	0.308	0.457	0.357
Cr	0.024	0.020	0.008	0.127	0.010
Fe^{2+}	0.773	0.767	0.747	0.697	0.773
Fe^{3+}	1.433	1.481	1.583	1.193	1.416
Mg	0.055	0.051	0.050	0.062	0.046
Mn	0.027	0.031	0.026	0.025	0.027
Ni	0.014	0.011	0.010	0.013	0.005
Zn	0.249	0.228	0.218	0.315	0.258
Total	**3.000**	**3.000**	**3.000**	**3.000**	**3.000**
Fe^{3+}/(Fe^{3+}+Al)	0.82	0.82	0.84	0.72	0.80
Zn/(Zn+Fe^{2+})	0.24	0.23	0.23	0.31	0.25

Table iv.59: EMP analyses of spinel *ss* from sample 12016(1) [Akllap].

Sample	**12016(2)**	**12016(2)**	**12016(2)**	**12016(2)**	**12016(2)**	**12016(2)**	**12016(2)**	**12016(2)**	**12016(2)**	**12016(2)**	**12016(2)**	**12016(2)**	**12016(2)**	**12016(2)**
No.	**#66**	**#68**	**#71**	**#73**	**#76**	**#78**	**#81**	**#84**	**#85**	**#88**	**#91**	**#93**	**#95**	**#98**
TiO_2	0.832	1.360	1.070	1.930	1.664	1.197	1.194	0.837	<0	0.063	1.422	0.547	2.140	0.340
Al_2O_3	3.410	3.700	2.940	6.130	3.060	3.270	2.720	4.220	0.218	1.630	3.490	2.840	3.260	2.780
Cr_2O_3	8.580	4.830	2.440	0.561	0.718	1.740	0.133	1.970	<0.024	0.221	0.099	18.360	1.490	0.185
FeO	27.106	27.625	27.159	28.141	28.842	28.118	27.823	27.647	27.983	27.276	27.747	24.619	29.263	27.407
Fe_2O_3	54.981	57.182	61.101	58.298	62.364	61.912	64.074	61.181	69.953	67.883	62.537	45.320	59.451	65.959
MgO	0.698	0.652	0.604	0.721	0.587	0.603	0.576	0.650	0.332	0.650	0.605	0.727	0.579	0.591
MnO	0.447	0.421	0.321	0.437	0.354	0.362	0.338	0.390	0.266	0.364	0.352	0.401	0.412	0.383
NiO	1.163	1.490	2.150	1.290	1.350	1.470	1.610	1.169	0.801	0.953	1.720	2.080	0.901	1.450
ZnO	3.140	2.740	2.280	3.600	2.270	2.450	2.510	2.960	2.280	2.480	2.680	4.230	2.290	2.370
Total	**100.356**	**100.000**	**100.064**	**101.108**	**101.209**	**101.123**	**100.978**	**101.023**	**101.833**	**101.520**	**100.651**	**99.124**	**99.786**	**101.465**
						Atoms per formula unit								
Ti	0.023	0.038	0.030	0.053	0.047	0.034	0.034	0.023	0.000	0.002	0.040	0.016	0.061	0.010
Al	0.150	0.164	0.131	0.265	0.135	0.144	0.120	0.185	0.010	0.072	0.154	0.127	0.145	0.122
Cr	0.254	0.143	0.073	0.016	0.021	0.051	0.004	0.058	0.000	0.007	0.003	0.550	0.044	0.005
Fe^{2+}	0.849	0.868	0.857	0.865	0.900	0.877	0.873	0.859	0.885	0.856	0.869	0.780	0.924	0.856
Fe^{3+}	1.549	1.616	1.736	1.612	1.751	1.738	1.808	1.711	1.990	1.918	1.763	1.292	1.689	1.853
Mg	0.039	0.037	0.034	0.039	0.033	0.034	0.032	0.036	0.019	0.036	0.034	0.041	0.033	0.033
Mn	0.014	0.013	0.010	0.014	0.011	0.011	0.011	0.012	0.009	0.012	0.011	0.013	0.013	0.012
Ni	0.035	0.045	0.065	0.038	0.041	0.044	0.049	0.035	0.024	0.029	0.052	0.063	0.027	0.044
Zn	0.087	0.076	0.064	0.098	0.063	0.067	0.069	0.081	0.064	0.069	0.074	0.118	0.064	0.065
Total	**3.000**	**3.000**	**3.000**	**3.000**	**3.000**	**3.000**	**3.000**	**3.000**	**3.000**	**3.000**	**3.000**	**3.000**	**3.000**	**3.000**
Fe^{3+}/(Fe^{3+}+Al)	0.91	0.91	0.93	0.86	0.93	0.92	0.94	0.90	1.00	0.96	0.92	0.91	0.92	0.94
Zn/(Zn+Fe^{2+})	0.09	0.08	0.07	0.10	0.06	0.07	0.07	0.09	0.07	0.07	0.08	0.13	0.06	0.07

Table iv.60: EMP analyses of spinel *ss* from sample 12016(2) [Akllap].

Sample	**13030(1)**	**13030(1)**	**13030(1)**	**13031(1)**	**13031(1)**	**13031(1)**	**13031(1)**	**13031(1)**	**13031(1)**	**13031(1)**	**13031(1)**
No.	**#51**	**#55**	**#61**	**#5**	**#9**	**#19**	**#23**	**#28**	**#33**	**#38**	**#45**
TiO_2	2.100	2.430	1.730	0.391	0.569	0.429	0.128	0.288	0.463	0.313	1.086
Al_2O_3	5.630	4.240	5.680	7.600	10.580	5.950	8.770	8.000	7.040	8.060	8.440
Cr_2O_3	3.960	0.265	5.460	<0.025	<0	<0	<0.028	<0.027	<0.025	0.036	0.028
FeO	26.133	27.563	25.479	16.481	11.684	13.650	5.106	8.539	17.330	15.469	21.859
Fe_2O_3	53.283	58.807	52.410	59.721	54.871	61.121	59.615	58.755	60.233	59.166	57.388
MgO	0.552	0.478	0.568	1.243	1.117	1.446	3.340	0.803	1.055	1.383	0.588
MnO	1.034	0.970	1.045	1.229	0.482	1.800	2.110	0.890	1.224	1.400	0.678
NiO	0.127	0.230	0.228	0.235	0.149	0.066	0.342	<0.044	0.156	0.255	<0.043
ZnO	6.010	4.900	6.240	14.460	21.370	16.260	22.330	24.610	13.930	15.050	11.490
Total	**98.829**	**99.883**	**98.840**	**101.359**	**100.822**	**100.722**	**101.741**	**101.886**	**101.430**	**101.133**	**101.558**
				Atoms per formula unit							
Ti	0.060	0.069	0.049	0.011	0.016	0.012	0.003	0.008	0.013	0.009	0.030
Al	0.250	0.188	0.252	0.329	0.457	0.261	0.373	0.349	0.305	0.348	0.363
Cr	0.118	0.008	0.163	0.000	0.000	0.000	0.000	0.000	0.000	0.001	0.001
Fe^{2+}	0.824	0.868	0.803	0.506	0.358	0.426	0.154	0.264	0.534	0.475	0.667
Fe^{3+}	1.512	1.666	1.487	1.650	1.512	1.715	1.620	1.635	1.669	1.633	1.576
Mg	0.031	0.027	0.032	0.068	0.061	0.080	0.180	0.044	0.058	0.076	0.032
Mn	0.033	0.031	0.033	0.038	0.015	0.057	0.065	0.028	0.038	0.043	0.021
Ni	0.004	0.007	0.007	0.007	0.004	0.002	0.010	0.000	0.005	0.008	0.000
Zn	0.167	0.136	0.174	0.392	0.578	0.447	0.595	0.672	0.379	0.407	0.310
Total	**3.000**	**3.000**	**3.000**	**3.000**	**3.000**	**3.000**	**3.000**	**3.000**	**3.000**	**3.000**	**3.000**
$Fe^{3+}/(Fe^{3+}+Al)$	0.86	0.90	0.85	0.83	0.77	0.87	0.81	0.82	0.85	0.82	0.81
$Zn/(Zn+Fe^{2+})$	0.17	0.14	0.18	0.44	0.62	0.51	0.79	0.72	0.41	0.46	0.32

Table iv.61: EMP analyses of spinel *ss* from samples 13030(1) and 13031(1) [Ostri Vrh].

Sample	**10021(2)**	**10021(2)**	**10021(2)**	**10021(2)**	**10021(2)**	**10021(2)**	**10021(2)**	**10021(2)**	**10021(2)**	**10021(2)**	**10021(2)**	**10-1A**	**10-1A**	**10-1A**
No.	**#37**	**#123**	**#124**	**#125**	**#126**	**#127**	**#128**	**#129**	**#130**	**#131**	**#132**	**#21**	**#24**	**#34**
SiO_2	0.407	0.384	0.398	0.387	0.375	0.415	0.402	0.451	0.400	0.379	0.429	0.537	0.510	0.522
TiO_2	1.018	1.197	1.224	1.308	1.153	0.948	1.020	1.021	0.794	0.744	1.157	0.087	0.058	0.083
Al_2O_3	1.281	1.212	1.179	1.228	1.075	1.137	1.265	1.212	1.006	0.908	1.243	0.225	0.195	0.263
Cr_2O_3	0.041	<0.026	0.042	<0.026	0.074	0.102	<0	<0	0.215	0.083	0.038	<0	<0	<0
MgO	0.024	0.028	<0.024	0.048	0.058	0.128	0.046	0.057	0.141	0.166	0.065	0.126	0.064	0.027
CaO	0.108	0.116	0.079	0.125	0.069	0.046	0.106	0.052	0.142	0.036	0.239	0.097	0.114	0.171
MnO	0.278	0.267	0.251	0.273	0.268	0.313	0.279	0.291	0.338	0.357	0.236	0.230	0.260	0.262
FeO	97.090	96.620	96.690	97.150	97.150	96.210	96.140	96.240	95.780	96.300	94.760	96.750	97.160	95.750
ZnO	0.739	0.860	1.027	0.952	1.250	1.700	0.899	0.571	1.620	1.243	2.120	1.810	1.770	2.300
Total	**100.986**	**100.684**	**100.890**	**101.471**	**101.472**	**100.999**	**100.157**	**99.895**	**100.436**	**100.216**	**100.287**	**99.862**	**100.131**	**99.378**
						Atoms per formula unit								
Si	0.005	0.004	0.005	0.004	0.004	0.005	0.005	0.005	0.005	0.004	0.005	0.006	0.006	0.006
Ti	0.009	0.010	0.011	0.011	0.010	0.008	0.009	0.009	0.007	0.007	0.010	0.001	0.001	0.001
Al	0.017	0.017	0.016	0.017	0.015	0.015	0.017	0.017	0.014	0.012	0.017	0.003	0.003	0.004
Cr	0.000	0.000	0.000	0.000	0.001	0.001	0.000	0.000	0.002	0.001	0.000	0.000	0.000	0.000
Mg	0.000	0.000	0.000	0.001	0.001	0.002	0.001	0.001	0.002	0.003	0.001	0.002	0.001	0.000
Ca	0.001	0.001	0.001	0.002	0.001	0.001	0.001	0.001	0.002	0.000	0.003	0.001	0.001	0.002
Mn	0.003	0.003	0.002	0.003	0.003	0.003	0.003	0.003	0.003	0.004	0.002	0.002	0.003	0.003
Fe	0.936	0.934	0.933	0.931	0.934	0.929	0.934	0.937	0.932	0.941	0.919	0.959	0.962	0.955
Zn	0.006	0.007	0.009	0.008	0.011	0.014	0.008	0.005	0.014	0.011	0.018	0.016	0.015	0.020
Total	**0.978**	**0.977**	**0.977**	**0.976**	**0.978**	**0.979**	**0.978**	**0.977**	**0.981**	**0.982**	**0.976**	**0.991**	**0.992**	**0.991**

Table iv.62: EMP analyses of wüstite from samples 10021(2) [Mramor Samakove] and 10-1A [Hajkobile].

Sample	**3(2)**	**3(2)**	**3(2)**	**3(2)**	**3(2)**	**3(2)**	**3(2)**	**3(2)**	**3(2)**	**3(2)**	**3(2)**	**3(2)**	**3(2)**	**3(2)**
No.	**#1**	**#3**	**#7**	**#9**	**#10**	**#13**	**#15**	**#17**	**#19**	**#21**	**#23**	**#24**	**#27**	**#29**
SiO_2	0.459	0.312	0.437	0.435	0.388	0.416	0.442	0.479	0.387	0.419	0.402	0.426	0.402	0.438
TiO_2	0.465	0.291	0.214	0.655	0.526	0.437	1.018	0.264	0.802	0.788	0.643	0.805	0.725	0.444
Al_2O_3	1.049	0.788	0.394	0.509	0.687	1.116	1.816	0.612	0.581	0.461	0.546	0.589	0.581	0.553
Cr_2O_3	<0.025	<0.026	<0.025	<0	<0.045	<0.025	0.024	0.032	0.029	<0.05	<0.025	<0	<0.025	<0.025
MgO	0.133	0.158	0.125	0.085	0.042	0.089	0.053	0.218	<0.023	<0.026	0.079	0.052	0.039	0.237
CaO	0.048	0.046	0.148	0.090	0.074	0.059	0.086	0.154	0.056	0.080	0.055	0.082	0.131	0.156
MnO	0.243	0.207	0.200	0.213	0.205	0.251	0.191	0.273	0.207	0.178	0.213	0.196	0.186	0.233
FeO	96.660	84.500	98.540	97.180	97.510	97.260	94.620	95.550	98.550	98.090	97.870	96.980	97.910	97.200
ZnO	0.799	13.080	0.767	0.972	0.919	1.100	1.057	2.680	0.461	0.742	0.714	1.183	0.913	1.161
Total	**99.856**	**99.382**	**100.825**	**100.139**	**100.351**	**100.728**	**99.307**	**100.262**	**101.073**	**100.758**	**100.522**	**100.313**	**100.887**	**100.422**
						Atoms per formula unit								
Si	0.005	0.004	0.005	0.005	0.005	0.005	0.005	0.006	0.004	0.005	0.005	0.005	0.005	0.005
Ti	0.004	0.003	0.002	0.006	0.005	0.004	0.009	0.002	0.007	0.007	0.006	0.007	0.006	0.004
Al	0.014	0.011	0.005	0.007	0.009	0.015	0.025	0.008	0.008	0.006	0.008	0.008	0.008	0.008
Cr	0.000	0.000	0.000	0.000	0.000	0.000	0.000	0.000	0.000	0.000	0.000	0.000	0.000	0.000
Mg	0.002	0.003	0.002	0.001	0.001	0.002	0.001	0.004	0.000	0.000	0.001	0.001	0.001	0.004
Ca	0.001	0.001	0.002	0.001	0.001	0.001	0.001	0.002	0.001	0.001	0.001	0.001	0.002	0.002
Mn	0.002	0.002	0.002	0.002	0.002	0.002	0.002	0.003	0.002	0.002	0.002	0.002	0.002	0.002
Fe	0.947	0.849	0.965	0.954	0.956	0.946	0.921	0.939	0.958	0.958	0.958	0.950	0.954	0.952
Zn	0.007	0.116	0.007	0.008	0.008	0.009	0.009	0.023	0.004	0.006	0.006	0.010	0.008	0.010
Total	**0.983**	**0.988**	**0.990**	**0.986**	**0.986**	**0.984**	**0.973**	**0.988**	**0.984**	**0.985**	**0.986**	**0.984**	**0.985**	**0.987**

Table iv.63: EMP analyses of wüstite from sample 3(2) [Hanroc].

Sample	**10-1A**	**10-1A**	**10-1A**	**10-1A**	**3(2)**
No.	**#2**	**#3**	**#9**	**#29**	**#5**
SiO_2	8.710	9.990	9.640	9.280	11.610
TiO_2	0.349	0.420	0.515	0.252	0.313
Al_2O_3	2.640	2.740	3.040	2.610	2.620
FeO	55.793	55.830	55.609	55.294	57.924
Fe_2O_3	29.023	25.893	25.973	27.333	21.944
MgO	1.203	1.579	1.517	0.442	0.960
CaO	0.159	0.127	0.123	0.224	1.510
MnO	0.469	0.550	0.507	0.484	0.375
ZnO	3.860	5.400	5.260	6.100	4.510
Total	**102.207**	**102.529**	**102.183**	**102.019**	**101.766**
		Atoms per formula unit			
Si	0.812	0.922	0.893	0.872	1.073
Ti	0.024	0.029	0.036	0.018	0.022
Al	0.290	0.298	0.332	0.289	0.285
Fe^{2+}	4.351	4.311	4.308	4.344	4.476
Fe^{3+}	2.037	1.799	1.810	1.932	1.526
Mg	0.167	0.217	0.209	0.062	0.132
Ca	0.016	0.013	0.012	0.023	0.149
Mn	0.037	0.043	0.040	0.039	0.029
Zn	0.266	0.368	0.360	0.423	0.308
Total	**8.000**	**8.000**	**8.000**	**8.000**	**8.000**

Table iv.64: EMP analyses of iscorite from samples 10-1A [Hajkobile] and 3(2) [Hanroc].

Sample	**12015(5)**	**12015(5)**
No.	**#63**	**#69**
SiO_2	38.750	39.840
TiO_2	0.284	0.263
Al_2O_3	10.170	10.990
MgO	0.052	0.065
CaO	12.080	9.300
MnO	0.532	0.540
FeO	17.080	16.720
NiO	<0	<0
CuO	0.085	0.102
ZnO	5.630	4.650
PbO	11.580	11.970
Na_2O	0.432	0.476
K_2O	1.390	2.860
P_2O_5	1.268	0.993
Total	**99.333**	**98.769**
	Atomic %	
SiO_2	47.319	49.519
TiO_2	0.261	0.246
Al_2O_3	7.318	8.050
MgO	0.095	0.120
CaO	15.805	12.385
MnO	0.550	0.569
FeO	17.443	17.380
NiO	0.000	0.000
CuO	0.078	0.096
ZnO	5.074	4.266
PbO	3.807	4.005
Na_2O	0.511	0.574
K_2O	1.083	2.268
P_2O_5	0.655	0.522
Total	**100.000**	**100.000**

Table iv.65: EMP analyses of glass from sample 12015(5) [Voguçincë].

Sample	12015(7)	12015(7)	12015(7)	12015(7)	12015(7)	12015(7)	12015(7)	12015(7)	12015(7)	12015(7)	12015(7)	12015(7)	12015(7)	12015(7)
No.	**#23**	**#26**	**#29**	**#32**	**#35**	**#38**	**#43**	**#47**	**#50**	**#53**	**#57**	**#60**	**#62**	**#67**
SiO_2	43.630	40.880	42.780	41.310	42.070	42.200	41.960	41.250	41.500	41.430	41.410	41.720	40.340	41.710
TiO_2	0.207	0.282	0.590	0.440	0.348	0.652	0.527	0.464	0.433	0.227	0.469	0.656	0.497	0.501
Al_2O_3	12.370	10.380	13.560	12.120	13.270	13.080	14.130	11.820	12.990	12.200	11.860	14.020	11.410	13.780
MgO	0.036	0.040	<0.017	0.035	0.017	<0.015	<0.016	<0	<0.016	0.015	<0.017	<0	<0.016	<0
CaO	11.640	10.890	13.170	10.370	13.630	16.040	16.510	16.970	16.550	13.720	16.630	15.520	16.290	11.930
MnO	0.289	0.406	0.247	0.377	0.300	0.252	0.232	0.279	0.230	0.255	0.231	0.260	0.248	0.322
FeO	21.200	27.470	18.370	23.780	20.950	17.460	17.030	19.260	17.910	19.870	18.920	17.510	21.090	22.460
NiO	<0	<0.041	<0	<0.041	<0	<0	<0.039	<0	<0.04	<0	<0.041	<0.041	<0	<0
CuO	<0	<0.052	<0	<0.054	<0.051	<0	<0.051	<0.052	<0.052	<0.053	<0	<0	0.058	<0.05
ZnO	2.820	4.000	3.640	3.540	3.160	4.410	3.350	4.400	4.390	3.650	3.930	3.780	4.350	3.160
PbO	1.900	1.710	2.360	1.530	2.080	1.800	1.480	1.770	1.740	2.140	2.090	2.010	1.480	1.750
Na_2O	0.578	0.651	0.932	1.232	1.390	1.092	1.360	1.017	1.079	1.120	1.015	1.303	1.317	1.580
K_2O	4.280	3.610	3.500	2.750	1.880	1.650	1.440	1.009	1.300	2.600	1.260	1.490	1.173	2.650
P_2O_5	0.785	0.597	0.733	0.704	1.010	0.832	1.282	1.035	1.000	1.033	0.911	1.051	1.046	0.842
Total	**99.735**	**100.916**	**99.882**	**98.188**	**100.105**	**99.468**	**99.301**	**99.274**	**99.122**	**98.260**	**98.726**	**99.320**	**99.299**	**100.685**
							Atomic %							
SiO_2	49.698	46.008	48.799	47.799	47.579	47.628	47.433	46.410	46.949	47.732	46.937	47.432	45.397	47.168
TiO_2	0.177	0.239	0.506	0.383	0.296	0.554	0.448	0.393	0.369	0.197	0.400	0.561	0.421	0.426
Al_2O_3	8.303	6.884	9.115	8.264	8.844	8.699	9.413	7.837	8.660	8.283	7.922	9.393	7.567	9.183
MgO	0.061	0.067	0.000	0.060	0.029	0.000	0.000	0.000	0.000	0.026	0.000	0.000	0.000	0.000
CaO	14.206	13.132	16.096	12.856	16.516	19.397	19.997	20.457	20.061	16.936	20.196	18.906	19.642	14.455
MnO	0.279	0.387	0.239	0.369	0.287	0.241	0.222	0.266	0.220	0.249	0.222	0.250	0.236	0.308
FeO	20.196	25.856	17.525	23.011	19.815	16.480	16.100	18.122	16.945	19.145	17.935	16.649	19.849	21.242
NiO	0.000	0.000	0.000	0.000	0.000	0.000	0.000	0.000	0.000	0.000	0.000	0.000	0.000	0.000
CuO	0.000	0.000	0.000	0.000	0.000	0.000	0.000	0.000	0.000	0.000	0.000	0.000	0.049	0.000
ZnO	2.371	3.323	3.065	3.023	2.638	3.674	2.795	3.654	3.666	3.104	3.288	3.172	3.613	2.637
PbO	0.583	0.518	0.725	0.477	0.633	0.547	0.450	0.536	0.530	0.664	0.638	0.615	0.448	0.533
Na_2O	0.638	0.710	1.031	1.382	1.524	1.195	1.490	1.109	1.183	1.251	1.115	1.436	1.437	1.732
K_2O	3.110	2.592	2.547	2.030	1.356	1.188	1.038	0.724	0.938	1.911	0.911	1.081	0.842	1.912
P_2O_5	0.379	0.284	0.354	0.345	0.484	0.397	0.613	0.493	0.479	0.504	0.437	0.506	0.498	0.403
Total	**100.000**	**100.000**	**100.000**	**100.000**	**100.000**	**100.000**	**100.000**	**100.000**	**100.000**	**100.000**	**100.000**	**100.000**	**100.000**	**100.000**

Table iv.66: EMP analyses of glass from sample 12015(7) [Voguçincë].

Sample	**14032**	**14032**	**14032**	**14032**	**14032**	**14032**	**14032**	**14032**	**14032**	**14032**	**14032**	**14032**	**14032**	**14032**	**14032**
No.	**#1**	**#2**	**#3**	**#4**	**#5**	**#7**	**#8**	**#10**	**#12**	**#14**	**#16**	**#18**	**#20**	**#22**	**#24**
SiO_2	37.400	36.770	36.670	38.090	37.980	40.810	36.800	44.480	39.860	41.200	40.460	40.090	39.490	37.990	40.150
TiO_2	0.414	0.401	0.375	0.396	0.401	0.216	0.363	0.269	0.370	0.246	0.584	0.779	0.506	0.675	0.260
Al_2O_3	7.340	7.360	7.250	7.560	7.620	9.280	7.110	11.330	10.220	9.590	10.460	10.920	9.370	8.750	9.260
MgO	1.520	1.556	1.566	1.084	1.325	0.415	1.720	0.237	0.207	0.210	0.149	0.244	0.128	0.141	0.579
CaO	7.280	6.060	6.120	7.420	7.400	7.790	5.340	11.840	10.510	11.850	14.040	10.100	11.640	13.430	5.930
MnO	0.700	0.640	0.657	0.602	0.577	0.634	0.663	0.330	0.348	0.386	0.290	0.281	0.400	0.288	0.605
FeO	34.530	37.380	37.890	33.520	33.710	29.830	39.240	17.700	21.260	20.460	18.530	25.740	23.240	22.460	33.780
NiO	<0.044	<0	<0.043	<0.046	<0	<0	<0.042	<0.042	<0.043	<0.043	<0.042	<0.044	<0.045	<0	<0
CuO	0.069	0.381	<0.055	0.168	0.195	0.073	0.141	<0.054	<0.056	<0.058	0.069	<0.054	0.065	<0.057	<0
ZnO	1.770	1.540	1.790	1.700	1.520	2.090	1.600	1.640	1.770	2.020	1.850	1.510	2.780	2.170	1.560
PbO	5.910	5.630	5.430	5.380	6.070	5.360	4.930	6.550	9.050	9.480	9.110	6.700	8.910	11.070	4.660
Na_2O	0.359	0.463	0.449	0.603	0.436	0.747	0.442	0.737	0.578	0.453	0.694	0.869	0.906	0.558	0.802
K_2O	2.530	2.920	2.810	3.310	3.030	3.420	2.780	3.980	3.880	3.590	2.000	3.180	1.930	1.260	3.520
P_2O_5	0.610	0.584	0.648	0.693	0.614	0.742	0.649	1.115	1.010	0.961	1.118	0.932	0.861	1.090	0.803
Total	**100.482**	**101.685**	**101.655**	**100.526**	**100.878**	**101.407**	**101.812**	**100.208**	**99.063**	**100.446**	**99.354**	**101.345**	**100.226**	**99.882**	**101.909**
							Atomic %								
SiO_2	43.106	42.012	41.839	43.897	43.718	46.827	41.803	51.613	48.018	48.664	47.960	46.484	46.567	45.405	45.859
TiO_2	0.359	0.345	0.322	0.343	0.347	0.186	0.310	0.235	0.335	0.219	0.521	0.680	0.449	0.607	0.223
Al_2O_3	4.985	4.955	4.875	5.134	5.169	6.275	4.759	7.747	7.255	6.675	7.307	7.461	6.511	6.163	6.233
MgO	2.612	2.650	2.664	1.862	2.274	0.710	2.913	0.410	0.372	0.370	0.263	0.422	0.225	0.251	0.986
CaO	8.990	7.419	7.482	9.162	9.127	9.577	6.499	14.720	13.566	14.997	17.832	12.548	14.707	17.198	7.257
MnO	0.683	0.619	0.635	0.588	0.563	0.616	0.638	0.324	0.355	0.386	0.291	0.276	0.400	0.292	0.585
FeO	33.284	35.718	36.155	32.307	32.451	28.625	37.279	17.177	21.419	20.211	18.369	24.960	22.919	22.450	32.268
NiO	0.000	0.000	0.000	0.000	0.000	0.000	0.000	0.000	0.000	0.000	0.000	0.000	0.000	0.000	0.000
CuO	0.060	0.328	0.000	0.146	0.169	0.063	0.121	0.000	0.000	0.000	0.062	0.000	0.058	0.000	0.000
ZnO	1.506	1.299	1.507	1.446	1.291	1.770	1.341	1.405	1.574	1.761	1.619	1.292	2.420	1.914	1.315
PbO	1.834	1.732	1.668	1.669	1.881	1.656	1.508	2.046	2.935	3.014	2.907	2.091	2.828	3.562	1.433
Na_2O	0.401	0.513	0.497	0.674	0.487	0.831	0.487	0.829	0.675	0.519	0.797	0.977	1.036	0.647	0.888
K_2O	1.860	2.128	2.045	2.433	2.225	2.503	2.014	2.946	2.981	2.705	1.512	2.352	1.452	0.961	2.565
P_2O_5	0.298	0.282	0.313	0.338	0.299	0.360	0.312	0.548	0.515	0.480	0.561	0.457	0.430	0.551	0.388
Total	**100.000**	**100.000**	**100.000**	**100.000**	**100.000**	**100.000**	**100.000**	**100.000**	**100.000**	**100.000**	**100.000**	**100.000**	**100.000**	**100.000**	**100.000**

Table iv.67: EMP analyses of glass from sample 14032 [Voguçincë].

Sample	11027(1)	11027(1)	11027(1)	11027(1)	11027(1)	11027(1)	11027(1)	11027(1)	11027(2)	11027(2)	11027(2)	11029(3)	11029(3)	11029(3)	11029(3)	11029(3)
No.	**#22**	**#28**	**#33**	**#38**	**#39**	**#42**	**#49**	**#53**	**#86**	**#88**	**#98**	**#3**	**#7**	**#10**	**#13**	**#16**
SiO_2	43.780	42.060	41.810	42.480	41.000	40.290	44.630	44.890	42.220	45.690	40.060	33.550	40.060	40.530	42.970	36.040
TiO_2	0.147	0.288	0.376	0.327	0.347	0.470	0.385	0.371	0.384	0.583	0.289	0.438	0.290	0.149	0.187	0.037
Al_2O_3	5.720	5.840	6.420	6.050	5.470	5.070	5.380	5.880	5.320	6.980	4.370	6.570	7.360	7.070	7.770	3.790
MgO	0.076	0.034	0.030	0.038	0.028	0.023	0.057	0.079	0.352	0.120	0.612	1.363	1.240	0.824	1.134	3.700
CaO	5.920	6.220	7.000	6.440	6.740	8.020	6.800	6.810	8.290	9.760	5.080	5.420	7.430	4.960	6.750	1.670
MnO	0.217	0.194	0.215	0.277	0.230	0.196	0.312	0.228	0.567	0.396	0.848	0.319	0.380	0.438	0.287	0.965
FeO	12.880	13.540	13.930	16.980	16.650	15.740	21.620	13.440	26.250	19.110	36.620	39.920	30.080	21.030	28.010	48.150
NiO	<0.049	<0	<0	<0	<0.086	<0.047	<0.044	<0	<0	<0.042	<0	<0	<0	<0	<0.042	<0.045
CuO	0.082	0.112	<0.062	<0.061	0.591	0.160	0.087	0.245	<0.057	<0.059	<0.056	0.061	<0.056	<0.058	0.057	<0.054
ZnO	4.380	5.030	5.500	5.690	6.140	7.070	4.930	3.520	4.670	4.480	4.390	1.260	1.310	1.330	1.129	1.410
PbO	23.490	25.300	23.220	19.680	21.750	22.060	14.360	21.090	9.940	9.500	6.220	7.530	9.900	17.190	8.930	3.170
Na_2O	<0.085	<0.172	<0	<0	<0	<0	<0	<0.072	<0	<0	<0.083	0.651	0.818	0.820	0.837	0.422
K_2O	1.870	1.680	1.630	1.650	1.250	0.930	1.340	1.860	1.490	1.940	1.840	2.070	2.430	2.940	3.200	1.760
P_2O_5	0.249	0.257	0.248	0.308	0.273	0.248	0.277	0.243	0.335	0.585	0.310	0.666	0.980	1.082	0.982	0.846
Total	**98.811**	**100.555**	**100.379**	**99.920**	**100.469**	**100.277**	**100.178**	**98.656**	**99.818**	**99.144**	**100.639**	**99.818**	**102.278**	**98.363**	**102.243**	**101.960**
								Atomic %								
SiO_2	57.918	55.555	54.506	54.209	52.826	51.944	54.197	58.124	49.847	54.043	46.167	39.712	46.423	51.930	49.488	39.834
TiO_2	0.146	0.286	0.369	0.314	0.336	0.456	0.352	0.361	0.341	0.519	0.251	0.390	0.253	0.144	0.162	0.031
Al_2O_3	4.459	4.546	4.932	4.550	4.153	3.852	3.850	4.487	3.701	4.865	2.968	4.583	5.026	5.338	5.273	2.469
MgO	0.150	0.067	0.058	0.072	0.054	0.044	0.103	0.152	0.620	0.212	1.051	2.405	2.142	1.574	1.947	6.096
CaO	8.391	8.803	9.778	8.805	9.305	11.079	8.848	9.448	10.487	12.369	6.273	6.874	9.225	6.809	8.329	1.978
MnO	0.243	0.217	0.237	0.299	0.251	0.214	0.321	0.250	0.567	0.397	0.828	0.320	0.373	0.475	0.280	0.903
FeO	14.250	14.957	15.187	18.121	17.941	16.971	21.957	14.554	25.919	18.904	35.295	39.518	29.152	22.535	26.978	44.507
NiO	0.000	0.000	0.000	0.000	0.000	0.000	0.000	0.000	0.000	0.000	0.000	0.000	0.000	0.000	0.000	0.000
CuO	0.082	0.112	0.000	0.000	0.574	0.156	0.080	0.239	0.000	0.000	0.000	0.054	0.000	0.000	0.050	0.000
ZnO	4.277	4.904	5.292	5.359	5.839	6.727	4.419	3.364	4.069	3.911	3.734	1.101	1.120	1.258	0.960	1.150
PbO	8.365	8.996	8.149	6.760	7.544	7.656	4.694	7.351	3.159	3.025	1.930	2.399	3.088	5.929	2.769	0.943
Na_2O	0.000	0.000	0.000	0.000	0.000	0.000	0.000	0.000	0.000	0.000	0.000	0.747	0.919	1.019	0.934	0.452
K_2O	1.578	1.415	1.355	1.343	1.027	0.765	1.038	1.536	1.122	1.464	1.353	1.563	1.796	2.403	2.351	1.241
P_2O_5	0.139	0.144	0.137	0.166	0.149	0.135	0.142	0.133	0.167	0.293	0.151	0.334	0.481	0.587	0.479	0.396
Total	**100.000**	**100.000**	**100.000**	**100.000**	**100.000**	**100.000**	**100.000**	**100.000**	**100.000**	**100.000**	**100.000**	**100.000**	**100.000**	**100.000**	**100.000**	**100.000**

Table iv.68: EMP analyses of glass from samples 11027(1) and 11027(2) [Mirash].

Sample	**11029(3)**	**11029(3)**	**11029(3)**	**11029(3)**	**11029(3)**
No.	**#3**	**#7**	**#10**	**#13**	**#16**
SiO_2	33.550	40.060	40.530	42.970	36.040
TiO_2	0.438	0.290	0.149	0.187	0.037
Al_2O_3	6.570	7.360	7.070	7.770	3.790
MgO	1.363	1.240	0.824	1.134	3.700
CaO	5.420	7.430	4.960	6.750	1.670
MnO	0.319	0.380	0.438	0.287	0.965
FeO	39.920	30.080	21.030	28.010	48.150
NiO	<0	<0	<0	<0.042	<0.045
CuO	0.061	<0.056	<0.058	0.057	<0.054
ZnO	1.260	1.310	1.330	1.129	1.410
PbO	7.530	9.900	17.190	8.930	3.170
Na_2O	0.651	0.818	0.820	0.837	0.422
K_2O	2.070	2.430	2.940	3.200	1.760
P_2O_5	0.666	0.980	1.082	0.982	0.846
Total	**99.818**	**102.278**	**98.363**	**102.243**	**101.960**
		Atomic %			
SiO_2	39.712	46.423	51.930	49.488	39.834
TiO_2	0.390	0.253	0.144	0.162	0.031
Al_2O_3	4.583	5.026	5.338	5.273	2.469
MgO	2.405	2.142	1.574	1.947	6.096
CaO	6.874	9.225	6.809	8.329	1.978
MnO	0.320	0.373	0.475	0.280	0.903
FeO	39.518	29.152	22.535	26.978	44.507
NiO	0.000	0.000	0.000	0.000	0.000
CuO	0.054	0.000	0.000	0.050	0.000
ZnO	1.101	1.120	1.258	0.960	1.150
PbO	2.399	3.088	5.929	2.769	0.943
Na_2O	0.747	0.919	1.019	0.934	0.452
K_2O	1.563	1.796	2.403	2.351	1.241
P_2O_5	0.334	0.481	0.587	0.479	0.396
Total	**100.000**	**100.000**	**100.000**	**100.000**	**100.000**

Table iv.69: EMP analyses of glass from sample 11029(3) [Mirash Novo].

Sample	**11029(4)**	**11029(4)**	**11029(4)**	**11029(4)**	**11029(4)**
No.	**#1**	**#2**	**#3**	**#4**	**#5**
SiO_2	45.210	44.490	45.420	45.740	47.110
TiO_2	0.112	0.140	0.065	0.196	0.079
Al_2O_3	7.190	7.230	7.080	9.860	6.570
MgO	0.794	0.885	0.705	0.277	1.800
CaO	5.710	6.820	5.850	13.140	7.790
MnO	0.590	0.715	0.653	0.552	0.981
FeO	33.370	32.220	31.100	23.310	32.420
NiO	<0	<0.043	<0	<0.069	<0
CuO	0.056	0.143	0.198	0.136	0.143
ZnO	0.855	1.098	1.039	1.056	0.796
PbO	1.990	2.550	2.400	3.330	1.330
Na_2O	0.785	0.799	0.839	0.603	0.358
K_2O	3.810	3.520	4.100	2.700	1.670
P_2O_5	0.423	0.384	0.489	0.542	0.432
Total	**100.895**	**100.994**	**99.938**	**101.442**	**101.479**
		Atomic %			
SiO_2	50.334	49.532	51.195	50.560	50.840
TiO_2	0.094	0.117	0.055	0.163	0.064
Al_2O_3	4.717	4.743	4.703	6.423	4.178
MgO	1.318	1.469	1.185	0.456	2.896
CaO	6.811	8.135	7.065	15.563	9.007
MnO	0.556	0.674	0.623	0.517	0.897
FeO	31.071	30.000	29.316	21.549	29.260
NiO	0.000	0.000	0.000	0.000	0.000
CuO	0.047	0.120	0.168	0.113	0.116
ZnO	0.703	0.902	0.864	0.862	0.634
PbO	0.596	0.764	0.728	0.991	0.386
Na_2O	0.847	0.862	0.917	0.646	0.375
K_2O	2.706	2.500	2.948	1.904	1.150
P_2O_5	0.199	0.181	0.233	0.254	0.197
Total	**100.000**	**100.000**	**100.000**	**100.000**	**100.000**

Table iv.70: EMP analyses of glass from sample 11029(4) [Mirash Novo].

Sample	**10021(21)**	**10021(21)**	**10021(21)**	**10021(21)**	**10021(21)**	**10021(21)**	**10021(21)**	**10021(21)**	**10021(21)**	**10021(21)**
No.	**#75**	**#78**	**#79**	**#87**	**#98**	**#99**	**#101**	**#103**	**#105**	**#110**
SiO_2	39.690	48.070	50.080	38.990	47.690	46.160	40.860	48.770	39.400	38.090
TiO_2	0.902	0.635	0.122	0.727	0.659	0.833	0.757	0.269	1.001	1.900
Al_2O_3	11.560	3.790	0.308	7.960	4.330	4.950	7.450	0.911	5.990	6.620
MgO	0.115	5.740	2.240	0.346	4.860	2.380	0.303	0.424	0.181	0.090
CaO	17.100	21.720	26.280	17.440	21.910	21.100	17.810	29.500	18.890	17.330
MnO	0.414	0.827	2.670	0.683	0.684	0.731	0.835	1.001	0.635	0.436
FeO	22.880	18.690	18.940	27.670	19.260	23.190	25.330	19.140	26.460	27.860
NiO	<0	<0	<0	<0	<0	<0.040	<0.040	<0	<0	<0
CuO	<0.094	<0	<0	<0	<0	<0.049	<0.050	<0	<0.051	<0.053
ZnO	2.660	0.783	0.612	2.470	0.725	0.820	3.180	0.747	3.840	2.470
PbO	<0.071	<0	<0	0.184	<0	<0	0.121	<0.052	0.153	0.182
Na_2O	1.490	0.121	<0	0.974	0.125	0.090	1.267	<0.043	0.938	2.020
K_2O	1.290	0.016	<0	0.872	<0	0.015	1.111	0.107	0.647	1.090
P_2O_5	1.581	0.467	0.098	1.543	0.072	0.297	1.995	0.285	2.030	2.700
Total	**99.682**	**101.435**	**101.350**	**99.859**	**101.062**	**100.634**	**101.019**	**101.154**	**100.165**	**100.788**
					Atomic %					
SiO_2	44.071	48.035	49.858	42.764	48.110	47.722	44.218	49.092	42.865	41.646
TiO_2	0.753	0.477	0.091	0.600	0.500	0.648	0.616	0.204	0.819	1.563
Al_2O_3	7.564	2.232	0.181	5.145	2.574	3.016	4.751	0.540	3.840	4.265
MgO	0.190	8.551	3.325	0.566	7.309	3.668	0.489	0.636	0.294	0.147
CaO	20.344	23.255	28.033	20.495	23.682	23.373	20.651	31.817	22.020	20.302
MnO	0.389	0.700	2.251	0.634	0.584	0.640	0.765	0.853	0.585	0.404
FeO	21.247	15.619	15.770	25.381	16.249	20.050	22.925	16.113	24.075	25.475
NiO	0.000	0.000	0.000	0.000	0.000	0.000	0.000	0.000	0.000	0.000
CuO	0.000	0.000	0.000	0.000	0.000	0.000	0.000	0.000	0.000	0.000
ZnO	2.180	0.577	0.450	1.999	0.540	0.626	2.540	0.555	3.083	1.993
PbO	0.000	0.000	0.000	0.054	0.000	0.000	0.035	0.000	0.045	0.054
Na_2O	1.604	0.117	0.000	1.036	0.122	0.090	1.329	0.000	0.989	2.141
K_2O	0.914	0.010	0.000	0.610	0.000	0.010	0.767	0.069	0.449	0.760
P_2O_5	0.743	0.198	0.041	0.716	0.031	0.130	0.914	0.121	0.935	1.250
Total	**100.000**	**100.000**	**100.000**	**100.000**	**100.000**	**100.000**	**100.000**	**100.000**	**100.000**	**100.000**

Table iv.71: EMP analyses of glass from sample 10021(21) [Mramor Samakove].

Sample	**10024(2)**	**10024(2)**	**10024(2)**	**10024(2)**	**10024(2)**	**10024(2)**	**10024(4)**	**10024(4)**	**10024(4)**	**10024(4)**	**10024(4)**	**10024(4)**	**10024(4)**	**10024(4)**
No.	**#3**	**#5**	**#9**	**#10**	**#17**	**#25**	**#35**	**#38**	**#43**	**#48**	**#49**	**#60**	**#62**	**#64**
SiO_2	36.740	38.050	35.940	36.100	38.640	37.520	37.690	38.840	37.800	36.590	38.590	38.340	37.160	36.730
TiO_2	0.037	0.044	<0.028	0.063	<0	0.120	0.206	0.201	0.404	0.403	0.424	0.230	0.285	0.368
Al_2O_3	5.070	6.040	4.110	5.660	6.310	5.780	7.700	8.490	9.660	9.980	9.470	10.030	8.590	8.460
MgO	2.960	0.115	6.240	1.880	0.080	1.081	0.145	0.092	0.097	0.101	0.043	0.058	0.087	0.083
CaO	2.820	8.060	2.650	2.800	4.820	7.840	16.670	18.150	16.380	14.580	17.460	18.020	17.650	17.500
MnO	3.820	1.500	4.220	3.550	1.780	2.340	0.539	0.441	0.394	0.434	0.370	0.381	0.400	0.402
FeO	29.790	10.950	33.330	26.280	9.860	15.780	25.850	21.080	20.790	23.350	21.010	20.940	23.160	23.830
NiO	<0.044	<0	0.044	<0	<0	0.051	<0	<0.041	<0	<0.040	<0	<0	<0.041	<0.041
CuO	0.072	<0.055	<0	0.098	0.062	<0.112	<0	<0.054	<0.052	<0.052	<0.055	<0	<0.053	<0
ZnO	9.400	13.780	8.110	10.200	14.170	11.570	3.320	4.370	4.010	3.630	4.390	3.710	4.260	4.060
PbO	7.180	15.200	3.230	10.880	17.850	13.080	2.520	3.230	3.080	2.950	2.880	1.550	2.680	2.660
Na_2O	0.438	<0.137	<0	<0.133	<0.151	<0.137	1.750	1.470	1.900	1.770	1.530	1.780	1.311	1.370
K_2O	2.510	3.250	2.420	3.470	4.080	2.800	1.300	0.692	1.031	1.410	0.872	0.855	0.777	0.780
P_2O_5	0.567	0.713	0.533	0.480	1.014	0.681	2.048	2.310	2.036	1.927	2.370	2.880	2.860	2.760
Total	**101.404**	**97.702**	**100.827**	**101.461**	**98.666**	**98.643**	**99.738**	**99.366**	**97.582**	**97.125**	**99.409**	**98.774**	**99.220**	**99.003**
							Atomic %							
SiO_2	42.459	49.087	39.664	43.380	51.018	46.677	42.321	43.877	43.769	42.872	43.751	43.421	42.214	41.813
TiO_2	0.032	0.043	0.000	0.057	0.000	0.112	0.174	0.171	0.352	0.355	0.362	0.196	0.244	0.315
Al_2O_3	3.453	4.592	2.673	4.008	4.910	4.237	5.095	5.652	6.591	6.891	6.327	6.694	5.750	5.675
MgO	5.100	0.221	10.266	3.368	0.157	2.005	0.243	0.155	0.167	0.176	0.073	0.098	0.147	0.141
CaO	3.492	11.141	3.134	3.605	6.819	10.450	20.056	21.969	20.322	18.304	21.210	21.866	21.483	21.345
MnO	3.739	1.639	3.945	3.613	1.991	2.466	0.513	0.422	0.386	0.431	0.355	0.365	0.385	0.388
FeO	28.792	11.814	30.762	26.410	10.888	16.418	24.275	19.916	20.133	22.881	19.921	19.833	22.003	22.687
NiO	0.000	0.000	0.039	0.000	0.000	0.051	0.000	0.000	0.000	0.000	0.000	0.000	0.000	0.000
CuO	0.063	0.000	0.000	0.089	0.062	0.000	0.000	0.000	0.000	0.000	0.000	0.000	0.000	0.000
ZnO	8.018	13.121	6.606	9.046	13.809	10.623	2.751	3.644	3.427	3.139	3.673	3.101	3.572	3.411
PbO	2.234	5.279	0.960	3.519	6.344	4.380	0.762	0.982	0.960	0.930	0.879	0.473	0.820	0.815
Na_2O	0.491	0.000	0.000	0.000	0.000	0.000	1.905	1.610	2.133	2.010	1.682	1.954	1.444	1.512
K_2O	1.850	2.674	1.704	2.660	3.436	2.222	0.931	0.499	0.761	1.054	0.631	0.618	0.563	0.566
P_2O_5	0.277	0.389	0.249	0.244	0.567	0.359	0.973	1.105	0.998	0.956	1.137	1.381	1.375	1.330
Total	**100.000**	**100.000**	**100.000**	**100.000**	**100.000**	**100.000**	**100.000**	**100.000**	**100.000**	**100.000**	**100.000**	**100.000**	**100.000**	**100.000**

Table iv.72: EMP analyses of glass from samples 10024(2) and 10024(4) [Mramor Proni Butoçit].

Sample	10024(5)	10024(5)	10024(5)	10024(5)	10024(5)	10024(5)	10024(5)	10024(5)	10024(5)	10024(5)	10024(5)
No.	**#66**	**#70**	**#74**	**#78**	**#82**	**#90**	**#94**	**#98**	**#103**	**#107**	**#110**
SiO_2	32.120	34.360	35.020	36.100	35.890	34.910	33.880	33.000	42.260	37.470	38.370
TiO_2	0.161	0.174	0.189	0.194	0.184	0.128	0.123	0.155	0.131	0.039	0.041
Al_2O_3	4.660	6.160	6.060	6.740	6.850	4.310	4.200	4.340	8.480	3.830	5.080
MgO	1.144	1.980	2.400	2.320	2.320	0.605	0.331	0.683	0.200	0.054	0.079
CaO	10.290	11.360	11.960	11.230	11.490	11.750	14.050	12.390	10.410	13.210	10.860
MnO	1.119	0.839	0.804	0.761	0.773	1.370	1.310	1.092	1.161	2.670	2.400
FeO	16.220	13.850	15.780	14.620	13.850	15.550	12.150	13.020	15.650	20.430	21.300
NiO	<0	<0	<0.045	<0.045	<0	<0.045	<0	<0.048	<0.043	<0.039	<0
CuO	0.126	<0.061	0.086	0.059	0.063	<0	0.062	0.064	<0.055	<0.101	<0
ZnO	2.780	2.030	1.910	1.810	1.760	2.760	2.580	2.210	4.270	6.710	6.340
PbO	25.550	21.840	19.200	18.590	18.990	22.220	24.490	26.630	7.130	4.250	4.830
Na_2O	1.062	1.051	0.735	1.012	0.757	1.760	1.920	1.346	3.830	4.630	4.680
K_2O	1.580	2.460	2.480	3.560	3.750	1.410	0.837	1.015	2.380	1.420	1.740
P_2O_5	0.974	0.955	0.888	0.969	0.912	1.450	1.561	1.359	1.611	3.710	2.670
Total	**97.786**	**97.059**	**97.512**	**97.965**	**97.589**	**98.223**	**97.494**	**97.304**	**97.513**	**98.423**	**98.390**
					Atomic %						
SiO_2	43.579	45.266	44.716	45.913	45.988	45.669	45.255	45.109	50.392	43.368	44.746
TiO_2	0.164	0.172	0.182	0.186	0.177	0.126	0.124	0.159	0.118	0.034	0.036
Al_2O_3	3.726	4.782	4.560	5.051	5.172	3.323	3.306	3.496	5.959	2.612	3.491
MgO	2.314	3.889	4.568	4.399	4.432	1.180	0.659	1.392	0.356	0.093	0.137
CaO	14.959	16.035	16.362	15.303	15.775	16.470	20.108	18.146	13.300	16.382	13.570
MnO	1.286	0.936	0.870	0.820	0.839	1.518	1.482	1.264	1.173	2.618	2.371
FeO	18.404	15.259	16.851	15.550	14.842	17.013	13.573	14.884	15.607	19.775	20.773
NiO	0.000	0.000	0.000	0.000	0.000	0.000	0.000	0.000	0.000	0.000	0.000
CuO	0.129	0.000	0.083	0.057	0.061	0.000	0.062	0.066	0.000	0.000	0.000
ZnO	2.784	1.974	1.800	1.699	1.664	2.665	2.543	2.230	3.758	5.732	5.457
PbO	9.332	7.745	6.599	6.365	6.550	7.825	8.806	9.799	2.289	1.324	1.516
Na_2O	1.397	1.342	0.910	1.248	0.940	2.232	2.486	1.784	4.427	5.195	5.291
K_2O	1.367	2.067	2.020	2.888	3.065	1.177	0.713	0.885	1.810	1.048	1.294
P_2O_5	0.559	0.533	0.480	0.522	0.495	0.803	0.883	0.786	0.813	1.818	1.318
Total	**100.000**	**100.000**	**100.000**	**100.000**	**100.000**	**100.000**	**100.000**	**100.000**	**100.000**	**100.000**	**100.000**

Table iv.73: EMP analyses of glass from sample 10024(5) [Mramor Proni Butoçit].

Sample	**10-6**	**10-6**	**10-6**	**10-6**	**10-6**	**10-6**	**10-6**	**10-6**	**10-6**	**10-6**	**10-6**	**10-6**	**10-6**	**10-6**	**10-6**	**10-6**
No.	**#111**	**#113**	**#115**	**#117**	**#119**	**#121**	**#123**	**#125**	**#127**	**#129**	**#131**	**#133**	**#135**	**#137**	**#139**	**#141**
SiO_2	40.920	42.550	38.260	40.970	38.680	38.420	36.900	39.280	38.610	38.580	38.370	38.580	38.280	39.480	40.490	43.080
TiO_2	1.890	1.760	2.460	1.341	2.480	1.720	1.840	1.278	1.597	1.840	1.277	0.779	0.878	1.259	1.980	0.982
Al_2O_3	11.870	12.860	11.390	11.760	11.230	10.470	10.350	8.890	9.770	10.950	10.720	8.000	8.380	9.440	12.230	10.430
MgO	<0.016	0.026	0.023	0.032	0.024	<0.017	<0.031	<0.016	0.017	<0.016	<0.032	0.052	0.103	0.028	<0	<0.020
CaO	12.180	8.750	10.050	7.310	9.680	9.640	8.960	11.120	9.790	10.430	8.290	6.950	5.820	11.180	10.790	11.780
MnO	0.042	0.047	0.052	0.047	<0.041	0.041	<0.042	0.057	0.068	0.045	0.048	0.065	0.110	0.067	0.052	<0.038
FeO	25.180	24.620	29.000	29.460	27.820	30.400	31.010	30.050	31.090	28.500	31.370	40.220	41.760	30.630	25.650	23.720
NiO	<0.04	<0.038	<0	<0	<0.038	<0.043	<0	<0.039	<0.041	<0	<0	<0	<0.040	<0.040	<0	<0
CuO	<0.052	<0.048	<0	0.059	<0.052	<0.054	<0.054	<0	<0.055	<0.052	<0.056	<0	<0	<0	<0	0.069
ZnO	2.910	2.470	3.100	2.500	2.990	3.270	3.650	1.830	3.300	2.930	3.010	3.360	2.680	2.860	2.620	3.730
PbO	2.100	1.880	1.590	3.880	1.930	2.410	3.710	1.990	1.920	1.790	4.010	0.960	0.987	2.080	0.963	1.390
Na_2O	0.403	0.546	0.395	0.573	0.358	0.332	0.290	0.333	0.301	0.367	0.426	0.277	0.343	0.306	0.440	0.074
K_2O	3.250	4.260	3.690	4.180	3.410	3.520	3.460	2.790	3.180	3.620	3.360	1.900	2.160	3.070	3.810	2.210
P_2O_5	0.389	0.355	0.381	0.319	0.389	0.332	0.330	0.307	0.289	0.341	0.348	0.266	0.213	0.380	0.383	0.354
Total	**101.134**	**100.124**	**100.391**	**102.431**	**98.991**	**100.555**	**100.500**	**97.925**	**99.932**	**99.393**	**101.229**	**101.409**	**101.714**	**100.780**	**99.408**	**97.819**
								Atomic %								
SiO_2	46.069	48.784	43.708	46.686	44.846	43.938	42.788	45.309	44.107	44.386	44.200	43.141	42.847	44.474	46.298	49.384
TiO_2	1.601	1.518	2.114	1.150	2.163	1.480	1.605	1.109	1.372	1.593	1.107	0.655	0.739	1.067	1.703	0.847
Al_2O_3	7.875	8.688	7.668	7.897	7.673	7.056	7.072	6.043	6.577	7.424	7.277	5.272	5.527	6.267	8.241	7.046
MgO	0.000	0.044	0.039	0.054	0.041	0.000	0.000	0.000	0.029	0.000	0.000	0.087	0.172	0.047	0.000	0.000
CaO	14.693	10.749	12.301	8.925	12.025	11.812	11.132	13.743	11.983	12.857	10.232	8.327	6.980	13.494	13.219	14.469
MnO	0.040	0.046	0.050	0.045	0.000	0.040	0.000	0.056	0.066	0.044	0.047	0.062	0.104	0.064	0.050	0.000
FeO	23.708	23.606	27.706	28.075	26.975	29.075	30.073	28.989	29.703	27.422	30.221	37.613	39.091	28.857	24.529	22.740
NiO	0.000	0.000	0.000	0.000	0.000	0.000	0.000	0.000	0.000	0.000	0.000	0.000	0.000	0.000	0.000	0.000
CuO	0.000	0.000	0.000	0.051	0.000	0.000	0.000	0.000	0.000	0.000	0.000	0.000	0.000	0.000	0.000	0.060
ZnO	2.418	2.090	2.614	2.103	2.559	2.760	3.124	1.558	2.782	2.488	2.559	2.773	2.214	2.378	2.211	3.156
PbO	0.636	0.580	0.489	1.190	0.602	0.742	1.158	0.618	0.590	0.554	1.243	0.289	0.297	0.631	0.296	0.429
Na_2O	0.440	0.607	0.437	0.633	0.402	0.368	0.326	0.372	0.333	0.409	0.476	0.300	0.372	0.334	0.488	0.082
K_2O	2.334	3.115	2.689	3.038	2.522	2.568	2.559	2.053	2.317	2.657	2.469	1.355	1.542	2.206	2.779	1.616
P_2O_5	0.185	0.172	0.184	0.154	0.191	0.161	0.162	0.150	0.140	0.166	0.170	0.126	0.101	0.181	0.185	0.172
Total	**100.000**	**100.000**	**100.000**	**100.000**	**100.000**	**100.000**	**100.000**	**100.000**	**100.000**	**100.000**	**100.000**	**100.000**	**100.000**	**100.000**	**100.000**	**100.000**

Sample	**10-6**	**10-6**	**10-6**	**10-6**	**10-6**	**10-6**	**10-6**	**10-6**	**10-6**	**10-6**	**10-6**	**10-6**	**10-6**	**10-6**	**10-6**	**10-6**
No.	**#143**	**#145**	**#147**	**#149**	**#151**	**#153**	**#155**	**#157**	**#159**	**#161**	**#163**	**#166**	**#168**	**#170**	**#172**	**#174**
SiO_2	38.830	38.660	39.960	38.840	40.360	37.960	40.300	40.310	42.380	39.040	42.860	42.010	40.580	38.350	27.790	36.010
TiO_2	2.360	1.910	1.585	1.440	0.870	1.820	1.910	1.623	0.975	2.170	0.826	1.595	1.103	2.660	3.650	1.670
Al_2O_3	11.760	9.830	12.470	10.190	11.180	10.770	12.460	11.880	11.880	11.830	10.990	13.180	10.500	11.300	8.410	8.620
MgO	<0.016	<0.017	<0.016	0.018	<0.019	0.021	0.018	<0.016	0.019	<0.016	0.025	0.019	0.017	<0.016	0.034	0.024
CaO	10.130	10.700	11.820	9.880	9.930	10.830	8.860	11.310	10.410	9.650	13.100	9.320	11.390	9.640	6.980	9.030
MnO	<0.04	<0.041	0.071	0.075	0.056	0.047	0.053	<0.039	0.048	0.042	0.067	<0.039	0.050	0.042	0.078	0.065
FeO	27.890	30.010	25.120	33.210	28.450	29.420	27.530	25.330	24.460	26.420	23.880	24.560	25.960	29.990	48.510	34.950
NiO	<0	<0	<0	<0	<0	<0.041	<0	<0	<0	<0.041	<0	<0.041	<0.043	<0	0.043	<0.041
CuO	<0	<0.054	<0	<0	<0	<0.054	<0	<0.05	<0.053	<0.05	<0	<0.052	<0	<0.051	0.083	<0.054
ZnO	2.940	4.880	3.600	3.890	3.500	3.220	2.760	3.120	3.240	3.400	3.240	2.770	3.410	3.330	2.980	3.390
PbO	1.740	1.560	1.280	1.690	1.680	1.940	2.000	1.620	1.780	1.880	1.640	1.450	2.610	1.460	2.730	2.060
Na_2O	0.401	0.256	0.443	0.351	0.491	0.287	0.481	0.422	0.453	0.378	0.340	0.576	0.326	0.352	0.098	0.247
K_2O	3.740	2.940	2.900	2.340	3.140	3.280	4.400	3.550	3.910	4.090	2.920	4.280	3.410	3.460	1.360	2.840
P_2O_5	0.371	0.335	0.429	0.355	0.409	0.421	0.382	0.378	0.418	0.364	0.458	0.419	0.342	0.307	0.197	0.312
Total	**100.162**	**101.081**	**99.678**	**102.279**	**100.066**	**100.016**	**101.154**	**99.543**	**99.973**	**99.264**	**100.346**	**100.179**	**99.698**	**100.891**	**102.943**	**99.218**
								Atomic %								
SiO_2	44.481	43.566	45.566	43.306	45.984	43.431	45.964	46.118	48.283	45.259	48.007	48.049	46.412	43.587	31.671	41.591
TiO_2	2.034	1.619	1.360	1.208	0.746	1.567	1.639	1.397	0.836	1.893	0.696	1.372	0.949	2.274	3.129	1.451
Al_2O_3	7.939	6.528	8.379	6.695	7.506	7.261	8.374	8.009	7.976	8.082	7.254	8.883	7.077	7.568	5.648	5.867
MgO	0.000	0.000	0.000	0.030	0.000	0.036	0.031	0.000	0.032	0.000	0.042	0.032	0.029	0.000	0.058	0.041
CaO	12.433	12.919	14.441	11.803	12.122	13.276	10.827	13.864	12.707	11.987	15.722	11.421	13.958	11.739	8.523	11.175
MnO	0.000	0.000	0.069	0.071	0.054	0.046	0.051	0.000	0.046	0.041	0.064	0.000	0.048	0.040	0.075	0.064
FeO	26.719	28.283	23.956	30.967	27.108	28.151	26.259	24.236	23.306	25.615	22.370	23.492	24.831	28.506	46.235	33.759
NiO	0.000	0.000	0.000	0.000	0.000	0.000	0.000	0.000	0.000	0.000	0.000	0.000	0.000	0.000	0.039	0.000
CuO	0.000	0.000	0.000	0.000	0.000	0.000	0.000	0.000	0.000	0.000	0.000	0.000	0.000	0.000	0.071	0.000
ZnO	2.486	4.059	3.030	3.201	2.943	2.719	2.323	2.635	2.724	2.909	2.679	2.338	2.878	2.793	2.507	2.890
PbO	0.537	0.473	0.393	0.507	0.515	0.598	0.614	0.499	0.546	0.587	0.494	0.446	0.804	0.447	0.838	0.640
Na_2O	0.445	0.280	0.490	0.379	0.542	0.318	0.532	0.468	0.500	0.425	0.369	0.639	0.361	0.388	0.108	0.277
K_2O	2.733	2.113	2.109	1.664	2.282	2.394	3.201	2.591	2.841	3.024	2.086	3.123	2.488	2.508	0.989	2.092
P_2O_5	0.180	0.160	0.207	0.168	0.197	0.204	0.184	0.183	0.202	0.179	0.217	0.203	0.166	0.148	0.095	0.153
Total	**100.000**	**100.000**	**100.000**	**100.000**	**100.000**	**100.000**	**100.000**	**100.000**	**100.000**	**100.000**	**100.000**	**100.000**	**100.000**	**100.000**	**100.000**	**100.000**

Table iv.74: EMP analyses of glass from sample 10-6 [Marec].

Sample	10-6	10032(1)	10032(1)	10032(1)	10032(1)	10032(1)	10032(1)	10032(1)	10032(1)	10032(1)	10032(1)	10032(1)	10032(1)
No.	**#176**	**#58**	**#62**	**#64**	**#66**	**#67**	**#70**	**#71**	**#73**	**#76**	**#78**	**#80**	**#82**
SiO_2	37.720	46.550	47.080	46.900	42.780	42.480	50.180	45.240	42.780	49.980	45.670	46.110	42.660
TiO_2	1.210	0.720	0.371	0.461	0.818	1.503	0.498	0.239	0.944	0.590	0.341	0.274	0.339
Al_2O_3	8.350	9.690	9.870	11.030	12.050	7.260	11.190	8.890	9.080	12.000	9.730	11.020	9.160
MgO	<0.017	0.095	0.049	0.029	0.059	0.171	0.049	0.365	0.140	0.064	0.085	0.041	0.071
CaO	10.890	14.390	10.950	10.160	5.950	14.260	10.740	5.040	5.270	7.990	5.170	4.920	5.360
MnO	0.057	0.080	0.081	0.060	<0.046	0.072	0.065	0.122	0.103	0.046	0.096	0.074	0.133
FeO	31.100	21.720	20.090	16.870	14.110	24.860	17.350	33.620	28.500	14.680	27.740	25.680	28.440
NiO	<0	<0	<0	<0	<0.047	<0	<0	<0	0.052	<0	<0.043	<0.040	<0.044
CuO	<0.054	0.081	<0.054	0.082	0.141	<0.055	<0	<0	<0.054	<0.055	<0.055	<0.053	<0
ZnO	3.190	2.720	4.680	5.580	1.820	4.840	3.350	4.230	3.000	2.350	5.060	4.320	5.760
PbO	2.180	1.620	3.710	4.890	17.770	2.540	2.590	1.630	5.400	6.600	2.760	3.260	6.310
Na_2O	0.110	0.269	0.315	0.236	0.575	0.117	0.463	0.497	0.496	0.568	0.377	0.583	0.308
K_2O	2.290	2.060	2.590	2.700	3.210	1.480	3.230	2.390	2.290	3.490	2.920	3.650	2.890
P_2O_5	0.299	0.376	0.475	0.413	0.289	0.253	0.449	0.274	0.310	0.393	0.191	0.263	0.364
Total	**97.396**	**100.371**	**100.261**	**99.411**	**99.572**	**99.836**	**100.154**	**102.537**	**98.365**	**98.751**	**100.140**	**100.195**	**101.795**
						Atomic %							
SiO_2	43.906	51.248	53.220	54.246	55.044	47.360	56.279	49.986	50.687	58.854	52.258	53.151	49.429
TiO_2	1.060	0.596	0.316	0.401	0.792	1.261	0.420	0.199	0.841	0.523	0.294	0.238	0.296
Al_2O_3	5.727	6.287	6.575	7.518	9.137	4.770	7.396	5.788	6.340	8.327	6.561	7.486	6.254
MgO	0.000	0.156	0.083	0.050	0.113	0.284	0.082	0.601	0.247	0.112	0.145	0.070	0.123
CaO	13.582	16.974	13.263	12.591	8.203	17.034	12.906	5.967	6.690	10.081	6.338	6.077	6.654
MnO	0.056	0.075	0.078	0.059	0.000	0.068	0.062	0.114	0.103	0.046	0.093	0.072	0.131
FeO	30.274	19.998	18.993	16.318	15.183	23.179	16.274	31.066	28.240	14.457	26.546	24.756	27.559
NiO	0.000	0.000	0.000	0.000	0.000	0.000	0.000	0.000	0.050	0.000	0.000	0.000	0.000
CuO	0.000	0.067	0.000	0.072	0.137	0.000	0.000	0.000	0.000	0.000	0.000	0.000	0.000
ZnO	2.741	2.210	3.905	4.763	1.728	3.983	2.773	3.449	2.623	2.042	4.273	3.675	4.926
PbO	0.683	0.480	1.129	1.523	6.155	0.762	0.782	0.485	1.722	2.092	0.850	1.012	1.968
Na_2O	0.124	0.287	0.345	0.265	0.717	0.126	0.503	0.532	0.570	0.648	0.418	0.651	0.346
K_2O	1.700	1.447	1.868	1.992	2.634	1.052	2.311	1.684	1.731	2.621	2.131	2.684	2.136
P_2O_5	0.147	0.175	0.227	0.202	0.157	0.119	0.213	0.128	0.155	0.196	0.093	0.128	0.179
Total	**100.000**	**100.000**	**100.000**	**100.000**	**100.000**	**100.000**	**100.000**	**100.000**	**100.000**	**100.000**	**100.000**	**100.000**	**100.000**

Table iv.75: EMP analyses of glass from samples 10-6 and 10032(1) [Marec].

Sample	10032(1)	10032(1)	10032(1)	10032(1)	10032(1)	10032(1)	10032(1)	10032(1)	10032(1)	10032(1)	10032(1)
No.	**#84**	**#86**	**#89**	**#92**	**#94**	**#98**	**#100**	**#103**	**#105**	**#107**	**#109**
SiO_2	45.140	47.620	44.570	44.060	30.630	45.990	43.800	42.250	40.720	43.750	42.800
TiO_2	0.463	0.235	0.412	0.297	1.820	1.373	1.265	1.940	1.420	1.470	2.110
Al_2O_3	9.760	9.760	9.430	9.390	8.510	12.350	10.350	9.520	8.890	9.760	9.680
MgO	0.036	0.050	0.100	0.030	0.038	0.030	0.118	0.034	0.042	0.034	0.038
CaO	11.270	7.830	5.860	6.490	4.650	10.050	6.010	8.130	6.830	8.020	8.230
MnO	0.081	0.053	0.122	0.106	0.075	0.070	0.101	0.100	0.131	0.130	0.095
FeO	20.280	21.280	27.850	28.500	38.230	16.360	25.820	25.720	33.840	27.080	27.740
NiO	<0	<0.044	<0	<0.041	<0.044	<0	<0	<0	<0.040	<0	<0.039
CuO	<0.053	<0.053	0.057	<0.054	0.103	0.076	<0.053	0.064	<0	<0.055	<0.055
ZnO	4.900	3.890	3.930	6.480	3.750	4.900	3.970	5.780	4.780	3.490	4.500
PbO	4.300	4.380	4.370	3.110	9.580	6.060	5.760	4.000	3.210	2.520	3.770
Na_2O	0.241	0.407	0.360	0.269	0.368	0.428	0.351	0.140	0.154	0.330	0.229
K_2O	2.320	3.530	2.690	2.540	2.160	2.390	2.750	1.950	1.830	1.780	1.900
P_2O_5	0.463	0.558	0.467	0.472	0.317	0.485	0.250	0.374	0.461	0.373	0.421
Total	**99.254**	**99.593**	**100.218**	**101.744**	**100.263**	**100.562**	**100.545**	**100.002**	**102.308**	**98.737**	**101.547**
					Atomic %						
SiO_2	51.837	54.870	51.442	49.819	37.632	53.288	51.033	48.785	45.896	50.359	48.522
TiO_2	0.400	0.204	0.358	0.253	1.682	1.197	1.109	1.685	1.204	1.273	1.800
Al_2O_3	6.605	6.627	6.414	6.257	6.161	8.433	7.106	6.478	5.905	6.620	6.467
MgO	0.062	0.086	0.172	0.051	0.070	0.052	0.205	0.059	0.071	0.058	0.064
CaO	13.867	9.667	7.247	7.863	6.121	12.477	7.503	10.058	8.248	9.891	9.997
MnO	0.079	0.052	0.119	0.102	0.078	0.069	0.100	0.098	0.125	0.127	0.091
FeO	19.477	20.506	26.882	26.950	39.281	15.853	25.160	24.837	31.898	26.069	26.301
NiO	0.000	0.000	0.000	0.000	0.000	0.000	0.000	0.000	0.000	0.000	0.000
CuO	0.000	0.000	0.050	0.000	0.095	0.066	0.000	0.056	0.000	0.000	0.000
ZnO	4.153	3.308	3.348	5.408	3.400	4.190	3.414	4.926	3.976	2.965	3.765
PbO	1.329	1.359	1.358	0.947	3.168	1.890	1.807	1.243	0.974	0.781	1.151
Na_2O	0.268	0.455	0.403	0.295	0.438	0.481	0.396	0.157	0.168	0.368	0.252
K_2O	1.699	2.594	1.980	1.832	1.693	1.766	2.044	1.436	1.316	1.307	1.374
P_2O_5	0.225	0.272	0.228	0.226	0.165	0.238	0.123	0.183	0.220	0.182	0.202
Total	**100.000**	**100.000**	**100.000**	**100.000**	**100.000**	**100.000**	**100.000**	**100.000**	**100.000**	**100.000**	**100.000**

Table iv.76: EMP analyses of glass from sample 10032(1) [Marec].

Sample	**3(1)**	**3(1)**	**3(1)**	**3(1)**	**3(1)**	**3(1)**	**3(1)**	**3(1)**	**3(1)**	**3(1)**	**3(1)**	**3(1)**	**3(1)**	**3(1)**	**3(1)**
No.	**#88**	**#89**	**#91**	**#93**	**#95**	**#97**	**#99**	**#101**	**#103**	**#105**	**#106**	**#113**	**#115**	**#117**	**#119**
SiO_2	46.680	43.700	45.010	45.590	42.560	47.790	46.720	41.710	41.800	42.460	36.320	42.580	41.030	43.740	44.380
TiO_2	0.438	0.349	0.483	0.349	0.361	0.352	0.230	0.327	0.304	0.295	0.191	0.263	0.264	0.303	0.342
Al_2O_3	6.210	5.070	5.500	6.120	5.500	6.730	6.200	5.200	5.000	5.120	3.800	5.080	4.950	5.470	5.810
MgO	0.073	0.075	0.083	0.103	0.087	0.075	0.094	0.070	0.089	0.098	0.039	0.071	0.083	0.085	0.090
CaO	5.660	6.450	7.540	5.520	5.640	5.090	5.470	4.650	5.010	4.590	3.350	4.800	4.990	5.500	5.140
MnO	0.392	0.484	0.472	0.493	0.454	0.338	0.361	0.483	0.572	0.580	0.441	0.479	0.476	0.427	0.403
FeO	13.210	15.670	16.140	14.950	14.820	11.160	11.620	15.600	16.340	19.220	10.840	15.080	15.710	13.760	13.520
NiO	<0	<0	<0	<0	<0	<0.046	<0.046	0.051	<0	<0	<0	<0	<0.047	<0.049	<0.046
CuO	0.079	<0.059	<0.059	<0.062	0.262	0.067	<0.061	<0.063	<0.061	<0.061	0.150	<0.060	<0.064	<0.062	0.073
ZnO	1.470	1.630	1.960	1.660	1.850	1.330	1.440	1.800	1.990	1.840	2.850	1.940	1.950	1.880	1.670
PbO	22.460	22.500	19.560	20.580	24.160	22.860	23.910	26.050	25.920	23.250	39.820	25.930	26.550	25.400	24.390
Na_2O	0.227	0.221	0.170	0.280	0.246	0.335	0.237	0.228	0.171	0.233	0.090	0.257	0.170	0.237	0.300
K_2O	1.690	1.350	1.220	1.990	1.630	2.390	2.050	1.590	1.240	1.590	0.607	1.640	1.430	1.520	1.920
P_2O_5	0.565	0.433	0.554	0.448	0.463	0.516	0.572	0.508	0.442	0.418	0.333	0.431	0.441	0.495	0.556
Total	**99.154**	**97.932**	**98.692**	**98.083**	**98.033**	**99.033**	**98.904**	**98.267**	**98.878**	**99.694**	**98.831**	**98.551**	**98.044**	**98.817**	**98.594**
							Atomic %								
SiO_2	60.663	57.495	57.261	59.252	57.078	62.504	61.595	56.830	56.322	55.603	55.585	57.597	56.200	58.543	59.209
TiO_2	0.428	0.345	0.462	0.341	0.364	0.346	0.228	0.335	0.308	0.291	0.220	0.268	0.272	0.305	0.343
Al_2O_3	4.756	3.931	4.123	4.687	4.347	5.187	4.817	4.175	3.970	3.951	3.427	4.049	3.995	4.314	4.568
MgO	0.141	0.147	0.157	0.200	0.174	0.146	0.185	0.142	0.179	0.191	0.089	0.143	0.169	0.170	0.179
CaO	7.881	9.093	10.278	7.687	8.104	7.133	7.727	6.788	7.233	6.440	5.493	6.957	7.323	7.887	7.347
MnO	0.431	0.539	0.509	0.543	0.516	0.374	0.403	0.557	0.653	0.643	0.572	0.549	0.552	0.484	0.455
FeO	14.357	17.242	17.172	16.250	16.622	12.207	12.812	17.776	18.413	21.050	13.874	17.059	17.996	15.402	15.085
NiO	0.000	0.000	0.000	0.000	0.000	0.000	0.000	0.056	0.000	0.000	0.000	0.000	0.000	0.000	0.000
CuO	0.077	0.000	0.000	0.000	0.265	0.066	0.000	0.000	0.000	0.000	0.173	0.000	0.000	0.000	0.073
ZnO	1.410	1.583	1.840	1.592	1.831	1.284	1.401	1.810	1.979	1.778	3.219	1.937	1.971	1.857	1.644
PbO	7.857	7.969	6.699	7.200	8.722	8.048	8.486	9.554	9.402	8.196	16.405	9.442	9.790	9.152	8.759
Na_2O	0.286	0.282	0.210	0.353	0.320	0.425	0.303	0.301	0.223	0.296	0.134	0.337	0.226	0.308	0.388
K_2O	1.401	1.133	0.990	1.650	1.394	1.994	1.724	1.382	1.066	1.328	0.593	1.415	1.249	1.298	1.634
P_2O_5	0.311	0.241	0.298	0.246	0.263	0.286	0.319	0.293	0.252	0.232	0.216	0.247	0.256	0.280	0.314
Total	**100.000**	**100.000**	**100.000**	**100.000**	**100.000**	**100.000**	**100.000**	**100.000**	**100.000**	**100.000**	**100.000**	**100.000**	**100.000**	**100.000**	**100.000**

Table iv.77: EMP analyses of glass from sample 3(1) [Hanroc].

Sample	12016(1)	12016(1)	12016(1)	12016(1)	12016(1)	12016(1)	12016(1)	12016(1)	12016(1)	12016(1)	12016(1)	12016(1)	12016(1)	12016(1)	12016(1)
No.	**#28**	**#31**	**#33**	**#34**	**#37**	**#40**	**#41**	**#43**	**#47**	**#50**	**#53**	**#55**	**#60**	**#61**	**#65**
SiO_2	37.610	37.270	40.030	36.940	37.610	36.300	36.300	37.330	39.100	39.710	37.780	38.190	40.890	37.550	38.530
TiO_2	0.122	0.106	<0	0.058	0.163	<0.033	0.116	0.087	0.195	0.232	0.338	0.274	0.529	0.297	0.376
Al_2O_3	6.420	6.150	6.540	5.870	6.110	5.540	5.510	6.360	7.550	7.500	8.070	8.010	9.490	7.550	8.380
MgO	0.352	0.325	0.361	0.326	0.283	0.219	0.257	0.208	0.212	0.190	0.153	0.114	0.119	0.153	0.144
CaO	6.870	6.550	4.600	4.440	6.640	3.800	4.090	6.070	8.700	8.490	5.510	6.500	9.980	7.750	8.450
MnO	1.174	1.153	1.360	1.380	1.151	1.430	1.243	1.005	0.851	0.707	1.021	0.959	0.858	0.925	0.766
FeO	13.530	12.690	12.400	12.400	12.740	13.080	12.200	10.960	11.690	10.050	12.560	12.480	12.520	12.800	11.760
NiO	<0.085	<0.046	<0	<0	<0.046	<0.075	<0	<0	<0.044	<0.046	<0.045	<0	<0	<0	<0
CuO	<0.06	<0.061	<0.058	<0.061	<0.061	<0.062	<0.059	<0.061	<0.059	<0	<0.059	<0.114	<0	<0.059	<0.058
ZnO	9.070	9.330	9.120	10.950	9.310	10.620	9.710	8.880	8.220	7.460	10.120	10.830	10.570	11.220	8.840
PbO	21.020	21.780	21.320	23.940	22.270	25.040	27.190	24.420	19.170	21.410	18.890	17.340	9.780	17.030	17.270
Na_2O	0.238	0.290	0.464	0.348	0.296	0.311	0.192	0.347	0.428	0.491	0.567	0.508	0.588	0.410	0.539
K_2O	2.030	2.070	2.950	2.230	2.060	2.190	1.860	2.250	2.070	2.310	2.680	2.870	2.950	2.270	2.640
P_2O_5	0.493	0.464	0.526	0.472	0.507	0.433	0.451	0.476	0.528	0.508	0.513	0.516	0.672	0.547	0.619
Total	**98.929**	**98.178**	**99.671**	**99.354**	**99.140**	**98.963**	**99.119**	**98.393**	**98.714**	**99.058**	**98.202**	**98.591**	**98.946**	**98.502**	**98.314**
							Atomic %								
SiO_2	49.639	49.951	52.742	50.115	50.026	50.018	50.624	51.084	50.768	52.166	50.159	49.790	49.794	48.649	49.945
TiO_2	0.121	0.107	0.000	0.059	0.163	0.000	0.122	0.090	0.190	0.229	0.338	0.269	0.485	0.289	0.367
Al_2O_3	4.993	4.857	5.078	4.693	4.789	4.498	4.528	5.129	5.777	5.806	6.314	6.154	6.810	5.764	6.401
MgO	0.693	0.649	0.709	0.659	0.561	0.450	0.534	0.424	0.410	0.372	0.303	0.222	0.216	0.296	0.278
CaO	9.715	9.406	6.494	6.454	9.463	5.610	6.112	8.900	12.103	11.950	7.838	9.080	13.022	10.758	11.736
MnO	1.312	1.309	1.518	1.586	1.297	1.669	1.468	1.165	0.936	0.787	1.148	1.059	0.885	1.015	0.841
FeO	14.934	14.224	13.664	14.069	14.172	15.073	14.229	12.543	12.694	11.041	13.946	13.607	12.751	13.869	12.749
NiO	0.000	0.000	0.000	0.000	0.000	0.000	0.000	0.000	0.000	0.000	0.000	0.000	0.000	0.000	0.000
CuO	0.000	0.000	0.000	0.000	0.000	0.000	0.000	0.000	0.000	0.000	0.000	0.000	0.000	0.000	0.000
ZnO	8.835	9.229	8.869	10.964	9.140	10.800	9.995	8.969	7.877	7.233	9.916	10.421	9.500	10.729	8.457
PbO	7.468	7.858	7.562	8.743	7.974	9.288	10.208	8.996	6.700	7.571	6.751	6.086	3.206	5.939	6.026
Na_2O	0.305	0.377	0.593	0.458	0.382	0.415	0.260	0.460	0.539	0.625	0.730	0.642	0.694	0.515	0.677
K_2O	1.709	1.770	2.479	1.930	1.748	1.925	1.655	1.964	1.714	1.936	2.270	2.387	2.291	1.876	2.183
P_2O_5	0.275	0.263	0.293	0.271	0.285	0.253	0.266	0.276	0.290	0.282	0.288	0.285	0.346	0.300	0.340
Total	**100.000**	**100.000**	**100.000**	**100.000**	**100.000**	**100.000**	**100.000**	**100.000**	**100.000**	**100.000**	**100.000**	**100.000**	**100.000**	**100.000**	**100.000**

Table iv.78: EMP analyses of glass from sample 12016(1) [Akllap].

Sample	**12016(2)**	**12016(2)**	**12016(2)**
No.	**#79**	**#90**	**#99**
SiO_2	37.480	32.850	33.320
TiO_2	0.041	0.035	0.065
Al_2O_3	4.420	3.770	4.110
MgO	0.282	0.260	0.145
CaO	4.080	2.520	2.180
MnO	0.822	0.600	0.702
FeO	12.050	15.730	14.010
NiO	<0.076	<0.050	<0.051
CuO	<0.066	<0.067	<0
ZnO	4.580	4.020	4.870
PbO	29.900	34.610	35.300
Na_2O	0.530	0.352	0.406
K_2O	2.300	1.980	1.840
P_2O_5	0.636	0.470	0.497
Total	**97.121**	**97.197**	**97.445**
	Atomic %		
SiO_2	54.036	49.821	50.848
TiO_2	0.044	0.040	0.075
Al_2O_3	3.755	3.369	3.696
MgO	0.606	0.588	0.330
CaO	6.303	4.095	3.565
MnO	1.004	0.771	0.907
FeO	14.529	19.951	17.880
NiO	0.000	0.000	0.000
CuO	0.000	0.000	0.000
ZnO	4.874	4.500	5.485
PbO	11.604	14.130	14.501
Na_2O	0.741	0.518	0.601
K_2O	2.115	1.915	1.791
P_2O_5	0.388	0.302	0.321
Total	**100.000**	**100.000**	**100.000**

Table iv.79: EMP analyses of glass from sample 12016(2) [Akllap].

Sample	**13030(1)**	**13030(1)**	**13030(1)**	**13030(1)**	**13030(1)**	**13030(1)**	**13030(1)**	**13030(1)**	**13030(1)**	**13030(1)**	**13030(1)**	**13030(1)**	**13030(1)**
No.	**#40**	**#41**	**#44**	**#47**	**#48**	**#49**	**#52**	**#53**	**#54**	**#57**	**#58**	**#59**	**#62**
SiO_2	33.700	34.380	33.650	33.450	33.570	33.250	34.530	33.990	33.200	34.120	33.290	33.360	33.620
TiO_2	0.181	0.174	0.094	0.123	0.201	0.161	0.205	0.214	0.200	0.205	0.173	0.153	0.166
Al_2O_3	6.290	6.300	6.380	6.240	6.220	6.150	6.520	6.380	6.210	6.350	6.280	6.350	6.300
MgO	0.214	0.431	0.080	0.102	0.287	0.191	0.438	0.272	0.172	0.351	0.293	0.265	0.264
CaO	5.270	6.980	3.350	3.610	6.050	4.710	7.210	5.730	4.580	6.810	6.140	6.040	5.530
MnO	1.290	1.190	1.171	1.194	1.117	1.300	1.254	1.263	1.251	1.330	1.232	1.222	1.124
FeO	10.520	11.470	9.660	10.370	10.520	10.930	11.250	11.310	10.640	11.610	10.220	10.180	9.890
NiO	<0.047	<0	<0.049	<0.049	<0.049	<0.048	<0	<0.047	<0	<0.049	0.072	<0.048	<0.050
CuO	<0.064	<0.065	<0	<0	<0.063	<0.064	<0	<0.063	<0	0.094	<0	<0	<0.065
ZnO	4.430	4.020	5.030	4.830	4.250	4.670	3.910	4.550	4.620	4.450	4.340	4.130	4.260
PbO	33.390	30.090	35.610	35.200	33.550	33.050	29.830	31.370	34.010	29.600	33.200	33.020	34.400
Na_2O	<0	<0	<0	<0	<0.085	<0	<0.087	<0.081	<0.078	<0	<0	<0	<0.078
K_2O	2.260	2.220	2.710	2.440	1.940	2.260	2.280	2.280	2.300	2.050	2.170	2.270	2.300
P_2O_5	0.548	0.671	0.543	0.592	0.550	0.590	0.607	0.641	0.558	0.593	0.568	0.566	0.613
Total	**98.093**	**97.926**	**98.278**	**98.151**	**98.255**	**97.262**	**98.034**	**98.000**	**97.741**	**97.563**	**97.978**	**97.556**	**98.467**
						Atomic %							
SiO_2	50.052	49.317	51.361	50.858	49.602	49.922	49.327	49.611	50.000	49.055	49.282	49.601	50.082
TiO_2	0.202	0.188	0.108	0.141	0.223	0.182	0.220	0.235	0.227	0.222	0.193	0.171	0.186
Al_2O_3	5.505	5.325	5.739	5.591	5.416	5.441	5.489	5.488	5.511	5.380	5.479	5.564	5.530
MgO	0.474	0.922	0.182	0.231	0.632	0.428	0.933	0.592	0.386	0.752	0.647	0.587	0.586
CaO	8.386	10.728	5.479	5.881	9.578	7.577	11.036	8.961	7.390	10.491	9.739	9.622	8.826
MnO	1.623	1.446	1.514	1.538	1.398	1.653	1.517	1.561	1.596	1.620	1.545	1.539	1.418
FeO	13.067	13.760	12.331	13.186	13.000	13.724	13.440	13.806	13.401	13.960	12.653	12.658	12.321
NiO	0.000	0.000	0.000	0.000	0.000	0.000	0.000	0.000	0.000	0.000	0.086	0.000	0.000
CuO	0.000	0.000	0.000	0.000	0.000	0.000	0.000	0.000	0.000	0.102	0.000	0.000	0.000
ZnO	4.856	4.256	5.666	5.420	4.635	5.175	4.122	4.902	5.135	4.722	4.742	4.532	4.684
PbO	13.350	11.619	14.631	14.407	13.344	13.358	11.471	12.326	13.788	11.456	13.231	13.216	13.794
Na_2O	0.000	0.000	0.000	0.000	0.000	0.000	0.000	0.000	0.000	0.000	0.000	0.000	0.000
K_2O	2.141	2.031	2.638	2.366	1.828	2.164	2.078	2.123	2.209	1.880	2.049	2.153	2.185
P_2O_5	0.345	0.407	0.351	0.381	0.344	0.375	0.367	0.396	0.356	0.361	0.356	0.356	0.387
Total	**100.000**	**100.000**	**100.000**	**100.000**	**100.000**	**100.000**	**100.000**	**100.000**	**100.000**	**100.000**	**100.000**	**100.000**	**100.000**

Table iv.80: EMP analyses of glass from sample 13030(1) [Ostri Vrh].

Sample	**13031(1)**	**13031(1)**	**13031(1)**	**13031(1)**	**13031(1)**	**13031(1)**	**13031(1)**
No.	**#4**	**#8**	**#12**	**#18**	**#27**	**#44**	**#51**
SiO_2	17.510	17.670	18.950	14.850	16.700	16.510	17.340
TiO_2	0.045	<0.039	<0.051	0.044	<0	<0.04	0.049
Al_2O_3	1.494	1.229	1.021	1.379	1.590	1.697	1.497
MgO	0.050	0.056	0.065	0.043	0.038	0.032	0.050
CaO	5.650	7.580	8.330	2.970	5.690	4.460	5.570
MnO	0.208	0.252	0.367	0.235	0.205	0.147	0.182
FeO	0.970	0.682	0.655	1.480	0.924	1.064	0.927
NiO	0.056	<0	<0.055	<0.054	<0.052	<0	<0
CuO	<0.07	<0.068	<0.072	0.072	<0	<0.069	<0.071
ZnO	0.299	0.197	0.151	0.516	0.285	0.308	0.125
PbO	71.630	69.590	68.430	74.710	71.740	72.520	71.740
Na_2O	0.069	0.071	0.075	0.069	0.079	0.066	0.068
K_2O	0.105	0.119	0.066	0.113	0.167	0.152	0.139
P_2O_5	0.513	0.699	0.246	0.559	0.702	0.538	0.609
Total	**98.599**	**98.145**	**98.356**	**97.040**	**98.120**	**97.494**	**98.296**
			Atomic %				
SiO_2	38.535	37.835	39.329	35.956	37.327	37.964	38.493
TiO_2	0.075	0.000	0.000	0.080	0.000	0.000	0.082
Al_2O_3	1.938	1.551	1.249	1.968	2.094	2.300	1.958
MgO	0.164	0.179	0.201	0.155	0.127	0.110	0.165
CaO	13.323	17.390	18.523	7.705	13.627	10.988	13.248
MnO	0.388	0.457	0.645	0.482	0.388	0.286	0.342
FeO	1.785	1.221	1.137	2.997	1.727	2.046	1.721
NiO	0.099	0.000	0.000	0.000	0.000	0.000	0.000
CuO	0.000	0.000	0.000	0.132	0.000	0.000	0.000
ZnO	0.486	0.311	0.231	0.922	0.470	0.523	0.205
PbO	42.436	40.112	38.231	48.695	43.166	44.890	42.870
Na_2O	0.147	0.147	0.151	0.162	0.171	0.147	0.146
K_2O	0.147	0.163	0.087	0.175	0.238	0.223	0.197
P_2O_5	0.478	0.634	0.216	0.573	0.664	0.524	0.572
Total	**100.000**	**100.000**	**100.000**	**100.000**	**100.000**	**100.000**	**100.000**

Table iv.81: EMP analyses of glass from sample 13031(1) [Ostri Vrh].

Sample	10021(21)	10021(21)	10021(21)	10021(21)
No.	**#1.66**	**#1.67**	**#1.73**	**#1.74**
Fe	61.887	61.768	61.552	60.967
Cu	0.706	0.740	0.588	0.831
Mn	0.055	0.034	0.059	0.054
Co	0.114	0.102	0.101	0.099
Ni	< 0.014	< 0	< 0.013	0.020
Zn	< 0.034	0.047	0.061	0.042
Cd	0.046	< 0.027	0.053	< 0.028
Sb	< 0	< 0	< 0	< 0
Pb	0.136	0.128	0.148	0.141
S	36.763	36.924	36.820	36.526
Total	**99.707**	**99.743**	**99.382**	**98.680**
		Atom-%		
Fe	48.823	48.662	48.670	48.559
Cu	0.489	0.512	0.409	0.582
Mn	0.044	0.027	0.047	0.044
Co	0.085	0.076	0.076	0.075
Ni	0.000	0.000	0.000	0.015
Zn	0.000	0.032	0.041	0.029
Cd	0.018	0.000	0.021	0.000
Sb	0.000	0.000	0.000	0.000
Pb	0.029	0.027	0.032	0.030
S	50.511	50.663	50.705	50.667
Total	**100.000**	**100.000**	**100.000**	**100.000**
		Normalised to 1 S atom		
Fe	0.967	0.961	0.960	0.958
Cu	0.010	0.010	0.008	0.011
Mn	0.001	0.001	0.001	0.001
Co	0.002	0.002	0.001	0.001
Ni	0.000	0.000	0.000	0.000
Zn	0.000	0.001	0.001	0.001
Cd	0.000	0.000	0.000	0.000
Sb	0.000	0.000	0.000	0.000
Pb	0.001	0.001	0.001	0.001
S	1.000	1.000	1.000	1.000
Total	**1.980**	**1.974**	**1.972**	**1.974**

Table iv.82.: EMP analyses of pyrrhotite from droplets in slag.

Sample	12015(7)	12015(7)	12015(7)	12015(7)	12015(7)	10-6	10-6	10-6	10-6	10-6
No.	**#60**	**#64**	**#69**	**#71**	**#73**	**#2**	**#3**	**#7**	**#9**	**#11**
Fe	61.409	60.768	60.538	60.283	61.087	58.996	60.438	61.345	62.163	61.186
Cu	0.750	1.002	0.798	0.846	0.825	0.658	0.574	0.678	0.550	0.427
Mn	0.034	0.033	0.027	0.040	0.038	0.013	0.021	0.024	0.012	0.012
Co	0.098	0.088	0.088	0.094	0.102	0.118	0.111	0.114	0.109	0.104
Ni	< 0	0.091	< 0.014	0.037	< 0.015	0.048	0.030	0.039	0.041	0.033
Zn	0.122	0.144	0.151	0.449	0.122	1.699	0.512	0.098	0.146	0.083
Cd	0.027	0.069	< 0.025	0.050	0.026	0.092	0.091	0.048	0.091	< 0.037
Sb	0.019	< 0.017	0.018	< 0.017	< 0	0.021	< 0.018	< 0.018	0.032	0.022
Pb	0.159	0.130	0.140	0.337	0.148	0.451	0.353	0.111	0.174	0.448
S	36.685	36.733	36.592	36.597	36.670	36.405	36.655	37.028	36.987	36.896
Total	**99.303**	**99.223**	**98.388**	**98.812**	**99.086**	**98.501**	**98.814**	**99.515**	**100.305**	**99.211**
					Atom-%					
Fe	48.638	48.221	48.332	48.062	48.494	47.282	48.152	48.404	48.775	48.497
Cu	0.522	0.699	0.560	0.593	0.576	0.463	0.402	0.470	0.379	0.297
Mn	0.027	0.027	0.022	0.032	0.031	0.011	0.017	0.019	0.010	0.010
Co	0.074	0.066	0.067	0.071	0.077	0.090	0.084	0.085	0.081	0.078
Ni	0.000	0.069	0.000	0.028	0.000	0.037	0.023	0.029	0.031	0.025
Zn	0.083	0.098	0.103	0.306	0.083	1.163	0.348	0.066	0.098	0.056
Cd	0.011	0.027	0.000	0.020	0.010	0.037	0.036	0.019	0.035	0.000
Sb	0.007	0.000	0.007	0.000	0.000	0.008	0.000	0.000	0.012	0.008
Pb	0.034	0.028	0.030	0.072	0.032	0.097	0.076	0.024	0.037	0.096
S	50.605	50.766	50.880	50.816	50.699	50.814	50.862	50.884	50.543	50.933
Total	**100.000**	**100.000**	**100.000**	**100.000**	**100.000**	**100.000**	**100.000**	**100.000**	**100.000**	**100.000**
					Normalised to 1 S atom					
Fe	0.961	0.950	0.950	0.946	0.956	0.930	0.947	0.951	0.965	0.952
Cu	0.010	0.014	0.011	0.012	0.011	0.009	0.008	0.009	0.008	0.006
Mn	0.001	0.001	0.000	0.001	0.001	0.000	0.000	0.000	0.000	0.000
Co	0.001	0.001	0.001	0.001	0.002	0.002	0.002	0.002	0.002	0.002
Ni	0.000	0.001	0.000	0.001	0.000	0.001	0.000	0.001	0.001	0.000
Zn	0.002	0.002	0.002	0.006	0.002	0.023	0.007	0.001	0.002	0.001
Cd	0.000	0.001	0.000	0.000	0.000	0.001	0.001	0.000	0.001	0.000
Sb	0.000	0.000	0.000	0.000	0.000	0.000	0.000	0.000	0.000	0.000
Pb	0.001	0.001	0.001	0.001	0.001	0.002	0.001	0.000	0.001	0.002
S	1.000	1.000	1.000	1.000	1.000	1.000	1.000	1.000	1.000	1.000
Total	**1.976**	**1.970**	**1.965**	**1.968**	**1.972**	**1.968**	**1.966**	**1.965**	**1.979**	**1.963**

Sample	10-6	10-6	10-6	10-6	10-6	10-6	10-6	10-6
No.	#11	#12	#15	#17	#19	#20	#22	#24
Fe	61.186	60.624	61.828	60.799	61.557	61.814	61.427	60.142
Cu	0.427	0.994	0.555	0.764	0.592	0.856	0.520	0.645
Mn	0.012	0.020	0.013	0.011	0.013	0.015	0.015	0.018
Co	0.104	0.113	0.106	0.112	0.117	0.122	0.117	0.117
Ni	0.033	0.063	0.029	0.074	0.056	0.060	0.020	0.021
Zn	0.083	0.589	0.119	0.077	0.170	0.078	0.109	0.144
Cd	< 0.037	0.050	0.065	0.048	0.067	0.046	< 0.038	< 0.037
Sb	0.022	0.021	0.027	< 0.017	< 0.018	0.029	0.021	0.025
Pb	0.448	0.475	0.213	0.184	0.185	0.113	0.511	0.292
S	36.896	36.923	37.488	36.796	36.931	36.957	37.184	37.369
Total	**99.211**	**99.872**	**100.471**	**98.865**	**99.688**	**100.110**	**100.005**	**98.773**
				Atom-%				
Fe	48.497	47.865	48.322	48.298	48.546	48.576	48.356	47.674
Cu	0.297	0.690	0.381	0.533	0.410	0.591	0.360	0.449
Mn	0.010	0.016	0.010	0.009	0.010	0.012	0.012	0.015
Co	0.078	0.085	0.079	0.084	0.087	0.091	0.087	0.088
Ni	0.025	0.047	0.022	0.056	0.042	0.045	0.015	0.016
Zn	0.056	0.397	0.079	0.052	0.114	0.052	0.073	0.097
Cd	0.000	0.020	0.025	0.019	0.026	0.018	0.000	0.000
Sb	0.008	0.008	0.010	0.000	0.000	0.010	0.008	0.009
Pb	0.096	0.101	0.045	0.039	0.039	0.024	0.108	0.062
S	50.933	50.772	51.027	50.909	50.724	50.581	50.980	51.590
Total	**100.000**	**100.000**	**100.000**	**100.000**	**100.000**	**100.000**	**100.000**	**100.000**
				Normalised to 1 S atom				
Fe	0.952	0.943	0.947	0.949	0.957	0.960	0.949	0.924
Cu	0.006	0.014	0.007	0.010	0.008	0.012	0.007	0.009
Mn	0.000	0.000	0.000	0.000	0.000	0.000	0.000	0.000
Co	0.002	0.002	0.002	0.002	0.002	0.002	0.002	0.002
Ni	0.000	0.001	0.000	0.001	0.001	0.001	0.000	0.000
Zn	0.001	0.008	0.002	0.001	0.002	0.001	0.001	0.002
Cd	0.000	0.000	0.000	0.000	0.001	0.000	0.000	0.000
Sb	0.000	0.000	0.000	0.000	0.000	0.000	0.000	0.000
Pb	0.002	0.002	0.001	0.001	0.001	0.000	0.002	0.001
S	1.000	1.000	1.000	1.000	1.000	1.000	1.000	1.000
Total	**1.963**	**1.970**	**1.960**	**1.964**	**1.971**	**1.977**	**1.962**	**1.938**

Table iv.83.: EMP analyses of pyrrhotite from interstitial sulphide clusters.

Sample	10-2B	10-2B	10-2B	10-2B	12015(5)	12015(5)	12015(5)	12015(5)	12015(5)	12015(5)
No.	**#84**	**#90**	**#91**	**#120**	**#6**	**#7**	**#8**	**#9**	**#18**	**#19**
Fe	60.769	59.132	60.779	60.295	60.468	60.823	60.975	60.960	60.773	60.576
Cu	1.331	2.568	1.106	1.426	1.931	1.470	1.504	1.106	0.737	0.917
Mn	0.145	0.125	0.134	0.142	0.083	0.081	0.076	0.083	0.080	0.068
Co	0.120	0.129	0.127	0.125	0.137	0.136	0.131	0.139	0.135	0.143
Ni	0.097	0.075	0.096	0.070	0.248	0.358	0.384	0.391	0.184	0.198
Zn	0.055	0.033	< 0.026	< 0.026	< 0.025	< 0	< 0.022	< 0.026	< 0	< 0
Cd	< 0.036	0.042	< 0.037	< 0.038	0.042	0.047	< 0.025	0.029	0.029	0.031
Sb	< 0.018	0.021	0.025	0.025	0.019	0.029	< 0.018	0.023	0.025	< 0.019
Pb	0.164	0.120	0.116	0.306	0.133	0.111	0.080	0.135	0.291	0.214
S	36.032	36.156	36.138	36.295	35.281	35.891	35.794	35.573	36.502	36.307
Total	**98.713**	**98.432**	**98.551**	**98.684**	**98.375**	**98.946**	**98.960**	**98.439**	**98.773**	**98.454**
					Atom-%					
Fe	48.562	47.393	48.592	48.165	48.715	48.564	48.693	48.950	48.432	48.429
Cu	0.935	1.809	0.777	1.001	1.367	1.031	1.055	0.780	0.516	0.644
Mn	0.118	0.102	0.109	0.115	0.068	0.066	0.062	0.068	0.065	0.055
Co	0.091	0.098	0.096	0.095	0.105	0.103	0.099	0.106	0.102	0.108
Ni	0.074	0.057	0.073	0.053	0.190	0.272	0.292	0.299	0.140	0.151
Zn	0.038	0.023	0.000	0.000	0.000	0.000	0.000	0.000	0.000	0.000
Cd	0.000	0.017	0.000	0.000	0.017	0.019	0.000	0.012	0.011	0.012
Sb	0.000	0.008	0.009	0.009	0.007	0.011	0.000	0.008	0.009	0.000
Pb	0.035	0.026	0.025	0.066	0.029	0.024	0.017	0.029	0.063	0.046
S	50.148	50.469	50.319	50.495	49.503	49.910	49.782	49.748	50.663	50.554
Total	**100.000**	**100.000**	**100.000**	**100.000**	**100.000**	**100.000**	**100.000**	**100.000**	**100.000**	**100.000**
					Normalised to 1 S atom					
Fe	0.968	0.939	0.966	0.954	0.984	0.973	0.978	0.984	0.956	0.958
Cu	0.019	0.036	0.015	0.020	0.028	0.021	0.021	0.016	0.010	0.013
Mn	0.002	0.002	0.002	0.002	0.001	0.001	0.001	0.001	0.001	0.001
Co	0.002	0.002	0.002	0.002	0.002	0.002	0.002	0.002	0.002	0.002
Ni	0.001	0.001	0.001	0.001	0.004	0.005	0.006	0.006	0.003	0.003
Zn	0.001	0.000	0.000	0.000	0.000	0.000	0.000	0.000	0.000	0.000
Cd	0.000	0.000	0.000	0.000	0.000	0.000	0.000	0.000	0.000	0.000
Sb	0.000	0.000	0.000	0.000	0.000	0.000	0.000	0.000	0.000	0.000
Pb	0.001	0.001	0.000	0.001	0.001	0.000	0.000	0.001	0.001	0.001
S	1.000	1.000	1.000	1.000	1.000	1.000	1.000	1.000	1.000	1.000
Total	**1.994**	**1.981**	**1.987**	**1.980**	**2.020**	**2.004**	**2.009**	**2.010**	**1.974**	**1.978**

Sample	14032	14032	14032	14032	14032	14032	14032	14032	14032	14032
No.	#7	#12	#14	#15	#25	#27	#32	#33	#37	#47
Fe	61.530	61.823	61.257	61.675	61.149	61.137	61.749	61.072	61.571	61.143
Cu	1.378	1.364	1.447	1.184	1.741	1.646	1.236	1.356	1.287	1.371
Mn	0.081	0.085	0.085	0.077	0.064	0.076	0.060	0.064	0.076	0.066
Co	0.123	0.104	0.121	0.116	0.115	0.129	0.113	0.129	0.117	0.111
Ni	0.074	0.059	0.082	0.053	0.053	0.063	0.101	0.127	0.129	0.078
Zn	0.032	< 0.025	< 0	< 0.025	< 0.022	0.030	0.029	< 0.025	< 0	0.026
Cd	< 0.024	0.028	< 0.025	< 0.025	0.028	< 0.025	0.045	0.033	< 0.027	0.038
Sb	< 0.016	0.027	< 0.018	0.021	0.044	< 0.019	< 0.018	0.032	0.022	< 0.019
Pb	0.069	0.081	0.137	0.197	0.099	0.109	0.099	0.073	0.132	0.129
S	36.801	36.901	37.157	37.148	36.922	37.066	37.181	37.085	37.132	37.024
Total	**100.088**	**100.472**	**100.305**	**100.497**	**100.215**	**100.256**	**100.632**	**99.997**	**100.466**	**100.018**
					Atom-%					
Fe	48.392	48.459	48.023	48.291	48.047	47.968	48.268	48.009	48.205	48.087
Cu	0.952	0.940	0.997	0.815	1.202	1.135	0.849	0.937	0.885	0.948
Mn	0.065	0.068	0.068	0.061	0.051	0.061	0.048	0.051	0.060	0.053
Co	0.092	0.077	0.090	0.086	0.086	0.096	0.084	0.096	0.087	0.083
Ni	0.055	0.044	0.061	0.039	0.040	0.047	0.075	0.095	0.096	0.058
Zn	0.021	0.000	0.000	0.000	0.000	0.020	0.019	0.000	0.000	0.017
Cd	0.000	0.011	0.000	0.000	0.011	0.000	0.017	0.013	0.000	0.015
Sb	0.000	0.010	0.000	0.008	0.016	0.000	0.000	0.012	0.008	0.000
Pb	0.015	0.017	0.029	0.042	0.021	0.023	0.021	0.015	0.028	0.027
S	50.408	50.375	50.732	50.658	50.526	50.650	50.618	50.772	50.631	50.712
Total	**100.000**	**100.000**	**100.000**	**100.000**	**100.000**	**100.000**	**100.000**	**100.000**	**100.000**	**100.000**
					Normalised to 1 S atom					
Fe	0.960	0.962	0.947	0.953	0.951	0.947	0.954	0.946	0.952	0.948
Cu	0.019	0.019	0.020	0.016	0.024	0.022	0.017	0.018	0.017	0.019
Mn	0.001	0.001	0.001	0.001	0.001	0.001	0.001	0.001	0.001	0.001
Co	0.002	0.002	0.002	0.002	0.002	0.002	0.002	0.002	0.002	0.002
Ni	0.001	0.001	0.001	0.001	0.001	0.001	0.001	0.002	0.002	0.001
Zn	0.000	0.000	0.000	0.000	0.000	0.000	0.000	0.000	0.000	0.000
Cd	0.000	0.000	0.000	0.000	0.000	0.000	0.000	0.000	0.000	0.000
Sb	0.000	0.000	0.000	0.000	0.000	0.000	0.000	0.000	0.000	0.000
Pb	0.000	0.000	0.001	0.001	0.000	0.000	0.000	0.000	0.001	0.001
S	1.000	1.000	1.000	1.000	1.000	1.000	1.000	1.000	1.000	1.000
Total	**1.984**	**1.985**	**1.971**	**1.974**	**1.979**	**1.974**	**1.976**	**1.970**	**1.975**	**1.972**

Sample	14032	11027(1)	11027(1)	11027(1)	11027(1)	11027(1)	11027(1)	11027(1)	11027(1)	11029(3)
No.	**#49**	**#2.16**	**#2.18**	**#2.21**	**#2.24**	**#2.30**	**#2.33**	**#2.34**	**#2.51**	**#20**
Fe	61.729	60.961	61.150	61.161	61.179	61.295	61.634	61.144	58.759	60.945
Cu	1.180	1.332	1.239	1.196	1.103	1.384	1.361	1.297	3.306	1.459
Mn	0.072	0.055	0.031	0.047	0.049	0.046	0.043	0.050	0.048	0.025
Co	0.114	0.163	0.153	0.145	0.156	0.161	0.152	0.158	0.155	0.177
Ni	0.124	0.114	0.083	0.087	0.123	0.145	0.176	0.161	0.177	0.282
Zn	< 0.022	< 0.025	0.035	0.030	0.047	< 0.025	0.027	< 0	0.035	< 0.026
Cd	0.029	< 0	0.034	< 0.025	0.037	0.032	0.046	< 0.026	0.028	< 0.025
Sb	0.021	0.027	0.023	< 0	< 0.019	0.027	0.022	< 0.013	< 0.017	< 0.02
Pb	0.105	0.092	0.090	0.103	0.086	0.083	0.082	0.133	0.186	0.168
S	36.933	35.861	36.361	36.317	36.343	36.370	35.955	36.225	36.233	36.634
Total	**100.307**	**98.623**	**99.199**	**99.103**	**99.140**	**99.563**	**99.518**	**99.168**	**98.954**	**99.690**
					Atom-%					
Fe	48.437	48.791	48.569	48.624	48.616	48.554	48.961	48.618	46.922	48.164
Cu	0.814	0.937	0.865	0.836	0.770	0.963	0.950	0.906	2.320	1.013
Mn	0.057	0.045	0.025	0.038	0.040	0.037	0.035	0.040	0.039	0.020
Co	0.085	0.124	0.115	0.109	0.117	0.121	0.114	0.119	0.117	0.133
Ni	0.093	0.087	0.063	0.066	0.093	0.109	0.133	0.122	0.134	0.212
Zn	0.000	0.000	0.024	0.020	0.032	0.000	0.018	0.000	0.024	0.000
Cd	0.011	0.000	0.013	0.000	0.015	0.013	0.018	0.000	0.011	0.000
Sb	0.008	0.010	0.008	0.000	0.000	0.010	0.008	0.000	0.000	0.000
Pb	0.022	0.020	0.019	0.022	0.018	0.018	0.018	0.029	0.040	0.036
S	50.473	49.987	50.298	50.285	50.298	50.176	49.744	50.166	50.392	50.422
Total	**100.000**	**100.000**	**100.000**	**100.000**	**100.000**	**100.000**	**100.000**	**100.000**	**100.000**	**100.000**
					Normalised to 1 S atom					
Fe	0.960	0.976	0.966	0.967	0.967	0.968	0.984	0.969	0.931	0.955
Cu	0.016	0.019	0.017	0.017	0.015	0.019	0.019	0.018	0.046	0.020
Mn	0.001	0.001	0.000	0.001	0.001	0.001	0.001	0.001	0.001	0.000
Co	0.002	0.002	0.002	0.002	0.002	0.002	0.002	0.002	0.002	0.003
Ni	0.002	0.002	0.001	0.001	0.002	0.002	0.003	0.002	0.003	0.004
Zn	0.000	0.000	0.000	0.000	0.001	0.000	0.000	0.000	0.000	0.000
Cd	0.000	0.000	0.000	0.000	0.000	0.000	0.000	0.000	0.000	0.000
Sb	0.000	0.000	0.000	0.000	0.000	0.000	0.000	0.000	0.000	0.000
Pb	0.000	0.000	0.000	0.000	0.000	0.000	0.000	0.001	0.001	0.001
S	1.000	1.000	1.000	1.000	1.000	1.000	1.000	1.000	1.000	1.000
Total	**1.981**	**2.001**	**1.988**	**1.989**	**1.988**	**1.993**	**2.010**	**1.993**	**1.984**	**1.983**

Sample	11029(5)	11029(5)	11029(5)	11029(5)	11029(5)	11029(5)	11029(5)	11029(5)	11029(5)	11029(5)
No.	**#1.19**	**#1.22**	**#1.25**	**#1.29**	**#1.42**	**#2.13**	**#2.17**	**#2.19**	**#2.22**	**#2.24**
Fe	60.529	60.734	60.167	60.414	60.412	61.025	61.200	61.085	60.941	61.327
Cu	1.187	1.224	1.213	0.966	1.125	1.307	1.249	1.320	1.298	1.049
Mn	0.196	0.176	0.193	0.203	0.248	0.182	0.183	0.208	0.161	0.160
Co	0.122	0.110	0.118	0.115	0.129	0.116	0.117	0.120	0.118	0.119
Ni	0.070	0.075	0.093	0.102	0.064	0.103	0.128	0.239	0.133	0.106
Zn	0.061	0.089	< 0.025	< 0.026	< 0.025	< 0	0.030	< 0.027	< 0	0.042
Cd	< 0.026	< 0.026	< 0.027	0.033	0.036	< 0.025	< 0.028	< 0.026	< 0.024	0.032
Sb	< 0	< 0	< 0	< 0	< 0	< 0.018	0.028	0.026	0.022	0.034
Pb	0.141	0.134	0.156	0.163	0.162	0.127	0.113	0.116	0.125	0.108
S	37.066	36.343	36.741	36.138	36.398	36.324	35.607	36.006	35.631	35.704
Total	**99.372**	**98.885**	**98.681**	**98.153**	**98.590**	**99.201**	**98.675**	**99.142**	**98.452**	**98.704**
					Atom-%					
Fe	47.812	48.366	47.881	48.457	48.218	48.485	49.039	48.654	48.916	49.099
Cu	0.824	0.857	0.848	0.681	0.789	0.913	0.880	0.924	0.916	0.738
Mn	0.157	0.142	0.156	0.166	0.201	0.147	0.149	0.168	0.131	0.130
Co	0.091	0.083	0.089	0.087	0.098	0.087	0.089	0.091	0.090	0.090
Ni	0.053	0.057	0.070	0.078	0.049	0.078	0.098	0.181	0.102	0.081
Zn	0.041	0.061	0.000	0.000	0.000	0.000	0.021	0.000	0.000	0.029
Cd	0.000	0.000	0.000	0.013	0.014	0.000	0.000	0.000	0.000	0.013
Sb	0.000	0.000	0.000	0.000	0.000	0.000	0.010	0.009	0.008	0.012
Pb	0.030	0.029	0.033	0.035	0.035	0.027	0.024	0.025	0.027	0.023
S	50.992	50.406	50.922	50.482	50.596	50.263	49.691	49.947	49.811	49.784
Total	**100.000**	**100.000**	**100.000**	**100.000**	**100.000**	**100.000**	**100.000**	**100.000**	**100.000**	**100.000**
					Normalised to 1 S atom					
Fe	0.938	0.960	0.940	0.960	0.953	0.965	0.987	0.974	0.982	0.986
Cu	0.016	0.017	0.017	0.013	0.016	0.018	0.018	0.018	0.018	0.015
Mn	0.003	0.003	0.003	0.003	0.004	0.003	0.003	0.003	0.003	0.003
Co	0.002	0.002	0.002	0.002	0.002	0.002	0.002	0.002	0.002	0.002
Ni	0.001	0.001	0.001	0.002	0.001	0.002	0.002	0.004	0.002	0.002
Zn	0.001	0.001	0.000	0.000	0.000	0.000	0.000	0.000	0.000	0.001
Cd	0.000	0.000	0.000	0.000	0.000	0.000	0.000	0.000	0.000	0.000
Sb	0.000	0.000	0.000	0.000	0.000	0.000	0.000	0.000	0.000	0.000
Pb	0.001	0.001	0.001	0.001	0.001	0.001	0.000	0.000	0.001	0.000
S	1.000	1.000	1.000	1.000	1.000	1.000	1.000	1.000	1.000	1.000
Total	**1.961**	**1.984**	**1.964**	**1.981**	**1.976**	**1.990**	**2.012**	**2.002**	**2.008**	**2.009**

Sample	11029(5)	11029(5)	11029(5)	11029(5)	11029(5)	11029(5)	11029(5)	11029(5)	11029(5)	11029(5)
No.	**#2.26**	**#2.30**	**#2.32**	**#2.33**	**#2.35**	**#2.37**	**#2.39**	**#2.40**	**#2.45**	**#2.47**
Fe	61.384	61.225	61.242	60.857	60.949	61.237	61.164	61.078	61.432	60.930
Cu	0.963	1.050	1.264	1.309	0.950	1.155	1.173	1.040	0.983	1.121
Mn	0.183	0.237	0.246	0.250	0.234	0.272	0.241	0.264	0.254	0.231
Co	0.119	0.114	0.111	0.107	0.108	0.107	0.114	0.112	0.115	0.108
Ni	0.075	0.105	0.122	0.089	0.039	0.162	0.149	0.062	0.051	0.043
Zn	< 0.026	0.051	< 0.026	0.032	0.028	< 0	< 0.025	< 0.024	< 0.024	< 0.026
Cd	0.028	< 0.024	< 0.026	< 0.025	0.038	0.037	0.034	< 0	0.028	0.028
Sb	0.029	< 0	0.022	< 0.018	< 0.019	< 0.018	0.033	0.023	< 0.019	0.036
Pb	0.116	0.131	0.073	0.115	0.164	0.096	0.113	0.114	0.125	0.131
S	36.349	36.100	36.444	36.303	36.480	36.402	36.364	36.479	36.526	36.580
Total	**99.268**	**99.013**	**99.553**	**99.062**	**98.990**	**99.502**	**99.385**	**99.172**	**99.514**	**99.208**
					Atom-%					
Fe	48.731	48.766	48.480	48.402	48.456	48.514	48.510	48.475	48.611	48.331
Cu	0.672	0.735	0.879	0.915	0.664	0.804	0.818	0.725	0.684	0.781
Mn	0.148	0.192	0.198	0.202	0.189	0.219	0.194	0.213	0.204	0.186
Co	0.090	0.086	0.083	0.081	0.081	0.080	0.086	0.084	0.086	0.081
Ni	0.057	0.080	0.092	0.067	0.030	0.122	0.112	0.047	0.038	0.032
Zn	0.000	0.035	0.000	0.022	0.019	0.000	0.000	0.000	0.000	0.000
Cd	0.011	0.000	0.000	0.000	0.015	0.015	0.013	0.000	0.011	0.011
Sb	0.011	0.000	0.008	0.000	0.000	0.000	0.012	0.008	0.000	0.013
Pb	0.025	0.028	0.016	0.025	0.035	0.020	0.024	0.024	0.027	0.028
S	50.257	50.078	50.244	50.286	50.511	50.226	50.230	50.423	50.338	50.535
Total	**100.000**	**100.000**	**100.000**	**100.000**	**100.000**	**100.000**	**100.000**	**100.000**	**100.000**	**100.000**
					Normalised to 1 S atom					
Fe	0.970	0.974	0.965	0.963	0.959	0.966	0.966	0.961	0.966	0.956
Cu	0.013	0.015	0.018	0.018	0.013	0.016	0.016	0.014	0.014	0.015
Mn	0.003	0.004	0.004	0.004	0.004	0.004	0.004	0.004	0.004	0.004
Co	0.002	0.002	0.002	0.002	0.002	0.002	0.002	0.002	0.002	0.002
Ni	0.001	0.002	0.002	0.001	0.001	0.002	0.002	0.001	0.001	0.001
Zn	0.000	0.001	0.000	0.000	0.000	0.000	0.000	0.000	0.000	0.000
Cd	0.000	0.000	0.000	0.000	0.000	0.000	0.000	0.000	0.000	0.000
Sb	0.000	0.000	0.000	0.000	0.000	0.000	0.000	0.000	0.000	0.000
Pb	0.000	0.001	0.000	0.000	0.001	0.000	0.000	0.000	0.001	0.001
S	1.000	1.000	1.000	1.000	1.000	1.000	1.000	1.000	1.000	1.000
Total	**1.990**	**1.997**	**1.990**	**1.989**	**1.980**	**1.991**	**1.991**	**1.983**	**1.987**	**1.979**

Sample	11029(5)	11029(5)	10024(4)	10024(4)	10024(4)	10024(4)	10024(4)	10024(4)	10024(4)	10024(4)
No.	**#2.50**	**#2.51**	**#1.45**	**#1.46**	**#1.49**	**#1.59**	**#1.60**	**#1.61**	**#1.68**	**#1.69**
Fe	61.142	60.593	60.860	60.981	61.098	60.939	60.712	60.254	60.381	60.958
Cu	1.266	1.280	1.297	1.127	1.267	1.504	1.275	1.325	1.319	1.569
Mn	0.267	0.247	0.094	0.097	0.095	0.106	0.107	0.094	0.117	0.127
Co	0.113	0.116	0.116	0.125	0.106	0.119	0.116	0.116	0.115	0.107
Ni	0.146	0.101	0.104	0.095	0.101	0.105	0.097	0.101	0.101	0.116
Zn	< 0	< 0	< 0	< 0.025	0.030	< 0.025	< 0	0.080	< 0.026	< 0.027
Cd	0.037	< 0.025	< 0.027	< 0.027	< 0	< 0.026	< 0	0.033	< 0.027	< 0.028
Sb	0.031	0.023	< 0	< 0	< 0	< 0	< 0	< 0	< 0	< 0
Pb	0.139	0.142	0.108	0.106	0.159	0.117	0.131	0.243	0.209	0.104
S	36.612	37.076	36.886	36.435	36.831	36.812	36.649	36.633	36.830	36.719
Total	**99.771**	**99.610**	**99.465**	**99.021**	**99.756**	**99.702**	**99.087**	**98.907**	**99.111**	**99.740**
					Atom-%					
Fe	48.293	47.788	48.082	48.489	48.215	48.088	48.181	47.946	47.897	48.129
Cu	0.879	0.887	0.901	0.788	0.879	1.043	0.889	0.927	0.919	1.089
Mn	0.214	0.198	0.075	0.078	0.076	0.085	0.086	0.076	0.094	0.102
Co	0.085	0.087	0.087	0.094	0.079	0.089	0.087	0.087	0.086	0.080
Ni	0.110	0.076	0.078	0.072	0.076	0.079	0.073	0.076	0.076	0.087
Zn	0.000	0.000	0.000	0.000	0.020	0.000	0.000	0.054	0.000	0.000
Cd	0.015	0.000	0.000	0.000	0.000	0.000	0.000	0.013	0.000	0.000
Sb	0.011	0.008	0.000	0.000	0.000	0.000	0.000	0.000	0.000	0.000
Pb	0.030	0.030	0.023	0.023	0.034	0.025	0.028	0.052	0.045	0.022
S	50.364	50.926	50.754	50.457	50.620	50.592	50.655	50.768	50.882	50.491
Total	**100.000**	**100.000**	**100.000**	**100.000**	**100.000**	**100.000**	**100.000**	**100.000**	**100.000**	**100.000**
					Normalised to 1 S atom					
Fe	0.959	0.938	0.947	0.961	0.952	0.951	0.951	0.944	0.941	0.953
Cu	0.017	0.017	0.018	0.016	0.017	0.021	0.018	0.018	0.018	0.022
Mn	0.004	0.004	0.001	0.002	0.002	0.002	0.002	0.001	0.002	0.002
Co	0.002	0.002	0.002	0.002	0.002	0.002	0.002	0.002	0.002	0.002
Ni	0.002	0.001	0.002	0.001	0.001	0.002	0.001	0.002	0.001	0.002
Zn	0.000	0.000	0.000	0.000	0.000	0.000	0.000	0.001	0.000	0.000
Cd	0.000	0.000	0.000	0.000	0.000	0.000	0.000	0.000	0.000	0.000
Sb	0.000	0.000	0.000	0.000	0.000	0.000	0.000	0.000	0.000	0.000
Pb	0.001	0.001	0.000	0.000	0.001	0.000	0.001	0.001	0.001	0.000
S	1.000	1.000	1.000	1.000	1.000	1.000	1.000	1.000	1.000	1.000
Total	**1.986**	**1.964**	**1.970**	**1.982**	**1.975**	**1.977**	**1.974**	**1.970**	**1.965**	**1.981**

Sample	10024(4)	10024(4)	10024(4)	10024(4)	10024(4)	10024(4)	10024(4)	10024(4)	10024(4)	10024(4)
No.	**#1.71**	**#1.74**	**#1.76**	**#1.77**	**#1.80**	**#1.82**	**#1.89**	**#1.91**	**#1.92**	**#1.97**
Fe	61.440	60.506	61.253	61.132	61.135	60.605	60.963	61.569	60.838	59.328
Cu	0.857	1.241	1.207	1.227	0.979	1.463	1.144	0.875	1.398	2.015
Mn	0.116	0.118	0.134	0.133	0.130	0.137	0.167	0.151	0.151	0.148
Co	0.131	0.099	0.125	0.119	0.112	0.122	0.107	0.113	0.117	0.115
Ni	0.081	0.078	0.067	0.073	0.069	0.049	0.085	0.089	0.082	0.044
Zn	< 0	0.027	0.037	< 0.025	0.075	0.032	< 0.026	< 0.025	< 0.026	< 0
Cd	0.030	0.032	0.036	0.043	0.044	< 0.024	< 0.032	0.031	0.037	0.044
Sb	< 0	< 0	< 0	< 0	< 0	< 0	< 0	< 0	< 0	< 0
Pb	0.140	0.471	0.137	0.150	0.153	0.198	0.129	0.109	0.122	0.791
S	36.845	35.933	37.144	36.988	36.993	36.922	37.014	36.595	36.865	35.771
Total	**99.640**	**98.611**	**100.186**	**99.917**	**99.750**	**99.590**	**99.653**	**99.532**	**99.667**	**98.277**
					Atom-%					
Fe	48.479	48.548	48.076	48.132	48.193	47.880	48.071	48.686	48.031	47.870
Cu	0.594	0.875	0.833	0.849	0.678	1.016	0.793	0.608	0.970	1.429
Mn	0.093	0.096	0.107	0.106	0.104	0.110	0.134	0.121	0.121	0.121
Co	0.098	0.075	0.093	0.089	0.084	0.091	0.080	0.085	0.088	0.088
Ni	0.061	0.060	0.050	0.055	0.052	0.037	0.064	0.067	0.062	0.034
Zn	0.000	0.018	0.025	0.000	0.050	0.022	0.000	0.000	0.000	0.000
Cd	0.012	0.013	0.014	0.017	0.017	0.000	0.000	0.012	0.015	0.018
Sb	0.000	0.000	0.000	0.000	0.000	0.000	0.000	0.000	0.000	0.000
Pb	0.030	0.102	0.029	0.032	0.033	0.042	0.027	0.023	0.026	0.172
S	50.633	50.213	50.774	50.720	50.789	50.802	50.832	50.398	50.689	50.268
Total	**100.000**	**100.000**	**100.000**	**100.000**	**100.000**	**100.000**	**100.000**	**100.000**	**100.000**	**100.000**
					Normalised to 1 S atom					
Fe	0.957	0.967	0.947	0.949	0.949	0.942	0.946	0.966	0.948	0.952
Cu	0.012	0.017	0.016	0.017	0.013	0.020	0.016	0.012	0.019	0.028
Mn	0.002	0.002	0.002	0.002	0.002	0.002	0.003	0.002	0.002	0.002
Co	0.002	0.001	0.002	0.002	0.002	0.002	0.002	0.002	0.002	0.002
Ni	0.001	0.001	0.001	0.001	0.001	0.001	0.001	0.001	0.001	0.001
Zn	0.000	0.000	0.000	0.000	0.001	0.000	0.000	0.000	0.000	0.000
Cd	0.000	0.000	0.000	0.000	0.000	0.000	0.000	0.000	0.000	0.000
Sb	0.000	0.000	0.000	0.000	0.000	0.000	0.000	0.000	0.000	0.000
Pb	0.001	0.002	0.001	0.001	0.001	0.001	0.001	0.000	0.001	0.003
S	1.000	1.000	1.000	1.000	1.000	1.000	1.000	1.000	1.000	1.000
Total	**1.975**	**1.992**	**1.970**	**1.972**	**1.969**	**1.968**	**1.967**	**1.984**	**1.973**	**1.989**

Sample	10024(4)	10024(4)	10024(4)	10024(4)	10024(4)	10024(4)	10024(4)	10024(4)	10024(4)	10024(4)
No.	**#1.154**	**#1.156**	**#1.158**	**#1.162**	**#1.163**	**#1.169**	**#2.13**	**#2.16**	**#2.18**	**#2.30**
Fe	61.031	61.080	61.203	61.071	61.557	60.909	62.116	61.868	62.056	61.534
Cu	1.155	1.273	1.476	1.509	1.243	1.942	0.870	0.911	0.874	1.117
Mn	0.095	0.095	0.102	0.103	0.145	0.154	0.053	0.091	0.088	0.127
Co	0.111	0.120	0.117	0.119	0.126	0.118	0.098	0.112	0.112	0.098
Ni	0.091	0.084	0.107	0.080	0.064	0.068	0.082	0.066	0.076	0.084
Zn	< 0.025	< 0	0.047	0.062	< 0.024	< 0.026	0.048	< 0.031	0.043	< 0.035
Cd	< 0.026	0.034	< 0.027	< 0.027	< 0.027	< 0.026	0.033	< 0.03	0.039	< 0.031
Sb	< 0	< 0	< 0	< 0	< 0	< 0	0.029	< 0.022	< 0.025	0.024
Pb	0.162	0.116	0.124	0.132	0.117	0.134	0.105	0.120	0.102	0.108
S	36.403	36.933	36.330	36.769	36.826	36.596	36.932	36.934	37.041	36.598
Total	**99.048**	**99.764**	**99.540**	**99.845**	**100.131**	**99.921**	**100.366**	**100.102**	**100.431**	**99.690**
					Atom-%					
Fe	48.523	48.147	48.511	48.157	48.415	48.065	48.709	48.605	48.600	48.606
Cu	0.807	0.882	1.028	1.046	0.859	1.347	0.600	0.629	0.602	0.775
Mn	0.077	0.076	0.082	0.083	0.116	0.124	0.042	0.073	0.070	0.102
Co	0.084	0.090	0.088	0.089	0.094	0.088	0.073	0.083	0.083	0.073
Ni	0.069	0.063	0.081	0.060	0.048	0.051	0.061	0.049	0.057	0.063
Zn	0.000	0.000	0.032	0.042	0.000	0.000	0.032	0.000	0.029	0.000
Cd	0.000	0.013	0.000	0.000	0.000	0.000	0.013	0.000	0.015	0.000
Sb	0.000	0.000	0.000	0.000	0.000	0.000	0.010	0.000	0.000	0.009
Pb	0.035	0.025	0.026	0.028	0.025	0.029	0.022	0.025	0.022	0.023
S	50.406	50.704	50.152	50.496	50.444	50.296	50.438	50.535	50.523	50.348
Total	**100.000**	**100.000**	**100.000**	**100.000**	**100.000**	**100.000**	**100.000**	**100.000**	**100.000**	**100.000**
					Normalised to 1 S atom					
Fe	0.963	0.950	0.967	0.954	0.960	0.956	0.966	0.962	0.962	0.965
Cu	0.016	0.017	0.021	0.021	0.017	0.027	0.012	0.012	0.012	0.015
Mn	0.002	0.002	0.002	0.002	0.002	0.002	0.001	0.001	0.001	0.002
Co	0.002	0.002	0.002	0.002	0.002	0.002	0.001	0.002	0.002	0.001
Ni	0.001	0.001	0.002	0.001	0.001	0.001	0.001	0.001	0.001	0.001
Zn	0.000	0.000	0.001	0.001	0.000	0.000	0.001	0.000	0.001	0.000
Cd	0.000	0.000	0.000	0.000	0.000	0.000	0.000	0.000	0.000	0.000
Sb	0.000	0.000	0.000	0.000	0.000	0.000	0.000	0.000	0.000	0.000
Pb	0.001	0.000	0.001	0.001	0.000	0.001	0.000	0.001	0.000	0.000
S	1.000	1.000	1.000	1.000	1.000	1.000	1.000	1.000	1.000	1.000
Total	**1.984**	**1.972**	**1.994**	**1.980**	**1.982**	**1.988**	**1.983**	**1.979**	**1.979**	**1.986**

Sample	10024(4)	10024(4)	10024(4)	10024(4)	10024(4)	10024(4)	10024(4)	10024(4)	10024(4)	10024(4)
No.	**#2.31**	**#2.32**	**#2.33**	**#2.36**	**#2.41**	**#2.42**	**#2.43**	**#2.45**	**#2.46**	**#2.48**
Fe	61.538	61.272	60.557	61.923	61.161	61.368	61.827	61.815	61.259	61.707
Cu	0.920	0.901	1.450	0.972	1.147	1.185	0.855	0.742	1.081	1.165
Mn	0.146	0.091	0.145	0.123	0.134	0.135	0.142	0.092	0.087	0.091
Co	0.106	0.131	0.115	0.110	0.122	0.112	0.108	0.112	0.112	0.114
Ni	0.067	0.069	0.085	0.033	0.062	0.071	0.058	0.094	0.068	0.046
Zn	0.036	< 0.031	< 0.031	0.036	0.058	0.064	< 0.032	0.055	0.065	0.084
Cd	0.061	0.055	< 0.031	0.044	0.054	< 0.031	< 0.032	< 0.031	<0	0.057
Sb	< 0.023	0.034	0.033	0.028	< 0.024	< 0.024	< 0.023	0.032	< 0.024	0.028
Pb	0.085	0.249	0.170	0.063	0.249	0.097	0.110	0.105	0.085	0.064
S	36.742	36.598	36.513	37.038	36.692	36.938	37.036	36.857	36.999	37.026
Total	**99.732**	**99.400**	**99.095**	**100.370**	**99.759**	**100.010**	**100.165**	**99.904**	**99.756**	**100.407**
					Atom-%					
Fe	48.557	48.553	48.129	48.519	48.338	48.271	48.525	48.659	48.241	48.363
Cu	0.638	0.627	1.013	0.669	0.797	0.819	0.590	0.513	0.748	0.802
Mn	0.117	0.073	0.117	0.098	0.108	0.108	0.113	0.074	0.070	0.072
Co	0.079	0.098	0.087	0.082	0.091	0.083	0.080	0.084	0.084	0.085
Ni	0.050	0.052	0.064	0.025	0.047	0.053	0.043	0.070	0.051	0.034
Zn	0.024	0.000	0.000	0.024	0.039	0.043	0.000	0.037	0.044	0.056
Cd	0.024	0.022	0.000	0.017	0.021	0.000	0.000	0.000	0.000	0.022
Sb	0.000	0.012	0.012	0.010	0.000	0.000	0.000	0.012	0.000	0.010
Pb	0.018	0.053	0.036	0.013	0.053	0.021	0.023	0.022	0.018	0.014
S	50.492	50.509	50.541	50.543	50.506	50.602	50.625	50.529	50.745	50.541
Total	**100.000**	**100.000**	**100.000**	**100.000**	**100.000**	**100.000**	**100.000**	**100.000**	**100.000**	**100.000**
					Normalised to 1 S atom					
Fe	0.962	0.961	0.952	0.960	0.957	0.954	0.959	0.963	0.951	0.957
Cu	0.013	0.012	0.020	0.013	0.016	0.016	0.012	0.010	0.015	0.016
Mn	0.002	0.001	0.002	0.002	0.002	0.002	0.002	0.001	0.001	0.001
Co	0.002	0.002	0.002	0.002	0.002	0.002	0.002	0.002	0.002	0.002
Ni	0.001	0.001	0.001	0.000	0.001	0.001	0.001	0.001	0.001	0.001
Zn	0.000	0.000	0.000	0.000	0.001	0.001	0.000	0.001	0.001	0.001
Cd	0.000	0.000	0.000	0.000	0.000	0.000	0.000	0.000	0.000	0.000
Sb	0.000	0.000	0.000	0.000	0.000	0.000	0.000	0.000	0.000	0.000
Pb	0.000	0.001	0.001	0.000	0.001	0.000	0.000	0.000	0.000	0.000
S	1.000	1.000	1.000	1.000	1.000	1.000	1.000	1.000	1.000	1.000
Total	**1.981**	**1.980**	**1.979**	**1.979**	**1.980**	**1.976**	**1.975**	**1.979**	**1.971**	**1.979**

Sample	10024(4)	10024(4)	10024(4)	10024(5)	10-1B	10-1B	10-1B	10-1B	10-1B	10-1B
No.	**#2.49**	**#2.60**	**#2.61**	**#1.203**	**#27**	**#29**	**#30**	**#33**	**#45**	**#57**
Fe	61.144	60.746	60.940	60.924	60.660	60.509	60.306	60.344	60.578	61.100
Cu	1.127	1.359	1.101	1.042	1.487	1.773	1.881	1.713	1.669	1.245
Mn	0.067	0.044	0.051	< 0.008	0.046	0.039	0.035	0.040	0.036	0.037
Co	0.110	0.109	0.120	< 0	0.115	0.128	0.127	0.120	0.126	0.122
Ni	0.061	0.087	0.070	< 0.016	0.104	0.081	0.089	0.082	0.125	0.117
Zn	0.091	< 0	< 0.03	< 0.033	0.051	0.037	0.029	0.054	< 0.025	0.032
Cd	< 0.031	< 0.032	< 0.031	< 0.028	< 0.037	< 0.038	0.046	< 0.038	0.050	< 0.036
Sb	< 0.024	< 0.021	0.039	< 0	0.026	0.019	0.027	< 0.019	0.025	< 0.019
Pb	0.124	0.235	0.140	0.120	0.148	0.129	0.115	0.114	0.130	0.139
S	37.068	36.634	36.961	36.614	36.596	36.664	36.743	36.841	36.516	36.423
Total	**99.792**	**99.214**	**99.422**	**98.742**	**99.251**	**99.406**	**99.415**	**99.335**	**99.255**	**99.215**
					Atom-%					
Fe	48.132	48.197	48.148	48.491	48.123	47.934	47.755	47.770	48.082	48.508
Cu	0.780	0.948	0.764	0.729	1.037	1.234	1.309	1.192	1.164	0.869
Mn	0.054	0.035	0.041	0.000	0.037	0.031	0.028	0.032	0.029	0.030
Co	0.082	0.082	0.090	0.000	0.086	0.096	0.095	0.090	0.095	0.092
Ni	0.046	0.066	0.053	0.000	0.079	0.061	0.067	0.062	0.094	0.088
Zn	0.061	0.000	0.000	0.000	0.035	0.025	0.020	0.036	0.000	0.022
Cd	0.000	0.000	0.000	0.000	0.000	0.000	0.018	0.000	0.020	0.000
Sb	0.000	0.000	0.014	0.000	0.009	0.007	0.010	0.000	0.009	0.000
Pb	0.026	0.050	0.030	0.026	0.032	0.028	0.025	0.024	0.028	0.030
S	50.820	50.622	50.860	50.754	50.563	50.584	50.674	50.793	50.479	50.362
Total	**100.000**	**100.000**	**100.000**	**100.000**	**100.000**	**100.000**	**100.000**	**100.000**	**100.000**	**100.000**
					Normalised to 1 S atom					
Fe	0.947	0.952	0.947	0.955	0.952	0.948	0.942	0.940	0.953	0.963
Cu	0.015	0.019	0.015	0.014	0.021	0.024	0.026	0.023	0.023	0.017
Mn	0.001	0.001	0.001	0.000	0.001	0.001	0.001	0.001	0.001	0.001
Co	0.002	0.002	0.002	0.000	0.002	0.002	0.002	0.002	0.002	0.002
Ni	0.001	0.001	0.001	0.000	0.002	0.001	0.001	0.001	0.002	0.002
Zn	0.001	0.000	0.000	0.000	0.001	0.000	0.000	0.001	0.000	0.000
Cd	0.000	0.000	0.000	0.000	0.000	0.000	0.000	0.000	0.000	0.000
Sb	0.000	0.000	0.000	0.000	0.000	0.000	0.000	0.000	0.000	0.000
Pb	0.001	0.001	0.001	0.001	0.001	0.001	0.000	0.000	0.001	0.001
S	1.000	1.000	1.000	1.000	1.000	1.000	1.000	1.000	1.000	1.000
Total	**1.968**	**1.975**	**1.966**	**1.970**	**1.978**	**1.977**	**1.973**	**1.969**	**1.981**	**1.986**

Sample	10-1B	10-1B	10-1B	10-1B
No.	**#58**	**#73**	**#77**	**#82**
Fe	60.958	60.771	60.306	60.423
Cu	1.291	1.328	1.666	1.307
Mn	0.039	0.037	0.051	0.026
Co	0.126	0.125	0.115	0.137
Ni	0.056	0.100	0.089	0.151
Zn	0.055	< 0.025	0.139	0.064
Cd	< 0.038	0.041	0.040	< 0.04
Sb	< 0.017	0.024	< 0.018	< 0.019
Pb	0.094	0.102	0.129	0.186
S	36.352	36.409	36.273	36.333
Total	**98.995**	**98.955**	**98.858**	**98.627**
		Atom-%		
Fe	48.499	48.362	48.105	48.240
Cu	0.903	0.929	1.168	0.917
Mn	0.032	0.030	0.041	0.021
Co	0.095	0.094	0.087	0.104
Ni	0.042	0.076	0.068	0.115
Zn	0.037	0.000	0.095	0.044
Cd	0.000	0.016	0.016	0.000
Sb	0.000	0.009	0.000	0.000
Pb	0.020	0.022	0.028	0.040
S	50.372	50.463	50.393	50.520
Total	**100.000**	**100.000**	**100.000**	**100.000**
		Normalised to 1 S atom		
Fe	0.963	0.958	0.955	0.955
Cu	0.018	0.018	0.023	0.018
Mn	0.001	0.001	0.001	0.000
Co	0.002	0.002	0.002	0.002
Ni	0.001	0.002	0.001	0.002
Zn	0.001	0.000	0.002	0.001
Cd	0.000	0.000	0.000	0.000
Sb	0.000	0.000	0.000	0.000
Pb	0.000	0.000	0.001	0.001
S	1.000	1.000	1.000	1.000
Total	**1.985**	**1.982**	**1.984**	**1.979**

Table iv.84.: EMP analyses of pyrrhotite from matte s.s.

Sample	**13030(1)**	**13030(1)**	**13030(1)**	**13030(1)**	**13030(1)**
Position	**Rim**	**Rim**	**Rim**	**Rim**	**Rim**
No.	**#84**	**#85**	**#86**	**#87**	**#88**
Zn	59.865	61.792	61.135	63.136	64.090
Fe	4.938	3.859	4.028	2.183	1.067
Cu	< 0	< 0	< 0	< 0	< 0
Pb	0.082	0.080	0.086	0.077	0.092
Mn	0.134	0.097	0.185	0.016	0.018
Co	< 0	< 0	< 0	< 0	< 0
Ni	< 0	< 0	< 0	< 0	< 0
Ag	0.022	0.018	< 0	< 0	< 0
Cd	0.232	0.186	0.234	0.183	0.256
Sb	0.025	0.030	0.048	0.048	0.032
S	33.311	33.587	33.534	33.375	33.050
Total	**98.609**	**99.649**	**99.250**	**99.018**	**98.605**
			Atom-%		
Zn	44.693	45.737	45.397	47.134	48.197
Fe	4.318	3.346	3.503	1.909	0.940
Cu	0.000	0.000	0.000	0.000	0.000
Pb	0.019	0.019	0.020	0.018	0.022
Mn	0.119	0.085	0.164	0.014	0.016
Co	0.000	0.000	0.000	0.000	0.000
Ni	0.000	0.000	0.000	0.000	0.000
Ag	0.010	0.008	0.000	0.000	0.000
Cd	0.101	0.080	0.101	0.079	0.112
Sb	0.010	0.012	0.019	0.019	0.013
S	50.730	50.713	50.796	50.826	50.700
Total	**100.000**	**100.000**	**100.000**	**100.000**	**100.000**
			Normalised to 1 S atom		
Zn	0.881	0.902	0.894	0.927	0.951
Fe	0.085	0.066	0.069	0.038	0.019
Cu	0.000	0.000	0.000	0.000	0.000
Pb	0.000	0.000	0.000	0.000	0.000
Mn	0.002	0.002	0.003	0.000	0.000
Co	0.000	0.000	0.000	0.000	0.000
Ni	0.000	0.000	0.000	0.000	0.000
Ag	0.000	0.000	0.000	0.000	0.000
Cd	0.002	0.002	0.002	0.002	0.002
Sb	0.000	0.000	0.000	0.000	0.000
S	1.000	1.000	1.000	1.000	1.000
Total	**1.971**	**1.972**	**1.969**	**1.967**	**1.972**
ZnS	91.19	93.18	92.84	96.11	98.09
CuS	0.00	0.00	0.00	0.00	0.00
FeS	8.81	6.82	7.16	3.89	1.91
Total	**100.00**	**100.00**	**100.00**	**100.00**	**100.00**

Table iv.85.: EMP analyses of (Zn,Fe)S from smelting residue.

Sample	13030(1)	13030(1)	13030(1)	13030(1)	13030(1)	13030(1)
Position	**Core**	**Core**	**Core**	**Core**	**Core**	**Core**
No.	**#99**	**#100**	**#101**	**#104**	**#105**	**#106**
Zn	59.514	58.763	59.727	59.431	56.689	52.611
Fe	4.820	5.161	5.361	4.827	7.389	10.729
Cu	0.172	0.067	0.090	0.156	0.064	0.125
Pb	0.133	0.150	0.123	0.142	0.132	0.099
Mn	0.174	0.156	0.178	0.178	0.187	0.202
Co	< 0	< 0	< 0	< 0	0.022	0.021
Ni	< 0	< 0	< 0	< 0	< 0	< 0
Ag	< 0	0.021	< 0	0.033	0.027	< 0
Cd	0.160	0.203	0.174	0.148	0.184	0.231
Sb	0.049	0.034	0.027	0.047	0.033	0.031
S	33.103	33.375	33.388	33.263	33.310	33.542
Total	**98.125**	**97.930**	**99.068**	**98.225**	**98.037**	**97.591**
			Atom-%			
Zn	44.670	44.070	44.383	44.522	42.372	39.211
Fe	4.237	4.533	4.666	4.235	6.469	9.366
Cu	0.133	0.052	0.069	0.120	0.049	0.096
Pb	0.032	0.036	0.029	0.034	0.031	0.023
Mn	0.155	0.139	0.157	0.159	0.166	0.179
Co	0.000	0.000	0.000	0.000	0.018	0.017
Ni	0.000	0.000	0.000	0.000	0.000	0.000
Ag	0.000	0.010	0.000	0.015	0.012	0.000
Cd	0.070	0.089	0.075	0.065	0.080	0.100
Sb	0.020	0.014	0.011	0.019	0.013	0.012
S	50.684	51.058	50.610	50.831	50.788	50.995
Total	**100.000**	**100.000**	**100.000**	**100.000**	**100.000**	**100.000**
			Normalised to 1 S atom			
Zn	0.881	0.863	0.877	0.876	0.834	0.769
Fe	0.084	0.089	0.092	0.083	0.127	0.184
Cu	0.003	0.001	0.001	0.002	0.001	0.002
Pb	0.001	0.001	0.001	0.001	0.001	0.000
Mn	0.003	0.003	0.003	0.003	0.003	0.004
Co	0.000	0.000	0.000	0.000	0.000	0.000
Ni	0.000	0.000	0.000	0.000	0.000	0.000
Ag	0.000	0.000	0.000	0.000	0.000	0.000
Cd	0.001	0.002	0.001	0.001	0.002	0.002
Sb	0.000	0.000	0.000	0.000	0.000	0.000
S	1.000	1.000	1.000	1.000	1.000	1.000
Total	**1.973**	**1.959**	**1.976**	**1.967**	**1.969**	**1.961**
ZnS	91.09	90.58	90.36	91.09	86.67	80.56
CuS	0.27	0.11	0.14	0.25	0.10	0.20
FeS	8.64	9.32	9.50	8.67	13.23	19.24
Total	**100.00**	**100.00**	**100.00**	**100.00**	**100.00**	**100.00**

Table iv.86.: EMP analyses of (Zn,Fe)S from smelting residue.

Sample	10024(4)	10024(4)	12015(7)	12015(12)	12015(12)	13030(1)	13030(1)
No.	**#2.51**	**#2.69**	**#66**	**#84**	**#107**	**#76**	**#78**
Zn	27.865	26.196	31.174	63.512	64.134	56.231	53.724
Fe	31.965	28.765	31.538	3.234	2.134	7.229	9.544
Cu	1.415	7.378	0.220	0.127	0.352	< 0.022	0.036
Pb	2.499	1.123	0.937	0.128	0.112	0.121	0.108
Mn	0.162	0.135	0.182	0.077	0.038	0.189	0.167
Co	0.064	0.034	0.040	< 0	< 0	< 0.012	0.022
Ni	< 0	< 0	< 0	< 0.013	< 0.011	< 0.013	< 0
Ag	0.024	0.045	< 0.018	< 0.018	0.020	< 0.018	< 0.017
Cd	0.066	< 0	< 0.029	< 0.029	< 0.028	0.034	< 0.027
Sb	< 0.024	0.202	0.036	< 0.02	0.021	0.043	0.041
S	34.336	33.870	34.111	33.783	34.312	33.619	34.000
Total	**98.396**	**97.748**	**98.238**	**100.861**	**101.123**	**97.466**	**97.642**
				Atom-%			
Zn	20.205	19.085	22.509	46.537	46.782	42.094	39.921
Fe	27.148	24.545	26.671	2.775	1.823	6.338	8.307
Cu	1.056	5.533	0.164	0.096	0.264	0.000	0.028
Pb	0.572	0.258	0.214	0.030	0.026	0.029	0.025
Mn	0.140	0.117	0.156	0.067	0.033	0.168	0.148
Co	0.052	0.027	0.032	0.000	0.000	0.000	0.018
Ni	0.000	0.000	0.000	0.000	0.000	0.000	0.000
Ag	0.011	0.020	0.000	0.000	0.009	0.000	0.000
Cd	0.028	0.000	0.000	0.000	0.000	0.015	0.000
Sb	0.000	0.079	0.014	0.000	0.008	0.017	0.016
S	50.789	50.335	50.241	50.495	51.055	51.338	51.537
Total	**100.000**	**100.000**	**100.000**	**100.000**	**100.000**	**100.000**	**100.000**
				Normalised to 1 S atom			
Zn	0.398	0.379	0.448	0.922	0.916	0.820	0.775
Fe	0.535	0.488	0.531	0.055	0.036	0.123	0.161
Cu	0.021	0.110	0.003	0.002	0.005	0.000	0.001
Pb	0.011	0.005	0.004	0.001	0.001	0.001	0.000
Mn	0.003	0.002	0.003	0.001	0.001	0.003	0.003
Co	0.001	0.001	0.001	0.000	0.000	0.000	0.000
Ni	0.000	0.000	0.000	0.000	0.000	0.000	0.000
Ag	0.000	0.000	0.000	0.000	0.000	0.000	0.000
Cd	0.001	0.000	0.000	0.000	0.000	0.000	0.000
Sb	0.000	0.002	0.000	0.000	0.000	0.000	0.000
S	1.000	1.000	1.000	1.000	1.000	1.000	1.000
Total	**1.969**	**1.987**	**1.990**	**1.980**	**1.959**	**1.948**	**1.940**
ZnS	41.74	38.82	45.62	94.19	95.73	86.91	82.73
CuS	2.18	11.25	0.33	0.19	0.54	0.00	0.06
FeS	56.08	49.93	54.05	5.62	3.73	13.09	17.21
Total	**100.00**	**100.00**	**100.00**	**100.00**	**100.00**	**100.00**	**100.00**

Table iv.87.: EMP analyses of (Zn,Fe)S from droplets in slag.

Sample	12015(7)	12015(7)	12015(7)	12015(7)	12015(7)	12015(7)	10032(1)	10032(1)	10032(1)	10032(1)
No.	**#40**	**#56**	**#59**	**#67**	**#75**	**#81**	**#71**	**#73**	**#75**	**#76**
Zn	28.540	26.924	28.544	28.366	28.148	28.512	35.474	31.335	33.344	36.623
Fe	33.363	32.804	33.848	32.727	33.183	33.989	28.333	30.489	29.133	26.143
Cu	1.462	3.553	0.298	1.174	0.443	0.446	0.678	1.928	1.626	0.217
Pb	0.128	0.871	0.592	0.399	1.586	0.164	0.131	0.208	0.128	1.582
Mn	0.130	0.101	0.157	0.138	0.155	0.150	0.037	0.036	0.030	0.028
Co	0.055	0.049	0.060	0.057	0.055	0.065	0.054	0.055	0.061	0.029
Ni	< 0	< 0.013	< 0	< 0.014	< 0.01	< 0.013	< 0.013	< 0.013	< 0.013	< 0
Ag	< 0.017	< 0.018	< 0.019	< 0.015	< 0.018	0.020	0.025	< 0.017	0.020	0.031
Cd	< 0	< 0	< 0	< 0	< 0	< 0	0.038	< 0.048	< 0	< 0
Sb	< 0.021	< 0.018	< 0.019	< 0.021	< 0.019	< 0	< 0.019	0.021	0.020	< 0.020
S	34.536	34.250	34.753	34.673	34.638	34.762	34.856	34.904	35.156	34.307
Total	**98.214**	**98.552**	**98.252**	**97.534**	**98.208**	**98.108**	**99.626**	**98.976**	**99.518**	**98.960**
					Atom-%					
Zn	20.411	19.325	20.414	20.409	20.269	20.365	25.223	22.317	23.645	26.532
Fe	27.946	27.578	28.353	27.579	27.986	28.434	23.596	25.433	24.197	22.183
Cu	1.076	2.625	0.219	0.869	0.328	0.328	0.496	1.413	1.187	0.162
Pb	0.029	0.197	0.134	0.091	0.361	0.037	0.029	0.047	0.029	0.362
Mn	0.111	0.086	0.134	0.118	0.133	0.128	0.031	0.031	0.025	0.024
Co	0.044	0.039	0.048	0.046	0.044	0.052	0.043	0.043	0.048	0.023
Ni	0.000	0.000	0.000	0.000	0.000	0.000	0.000	0.000	0.000	0.000
Ag	0.000	0.000	0.000	0.000	0.000	0.009	0.011	0.000	0.009	0.014
Cd	0.000	0.000	0.000	0.000	0.000	0.000	0.016	0.000	0.000	0.000
Sb	0.000	0.000	0.000	0.000	0.000	0.000	0.000	0.008	0.008	0.000
S	50.383	50.148	50.700	50.888	50.879	50.648	50.556	50.708	50.854	50.700
Total	**100.000**	**100.000**	**100.000**	**100.000**	**100.000**	**100.000**	**100.000**	**100.000**	**100.000**	**100.000**
					Normalised to 1 S atom					
Zn	0.405	0.385	0.403	0.401	0.398	0.402	0.499	0.440	0.465	0.523
Fe	0.555	0.550	0.559	0.542	0.550	0.561	0.467	0.502	0.476	0.438
Cu	0.021	0.052	0.004	0.017	0.006	0.006	0.010	0.028	0.023	0.003
Pb	0.001	0.004	0.003	0.002	0.007	0.001	0.001	0.001	0.001	0.007
Mn	0.002	0.002	0.003	0.002	0.003	0.003	0.001	0.001	0.000	0.000
Co	0.001	0.001	0.001	0.001	0.001	0.001	0.001	0.001	0.001	0.000
Ni	0.000	0.000	0.000	0.000	0.000	0.000	0.000	0.000	0.000	0.000
Ag	0.000	0.000	0.000	0.000	0.000	0.000	0.000	0.000	0.000	0.000
Cd	0.000	0.000	0.000	0.000	0.000	0.000	0.000	0.000	0.000	0.000
Sb	0.000	0.000	0.000	0.000	0.000	0.000	0.000	0.000	0.000	0.000
S	1.000	1.000	1.000	1.000	1.000	1.000	1.000	1.000	1.000	1.000
Total	**1.985**	**1.994**	**1.972**	**1.965**	**1.965**	**1.974**	**1.978**	**1.972**	**1.966**	**1.972**
ZnS	41.29	39.02	41.67	41.77	41.72	41.45	51.15	45.39	48.23	54.28
CuS	2.18	5.30	0.45	1.78	0.68	0.67	1.01	2.87	2.42	0.33
FeS	56.53	55.68	57.88	56.45	57.60	57.88	47.85	51.73	49.35	45.39
Total	**100.00**	**100.00**	**100.00**	**100.00**	**100.00**	**100.00**	**100.00**	**100.00**	**100.00**	**100.00**

Sample	10032(1)	10032(1)	10032(1)	10032(1)	10032(1)	10032(1)	10032(1)	10032(1)	10032(1)
No.	**#80**	**#87**	**#90**	**#92**	**#94**	**#96**	**#98**	**#100**	**#102**
Zn	38.209	30.586	31.523	29.363	30.806	34.689	32.145	31.479	30.482
Fe	25.124	30.107	29.763	31.594	31.773	27.562	28.889	30.244	29.728
Cu	0.579	1.861	1.716	2.283	1.507	0.995	1.276	1.467	3.084
Pb	0.160	0.630	0.196	0.204	0.205	2.274	1.900	1.301	0.155
Mn	0.023	0.036	0.030	0.031	0.040	0.021	0.027	0.031	0.028
Co	0.046	0.051	0.054	0.060	0.058	0.051	0.062	0.073	0.065
Ni	< 0.013	< 0.013	< 0.014	0.019	< 0.012	< 0.013	< 0.013	< 0.013	< 0.012
Ag	0.025	< 0	0.024	< 0.014	< 0.017	0.030	0.023	0.019	< 0.018
Cd	< 0.027	< 0	< 0	< 0	< 0	< 0	< 0.029	< 0	< 0
Sb	< 0.020	< 0.020	< 0.020	0.037	0.020	< 0.019	< 0.022	< 0.020	0.028
S	34.796	34.888	34.850	34.958	35.211	33.877	34.540	34.704	34.991
Total	**98.962**	**98.159**	**98.156**	**98.549**	**99.620**	**99.499**	**98.862**	**99.318**	**98.561**
				Atom-%					
Zn	27.418	21.968	22.611	20.938	21.758	25.152	23.215	22.526	21.769
Fe	21.116	25.327	25.005	26.387	26.284	23.407	24.436	25.349	24.867
Cu	0.428	1.376	1.267	1.676	1.096	0.743	0.949	1.081	2.267
Pb	0.036	0.143	0.044	0.046	0.046	0.520	0.433	0.294	0.035
Mn	0.020	0.031	0.026	0.026	0.034	0.018	0.023	0.026	0.024
Co	0.037	0.041	0.043	0.047	0.045	0.041	0.050	0.058	0.052
Ni	0.000	0.000	0.000	0.015	0.000	0.000	0.000	0.000	0.000
Ag	0.011	0.000	0.010	0.000	0.000	0.013	0.010	0.008	0.000
Cd	0.000	0.000	0.000	0.000	0.000	0.000	0.000	0.000	0.000
Sb	0.000	0.000	0.000	0.014	0.008	0.000	0.000	0.000	0.011
S	50.934	51.115	50.993	50.850	50.730	50.106	50.884	50.658	50.976
Total	**100.000**	**100.000**	**100.000**	**100.000**	**100.000**	**100.000**	**100.000**	**100.000**	**100.000**
				Normalised to 1 S atom					
Zn	0.538	0.430	0.443	0.412	0.429	0.502	0.456	0.445	0.427
Fe	0.415	0.495	0.490	0.519	0.518	0.467	0.480	0.500	0.488
Cu	0.008	0.027	0.025	0.033	0.022	0.015	0.019	0.021	0.044
Pb	0.001	0.003	0.001	0.001	0.001	0.010	0.009	0.006	0.001
Mn	0.000	0.001	0.001	0.001	0.001	0.000	0.000	0.001	0.000
Co	0.001	0.001	0.001	0.001	0.001	0.001	0.001	0.001	0.001
Ni	0.000	0.000	0.000	0.000	0.000	0.000	0.000	0.000	0.000
Ag	0.000	0.000	0.000	0.000	0.000	0.000	0.000	0.000	0.000
Cd	0.000	0.000	0.000	0.000	0.000	0.000	0.000	0.000	0.000
Sb	0.000	0.000	0.000	0.000	0.000	0.000	0.000	0.000	0.000
S	1.000	1.000	1.000	1.000	1.000	1.000	1.000	1.000	1.000
Total	**1.963**	**1.956**	**1.961**	**1.967**	**1.971**	**1.996**	**1.965**	**1.974**	**1.962**
ZnS	56.00	45.14	46.26	42.73	44.28	51.02	47.77	46.01	44.52
CuS	0.87	2.83	2.59	3.42	2.23	1.51	1.95	2.21	4.64
FeS	43.13	52.04	51.15	53.85	53.49	47.48	50.28	51.78	50.85
Total	**100.00**	**100.00**	**100.00**	**100.00**	**100.00**	**100.00**	**100.00**	**100.00**	**100.00**

Table iv.88.: EMP analyses of (Zn,Fe)S from pyrrhotite-bearing interstitial sulphide cluster.

Sample	12015(12)	12015(12)	12015(12)	12015(12)	12015(12)	12015(12)	12015(12)	12015(12)
No.	**#85**	**#89**	**#92**	**#94**	**#100**	**#103**	**#107**	**#109**
Zn	64.015	63.099	62.511	62.030	61.758	57.963	64.134	62.591
Fe	3.058	3.323	4.034	4.129	4.496	6.622	2.134	3.843
Cu	0.170	0.052	0.182	0.176	0.122	0.775	0.352	0.265
Pb	0.222	0.131	0.120	0.096	1.799	2.333	0.112	0.145
Mn	0.048	0.064	0.054	0.062	0.089	0.073	0.038	0.053
Co	< 0.011	< 0.011	< 0.011	< 0.013	< 0.011	< 0.011	< 0	< 0.012
Ni	0.015	< 0.011	< 0.011	0.029	< 0	< 0.012	< 0.011	< 0.011
Ag	0.025	0.019	< 0.018	< 0.017	0.030	0.055	0.020	< 0.02
Cd	0.077	< 0.028	< 0.028	< 0.028	0.060	0.056	< 0.028	< 0
Sb	0.034	0.029	0.043	< 0.019	< 0.02	0.033	0.021	0.032
S	34.074	34.074	33.593	34.256	33.558	33.736	34.312	34.040
Total	**101.738**	**100.791**	**100.537**	**100.778**	**101.912**	**101.646**	**101.123**	**100.969**
				Atom-%				
Zn	46.556	46.160	45.939	45.257	45.300	42.544	46.782	45.711
Fe	2.605	2.847	3.472	3.528	3.863	5.693	1.823	3.287
Cu	0.127	0.039	0.138	0.132	0.092	0.586	0.264	0.199
Pb	0.051	0.030	0.028	0.022	0.417	0.541	0.026	0.033
Mn	0.042	0.056	0.047	0.054	0.078	0.064	0.033	0.046
Co	0.000	0.000	0.000	0.000	0.000	0.000	0.000	0.000
Ni	0.012	0.000	0.000	0.024	0.000	0.000	0.000	0.000
Ag	0.011	0.008	0.000	0.000	0.013	0.024	0.009	0.000
Cd	0.033	0.000	0.000	0.000	0.026	0.024	0.000	0.000
Sb	0.013	0.011	0.017	0.000	0.000	0.013	0.008	0.013
S	50.550	50.848	50.359	50.983	50.212	50.512	51.055	50.711
Total	**100.000**	**100.000**	**100.000**	**100.000**	**100.000**	**100.000**	**100.000**	**100.000**
				Normalised to 1 S atom				
Zn	0.921	0.908	0.912	0.888	0.902	0.842	0.916	0.901
Fe	0.052	0.056	0.069	0.069	0.077	0.113	0.036	0.065
Cu	0.003	0.001	0.003	0.003	0.002	0.012	0.005	0.004
Pb	0.001	0.001	0.001	0.000	0.008	0.011	0.001	0.001
Mn	0.001	0.001	0.001	0.001	0.002	0.001	0.001	0.001
Co	0.000	0.000	0.000	0.000	0.000	0.000	0.000	0.000
Ni	0.000	0.000	0.000	0.000	0.000	0.000	0.000	0.000
Ag	0.000	0.000	0.000	0.000	0.000	0.000	0.000	0.000
Cd	0.001	0.000	0.000	0.000	0.001	0.000	0.000	0.000
Sb	0.000	0.000	0.000	0.000	0.000	0.000	0.000	0.000
S	1.000	1.000	1.000	1.000	1.000	1.000	1.000	1.000
Total	**1.978**	**1.967**	**1.986**	**1.961**	**1.992**	**1.980**	**1.959**	**1.972**
ZnS	94.46	94.11	92.71	92.52	91.97	87.14	95.73	92.91
CuS	0.26	0.08	0.28	0.27	0.19	1.20	0.54	0.40
FeS	5.28	5.81	7.01	7.21	7.84	11.66	3.73	6.68
Total	**100.00**	**100.00**	**100.00**	**100.00**	**100.00**	**100.00**	**100.00**	**100.00**

Table iv.89.: EMP analyses of (Zn,Fe)S from pyrrhotite-free interstitial sulphide cluster.

Sample	10-2B	14032	11027(1)	11027(1)	11027(1)	11027(1)	11027(1)	11027(1)	11029(3)	11029(3)
No.	**#112**	**#23**	**#1.60**	**#1.61**	**#1.77**	**#2.55**	**#2.56**	**#2.58**	**#19**	**#22**
Zn	31.382	26.086	27.697	27.829	27.602	28.275	29.646	28.125	27.530	30.595
Fe	29.792	35.299	31.045	31.063	33.259	33.663	32.703	33.210	35.394	31.362
Cu	0.650	1.588	2.937	3.015	1.164	1.314	0.786	1.318	0.743	0.917
Pb	0.122	0.116	1.155	1.200	0.155	0.103	0.137	0.141	0.165	0.172
Mn	0.485	0.380	< 0.008	< 0.009	0.025	0.232	0.215	0.243	0.135	0.134
Co	0.065	0.070	< 0	< 0	< 0	0.100	0.100	0.096	0.115	0.095
Ni	< 0	< 0.011	< 0.015	< 0	< 0	< 0	0.017	< 0.015	0.030	< 0
Ag	< 0.025	< 0.017	< 0.018	< 0.014	< 0.019	0.025	0.024	< 0.017	< 0.017	0.028
Cd	0.039	< 0	0.044	0.039	0.055	< 0	< 0	< 0	< 0	< 0
Sb	< 0.020	< 0.019	< 0.019	< 0	< 0	< 0	< 0	< 0	< 0	< 0
S	33.848	34.964	34.365	34.280	35.238	34.398	35.159	35.097	34.942	35.179
Total	**96.383**	**98.503**	**97.243**	**97.426**	**97.498**	**98.110**	**98.787**	**98.230**	**99.054**	**98.482**
					Atom-%					
Zn	22.956	18.507	20.133	20.218	19.751	20.246	21.037	20.030	19.469	21.796
Fe	25.526	29.332	26.431	26.433	27.875	28.232	27.181	27.702	29.318	26.169
Cu	0.489	1.160	2.197	2.255	0.857	0.968	0.574	0.966	0.541	0.672
Pb	0.028	0.026	0.265	0.275	0.035	0.023	0.031	0.032	0.037	0.039
Mn	0.422	0.321	0.000	0.000	0.021	0.198	0.182	0.206	0.114	0.114
Co	0.053	0.055	0.000	0.000	0.000	0.079	0.079	0.076	0.090	0.075
Ni	0.000	0.000	0.000	0.000	0.000	0.000	0.013	0.000	0.024	0.000
Ag	0.000	0.000	0.000	0.000	0.000	0.011	0.010	0.000	0.000	0.012
Cd	0.017	0.000	0.019	0.016	0.023	0.000	0.000	0.000	0.000	0.000
Sb	0.000	0.000	0.000	0.000	0.000	0.000	0.000	0.000	0.000	0.000
S	50.508	50.600	50.955	50.803	51.437	50.243	50.893	50.988	50.408	51.123
Total	**100.000**	**100.000**	**100.000**	**100.000**	**100.000**	**100.000**	**100.000**	**100.000**	**100.000**	**100.000**
					Normalised to 1 S atom					
Zn	0.455	0.366	0.395	0.398	0.384	0.403	0.413	0.393	0.386	0.426
Fe	0.505	0.580	0.519	0.520	0.542	0.562	0.534	0.543	0.582	0.512
Cu	0.010	0.023	0.043	0.044	0.017	0.019	0.011	0.019	0.011	0.013
Pb	0.001	0.001	0.005	0.005	0.001	0.000	0.001	0.001	0.001	0.001
Mn	0.008	0.006	0.000	0.000	0.000	0.004	0.004	0.004	0.002	0.002
Co	0.001	0.001	0.000	0.000	0.000	0.002	0.002	0.001	0.002	0.001
Ni	0.000	0.000	0.000	0.000	0.000	0.000	0.000	0.000	0.000	0.000
Ag	0.000	0.000	0.000	0.000	0.000	0.000	0.000	0.000	0.000	0.000
Cd	0.000	0.000	0.000	0.000	0.000	0.000	0.000	0.000	0.000	0.000
Sb	0.000	0.000	0.000	0.000	0.000	0.000	0.000	0.000	0.000	0.000
S	1.000	1.000	1.000	1.000	1.000	1.000	1.000	1.000	1.000	1.000
Total	**1.980**	**1.976**	**1.963**	**1.968**	**1.944**	**1.990**	**1.965**	**1.961**	**1.984**	**1.956**
ZnS	46.88	37.77	41.29	41.34	40.74	40.95	43.12	41.13	39.47	44.81
CuS	1.00	2.37	4.51	4.61	1.77	1.96	1.18	1.98	1.10	1.38
FeS	52.12	59.86	54.21	54.05	57.49	57.10	55.71	56.89	59.43	53.80
Total	**100.00**	**100.00**	**100.00**	**100.00**	**100.00**	**100.00**	**100.00**	**100.00**	**100.00**	**100.00**

Sample	11029(3)	11029(3)	11029(5)	10024(4)	10024(4)	10024(4)	10024(4)	10-1B	10-1B	10-1B
No.	**#23**	**#24**	**#2.44**	**#1.67**	**#2.21**	**#2.24**	**#2.27**	**#31**	**#39**	**#40**
Zn	35.985	30.444	27.703	26.862	26.380	26.112	26.724	26.345	26.786	26.343
Fe	26.080	31.134	31.695	33.985	34.844	36.089	34.573	34.143	34.369	35.187
Cu	0.647	1.080	2.408	1.905	1.273	0.819	0.794	3.513	2.130	2.597
Pb	0.208	0.195	0.139	0.185	0.146	0.114	0.124	0.143	0.164	0.158
Mn	0.104	0.124	1.804	0.685	0.569	0.630	0.776	0.142	0.125	0.136
Co	0.075	0.081	0.044	0.073	0.071	0.061	0.068	0.067	0.057	0.078
Ni	< 0	0.019	0.095	< 0	< 0	< 0.017	0.029	< 0.01	< 0.013	< 0.013
Ag	< 0.019	0.019	0.021	< 0	< 0.022	0.027	< 0.015	< 0.024	< 0.024	< 0.025
Cd	< 0	< 0	< 0	< 0	< 0	< 0	< 0	0.076	0.068	0.060
Sb	< 0.020	< 0	< 0	< 0	< 0.022	< 0	0.026	< 0	< 0	< 0.016
S	34.203	35.005	34.333	34.285	35.086	35.146	35.066	34.515	35.491	34.789
Total	**97.302**	**98.101**	**99.054**	**97.980**	**98.369**	**98.998**	**98.180**	**98.944**	**99.190**	**99.348**
					Atom-%					
Zn	26.220	21.783	19.830	19.253	18.726	18.416	19.000	18.725	18.872	18.613
Fe	22.258	26.092	26.574	28.530	28.970	29.812	28.790	28.424	28.362	29.120
Cu	0.485	0.795	1.774	1.405	0.930	0.595	0.581	2.570	1.545	1.889
Pb	0.048	0.044	0.031	0.042	0.033	0.025	0.028	0.032	0.036	0.035
Mn	0.090	0.106	1.537	0.585	0.481	0.529	0.657	0.120	0.105	0.114
Co	0.061	0.064	0.035	0.058	0.056	0.048	0.054	0.053	0.045	0.061
Ni	0.000	0.015	0.076	0.000	0.000	0.000	0.023	0.000	0.000	0.000
Ag	0.000	0.008	0.009	0.000	0.000	0.012	0.000	0.000	0.000	0.000
Cd	0.000	0.000	0.000	0.000	0.000	0.000	0.000	0.031	0.028	0.025
Sb	0.000	0.000	0.000	0.000	0.000	0.000	0.010	0.000	0.000	0.000
S	50.838	51.092	50.133	50.127	50.805	50.564	50.857	50.044	51.008	50.142
Total	**100.000**	**100.000**	**100.000**	**100.000**	**100.000**	**100.000**	**100.000**	**100.000**	**100.000**	**100.000**
					Normalised to 1 S atom					
Zn	0.516	0.426	0.396	0.384	0.369	0.364	0.374	0.374	0.370	0.371
Fe	0.438	0.511	0.530	0.569	0.570	0.590	0.566	0.568	0.556	0.581
Cu	0.010	0.016	0.035	0.028	0.018	0.012	0.011	0.051	0.030	0.038
Pb	0.001	0.001	0.001	0.001	0.001	0.001	0.001	0.001	0.001	0.001
Mn	0.002	0.002	0.031	0.012	0.009	0.010	0.013	0.002	0.002	0.002
Co	0.001	0.001	0.001	0.001	0.001	0.001	0.001	0.001	0.001	0.001
Ni	0.000	0.000	0.002	0.000	0.000	0.000	0.000	0.000	0.000	0.000
Ag	0.000	0.000	0.000	0.000	0.000	0.000	0.000	0.000	0.000	0.000
Cd	0.000	0.000	0.000	0.000	0.000	0.000	0.000	0.001	0.001	0.000
Sb	0.000	0.000	0.000	0.000	0.000	0.000	0.000	0.000	0.000	0.000
S	1.000	1.000	1.000	1.000	1.000	1.000	1.000	1.000	1.000	1.000
Total	**1.967**	**1.957**	**1.995**	**1.995**	**1.968**	**1.978**	**1.966**	**1.998**	**1.960**	**1.994**
ZnS	53.55	44.76	41.16	39.14	38.51	37.72	39.28	37.66	38.69	37.51
CuS	0.99	1.63	3.68	2.86	1.91	1.22	1.20	5.17	3.17	3.81
FeS	45.46	53.61	55.16	58.00	59.58	61.06	59.52	57.17	58.14	58.68
Total	**100.00**	**100.00**	**100.00**	**100.00**	**100.00**	**100.00**	**100.00**	**100.00**	**100.00**	**100.00**

Sample	10-1B	10-1B	10-1B	10-1B	10-1B	10-1B	10-1B	10-1B	10-1B
No.	**#44**	**#49**	**#52**	**#56**	**#62**	**#65**	**#74**	**#75**	**#78**
Zn	25.664	28.911	33.869	26.460	26.155	26.514	26.117	25.776	26.296
Fe	34.660	33.235	29.193	34.074	35.577	34.835	35.339	34.694	35.778
Cu	3.398	1.724	1.112	3.244	2.101	2.307	2.383	3.224	2.065
Pb	0.355	0.126	0.117	0.127	0.149	0.149	0.165	0.171	0.091
Mn	0.129	0.130	0.112	0.136	0.140	0.134	0.142	0.130	0.132
Co	0.081	0.077	0.065	0.075	0.072	0.078	0.078	0.084	0.074
Ni	< 0	< 0.013	< 0.012	0.015	0.016	< 0.011	< 0.013	< 0	< 0.019
Ag	< 0.027	0.026	< 0.024	< 0	0.030	< 0.022	< 0.027	< 0.024	< 0.024
Cd	0.061	0.061	0.059	0.057	0.053	0.054	0.054	0.060	0.060
Sb	< 0.020	< 0.019	< 0.019	< 0.021	< 0	< 0.019	< 0.020	< 0.020	< 0
S	33.310	34.342	34.328	34.386	34.555	34.237	34.460	34.131	34.216
Total	**97.658**	**98.632**	**98.855**	**98.574**	**98.848**	**98.308**	**98.738**	**98.270**	**98.712**
				Atom-%					
Zn	18.584	20.651	24.277	18.875	18.571	18.958	18.576	18.452	18.726
Fe	29.397	27.805	24.509	28.469	29.587	29.174	29.440	29.090	29.841
Cu	2.533	1.268	0.820	2.382	1.536	1.698	1.745	2.376	1.514
Pb	0.081	0.028	0.026	0.029	0.033	0.034	0.037	0.039	0.020
Mn	0.111	0.111	0.096	0.116	0.118	0.114	0.120	0.111	0.112
Co	0.065	0.061	0.052	0.059	0.057	0.062	0.062	0.067	0.058
Ni	0.000	0.000	0.000	0.012	0.013	0.000	0.000	0.000	0.000
Ag	0.000	0.011	0.000	0.000	0.013	0.000	0.000	0.000	0.000
Cd	0.026	0.025	0.025	0.024	0.022	0.022	0.022	0.025	0.025
Sb	0.000	0.000	0.000	0.000	0.000	0.000	0.000	0.000	0.000
S	49.204	50.039	50.194	50.036	50.050	49.938	49.998	49.841	49.703
Total	**100.000**	**100.000**	**100.000**	**100.000**	**100.000**	**100.000**	**100.000**	**100.000**	**100.000**
				Normalised to 1 S atom					
Zn	0.378	0.413	0.484	0.377	0.371	0.380	0.372	0.370	0.377
Fe	0.597	0.556	0.488	0.569	0.591	0.584	0.589	0.584	0.600
Cu	0.051	0.025	0.016	0.048	0.031	0.034	0.035	0.048	0.030
Pb	0.002	0.001	0.001	0.001	0.001	0.001	0.001	0.001	0.000
Mn	0.002	0.002	0.002	0.002	0.002	0.002	0.002	0.002	0.002
Co	0.001	0.001	0.001	0.001	0.001	0.001	0.001	0.001	0.001
Ni	0.000	0.000	0.000	0.000	0.000	0.000	0.000	0.000	0.000
Ag	0.000	0.000	0.000	0.000	0.000	0.000	0.000	0.000	0.000
Cd	0.001	0.001	0.000	0.000	0.000	0.000	0.000	0.001	0.001
Sb	0.000	0.000	0.000	0.000	0.000	0.000	0.000	0.000	0.000
S	1.000	1.000	1.000	1.000	1.000	1.000	1.000	1.000	1.000
Total	**2.032**	**1.998**	**1.992**	**1.999**	**1.998**	**2.002**	**2.000**	**2.006**	**2.012**
ZnS	36.79	41.53	48.94	37.96	37.37	38.05	37.33	36.97	37.39
CuS	5.01	2.55	1.65	4.79	3.09	3.41	3.51	4.76	3.02
FeS	58.20	55.92	49.41	57.25	59.54	58.55	59.16	58.28	59.59
Total	**100.00**	**100.00**	**100.00**	**100.00**	**100.00**	**100.00**	**100.00**	**100.00**	**100.00**

Table iv.90.: EMP analyses of (Zn,Fe)S from matte s.s.

Sample	13030(1)	13030(1)	13030(1)	13030(1)	13030(1)	13030(1)	13030(1)	13030(1)	13030(1)
Position	Rim	Rim	Rim	Rim	Core	Core	Core	Core	Core
No.	#89	#90	#91	#92	#94	#95	#96	#97	#98
Pb	86.547	86.355	86.999	86.667	86.734	86.178	85.137	85.767	85.919
Cu	0.341	0.425	0.551	0.546	0.417	0.408	1.174	0.405	0.283
Fe	0.129	0.053	0.069	0.188	0.111	0.079	0.318	0.059	0.025
Mn	< 0.015	0.024	0.019	0.033	0.033	0.037	0.026	0.022	0.029
Zn	0.543	0.243	1.129	0.795	0.359	0.259	0.052	0.161	0.247
As	< 0	< 0	< 0	< 0	< 0	< 0	< 0	< 0	< 0
Ag	< 0	< 0	< 0	< 0	< 0	< 0	< 0	< 0	< 0
Cd	0.076	0.042	0.073	0.094	0.044	0.083	0.060	0.071	0.067
Sb	0.059	0.047	0.066	0.049	0.057	0.053	0.061	0.068	0.062
S	13.612	13.645	13.695	13.695	13.439	13.588	13.799	13.642	13.470
Total	**101.307**	**100.834**	**102.601**	**102.067**	**101.194**	**100.685**	**100.627**	**100.195**	**100.102**
				Atom-%					
Pb	48.606	48.753	47.949	48.004	49.061	48.741	47.354	48.649	49.069
Cu	0.624	0.782	0.990	0.986	0.769	0.752	2.129	0.749	0.527
Fe	0.269	0.111	0.141	0.386	0.233	0.166	0.656	0.124	0.053
Mn	0.000	0.051	0.039	0.069	0.070	0.079	0.055	0.047	0.062
Zn	0.966	0.435	1.971	1.395	0.643	0.464	0.092	0.289	0.447
As	0.000	0.000	0.000	0.000	0.000	0.000	0.000	0.000	0.000
Ag	0.000	0.000	0.000	0.000	0.000	0.000	0.000	0.000	0.000
Cd	0.079	0.044	0.074	0.096	0.046	0.087	0.062	0.074	0.071
Sb	0.056	0.045	0.062	0.046	0.055	0.051	0.058	0.066	0.060
S	49.399	49.779	48.773	49.017	49.122	49.660	49.595	50.002	49.710
Total	**100.000**	**100.000**	**100.000**	**100.000**	**100.000**	**100.000**	**100.000**	**100.000**	**100.000**
				Normalised to 1 S atom					
Pb	0.984	0.979	0.983	0.979	0.999	0.981	0.955	0.973	0.987
Cu	0.013	0.016	0.020	0.020	0.016	0.015	0.043	0.015	0.011
Fe	0.005	0.002	0.003	0.008	0.005	0.003	0.013	0.002	0.001
Mn	0.000	0.001	0.001	0.001	0.001	0.002	0.001	0.001	0.001
Zn	0.020	0.009	0.040	0.028	0.013	0.009	0.002	0.006	0.009
As	0.000	0.000	0.000	0.000	0.000	0.000	0.000	0.000	0.000
Ag	0.000	0.000	0.000	0.000	0.000	0.000	0.000	0.000	0.000
Cd	0.002	0.001	0.002	0.002	0.001	0.002	0.001	0.001	0.001
Sb	0.001	0.001	0.001	0.001	0.001	0.001	0.001	0.001	0.001
S	1.000	1.000	1.000	1.000	1.000	1.000	1.000	1.000	1.000
Total	**2.024**	**2.009**	**2.050**	**2.040**	**2.036**	**2.014**	**2.016**	**2.000**	**2.012**

Sample	10-2B	10-2B	10-2B	12015(5)	12015(5)	12015(5)	12015(5)	12015(5)	12015(5)	12015(5)
No.	**#124**	**#125**	**#126**	**#20**	**#21**	**#22**	**#24**	**#26**	**#27**	**#29**
Pb	85.602	84.742	86.298	87.951	88.100	88.495	87.757	87.997	88.195	88.046
Cu	0.820	0.548	0.808	0.540	0.444	0.542	0.952	0.721	0.938	0.400
Fe	1.092	0.815	0.987	1.270	1.332	1.281	0.855	0.794	0.801	0.956
Mn	0.061	0.069	0.066	0.050	0.043	0.050	0.043	0.035	0.035	0.046
Zn	0.620	0.497	0.554	0.267	0.378	0.443	0.204	0.242	0.132	0.285
As	0.015	0.032	0.030	< 0.015	0.020	< 0.014	< 0.015	< 0.016	< 0.014	< 0.014
Ag	< 0	< 0	< 0.035	< 0	< 0	0.060	< 0	< 0	< 0	< 0
Cd	0.100	0.118	0.179	0.038	0.063	0.066	0.067	0.038	0.085	0.076
Sb	0.047	0.033	0.050	0.052	0.047	0.043	0.052	0.045	< 0.027	0.063
S	13.435	13.461	13.618	13.551	13.714	13.596	13.489	13.653	13.749	13.716
Total	**101.792**	**100.315**	**102.590**	**103.719**	**104.141**	**104.576**	**103.419**	**103.525**	**103.935**	**103.588**
					Normalised to 100 %					
Pb	84.095	84.476	84.119	84.797	84.597	84.623	84.856	85.001	84.856	84.996
Cu	0.806	0.546	0.788	0.521	0.426	0.518	0.921	0.696	0.902	0.386
Fe	1.073	0.812	0.962	1.224	1.279	1.225	0.827	0.767	0.771	0.923
Mn	0.060	0.069	0.064	0.048	0.041	0.048	0.042	0.034	0.034	0.044
Zn	0.609	0.495	0.540	0.257	0.363	0.424	0.197	0.234	0.127	0.275
As	0.015	0.032	0.029	-	0.019	-	-	-	-	-
Ag	-	-	-	-	-	0.057	-	-	-	-
Cd	0.098	0.118	0.174	0.037	0.060	0.063	0.065	0.037	0.082	0.073
Sb	0.046	0.033	0.049	0.050	0.045	0.041	0.050	0.043	-	0.061
S	13.198	13.419	13.274	13.065	13.169	13.001	13.043	13.188	13.228	13.241
Total	**100.000**	**100.000**	**100.000**	**100.000**	**100.000**	**100.000**	**100.000**	**100.000**	**100.000**	**100.000**
					Atom-%					
Pb	47.127	47.413	47.133	48.013	47.694	47.894	48.160	48.201	47.990	48.152
Cu	1.472	1.000	1.439	0.961	0.784	0.956	1.704	1.288	1.664	0.713
Fe	2.231	1.692	2.000	2.572	2.675	2.572	1.741	1.614	1.617	1.940
Mn	0.127	0.146	0.136	0.103	0.088	0.102	0.089	0.072	0.072	0.095
Zn	1.081	0.881	0.958	0.462	0.648	0.759	0.355	0.420	0.228	0.494
As	0.023	0.050	0.045	0.000	0.030	0.000	0.000	0.000	0.000	0.000
Ag	0.000	0.000	0.000	0.000	0.000	0.062	0.000	0.000	0.000	0.000
Cd	0.101	0.122	0.180	0.038	0.063	0.066	0.068	0.038	0.085	0.077
Sb	0.044	0.031	0.046	0.048	0.043	0.040	0.049	0.042	0.000	0.059
S	47.795	48.667	48.061	47.802	47.975	47.548	47.835	48.325	48.344	48.471
Total	**100.000**	**100.000**	**100.000**	**100.000**	**100.000**	**100.000**	**100.000**	**100.000**	**100.000**	**100.000**
					Normalised to 1 S atom					
Pb	0.986	0.974	0.981	1.004	0.994	1.007	1.007	0.997	0.993	0.993
Cu	0.031	0.021	0.030	0.020	0.016	0.020	0.036	0.027	0.034	0.015
Fe	0.047	0.035	0.042	0.054	0.056	0.054	0.036	0.033	0.033	0.040
Mn	0.003	0.003	0.003	0.002	0.002	0.002	0.002	0.001	0.001	0.002
Zn	0.023	0.018	0.020	0.010	0.014	0.016	0.007	0.009	0.005	0.010
As	0.000	0.001	0.001	0.000	0.001	0.000	0.000	0.000	0.000	0.000
Ag	0.000	0.000	0.000	0.000	0.000	0.001	0.000	0.000	0.000	0.000
Cd	0.002	0.003	0.004	0.001	0.001	0.001	0.001	0.001	0.002	0.002
Sb	0.001	0.001	0.001	0.001	0.001	0.001	0.001	0.001	0.000	0.001
S	1.000	1.000	1.000	1.000	1.000	1.000	1.000	1.000	1.000	1.000
Total	**2.092**	**2.055**	**2.081**	**2.092**	**2.084**	**2.103**	**2.091**	**2.069**	**2.069**	**2.063**

Sample	12015(5)	12015(5)	12015(5)	12015(5)	12015(5)	12015(12)	14032	11027(1)	11027(1)	11027(1)
No.	**#30**	**#31**	**#32**	**#33**	**#34**	**#105**	**#70**	**#1.79**	**#2.37**	**#2.40**
Pb	87.669	88.191	88.261	87.554	88.200	89.718	85.970	87.113	87.380	87.740
Cu	0.439	0.529	0.501	1.586	0.650	0.351	0.919	0.923	0.615	0.474
Fe	0.809	0.831	0.854	0.897	0.812	0.430	1.727	0.702	0.849	1.249
Mn	0.036	0.035	0.036	0.047	0.056	0.028	0.040	0.040	0.045	0.044
Zn	0.291	0.324	0.312	0.269	0.280	0.703	0.155	0.225	0.355	0.498
As	< 0.015	< 0.015	< 0	0.016	< 0.016	< 0	0.030	0.032	0.027	< 0.023
Ag	< 0	< 0	< 0	< 0	0.048	< 0	< 0	< 0	< 0	< 0
Cd	0.087	0.068	0.078	0.069	0.069	0.060	0.141	< 0	0.073	0.068
Sb	0.070	0.029	0.037	0.050	0.064	0.065	0.072	< 0.027	0.045	0.058
S	13.522	13.730	13.768	13.694	13.651	13.866	13.570	13.679	13.577	13.648
Total	**102.923**	**103.737**	**103.847**	**104.182**	**103.830**	**105.221**	**102.624**	**102.714**	**102.966**	**103.779**
					Normalised to 100 %					
Pb	85.179	85.014	84.991	84.039	84.947	85.266	83.772	84.811	84.863	84.545
Cu	0.427	0.510	0.482	1.522	0.626	0.334	0.896	0.899	0.597	0.457
Fe	0.786	0.801	0.822	0.861	0.782	0.409	1.683	0.683	0.825	1.204
Mn	0.035	0.034	0.035	0.045	0.054	0.027	0.039	0.039	0.044	0.042
Zn	0.283	0.312	0.300	0.258	0.270	0.668	0.151	0.219	0.345	0.480
As	-	-	-	0.015	-	-	0.029	0.031	0.026	-
Ag	-	-	-	-	0.046	-	-	-	-	-
Cd	0.085	0.066	0.075	0.066	0.066	0.057	0.137	-	0.071	0.066
Sb	0.068	0.028	0.036	0.048	0.062	0.062	0.070	-	0.044	0.056
S	13.138	13.235	13.258	13.144	13.147	13.178	13.223	13.318	13.186	13.151
Total	**100.000**	**100.000**	**100.000**	**100.000**	**100.000**	**100.000**	**100.000**	**100.000**	**100.000**	**100.000**
					Atom-%					
Pb	48.485	48.178	48.135	47.116	48.205	48.598	46.680	47.846	48.051	47.664
Cu	0.792	0.942	0.891	2.783	1.158	0.620	1.627	1.653	1.103	0.840
Fe	1.660	1.684	1.728	1.791	1.647	0.864	3.479	1.431	1.732	2.517
Mn	0.075	0.072	0.074	0.095	0.115	0.057	0.082	0.083	0.093	0.090
Zn	0.510	0.561	0.539	0.459	0.485	1.206	0.267	0.391	0.618	0.857
As	0.000	0.000	0.000	0.024	0.000	0.000	0.045	0.049	0.041	0.000
Ag	0.000	0.000	0.000	0.000	0.050	0.000	0.000	0.000	0.000	0.000
Cd	0.089	0.068	0.078	0.068	0.070	0.060	0.141	0.000	0.074	0.068
Sb	0.066	0.027	0.034	0.046	0.060	0.060	0.067	0.000	0.042	0.054
S	48.324	48.467	48.520	47.619	48.211	48.534	47.613	48.548	48.245	47.910
Total	**100.000**	**100.000**	**100.000**	**100.000**	**100.000**	**100.000**	**100.000**	**100.000**	**100.000**	**100.000**
					Normalised to 1 S atom					
Pb	1.003	0.994	0.992	0.989	1.000	1.001	0.980	0.986	0.996	0.995
Cu	0.016	0.019	0.018	0.058	0.024	0.013	0.034	0.034	0.023	0.018
Fe	0.034	0.035	0.036	0.038	0.034	0.018	0.073	0.029	0.036	0.053
Mn	0.002	0.001	0.002	0.002	0.002	0.001	0.002	0.002	0.002	0.002
Zn	0.011	0.012	0.011	0.010	0.010	0.025	0.006	0.008	0.013	0.018
As	0.000	0.000	0.000	0.001	0.000	0.000	0.001	0.001	0.001	0.000
Ag	0.000	0.000	0.000	0.000	0.001	0.000	0.000	0.000	0.000	0.000
Cd	0.002	0.001	0.002	0.001	0.001	0.001	0.003	0.000	0.002	0.001
Sb	0.001	0.001	0.001	0.001	0.001	0.001	0.001	0.000	0.001	0.001
S	1.000	1.000	1.000	1.000	1.000	1.000	1.000	1.000	1.000	1.000
Total	**2.069**	**2.063**	**2.061**	**2.100**	**2.074**	**2.060**	**2.100**	**2.060**	**2.073**	**2.087**

Sample	11027(2)	11027(2)	11027(2)	11029(4)	11029(4)	11029(4)	11029(5)	11029(5)	11029(5)	11029(5)
No.	**#2.12**	**#2.13**	**#2.14**	**#2.57**	**#2.58**	**#2.63**	**#1.11**	**#1.17**	**#2.53**	**#2.56**
Pb	87.630	87.668	85.580	86.722	86.701	86.951	87.504	86.507	87.313	88.484
Cu	1.146	0.696	1.592	0.983	0.592	0.924	0.872	1.440	0.956	0.206
Fe	0.757	0.532	0.717	1.249	1.698	1.442	0.139	1.048	1.423	1.764
Mn	0.032	0.030	< 0.015	0.040	0.034	0.039	0.040	0.096	0.127	0.183
Zn	0.337	0.218	0.351	0.052	0.037	0.331	< 0.032	0.146	0.164	0.092
As	< 0.018	0.022	< 0.013	0.120	0.077	0.083	0.044	0.074	< 0.023	< 0.015
Ag	< 0.024	0.029	0.033	< 0	< 0	< 0	< 0.023	0.176	< 0	< 0.025
Cd	0.053	0.056	0.056	0.064	0.077	< 0.034	0.071	0.108	0.058	0.060
Sb	0.099	0.082	0.063	< 0.027	0.029	0.078	< 0.027	< 0.027	0.056	0.042
S	13.708	13.364	13.648	13.876	13.824	13.896	13.535	13.727	13.675	13.712
Total	**103.762**	**102.697**	**102.040**	**103.806**	**103.785**	**104.279**	**102.224**	**103.322**	**103.772**	**104.543**
				Normalised to 100 %						
Pb	84.453	85.366	83.869	83.542	83.539	83.383	85.600	83.726	84.139	84.639
Cu	1.104	0.678	1.560	0.947	0.570	0.886	0.853	1.394	0.921	0.197
Fe	0.730	0.518	0.703	1.203	1.636	1.383	0.136	1.014	1.371	1.687
Mn	0.031	0.029	-	0.039	0.033	0.037	0.039	0.093	0.122	0.175
Zn	0.325	0.212	0.344	0.050	0.036	0.317	-	0.141	0.158	0.088
As	-	0.021	-	0.116	0.074	0.080	0.043	0.072	-	-
Ag	-	0.028	0.032	-	-	-	-	0.170	-	-
Cd	0.051	0.055	0.055	0.062	0.074	-	0.069	0.105	0.056	0.057
Sb	0.095	0.080	0.062	-	0.028	0.075	-	-	0.054	0.040
S	13.211	13.013	13.375	13.367	13.320	13.326	13.241	13.286	13.178	13.116
Total	**100.000**	**100.000**	**100.000**	**100.000**	**100.000**	**100.000**	**100.000**	**100.000**	**100.000**	**100.000**
				Atom-%						
Pb	47.571	48.859	46.763	46.571	46.573	46.349	48.941	46.670	47.126	47.708
Cu	2.029	1.265	2.836	1.721	1.037	1.606	1.590	2.533	1.682	0.362
Fe	1.525	1.100	1.454	2.489	3.384	2.852	0.288	2.098	2.850	3.529
Mn	0.066	0.063	0.000	0.081	0.069	0.078	0.084	0.195	0.259	0.372
Zn	0.580	0.385	0.608	0.088	0.063	0.559	0.000	0.250	0.280	0.157
As	0.000	0.034	0.000	0.178	0.114	0.122	0.068	0.110	0.000	0.000
Ag	0.000	0.031	0.035	0.000	0.000	0.000	0.000	0.182	0.000	0.000
Cd	0.053	0.058	0.056	0.063	0.076	0.000	0.073	0.107	0.058	0.060
Sb	0.091	0.078	0.059	0.000	0.027	0.071	0.000	0.000	0.051	0.039
S	48.086	48.128	48.190	48.152	47.985	47.865	48.917	47.854	47.694	47.773
Total	**100.000**	**100.000**	**100.000**	**100.000**	**100.000**	**100.000**	**100.000**	**100.000**	**100.000**	**100.000**
				Normalised to 1 S atom						
Pb	0.989	1.015	0.970	0.967	0.971	0.968	1.000	0.975	0.988	0.999
Cu	0.042	0.026	0.059	0.036	0.022	0.034	0.033	0.053	0.035	0.008
Fe	0.032	0.023	0.030	0.052	0.071	0.060	0.006	0.044	0.060	0.074
Mn	0.001	0.001	0.000	0.002	0.001	0.002	0.002	0.004	0.005	0.008
Zn	0.012	0.008	0.013	0.002	0.001	0.012	0.000	0.005	0.006	0.003
As	0.000	0.001	0.000	0.004	0.002	0.003	0.001	0.002	0.000	0.000
Ag	0.000	0.001	0.001	0.000	0.000	0.000	0.000	0.004	0.000	0.000
Cd	0.001	0.001	0.001	0.001	0.002	0.000	0.001	0.002	0.001	0.001
Sb	0.002	0.002	0.001	0.000	0.001	0.001	0.000	0.000	0.001	0.001
S	1.000	1.000	1.000	1.000	1.000	1.000	1.000	1.000	1.000	1.000
Total	**2.080**	**2.078**	**2.075**	**2.077**	**2.084**	**2.089**	**2.044**	**2.090**	**2.097**	**2.093**

Sample	11029(5)	11029(5)	11029(5)	10024(2)	10024(2)	10024(2)	10024(2)	10024(2)	10024(2)	10024(4)
No.	**#2.63**	**#2.64**	**#2.67**	**#101**	**#103**	**#106**	**#109**	**#112**	**#115**	**#2.52**
Pb	86.134	85.656	87.229	88.235	88.610	88.637	88.515	88.544	88.024	86.813
Cu	1.863	2.009	1.983	0.499	0.350	0.405	0.597	0.453	0.481	0.303
Fe	0.782	1.059	1.101	0.675	0.615	1.077	0.353	1.451	0.438	1.657
Mn	0.083	0.130	0.096	0.082	0.050	0.094	0.042	0.135	0.034	0.045
Zn	0.086	0.094	0.060	0.583	0.509	0.765	0.298	0.961	0.320	0.339
As	0.034	0.038	< 0	< 0	< 0	< 0	< 0	< 0	< 0	< 0.018
Ag	0.084	0.080	0.100	< 0	< 0	< 0	< 0	< 0	< 0	< 0
Cd	0.076	0.038	0.085	0.074	0.040	0.080	0.062	0.106	0.058	< 0.044
Sb	0.054	0.081	0.095	0.044	0.049	0.049	0.064	0.092	0.042	0.045
S	13.719	13.883	13.958	13.855	13.819	13.880	13.766	13.944	13.842	13.984
Total	**102.915**	**103.068**	**104.729**	**104.047**	**104.042**	**104.987**	**103.755**	**105.686**	**103.239**	**103.186**
				Normalised to 100 %						
Pb	83.694	83.106	83.290	84.803	85.168	84.427	85.312	83.780	85.262	84.133
Cu	1.810	1.949	1.893	0.480	0.336	0.386	0.575	0.429	0.466	0.294
Fe	0.760	1.027	1.051	0.649	0.591	1.026	0.340	1.373	0.424	1.606
Mn	0.081	0.126	0.092	0.079	0.048	0.090	0.040	0.128	0.033	0.044
Zn	0.084	0.091	0.057	0.560	0.489	0.729	0.287	0.909	0.310	0.329
As	0.033	0.037	-	-	-	-	-	-	-	-
Ag	0.082	0.078	0.095	-	-	-	-	-	-	-
Cd	0.074	0.037	0.081	0.071	0.038	0.076	0.060	0.100	0.056	-
Sb	0.052	0.079	0.091	0.042	0.047	0.047	0.062	0.087	0.041	0.044
S	13.330	13.470	13.328	13.316	13.282	13.221	13.268	13.194	13.408	13.552
Total	**100.000**	**100.000**	**100.000**	**100.000**	**100.000**	**100.000**	**100.000**	**100.000**	**100.000**	**100.000**
					Atom-%					
Pb	46.601	45.781	46.125	47.885	48.345	47.488	48.566	46.746	48.369	46.766
Cu	3.287	3.501	3.419	0.883	0.623	0.707	1.068	0.780	0.862	0.532
Fe	1.570	2.100	2.160	1.359	1.245	2.141	0.719	2.842	0.893	3.312
Mn	0.169	0.262	0.191	0.168	0.103	0.190	0.087	0.269	0.070	0.091
Zn	0.147	0.159	0.101	1.002	0.880	1.298	0.518	1.607	0.557	0.578
As	0.051	0.056	0.000	0.000	0.000	0.000	0.000	0.000	0.000	0.000
Ag	0.087	0.082	0.102	0.000	0.000	0.000	0.000	0.000	0.000	0.000
Cd	0.076	0.037	0.083	0.074	0.040	0.079	0.063	0.103	0.059	0.000
Sb	0.050	0.074	0.085	0.041	0.045	0.045	0.060	0.083	0.039	0.041
S	47.962	47.948	47.693	48.588	48.719	48.052	48.807	47.570	49.150	48.679
Total	**100.000**	**100.000**	**100.000**	**100.000**	**100.000**	**100.000**	**100.000**	**100.000**	**100.000**	**100.000**
					Normalised to 1 S atom					
Pb	0.972	0.955	0.967	0.986	0.992	0.988	0.995	0.983	0.984	0.961
Cu	0.069	0.073	0.072	0.018	0.013	0.015	0.022	0.016	0.018	0.011
Fe	0.033	0.044	0.045	0.028	0.026	0.045	0.015	0.060	0.018	0.068
Mn	0.004	0.005	0.004	0.003	0.002	0.004	0.002	0.006	0.001	0.002
Zn	0.003	0.003	0.002	0.021	0.018	0.027	0.011	0.034	0.011	0.012
As	0.001	0.001	0.000	0.000	0.000	0.000	0.000	0.000	0.000	0.000
Ag	0.002	0.002	0.002	0.000	0.000	0.000	0.000	0.000	0.000	0.000
Cd	0.002	0.001	0.002	0.002	0.001	0.002	0.001	0.002	0.001	0.000
Sb	0.001	0.002	0.002	0.001	0.001	0.001	0.001	0.002	0.001	0.001
S	1.000	1.000	1.000	1.000	1.000	1.000	1.000	1.000	1.000	1.000
Total	**2.085**	**2.086**	**2.097**	**2.058**	**2.053**	**2.081**	**2.049**	**2.102**	**2.035**	**2.054**

Sample	10024(4)	10024(4)	10032(4)	10032(4)	10032(4)	10032(4)	10032(4)	3(1)	3(1)	3(1)
No.	**#2.53**	**#2.67**	**#30**	**#34**	**#39**	**#43**	**#44**	**#37**	**#38**	**#39**
Pb	87.792	87.765	87.878	87.548	87.891	87.351	86.437	88.082	88.168	87.600
Cu	0.276	0.271	0.164	1.281	1.366	0.713	1.249	0.579	1.489	0.825
Fe	1.610	0.683	0.149	1.474	0.304	1.118	0.333	1.379	1.324	1.565
Mn	0.057	0.026	0.017	0.045	0.031	0.036	0.027	0.048	0.051	0.050
Zn	0.212	0.080	< 0.032	0.103	< 0.028	0.049	0.042	0.231	0.249	0.269
As	0.032	< 0	< 0.014	0.028	< 0	0.094	< 0	0.023	< 0	0.027
Ag	< 0	< 0	< 0	0.073	< 0	< 0	< 0	0.030	0.127	0.032
Cd	0.062	0.078	0.079	0.070	0.038	< 0.034	0.064	0.144	0.086	0.060
Sb	0.051	< 0.035	0.054	0.068	0.072	0.083	0.064	0.069	0.070	0.065
S	13.873	13.656	13.482	13.865	13.632	13.644	13.127	13.783	14.129	13.826
Total	**103.965**	**102.559**	**101.823**	**104.555**	**103.334**	**103.109**	**101.343**	**104.368**	**105.693**	**104.319**
				Normalised to 100 %						
Pb	84.444	85.575	86.305	83.734	85.055	84.717	85.292	84.396	83.419	83.973
Cu	0.265	0.264	0.161	1.225	1.322	0.692	1.232	0.555	1.409	0.791
Fe	1.549	0.666	0.146	1.410	0.294	1.084	0.329	1.321	1.253	1.500
Mn	0.055	0.025	0.017	0.043	0.030	0.035	0.027	0.046	0.048	0.048
Zn	0.204	0.078	-	0.099	-	0.048	0.041	0.221	0.236	0.258
As	0.031	-	-	0.027	-	0.091	-	0.022	-	0.026
Ag	-	-	-	0.070	-	-	-	0.029	0.120	0.031
Cd	0.060	0.076	0.078	0.067	0.037	-	0.063	0.138	0.081	0.058
Sb	0.049	-	0.053	0.065	0.070	0.080	0.063	0.066	0.066	0.062
S	13.344	13.315	13.241	13.261	13.192	13.233	12.953	13.206	13.368	13.254
Total	**100.000**	**100.000**	**100.000**	**100.000**	**100.000**	**100.000**	**100.000**	**100.000**	**100.000**	**100.000**
				Atom-%						
Pb	47.331	48.780	49.821	46.631	48.326	47.797	48.826	47.466	46.225	46.886
Cu	0.485	0.491	0.303	2.225	2.449	1.272	2.300	1.017	2.545	1.440
Fe	3.220	1.408	0.313	2.913	0.620	2.270	0.698	2.757	2.575	3.108
Mn	0.116	0.055	0.036	0.090	0.064	0.074	0.058	0.098	0.101	0.101
Zn	0.362	0.141	0.000	0.174	0.000	0.085	0.075	0.394	0.414	0.456
As	0.048	0.000	0.000	0.041	0.000	0.142	0.000	0.034	0.000	0.040
Ag	0.000	0.000	0.000	0.075	0.000	0.000	0.000	0.031	0.128	0.033
Cd	0.062	0.080	0.083	0.069	0.039	0.000	0.067	0.143	0.083	0.059
Sb	0.047	0.000	0.052	0.062	0.067	0.077	0.062	0.063	0.062	0.059
S	48.330	49.046	49.391	47.721	48.435	48.242	47.915	47.996	47.867	47.818
Total	**100.000**	**100.000**	**100.000**	**100.000**	**100.000**	**100.000**	**100.000**	**100.000**	**100.000**	**100.000**
				Normalised to 1 S atom						
Pb	0.979	0.995	1.009	0.977	0.998	0.991	1.019	0.989	0.966	0.981
Cu	0.010	0.010	0.006	0.047	0.051	0.026	0.048	0.021	0.053	0.030
Fe	0.067	0.029	0.006	0.061	0.013	0.047	0.015	0.057	0.054	0.065
Mn	0.002	0.001	0.001	0.002	0.001	0.002	0.001	0.002	0.002	0.002
Zn	0.007	0.003	0.000	0.004	0.000	0.002	0.002	0.008	0.009	0.010
As	0.001	0.000	0.000	0.001	0.000	0.003	0.000	0.001	0.000	0.001
Ag	0.000	0.000	0.000	0.002	0.000	0.000	0.000	0.001	0.003	0.001
Cd	0.001	0.002	0.002	0.001	0.001	0.000	0.001	0.003	0.002	0.001
Sb	0.001	0.000	0.001	0.001	0.001	0.002	0.001	0.001	0.001	0.001
S	1.000	1.000	1.000	1.000	1.000	1.000	1.000	1.000	1.000	1.000
Total	**2.069**	**2.039**	**2.025**	**2.096**	**2.065**	**2.073**	**2.087**	**2.084**	**2.089**	**2.091**

Sample	3(1)	3(1)	3(1)	3(1)	3(1)	3(1)	3(1)	3(1)	3(1)	3(1)
No.	**#41**	**#42**	**#43**	**#45**	**#46**	**#47**	**#48**	**#49**	**#50**	**#51**
Pb	86.872	86.985	87.838	87.642	87.430	87.496	87.944	88.046	86.882	87.149
Cu	1.300	1.183	0.548	0.673	0.960	1.266	1.008	0.915	1.107	0.936
Fe	1.198	1.420	1.649	1.916	1.784	1.418	1.278	1.926	1.432	1.465
Mn	0.059	0.051	0.063	0.076	0.068	0.055	0.059	0.062	0.064	0.052
Zn	0.218	0.231	0.275	0.226	0.269	0.224	0.236	0.244	0.230	0.251
As	< 0	< 0	< 0	< 0.023	< 0.017	< 0	< 0.016	< 0	< 0	< 0
Ag	0.220	0.510	0.108	0.157	0.350	0.129	0.091	0.084	0.115	0.532
Cd	0.073	0.077	0.087	0.087	0.094	0.081	0.093	0.064	0.047	0.067
Sb	0.066	0.064	0.047	0.073	0.062	0.093	0.085	0.082	0.071	0.057
S	13.980	14.052	13.848	13.894	13.958	13.907	13.799	13.955	13.961	13.972
Total	**103.986**	**104.573**	**104.463**	**104.744**	**104.975**	**104.669**	**104.593**	**105.378**	**103.909**	**104.481**
					Normalised to 100 %					
Pb	83.542	83.181	84.085	83.673	83.286	83.593	84.082	83.553	83.614	83.411
Cu	1.250	1.131	0.525	0.643	0.915	1.210	0.964	0.868	1.065	0.896
Fe	1.152	1.358	1.579	1.829	1.699	1.355	1.222	1.828	1.378	1.402
Mn	0.057	0.049	0.060	0.073	0.065	0.053	0.056	0.059	0.062	0.050
Zn	0.210	0.221	0.263	0.216	0.256	0.214	0.226	0.232	0.221	0.240
As	-	-	-	-	-	-	-	-	-	-
Ag	0.212	0.488	0.103	0.150	0.333	0.123	0.087	0.080	0.111	0.509
Cd	0.070	0.074	0.083	0.083	0.090	0.077	0.089	0.061	0.045	0.064
Sb	0.063	0.061	0.045	0.070	0.059	0.089	0.081	0.078	0.068	0.055
S	13.444	13.438	13.256	13.265	13.296	13.287	13.193	13.243	13.436	13.373
Total	**100.000**	**100.000**	**100.000**	**100.000**	**100.000**	**100.000**	**100.000**	**100.000**	**100.000**	**100.000**
					Atom-%					
Pb	46.338	46.007	47.027	46.540	46.153	46.485	47.129	46.395	46.358	46.318
Cu	2.261	2.040	0.957	1.165	1.652	2.193	1.761	1.572	1.926	1.622
Fe	2.371	2.787	3.276	3.775	3.494	2.795	2.541	3.765	2.835	2.889
Mn	0.119	0.102	0.127	0.152	0.135	0.110	0.119	0.123	0.129	0.104
Zn	0.368	0.387	0.466	0.380	0.450	0.377	0.401	0.407	0.389	0.423
As	0.000	0.000	0.000	0.000	0.000	0.000	0.000	0.000	0.000	0.000
Ag	0.225	0.518	0.111	0.160	0.355	0.132	0.094	0.085	0.118	0.543
Cd	0.072	0.075	0.086	0.085	0.091	0.079	0.092	0.062	0.046	0.066
Sb	0.060	0.058	0.043	0.066	0.056	0.084	0.078	0.074	0.064	0.052
S	48.186	48.026	47.908	47.676	47.613	47.744	47.785	47.517	48.136	47.984
Total	**100.000**	**100.000**	**100.000**	**100.000**	**100.000**	**100.000**	**100.000**	**100.000**	**100.000**	**100.000**
					Normalised to 1 S atom					
Pb	0.962	0.958	0.982	0.976	0.969	0.974	0.986	0.976	0.963	0.965
Cu	0.047	0.042	0.020	0.024	0.035	0.046	0.037	0.033	0.040	0.034
Fe	0.049	0.058	0.068	0.079	0.073	0.059	0.053	0.079	0.059	0.060
Mn	0.002	0.002	0.003	0.003	0.003	0.002	0.002	0.003	0.003	0.002
Zn	0.008	0.008	0.010	0.008	0.009	0.008	0.008	0.009	0.008	0.009
As	0.000	0.000	0.000	0.000	0.000	0.000	0.000	0.000	0.000	0.000
Ag	0.005	0.011	0.002	0.003	0.007	0.003	0.002	0.002	0.002	0.011
Cd	0.001	0.002	0.002	0.002	0.002	0.002	0.002	0.001	0.001	0.001
Sb	0.001	0.001	0.001	0.001	0.001	0.002	0.002	0.002	0.001	0.001
S	1.000	1.000	1.000	1.000	1.000	1.000	1.000	1.000	1.000	1.000
Total	**2.075**	**2.082**	**2.087**	**2.097**	**2.100**	**2.094**	**2.093**	**2.105**	**2.077**	**2.084**

Sample	3(1)	3(1)	3(1)	3(2)	3(2)	3(2)	3(2)	3(2)	12016(1)	12016(1)
No.	**#52**	**#53**	**#54**	**#66**	**#67**	**#68**	**#69**	**#72**	**#53**	**#54**
Pb	88.261	86.737	86.899	88.767	88.219	86.602	86.525	87.947	86.378	86.358
Cu	0.433	1.436	1.461	< 0.027	0.042	< 0	< 0.027	0.028	0.973	0.381
Fe	2.039	0.400	0.705	0.351	0.287	0.343	0.573	1.013	0.543	1.053
Mn	0.072	0.027	0.030	0.028	0.025	0.018	0.034	0.018	0.049	0.091
Zn	0.232	0.065	0.089	0.128	0.105	0.139	0.187	0.210	0.603	0.883
As	< 0	< 0	< 0	< 0.014	< 0	< 0	< 0	< 0	0.019	0.020
Ag	0.083	0.188	0.245	< 0	< 0	< 0	< 0	< 0	< 0	< 0
Cd	0.094	0.060	< 0.035	0.042	0.058	0.062	0.058	< 0.033	0.081	0.278
Sb	0.087	0.046	0.058	0.057	0.044	0.046	0.034	< 0.027	0.050	0.071
S	13.942	13.940	13.920	13.782	13.597	13.371	13.351	13.477	13.613	13.685
Total	**105.243**	**102.899**	**103.407**	**103.155**	**102.377**	**100.581**	**100.762**	**102.693**	**102.335**	**102.820**
				Normalised to 100 %						
Pb	83.864	84.293	84.036	86.052	86.171	86.102	85.871	85.641	84.407	83.989
Cu	0.411	1.396	1.413	-	0.041	-	-	0.027	0.951	0.371
Fe	1.937	0.389	0.682	0.340	0.280	0.341	0.569	0.986	0.531	1.024
Mn	0.068	0.026	0.029	0.027	0.024	0.018	0.034	0.018	0.048	0.089
Zn	0.220	0.063	0.086	0.124	0.103	0.138	0.186	0.204	0.589	0.859
As	-	-	-	-	-	-	-	-	0.019	0.019
Ag	0.079	0.183	0.237	-	-	-	-	-	-	-
Cd	0.089	0.058	-	0.041	0.057	0.062	0.058	-	0.079	0.270
Sb	0.083	0.045	0.056	0.055	0.043	0.046	0.034	-	0.049	0.069
S	13.247	13.547	13.461	13.360	13.281	13.294	13.250	13.124	13.302	13.310
Total	**100.000**	**100.000**	**100.000**	**100.000**	**100.000**	**100.000**	**100.000**	**100.000**	**100.000**	**100.000**
					Atom-%					
Pb	46.744	47.181	46.924	49.366	49.591	49.493	49.215	48.964	47.459	46.993
Cu	0.748	2.547	2.572	0.000	0.077	0.000	0.000	0.051	1.743	0.676
Fe	4.007	0.807	1.412	0.724	0.599	0.727	1.209	2.093	1.107	2.126
Mn	0.144	0.055	0.061	0.059	0.053	0.039	0.073	0.038	0.102	0.187
Zn	0.389	0.112	0.152	0.225	0.187	0.252	0.337	0.370	1.050	1.522
As	0.000	0.000	0.000	0.000	0.000	0.000	0.000	0.000	0.029	0.030
Ag	0.084	0.196	0.254	0.000	0.000	0.000	0.000	0.000	0.000	0.000
Cd	0.092	0.060	0.000	0.043	0.060	0.065	0.061	0.000	0.082	0.279
Sb	0.078	0.043	0.053	0.054	0.042	0.045	0.033	0.000	0.047	0.066
S	47.714	48.998	48.571	49.528	49.391	49.379	49.072	48.485	48.332	48.121
Total	**100.000**	**100.000**	**100.000**	**100.000**	**100.000**	**100.000**	**100.000**	**100.000**	**100.000**	**100.000**
					Normalised to 1 S atom					
Pb	0.980	0.963	0.966	0.997	1.004	1.002	1.003	1.010	0.982	0.977
Cu	0.016	0.052	0.053	0.000	0.002	0.000	0.000	0.001	0.036	0.014
Fe	0.084	0.016	0.029	0.015	0.012	0.015	0.025	0.043	0.023	0.044
Mn	0.003	0.001	0.001	0.001	0.001	0.001	0.001	0.001	0.002	0.004
Zn	0.008	0.002	0.003	0.005	0.004	0.005	0.007	0.008	0.022	0.032
As	0.000	0.000	0.000	0.000	0.000	0.000	0.000	0.000	0.001	0.001
Ag	0.002	0.004	0.005	0.000	0.000	0.000	0.000	0.000	0.000	0.000
Cd	0.002	0.001	0.000	0.001	0.001	0.001	0.001	0.000	0.002	0.006
Sb	0.002	0.001	0.001	0.001	0.001	0.001	0.001	0.000	0.001	0.001
S	1.000	1.000	1.000	1.000	1.000	1.000	1.000	1.000	1.000	1.000
Total	**2.096**	**2.041**	**2.059**	**2.019**	**2.025**	**2.025**	**2.038**	**2.063**	**2.069**	**2.078**

Sample	12016(1)	12016(1)	12016(1)	12016(1)	12016(1)	12016(1)	12016(1)	12016(1)	12016(1)	12016(1)
No.	**#56**	**#57**	**#59**	**#61**	**#62**	**#64**	**#66**	**#67**	**#68**	**#69**
Pb	86.929	87.722	86.838	87.104	86.752	87.146	85.660	86.533	86.451	86.931
Cu	0.640	0.411	0.851	0.661	0.616	0.496	0.839	0.527	0.794	0.760
Fe	0.698	1.110	1.178	0.870	0.953	0.977	0.534	0.579	0.783	1.042
Mn	0.049	0.075	0.075	0.053	0.062	0.062	0.040	0.052	0.060	0.055
Zn	0.642	1.182	0.858	1.005	0.969	1.320	0.761	0.766	0.796	0.888
As	0.102	< 0.015	0.016	0.028	0.026	0.019	0.027	< 0.015	< 0.015	0.022
Ag	< 0.033	< 0	< 0	< 0.033	< 0	< 0	< 0	< 0	< 0	< 0
Cd	0.090	0.085	0.098	0.095	0.117	0.121	0.112	0.087	0.117	0.135
Sb	0.040	0.051	0.044	0.036	0.042	0.066	0.047	0.051	0.037	0.056
S	13.770	13.795	13.653	13.769	13.687	13.796	13.599	13.632	13.706	13.739
Total	**103.114**	**104.431**	**103.611**	**103.621**	**103.224**	**104.003**	**101.619**	**102.227**	**102.744**	**103.628**
					Normalised to 100 %					
Pb	84.304	84.000	83.812	84.060	84.042	83.792	84.295	84.648	84.142	83.888
Cu	0.621	0.394	0.821	0.638	0.597	0.477	0.826	0.516	0.773	0.733
Fe	0.677	1.063	1.137	0.840	0.923	0.939	0.525	0.566	0.762	1.006
Mn	0.048	0.072	0.072	0.051	0.060	0.060	0.039	0.051	0.058	0.053
Zn	0.623	1.132	0.828	0.970	0.939	1.269	0.749	0.749	0.775	0.857
As	0.099	-	0.015	0.027	0.025	0.018	0.027	-	-	0.021
Ag	-	-	-	-	-	-	-	-	-	-
Cd	0.087	0.081	0.095	0.092	0.113	0.116	0.110	0.085	0.114	0.130
Sb	0.039	0.049	0.042	0.035	0.041	0.063	0.046	0.050	0.036	0.054
S	13.354	13.210	13.177	13.288	13.260	13.265	13.382	13.335	13.340	13.258
Total	**100.000**	**100.000**	**100.000**	**100.000**	**100.000**	**100.000**	**100.000**	**100.000**	**100.000**	**100.000**
					Atom-%					
Pb	47.279	47.013	46.811	47.043	47.045	46.767	47.280	47.714	47.103	46.868
Cu	1.135	0.718	1.496	1.164	1.089	0.868	1.510	0.947	1.411	1.336
Fe	1.409	2.207	2.356	1.743	1.917	1.945	1.094	1.185	1.583	2.084
Mn	0.101	0.152	0.152	0.108	0.127	0.125	0.083	0.108	0.123	0.112
Zn	1.106	2.007	1.465	1.719	1.665	2.244	1.331	1.338	1.374	1.517
As	0.153	0.000	0.024	0.042	0.039	0.028	0.041	0.000	0.000	0.033
Ag	0.000	0.000	0.000	0.000	0.000	0.000	0.000	0.000	0.000	0.000
Cd	0.090	0.084	0.097	0.095	0.117	0.120	0.114	0.088	0.118	0.134
Sb	0.037	0.047	0.040	0.033	0.039	0.060	0.044	0.048	0.034	0.051
S	48.395	47.773	47.558	48.053	47.962	47.842	48.503	48.572	48.255	47.865
Total	**100.000**	**100.000**	**100.000**	**100.000**	**100.000**	**100.000**	**100.000**	**100.000**	**100.000**	**100.000**
					Normalised to 1 S atom					
Pb	0.977	0.984	0.984	0.979	0.981	0.978	0.975	0.982	0.976	0.979
Cu	0.023	0.015	0.031	0.024	0.023	0.018	0.031	0.020	0.029	0.028
Fe	0.029	0.046	0.050	0.036	0.040	0.041	0.023	0.024	0.033	0.044
Mn	0.002	0.003	0.003	0.002	0.003	0.003	0.002	0.002	0.003	0.002
Zn	0.023	0.042	0.031	0.036	0.035	0.047	0.027	0.028	0.028	0.032
As	0.003	0.000	0.001	0.001	0.001	0.001	0.001	0.000	0.000	0.001
Ag	0.000	0.000	0.000	0.000	0.000	0.000	0.000	0.000	0.000	0.000
Cd	0.002	0.002	0.002	0.002	0.002	0.003	0.002	0.002	0.002	0.003
Sb	0.001	0.001	0.001	0.001	0.001	0.001	0.001	0.001	0.001	0.001
S	1.000	1.000	1.000	1.000	1.000	1.000	1.000	1.000	1.000	1.000
Total	**2.066**	**2.093**	**2.103**	**2.081**	**2.085**	**2.090**	**2.062**	**2.059**	**2.072**	**2.089**

Sample	12016(1)	12016(2)	13030(1)	13030(1)	13030(1)	13030(1)	13031(1)	13031(1)
No.	**#70**	**#46**	**#74**	**#75**	**#77**	**#81**	**#64**	**#66**
Pb	84.902	87.561	87.115	86.428	86.974	86.405	88.032	88.525
Cu	2.077	0.353	0.557	0.743	0.440	0.815	0.910	0.696
Fe	0.424	0.674	0.280	0.337	0.352	0.368	< 0	< 0
Mn	0.034	0.023	0.034	0.027	0.021	0.033	0.016	0.016
Zn	0.463	0.141	0.293	0.355	0.698	0.151	< 0.031	< 0.033
As	< 0.011	< 0.014	< 0	< 0	< 0	< 0	< 0.015	< 0
Ag	0.077	< 0	0.036	0.307	< 0.024	0.053	< 0	< 0.025
Cd	0.070	0.150	0.054	0.126	0.047	0.042	0.037	0.053
Sb	0.047	0.077	0.082	0.060	0.060	0.035	0.053	0.034
S	13.520	13.759	13.744	13.858	13.720	13.661	13.838	13.913
Total	**101.614**	**102.850**	**102.195**	**102.241**	**102.312**	**101.563**	**102.886**	**103.237**
				Normalised to 100 %				
Pb	83.553	85.135	85.244	84.534	85.009	85.075	85.563	85.749
Cu	2.044	0.343	0.545	0.727	0.430	0.802	0.884	0.674
Fe	0.417	0.655	0.274	0.330	0.344	0.362	-	-
Mn	0.033	0.022	0.033	0.026	0.021	0.032	0.016	0.015
Zn	0.456	0.137	0.287	0.347	0.682	0.149	-	-
As	-	-	-	-	-	-	-	-
Ag	0.076	-	0.035	0.300	-	0.052	-	-
Cd	0.069	0.146	0.053	0.123	0.046	0.041	0.036	0.051
Sb	0.046	0.075	0.080	0.059	0.059	0.034	0.052	0.033
S	13.305	13.378	13.449	13.554	13.410	13.451	13.450	13.477
Total	**100.000**	**100.000**	**100.000**	**100.000**	**100.000**	**100.000**	**100.000**	**100.000**
				Atom-%				
Pb	46.505	48.254	48.358	47.540	48.092	48.124	48.734	48.932
Cu	3.710	0.634	1.008	1.333	0.793	1.480	1.643	1.254
Fe	0.862	1.378	0.577	0.688	0.722	0.760	0.000	0.000
Mn	0.070	0.048	0.071	0.056	0.044	0.069	0.033	0.033
Zn	0.803	0.246	0.515	0.619	1.223	0.266	0.000	0.000
As	0.000	0.000	0.000	0.000	0.000	0.000	0.000	0.000
Ag	0.081	0.000	0.038	0.324	0.000	0.057	0.000	0.000
Cd	0.071	0.152	0.055	0.128	0.048	0.043	0.038	0.054
Sb	0.044	0.072	0.077	0.056	0.056	0.033	0.050	0.032
S	47.854	48.997	49.300	49.257	49.022	49.166	49.502	49.694
Total	**100.000**	**100.000**	**100.000**	**100.000**	**100.000**	**100.000**	**100.000**	**100.000**
				Normalised to 1 S atom				
Pb	0.972	0.985	0.981	0.965	0.981	0.979	0.984	0.985
Cu	0.078	0.013	0.020	0.027	0.016	0.030	0.033	0.025
Fe	0.018	0.028	0.012	0.014	0.015	0.015	0.000	0.000
Mn	0.001	0.001	0.001	0.001	0.001	0.001	0.001	0.001
Zn	0.017	0.005	0.010	0.013	0.025	0.005	0.000	0.000
As	0.000	0.000	0.000	0.000	0.000	0.000	0.000	0.000
Ag	0.002	0.000	0.001	0.007	0.000	0.001	0.000	0.000
Cd	0.001	0.003	0.001	0.003	0.001	0.001	0.001	0.001
Sb	0.001	0.001	0.002	0.001	0.001	0.001	0.001	0.001
S	1.000	1.000	1.000	1.000	1.000	1.000	1.000	1.000
Total	**2.090**	**2.041**	**2.028**	**2.030**	**2.040**	**2.034**	**2.020**	**2.012**

Table iv.91.: EMP analyses of galena droplets from slag.

Sample	12015(7)	12015(7)	12015(7)	12015(7)	12015(7)	12015(7)	12015(7)	12015(7)	12015(7)	12015(7)
No.	**#39**	**#47**	**#49**	**#51**	**#53**	**#55**	**#62**	**#70**	**#72**	**#74**
Pb	89.031	87.201	87.940	87.645	87.576	88.037	88.569	88.739	86.024	88.817
Cu	0.217	0.564	0.395	0.269	0.361	0.262	0.458	0.220	0.732	0.149
Fe	1.608	0.110	0.380	0.041	0.375	0.334	1.988	1.648	1.876	1.448
Mn	0.032	0.025	0.021	0.027	0.029	0.018	0.033	0.024	0.055	0.044
Zn	0.506	0.209	0.504	0.072	0.165	0.088	0.333	0.592	0.198	0.540
As	0.016	< 0	0.015	< 0.015	0.025	0.034	< 0.014	0.016	0.026	0.018
Ag	0.049	< 0	< 0	< 0	< 0	< 0	< 0	< 0	< 0.023	< 0
Cd	< 0.034	0.054	0.065	< 0.034	0.048	0.043	0.055	0.037	0.089	< 0.035
Sb	0.065	0.048	0.067	0.045	0.044	0.043	0.085	0.065	0.061	0.055
S	13.801	13.623	13.537	13.766	13.742	13.710	13.912	13.838	13.947	13.907
Total	**105.325**	**101.834**	**102.924**	**101.865**	**102.365**	**102.569**	**105.433**	**105.179**	**103.008**	**104.978**
					Normalised to 100 %					
Pb	84.530	85.631	85.442	86.040	85.553	85.832	84.005	84.370	83.512	84.605
Cu	0.206	0.554	0.384	0.264	0.353	0.255	0.434	0.209	0.711	0.142
Fe	1.527	0.108	0.369	0.040	0.366	0.326	1.886	1.567	1.821	1.379
Mn	0.030	0.025	0.020	0.027	0.028	0.018	0.031	0.023	0.053	0.042
Zn	0.480	0.205	0.490	0.071	0.161	0.086	0.316	0.563	0.192	0.514
As	0.015	-	0.015	-	0.024	0.033	-	0.015	0.025	0.017
Ag	0.047	-	-	-	-	-	-	-	-	-
Cd	-	0.053	0.063	-	0.047	0.042	0.052	0.035	0.086	-
Sb	0.062	0.047	0.065	0.044	0.043	0.042	0.081	0.062	0.059	0.052
S	13.103	13.378	13.152	13.514	13.425	13.367	13.195	13.157	13.540	13.248
Total	**100.000**	**100.000**	**100.000**	**100.000**	**100.000**	**100.000**	**100.000**	**100.000**	**100.000**	**100.000**
					Atom-%					
Pb	47.646	48.875	48.838	49.229	48.705	49.096	46.921	47.409	46.084	47.608
Cu	0.379	1.031	0.715	0.493	0.655	0.476	0.791	0.383	1.279	0.260
Fe	3.193	0.229	0.783	0.085	0.774	0.691	3.908	3.267	3.729	2.880
Mn	0.065	0.053	0.044	0.057	0.061	0.038	0.066	0.048	0.111	0.089
Zn	0.858	0.371	0.887	0.128	0.291	0.155	0.559	1.002	0.336	0.917
As	0.024	0.000	0.023	0.000	0.038	0.052	0.000	0.024	0.039	0.027
Ag	0.050	0.000	0.000	0.000	0.000	0.000	0.000	0.000	0.000	0.000
Cd	0.000	0.056	0.067	0.000	0.049	0.044	0.054	0.036	0.088	0.000
Sb	0.059	0.046	0.063	0.043	0.042	0.041	0.077	0.059	0.056	0.050
S	47.726	49.340	48.580	49.964	49.385	49.406	47.625	47.772	48.280	48.170
Total	**100.000**	**100.000**	**100.000**	**100.000**	**100.000**	**100.000**	**100.000**	**100.000**	**100.000**	**100.000**
					Normalised to 1 S atom					
Pb	0.998	0.991	1.005	0.985	0.986	0.994	0.985	0.992	0.955	0.988
Cu	0.008	0.021	0.015	0.010	0.013	0.010	0.017	0.008	0.026	0.005
Fe	0.067	0.005	0.016	0.002	0.016	0.014	0.082	0.068	0.077	0.060
Mn	0.001	0.001	0.001	0.001	0.001	0.001	0.001	0.001	0.002	0.002
Zn	0.018	0.008	0.018	0.003	0.006	0.003	0.012	0.021	0.007	0.019
As	0.000	0.000	0.000	0.000	0.001	0.001	0.000	0.000	0.001	0.001
Ag	0.001	0.000	0.000	0.000	0.000	0.000	0.000	0.000	0.000	0.000
Cd	0.000	0.001	0.001	0.000	0.001	0.001	0.001	0.001	0.002	0.000
Sb	0.001	0.001	0.001	0.001	0.001	0.001	0.002	0.001	0.001	0.001
S	1.000	1.000	1.000	1.000	1.000	1.000	1.000	1.000	1.000	1.000
Total	**2.095**	**2.027**	**2.058**	**2.001**	**2.025**	**2.024**	**2.100**	**2.093**	**2.071**	**2.076**

Sample	12015(7)	12015(7)	12015(7)	10-6	10032(1)	10032(1)	10032(1)	10032(1)	10032(1)	10032(1)
No.	**#78**	**#80**	**#82**	**#16**	**#72**	**#74**	**#77**	**#78**	**#81**	**#84**
Pb	88.088	88.234	88.194	83.656	88.243	88.321	88.022	87.921	88.482	88.610
Cu	0.209	0.215	0.220	0.146	0.091	0.116	0.334	0.190	0.067	0.088
Fe	1.699	1.499	1.610	1.931	1.523	1.271	1.070	1.188	1.832	0.789
Mn	0.018	0.034	0.040	0.016	< 0.015	0.016	< 0.015	0.023	0.030	0.023
Zn	0.205	0.242	0.697	0.260	0.611	0.563	0.353	0.941	0.706	0.715
As	0.021	0.016	< 0.015	0.024	< 0.015	< 0.014	0.029	< 0.014	< 0	0.015
Ag	< 0	< 0	< 0.025	< 0.035	0.029	0.034	< 0.025	0.129	< 0.024	0.033
Cd	0.036	< 0.037	0.052	0.077	0.054	0.077	0.037	0.054	0.061	0.058
Sb	0.047	0.070	0.048	0.062	0.124	0.167	0.095	0.184	0.109	0.118
S	13.688	13.782	13.741	13.287	13.779	13.779	13.828	13.833	13.777	13.756
Total	**104.011**	**104.092**	**104.602**	**99.459**	**104.454**	**104.344**	**103.768**	**104.463**	**105.064**	**104.205**
				Normalised to 100 %						
Pb	84.691	84.765	84.314	84.111	84.480	84.644	84.826	84.165	84.217	85.034
Cu	0.201	0.207	0.210	0.147	0.087	0.111	0.322	0.182	0.064	0.084
Fe	1.633	1.440	1.539	1.942	1.458	1.218	1.031	1.137	1.744	0.757
Mn	0.017	0.033	0.038	0.016	-	0.015	-	0.022	0.029	0.022
Zn	0.197	0.232	0.666	0.261	0.585	0.540	0.340	0.901	0.672	0.686
As	0.020	0.015	-	0.024	-	-	0.028	-	-	0.014
Ag	-	-	-	-	0.028	0.033	-	0.123	-	0.032
Cd	0.035	-	0.050	0.077	0.052	0.074	0.036	0.052	0.058	0.056
Sb	0.045	0.067	0.046	0.062	0.119	0.160	0.092	0.176	0.104	0.113
S	13.160	13.240	13.136	13.359	13.191	13.205	13.326	13.242	13.113	13.201
Total	**100.000**	**100.000**	**100.000**	**100.000**	**100.000**	**100.000**	**100.000**	**100.000**	**100.000**	**100.000**
					Atom-%					
Pb	47.758	47.794	47.362	46.905	47.563	47.796	47.873	47.253	47.273	48.295
Cu	0.369	0.380	0.385	0.267	0.160	0.205	0.592	0.333	0.117	0.156
Fe	3.418	3.013	3.208	4.017	3.046	2.552	2.159	2.369	3.632	1.596
Mn	0.037	0.069	0.081	0.034	0.000	0.033	0.000	0.047	0.060	0.047
Zn	0.352	0.415	1.186	0.462	1.043	0.965	0.608	1.602	1.195	1.234
As	0.031	0.024	0.000	0.037	0.000	0.000	0.044	0.000	0.000	0.023
Ag	0.000	0.000	0.000	0.000	0.030	0.035	0.000	0.133	0.000	0.035
Cd	0.036	0.000	0.051	0.080	0.054	0.077	0.037	0.053	0.060	0.058
Sb	0.043	0.065	0.044	0.059	0.114	0.154	0.088	0.168	0.099	0.109
S	47.955	48.240	47.683	48.140	47.991	48.184	48.598	48.041	47.564	48.447
Total	**100.000**	**100.000**	**100.000**	**100.000**	**100.000**	**100.000**	**100.000**	**100.000**	**100.000**	**100.000**
					Normalised to 1 S atom					
Pb	0.996	0.991	0.993	0.974	0.991	0.992	0.985	0.984	0.994	0.997
Cu	0.008	0.008	0.008	0.006	0.003	0.004	0.012	0.007	0.002	0.003
Fe	0.071	0.062	0.067	0.083	0.063	0.053	0.044	0.049	0.076	0.033
Mn	0.001	0.001	0.002	0.001	0.000	0.001	0.000	0.001	0.001	0.001
Zn	0.007	0.009	0.025	0.010	0.022	0.020	0.013	0.033	0.025	0.025
As	0.001	0.000	0.000	0.001	0.000	0.000	0.001	0.000	0.000	0.000
Ag	0.000	0.000	0.000	0.000	0.001	0.001	0.000	0.003	0.000	0.001
Cd	0.001	0.000	0.001	0.002	0.001	0.002	0.001	0.001	0.001	0.001
Sb	0.001	0.001	0.001	0.001	0.002	0.003	0.002	0.004	0.002	0.002
S	1.000	1.000	1.000	1.000	1.000	1.000	1.000	1.000	1.000	1.000
Total	**2.085**	**2.073**	**2.097**	**2.077**	**2.084**	**2.075**	**2.058**	**2.082**	**2.102**	**2.064**

Sample	10032(1)	10032(1)
No.	#86	#89
Pb	88.453	87.741
Cu	0.138	0.151
Fe	0.664	2.003
Mn	0.018	0.023
Zn	0.457	1.219
As	< 0.015	< 0.014
Ag	0.046	0.073
Cd	< 0.033	0.071
Sb	0.111	0.223
S	13.903	14.221
Total	**103.790**	**105.725**
Normalised to 100 %		
Pb	85.223	82.990
Cu	0.133	0.143
Fe	0.640	1.895
Mn	0.017	0.022
Zn	0.440	1.153
As	-	-
Ag	0.044	0.069
Cd	-	0.067
Sb	0.107	0.211
S	13.395	13.451
Total	**100.000**	**100.000**
Atom-%		
Pb	48.335	45.661
Cu	0.246	0.256
Fe	1.346	3.867
Mn	0.037	0.045
Zn	0.791	2.010
As	0.000	0.000
Ag	0.048	0.073
Cd	0.000	0.068
Sb	0.103	0.197
S	49.093	47.822
Total	**100.000**	**100.000**
Normalised to 1 S atom		
Pb	0.985	0.955
Cu	0.005	0.005
Fe	0.027	0.081
Mn	0.001	0.001
Zn	0.016	0.042
As	0.000	0.000
Ag	0.001	0.002
Cd	0.000	0.001
Sb	0.002	0.004
S	1.000	1.000
Total	**2.037**	**2.091**

Table iv.92.: EMP analyses of galena from pyrrhotite-bearing interstitial sulphide cluster.

Sample	10032(1)	12015(12)	12015(12)	12015(12)	12015(12)
No.	#101	#87	#88	#95	#108
Pb	88.060	88.275	88.915	88.187	89.276
Cu	0.089	0.626	0.377	0.624	0.597
Fe	0.699	0.474	1.018	0.945	0.696
Mn	0.023	0.018	0.042	0.023	0.035
Zn	0.470	0.608	1.222	1.285	1.084
As	0.016	< 0	< 0	< 0.023	0.019
Ag	0.154	< 0	< 0	< 0	< 0
Cd	0.060	< 0.034	0.083	0.089	0.105
Sb	0.442	0.058	0.059	0.035	0.039
S	13.876	13.871	13.836	13.953	13.835
Total	**103.889**	**103.930**	**105.552**	**105.141**	**105.686**
		Normalised to 100 %			
Pb	84.764	84.937	84.238	83.875	84.473
Cu	0.086	0.602	0.357	0.593	0.565
Fe	0.673	0.456	0.964	0.899	0.659
Mn	0.022	0.017	0.040	0.022	0.033
Zn	0.452	0.585	1.158	1.222	1.026
As	0.015	-	0.000	-	0.018
Ag	0.148	-	-	-	-
Cd	0.058	-	0.079	0.085	0.099
Sb	0.425	0.056	0.056	0.033	0.037
S	13.357	13.346	13.108	13.271	13.091
Total	**100.000**	**100.000**	**100.000**	**100.000**	**100.000**
		Atom-%			
Pb	48.019	48.028	47.393	46.840	47.720
Cu	0.158	1.111	0.655	1.081	1.040
Fe	1.414	0.957	2.013	1.862	1.380
Mn	0.047	0.037	0.084	0.046	0.071
Zn	0.812	1.048	2.063	2.162	1.835
As	0.024	0.000	0.000	0.000	0.028
Ag	0.161	0.000	0.000	0.000	0.000
Cd	0.060	0.000	0.082	0.087	0.103
Sb	0.410	0.054	0.054	0.032	0.035
S	48.894	48.766	47.655	47.890	47.786
Total	**100.000**	**100.000**	**100.000**	**100.000**	**100.000**
		Normalised to 1 S atom			
Pb	0.982	0.985	0.995	0.978	0.999
Cu	0.003	0.023	0.014	0.023	0.022
Fe	0.029	0.020	0.042	0.039	0.029
Mn	0.001	0.001	0.002	0.001	0.001
Zn	0.017	0.021	0.043	0.045	0.038
As	0.000	0.000	0.000	0.000	0.001
Ag	0.003	0.000	0.000	0.000	0.000
Cd	0.001	0.000	0.002	0.002	0.002
Sb	0.008	0.001	0.001	0.001	0.001
S	1.000	1.000	1.000	1.000	1.000
Total	**2.045**	**2.051**	**2.098**	**2.088**	**2.093**

Table iv.93.: EMP analyses of galena from pyrrhotite-bearing [10032(1)] and pyrrhotite-free interstitial sulphide cluster [12015(12)].

Sample	10024(5)	10024(5)	10024(5)	10024(5)	10024(5)	10024(5)	10024(5)	10024(5)	10024(5)	10024(5)
No.	**#1.101**	**#1.102**	**#1.106**	**#1.107**	**#1.108**	**#1.109**	**#1.112**	**#1.113**	**#1.116**	**#1.118**
Pb	88.719	87.508	88.580	88.568	87.954	87.537	87.665	88.187	88.555	88.378
Cu	1.398	2.485	0.584	1.402	0.547	0.811	1.763	1.077	1.026	1.197
Fe	< 0	< 0	< 0.027	< 0	< 0.021	0.025	< 0.017	< 0	< 0.023	< 0
Mn	< 0.011	< 0.011	0.015	0.021	< 0.014	0.015	< 0.01	0.015	0.029	0.024
Zn	< 0.031	< 0.028	< 0.032	< 0.032	< 0	< 0.032	< 0.032	< 0	< 0.034	0.036
As	0.041	0.030	0.129	0.040	0.051	0.028	0.129	0.058	0.103	0.042
Ag	< 0.025	0.027	< 0	< 0	< 0	< 0	< 0	< 0	< 0	< 0
Cd	< 0.038	0.061	0.052	0.082	0.058	0.041	0.066	< 0.038	0.053	0.044
Sb	< 0.034	< 0.034	< 0.028	< 0.027	< 0	0.028	< 0.027	0.037	< 0.028	< 0.027
S	13.704	13.723	13.653	13.901	13.499	13.493	13.846	13.541	13.623	13.683
Total	**103.862**	**103.834**	**103.013**	**104.014**	**102.109**	**101.978**	**103.469**	**102.915**	**103.389**	**103.404**
					Normalised to 100 %					
Pb	85.420	84.277	85.989	85.150	86.137	85.839	84.726	85.689	85.652	85.469
Cu	1.346	2.393	0.567	1.348	0.536	0.795	1.704	1.046	0.992	1.158
Fe	-	-	-	-	-	0.025	-	0.000	-	-
Mn	-	-	0.015	0.020	-	0.015	-	0.015	0.028	0.023
Zn	-	-	-	-	-	-	-	-	-	0.035
As	0.039	0.029	0.125	0.038	0.050	0.027	0.125	0.056	0.100	0.041
Ag	-	0.026	-	-	-	-	-	-	-	-
Cd	-	0.059	0.050	0.079	0.057	0.040	0.064	-	0.051	0.043
Sb	-	-	-	-	-	0.027	-	0.036	-	-
S	13.194	13.216	13.254	13.365	13.220	13.231	13.382	13.157	13.176	13.233
Total	**100.000**	**100.000**	**100.000**	**100.000**	**100.000**	**100.000**	**100.000**	**100.000**	**100.000**	**100.000**
					Atom-%					
Pb	48.762	47.421	49.426	48.317	49.631	49.255	47.810	49.135	49.082	48.800
Cu	2.505	4.391	1.063	2.494	1.006	1.488	3.135	1.957	1.854	2.155
Fe	0.000	0.000	0.000	0.000	0.000	0.052	0.000	0.000	0.000	0.000
Mn	0.000	0.000	0.032	0.043	0.000	0.032	0.000	0.032	0.061	0.050
Zn	0.000	0.000	0.000	0.000	0.000	0.000	0.000	0.000	0.000	0.063
As	0.062	0.045	0.199	0.060	0.080	0.044	0.195	0.089	0.158	0.064
Ag	0.000	0.028	0.000	0.000	0.000	0.000	0.000	0.000	0.000	0.000
Cd	0.000	0.061	0.053	0.082	0.060	0.043	0.066	0.000	0.054	0.045
Sb	0.000	0.000	0.000	0.000	0.000	0.027	0.000	0.035	0.000	0.000
S	48.671	48.054	49.227	49.003	49.222	49.060	48.795	48.752	48.791	48.822
Total	**100.000**	**100.000**	**100.000**	**100.000**	**100.000**	**100.000**	**100.000**	**100.000**	**100.000**	**100.000**
					Normalised to 1 S atom					
Pb	1.002	0.987	1.004	0.986	1.008	1.004	0.980	1.008	1.006	1.000
Cu	0.051	0.091	0.022	0.051	0.020	0.030	0.064	0.040	0.038	0.044
Fe	0.000	0.000	0.000	0.000	0.000	0.001	0.000	0.000	0.000	0.000
Mn	0.000	0.000	0.001	0.001	0.000	0.001	0.000	0.001	0.001	0.001
Zn	0.000	0.000	0.000	0.000	0.000	0.000	0.000	0.000	0.000	0.001
As	0.001	0.001	0.004	0.001	0.002	0.001	0.004	0.002	0.003	0.001
Ag	0.000	0.001	0.000	0.000	0.000	0.000	0.000	0.000	0.000	0.000
Cd	0.000	0.001	0.001	0.002	0.001	0.001	0.001	0.000	0.001	0.001
Sb	0.000	0.000	0.000	0.000	0.000	0.001	0.000	0.001	0.000	0.000
S	1.000	1.000	1.000	1.000	1.000	1.000	1.000	1.000	1.000	1.000
Total	**2.055**	**2.081**	**2.031**	**2.041**	**2.032**	**2.038**	**2.049**	**2.051**	**2.050**	**2.048**

Sample	10024(5)	10024(5)	10024(5)	10024(5)	10024(5)	10024(5)	10024(5)	10024(5)	10024(5)	10024(5)
No.	**#1.119**	**#1.136**	**#1.172**	**#1.173**	**#1.175**	**#1.177**	**#1.178**	**#1.180**	**#1.181**	**#1.183**
Pb	88.537	89.612	88.654	88.487	88.512	88.331	87.692	87.680	88.285	89.260
Cu	1.658	1.994	1.578	2.084	0.473	0.648	0.999	0.970	0.576	2.282
Fe	< 0	< 0	< 0	< 0.023	< 0	< 0.023	< 0	0.141	< 0.022	< 0
Mn	0.012	0.018	< 0.011	< 0.01	0.017	0.025	0.022	0.019	0.033	0.015
Zn	< 0	< 0.032	< 0	< 0	< 0	< 0.032	< 0.034	< 0.032	< 0.033	< 0
As	0.032	0.048	0.026	0.049	0.040	0.145	0.027	0.041	0.022	0.099
Ag	< 0.024	< 0.024	< 0.023	0.027	< 0	< 0	< 0	< 0	< 0	< 0.024
Cd	0.074	< 0.039	0.040	0.123	0.054	0.087	0.068	0.052	0.054	0.058
Sb	< 0	< 0.027	< 0	< 0	< 0	< 0	< 0	< 0.028	< 0.029	< 0.029
S	13.796	13.778	13.727	13.612	13.457	13.511	13.679	13.499	13.498	13.646
Total	**104.109**	**105.450**	**104.025**	**104.382**	**102.553**	**102.747**	**102.487**	**102.402**	**102.468**	**105.360**
				Normalised to 100 %						
Pb	85.043	84.981	85.224	84.772	86.309	85.969	85.564	85.623	86.159	84.719
Cu	1.593	1.891	1.517	1.997	0.461	0.631	0.975	0.947	0.562	2.166
Fe	-	-	-	-	-	-	-	0.138	-	-
Mn	0.012	0.017	-	-	0.017	0.024	0.021	0.019	0.032	0.014
Zn	-	-	-	-	-	-	-	-	-	-
As	0.031	0.046	0.025	0.047	0.039	0.141	0.026	0.040	0.021	0.094
Ag	-	-	-	0.026	-	-	-	-	-	-
Cd	0.071	-	0.038	0.118	0.053	0.085	0.066	0.051	0.053	0.055
Sb	-	-	-	-	-	-	-	-	-	-
S	13.251	13.066	13.196	13.041	13.122	13.150	13.347	13.182	13.173	12.952
Total	**100.000**	**100.000**	**100.000**	**100.000**	**100.000**	**100.000**	**100.000**	**100.000**	**100.000**	**100.000**
					Atom-%					
Pb	48.286	48.348	48.538	48.181	49.926	49.511	48.820	49.017	49.690	48.166
Cu	2.948	3.508	2.817	3.700	0.870	1.184	1.813	1.768	1.057	4.015
Fe	0.000	0.000	0.000	0.000	0.000	0.000	0.000	0.292	0.000	0.000
Mn	0.025	0.037	0.000	0.000	0.036	0.053	0.046	0.040	0.070	0.031
Zn	0.000	0.000	0.000	0.000	0.000	0.000	0.000	0.000	0.000	0.000
As	0.048	0.072	0.039	0.074	0.062	0.225	0.042	0.063	0.034	0.148
Ag	0.000	0.000	0.000	0.028	0.000	0.000	0.000	0.000	0.000	0.000
Cd	0.074	0.000	0.040	0.123	0.056	0.090	0.070	0.054	0.056	0.058
Sb	0.000	0.000	0.000	0.000	0.000	0.000	0.000	0.000	0.000	0.000
S	48.619	48.035	48.565	47.894	49.049	48.937	49.209	48.765	49.092	47.583
Total	**100.000**	**100.000**	**100.000**	**100.000**	**100.000**	**100.000**	**100.000**	**100.000**	**100.000**	**100.000**
					Normalised to 1 S atom					
Pb	0.993	1.007	0.999	1.006	1.018	1.012	0.992	1.005	1.012	1.012
Cu	0.061	0.073	0.058	0.077	0.018	0.024	0.037	0.036	0.022	0.084
Fe	0.000	0.000	0.000	0.000	0.000	0.000	0.000	0.006	0.000	0.000
Mn	0.001	0.001	0.000	0.000	0.001	0.001	0.001	0.001	0.001	0.001
Zn	0.000	0.000	0.000	0.000	0.000	0.000	0.000	0.000	0.000	0.000
As	0.001	0.001	0.001	0.002	0.001	0.005	0.001	0.001	0.001	0.003
Ag	0.000	0.000	0.000	0.001	0.000	0.000	0.000	0.000	0.000	0.000
Cd	0.002	0.000	0.001	0.003	0.001	0.002	0.001	0.001	0.001	0.001
Sb	0.000	0.000	0.000	0.000	0.000	0.000	0.000	0.000	0.000	0.000
S	1.000	1.000	1.000	1.000	1.000	1.000	1.000	1.000	1.000	1.000
Total	**2.057**	**2.082**	**2.059**	**2.088**	**2.039**	**2.043**	**2.032**	**2.051**	**2.037**	**2.102**

Sample	10024(5)	10024(5)	10024(5)	10024(5)	10024(5)	10024(5)
No.	**#1.184**	**#1.186**	**#1.187**	**#1.189**	**#1.190**	**#1.202**
Pb	88.635	88.390	88.358	88.189	88.149	87.767
Cu	1.157	1.971	0.947	1.307	1.736	1.049
Fe	< 0.033	< 0	< 0	< 0	< 0	< 0.023
Mn	0.014	0.013	0.018	< 0.011	0.015	0.051
Zn	< 0.028	< 0	< 0	< 0	< 0.033	< 0
As	0.064	0.136	0.097	0.028	0.033	0.038
Ag	< 0	< 0.023	< 0	< 0	< 0	< 0
Cd	0.078	0.051	0.048	0.057	0.041	< 0.041
Sb	< 0	< 0.026	< 0.028	< 0.026	< 0	< 0
S	13.465	13.614	13.629	13.541	13.515	13.533
Total	**103.413**	**104.175**	**103.097**	**103.122**	**103.489**	**102.438**
			Normalised to 100 %			
Pb	85.710	84.848	85.704	85.519	85.177	85.678
Cu	1.119	1.892	0.919	1.267	1.677	1.024
Fe	-	-	-	-	-	-
Mn	0.014	0.012	0.017	-	0.014	0.050
Zn	-	-	-	-	-	-
As	0.062	0.131	0.094	0.027	0.032	0.037
Ag	-	-	0.000	-	-	-
Cd	0.075	0.049	0.047	0.055	0.040	-
Sb	0.000	-	-	-	-	-
S	13.021	13.068	13.220	13.131	13.059	13.211
Total	**100.000**	**100.000**	**100.000**	**100.000**	**100.000**	**100.000**
			Atom-%			
Pb	49.299	48.219	49.104	48.958	48.603	49.050
Cu	2.098	3.506	1.716	2.366	3.121	1.912
Fe	0.000	0.000	0.000	0.000	0.000	0.000
Mn	0.029	0.027	0.038	0.000	0.031	0.107
Zn	0.000	0.000	0.000	0.000	0.000	0.000
As	0.098	0.205	0.149	0.043	0.050	0.059
Ag	0.000	0.000	0.000	0.000	0.000	0.000
Cd	0.080	0.051	0.049	0.058	0.042	0.000
Sb	0.000	0.000	0.000	0.000	0.000	0.000
S	48.395	47.991	48.944	48.575	48.153	48.872
Total	**100.000**	**100.000**	**100.000**	**100.000**	**100.000**	**100.000**
			Normalised to 1 S atom			
Pb	1.019	1.005	1.003	1.008	1.009	1.004
Cu	0.043	0.073	0.035	0.049	0.065	0.039
Fe	0.000	0.000	0.000	0.000	0.000	0.000
Mn	0.001	0.001	0.001	0.000	0.001	0.002
Zn	0.000	0.000	0.000	0.000	0.000	0.000
As	0.002	0.004	0.003	0.001	0.001	0.001
Ag	0.000	0.000	0.000	0.000	0.000	0.000
Cd	0.002	0.001	0.001	0.001	0.001	0.000
Sb	0.000	0.000	0.000	0.000	0.000	0.000
S	1.000	1.000	1.000	1.000	1.000	1.000
Total	**2.066**	**2.084**	**2.043**	**2.059**	**2.077**	**2.046**

Table iv.94.: EMP analyses of segregated galena from Pb-Cu matte.

Sample	12015(5)	12015(5)	12015(5)	12015(5)	12015(5)	14032	14032	14032	14032	14032
No.	**#10**	**#11**	**#12**	**#13**	**#14**	**#38**	**#39**	**#40**	**#54**	**#55**
Pb	87.908	88.286	87.808	88.617	88.482	87.865	88.115	88.116	88.847	87.981
Cu	1.050	0.978	1.015	1.192	1.211	0.385	0.293	0.595	0.310	0.212
Fe	0.351	0.143	0.190	0.254	0.238	0.193	0.128	0.314	0.138	0.216
Mn	0.024	0.023	0.026	0.029	0.024	0.019	0.018	0.027	0.024	0.024
Zn	0.096	< 0.032	< 0.031	< 0.033	< 0.031	< 0	< 0	0.040	< 0.033	< 0
As		< 0	< 0	< 0.014	< 0.015	< 0	< 0	< 0	< 0	< 0
Ag	< 0	< 0	< 0	< 0	< 0	< 0	< 0	< 0	< 0	< 0
Cd	0.052	0.046	0.047	0.051	0.047	0.067	0.042	0.056	0.046	0.064
Sb	< 0.028	0.049	0.056	0.048	0.040	0.064	0.046	0.055	0.079	0.063
S	13.409	13.397	13.529	13.595	13.470	13.693	13.809	13.617	13.901	13.560
Total	**102.890**	**102.922**	**102.671**	**103.786**	**103.512**	**102.286**	**102.451**	**102.820**	**103.345**	**102.120**
					Normalised to 100 %					
Pb	85.439	85.780	85.524	85.384	85.480	85.901	86.007	85.699	85.971	86.155
Cu	1.021	0.950	0.989	1.149	1.170	0.376	0.286	0.579	0.300	0.208
Fe	0.341	0.139	0.185	0.245	0.230	0.189	0.125	0.305	0.134	0.212
Mn	0.023	0.022	0.025	0.028	0.023	0.019	0.018	0.026	0.023	0.024
Zn	0.093	-	-	-	-	-	-	0.039	-	-
As	0.000	-	-	-	-	-	-	-	-	-
Ag	-	-	-	-	-	-	-	-	-	-
Cd	0.051	0.045	0.046	0.049	0.045	0.066	0.041	0.054	0.045	0.063
Sb	-	0.048	0.055	0.046	0.039	0.063	0.045	0.053	0.076	0.062
S	13.032	13.017	13.177	13.099	13.013	13.387	13.479	13.244	13.451	13.278
Total	**100.000**	**100.000**	**100.000**	**100.000**	**100.000**	**100.000**	**100.000**	**100.000**	**100.000**	**100.000**
					Atom-%					
Pb	48.900	49.369	48.911	48.803	48.993	49.190	49.226	49.052	49.221	49.591
Cu	1.904	1.783	1.843	2.140	2.186	0.703	0.534	1.080	0.560	0.390
Fe	0.724	0.297	0.393	0.519	0.489	0.401	0.265	0.649	0.284	0.452
Mn	0.050	0.049	0.055	0.060	0.050	0.040	0.038	0.057	0.050	0.051
Zn	0.169	0.000	0.000	0.000	0.000	0.000	0.000	0.071	0.000	0.000
As	0.000	0.000	0.000	0.000	0.000	0.000	0.000	0.000	0.000	0.000
Ag	0.000	0.000	0.000	0.000	0.000	0.000	0.000	0.000	0.000	0.000
Cd	0.053	0.047	0.048	0.052	0.048	0.069	0.043	0.057	0.047	0.066
Sb	0.000	0.047	0.053	0.045	0.038	0.061	0.044	0.052	0.074	0.060
S	48.199	48.409	48.697	48.380	48.196	49.536	49.850	48.983	49.764	49.389
Total	**100.000**	**100.000**	**100.000**	**100.000**	**100.000**	**100.000**	**100.000**	**100.000**	**100.000**	**100.000**
					Normalised to 1 S atom					
Pb	1.015	1.020	1.004	1.009	1.017	0.993	0.987	1.001	0.989	1.004
Cu	0.040	0.037	0.038	0.044	0.045	0.014	0.011	0.022	0.011	0.008
Fe	0.015	0.006	0.008	0.011	0.010	0.008	0.005	0.013	0.006	0.009
Mn	0.001	0.001	0.001	0.001	0.001	0.001	0.001	0.001	0.001	0.001
Zn	0.004	0.000	0.000	0.000	0.000	0.000	0.000	0.001	0.000	0.000
As	0.000	0.000	0.000	0.000	0.000	0.000	0.000	0.000	0.000	0.000
Ag	0.000	0.000	0.000	0.000	0.000	0.000	0.000	0.000	0.000	0.000
Cd	0.001	0.001	0.001	0.001	0.001	0.001	0.001	0.001	0.001	0.001
Sb	0.000	0.001	0.001	0.001	0.001	0.001	0.001	0.001	0.001	0.001
S	1.000	1.000	1.000	1.000	1.000	1.000	1.000	1.000	1.000	1.000
Total	**2.075**	**2.066**	**2.054**	**2.067**	**2.075**	**2.019**	**2.006**	**2.042**	**2.009**	**2.025**

Sample	14032	14032	14032	11027(1)	11027(1)	11029(3)	11029(3)	11029(3)	11029(3)	11029(3)
No.	**#56**	**#57**	**#58**	**#2.42**	**#2.43**	**#11**	**#12**	**#13**	**#17**	**#18**
Pb	87.856	87.963	87.641	87.576	87.675	87.032	86.520	86.657	87.157	87.320
Cu	0.223	0.647	0.349	1.406	0.824	0.714	0.782	0.531	0.731	0.755
Fe	0.179	0.525	0.167	0.636	0.448	0.106	0.090	0.081	0.115	0.097
Mn	< 0.015	< 0.016	< 0.015	0.024	0.018	0.026	0.023	< 0.015	< 0.015	0.017
Zn	0.034	0.050	< 0.030	0.310	0.189	< 0	< 0	< 0	< 0.035	< 0.032
As	< 0	< 0	< 0	< 0.017	< 0.015	0.027	< 0.014	0.016	0.017	< 0.014
Ag	< 0	< 0	< 0	< 0	< 0	< 0	< 0	< 0	< 0	< 0
Cd	0.045	0.046	0.045	0.058	0.051	< 0.035	0.042	0.044	0.079	< 0.035
Sb	0.045	0.055	0.039	0.048	0.041	0.037	0.051	0.052	0.073	0.049
S	13.617	13.752	13.702	13.775	13.489	13.827	13.739	13.633	13.756	13.843
Total	**101.999**	**103.038**	**101.943**	**103.833**	**102.735**	**101.769**	**101.247**	**101.014**	**101.928**	**102.081**
					Normalised to 100 %					
Pb	86.134	85.369	85.971	84.343	85.341	85.519	85.454	85.787	85.508	85.540
Cu	0.219	0.628	0.342	1.354	0.802	0.702	0.772	0.526	0.717	0.740
Fe	0.175	0.510	0.164	0.613	0.436	0.104	0.089	0.080	0.113	0.095
Mn	-	-	-	0.023	0.018	0.026	0.023	-	-	0.017
Zn	0.033	0.049	-	0.299	0.184	-	-	-	-	-
As	-	-	-	-	-	0.027	-	0.016	0.017	-
Ag	-	-	-	-	-	-	-	-	-	-
Cd	0.044	0.045	0.044	0.056	0.050	-	0.041	0.044	0.078	-
Sb	0.044	0.053	0.038	0.046	0.040	0.036	0.050	0.051	0.072	0.048
S	13.350	13.347	13.441	13.266	13.130	13.587	13.570	13.496	13.496	13.561
Total	**100.000**	**100.000**	**100.000**	**100.000**	**100.000**	**100.000**	**100.000**	**100.000**	**100.000**	**100.000**
					Atom-%					
Pb	49.495	48.539	49.212	47.391	48.703	48.530	48.488	48.959	48.644	48.581
Cu	0.410	1.164	0.639	2.481	1.492	1.298	1.429	0.978	1.330	1.370
Fe	0.374	1.075	0.348	1.277	0.923	0.219	0.187	0.170	0.238	0.200
Mn	0.000	0.000	0.000	0.049	0.038	0.055	0.049	0.000	0.000	0.036
Zn	0.061	0.087	0.000	0.531	0.333	0.000	0.000	0.000	0.000	0.000
As	0.000	0.000	0.000	0.000	0.000	0.042	0.000	0.025	0.026	0.000
Ag	0.000	0.000	0.000	0.000	0.000	0.000	0.000	0.000	0.000	0.000
Cd	0.047	0.047	0.047	0.058	0.052	0.000	0.043	0.046	0.081	0.000
Sb	0.043	0.052	0.037	0.044	0.039	0.035	0.049	0.050	0.069	0.046
S	49.571	49.036	49.717	48.169	48.420	49.821	49.755	49.772	49.611	49.767
Total	**100.000**	**100.000**	**100.000**	**100.000**	**100.000**	**100.000**	**100.000**	**100.000**	**100.000**	**100.000**
					Normalised to 1 S atom					
Pb	0.998	0.990	0.990	0.984	1.006	0.974	0.975	0.984	0.981	0.976
Cu	0.008	0.024	0.013	0.052	0.031	0.026	0.029	0.020	0.027	0.028
Fe	0.008	0.022	0.007	0.027	0.019	0.004	0.004	0.003	0.005	0.004
Mn	0.000	0.000	0.000	0.001	0.001	0.001	0.001	0.000	0.000	0.001
Zn	0.001	0.002	0.000	0.011	0.007	0.000	0.000	0.000	0.000	0.000
As	0.000	0.000	0.000	0.000	0.000	0.001	0.000	0.001	0.001	0.000
Ag	0.000	0.000	0.000	0.000	0.000	0.000	0.000	0.000	0.000	0.000
Cd	0.001	0.001	0.001	0.001	0.001	0.000	0.001	0.001	0.002	0.000
Sb	0.001	0.001	0.001	0.001	0.001	0.001	0.001	0.001	0.001	0.001
S	1.000	1.000	1.000	1.000	1.000	1.000	1.000	1.000	1.000	1.000
Total	**2.017**	**2.039**	**2.011**	**2.076**	**2.065**	**2.007**	**2.010**	**2.009**	**2.016**	**2.009**

Sample	11029(5)	10024(4)	10024(4)	10024(4)	10024(4)	10024(4)	10024(4)
No.	**#1.37**	**#1.166**	**#2.55**	**#2.56**	**#2.57**	**#2.58**	**#2.59**
Pb	87.674	87.893	87.198	86.939	87.838	87.346	87.367
Cu	1.414	1.302	0.774	0.818	0.826	0.705	0.894
Fe	0.236	0.848	0.305	0.574	0.252	0.245	0.240
Mn	0.048	0.024	0.026	< 0.018	0.043	0.021	0.031
Zn	< 0.032	0.134	0.118	< 0.039	0.064	0.182	0.052
As	0.056	< 0.014	< 0.018	< 0	0.024	< 0	< 0
Ag	< 0.024	< 0	< 0	< 0	< 0	< 0	< 0.030
Cd	0.089	0.056	< 0.044	< 0.043	0.053	0.065	0.051
Sb	< 0.028	0.134	0.080	0.044	0.048	0.066	< 0.033
S	13.630	13.608	13.820	13.773	13.687	13.796	13.813
Total	**103.147**	**103.999**	**102.321**	**102.148**	**102.835**	**102.426**	**102.448**
			Normalised to 100 %				
Pb	84.999	84.513	85.220	85.111	85.416	85.277	85.279
Cu	1.371	1.252	0.756	0.801	0.803	0.688	0.873
Fe	0.229	0.815	0.298	0.562	0.245	0.239	0.234
Mn	0.047	0.023	0.025	-	0.042	0.021	0.030
Zn	-	0.129	0.115	-	0.062	0.178	0.051
As	0.054	-	-	-	0.023	-	-
Ag	-	-	-	-	-	-	-
Cd	0.086	0.054	-	-	0.052	0.063	0.050
Sb	-	0.129	0.078	0.043	0.047	0.064	-
S	13.214	13.085	13.507	13.483	13.310	13.469	13.483
Total	**100.000**	**100.000**	**100.000**	**100.000**	**100.000**	**100.000**	**100.000**
			Atom-%				
Pb	48.243	47.751	48.238	48.083	48.658	48.367	48.321
Cu	2.537	2.306	1.396	1.475	1.492	1.273	1.612
Fe	0.482	1.709	0.626	1.178	0.518	0.503	0.492
Mn	0.100	0.049	0.054	0.000	0.090	0.044	0.065
Zn	0.000	0.231	0.207	0.000	0.112	0.319	0.091
As	0.085	0.000	0.000	0.000	0.037	0.000	0.000
Ag	0.000	0.000	0.000	0.000	0.000	0.000	0.000
Cd	0.090	0.056	0.000	0.000	0.054	0.066	0.052
Sb	0.000	0.124	0.075	0.041	0.045	0.062	0.000
S	48.463	47.773	49.403	49.223	48.994	49.365	49.367
Total	**100.000**	**100.000**	**100.000**	**100.000**	**100.000**	**100.000**	**100.000**
			Normalised to 1 S atom				
Pb	0.995	1.000	0.976	0.977	0.993	0.980	0.979
Cu	0.052	0.048	0.028	0.030	0.030	0.026	0.033
Fe	0.010	0.036	0.013	0.024	0.011	0.010	0.010
Mn	0.002	0.001	0.001	0.000	0.002	0.001	0.001
Zn	0.000	0.005	0.004	0.000	0.002	0.006	0.002
As	0.002	0.000	0.000	0.000	0.001	0.000	0.000
Ag	0.000	0.000	0.000	0.000	0.000	0.000	0.000
Cd	0.002	0.001	0.000	0.000	0.001	0.001	0.001
Sb	0.000	0.003	0.002	0.001	0.001	0.001	0.000
S	1.000	1.000	1.000	1.000	1.000	1.000	1.000
Total	**2.063**	**2.093**	**2.024**	**2.032**	**2.041**	**2.026**	**2.026**

Table iv.95.: EMP analyses of segregated galena from matte s.s.

Sample	12015(5)	12015(5)	14032	14032	11027(1)	11027(1)	11029(3)	11029(3)	11029(3)	11029(3)
No.	**#2**	**#5**	**#128**	**#134**	**#2.9**	**#2.11**	**#1**	**#4**	**#6**	**#7**
Pb	82.503	75.993	86.685	78.337	88.882	88.425	86.987	87.616	86.896	85.153
Cu	5.619	6.820	3.006	6.186	2.274	2.423	1.996	2.844	2.216	1.293
Fe	1.196	2.333	0.762	1.932	0.490	0.530	0.317	0.464	0.392	1.631
Mn	0.022	0.018	0.025	0.039	0.034	< 0.015	0.017	0.015	< 0.016	0.018
Zn	< 0.036	< 0.031	< 0	< 0.048	0.099	0.093	< 0.031	< 0.032	< 0.032	0.057
As	< 0.016	< 0.015	< 0	< 0	0.017	0.019	< 0.015	< 0.016	< 0.016	0.044
Ag	< 0	< 0	< 0	< 0	< 0	< 0	< 0	< 0	< 0	< 0
Cd	0.165	0.072	0.104	0.122	0.096	0.080	0.053	0.054	< 0.034	0.090
Sb	0.054	0.028	0.056	0.042	0.063	0.050	0.051	0.032	0.046	0.066
S	15.218	15.168	14.179	14.892	13.869	13.957	13.889	13.886	13.782	13.487
Total	**104.777**	**100.432**	**104.817**	**101.550**	**105.824**	**105.577**	**103.310**	**104.911**	**103.332**	**101.839**
				Normalised to 100 %						
Pb	78.742	75.666	82.701	77.141	83.990	83.754	84.200	83.515	84.094	83.615
Cu	5.363	6.791	2.868	6.092	2.149	2.295	1.932	2.711	2.145	1.270
Fe	1.141	2.323	0.727	1.903	0.463	0.502	0.307	0.442	0.379	1.602
Mn	0.021	0.018	0.024	0.038	0.032	-	0.016	0.014	-	0.018
Zn	-	-	-	-	0.094	0.088	-	-	-	0.056
As	-	-	-	-	0.016	0.018	-	-	-	0.043
Ag	-	-	-	-	-	-	-	-	-	-
Cd	0.157	0.072	0.099	0.120	0.091	0.076	0.051	0.051	-	0.088
Sb	0.052	0.028	0.053	0.041	0.060	0.047	0.049	0.031	0.045	0.065
S	14.524	15.103	13.527	14.665	13.106	13.220	13.444	13.236	13.338	13.243
Total	**100.000**	**100.000**	**100.000**	**100.000**	**100.000**	**100.000**	**100.000**	**100.000**	**100.000**	**100.000**
					Atom-%					
Pb	40.427	37.043	45.309	38.714	47.150	46.771	47.104	46.468	47.044	46.476
Cu	8.978	10.840	5.123	9.968	3.933	4.179	3.524	4.918	3.912	2.301
Fe	2.174	4.219	1.478	3.543	0.964	1.040	0.637	0.913	0.787	3.303
Mn	0.041	0.033	0.049	0.073	0.068	0.000	0.035	0.030	0.000	0.037
Zn	0.000	0.000	0.000	0.000	0.166	0.156	0.000	0.000	0.000	0.099
As	0.000	0.000	0.000	0.000	0.025	0.028	0.000	0.000	0.000	0.066
Ag	0.000	0.000	0.000	0.000	0.000	0.000	0.000	0.000	0.000	0.000
Cd	0.149	0.065	0.100	0.111	0.094	0.078	0.053	0.053	0.000	0.091
Sb	0.045	0.023	0.050	0.035	0.057	0.045	0.047	0.029	0.042	0.061
S	48.186	47.777	47.890	47.557	47.542	47.704	48.600	47.589	48.214	47.566
Total	**100.000**	**100.000**	**100.000**	**100.000**	**100.000**	**100.000**	**100.000**	**100.000**	**100.000**	**100.000**
					Normalised to 1 S atom					
Pb	0.839	0.775	0.946	0.814	0.992	0.980	0.969	0.976	0.976	0.977
Cu	0.186	0.227	0.107	0.210	0.083	0.088	0.073	0.103	0.081	0.048
Fe	0.045	0.088	0.031	0.074	0.020	0.022	0.013	0.019	0.016	0.069
Mn	0.001	0.001	0.001	0.002	0.001	0.000	0.001	0.001	0.000	0.001
Zn	0.000	0.000	0.000	0.000	0.003	0.003	0.000	0.000	0.000	0.002
As	0.000	0.000	0.000	0.000	0.001	0.001	0.000	0.000	0.000	0.001
Ag	0.000	0.000	0.000	0.000	0.000	0.000	0.000	0.000	0.000	0.000
Cd	0.003	0.001	0.002	0.002	0.002	0.002	0.001	0.001	0.000	0.002
Sb	0.001	0.000	0.001	0.001	0.001	0.001	0.001	0.001	0.001	0.001
S	1.000	1.000	1.000	1.000	1.000	1.000	1.000	1.000	1.000	1.000
Total	**2.075**	**2.093**	**2.088**	**2.103**	**2.103**	**2.096**	**2.058**	**2.101**	**2.074**	**2.102**

Sample	11029(5)	10024(4)	10024(4)	10024(4)	10-1B
No.	**#2.6**	**#2.1**	**#2.7**	**#2.9**	**#46**
Pb	83.594	84.974	85.062	83.320	72.927
Cu	3.723	3.356	3.816	3.993	8.570
Fe	1.493	1.659	1.283	1.838	2.258
Mn	0.071	0.028	0.032	0.020	0.018
Zn	0.646	< 0.046	< 0.031	< 0.032	0.042
As	< 0	< 0	< 0	< 0	0.034
Ag	< 0	< 0	< 0	< 0	< 0.034
Cd	0.068	0.095	0.040	0.059	0.104
Sb	0.060	0.073	0.064	0.030	< 0
S	14.579	14.462	14.532	14.765	15.597
Total	**104.234**	**104.647**	**104.829**	**104.025**	**99.607**
		Normalised to 100 %			
Pb	80.198	81.201	81.144	80.096	73.215
Cu	3.572	3.207	3.640	3.839	8.604
Fe	1.432	1.585	1.224	1.767	2.267
Mn	0.068	0.027	0.031	0.019	0.018
Zn	0.620	-	-	-	0.042
As	-	-	-	-	0.034
Ag	-	-	-	-	-
Cd	0.065	0.091	0.038	0.057	0.104
Sb	0.058	0.070	0.061	0.029	-
S	13.987	13.820	13.863	14.194	15.659
Total	**100.000**	**100.000**	**100.000**	**100.000**	**100.000**
		Atom-%			
Pb	42.214	43.370	43.295	41.911	34.608
Cu	6.130	5.585	6.333	6.549	13.261
Fe	2.797	3.142	2.423	3.430	3.976
Mn	0.135	0.054	0.061	0.038	0.032
Zn	1.033	0.000	0.000	0.000	0.063
As	0.000	0.000	0.000	0.000	0.045
Ag	0.000	0.000	0.000	0.000	0.000
Cd	0.063	0.089	0.038	0.055	0.091
Sb	0.052	0.063	0.055	0.026	0.000
S	47.574	47.697	47.795	47.992	47.829
Total	**100.000**	**100.000**	**100.000**	**100.000**	**100.000**
		Normalised to 1 S atom			
Pb	0.887	0.909	0.906	0.873	0.724
Cu	0.129	0.117	0.133	0.136	0.277
Fe	0.059	0.066	0.051	0.071	0.083
Mn	0.003	0.001	0.001	0.001	0.001
Zn	0.022	0.000	0.000	0.000	0.001
As	0.000	0.000	0.000	0.000	0.001
Ag	0.000	0.000	0.000	0.000	0.000
Cd	0.001	0.002	0.001	0.001	0.002
Sb	0.001	0.001	0.001	0.001	0.000
S	1.000	1.000	1.000	1.000	1.000
Total	**2.102**	**2.097**	**2.092**	**2.084**	**2.091**

Table iv.96.: EMP analyses of eutectoid galena from matte s.s.

Sample	**11027(1)**	**10032(4)**
No.	**#1.102**	**#41**
Cu	63.746	52.456
Fe	9.208	15.874
Pb	0.204	0.986
Ag	0.608	0.045
Mn	< 0.008	0.033
Co	< 0	0.018
Zn	0.054	< 0.019
As	< 0	< 0.018
Cd	0.040	< 0.026
Sb	< 0.027	0.038
S	26.110	28.474
Total	**99.970**	**97.947**
	Atom-%	
Cu	50.406	41.189
Fe	8.285	14.183
Pb	0.049	0.237
Ag	0.283	0.021
Mn	0.000	0.030
Co	0.000	0.015
Zn	0.041	0.000
As	0.000	0.000
Cd	0.018	0.000
Sb	0.000	0.016
S	40.916	44.309
Total	**100.000**	**100.000**
	Normalised to 4 S atoms	
Cu	4.928	3.718
Fe	0.810	1.280
Pb	0.005	0.021
Ag	0.028	0.002
Mn	0.000	0.003
Co	0.000	0.001
Zn	0.004	0.000
As	0.000	0.000
Cd	0.002	0.000
Sb	0.000	0.001
S	4.000	4.000
Total	**9.776**	**9.028**

Table iv.97.: EMP analyses of bornite *ss* droplets in slag.

Sample	10-2B	10-2B	10-2B	10-2B	10-2B	10-2B	10-2B	14032	14032	14032
No.	**#83**	**#89**	**#92**	**#93**	**#94**	**#96**	**#107**	**#5**	**#9**	**#11**
Cu	55.497	56.956	52.090	52.870	56.901	55.567	53.491	50.809	53.310	51.111
Fe	14.454	13.582	17.502	16.825	14.163	14.873	15.424	17.449	15.891	17.534
Pb	0.154	0.202	0.194	0.220	0.244	0.244	0.462	0.151	0.177	0.221
Ag	0.079	0.068	0.056	0.073	0.081	0.067	0.066	0.174	0.079	0.110
Mn	0.024	0.023	0.027	0.013	0.022	0.024	0.019	0.016	0.015	< 0.011
Co	0.019	0.015	0.030	0.020	0.018	0.025	0.017	0.032	0.035	0.026
Zn	0.065	0.092	0.185	0.228	0.116	0.089	< 0.029	< 0.027	< 0	< 0.027
As	0.116	0.113	0.181	0.123	0.201	0.103	0.044	0.130	0.086	0.092
Cd	0.114	0.089	0.097	0.123	0.138	0.092	0.110	0.051	0.108	0.086
Sb	0.025	0.055	0.033	0.026	0.043	0.045	0.032	0.043	0.046	0.023
S	27.900	27.504	28.952	28.760	27.279	28.708	28.583	31.210	30.133	30.529
Total	**98.447**	**98.699**	**99.347**	**99.281**	**99.206**	**99.856**	**98.248**	**100.065**	**99.880**	**99.732**
					Atom-%					
Cu	40.130	39.526	43.487	44.732	40.087	40.805	44.583	39.295	44.863	38.237
Fe	13.563	14.173	12.888	12.138	15.326	14.776	12.627	14.642	10.875	14.942
Pb	0.093	0.108	0.037	0.049	0.046	0.052	0.059	0.056	0.042	0.035
Ag	0.027	0.033	0.036	0.031	0.025	0.033	0.037	0.044	0.057	0.077
Mn	0.013	0.000	0.022	0.021	0.024	0.012	0.020	0.018	0.012	0.014
Co	0.018	0.012	0.016	0.013	0.025	0.017	0.015	0.016	0.010	0.026
Zn	0.076	0.182	0.049	0.070	0.138	0.171	0.088	0.000	0.000	0.000
As	0.111	0.102	0.077	0.075	0.118	0.081	0.134	0.038	0.065	0.083
Cd	0.053	0.052	0.050	0.040	0.042	0.054	0.061	0.022	0.017	0.022
Sb	0.017	0.010	0.010	0.023	0.013	0.010	0.018	0.017	0.013	0.017
S	45.898	45.803	43.326	42.809	44.155	43.990	42.358	45.853	44.047	46.547
Total	**100.000**	**100.000**	**100.000**	**100.000**	**100.000**	**100.000**	**100.000**	**100.000**	**100.000**	**100.000**
					Normalised to 4 S atoms					
Cu	3.497	3.452	4.015	4.180	3.631	3.710	4.210	3.428	4.074	3.286
Fe	1.182	1.238	1.190	1.134	1.388	1.344	1.192	1.277	0.988	1.284
Pb	0.008	0.009	0.003	0.005	0.004	0.005	0.006	0.005	0.004	0.003
Ag	0.002	0.003	0.003	0.003	0.002	0.003	0.004	0.004	0.005	0.007
Mn	0.001	0.000	0.002	0.002	0.002	0.001	0.002	0.002	0.001	0.001
Co	0.002	0.001	0.001	0.001	0.002	0.002	0.001	0.001	0.001	0.002
Zn	0.007	0.016	0.005	0.007	0.013	0.016	0.008	0.000	0.000	0.000
As	0.010	0.009	0.007	0.007	0.011	0.007	0.013	0.003	0.006	0.007
Cd	0.005	0.005	0.005	0.004	0.004	0.005	0.006	0.002	0.002	0.002
Sb	0.001	0.001	0.001	0.002	0.001	0.001	0.002	0.001	0.001	0.001
S	4.000	4.000	4.000	4.000	4.000	4.000	4.000	4.000	4.000	4.000
Total	**8.715**	**8.733**	**9.232**	**9.344**	**9.059**	**9.093**	**9.443**	**8.724**	**9.081**	**8.593**

Sample	14032	14032	14032	14032	14032	14032	14032	14032	14032	14032
No.	**#20**	**#24**	**#28**	**#29**	**#31**	**#36**	**#41**	**#46**	**#48**	**#59**
Cu	50.490	56.803	51.264	51.293	51.055	49.472	49.067	50.562	49.844	46.230
Fe	17.910	13.621	16.694	15.873	16.461	17.882	18.291	16.714	17.518	18.849
Pb	0.236	0.199	0.221	0.183	0.211	0.181	0.181	0.208	0.249	0.300
Ag	0.181	0.116	0.128	0.162	0.176	0.138	0.157	0.155	0.154	0.173
Mn	0.017	0.014	0.021	0.015	0.017	0.017	0.022	0.022	< 0.01	0.015
Co	0.029	0.027	0.020	0.030	0.023	0.028	0.025	0.022	0.030	0.023
Zn	0.036	0.121	< 0.027	< 0.026	< 0.027	0.057	< 0.026	0.044	0.035	< 0
As	0.104	0.122	0.084	0.088	0.072	0.105	0.108	0.065	0.022	0.040
Cd	0.043	0.097	0.074	0.192	0.086	0.185	0.095	0.076	0.065	0.086
Sb	0.031	0.033	0.025	0.033	0.037	0.041	< 0.020	0.033	0.031	0.030
S	30.802	29.838	30.445	31.701	31.386	31.721	31.534	32.304	31.910	33.866
Total	**99.879**	**101.005**	**98.990**	**99.570**	**99.524**	**99.827**	**99.480**	**100.205**	**99.858**	**99.612**
					Atom-%					
Cu	40.564	38.760	38.975	40.130	39.526	43.487	44.732	40.087	40.805	44.583
Fe	13.759	15.131	14.845	13.563	14.173	12.888	12.138	15.326	14.776	12.627
Pb	0.041	0.051	0.076	0.093	0.108	0.037	0.049	0.046	0.052	0.059
Ag	0.035	0.049	0.036	0.027	0.033	0.036	0.031	0.025	0.033	0.037
Mn	0.013	0.000	0.000	0.013	0.000	0.022	0.021	0.024	0.012	0.020
Co	0.029	0.021	0.021	0.018	0.012	0.016	0.013	0.025	0.017	0.015
Zn	0.000	0.000	0.094	0.076	0.182	0.049	0.070	0.138	0.171	0.088
As	0.056	0.059	0.118	0.111	0.102	0.077	0.075	0.118	0.081	0.134
Cd	0.046	0.037	0.069	0.053	0.052	0.050	0.040	0.042	0.054	0.061
Sb	0.018	0.009	0.013	0.017	0.010	0.010	0.023	0.013	0.010	0.018
S	45.439	45.882	45.754	45.898	45.803	43.326	42.809	44.155	43.990	42.358
Total	**100.000**	**100.000**	**100.000**	**100.000**	**100.000**	**100.000**	**100.000**	**100.000**	**100.000**	**100.000**
					Normalised to 4 S atoms					
Cu	3.571	3.379	3.407	3.497	3.452	4.015	4.180	3.631	3.710	4.210
Fe	1.211	1.319	1.298	1.182	1.238	1.190	1.134	1.388	1.344	1.192
Pb	0.004	0.004	0.007	0.008	0.009	0.003	0.005	0.004	0.005	0.006
Ag	0.003	0.004	0.003	0.002	0.003	0.003	0.003	0.002	0.003	0.004
Mn	0.001	0.000	0.000	0.001	0.000	0.002	0.002	0.002	0.001	0.002
Co	0.003	0.002	0.002	0.002	0.001	0.001	0.001	0.002	0.002	0.001
Zn	0.000	0.000	0.008	0.007	0.016	0.005	0.007	0.013	0.016	0.008
As	0.005	0.005	0.010	0.010	0.009	0.007	0.007	0.011	0.007	0.013
Cd	0.004	0.003	0.006	0.005	0.005	0.005	0.004	0.004	0.005	0.006
Sb	0.002	0.001	0.001	0.001	0.001	0.001	0.002	0.001	0.001	0.002
S	4.000	4.000	4.000	4.000	4.000	4.000	4.000	4.000	4.000	4.000
Total	**8.803**	**8.718**	**8.742**	**8.715**	**8.733**	**9.232**	**9.344**	**9.059**	**9.093**	**9.443**

Sample	14032	14032	11027(1)	11027(1)	11027(1)	11027(1)	11027(1)	11027(1)	11027(1)	11027(1)
No.	**#60**	**#62**	**#1.43**	**#1.48**	**#1.71**	**#1.73**	**#1.74**	**#1.83**	**#1.107**	**#2.20**
Cu	47.194	52.869	50.549	48.504	50.094	48.214	50.953	50.623	52.128	47.390
Fe	17.549	12.839	16.864	17.376	14.961	17.460	13.687	16.748	15.794	19.109
Pb	0.233	0.175	0.223	0.330	0.781	0.244	0.650	0.322	0.297	0.213
Ag	0.147	0.275	0.241	0.313	0.305	0.278	0.265	0.234	0.332	0.315
Mn	< 0	< 0.010	< 0.010	0.017	< 0	0.014	0.020	0.009	0.010	0.019
Co	0.026	0.022	< 0	< 0	< 0	< 0	< 0	< 0	< 0	0.037
Zn	0.036	0.145	0.036	0.039	0.073	0.041	< 0.029	< 0.027	< 0	0.137
As	0.048	0.036	0.065	0.105	0.070	0.027	0.070	< 0.019	< 0.02	0.080
Cd	0.088	0.059	< 0.03	0.031	< 0.029	< 0.036	0.064	0.046	0.036	0.064
Sb	0.029	0.032	< 0.019	< 0.02	< 0.02	< 0	< 0.018	< 0.02	< 0	0.027
S	33.981	33.631	32.368	33.061	32.753	33.470	33.581	31.137	30.941	31.126
Total	**99.345**	**100.083**	**100.346**	**99.776**	**99.037**	**99.748**	**99.290**	**99.119**	**99.538**	**98.517**
					Atom-%					
Cu	42.809	41.782	35.893	48.653	37.671	36.131	37.785	35.786	38.152	38.450
Fe	13.038	13.709	14.482	9.038	14.301	14.728	12.841	14.746	11.662	14.475
Pb	0.058	0.111	0.082	0.033	0.051	0.075	0.181	0.056	0.149	0.075
Ag	0.030	0.030	0.203	0.044	0.106	0.137	0.136	0.122	0.117	0.105
Mn	0.021	0.017	0.018	0.000	0.000	0.015	0.000	0.012	0.017	0.008
Co	0.021	0.014	0.026	0.020	0.000	0.000	0.000	0.000	0.000	0.000
Zn	0.067	0.000	0.000	0.000	0.026	0.028	0.053	0.030	0.000	0.000
As	0.067	0.029	0.117	0.042	0.041	0.066	0.045	0.017	0.044	0.000
Cd	0.040	0.049	0.019	0.038	0.000	0.013	0.000	0.000	0.027	0.020
Sb	0.018	0.013	0.000	0.000	0.000	0.000	0.000	0.000	0.000	0.000
S	43.831	44.246	49.159	42.131	47.804	48.806	48.960	49.232	49.831	46.868
Total	**100.000**	**100.000**	**100.000**	**100.000**	**100.000**	**100.000**	**100.000**	**100.000**	**100.000**	**100.000**
					Normalised to 4 S atoms					
Cu	3.907	3.777	2.921	4.619	3.152	2.961	3.087	2.908	3.063	3.282
Fe	1.190	1.239	1.178	0.858	1.197	1.207	1.049	1.198	0.936	1.235
Pb	0.005	0.010	0.007	0.003	0.004	0.006	0.015	0.005	0.012	0.006
Ag	0.003	0.003	0.017	0.004	0.009	0.011	0.011	0.010	0.009	0.009
Mn	0.002	0.002	0.001	0.000	0.000	0.001	0.000	0.001	0.001	0.001
Co	0.002	0.001	0.002	0.002	0.000	0.000	0.000	0.000	0.000	0.000
Zn	0.006	0.000	0.000	0.000	0.002	0.002	0.004	0.002	0.000	0.000
As	0.006	0.003	0.010	0.004	0.003	0.005	0.004	0.001	0.004	0.000
Cd	0.004	0.004	0.002	0.004	0.000	0.001	0.000	0.000	0.002	0.002
Sb	0.002	0.001	0.000	0.000	0.000	0.000	0.000	0.000	0.000	0.000
S	4.000	4.000	4.000	4.000	4.000	4.000	4.000	4.000	4.000	4.000
Total	**9.126**	**9.040**	**8.137**	**9.494**	**8.367**	**8.196**	**8.170**	**8.125**	**8.027**	**8.535**

Sample	11027(1)	11027(1)	11027(1)	11027(1)	11027(1)	11027(1)	11027(1)	11027(2)	11027(2)	11027(2)
No.	**#2.25**	**#2.26**	**#2.27**	**#2.32**	**#2.50**	**#2.52**	**#2.53**	**#1.122**	**#1.123**	**#2.23**
Cu	48.117	55.053	50.350	50.016	61.496	52.575	52.749	49.905	46.959	49.928
Fe	18.101	12.461	17.409	17.831	9.923	16.400	16.331	14.678	17.019	13.790
Pb	0.228	0.176	0.252	0.223	0.796	0.301	0.273	0.182	0.281	0.137
Ag	0.328	0.503	0.195	0.209	0.183	0.162	0.194	0.334	0.236	0.298
Mn	0.020	< 0.01	0.014	< 0.01	0.013	0.023	< 0.01	< 0	0.016	0.019
Co	0.033	0.015	0.029	0.043	0.021	0.029	0.029	< 0	< 0	0.020
Zn	< 0.027	0.123	< 0.028	0.043	< 0.028	0.035	< 0.028	0.067	0.051	< 0.027
As	0.072	0.081	< 0.019	< 0	0.050	0.033	0.059	0.158	0.075	0.102
Cd	0.087	0.098	0.054	0.036	0.030	< 0.026	< 0.026	< 0.033	0.052	0.052
Sb	0.035	0.024	0.035	0.024	0.030	0.041	< 0.019	< 0	< 0.02	0.041
S	31.221	30.386	30.696	31.173	26.681	28.888	29.260	34.815	34.055	33.718
Total	**98.242**	**98.920**	**99.034**	**99.598**	**99.223**	**98.487**	**98.912**	**100.139**	**98.744**	**98.105**
					Atom-%					
Cu	39.570	36.070	36.720	42.325	38.353	37.777	48.757	40.814	40.702	36.680
Fe	13.642	16.550	15.718	10.901	15.090	15.325	8.952	14.487	14.339	12.276
Pb	0.069	0.050	0.053	0.041	0.059	0.052	0.194	0.072	0.065	0.041
Ag	0.148	0.141	0.147	0.228	0.088	0.093	0.085	0.074	0.088	0.145
Mn	0.009	0.017	0.018	0.000	0.012	0.000	0.012	0.021	0.000	0.000
Co	0.000	0.030	0.027	0.012	0.024	0.035	0.018	0.024	0.024	0.000
Zn	0.000	0.101	0.000	0.092	0.000	0.032	0.000	0.026	0.000	0.048
As	0.000	0.052	0.047	0.053	0.000	0.000	0.034	0.022	0.039	0.098
Cd	0.015	0.028	0.038	0.043	0.023	0.015	0.013	0.000	0.000	0.000
Sb	0.000	0.011	0.014	0.010	0.014	0.009	0.012	0.017	0.000	0.000
S	46.546	46.951	47.218	46.296	46.338	46.661	41.923	44.443	44.744	50.712
Total	**100.000**	**100.000**	**100.000**	**100.000**	**100.000**	**100.000**	**100.000**	**100.000**	**100.000**	**100.000**
					Normalised to 4 S atoms					
Cu	3.400	3.073	3.111	3.657	3.311	3.238	4.652	3.673	3.639	2.893
Fe	1.172	1.410	1.332	0.942	1.303	1.314	0.854	1.304	1.282	0.968
Pb	0.006	0.004	0.005	0.004	0.005	0.004	0.018	0.006	0.006	0.003
Ag	0.013	0.012	0.012	0.020	0.008	0.008	0.008	0.007	0.008	0.011
Mn	0.001	0.001	0.001	0.000	0.001	0.000	0.001	0.002	0.000	0.000
Co	0.000	0.003	0.002	0.001	0.002	0.003	0.002	0.002	0.002	0.000
Zn	0.000	0.009	0.000	0.008	0.000	0.003	0.000	0.002	0.000	0.004
As	0.000	0.004	0.004	0.005	0.000	0.000	0.003	0.002	0.003	0.008
Cd	0.001	0.002	0.003	0.004	0.002	0.001	0.001	0.000	0.000	0.000
Sb	0.000	0.001	0.001	0.001	0.001	0.001	0.001	0.001	0.000	0.000
S	4.000	4.000	4.000	4.000	4.000	4.000	4.000	4.000	4.000	4.000
Total	**8.594**	**8.520**	**8.471**	**8.640**	**8.632**	**8.572**	**9.541**	**9.000**	**8.940**	**7.888**

Sample	11027(2)	11027(2)	11027(2)	11027(2)	11029(3)	11029(3)	11029(5)	11029(5)	11029(5)	11029(5)
No.	**#2.24**	**#2.25**	**#2.26**	**#2.29**	**#25**	**#28**	**#1.26**	**#1.30**	**#1.33**	**#1.34**
Cu	49.251	45.332	46.819	47.308	49.803	56.044	53.938	62.467	54.643	56.330
Fe	14.574	18.496	17.273	16.149	17.905	13.857	16.375	10.196	15.888	14.450
Pb	0.626	0.238	0.198	0.217	0.437	0.444	0.349	0.641	0.251	0.206
Ag	0.231	0.243	0.264	0.449	0.196	0.244	0.081	0.038	0.129	0.125
Mn	0.017	0.018	< 0.011	0.017	0.027	0.011	0.054	0.091	0.024	0.020
Co	0.031	0.025	0.031	0.029	0.033	0.024	0.033	< 0.011	0.028	0.027
Zn	< 0.028	0.027	0.029	< 0.027	0.414	< 0.026	0.092	< 0.029	< 0	< 0.029
As	< 0.019	0.163	0.125	0.086	< 0	0.080	0.131	0.185	0.126	0.090
Cd	0.032	< 0.027	0.050	0.068	< 0.026	0.036	0.031	0.081	0.033	0.050
Sb	0.035	0.036	0.035	0.022	0.024	0.040	< 0.019	< 0.019	< 0	< 0.019
S	33.630	34.161	33.880	33.810	29.423	28.122	29.157	27.294	29.461	29.085
Total	**98.427**	**98.739**	**98.704**	**98.155**	**98.262**	**98.902**	**100.241**	**100.993**	**100.583**	**100.383**
					Atom-%					
Cu	34.992	37.585	37.059	33.698	34.927	35.518	38.542	43.794	41.229	48.542
Fe	14.431	11.812	12.478	15.645	14.663	13.796	15.767	12.321	14.243	9.016
Pb	0.064	0.032	0.144	0.054	0.045	0.050	0.104	0.106	0.082	0.153
Ag	0.104	0.132	0.102	0.106	0.116	0.199	0.089	0.112	0.036	0.017
Mn	0.014	0.017	0.015	0.015	0.000	0.015	0.024	0.010	0.048	0.082
Co	0.000	0.016	0.025	0.020	0.025	0.023	0.028	0.020	0.027	0.000
Zn	0.037	0.000	0.000	0.019	0.021	0.000	0.311	0.000	0.068	0.000
As	0.047	0.065	0.000	0.103	0.079	0.055	0.000	0.053	0.085	0.122
Cd	0.022	0.022	0.014	0.000	0.021	0.029	0.000	0.016	0.013	0.036
Sb	0.000	0.016	0.014	0.014	0.014	0.009	0.010	0.016	0.000	0.000
S	50.290	50.303	50.149	50.325	50.089	50.306	45.125	43.550	44.168	42.033
Total	**100.000**	**100.000**	**100.000**	**100.000**	**100.000**	**100.000**	**100.000**	**100.000**	**100.000**	**100.000**
					Normalised to 4 S atoms					
Cu	2.783	2.989	2.956	2.678	2.789	2.824	3.416	4.022	3.734	4.619
Fe	1.148	0.939	0.995	1.244	1.171	1.097	1.398	1.132	1.290	0.858
Pb	0.005	0.003	0.012	0.004	0.004	0.004	0.009	0.010	0.007	0.015
Ag	0.008	0.011	0.008	0.008	0.009	0.016	0.008	0.010	0.003	0.002
Mn	0.001	0.001	0.001	0.001	0.000	0.001	0.002	0.001	0.004	0.008
Co	0.000	0.001	0.002	0.002	0.002	0.002	0.002	0.002	0.002	0.000
Zn	0.003	0.000	0.000	0.002	0.002	0.000	0.028	0.000	0.006	0.000
As	0.004	0.005	0.000	0.008	0.006	0.004	0.000	0.005	0.008	0.012
Cd	0.002	0.002	0.001	0.000	0.002	0.002	0.000	0.001	0.001	0.003
Sb	0.000	0.001	0.001	0.001	0.001	0.001	0.001	0.001	0.000	0.000
S	4.000	4.000	4.000	4.000	4.000	4.000	4.000	4.000	4.000	4.000
Total	**7.954**	**7.952**	**7.976**	**7.948**	**7.986**	**7.951**	**8.864**	**9.185**	**9.056**	**9.516**

Sample	11029(5)	11029(5)	11029(5)	11029(5)	11029(5)	11029(5)	11029(5)	11029(5)	11029(5)	11029(5)
No.	**#1.36**	**#1.43**	**#1.44**	**#1.45**	**#1.47**	**#1.48**	**#2.14**	**#2.20**	**#2.23**	**#2.29**
Cu	69.293	58.180	57.106	51.682	59.907	56.893	55.577	50.728	60.075	59.436
Fe	5.146	12.387	12.060	16.625	11.266	13.351	14.350	17.405	9.836	10.916
Pb	0.820	0.660	0.782	0.272	0.200	0.279	0.259	0.404	0.255	0.206
Ag	0.201	0.083	0.127	0.074	0.133	0.136	0.083	0.075	0.101	0.115
Mn	0.018	0.020	0.010	0.020	< 0.008	0.016	0.017	0.028	0.015	< 0.011
Co	< 0.01	0.028	0.019	0.030	0.028	0.024	0.022	0.026	0.014	0.025
Zn	< 0	0.105	< 0	< 0.022	< 0	< 0	< 0	< 0.027	0.046	< 0.027
As	0.180	0.175	0.080	0.077	0.079	0.063	0.036	< 0.016	< 0	0.025
Cd	< 0.027	0.033	0.041	0.036	0.062	0.044	0.107	0.029	0.062	0.074
Sb	< 0.020	< 0	< 0.020	< 0.020	< 0.017	< 0.020	0.027	< 0.019	< 0.019	0.033
S	25.770	28.819	29.072	31.020	28.896	29.857	28.945	29.863	27.670	27.779
Total	**101.428**	**100.509**	**99.297**	**99.836**	**100.571**	**100.663**	**99.423**	**98.558**	**98.074**	**98.609**
					Atom-%					
Cu	41.571	43.097	54.664	44.767	44.309	39.052	45.989	43.250	42.902	39.034
Fe	13.754	12.580	4.619	10.846	10.648	14.294	9.841	11.549	12.605	15.239
Pb	0.059	0.048	0.198	0.156	0.186	0.063	0.047	0.065	0.061	0.095
Ag	0.058	0.056	0.093	0.038	0.058	0.033	0.060	0.061	0.038	0.034
Mn	0.021	0.018	0.016	0.018	0.009	0.017	0.000	0.014	0.015	0.025
Co	0.023	0.022	0.000	0.023	0.016	0.024	0.023	0.020	0.018	0.022
Zn	0.000	0.000	0.000	0.078	0.000	0.000	0.000	0.000	0.000	0.000
As	0.081	0.058	0.120	0.114	0.053	0.049	0.051	0.041	0.024	0.000
Cd	0.014	0.022	0.000	0.014	0.018	0.015	0.027	0.019	0.047	0.013
Sb	0.000	0.000	0.000	0.000	0.000	0.000	0.000	0.000	0.011	0.000
S	44.419	44.099	40.288	43.946	44.704	46.451	43.961	44.981	44.280	45.539
Total	**100.000**	**100.000**	**100.000**	**100.000**	**100.000**	**100.000**	**100.000**	**100.000**	**100.000**	**100.000**
					Normalised to 4 S atoms					
Cu	3.744	3.909	5.427	4.075	3.965	3.363	4.184	3.846	3.875	3.429
Fe	1.239	1.141	0.459	0.987	0.953	1.231	0.895	1.027	1.139	1.339
Pb	0.005	0.004	0.020	0.014	0.017	0.005	0.004	0.006	0.006	0.008
Ag	0.005	0.005	0.009	0.003	0.005	0.003	0.005	0.005	0.003	0.003
Mn	0.002	0.002	0.002	0.002	0.001	0.002	0.000	0.001	0.001	0.002
Co	0.002	0.002	0.000	0.002	0.001	0.002	0.002	0.002	0.002	0.002
Zn	0.000	0.000	0.000	0.007	0.000	0.000	0.000	0.000	0.000	0.000
As	0.007	0.005	0.012	0.010	0.005	0.004	0.005	0.004	0.002	0.000
Cd	0.001	0.002	0.000	0.001	0.002	0.001	0.002	0.002	0.004	0.001
Sb	0.000	0.000	0.000	0.000	0.000	0.000	0.000	0.000	0.001	0.000
S	4.000	4.000	4.000	4.000	4.000	4.000	4.000	4.000	4.000	4.000
Total	**9.005**	**9.071**	**9.928**	**9.102**	**8.948**	**8.611**	**9.099**	**8.893**	**9.033**	**8.784**

Sample	11029(5)	11029(5)	11029(5)	11029(5)	11029(5)	11029(5)	11029(5)	10024(4)	10024(4)	10024(4)
No.	**#2.31**	**#2.36**	**#2.38**	**#2.41**	**#2.43**	**#2.48**	**#2.52**	**#1.88**	**#1.100**	**#2.47**
Cu	54.295	58.566	50.387	50.420	59.791	51.321	58.275	57.830	48.784	62.281
Fe	14.993	11.637	17.733	17.445	10.508	16.806	12.414	12.667	17.298	10.168
Pb	0.195	0.407	0.221	0.248	0.184	0.237	0.177	0.189	0.364	0.137
Ag	0.105	0.074	0.113	0.098	0.152	0.098	0.126	0.160	0.468	0.095
Mn	0.019	0.026	0.026	0.014	0.012	0.020	0.013	0.010	0.021	< 0.013
Co	0.021	< 0.011	0.022	0.025	0.013	0.019	0.012	0.015	0.033	0.024
Zn	< 0	< 0	< 0.027	< 0.027	< 0.029	< 0.038	< 0	< 0	< 0.027	< 0.035
As	0.041	0.033	0.047	0.071	0.141	0.058	0.100	0.138	0.188	0.063
Cd	0.044	0.046	0.060	0.077	0.133	0.050	0.038	< 0.028	0.045	0.087
Sb	0.032	0.033	0.024	0.019	0.045	0.042	0.032	< 0	< 0.02	< 0.023
S	29.446	28.189	30.490	30.680	27.571	30.218	28.870	30.018	33.714	27.214
Total	**99.191**	**99.011**	**99.123**	**99.097**	**98.550**	**98.869**	**100.057**	**101.027**	**100.915**	**100.069**
					Atom-%					
Cu	47.545	46.746	41.780	45.775	38.386	38.382	47.161	42.809	41.782	43.801
Fe	8.858	9.769	13.128	10.350	15.372	15.111	9.431	13.038	13.709	10.917
Pb	0.062	0.050	0.046	0.098	0.052	0.058	0.045	0.058	0.111	0.044
Ag	0.047	0.053	0.048	0.034	0.051	0.044	0.071	0.030	0.030	0.071
Mn	0.014	0.000	0.017	0.024	0.023	0.012	0.011	0.021	0.017	0.009
Co	0.012	0.021	0.017	0.000	0.018	0.021	0.011	0.021	0.014	0.012
Zn	0.035	0.000	0.000	0.000	0.000	0.000	0.000	0.067	0.000	0.000
As	0.000	0.017	0.027	0.022	0.030	0.046	0.094	0.067	0.029	0.089
Cd	0.028	0.033	0.019	0.020	0.026	0.033	0.059	0.040	0.049	0.000
Sb	0.000	0.014	0.013	0.013	0.010	0.008	0.019	0.018	0.013	0.000
S	43.399	43.298	44.905	43.664	46.033	46.285	43.098	43.831	44.246	45.057
Total	**100.000**	**100.000**	**100.000**	**100.000**	**100.000**	**100.000**	**100.000**	**100.000**	**100.000**	**100.000**
					Normalised to 4 S atoms					
Cu	4.382	4.319	3.722	4.193	3.336	3.317	4.377	3.907	3.777	3.888
Fe	0.816	0.903	1.169	0.948	1.336	1.306	0.875	1.190	1.239	0.969
Pb	0.006	0.005	0.004	0.009	0.004	0.005	0.004	0.005	0.010	0.004
Ag	0.004	0.005	0.004	0.003	0.004	0.004	0.007	0.003	0.003	0.006
Mn	0.001	0.000	0.002	0.002	0.002	0.001	0.001	0.002	0.002	0.001
Co	0.001	0.002	0.002	0.000	0.002	0.002	0.001	0.002	0.001	0.001
Zn	0.003	0.000	0.000	0.000	0.000	0.000	0.000	0.006	0.000	0.000
As	0.000	0.002	0.002	0.002	0.003	0.004	0.009	0.006	0.003	0.008
Cd	0.003	0.003	0.002	0.002	0.002	0.003	0.006	0.004	0.004	0.000
Sb	0.000	0.001	0.001	0.001	0.001	0.001	0.002	0.002	0.001	0.000
S	4.000	4.000	4.000	4.000	4.000	4.000	4.000	4.000	4.000	4.000
Total	**9.217**	**9.238**	**8.908**	**9.161**	**8.689**	**8.642**	**9.281**	**9.126**	**9.040**	**8.878**

Sample	10-1B	10-1B	10-1B
No.	**#32**	**#54**	**#55**
Cu	51.406	52.561	51.845
Fe	17.207	15.611	16.337
Pb	0.326	0.398	0.463
Ag	0.081	0.061	0.073
Mn	< 0.009	0.015	< 0.008
Co	0.026	0.022	0.014
Zn	0.127	0.102	0.246
As	0.183	0.171	0.157
Cd	0.160	0.123	0.120
Sb	0.034	0.043	0.024
S	30.451	30.334	30.315
Total	**100.001**	**99.441**	**99.594**
	Atom-%		
Cu	38.975	40.130	38.975
Fe	14.845	13.563	14.845
Pb	0.076	0.093	0.076
Ag	0.036	0.027	0.036
Mn	0.000	0.013	0.000
Co	0.021	0.018	0.021
Zn	0.094	0.076	0.094
As	0.118	0.111	0.118
Cd	0.069	0.053	0.069
Sb	0.013	0.017	0.013
S	45.754	45.898	45.754
Total	**100.000**	**100.000**	**100.000**
	Normalised to 4 S atoms		
Cu	3.407	3.497	3.407
Fe	1.298	1.182	1.298
Pb	0.007	0.008	0.007
Ag	0.003	0.002	0.003
Mn	0.000	0.001	0.000
Co	0.002	0.002	0.002
Zn	0.008	0.007	0.008
As	0.010	0.010	0.010
Cd	0.006	0.005	0.006
Sb	0.001	0.001	0.001
S	4.000	4.000	4.000
Total	**8.742**	**8.715**	**8.742**

Table iv.98.: EMP analyses of segregated bornite *ss* from matte s.s.

Sample	10-2B	11029(3)	11029(3)	11029(3)	11029(3)	10024(4)	10-1B	10-1B
No.	#110	#3	#5	#21	#26	#2.2	#42	#59
Cu	59.250	53.640	60.489	50.075	57.317	50.226	52.123	54.794
Fe	12.007	15.150	10.611	17.992	11.683	15.007	15.837	12.971
Pb	0.326	0.272	0.332	0.309	1.511	0.220	0.339	2.631
Ag	0.053	0.226	0.253	0.196	0.185	0.237	0.042	0.074
Mn	0.011	< 0.010	0.015	0.013	0.022	0.019	< 0.009	0.009
Co	0.026	0.025	0.016	0.015	0.023	0.030	0.023	0.030
Zn	0.039	< 0.028	< 0.029	< 0.027	< 0.029	0.041	0.046	0.493
As	0.045	0.045	0.055	< 0	0.032	< 0	0.117	0.058
Cd	0.082	0.078	0.030	0.036	0.036	0.041	0.179	0.198
Sb	0.038	0.033	0.055	0.029	0.042	0.034	0.037	0.031
S	27.217	29.205	26.502	30.042	27.323	33.180	30.020	28.576
Total	**99.131**	**98.674**	**98.358**	**98.707**	**98.191**	**99.035**	**98.763**	**99.865**
				Atom-%				
Cu	46.578	41.549	48.213	38.412	45.682	37.651	40.078	42.897
Fe	10.741	13.353	9.624	15.705	10.595	12.801	13.856	11.555
Pb	0.079	0.065	0.081	0.073	0.369	0.051	0.080	0.632
Ag	0.025	0.103	0.119	0.089	0.087	0.105	0.019	0.034
Mn	0.010	0.000	0.014	0.012	0.020	0.016	0.000	0.008
Co	0.022	0.021	0.014	0.012	0.020	0.024	0.019	0.025
Zn	0.030	0.000	0.000	0.000	0.000	0.030	0.034	0.375
As	0.030	0.030	0.037	0.000	0.022	0.000	0.076	0.039
Cd	0.036	0.034	0.014	0.016	0.016	0.017	0.078	0.088
Sb	0.016	0.013	0.023	0.012	0.017	0.013	0.015	0.013
S	42.403	44.832	41.862	45.670	43.156	49.292	45.745	44.335
Total	**100.000**	**100.000**	**100.000**	**100.000**	**100.000**	**100.000**	**100.000**	**100.000**
				Normalised to 4 S atoms				
Cu	4.394	3.707	4.607	3.364	4.234	3.055	3.504	3.870
Fe	1.013	1.191	0.920	1.375	0.982	1.039	1.212	1.043
Pb	0.007	0.006	0.008	0.006	0.034	0.004	0.007	0.057
Ag	0.002	0.009	0.011	0.008	0.008	0.008	0.002	0.003
Mn	0.001	0.000	0.001	0.001	0.002	0.001	0.000	0.001
Co	0.002	0.002	0.001	0.001	0.002	0.002	0.002	0.002
Zn	0.003	0.000	0.000	0.000	0.000	0.002	0.003	0.034
As	0.003	0.003	0.004	0.000	0.002	0.000	0.007	0.003
Cd	0.003	0.003	0.001	0.001	0.002	0.001	0.007	0.008
Sb	0.001	0.001	0.002	0.001	0.002	0.001	0.001	0.001
S	4.000	4.000	4.000	4.000	4.000	4.000	4.000	4.000
Total	**9.433**	**8.922**	**9.555**	**8.758**	**9.269**	**8.115**	**8.744**	**9.022**

Table iv.99.: EMP analyses of eutectoid bornite *ss* from matte s.s.

Sample	10032(4)	10024(4)	10024(4)	10024(4)	10024(4)	10024(4)	10024(4)
No.	**#47**	**#1.33**	**#1.34**	**#1.37**	**#1.40**	**#1.147**	**#1.148**
Fe	35.600	39.855	39.568	40.065	31.294	38.834	34.829
Cu	26.083	21.687	20.643	22.843	30.094	23.278	18.476
Zn	0.362	2.417	1.816	0.820	1.840	1.918	10.615
Pb	1.085	0.127	0.170	0.132	0.192	0.108	0.150
Mn	0.044	0.135	0.138	0.138	0.128	0.149	0.275
Co	0.053	0.081	0.086	0.070	0.062	0.075	0.070
Ni	< 0	0.083	0.087	0.063	0.043	0.068	0.047
Ag	< 0.017	< 0	< 0.016	< 0	0.586	< 0.016	0.146
Cd	< 0.026	0.035	0.056	0.058	0.048	0.038	< 0
S	34.293	35.730	35.101	35.474	33.522	35.429	34.857
Total	**97.543**	**100.150**	**97.665**	**99.663**	**97.809**	**99.897**	**99.465**
			Atom-%				
Fe	29.927	32.258	32.763	32.586	26.452	31.581	28.703
Cu	19.270	15.426	15.021	16.327	22.355	16.636	13.381
Zn	0.260	1.670	1.284	0.569	1.328	1.332	7.469
Pb	0.246	0.028	0.038	0.029	0.044	0.024	0.033
Mn	0.038	0.111	0.116	0.114	0.110	0.123	0.230
Co	0.042	0.062	0.067	0.054	0.050	0.058	0.055
Ni	0.000	0.064	0.069	0.049	0.035	0.053	0.037
Ag	0.000	0.000	0.000	0.000	0.256	0.000	0.062
Cd	0.000	0.014	0.023	0.023	0.020	0.015	0.000
S	50.209	50.367	50.619	50.249	49.350	50.179	50.030
Total	**100.000**	**100.000**	**100.000**	**100.000**	**100.000**	**100.000**	**100.000**
			Normalised to 3 S atoms				
Fe	1.788	1.921	1.942	1.945	1.608	1.888	1.721
Cu	1.151	0.919	0.890	0.975	1.359	0.995	0.802
Zn	0.016	0.099	0.076	0.034	0.081	0.080	0.448
Pb	0.015	0.002	0.002	0.002	0.003	0.001	0.002
Mn	0.002	0.007	0.007	0.007	0.007	0.007	0.014
Co	0.003	0.004	0.004	0.003	0.003	0.003	0.003
Ni	0.000	0.004	0.004	0.003	0.002	0.003	0.002
Ag	0.000	0.000	0.000	0.000	0.016	0.000	0.004
Cd	0.000	0.001	0.001	0.001	0.001	0.001	0.000
S	3.000	3.000	3.000	3.000	3.000	3.000	3.000
Total	**5.975**	**5.956**	**5.927**	**5.970**	**6.079**	**5.979**	**5.996**

Table iv.100.: EMP analyses of iss droplets in slag [10032(4)] and segregated iss from matte s.s. [10024(4)].

Sample	10024(5)	10024(5)	11027(1)	11027(1)	11027(1)	11027(1)	11027(1)	11027(1)	11027(1)	10024(4)
No.	**#115**	**#185**	**#45**	**#46**	**#62**	**#63**	**#104**	**#106**	**#109**	**#58**
Cu	47.851	57.283	57.421	57.315	60.417	61.744	63.530	64.835	61.081	50.893
Fe	< 0.017	0.049	2.105	4.046	1.798	1.260	0.350	0.551	0.293	7.725
Pb	22.197	11.494	8.508	5.858	3.755	3.003	3.933	2.589	6.468	9.045
Ag	0.258	0.277	0.269	0.142	0.171	0.166	0.307	0.369	0.350	0.316
Mn	0.013	< 0.007	0.017	0.024	0.013	< 0.007	0.010	0.014	0.017	0.026
Zn	< 0	< 0	< 0.029	0.106	0.138	0.031	< 0	< 0	< 0.030	< 0.028
As	1.337	0.501	0.155	0.069	0.022	0.108	< 0	< 0	< 0	0.044
Cd	0.032	0.071	< 0.030	0.048	< 0	0.044	< 0.031	0.035	< 0.031	0.106
Sb	0.073	0.412	< 0.020	0.086	0.053	0.054	< 0.018	< 0	< 0.019	< 0.019
S	24.440	27.528	29.709	29.582	31.446	32.117	31.781	30.315	31.204	28.752
Total	**96.201**	**97.615**	**98.184**	**97.276**	**97.813**	**98.527**	**99.911**	**98.708**	**99.413**	**96.907**
					Atom-%					
Cu	45.812	49.271	47.217	46.717	47.863	48.230	49.513	51.218	48.684	42.499
Fe	0.000	0.048	1.970	3.753	1.621	1.120	0.310	0.495	0.266	7.340
Pb	6.518	3.032	2.146	1.464	0.912	0.719	0.940	0.627	1.581	2.316
Ag	0.146	0.140	0.130	0.068	0.080	0.076	0.141	0.172	0.164	0.155
Mn	0.014	0.000	0.016	0.023	0.012	0.000	0.009	0.013	0.016	0.025
Zn	0.000	0.000	0.000	0.084	0.106	0.024	0.000	0.000	0.000	0.000
As	1.086	0.365	0.108	0.048	0.015	0.072	0.000	0.000	0.000	0.031
Cd	0.017	0.035	0.000	0.022	0.000	0.019	0.000	0.016	0.000	0.050
Sb	0.036	0.185	0.000	0.037	0.022	0.022	0.000	0.000	0.000	0.000
S	46.371	46.924	48.414	47.785	49.370	49.718	49.087	47.460	49.289	47.582
Total	**100.000**	**100.000**	**100.000**	**100.000**	**100.000**	**100.000**	**100.000**	**100.000**	**100.000**	**100.000**
					Normalised to 1 S atom					
Cu	0.988	1.050	0.975	0.978	0.969	0.970	1.009	1.079	0.988	0.893
Fe	0.000	0.001	0.041	0.079	0.033	0.023	0.006	0.010	0.005	0.154
Pb	0.141	0.065	0.044	0.031	0.018	0.014	0.019	0.013	0.032	0.049
Ag	0.003	0.003	0.003	0.001	0.002	0.002	0.003	0.004	0.003	0.003
Mn	0.000	0.000	0.000	0.000	0.000	0.000	0.000	0.000	0.000	0.001
Zn	0.000	0.000	0.000	0.002	0.002	0.000	0.000	0.000	0.000	0.000
As	0.023	0.008	0.002	0.001	0.000	0.001	0.000	0.000	0.000	0.001
Cd	0.000	0.001	0.000	0.000	0.000	0.000	0.000	0.000	0.000	0.001
Sb	0.001	0.004	0.000	0.001	0.000	0.000	0.000	0.000	0.000	0.000
S	1.000	1.000	1.000	1.000	1.000	1.000	1.000	1.000	1.000	1.000
Total	**2.157**	**2.131**	**2.066**	**2.093**	**2.026**	**2.011**	**2.037**	**2.107**	**2.029**	**2.102**

Table iv.101.: EMP analyses of secondary covellite from Pb-Cu matte [10024(5)] and matte s.s. [11027(1), 10024(4)].

Sample	**10021(2)**	**10021(21)**	**10021(21)**	**10021(21)**	**10021(21)**	**10021(21)**	**10021(21)**	**10021(21)**	**10021(21)**	**10021(21)**
No.	**#85**	**#1.65**	**#1.68**	**#2.92**	**#2.93**	**#2.94**	**#2.95**	**#2.96**	**#2.97**	**#2.98**
Fe	40.092	57.884	51.838	59.417	62.153	61.000	52.339	54.647	57.203	59.998
Cu	0.930	1.086	0.928	2.939	0.530	0.461	3.186	2.302	0.744	0.663
Zn	20.790	1.073	0.051	1.333	0.275	0.080	0.325	1.111	1.311	0.715
Pb	2.713	2.406	13.105	7.671	3.020	2.710	9.695	10.709	7.275	3.583
Mn	0.112	0.080	0.033	0.089	0.083	0.061	0.078	0.129	0.099	0.091
Co	0.068	0.091	0.084	0.094	0.101	0.088	0.081	0.084	0.098	0.087
Cd	< 0	0.111	< 0.029	0.308	0.251	0.218	0.094	0.427	0.079	0.215
Sn	< 0.025	0.069	< 0.028	0.736	0.099	0.085	0.252	0.134	0.205	0.076
Sb	< 0	< 0	0.067	0.082	0.028	0.031	0.047	0.048	0.087	0.073
S	32.426	33.506	30.997	24.801	30.742	30.752	30.274	29.563	30.622	32.708
Total	**97.131**	**96.306**	**97.103**	**97.470**	**97.282**	**95.486**	**96.371**	**99.154**	**97.723**	**98.209**
					Atomic %					
Fe	34.549	48.637	46.973	54.453	52.864	52.554	47.111	48.575	49.899	50.219
Cu	0.704	0.802	0.739	2.367	0.396	0.349	2.520	1.798	0.570	0.488
Zn	15.296	0.770	0.039	1.043	0.200	0.059	0.250	0.843	0.976	0.511
Pb	0.630	0.545	3.201	1.895	0.692	0.629	2.352	2.566	1.710	0.808
Mn	0.098	0.068	0.030	0.083	0.072	0.053	0.071	0.117	0.088	0.077
Co	0.056	0.072	0.072	0.082	0.081	0.072	0.069	0.071	0.081	0.069
Cd	0.000	0.046	0.000	0.140	0.106	0.093	0.042	0.189	0.034	0.089
Sn	0.000	0.027	0.000	0.317	0.040	0.034	0.107	0.056	0.084	0.030
Sb	0.000	0.000	0.028	0.034	0.011	0.012	0.019	0.020	0.035	0.028
S	48.666	49.032	48.918	39.585	45.539	46.143	47.459	45.767	46.522	47.680
Total	**100.000**	**100.000**	**100.000**	**100.000**	**100.000**	**100.000**	**100.000**	**100.000**	**100.000**	**100.000**

Table iv.102.: EMP analyses of base metal sulphide melt.

Sample	**10021(2)**	**10021(2)**	**10021(2)**	**10021(2)**	**10021(2)**	**10024(4)**	**10024(4)**	**10024(4)**	**10024(4)**	**10024(4)**	**10024(4)**	**10024(4)**	**10024(4)**	**10024(4)**	**10024(4)**	**10-1B**
No.	**#2.110**	**#2.112**	**#2.115**	**#2.125**	**#2.126**	**#1.41**	**#1.47**	**#1.51**	**#1.52**	**#1.63**	**#1.64**	**#1.78**	**#1.83**	**#2.26**	**#2.35**	**#79**
FeO	88.000	88.462	89.146	88.799	88.957	88.693	89.545	88.531	85.236	89.342	89.906	89.623	89.362	91.006	90.669	90.092
MnO	0.278	0.265	0.275	0.222	0.267	1.453	0.671	0.766	0.465	0.714	0.706	0.896	0.915	1.073	0.941	0.258
CoO	0.161	0.137	0.142	0.158	0.145	0.150	0.150	0.141	0.132	0.146	0.149	0.165	0.146	0.155	0.125	0.140
CuO	<0	0.043	0.063	<0	<0	0.493	0.224	0.334	0.378	0.134	0.144	0.193	0.166	0.176	0.562	0.176
ZnO	0.923	0.533	0.442	0.587	0.546	0.563	0.442	0.332	0.597	0.366	0.380	0.375	0.387	0.352	0.309	0.748
Total	**89.362**	**89.439**	**90.068**	**89.766**	**89.915**	**91.352**	**91.032**	**90.104**	**86.809**	**90.702**	**91.285**	**91.252**	**90.977**	**92.763**	**92.606**	**91.414**

Table iv.103.: EMP analyses of Fe-rich oxides from Fe oxide clusters [10021(2)] and from matte s.s. [10024(4), 10-1B].

Sample	11029(7)	11029(7)	11029(7)	11029(7)	11029(7)	11029(7)	11029(7)
No.	**#75**	**#77**	**#83**	**#85**	**#86**	**#88**	**#91**
Fe	87.861	87.115	87.499	87.081	87.889	87.563	87.688
As	9.131	9.636	9.876	9.769	9.580	9.787	9.963
Cu	0.916	0.864	0.819	0.890	0.874	0.876	0.884
Mn	0.015	0.029	0.028	< 0.012	0.012	0.023	0.019
Co	0.174	0.165	0.179	0.178	0.179	0.164	0.176
Ni	0.054	0.051	0.058	0.053	0.047	0.056	0.058
Zn	0.053	0.037	0.042	0.031	0.034	0.027	0.041
Sn	0.149	0.154	0.151	0.144	0.143	0.177	0.154
Pb	< 0.051	< 0.052	< 0.048	< 0.051	0.001	< 0.046	< 0.049
S	0.013	0.006	< 0.006	0.009	0.009	0.018	< 0.006
Total	**98.366**	**98.057**	**98.652**	**98.155**	**98.768**	**98.691**	**98.983**
			Atom-%				
Fe	91.674	91.311	91.203	91.210	91.422	91.215	91.115
As	7.102	7.529	7.673	7.627	7.428	7.599	7.717
Cu	0.839	0.795	0.749	0.818	0.798	0.801	0.806
Mn	0.016	0.031	0.030	0.000	0.013	0.024	0.020
Co	0.172	0.164	0.177	0.177	0.176	0.162	0.173
Ni	0.054	0.051	0.058	0.053	0.047	0.056	0.057
Zn	0.047	0.033	0.037	0.028	0.030	0.024	0.036
Sn	0.073	0.076	0.074	0.071	0.070	0.087	0.075
Sb	0.000	0.000	0.000	0.000	0.000	0.000	0.000
S	0.024	0.011	0.000	0.016	0.016	0.033	0.000
Total	**100.000**	**100.000**	**100.000**	**100.000**	**100.000**	**100.000**	**100.000**
			Normalised to 1 apfu				
Fe	0.917	0.913	0.912	0.912	0.914	0.912	0.911
As	0.071	0.075	0.077	0.076	0.074	0.076	0.077
Cu	0.008	0.008	0.007	0.008	0.008	0.008	0.008
Mn	0.000	0.000	0.000	0.000	0.000	0.000	0.000
Co	0.002	0.002	0.002	0.002	0.002	0.002	0.002
Ni	0.001	0.001	0.001	0.001	0.000	0.001	0.001
Zn	0.000	0.000	0.000	0.000	0.000	0.000	0.000
Sn	0.001	0.001	0.001	0.001	0.001	0.001	0.001
Sb	0.000	0.000	0.000	0.000	0.000	0.000	0.000
S	0.000	0.000	0.000	0.000	0.000	0.000	0.000
Total	**1.000**	**1.000**	**1.000**	**1.000**	**1.000**	**1.000**	**1.000**

Table iv.104.: EMP analyses of segregated Fe_9As from ferrous speiss.

Sample	11029(7)	11029(7)	11029(7)
No.	**#78**	**#84**	**#92**
Fe	87.992	86.712	87.540
As	9.790	10.120	10.030
Cu	0.797	0.838	0.843
Mn	0.013	< 0.011	0.014
Co	0.177	0.184	0.163
Ni	0.064	0.058	0.061
Zn	< 0.027	< 0.027	< 0.027
Sn	0.442	0.183	0.161
Pb	< 0.04	0.051	0.056
S	< 0.005	< 0.006	0.008
Total	**99.343**	**98.146**	**98.915**
	Atom-%		
Fe	91.212	90.969	91.086
As	7.564	7.914	7.779
Cu	0.725	0.771	0.770
Mn	0.014	0.000	0.015
Co	0.174	0.183	0.161
Ni	0.063	0.058	0.060
Zn	0.000	0.000	0.000
Sn	0.216	0.090	0.079
Sb	0.000	0.014	0.016
S	0.000	0.000	0.014
Total	**100.000**	**100.000**	**100.000**
	Normalised to 1 apfu		
Fe	0.912	0.910	0.911
As	0.076	0.079	0.078
Cu	0.007	0.008	0.008
Mn	0.000	0.000	0.000
Co	0.002	0.002	0.002
Ni	0.001	0.001	0.001
Zn	0.000	0.000	0.000
Sn	0.002	0.001	0.001
Sb	0.000	0.000	0.000
S	0.000	0.000	0.000
Total	**1.000**	**1.000**	**1.000**

Table iv.105.: EMP analyses of eutectoid Fe_9As from ferrous speiss.

Sample	11029(4)	11029(4)	11029(4)	11029(4)	11029(4)	11029(4)	11029(4)	11029(4)	11029(4)	11029(4)
No.	**#1.6**	**#1.10**	**#1.20**	**#1.22**	**#1.25**	**#1.29**	**#2.1**	**#2.2**	**#2.3**	**#2.21**
Fe	55.304	55.025	55.392	54.746	55.254	55.716	55.469	54.602	53.437	55.608
As	35.854	36.193	35.948	35.462	35.963	36.131	36.088	36.640	36.009	35.901
Cu	5.860	6.307	5.483	6.076	5.944	5.587	5.703	5.854	7.682	5.693
Mn	0.024	0.024	0.023	0.019	0.022	0.033	0.031	0.022	0.024	0.025
Co	0.130	0.123	0.128	0.125	0.127	0.117	0.121	0.117	0.113	0.116
Ni	0.266	0.198	0.294	0.295	0.191	0.233	0.215	0.218	0.245	0.219
Cd	< 0.028	0.032	< 0.028	0.032	0.069	0.034	< 0.027	< 0.026	< 0.027	0.034
Sn	0.070	0.034	0.095	0.160	0.039	0.034	0.057	0.062	< 0.028	0.050
Sb	0.485	0.293	0.669	0.938	0.322	0.273	0.433	0.358	0.316	0.325
S	0.242	0.244	0.247	0.246	0.295	0.229	0.221	0.281	0.220	0.210
Total	**98.281**	**98.473**	**98.279**	**98.099**	**98.226**	**98.387**	**98.338**	**98.154**	**98.046**	**98.209**
					Atom-%					
Fe	62.660	62.205	62.800	62.297	62.565	62.975	62.795	61.996	60.786	62.993
As	30.280	30.498	30.378	30.079	30.353	30.440	30.452	31.009	30.532	30.314
Cu	5.826	6.256	5.454	6.067	5.906	5.541	5.665	5.832	7.667	5.659
Mn	0.028	0.028	0.027	0.022	0.025	0.038	0.036	0.025	0.028	0.029
Co	0.140	0.132	0.138	0.135	0.136	0.125	0.130	0.126	0.122	0.125
Ni	0.287	0.213	0.317	0.319	0.206	0.251	0.232	0.236	0.265	0.236
Cd	0.000	0.018	0.000	0.018	0.039	0.019	0.000	0.000	0.000	0.019
Sn	0.037	0.018	0.051	0.086	0.021	0.018	0.030	0.033	0.000	0.027
Sb	0.252	0.152	0.348	0.490	0.167	0.142	0.225	0.186	0.165	0.169
S	0.478	0.480	0.488	0.488	0.582	0.451	0.436	0.556	0.436	0.414
Total	**100.000**	**100.000**	**100.000**	**100.000**	**100.000**	**100.000**	**100.000**	**100.000**	**100.000**	**100.000**
					Normalised to 3 apfu					
Fe	1.880	1.866	1.884	1.869	1.877	1.889	1.884	1.860	1.824	1.890
As	0.908	0.915	0.911	0.902	0.911	0.913	0.914	0.930	0.916	0.909
Cu	0.175	0.188	0.164	0.182	0.177	0.166	0.170	0.175	0.230	0.170
Mn	0.001	0.001	0.001	0.001	0.001	0.001	0.001	0.001	0.001	0.001
Co	0.004	0.004	0.004	0.004	0.004	0.004	0.004	0.004	0.004	0.004
Ni	0.009	0.006	0.010	0.010	0.006	0.008	0.007	0.007	0.008	0.007
Cd	0.000	0.001	0.000	0.001	0.001	0.001	0.000	0.000	0.000	0.001
Sn	0.001	0.001	0.002	0.003	0.001	0.001	0.001	0.001	0.000	0.001
Sb	0.008	0.005	0.010	0.015	0.005	0.004	0.007	0.006	0.005	0.005
S	0.014	0.014	0.015	0.015	0.017	0.014	0.013	0.017	0.013	0.012
Total	**3.000**	**3.000**	**3.000**	**3.000**	**3.000**	**3.000**	**3.000**	**3.000**	**3.000**	**3.000**

Sample	11029(4)	11029(4)	11029(4)	11029(4)
No.	**#2.27**	**#2.28**	**#2.30**	**#2.35**
Fe	55.809	55.949	55.748	56.032
As	35.782	35.664	35.900	35.884
Cu	5.496	5.583	5.563	5.349
Mn	0.022	0.029	0.027	0.028
Co	0.103	0.121	0.107	0.108
Ni	0.214	0.229	0.228	0.244
Cd	0.031	0.034	0.028	0.043
Sn	0.069	0.032	0.030	0.033
Sb	0.340	0.299	0.382	0.335
S	0.230	0.206	0.202	0.199
Total	**98.096**	**98.146**	**98.215**	**98.255**
		Atom-%		
Fe	63.254	63.347	63.142	63.404
As	30.229	30.099	30.309	30.267
Cu	5.466	5.546	5.529	5.311
Mn	0.025	0.033	0.031	0.032
Co	0.111	0.130	0.115	0.116
Ni	0.231	0.247	0.246	0.263
Cd	0.017	0.019	0.016	0.024
Sn	0.037	0.017	0.016	0.018
Sb	0.177	0.155	0.198	0.174
S	0.454	0.406	0.398	0.392
Total	**100.000**	**100.000**	**100.000**	**100.000**
		Normalised to 3 apfu		
Fe	1.898	1.900	1.894	1.902
As	0.907	0.903	0.909	0.908
Cu	0.164	0.166	0.166	0.159
Mn	0.001	0.001	0.001	0.001
Co	0.003	0.004	0.003	0.003
Ni	0.007	0.007	0.007	0.008
Cd	0.001	0.001	0.000	0.001
Sn	0.001	0.001	0.000	0.001
Sb	0.005	0.005	0.006	0.005
S	0.014	0.012	0.012	0.012
Total	**3.000**	**3.000**	**3.000**	**3.000**

Table iv.106.: EMP analyses of segregated Fe_2As from ferrous speiss.

Sample	11029(7)	11029(7)	11029(7)	11029(7)	11029(7)
No.	**#76**	**#82**	**#89**	**#90**	**#93**
Fe	61.518	64.490	56.320	58.261	64.625
As	31.140	26.739	35.970	28.704	26.845
Cu	3.223	2.852	3.742	3.139	2.783
Mn	0.025	0.014	0.028	0.020	0.013
Co	0.130	0.138	0.109	0.120	0.132
Ni	0.122	0.122	0.154	0.130	0.098
Cd	< 0.039	0.066	< 0.039	0.052	0.064
Sn	0.220	0.260	0.073	0.072	0.236
Sb	0.355	0.344	0.356	0.340	0.334
S	2.188	2.635	0.326	7.029	2.679
Total	**98.921**	**97.660**	**97.078**	**97.867**	**97.809**
			Atom-%		
Fe	66.941	70.032	64.396	61.246	70.039
As	25.257	21.644	30.656	22.492	21.686
Cu	3.077	2.717	3.754	2.895	2.646
Mn	0.028	0.015	0.033	0.021	0.014
Co	0.134	0.142	0.118	0.120	0.136
Ni	0.126	0.126	0.168	0.130	0.101
Cd	0.000	0.036	0.000	0.027	0.034
Sn	0.113	0.133	0.039	0.036	0.120
Sb	0.177	0.171	0.187	0.164	0.166
S	4.147	4.984	0.649	12.869	5.057
Total	**100.000**	**100.000**	**100.000**	**100.000**	**100.000**
			Normalised to 3 apfu		
Fe	2.008	2.101	1.932	1.837	2.101
As	0.758	0.649	0.920	0.675	0.651
Cu	0.092	0.082	0.113	0.087	0.079
Mn	0.001	0.000	0.001	0.001	0.000
Co	0.004	0.004	0.004	0.004	0.004
Ni	0.004	0.004	0.005	0.004	0.003
Cd	0.000	0.001	0.000	0.001	0.001
Sn	0.003	0.004	0.001	0.001	0.004
Sb	0.005	0.005	0.006	0.005	0.005
S	0.124	0.150	0.019	0.386	0.152
Total	**3.000**	**3.000**	**3.000**	**3.000**	**3.000**

Table iv.107.: EMP analyses of eutectoid Fe_2As from ferrous speiss.

Sample	11029(4)	11029(4)	10-2B	10-2B	10-2B	10032(4)
Occurrence	Ferrous speiss	Ferrous speiss	Matte s.s.	Matte s.s.	Matte s.s.	Slag droplet
No.	#2.4	#2.5	#98	#101	#102	#46
Fe	46.510	46.562	29.336	33.899	31.013	37.574
As	32.839	32.072	33.280	36.051	33.502	47.155
Cu	15.023	15.349	6.402	6.996	7.395	0.143
Mn	0.024	0.030	0.027	0.028	0.024	0.049
Co	0.106	0.117	0.466	0.632	0.434	0.301
Zn	< 0.027	< 0	0.132	< 0.028	0.104	0.054
Ni	0.255	0.251	23.145	18.234	20.419	2.972
Ag	0.024	< 0.019	< 0.027	< 0.025	0.031	< 0.022
Cd	0.048	0.042	< 0.040	< 0.040	0.056	0.033
Sn	0.100	0.030	< 0.021	< 0.019	0.030	< 0
Sb	0.687	0.406	1.677	1.377	1.238	1.214
Pb	0.040	< 0	0.937	0.704	0.930	5.494
S	1.264	1.319	1.171	1.139	1.914	0.324
Total	**96.920**	**96.178**	**96.573**	**99.060**	**97.090**	**95.313**
			Atom-%			
Fe	53.357	53.609	34.338	38.653	35.793	47.759
As	28.081	27.524	29.036	30.640	28.820	44.675
Cu	15.146	15.530	6.585	7.010	7.500	0.160
Mn	0.028	0.035	0.032	0.032	0.028	0.063
Co	0.115	0.128	0.517	0.683	0.475	0.363
Zn	0.000	0.000	0.132	0.000	0.102	0.059
Ni	0.278	0.275	25.777	19.782	22.423	3.594
Ag	0.014	0.000	0.000	0.000	0.019	0.000
Cd	0.027	0.024	0.000	0.000	0.032	0.021
Sn	0.054	0.016	0.000	0.000	0.016	0.000
Sb	0.361	0.214	0.900	0.720	0.655	0.708
Pb	0.012	0.000	0.296	0.216	0.289	1.882
S	2.525	2.645	2.387	2.262	3.847	0.717
Total	**100.000**	**100.000**	**100.000**	**100.000**	**100.000**	**100.000**
			Normalised to 1 apfu			
Fe	0.534	0.536	0.343	0.387	0.358	0.478
As	0.281	0.275	0.290	0.306	0.288	0.447
Cu	0.151	0.155	0.066	0.070	0.075	0.002
Mn	0.000	0.000	0.000	0.000	0.000	0.001
Co	0.001	0.001	0.005	0.007	0.005	0.004
Zn	0.000	0.000	0.001	0.000	0.001	0.001
Ni	0.003	0.003	0.258	0.198	0.224	0.036
Ag	0.000	0.000	0.000	0.000	0.000	0.000
Cd	0.000	0.000	0.000	0.000	0.000	0.000
Sn	0.001	0.000	0.000	0.000	0.000	0.000
Sb	0.004	0.002	0.009	0.007	0.007	0.007
Pb	0.000	0.000	0.003	0.002	0.003	0.019
S	0.025	0.026	0.024	0.023	0.038	0.007
Total	**1.000**	**1.000**	**1.000**	**1.000**	**1.000**	**1.000**

Table iv.108.: EMP analyses of FeAs from ferrous speiss [11029(4)], matte s.s. [10-2B] and droplets in slag [10032(4)].

Sample	10021(4)	10021(4)	10021(4)	10021(4)	10021(4)	10021(4)	10021(4)	10021(4)	10021(4)	10021(4)
No.	**#11**	**#12**	**#13**	**#14**	**#15**	**#16**	**#17**	**#18**	**#19**	**#20**
Fe	91.972	92.362	92.366	90.539	92.845	92.419	91.171	91.035	91.642	90.558
As	6.286	6.646	6.080	7.516	5.585	7.074	7.268	7.024	6.380	6.510
Cu	0.557	0.667	0.561	0.600	0.637	0.560	0.502	0.533	0.568	0.625
Mn	0.012	0.014	0.022	0.015	0.015	0.022	< 0.009	0.012	< 0.009	0.019
Co	0.160	0.168	0.185	0.165	0.177	0.175	0.169	0.180	0.184	0.172
Ni	0.153	0.171	0.137	0.185	0.159	0.169	0.157	0.167	0.158	0.166
Zn	0.057	0.036	0.030	< 0.026	< 0.027	0.035	0.038	0.064	0.051	0.039
Cd	0.043	0.089	< 0.038	< 0.037	0.049	0.054	< 0.039	0.044	0.051	0.047
Sn	0.104	0.129	0.158	0.103	0.109	0.125	0.133	0.129	0.119	0.127
Sb	0.140	0.175	0.170	0.162	0.137	0.162	0.177	0.180	0.141	0.146
Pb	0.037	0.048	< 0.031	0.062	< 0.034	< 0.032	0.069	< 0.036	0.063	0.055
S	0.048	0.012	0.010	0.008	0.012	< 0.006	0.020	0.013	0.012	0.014
Total	**99.569**	**100.517**	**99.719**	**99.391**	**99.725**	**100.795**	**99.704**	**99.381**	**99.398**	**98.478**
					Atom-%					
Fe	94.106	93.781	94.334	93.159	94.681	93.615	93.443	93.540	94.027	93.821
As	4.794	5.030	4.629	5.764	4.245	5.341	5.552	5.380	4.879	5.027
Cu	0.500	0.594	0.503	0.542	0.570	0.498	0.451	0.481	0.511	0.568
Mn	0.012	0.014	0.023	0.016	0.016	0.023	0.000	0.013	0.000	0.020
Co	0.155	0.162	0.179	0.161	0.171	0.168	0.164	0.175	0.179	0.169
Ni	0.149	0.165	0.133	0.181	0.154	0.163	0.153	0.163	0.154	0.164
Zn	0.050	0.031	0.026	0.000	0.000	0.030	0.033	0.056	0.045	0.034
Cd	0.022	0.045	0.000	0.000	0.025	0.027	0.000	0.022	0.026	0.024
Sn	0.050	0.062	0.076	0.050	0.052	0.060	0.064	0.062	0.057	0.062
Sb	0.066	0.081	0.080	0.076	0.064	0.075	0.083	0.085	0.066	0.069
Pb	0.010	0.013	0.000	0.017	0.000	0.000	0.019	0.000	0.017	0.015
S	0.086	0.021	0.018	0.014	0.021	0.000	0.036	0.023	0.021	0.025
Total	**100.000**	**100.000**	**100.000**	**100.000**	**100.000**	**100.000**	**100.000**	**100.000**	**100.000**	**100.000**
					Normalised to 1 apfu					
Fe	0.941	0.938	0.943	0.932	0.947	0.936	0.934	0.935	0.940	0.938
As	0.048	0.050	0.046	0.058	0.042	0.053	0.056	0.054	0.049	0.050
Cu	0.005	0.006	0.005	0.005	0.006	0.005	0.005	0.005	0.005	0.006
Mn	0.000	0.000	0.000	0.000	0.000	0.000	0.000	0.000	0.000	0.000
Co	0.002	0.002	0.002	0.002	0.002	0.002	0.002	0.002	0.002	0.002
Ni	0.001	0.002	0.001	0.002	0.002	0.002	0.002	0.002	0.002	0.002
Zn	0.000	0.000	0.000	0.000	0.000	0.000	0.000	0.001	0.000	0.000
Cd	0.000	0.000	0.000	0.000	0.000	0.000	0.000	0.000	0.000	0.000
Sn	0.001	0.001	0.001	0.000	0.001	0.001	0.001	0.001	0.001	0.001
Sb	0.001	0.001	0.001	0.001	0.001	0.001	0.001	0.001	0.001	0.001
Pb	0.000	0.000	0.000	0.000	0.000	0.000	0.000	0.000	0.000	0.000
S	0.001	0.000	0.000	0.000	0.000	0.000	0.000	0.000	0.000	0.000
Total	**1.000**	**1.000**	**1.000**	**1.000**	**1.000**	**1.000**	**1.000**	**1.000**	**1.000**	**1.000**

Sample	10021(4)	10021(4)	10021(4)	10021(4)	10021(4)	10021(4)
No.	**#21**	**#22**	**#23**	**#24**	**#25**	**#26**
Fe	91.119	89.680	89.889	91.139	89.842	88.951
As	6.753	8.411	7.587	6.935	8.434	8.517
Cu	0.473	0.325	0.524	0.511	0.467	0.502
Mn	0.021	0.020	0.014	< 0.011	0.019	0.016
Co	0.167	0.163	0.173	0.175	0.173	0.159
Ni	0.123	0.183	0.159	0.118	0.198	0.177
Zn	0.030	0.039	< 0.027	0.033	0.043	0.065
Cd	< 0.038	0.055	< 0.039	0.050	0.051	0.046
Sn	0.134	0.194	0.168	0.137	0.158	0.141
Sb	0.136	0.330	0.239	0.207	0.169	0.177
Pb	0.065	0.062	0.049	0.038	0.069	0.049
S	0.011	0.014	0.015	0.015	0.012	0.040
Total	**99.032**	**99.476**	**98.817**	**99.358**	**99.635**	**98.840**
			Atom-%			
Fe	93.887	92.522	93.090	93.684	92.465	92.288
As	5.186	6.468	5.857	5.314	6.470	6.587
Cu	0.428	0.294	0.476	0.461	0.422	0.457
Mn	0.022	0.021	0.015	0.000	0.020	0.017
Co	0.163	0.159	0.170	0.170	0.169	0.156
Ni	0.121	0.180	0.157	0.115	0.194	0.175
Zn	0.026	0.034	0.000	0.029	0.038	0.058
Cd	0.000	0.028	0.000	0.026	0.026	0.024
Sn	0.065	0.094	0.082	0.066	0.076	0.069
Sb	0.064	0.156	0.114	0.098	0.080	0.084
Pb	0.018	0.017	0.014	0.011	0.019	0.014
S	0.020	0.025	0.027	0.027	0.022	0.072
Total	**100.000**	**100.000**	**100.000**	**100.000**	**100.000**	**100.000**
			Normalised to 1 apfu			
Fe	0.939	0.925	0.931	0.937	0.925	0.923
As	0.052	0.065	0.059	0.053	0.065	0.066
Cu	0.004	0.003	0.005	0.005	0.004	0.005
Mn	0.000	0.000	0.000	0.000	0.000	0.000
Co	0.002	0.002	0.002	0.002	0.002	0.002
Ni	0.001	0.002	0.002	0.001	0.002	0.002
Zn	0.000	0.000	0.000	0.000	0.000	0.001
Cd	0.000	0.000	0.000	0.000	0.000	0.000
Sn	0.001	0.001	0.001	0.001	0.001	0.001
Sb	0.001	0.002	0.001	0.001	0.001	0.001
Pb	0.000	0.000	0.000	0.000	0.000	0.000
S	0.000	0.000	0.000	0.000	0.000	0.001
Total	**1.000**	**1.000**	**1.000**	**1.000**	**1.000**	**1.000**

Table iv.109.: EMP analyses of grains of arsenical Fe from a lump of pig iron.

Sample	10021(21)	10021(21)
No.	**#1.63**	**#2.81**
Fe	97.521	95.383
As	0.331	3.124
Cu	0.210	0.157
Co	0.173	0.149
Mn	0.019	0.094
Ni	0.040	0.053
Sn	0.091	0.189
Sb	0.029	0.222
S	0.012	0.016
Total	**98.426**	**99.387**
	Atom-%	
Fe	99.257	96.978
As	0.251	2.368
Cu	0.188	0.140
Co	0.167	0.144
Mn	0.020	0.097
Ni	0.039	0.051
Sn	0.044	0.090
Sb	0.014	0.104
S	0.021	0.028
Total	**100.000**	**100.000**
	Normalised to 1 apfu	
Fe	0.993	0.970
As	0.003	0.024
Cu	0.002	0.001
Co	0.002	0.001
Mn	0.000	0.001
Ni	0.000	0.001
Sn	0.000	0.001
Sb	0.000	0.001
S	0.000	0.000
Total	**1.000**	**1.000**

Table iv.110.: EMP analyses of droplets of arsenical Fe from a furnace slag.

Sample	12016(2)	12016(2)	12016(2)	12016(2)	12016(2)	12016(2)	12016(2)
No.	**#30**	**#38**	**#41**	**#44**	**#48**	**#50**	**#51**
Ni	31.407	28.454	30.916	30.123	33.562	32.221	31.776
Sb	51.013	59.858	47.781	52.373	30.456	46.959	48.821
As	12.903	4.729	11.402	8.819	23.719	14.756	11.989
Pb	1.108	0.899	1.092	4.671	6.613	0.805	1.240
Cu	2.463	3.916	5.134	2.793	2.518	3.546	3.897
Fe	0.517	1.108	0.618	0.829	0.439	0.737	0.854
Mn	0.027	0.036	0.036	0.036	0.031	0.028	0.043
Zn	0.150	0.218	0.101	0.125	0.085	0.128	0.110
Ag	0.038	< 0.025	< 0.025	0.034	0.038	< 0.025	0.041
Cd	0.112	0.119	0.080	0.084	0.054	0.055	0.076
Sn	0.249	0.282	0.275	0.257	0.150	0.217	0.230
S	0.047	0.068	0.608	0.015	0.835	0.145	0.568
Total	**100.034**	**99.687**	**98.043**	**100.159**	**98.500**	**99.597**	**99.645**
			Atom-%				
Ni	45.067	42.718	44.165	44.680	45.821	45.228	44.812
Sb	35.286	43.318	32.903	37.446	20.044	31.774	33.188
As	14.504	5.562	12.760	10.247	25.368	16.226	13.245
Pb	0.450	0.382	0.442	1.963	2.557	0.320	0.495
Cu	3.264	5.430	6.774	3.826	3.175	4.597	5.076
Fe	0.780	1.748	0.928	1.292	0.630	1.087	1.266
Mn	0.041	0.058	0.055	0.057	0.045	0.042	0.065
Zn	0.193	0.294	0.129	0.166	0.104	0.161	0.139
Ag	0.030	0.000	0.000	0.027	0.028	0.000	0.031
Cd	0.084	0.093	0.060	0.065	0.038	0.040	0.056
Sn	0.177	0.209	0.194	0.188	0.101	0.151	0.160
S	0.123	0.187	1.590	0.041	2.087	0.373	1.466
Total	**100.000**	**100.000**	**100.000**	**100.000**	**100.000**	**100.000**	**100.000**
			Normalised to 1 apfu				
Ni	0.451	0.427	0.442	0.447	0.458	0.452	0.448
Sb	0.353	0.433	0.329	0.374	0.200	0.318	0.332
As	0.145	0.056	0.128	0.102	0.254	0.162	0.132
Pb	0.005	0.004	0.004	0.020	0.026	0.003	0.005
Cu	0.033	0.054	0.068	0.038	0.032	0.046	0.051
Fe	0.008	0.017	0.009	0.013	0.006	0.011	0.013
Mn	0.000	0.001	0.001	0.001	0.000	0.000	0.001
Zn	0.002	0.003	0.001	0.002	0.001	0.002	0.001
Ag	0.000	0.000	0.000	0.000	0.000	0.000	0.000
Cd	0.001	0.001	0.001	0.001	0.000	0.000	0.001
Sn	0.002	0.002	0.002	0.002	0.001	0.002	0.002
S	0.001	0.002	0.016	0.000	0.021	0.004	0.015
Total	**1.000**	**1.000**	**1.000**	**1.000**	**1.000**	**1.000**	**1.000**

Table iv.111.: EMP analyses of (Ni,Cu)(Sb,As) droplets from slag.

Sample	11029(4)	11029(4)
No.	**#1.15**	**#2.29**
Cu	60.909	61.528
Fe	3.451	1.299
Sn	25.505	26.484
Sb	11.327	10.721
Ni	0.474	0.479
Ag	0.062	0.097
As	0.304	0.151
Pb	0.366	0.100
S	0.024	0.047
Total	**102.422**	**100.906**
	Atom-%	
Cu	71.349	73.593
Fe	4.600	1.768
Sn	15.993	16.957
Sb	6.925	6.692
Ni	0.601	0.620
Ag	0.043	0.068
As	0.302	0.153
Pb	0.131	0.037
S	0.056	0.111
Total	**100.000**	**100.000**
	Normalised to 4 apfu	
Cu	2.854	2.944
Fe	0.184	0.071
Sn	0.640	0.678
Sb	0.277	0.268
Ni	0.024	0.025
Ag	0.002	0.003
As	0.012	0.006
Pb	0.005	0.001
S	0.002	0.004
Total	**4.000**	**4.000**

Table iv.112.: EMP analyses of $(Cu,Fe)_3(Sn,Sb)$ from ferrous speiss.

Sample	**10032(4)**	**10032(4)**	**10032(4)**	**10032(4)**	**10032(4)**
No.	**#31**	**#35**	**#37**	**#38**	**#45**
Cu	47.806	46.077	49.292	49.291	48.210
Ni	1.613	3.482	1.338	1.311	1.788
Sb	49.849	49.507	50.301	49.932	50.034
Mn	0.022	0.020	< 0.013	0.016	0.019
Fe	0.505	0.193	0.159	0.248	0.352
Ag	0.557	0.191	0.201	0.245	0.350
As	0.223	0.348	0.209	0.239	0.203
Cd	0.057	< 0.027	0.038	0.029	0.050
Sn	0.244	0.242	0.236	0.234	0.249
Pb	0.355	0.543	0.115	0.167	0.126
S	0.056	0.053	0.008	< 0.006	< 0.007
Total	**101.287**	**100.656**	**101.897**	**101.712**	**101.381**
			Atom %		
Cu	62.031	60.046	63.465	63.511	62.400
Ni	2.266	4.913	1.865	1.829	2.506
Sb	33.757	33.671	33.800	33.577	33.798
Mn	0.033	0.030	0.000	0.024	0.028
Fe	0.746	0.286	0.233	0.364	0.518
Ag	0.426	0.147	0.152	0.186	0.267
As	0.245	0.385	0.228	0.261	0.223
Cd	0.042	0.000	0.028	0.021	0.037
Sn	0.169	0.169	0.163	0.161	0.173
Pb	0.141	0.217	0.045	0.066	0.050
S	0.144	0.137	0.020	0.000	0.000
Total	**100.000**	**100.000**	**100.000**	**100.000**	**100.000**
			Normalised to 3 apfu		
Cu	1.861	1.801	1.904	1.905	1.872
Ni	0.068	0.147	0.056	0.055	0.075
Sb	1.013	1.010	1.014	1.007	1.014
Mn	0.001	0.001	0.000	0.001	0.001
Fe	0.022	0.009	0.007	0.011	0.016
Ag	0.013	0.004	0.005	0.006	0.008
As	0.007	0.012	0.007	0.008	0.007
Cd	0.001	0.000	0.001	0.001	0.001
Sn	0.005	0.005	0.005	0.005	0.005
Pb	0.004	0.007	0.001	0.002	0.002
S	0.004	0.004	0.001	0.000	0.000
Total	**3.000**	**3.000**	**3.000**	**3.000**	**3.000**

Table iv.113.: EMP analyses of $(Cu,Ni)_2Sb$ from droplets in slag.

Sample	14032	11027(1)	11029(4)	10024(2)	10024(2)	10024(2)	10024(2)	10024(4)	10024(4)	10024(4)
No.	**#65**	**#2.44**	**#2.59**	**#2.102**	**#2.104**	**#2.110**	**#2.117**	**#2.65**	**#2.66**	**#2.70**
Pb	97.505	90.401	90.730	96.863	93.673	88.628	94.992	92.254	92.089	88.428
Sb	1.365	0.574	1.125	1.445	2.115	1.502	1.620	0.787	0.597	0.348
As	< 0.014	0.038	0.081	0.029	0.043	0.022	0.038	0.057	0.023	0.025
Mn	0.025	0.027	0.020	0.034	0.047	0.033	0.030	0.045	0.034	0.030
Fe	0.051	0.331	0.611	0.348	0.464	0.239	0.198	0.319	0.054	0.248
Cu	0.241	0.712	0.054	0.034	0.036	< 0.027	0.048	0.106	0.040	0.055
Zn	< 0.033	0.087	0.035	0.292	0.392	0.176	0.167	0.097	< 0.037	0.068
Ag	< 0	< 0	< 0	< 0	< 0	< 0	< 0	< 0	< 0	< 0
Cd	0.079	0.062	0.537	0.086	0.273	0.064	0.112	0.114	0.084	0.079
Sn	< 0	< 0	0.104	< 0	< 0.041	< 0	< 0	< 0	< 0	< 0
S	0.185	0.356	0.132	0.093	0.142	1.356	0.258	0.643	0.311	1.359
Total	**99.451**	**92.588**	**93.429**	**99.224**	**97.185**	**92.020**	**97.463**	**94.422**	**93.232**	**90.640**
					Normalised to 100 wt %					
Pb	98.043	97.638	97.111	97.621	96.386	96.314	97.465	97.704	98.774	97.560
Sb	1.373	0.620	1.204	1.456	2.176	1.632	1.662	0.833	0.640	0.384
As	-	0.041	0.087	0.029	0.044	0.024	0.039	0.060	0.025	0.028
Mn	0.025	0.029	0.021	0.034	0.048	0.036	0.031	0.048	0.036	0.033
Fe	0.051	0.357	0.654	0.351	0.477	0.260	0.203	0.338	0.058	0.274
Cu	0.242	0.769	0.058	0.034	0.037	-	0.049	0.112	0.043	0.061
Zn	-	0.094	0.037	0.294	0.403	0.191	0.171	0.103	-	0.075
Ag	-	-	-	-	-	-	-	-	-	-
Cd	0.079	0.067	0.575	0.087	0.281	0.070	0.115	0.121	0.090	0.087
Sn	-	-	0.111	-	-	-	-	-	-	-
S	0.186	0.384	0.141	0.094	0.146	1.474	0.265	0.681	0.334	1.499
Total	**100.000**	**100.000**	**100.000**	**100.000**	**100.000**	**100.000**	**100.000**	**100.000**	**100.000**	**100.000**
					Atom %					
Pb	95.370	92.411	93.035	94.393	91.773	87.152	93.809	92.141	96.134	88.922
Sb	2.272	0.999	1.963	2.396	3.526	2.513	2.722	1.338	1.061	0.596
As	0.000	0.107	0.230	0.078	0.117	0.060	0.104	0.157	0.066	0.070
Mn	0.092	0.104	0.077	0.125	0.174	0.122	0.112	0.170	0.134	0.114
Fe	0.185	1.255	2.325	1.258	1.687	0.872	0.725	1.182	0.209	0.925
Cu	0.769	2.373	0.181	0.108	0.115	0.000	0.155	0.345	0.136	0.180
Zn	0.000	0.282	0.114	0.901	1.217	0.548	0.522	0.307	0.000	0.217
Ag	0.000	0.000	0.000	0.000	0.000	0.000	0.000	0.000	0.000	0.000
Cd	0.142	0.117	1.015	0.154	0.493	0.116	0.204	0.210	0.162	0.146
Sn	0.000	0.000	0.186	0.000	0.000	0.000	0.000	0.000	0.000	0.000
S	1.169	2.352	0.875	0.586	0.899	8.616	1.646	4.150	2.098	8.831
Total	**100.000**	**100.000**	**100.000**	**100.000**	**100.000**	**100.000**	**100.000**	**100.000**	**100.000**	**100.000**

Sample	10024(5)	10024(5)	10024(5)	10024(5)	10024(5)	10024(5)	10024(5)	10024(5)	10024(5)	10024(5)
No.	**#1.198**	**#2.72**	**#2.76**	**#2.80**	**#2.81**	**#2.82**	**#2.83**	**#2.85**	**#2.88**	**#2.90**
Pb	93.997	93.055	96.227	92.724	91.723	91.282	95.235	96.252	93.567	95.799
Sb	1.010	1.167	1.439	1.319	0.564	0.640	0.543	0.758	1.353	0.850
As	1.228	0.037	0.059	0.047	0.036	0.053	0.047	0.032	0.069	0.070
Mn	0.035	0.045	0.041	0.041	0.027	0.037	0.020	0.038	0.045	0.017
Fe	0.276	0.241	0.213	0.330	0.045	0.095	0.059	0.089	0.199	0.103
Cu	0.062	0.229	0.096	0.171	0.210	0.061	0.073	0.126	0.194	0.061
Zn	< 0	0.068	0.093	0.085	< 0.031	< 0	0.036	0.040	0.059	< 0
Ag	< 0	< 0	< 0	< 0	< 0	< 0	< 0	< 0	< 0	< 0
Cd	< 0	0.130	0.239	0.184	< 0.034	0.068	0.063	0.087	0.103	0.061
Sn	< 0	< 0	< 0	< 0.035	< 0	< 0.037	< 0	< 0	< 0.035	< 0
S	< 0.012	0.141	0.160	0.143	0.040	0.083	0.077	0.061	0.200	0.113
Total	**96.608**	**95.113**	**98.567**	**95.044**	**92.645**	**92.319**	**96.153**	**97.483**	**95.789**	**97.074**
					Normalised to 100 wt %					
Pb	97.297	97.836	97.626	97.559	99.005	98.877	99.045	98.737	97.680	98.687
Sb	1.045	1.227	1.460	1.388	0.609	0.693	0.565	0.778	1.412	0.876
As	1.271	0.039	0.060	0.049	0.039	0.057	0.049	0.033	0.072	0.072
Mn	0.036	0.047	0.042	0.043	0.029	0.040	0.021	0.039	0.047	0.018
Fe	0.286	0.253	0.216	0.347	0.049	0.103	0.061	0.091	0.208	0.106
Cu	0.064	0.241	0.097	0.180	0.227	0.066	0.076	0.129	0.203	0.063
Zn	-	0.071	0.094	0.089	-	-	0.037	0.041	0.062	-
Ag	-	-	-	-	-	-	-	-	-	-
Cd	-	0.137	0.242	0.194	-	0.074	0.066	0.089	0.108	0.063
Sn	-	-	-	-	-	-	-	-	-	-
S	-	0.148	0.162	0.150	0.043	0.090	0.080	0.063	0.209	0.116
Total	**100.000**	**100.000**	**100.000**	**100.000**	**100.000**	**100.000**	**100.000**	**100.000**	**100.000**	**100.000**
					Atom %					
Pb	93.557	94.645	94.464	94.071	97.584	97.243	97.628	97.032	94.255	96.838
Sb	1.711	2.020	2.404	2.277	1.021	1.160	0.947	1.300	2.319	1.462
As	3.380	0.104	0.160	0.132	0.106	0.156	0.133	0.089	0.192	0.196
Mn	0.131	0.173	0.152	0.157	0.108	0.149	0.077	0.144	0.171	0.065
Fe	1.019	0.909	0.776	1.242	0.178	0.375	0.224	0.333	0.744	0.386
Cu	0.201	0.759	0.307	0.566	0.728	0.212	0.244	0.414	0.637	0.201
Zn	0.000	0.219	0.289	0.273	0.000	0.000	0.117	0.128	0.188	0.000
Ag	0.000	0.000	0.000	0.000	0.000	0.000	0.000	0.000	0.000	0.000
Cd	0.000	0.244	0.432	0.344	0.000	0.134	0.119	0.162	0.191	0.114
Sn	0.000	0.000	0.000	0.000	0.000	0.000	0.000	0.000	0.000	0.000
S	0.000	0.927	1.015	0.937	0.275	0.571	0.510	0.397	1.302	0.738
Total	**100.000**	**100.000**	**100.000**	**100.000**	**100.000**	**100.000**	**100.000**	**100.000**	**100.000**	**100.000**

Sample	10024(5)	10024(5)	10024(5)	10024(5)	10024(5)	10024(5)	10024(5)	10024(5)	10024(5)	10024(5)
No.	**#2.93**	**#2.94**	**#2.95**	**#2.96**	**#2.97**	**#2.98**	**#2.99**	**#2.100**	**#2.103**	**#2.104**
Pb	89.821	94.383	93.624	94.576	92.809	91.730	93.343	90.394	95.710	89.507
Sb	0.456	0.617	0.458	0.486	0.487	1.061	1.403	1.304	0.491	0.774
As	0.073	0.053	0.043	0.042	0.038	0.069	0.023	0.052	0.046	0.052
Mn	0.041	0.026	0.034	0.027	0.031	0.067	0.025	0.034	0.020	0.049
Fe	0.263	0.041	0.065	0.059	< 0.024	0.403	0.046	0.121	0.032	0.172
Cu	0.142	0.048	0.064	0.043	0.033	0.137	0.293	0.387	0.047	0.085
Zn	0.060	< 0	0.036	< 0	< 0.029	0.081	< 0	0.075	< 0.030	0.049
Ag	< 0	< 0	< 0	0.066	< 0	< 0	< 0	< 0	< 0	< 0.023
Cd	0.107	0.070	0.093	0.058	0.041	0.185	0.052	0.482	< 0.034	0.314
Sn	< 0	< 0	< 0	< 0	< 0.033	0.038	< 0	< 0.040	< 0	< 0
S	0.210	0.065	0.086	0.084	0.072	0.249	0.097	0.223	0.061	0.150
Total	**91.173**	**95.303**	**94.503**	**95.441**	**93.511**	**94.020**	**95.282**	**93.072**	**96.407**	**91.152**
					Normalised to 100 wt %					
Pb	98.517	99.035	99.070	99.094	99.249	97.564	97.965	97.123	99.277	98.195
Sb	0.500	0.647	0.485	0.509	0.521	1.128	1.472	1.401	0.509	0.849
As	0.080	0.056	0.046	0.044	0.041	0.073	0.024	0.056	0.048	0.057
Mn	0.045	0.027	0.036	0.028	0.033	0.071	0.026	0.037	0.021	0.054
Fe	0.288	0.043	0.069	0.062	-	0.429	0.048	0.130	0.033	0.189
Cu	0.156	0.050	0.068	0.045	0.035	0.146	0.308	0.416	0.049	0.093
Zn	0.066	-	0.038	0.000	-	0.086	-	0.081	-	0.054
Ag	-	-	-	0.069	-	-	-	-	-	-
Cd	0.117	0.073	0.098	0.061	0.044	0.197	0.055	0.518	-	0.344
Sn	-	-	-	-	-	0.040	-	-	-	-
S	0.230	0.068	0.091	0.088	0.077	0.265	0.102	0.240	0.063	0.165
Total	**100.000**	**100.000**	**100.000**	**100.000**	**100.000**	**100.000**	**100.000**	**100.000**	**100.000**	**100.000**
					Atom %					
Pb	95.416	97.770	97.584	97.746	98.202	93.417	95.504	93.033	98.250	95.452
Sb	0.824	1.088	0.812	0.855	0.877	1.839	2.443	2.284	0.858	1.405
As	0.214	0.152	0.124	0.120	0.111	0.194	0.065	0.148	0.131	0.153
Mn	0.164	0.102	0.134	0.105	0.124	0.257	0.096	0.132	0.077	0.197
Fe	1.037	0.158	0.251	0.226	0.000	1.523	0.175	0.462	0.122	0.681
Cu	0.492	0.162	0.218	0.145	0.114	0.455	0.977	1.299	0.157	0.296
Zn	0.202	0.000	0.119	0.000	0.000	0.261	0.000	0.245	0.000	0.166
Ag	0.000	0.000	0.000	0.131	0.000	0.000	0.000	0.000	0.000	0.000
Cd	0.210	0.134	0.179	0.110	0.080	0.347	0.098	0.914	0.000	0.617
Sn	0.000	0.000	0.000	0.000	0.000	0.068	0.000	0.000	0.000	0.000
S	1.442	0.435	0.579	0.561	0.492	1.639	0.641	1.483	0.405	1.034
Total	**100.000**	**100.000**	**100.000**	**100.000**	**100.000**	**100.000**	**100.000**	**100.000**	**100.000**	**100.000**

Sample	10024(5)	10024(5)	10024(5)	10021(2)	10021(21)	10021(21)	13030(1)	13030(1)	13030(1)	13031(1)
No.	**#2.105**	**#2.106**	**#2.109**	**#2.123**	**#1.60**	**#2.75**	**#80**	**#82**	**#83**	**#69**
Pb	91.879	95.056	92.444	93.918	88.535	93.549	91.804	89.546	96.886	88.807
Sb	0.459	0.488	0.081	0.376	1.335	0.891	0.164	0.764	0.433	0.067
As	0.043	0.056	0.025	0.015	0.052	0.025	0.041	0.063	0.028	0.027
Mn	0.037	0.029	0.019	0.023	0.035	0.027	0.038	0.038	< 0.015	0.020
Fe	0.090	0.044	0.057	2.214	0.856	0.183	0.299	0.168	0.135	< 0.023
Cu	0.056	0.028	0.029	0.041	0.040	< 0	0.182	0.079	< 0.027	0.077
Zn	< 0.025	< 0.033	0.042	0.170	0.096	0.041	0.177	0.078	0.072	0.036
Ag	< 0	< 0	< 0	< 0	< 0.024	< 0	< 0	< 0	< 0	0.604
Cd	0.097	0.111	0.079	0.249	< 0	< 0.035	0.091	0.067	0.062	0.069
Sn	< 0.040	< 0	< 0	0.619	0.877	0.406	< 0	< 0.034	< 0	< 0
S	0.103	0.068	0.070	0.100	0.216	0.991	0.146	0.139	0.075	0.352
Total	**92.764**	**95.880**	**92.846**	**97.725**	**92.042**	**96.113**	**92.942**	**90.942**	**97.691**	**90.059**
					Normalised to 100 wt %					
Pb	99.046	99.141	99.567	96.104	96.190	97.332	98.776	98.465	99.176	98.610
Sb	0.495	0.509	0.087	0.385	1.450	0.927	0.176	0.840	0.443	0.074
As	0.046	0.058	0.027	0.015	0.056	0.026	0.044	0.069	0.029	0.030
Mn	0.040	0.030	0.020	0.024	0.038	0.028	0.041	0.042	-	0.022
Fe	0.097	0.046	0.061	2.266	0.930	0.190	0.322	0.185	0.138	-
Cu	0.060	0.029	0.031	0.042	0.043	-	0.196	0.087	-	0.085
Zn	-	-	0.045	0.174	0.104	0.043	0.190	0.086	0.074	0.040
Ag	-	-	-	-	-	-	-	-	-	0.671
Cd	0.105	0.116	0.085	0.255	-	-	0.098	0.074	0.063	0.077
Sn	-	-	-	0.633	0.953	0.422	-	-	-	-
S	0.111	0.071	0.075	0.102	0.235	1.031	0.157	0.153	0.077	0.391
Total	**100.000**	**100.000**	**100.000**	**100.000**	**100.000**	**100.000**	**100.000**	**100.000**	**100.000**	**100.000**
					Atom %					
Pb	97.454	97.946	98.597	88.804	90.694	90.686	95.914	95.963	97.837	95.493
Sb	0.828	0.856	0.147	0.605	2.327	1.470	0.292	1.393	0.744	0.123
As	0.126	0.160	0.074	0.039	0.147	0.067	0.118	0.187	0.078	0.080
Mn	0.148	0.113	0.076	0.082	0.135	0.099	0.150	0.154	0.000	0.081
Fe	0.354	0.168	0.226	7.767	3.253	0.658	1.159	0.668	0.506	0.000
Cu	0.194	0.094	0.101	0.126	0.134	0.000	0.620	0.276	0.000	0.270
Zn	0.000	0.000	0.142	0.509	0.312	0.126	0.586	0.265	0.230	0.123
Ag	0.000	0.000	0.000	0.000	0.000	0.000	0.000	0.000	0.000	1.248
Cd	0.190	0.211	0.155	0.434	0.000	0.000	0.175	0.132	0.115	0.137
Sn	0.000	0.000	0.000	1.022	1.568	0.687	0.000	0.000	0.000	0.000
S	0.706	0.453	0.482	0.611	1.430	6.208	0.986	0.963	0.489	2.446
Total	**100.000**	**100.000**	**100.000**	**100.000**	**100.000**	**100.000**	**100.000**	**100.000**	**100.000**	**100.000**

Table iv.114.: EMP analyses of crude Pb from slag samples.

Sample	**10-5**	**10-5**	**10-5**	**10-5**	**10-5**	**10-5**	**10-5**	**10-5**	**10-5**	**10-5**
No.	**#16**	**#17**	**#18**	**#19**	**#20**	**#21**	**#22**	**#23**	**#24**	**#25**
PbO	100.169	96.330	96.450	98.672	96.456	97.982	95.971	98.172	99.506	96.953
As_2O_3	0.079	<0.018	0.069	0.085	<0.019	0.077	0.066	0.092	0.061	0.053
Sb_2O_3	<0.036	0.110	0.103	0.096	<0.035	0.089	0.110	0.122	<0.037	0.148
SO_3	0.080	0.100	0.102	0.077	0.090	0.092	0.122	0.105	0.065	0.162
Total	**100.328**	**96.540**	**96.724**	**98.930**	**96.546**	**98.239**	**96.269**	**98.492**	**99.632**	**97.317**

Table iv.115.: EMP analyses of litharge from cupellation remains.

Sample	**I.1**	**I.1**	**I.1**	**I.1**	**I.1**	**I.1**	**I.1**	**I.1**	**I.1**	**I.1**	**I.1**
No.	**#1**	**#3**	**#5**	**#6**	**#8**	**#9**	**#10**	**#12**	**#13**	**#14**	**#15**
Pb	99.797	96.064	92.832	100.068	94.329	93.392	96.806	97.748	92.753	94.299	96.012
Sb	0.093	0.089	0.102	0.063	0.065	0.079	0.041	0.066	0.070	0.047	0.114
As	0.181	0.039	0.023	0.018	< 0	0.023	0.021	0.030	0.038	0.015	0.026
Mn	0.022	0.022	0.021	< 0.016	0.018	0.017	0.027	0.026	0.024	< 0.015	< 0.016
Cu	0.081	< 0.027	< 0.027	< 0	< 0	< 0.026	< 0.053	< 0	< 0.027	< 0.027	< 0.028
Ag	< 0	< 0	< 0	< 0	< 0	< 0.023	< 0	< 0	< 0	< 0	< 0
Cd	< 0.035	0.041	< 0.034	< 0.034	0.046	0.034	0.040	0.044	0.042	0.035	0.048
S	0.108	0.050	0.120	0.074	0.068	0.144	0.057	0.147	0.074	0.112	0.102
Total	**100.282**	**96.305**	**93.098**	**100.223**	**94.526**	**93.689**	**96.992**	**98.061**	**93.001**	**94.508**	**96.302**
					Normalised to 100 wt %						
Pb	99.516	99.750	99.714	99.845	99.792	99.683	99.808	99.681	99.733	99.779	99.699
Sb	0.093	0.092	0.110	0.063	0.069	0.084	0.042	0.067	0.075	0.050	0.118
As	0.180	0.040	0.025	0.018	-	0.025	0.022	0.031	0.041	0.016	0.027
Mn	0.022	0.023	0.023	-	0.019	0.018	0.028	0.027	0.026	-	-
Cu	0.081	-	-	-	-	-	-	-	-	-	-
Ag	-	-	-	-	-	-	-	-	-	-	-
Cd	-	0.043	-	-	0.049	0.036	0.041	0.045	0.045	0.037	0.050
S	0.108	0.052	0.129	0.074	0.072	0.154	0.059	0.150	0.080	0.119	0.106
Total	**100.000**	**100.000**	**100.000**	**100.000**	**100.000**	**100.000**	**100.000**	**100.000**	**100.000**	**100.000**	**100.000**
					Atom %						
Pb	98.321	99.235	98.838	99.369	99.261	98.674	99.311	98.663	99.070	99.045	98.955
Sb	0.156	0.156	0.185	0.106	0.116	0.142	0.072	0.113	0.127	0.084	0.200
As	0.493	0.111	0.068	0.049	0.000	0.067	0.060	0.084	0.112	0.044	0.074
Mn	0.082	0.086	0.084	0.000	0.071	0.068	0.104	0.099	0.097	0.000	0.000
Cu	0.260	0.000	0.000	0.000	0.000	0.000	0.000	0.000	0.000	0.000	0.000
Ag	0.000	0.000	0.000	0.000	0.000	0.000	0.000	0.000	0.000	0.000	0.000
Cd	0.000	0.078	0.000	0.000	0.089	0.066	0.076	0.082	0.083	0.068	0.091
S	0.688	0.334	0.826	0.475	0.462	0.983	0.378	0.959	0.511	0.760	0.679
Total	**100.000**	**100.000**	**100.000**	**100.000**	**100.000**	**100.000**	**100.000**	**100.000**	**100.000**	**100.000**	**100.000**

Table iv.116.: EMP analyses of lead artefact sample I.1.

Sample	**I.2**	**I.2**	**I.2**	**I.2**	**I.2**	**I.2**	**I.2**	**I.2**	**I.2**	**I.2**	**I.2**
No.	**#1**	**#2**	**#3**	**#4**	**#6**	**#7**	**#8**	**#9**	**#10**	**#11**	**#12**
Pb	92.131	94.174	91.721	95.143	97.891	93.416	91.110	93.316	91.570	93.175	95.159
Sb	0.081	0.064	0.113	0.081	0.071	0.079	0.040	0.083	0.081	0.082	0.110
As	0.036	0.029	0.044	0.055	0.036	0.024	0.024	0.022	0.030	0.019	0.062
Mn	0.023	0.018	0.020	0.019	0.023	< 0.015	0.024	0.019	0.021	0.030	< 0.015
Cu	< 0.026	0.061	0.032	< 0.027	< 0	< 0.026	< 0.026	< 0.029	0.036	< 0	< 0.027
Ag	< 0	< 0.027	< 0	< 0	< 0	< 0.024	< 0.023	< 0.026	< 0	< 0	< 0
Cd	< 0.033	0.035	< 0.033	< 0.034	0.064	0.050	0.037	0.044	0.078	0.072	0.042
S	0.085	0.067	0.083	0.073	0.075	0.062	0.087	0.102	0.089	0.074	0.051
Total	**92.356**	**94.482**	**92.013**	**95.371**	**98.160**	**93.631**	**91.322**	**93.586**	**91.905**	**93.452**	**95.424**
					Normalised to 100 wt %						
Pb	99.756	99.674	99.683	99.761	99.726	99.770	99.768	99.711	99.635	99.704	99.722
Sb	0.088	0.068	0.123	0.085	0.072	0.084	0.044	0.089	0.088	0.088	0.115
As	0.039	0.031	0.048	0.058	0.037	0.026	0.026	0.024	0.033	0.020	0.065
Mn	0.025	0.019	0.022	0.020	0.023	-	0.026	0.020	0.023	0.032	-
Cu	-	0.065	0.035	-	-	-	-	-	0.039	-	-
Ag	-	-	-	-	-	-	-	-	-	-	-
Cd	-	0.037	-	-	0.065	0.053	0.041	0.047	0.085	0.077	0.044
S	0.092	0.071	0.090	0.077	0.076	0.066	0.095	0.109	0.097	0.079	0.053
Total	**100.000**	**99.964**	**100.000**	**100.000**	**100.000**	**100.000**	**100.000**	**100.000**	**100.000**	**100.000**	**100.000**
					Atom %						
Pb	99.061	98.998	98.889	99.132	99.079	99.263	99.070	98.925	98.774	99.026	99.202
Sb	0.148	0.114	0.207	0.144	0.122	0.143	0.074	0.150	0.149	0.148	0.195
As	0.107	0.084	0.131	0.158	0.101	0.071	0.072	0.064	0.089	0.056	0.179
Mn	0.093	0.071	0.081	0.075	0.088	0.000	0.098	0.076	0.085	0.120	0.000
Cu	0.000	0.209	0.112	0.000	0.000	0.000	0.000	0.000	0.127	0.000	0.000
Ag	0.000	0.000	0.000	0.000	0.000	0.000	0.000	0.000	0.000	0.000	0.000
Cd	0.000	0.068	0.000	0.000	0.119	0.098	0.074	0.086	0.155	0.141	0.081
S	0.591	0.455	0.578	0.491	0.491	0.426	0.611	0.699	0.620	0.508	0.344
Total	**100.000**	**100.000**	**100.000**	**100.000**	**100.000**	**100.000**	**100.000**	**100.000**	**100.000**	**100.000**	**100.000**

Table iv.117.: EMP analyses of lead artefact sample I.2.

Sample	**I.3**	**I.3**	**I.3**	**I.3**	**I.3**	**I.3**	**I.3**	**I.3**
No.	**#1**	**#4**	**#6**	**#8**	**#9**	**#10**	**#11**	**#15**
Pb	96.221	93.757	96.933	96.018	90.031	98.173	94.917	93.806
Sb	0.125	0.131	0.096	0.089	0.097	0.189	0.105	0.092
As	0.047	0.038	0.056	0.034	0.049	0.055	0.046	0.025
Mn	0.021	0.016	< 0.015	0.019	0.021	0.017	0.025	< 0.015
Cu	< 0.026	< 0.027	0.057	< 0.026	< 0.027	< 0.027	0.040	< 0.028
Ag	< 0	< 0	0.301	< 0	< 0	0.027	< 0	< 0
Cd	0.058	0.044	0.147	< 0.034	< 0.032	0.065	0.041	0.062
S	0.168	0.087	0.086	0.109	0.084	0.107	0.069	0.072
Total	**96.640**	**94.073**	**97.676**	**96.269**	**90.282**	**98.633**	**95.243**	**94.057**
				Normalised to 100 wt %				
Pb	99.566	99.664	99.239	99.739	99.722	99.534	99.658	99.733
Sb	0.129	0.139	0.098	0.092	0.107	0.192	0.110	0.098
As	0.049	0.040	0.057	0.035	0.054	0.056	0.048	0.027
Mn	0.022	0.017	-	0.020	0.023	0.017	0.026	-
Cu	-	-	0.058	-	-	-	0.042	-
Ag	-	-	0.308	-	-	0.027	-	-
Cd	0.060	0.047	0.150	-	-	0.066	0.043	0.066
S	0.174	0.092	0.088	0.113	0.093	0.108	0.072	0.077
Total	**100.000**	**100.000**	**100.000**	**100.000**	**100.000**	**100.000**	**100.000**	**100.000**
				Atom %				
Pb	98.350	98.912	98.069	98.947	98.986	98.593	98.904	99.149
Sb	0.217	0.235	0.165	0.156	0.181	0.323	0.186	0.165
As	0.133	0.111	0.157	0.097	0.149	0.153	0.133	0.073
Mn	0.081	0.064	0.000	0.074	0.087	0.064	0.098	0.000
Cu	0.000	0.000	0.188	0.000	0.000	0.000	0.136	0.000
Ag	0.000	0.000	0.585	0.000	0.000	0.052	0.000	0.000
Cd	0.109	0.086	0.274	0.000	0.000	0.120	0.079	0.121
S	1.110	0.593	0.562	0.726	0.597	0.694	0.465	0.492
Total	**100.000**	**100.000**	**100.000**	**100.000**	**100.000**	**100.000**	**100.000**	**100.000**

Table iv.118.: EMP analyses of lead artefact sample I.3.

Sample	**II.1**	**II.1**	**II.1**	**II.1**	**II.1**	**II.2**	**II.3**	**II.3**
No.	**#3**	**#5**	**#9**	**#13**	**#15**	**#13**	**#1**	**#2**
Pb	94.558	92.204	94.767	90.304	90.113	93.460	90.443	95.115
Sb	0.063	0.054	0.096	0.106	0.141	0.072	0.129	0.171
As	0.027	0.030	0.037	0.027	0.036	0.018	0.039	0.027
Mn	0.021	0.024	0.021	0.015	0.019	0.018	0.032	0.025
Cu	< 0.022	0.029	0.057	0.028	0.038	0.034	0.041	< 0.027
Ag	< 0	< 0	< 0	< 0	< 0.025	< 0	< 0	< 0
Cd	0.151	0.092	< 0.034	0.055	0.044	0.076	0.093	0.092
S	0.095	0.064	0.105	0.143	0.056	0.085	0.101	0.070
Total	**94.915**	**92.497**	**95.083**	**90.678**	**90.447**	**93.763**	**90.878**	**95.500**
				Normalised to 100 wt %				
Pb	99.624	99.683	99.668	99.588	99.631	99.677	99.521	99.597
Sb	0.066	0.058	0.101	0.117	0.156	0.077	0.142	0.179
As	0.028	0.032	0.039	0.030	0.040	0.019	0.043	0.028
Mn	0.022	0.026	0.022	0.017	0.021	0.019	0.035	0.026
Cu	-	0.031	0.060	0.031	0.042	0.036	0.045	-
Ag	-	-	-	-	-	-	-	-
Cd	0.159	0.099	-	0.061	0.049	0.081	0.102	0.096
S	0.100	0.069	0.110	0.158	0.062	0.091	0.111	0.073
Total	**100.000**	**100.000**	**100.000**	**100.000**	**100.000**	**100.000**	**100.000**	**100.000**
				Atom %				
Pb	98.795	98.988	98.740	98.443	98.926	98.899	98.469	98.875
Sb	0.112	0.099	0.170	0.197	0.263	0.130	0.239	0.302
As	0.078	0.089	0.107	0.081	0.109	0.053	0.117	0.078
Mn	0.083	0.097	0.083	0.062	0.079	0.072	0.131	0.098
Cu	0.000	0.102	0.194	0.100	0.136	0.117	0.146	0.000
Ag	0.000	0.000	0.000	0.000	0.000	0.000	0.000	0.000
Cd	0.291	0.182	0.000	0.111	0.089	0.148	0.187	0.176
S	0.641	0.444	0.707	1.007	0.397	0.581	0.711	0.470
Total	**100.000**	**100.000**	**100.000**	**100.000**	**100.000**	**100.000**	**100.000**	**100.000**

Table iv.119.: EMP analyses of lead artefact samples II.1, II.2 and II.3.

Sample	IV	IV	IV	V	V	V	V	V	V	V
No.	**#7**	**#16**	**#18**	**#1**	**#5**	**#8**	**#16**	**#18**	**#19**	**#20**
Pb	95.776	97.720	93.488	91.503	92.766	94.321	93.902	89.713	95.568	94.857
Sb	0.110	0.079	0.098	0.070	0.072	0.069	0.064	0.072	0.035	0.048
As	0.027	< 0.013	< 0.014	0.030	0.017	0.020	0.028	0.019	0.026	0.016
Mn	< 0.015	0.026	0.019	0.027	0.019	0.023	< 0.015	0.028	0.026	0.015
Cu	0.041	< 0.028	0.027	< 0.027	< 0.027	< 0.027	< 0	< 0.026	< 0	0.035
Ag	< 0	< 0	< 0	< 0	< 0	< 0	< 0	< 0	< 0	< 0
Cd	0.061	0.068	< 0.034	0.039	0.060	0.048	< 0.033	0.054	< 0.033	0.051
S	0.219	0.216	0.154	0.098	0.146	0.052	0.160	0.158	0.100	0.150
Total	**96.234**	**98.109**	**93.786**	**91.767**	**93.080**	**94.533**	**94.154**	**90.044**	**95.755**	**95.172**
				Normalised to 100 wt %						
Pb	99.524	99.604	99.682	99.712	99.663	99.776	99.732	99.632	99.805	99.669
Sb	0.114	0.081	0.104	0.076	0.077	0.073	0.068	0.080	0.037	0.050
As	0.028	-	-	0.033	0.018	0.021	0.030	0.021	0.027	0.017
Mn	-	0.027	0.020	0.029	0.020	0.024	-	0.031	0.027	0.016
Cu	0.043	-	0.029	-	-	-	-	-	-	0.037
Ag	-	-	-	-	-	-	-	-	-	-
Cd	0.063	0.069	-	0.042	0.064	0.051	-	0.060	-	0.054
S	0.228	0.220	0.164	0.107	0.157	0.055	0.170	0.175	0.104	0.158
Total	**100.000**	**100.000**	**100.000**	**100.000**	**100.000**	**100.000**	**100.000**	**100.000**	**100.000**	**100.000**
				Atom %						
Pb	98.032	98.237	98.606	98.909	98.623	99.280	98.717	98.462	99.092	98.587
Sb	0.192	0.135	0.176	0.129	0.130	0.124	0.114	0.134	0.062	0.085
As	0.076	0.000	0.000	0.090	0.050	0.058	0.081	0.058	0.075	0.046
Mn	0.000	0.099	0.076	0.110	0.076	0.091	0.000	0.116	0.102	0.059
Cu	0.137	0.000	0.093	0.000	0.000	0.000	0.000	0.000	0.000	0.119
Ag	0.000	0.000	0.000	0.000	0.000	0.000	0.000	0.000	0.000	0.000
Cd	0.115	0.126	0.000	0.078	0.118	0.093	0.000	0.109	0.000	0.098
S	1.448	1.403	1.050	0.685	1.003	0.354	1.087	1.121	0.670	1.007
Total	**100.000**	**100.000**	**100.000**	**100.000**	**100.000**	**100.000**	**100.000**	**100.000**	**100.000**	**100.000**

Table iv.120.: EMP analyses of lead artefact samples IV and V.

Sample	**III**	**III**	**III**	**III**	**III**	**III**	**III**	**III**	**III**	**III**	**III**	**III**	**III**	**III**	**III**
No.	**#1**	**#2**	**#3**	**#4**	**#5**	**#6**	**#7**	**#8**	**#9**	**#10**	**#11**	**#12**	**#13**	**#14**	**#15**
Cu	91.332	91.094	88.733	91.718	90.566	90.988	92.148	90.303	91.990	90.419	90.395	91.410	91.612	90.540	90.352
Sn	5.937	6.194	6.302	6.095	6.275	5.711	5.359	6.212	5.915	6.672	6.148	5.902	5.991	6.315	6.278
Ag	2.468	2.392	3.031	1.923	2.517	2.503	2.201	2.615	2.294	2.446	2.697	2.421	2.529	2.647	2.916
Fe	0.116	0.088	0.095	0.055	0.101	0.084	0.094	0.077	0.106	0.085	0.098	0.093	0.101	0.078	0.082
Ni	0.053	0.038	0.045	0.044	0.043	0.050	0.048	0.043	0.033	0.036	0.045	0.052	0.043	0.047	0.042
Zn	0.052	< 0	0.047	< 0	0.041	0.056	0.032	0.032	0.059	0.062	0.049	< 0.029	0.060	< 0.030	0.048
As	0.103	0.119	0.104	0.124	0.120	0.114	0.108	0.102	0.106	0.111	0.098	0.114	0.075	0.119	0.115
Cd	< 0.018	< 0.027	< 0	< 0.027	< 0	< 0.028	< 0.027	< 0.027	< 0.028	< 0.028	< 0.027	< 0	< 0.030	< 0.027	< 0.028
Sb	0.113	0.129	0.132	0.128	0.139	0.104	0.131	0.110	0.114	0.120	0.123	0.131	0.130	0.118	0.121
Pb	< 0.026	0.784	2.568	0.061	< 0.034	< 0.032	< 0	< 0.028	< 0.034	0.047	< 0.040	< 0.030	0.001	< 0.038	< 0.033
S	0.012	0.012	0.013	0.007	0.013	0.018	0.007	0.021	0.017	0.040	0.012	0.010	0.017	0.013	0.014
Total	**100.186**	**100.861**	**101.070**	**100.155**	**99.840**	**99.639**	**100.128**	**99.515**	**100.649**	**100.038**	**99.677**	**100.151**	**100.581**	**99.877**	**99.968**
							Atom %								
Cu	94.768	94.491	93.339	95.115	94.500	94.855	95.315	94.539	94.912	94.306	94.489	94.860	94.719	94.502	94.309
Sn	3.298	3.439	3.549	3.384	3.505	3.187	2.967	3.481	3.267	3.725	3.440	3.279	3.316	3.528	3.508
Ag	1.509	1.462	1.878	1.175	1.547	1.537	1.341	1.613	1.394	1.503	1.661	1.480	1.540	1.628	1.793
Fe	0.137	0.104	0.114	0.065	0.120	0.100	0.111	0.092	0.124	0.101	0.117	0.110	0.119	0.093	0.097
Ni	0.060	0.043	0.051	0.049	0.049	0.056	0.054	0.049	0.037	0.041	0.051	0.058	0.048	0.053	0.047
Zn	0.052	0.000	0.048	0.000	0.042	0.057	0.032	0.033	0.059	0.063	0.050	0.000	0.060	0.000	0.049
As	0.091	0.105	0.093	0.109	0.106	0.101	0.095	0.091	0.093	0.098	0.087	0.100	0.066	0.105	0.102
Cd	0.000	0.000	0.000	0.000	0.000	0.000	0.000	0.000	0.000	0.000	0.000	0.000	0.000	0.000	0.000
Sb	0.061	0.070	0.072	0.069	0.076	0.057	0.071	0.060	0.061	0.065	0.067	0.071	0.070	0.064	0.066
Pb	0.000	0.249	0.828	0.019	0.000	0.000	0.000	0.000	0.000	0.015	0.000	0.000	0.000	0.000	0.000
S	0.025	0.025	0.027	0.014	0.027	0.037	0.014	0.044	0.035	0.083	0.025	0.021	0.035	0.027	0.029
Total	**100.000**	**100.000**	**100.000**	**100.000**	**100.000**	**100.000**	**100.000**	**100.000**	**100.000**	**100.000**	**100.000**	**100.000**	**100.000**	**100.000**	**100.000**

Table iv.121.: EMP analyses of bronze coin sample III.

Sample	**VI**	**VI**	**VI**	**VI**	**VI**	**VI**	**VI**	**VI**	**VI**	**VI**	**VI**	**VI**	**VI**	**VI**
No.	**#1**	**#2**	**#3**	**#4**	**#5**	**#6**	**#7**	**#8**	**#9**	**#10**	**#11**	**#12**	**#14**	**#15**
Cu	97.485	97.693	98.449	98.410	98.492	97.071	96.902	96.855	96.408	90.606	98.290	97.239	97.659	98.455
Sn	0.514	0.648	0.307	0.651	0.551	0.588	0.680	0.413	0.500	0.727	0.223	0.642	0.833	0.377
Ag	1.593	2.054	1.323	1.192	1.264	1.693	2.223	1.859	2.027	2.407	1.195	2.211	1.412	1.441
Fe	< 0	< 0.016	< 0.014	< 0.015	< 0.015	< 0.015	< 0.014	< 0.018	< 0	< 0.015	< 0.012	0.021	< 0.016	0.018
Ni	0.041	0.051	0.074	0.043	0.047	0.061	0.041	0.067	0.045	0.039	0.061	0.053	0.053	0.056
Zn	< 0	< 0	< 0	< 0	< 0	< 0	< 0	< 0	< 0	< 0	< 0	< 0	< 0	< 0
As	0.089	0.095	0.079	0.113	0.081	0.100	0.081	0.050	0.072	0.109	0.044	0.094	0.099	0.064
Cd	0.037	0.043	< 0.027	0.031	0.027	0.067	0.030	0.058	< 0.027	0.040	0.042	< 0.026	0.036	0.037
Sb	0.094	0.116	0.083	0.122	0.107	0.128	0.116	0.095	0.110	0.138	0.057	0.113	0.143	0.097
Pb	0.370	0.033	< 0.026	< 0	0.062	0.674	0.058	< 0.032	< 0	7.489	0.065	< 0.034	< 0	< 0.038
S	0.020	< 0	< 0.006	0.008	0.018	0.009	0.011	0.042	< 0.006	0.013	0.019	0.012	< 0.006	< 0.006
Total	**100.260**	**100.733**	**100.330**	**100.570**	**100.661**	**100.391**	**100.153**	**99.439**	**99.162**	**101.568**	**99.996**	**100.399**	**100.248**	**100.545**
							Atom %							
Cu	98.409	98.203	98.844	98.706	98.698	98.187	98.061	98.378	98.338	95.410	98.955	98.077	98.458	98.739
Sn	0.278	0.349	0.165	0.350	0.296	0.318	0.368	0.225	0.273	0.410	0.120	0.347	0.450	0.202
Ag	0.947	1.216	0.783	0.704	0.746	1.009	1.325	1.112	1.218	1.493	0.709	1.314	0.839	0.851
Fe	0.000	0.000	0.000	0.000	0.000	0.000	0.000	0.000	0.000	0.000	0.000	0.024	0.000	0.021
Ni	0.045	0.056	0.080	0.047	0.051	0.067	0.045	0.074	0.050	0.044	0.066	0.058	0.058	0.061
Zn	0.000	0.000	0.000	0.000	0.000	0.000	0.000	0.000	0.000	0.000	0.000	0.000	0.000	0.000
As	0.076	0.081	0.067	0.096	0.069	0.086	0.070	0.043	0.062	0.097	0.038	0.080	0.085	0.054
Cd	0.021	0.024	0.000	0.018	0.015	0.038	0.017	0.033	0.000	0.024	0.024	0.000	0.021	0.021
Sb	0.050	0.061	0.043	0.064	0.056	0.068	0.061	0.050	0.059	0.076	0.030	0.059	0.075	0.051
Pb	0.115	0.010	0.000	0.000	0.019	0.209	0.018	0.000	0.000	2.419	0.020	0.000	0.000	0.000
S	0.040	0.000	0.000	0.016	0.036	0.018	0.022	0.085	0.000	0.027	0.038	0.024	0.000	0.000
Total	**100.000**	**100.000**	**100.000**	**100.000**	**100.000**	**100.000**	**100.000**	**100.000**	**100.000**	**100.000**	**100.000**	**100.000**	**100.000**	**100.000**

Table iv.122.: EMP analyses of impure copper coin sample VI.

v. Isotope analyses

Sample	$^{206}Pb/^{204}Pb$	2σ	$^{207}Pb/^{204}Pb$	2σ	$^{208}Pb/^{204}Pb$	2σ	$^{207}Pb/^{206}Pb$	2σ	$^{208}Pb/^{206}Pb$	2σ
11015	18.793	0.080	15.670	0.013	38.953	0.033	0.83382	0.00021	2.07268	0.00077
11043(2)	18.787	0.079	15.670	0.013	38.968	0.037	0.83409	0.00017	2.07410	0.00058
11043(3)	18.788	0.115	15.668	0.018	38.985	0.047	0.83395	0.00024	2.07484	0.00075
11079	18.789	0.079	15.675	0.014	38.966	0.036	0.83426	0.00018	2.07386	0.00057
11090(6)	18.781	0.061	15.665	0.011	38.954	0.031	0.83412	0.00022	2.07419	0.00080
12055(1)	18.789	0.048	15.674	0.008	39.004	0.025	0.83420	0.00014	2.07595	0.00057
13020(1)	18.788	0.075	15.673	0.013	38.974	0.038	0.83417	0.00021	2.07438	0.00069
13098(1)	18.788	0.056	15.669	0.010	38.950	0.029	0.83402	0.00024	2.07319	0.00072
13099(2)	18.788	0.091	15.672	0.016	38.975	0.041	0.83418	0.00025	2.07454	0.00084
14018	18.786	0.087	15.673	0.015	38.964	0.042	0.83433	0.00022	2.07419	0.00069
13105(1)	18.734	0.051	15.669	0.015	38.899	0.046	0.83645	0.00023	2.07650	0.00063
13105(2)	18.732	0.027	15.666	0.009	38.892	0.024	0.83637	0.00018	2.07622	0.00059
13105(3)	18.735	0.029	15.669	0.012	38.901	0.028	0.83640	0.00015	2.07649	0.00050
13130(1)	18.617	0.042	15.656	0.012	38.789	0.034	0.84096	0.00016	2.08350	0.00062
13130(2)	18.625	0.033	15.659	0.011	38.800	0.031	0.84076	0.00018	2.08319	0.00052
13130(3)	18.620	0.035	15.657	0.011	38.788	0.032	0.84085	0.00013	2.08308	0.00060

Table v.1.: Pb isotope data of ores.

Sample	$^{206}Pb/^{204}Pb$	2σ	$^{207}Pb/^{204}Pb$	2σ	$^{208}Pb/^{204}Pb$	2σ	$^{207}Pb/^{206}Pb$	2σ	$^{208}Pb/^{206}Pb$	2σ
10-2B	18.780	0.013	15.668	0.015	38.975	0.040	0.83434	0.00027	2.07546	0.00089
12015(5)	18.775	0.012	15.669	0.012	38.975	0.034	0.83459	0.00017	2.07592	0.00067
12015(7)	18.699	0.013	15.661	0.014	38.866	0.033	0.83754	0.00022	2.07843	0.00078
12015(12)	18.715	0.015	15.664	0.015	38.902	0.041	0.83694	0.00019	2.07861	0.00070
14032	18.779	0.015	15.673	0.013	38.962	0.033	0.83457	0.00020	2.07469	0.00060
11027(1)	18.713	0.025	15.669	0.022	38.893	0.059	0.83736	0.00034	2.07839	0.00086
11027(2)	18.757	0.012	15.672	0.009	38.961	0.029	0.83553	0.00021	2.07723	0.00085
11029(3)	18.739	0.013	15.665	0.012	38.929	0.035	0.83595	0.00024	2.07735	0.00090
11029(4)	18.681	0.023	15.665	0.019	38.888	0.052	0.83852	0.00025	2.08156	0.00079
11029(5)	18.775	0.013	15.670	0.011	38.969	0.032	0.83462	0.00021	2.07551	0.00088
11029(7)	18.625	0.017	15.663	0.016	38.834	0.049	0.84096	0.00023	2.08491	0.00088
10024(2)	18.788	0.012	15.668	0.012	38.972	0.036	0.83393	0.00019	2.07426	0.00081
10024(4)	18.785	0.015	15.671	0.014	38.996	0.039	0.83422	0.00022	2.07587	0.00076
10024(5)	18.788	0.041	15.675	0.033	39.010	0.090	0.83427	0.00034	2.07634	0.00084
10021(2)	18.720	0.020	15.668	0.019	38.938	0.054	0.83696	0.00022	2.07995	0.00079
10021(4)	18.711	0.016	15.670	0.013	38.938	0.037	0.83749	0.00023	2.08109	0.00073
10021(21)	18.720	0.014	15.672	0.012	38.947	0.034	0.83717	0.00026	2.08050	0.00082
MrS_gn	18.786	0.013	15.668	0.013	38.985	0.037	0.83402	0.00019	2.07516	0.00076
MrS_Pb	18.787	0.011	15.670	0.011	38.989	0.034	0.83410	0.00019	2.07529	0.00079
10-5	18.670	0.012	15.663	0.011	38.822	0.031	0.83892	0.00018	2.07936	0.00056
10-6	18.620	0.012	15.659	0.012	38.798	0.034	0.84101	0.00020	2.08365	0.00080
10032(1)	18.616	0.013	15.657	0.012	38.788	0.033	0.84107	0.00021	2.08359	0.00081
10032(4)	18.634	0.019	15.656	0.017	38.781	0.047	0.84019	0.00027	2.08120	0.00077
10-1A	18.619	0.015	15.665	0.013	38.786	0.037	0.84132	0.00022	2.08306	0.00086
10-1B	18.659	0.017	15.674	0.016	38.848	0.046	0.83997	0.00027	2.08201	0.00080
3(1)	18.645	0.011	15.655	0.010	38.780	0.031	0.83966	0.00021	2.07997	0.00070
3(2)	18.666	0.014	15.663	0.013	38.851	0.038	0.83914	0.00023	2.08141	0.00082
12016(1)	18.703	0.013	15.663	0.011	38.882	0.035	0.83742	0.00016	2.07888	0.00073
12016(2)	18.785	0.010	15.668	0.011	38.976	0.030	0.83410	0.00016	2.07490	0.00063
13030(1)	18.792	0.018	15.673	0.016	38.992	0.043	0.83401	0.00021	2.07493	0.00075
13031(1)	18.786	0.016	15.669	0.014	38.976	0.044	0.83405	0.00020	2.07471	0.00078

Table v.2.: Pb isotope data of metallurgical (by-) products.

Sample	$^{206}Pb/^{204}Pb$	2σ	$^{207}Pb/^{204}Pb$	2σ	$^{208}Pb/^{204}Pb$	2σ	$^{207}Pb/^{206}Pb$	2σ	$^{208}Pb/^{206}Pb$	2σ
I.1	18.681	0.019	15.664	0.018	38.844	0.049	0.83848	0.00028	2.07917	0.00101
I.2	18.683	0.013	15.664	0.014	38.841	0.040	0.83841	0.00021	2.07895	0.00091
I.3	18.683	0.014	15.664	0.014	38.843	0.040	0.83846	0.00022	2.07904	0.00090
II.1	18.731	0.016	15.665	0.016	38.861	0.046	0.83632	0.00026	2.07475	0.00110
II.2	18.735	0.012	15.668	0.012	38.869	0.038	0.83633	0.00025	2.07480	0.00087
II.3	18.731	0.015	15.665	0.014	38.860	0.041	0.83630	0.00029	2.07465	0.00101
IV	18.765	0.020	15.667	0.018	38.917	0.052	0.83488	0.00029	2.07395	0.00113
V	18.693	0.021	15.660	0.020	38.823	0.056	0.83775	0.00028	2.07670	0.00092
III	18.495	0.014	15.653	0.014	38.623	0.044	0.84634	0.00028	2.08831	0.00109
VI	18.652	0.012	15.668	0.012	38.757	0.038	0.83998	0.00021	2.07781	0.00085

Table v.3.: Pb isotope data of metal artefacts.

Sample	$\delta^{65}Cu$	2σ
11015	-1.410	0.196
11043(2)	9.979	0.243
11043(3)	-4.290	2.850
11079	0.257	0.121
11090(6)	6.160	0.185
12055(1)	-0.728	0.154
13020(1)	11.898	0.177
13098(1)	0.019	0.283
13099(2)	-1.250	0.133
14018	na	na
MrS_gn	-0.720	0.170
MrS_Pb	1.429	0.218
I.1	-0.549	0.247
I.2	-0.749	0.289
I.3	-0.626	0.237
II.1	-0.716	0.159
II.2	-0.735	0.304
II.3	-0.651	0.241
IV	-0.327	0.265
V	0.437	0.324
III	-0.772	0.172
VI	0.440	0.536

Table v.4.: Cu isotope data of ores and metal artefacts.